INTERNATIONAL COUNCIL FOR BUILDING RESEARCH STUDIES AND DOCUMENTATION

WORKING COMMISSION W18 - TIMBER STRUCTURES

INTERNATIONAL UNION OF FOREST RESEARCH ORGANISATIONS

GROUP S 5.02 - TIMBER ENGINEERING

CIB-W18
IUFRO S 5.02

Volume II

MEETING NINETEEN

FLORENCE

ITALY

SEPTEMBER 1986

CONTENTS VOLUME II

List of CIB-W18 Papers/Florence 1986
CIB Papers 19-9-1 up to 19-105-1
Minutes of IUFRO S 5.02 Meeting, Ljubljiana, Jougoslavia
List of IUFRO S 5.02 Papers/Ljubljiana 1986
IUFRO Papers

CONTENTS VOLUME I

1 List of Participants
2 Chairman's Introduction
3 Cooperation with other Organisations
4 CIB-W18B: Tropical Timbers
5 Trussed Rafter Sub-Group
6 Sampling Sub-Group
7 Reports on Current Research
8 Duration of Load and Creep
9 Eurocode
10 Questions Related to Strength Distributions
11 Joints
12 Trussed Rafters
13 Stability
14 Seismic Design
15 Address by Mr. Marchi
16 Material Strength
17 Design with Wood-Based Panels
18 Future IUFRO S 5.02 Meeting
19 Future CIB-W18A Meeting
20 Testing of Truss Plates
21 Trussed Rafter Sub-Group
22 Sampling Sub-Group
23 Column Interaction
24 Other Business
25 Report on Current Reserach
26 Report on Session on Duration of Load and Creep
27 Report on Session on Eurocode 5
28 List of CIB-W18 Papers/Florence 1986
29 Current List of CIB Papers

CIB Papers 19-1-1 up to 19-8-1

List of CIB-W18 Papers/Florence 1986

19-1-1	Duration of Load Effects and Reliability Based Design (Single Member) - R O Foschi and Z C Yao
19-2-1	Creep Buckling Strength of Timber Beams and Columns - R H Leicester
19-5-1	Stress-Grading by ECE Standards of Italian-Grown Douglas-Fir Dimension Lumber from Young Thinnings - L Uzielli
19-5-2	Structural Softwood from Afforestation Regions in Western Norway - R Lackner
19-6-1	Effect of Age and/or Load on Timber Strength - J Kuipers
19-6-2	Confidence in Estimates of Characteristic Values - R H Leicester
19-6-3	Fracture Toughness of Wood - Mode I - K Wright and M Fonselius
19-6-4	Fracture Toughness of Pine - Mode II - K Wright
19-6-5	Drying Stresses in Round Timber - A Ranta-Maunus
19-6-6	A Dynamic Method for Determining Elastic Properties of Wood - R Görlacher
19-7-1	Behaviour of Nailed and Bolted Joints under Short-Term Lateral Load - Conslusions from Some Recent Research - L R J Whale, I Smith B O Hilson
19-7-2	Glued Bolts in Glulam - H Riberholt
19-7-3	Effectiveness of Multiple Fastener Joints According to National Codes and Eurocode 5 (Draft) - G Steck
19-7-4	The Prediction of the Long-Term Load Carrying Capacity of Joints in Wood Structures - Y M Ivanov and Y Y Slavic
19-7-5	Slip in Joints under Long-Term Loading - T Feldborg and M Johansen
19-7-6	The Derivation of Design Clauses for Nailed and Bolted Joints in Eurocode 5 - L R J Whale and I Smith
19-7-7	Design of Joints with Nail Plates - Principles - B Norén
19-7-8	Shear Tests for Nail Plates - B Norén
19-7-9	Advances in Technology of Joints for Laminated Timber - Analyses of the Structural Behaviour - M Piazza and G Turrini

19-8-1	Predicting the Natural Frequencies of Light-Weight Wooden Floors - I Smith an Y H Chui
19-9-1	Another Look at Three Duration of Load Models - R O Foschi and Z C Yao
19-9-2	Duration of Load Effects for Spruce Timber with Special Reference to Moisture Influence - A Status Report - P Hoffmeyer
19-9-3	A Model of Deformation and Damage Processes Based on the Reaction Kinetics of Bond Exchange - T A C M van der Put
19-9-4	Non-Linear Creep Superposition - U Korin
19-9-5	Determination of Creep Data for the Component Parts of Stressed-Skin Panels - R Kliger
19-9-6	Creep and Lifetime of Timber Loaded in Tension and Compression - P Glos
19-10-1	Possible Code Approaches to Lateral Buckling in Beams - H J Burgess
19-11-1	Experimental Analysis on Ancient Downgraded Timber Structures - B Leggeri and L Paolini
19-12-1	Strength of Glued Laminated Timber - J Ehlbeck and F Colling
19-12-2	Strength Model for Glulam Columns - H J Blaß
19-12-3	Influence of Volume and Stress Distribution on the Shear Strength and Tensile Strength Perpendicular to Grain - F Colling
19-12-4	Time-Dependent Behaviour of Glued-Laminated Beams - F Zaupa
19-14-1	Annex on Simplified Design of W-Trusses - H J Larsen
19-14-2	Simplified Static Analysis and Dimensioning of Trussed Rafters - Part 2 - H Riberholt
19-14-3	Joint Eccentricity in Trussed Rafters - T Poutanen
19-15-1	Connections Deformability in Timber Structures: a Theoretical Evaluation of its Influence on Seismic Effects - A Ceccotti and A Vignoli
19-15-2	The Bracing of Trussed Beams - M H Kessel and J Natterer
19-15-3	Racking Resistance of Wooden Frame Walls with Various Openings - M Yasumura

19-15-4 Some Experiences of Restoration of Timber Structures for Country Buildings - G Cardinale and P Spinelli

19-15-5 Non-Destructive Vibration Tests on Existing Wooden Dwellings - Y Hirashima

19-16-1 Simulation of Fire in Tests of Axially Loaded Wood Wall Studs - J König

19-17-1 Load Factors for Proof and Prototype Testing - R H Leicester

19-102-1 Eurocode 5 - Requirements to Timber - Drafting Panel Eurocode 5

19-102-2 Eurocode 5 and CIB Structural Timber Design Code - H J Larsen

19-102-3 Comments on the Format of Eurocode 5 - A R Fewell

19-102-4 New Developments of Limit States Design for the New GDR Timber Design Code - W Rug and M Badstube

19-105-1 Tropical and Hardwood Timbers Structures - R H Leicester

CIB-W18/19-9-1

INTERNATIONAL COUNCIL FOR BUILDING RESEARCH STUDIES AND DOCUMENTATION

WORKING COMMISSION W18 - TIMBER STRUCTURES

ANOTHER LOOK AT THREE DURATION OF LOAD MODELS

by

R O Foschi and Z C Yao
University of British Columbia
Canada

MEETING NINETEEN
FLORENCE
ITALY
SEPTEMBER 1986

INTRODUCTION

The problem of load duration effects in timber and wood-based products has attracted considerable attention during the last decade. In particular, the research effort has concentrated on determining the differences between the behaviour of material in structural sizes and that of small, clear specimens. Results reported by Madsen and Barrett (1976) first showed that Douglas fir lumber in bending did not follow the trend of the "Madison curve", derived from small clears and traditionally used to quantify duration of load effects for all structural applications of wood. Tests were subsequently started at the Western Forest Products Laboratory in Vancouver using Western hemlock lumber in bending. The results have been reported by Foschi and Barrett (1982), and they not only confirmed the experimental trend observed by Madsen but the conclusions were reinforced by a substantially larger sample size. In the U.S., tests were started at the Madison Laboratory by Gerhards (1977,1986), using a sample of 2 x 4 lumber particularly selected to provide low short-term strength material. As a result of this activity, a joint Canada-U.S. project was begun between Forintek Canada Corp. and the Madison laboratory. The planning included testing of spruce lumber in Canada and Douglas fir in the U.S., in two sizes, two lumber qualities, in bending, tension and fully-restrained compression. The Canadian part of the project is well underway, with the bending testing almost complete for 2 x 8's and continuing for 2 x 4's. Testing in tension and compression is equally advanced. Preliminary results from the bending tests were presented during a symposium on load duration organized by Forintek Canada Corp.,(Foschi and Barrett, 1985).

Experimental programs are also underway in Europe, particularly in the U.K, Denmark and West Germany.

The interpretation of the experimental results has also received substantial attention. The development of "duration of load models" is required to link the conclusions from the tests, performed under constant loads, to the more general design situation of loads varying over time.

Essentially two approaches have been used in the development of load duration models: 1) accumulation of damage and 2) fracture mechanics or crack propagation. The work of Gerhards (1977,1986) and Foschi and Barrett (1982,1985) uses the concept of damage accumulation, while Nielsen's (1980,1982,1985) is based on crack propagation in a material with viscoelastic properties.

In the first approach, "damage" is seen as a state variable ranging from 0 at the beginning of load application to 1 at failure. Several types of damage accumulation laws could be postulated, depending on whether the accumulation rate is assumed to depend only on the stress level or also on the previously accumulated damage. Election of a particular form for the damage law must rely on how well it will match the experimental results when the corresponding test load histories are entered. Although "damage" cannot be measured directly, one can think of it as being implicitly related to more "physical variables". For example, an admissible definition of damage would be the ratio between the current crack length and the crack length at failure, since it satisfies the range conditions (0-1). Simple damage accumulation laws, depending only on stress level, have long been used in the study of fatigue in metals: Miner's rule of linear damage accumulation is a well known example.

The fracture mechanics approach postulates a law for the speed at which a crack will grow under stress. In linear, elastic fracture mechanics the law commonly used is an empirical relationship between speed and level of the stress intensity factor, derived from tests. Since the stress intensity factor depends on the crack length, this law implies that the crack speed is controlled both by stress level and the current length of the crack. Nielsen has proposed a similar model but, instead of making the assumptions of linear, elastic materials, he considers a material which behaves viscoelastically around the crack tip. Thus, upon load application, the material around the tip deforms (without the crack propagating) until a critical deformation is achieved. At this time, the crack advances and the process repeats itself until the crack achieves a critical length at which very rapid failure follows.

One objective of this paper is to discuss briefly these three models and their ability to represent data from an experiment on Western hemlock lumber in bending (Foschi and Barrett, 1982). A second objective is to discuss the problems which each of these models present when they are used in the development of reliability-based design procedures.

THE U.S DAMAGE MODEL (GERHARDS)

In this model the rate of damage accumulation is written as

$$(1) \qquad d\alpha/dt = \exp(-a + b\,\tau(t)/\tau_s)$$

where $\alpha(t)$ is the damage, $\tau(t)$ the applied stress, a and b are constants

and τ_s is the short-term strength measured in a ramp test. It is assumed that while a and b are constants for the population, τ_s is lognormally distributed.

This is an example of a law which only depends on stress level. Let us consider the integration of Eq.(1) for the ramp stress history used in determining τ_s. For $\tau(t) = \bar{\tau}_s\ (t/\bar{T}_s)$, and integrating between t=0 ($\alpha = 0$) and $t = T_s$ ($\alpha = 1$), one gets (for $k = \bar{\tau}_s / \bar{T}_s$) ,

$$1 = \tau_s \exp(-a)\ [\exp(b) - 1.0] / (b\ k) \qquad (2)$$

This equation points to a first flaw in the formulation of the model. It is apparent that if a and b are constants, since k is constant, τ_s must also be constant, contrary to the its definition as a random variable. Nevertheless, for the test load history of Fig.1, the time-to-failure T_f is given by

$$T_f = T_o + \tau_s\ \{\ \exp[b(1 - \tau_a/\ \tau_s)] - 1\ \} / (b\ k) \qquad (3)$$

where τ_a is the applied constant stress and T_o the time needed to apply it.

Eq.(3) can be fitted to cumulative distribution data of times-to-failure. Given τ_s , the constants a and b can be found

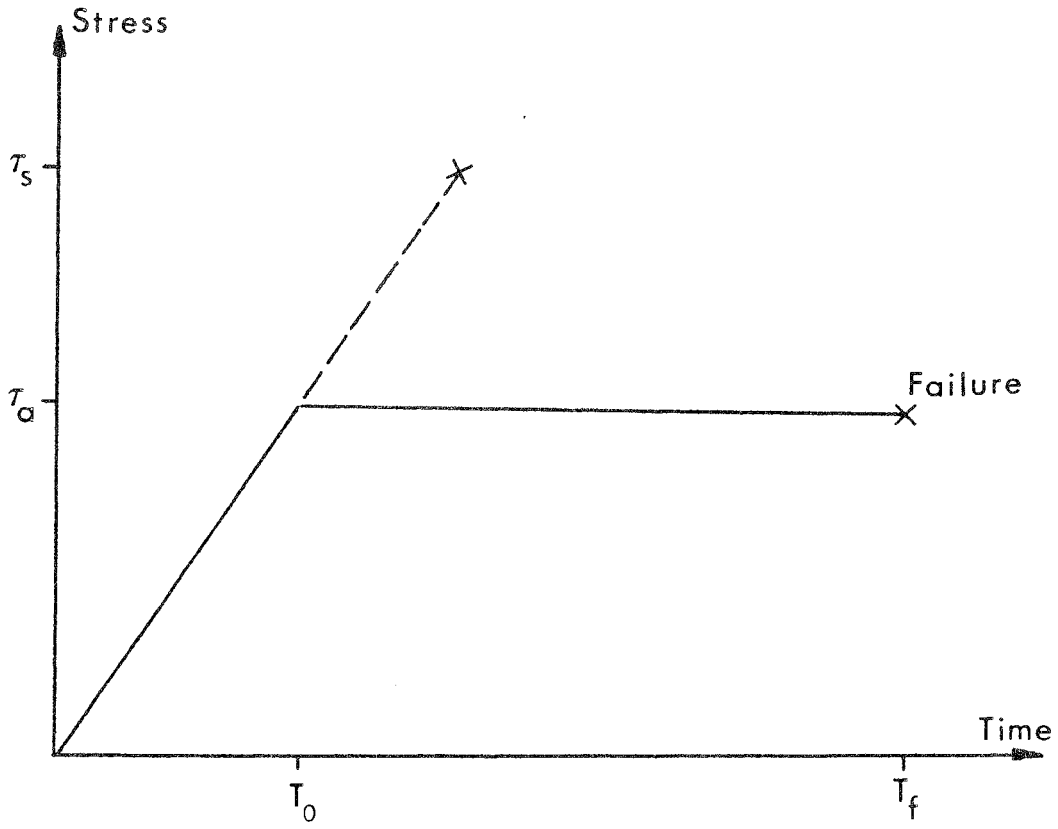


FIGURE 1. Experimental Stress History

from the minimization of the function

$$(4) \qquad \psi = \sum_{i=1}^{N} (1.0 - T_{fi}/T_{di})^2$$

where T_{fi} and T_{di} are, respectively, the predicted and the measured time-to-failure at the same probability level.

Fig. 2 shows a fit of the model to cumulative probability distributions for Western hemlock lumber in bending. It is apparent that the model is too rigid to represent the data trend. If a better fit is obtained for the shorter times, as in Fig. 3, the model is not able at all to follow the data trend at longer times.

The model, whether from Fig. 2 or 3, would predict much longer times-to-failure than observed from the data. This non-conservative feature, coupled with flaws in its definition, do not make this model suitable for either data representation or further reliability studies.

THE FRACTURE MECHANICS MODEL (NIELSEN)

L. Nielsen's model of crack propagation in a material with viscoelastic properties must be considered in two parts: 1) while the crack tip is viscoelastically deforming without crack extension and 2) after crack extension takes place.

TIME–to–FAILURE CUMULATIVE DISTRIBUTION
from experiment and from theory

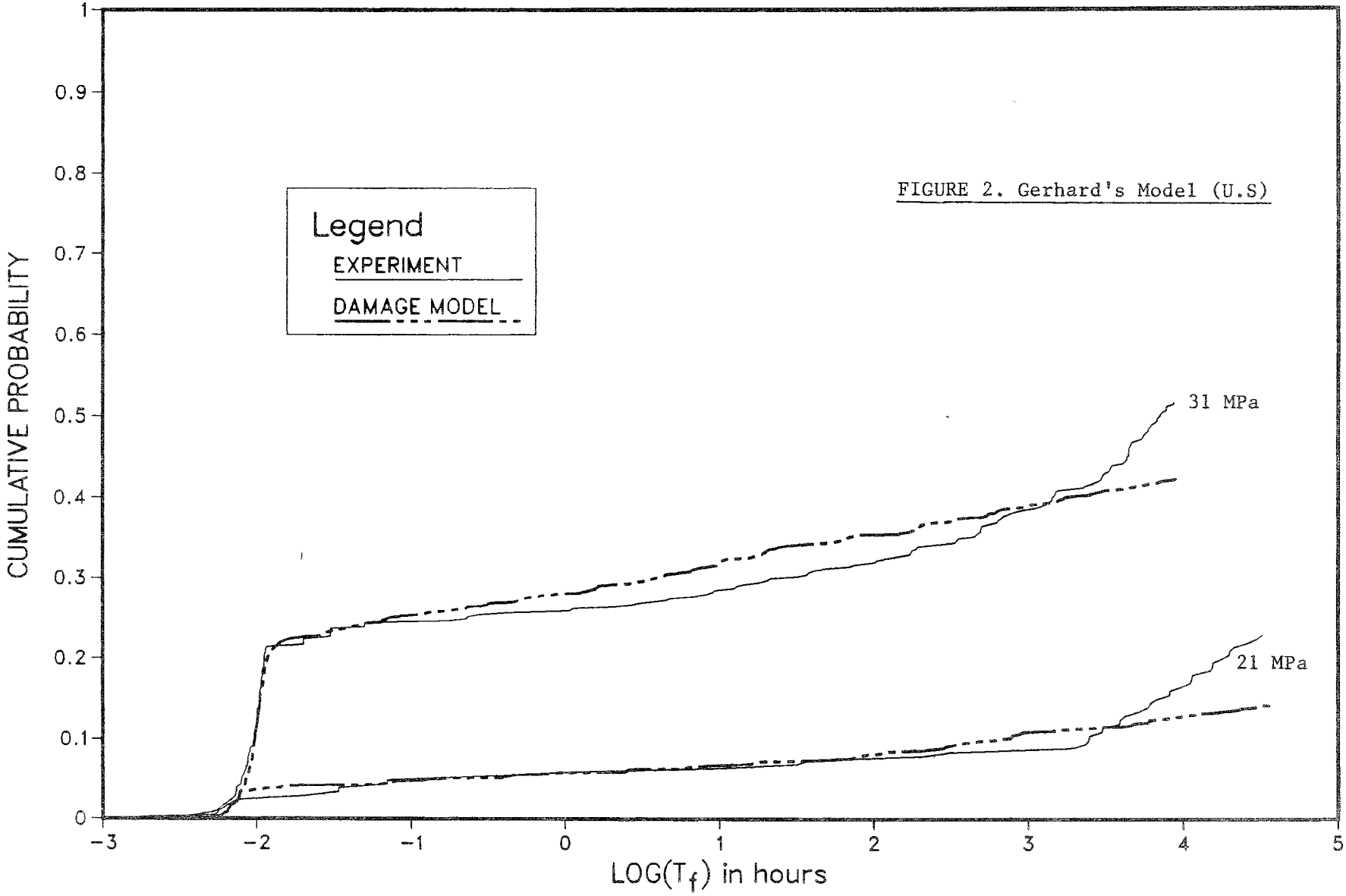


FIGURE 2. Gerhard's Model (U.S)

TIME–to–FAILURE CUMULATIVE DISTRIBUTION
from experiment and from theory

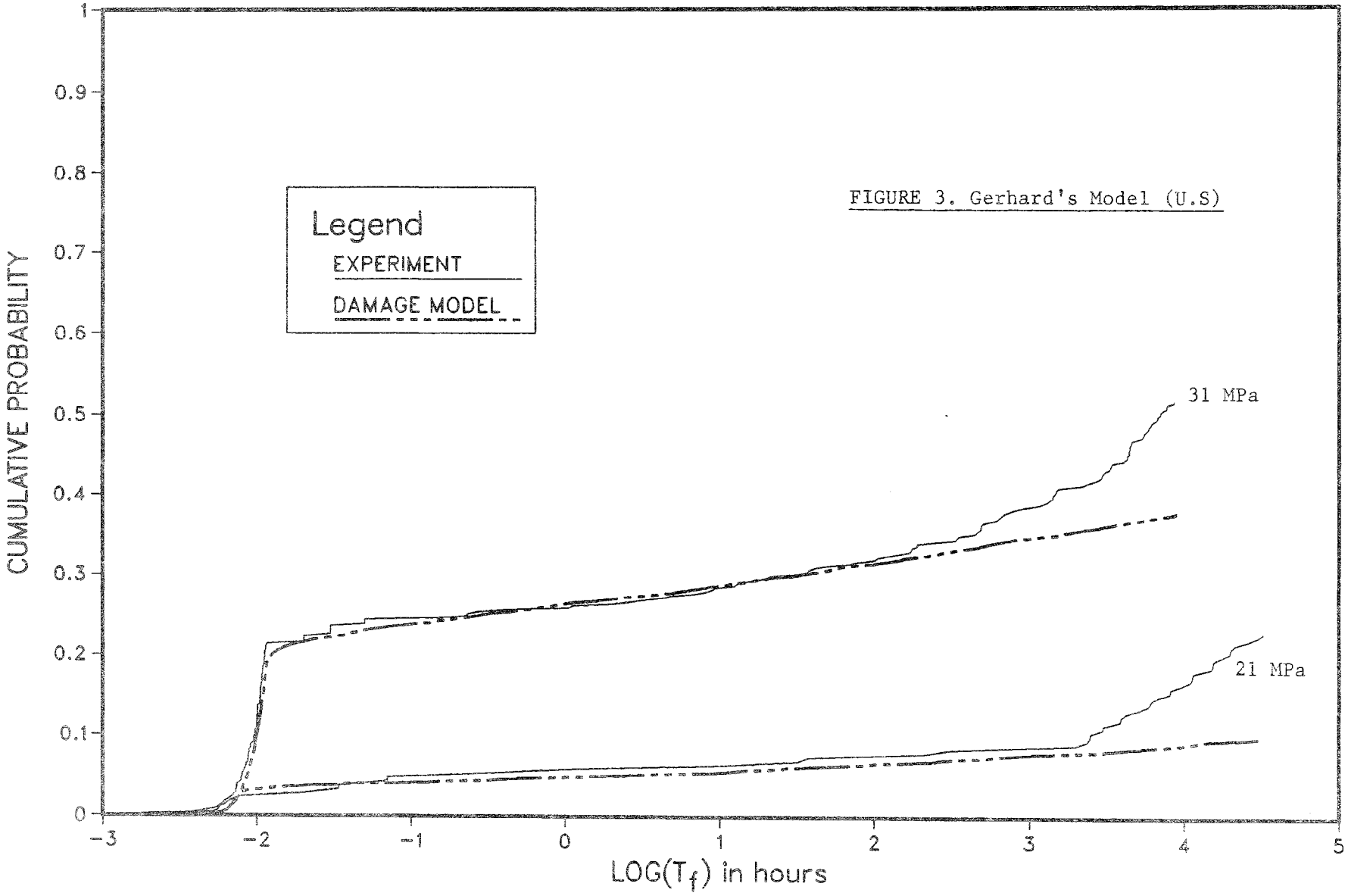


FIGURE 3. Gerhard's Model (U.S)

Nielsen shows the calculation of the time T_s required to start crack propagation. This time depends on the load history, satisfying

$$(5) \qquad [1.0 + 2.0\ (T_s/\tau)^b/(b+1)(b+2)] = [\ \sigma_{cr}/(k\ T_s)]^2$$

for a ramp load, and

$$(6) \qquad [1.0 + (T_s/\tau\ )^b] \ = \ (\ \sigma_{cr}/\ \tau_a)^2$$

for a constant, step-function stress τ_a. The parameters b and τ correspond to the creep function J(t),

$$(7) \qquad J(t) = [1.0 + (t/\tau\ )^b]/E$$

where τ is then the deformation doubling time and E the initial modulus of elasticity.

After the time T_s, the model results in the following relationship for the rate of crack growth:

$$(8) \qquad d\ \kappa(t)/dt = \frac{\pi^2}{8\ q\ \tau}\left(\frac{\sigma_{cr}}{\sigma_L}\right)^2 \frac{\left[\kappa(t)\left\{\frac{\sigma(t)}{\sigma_{cr}}\right\}^2\right]^{(b+1)/b}}{\left[1.0 - \kappa(t)\left\{\frac{\sigma(t)}{\sigma_{cr}}\right\}^2\right]^{1/b}}$$

where $\kappa(t)$ is the non-dimensional crack length ratio, σ_L the inherent strength of the material without flaws, and σ_{cr} is the short-term strength measured in a very fast ramp test (actually, under an infinite rate of loading). The constant q in Eq.(8) is defined as

$$q = [(b+1)(b+2)/2]^{1/b} \tag{9}$$

and, if c(t) and c_o are, respectively, the current and the original crack length,

$$\kappa(t) = c(t) / c_o \tag{10}$$

Eq.(8) is identical with Eq.(31) shown by Nielsen (1985). It is apparent that, given any stress history $\sigma(t)$, a solution for $\kappa(t)$ is quite difficult to obtain without resorting to numerical integration.

What is the condition at failure when the crack speed grows without bounds? From the denominator of Eq.(8), the time-to-failure T_f will be such that

$$\kappa(Tf)\left(\frac{\sigma(T_f)}{\sigma_{cr}}\right)^2 = 1 \tag{11}$$

When the applied stress is constant (a step function τ_a), the variables t and $\kappa(t)$ can be separated and Eq.(8) can be integrated between the lower limit $\kappa = 1$ and the upper limit given by Eq.(11). The resulting time-to-failure T_f is given by

$$(12) \qquad T_f = T_s + \frac{8\, q\, \tau}{\pi^2}\left(\frac{\sigma_{cr}}{\tau_a}\right)^2\left(\frac{\sigma_L}{\sigma_{cr}}\right)^2 \int_1^{(\sigma_{cr}/\tau_a)^2} \frac{(\theta - 1)^{1/b}}{\theta}\, d\theta$$

This equation was used to fit the model to the same Western hemlock data previously considered. The calibration parameters were the exponent b, the doubling time τ and the ratio $r = (\sigma_L / \sigma_{cr})$. Each of these were assumed to be independent, random variables. To satisfy the condition that r and τ be positive, they were assumed to be lognormally distributed. The exponent b, on the other hand, was assumed normally distributed. The model was calibrated by minimizing the same function of Eq.(4), with the actual variables being the mean and standard deviations of each of the three unknown distributions. The minimization itself was carried out with a nonlinear optimization routine (Fletcher and Powell, 1963).

The results of the minimization were as follows:

Variable	Distribution	Mean	Std. Deviation
Doubling time, τ	Lognormal	1017.38 hours	536.11 hours
Creep exponent, b	Normal	0.249	0.0415
Ratio, r*	Lognormal	2.764	2.883

with the ratio $r = \sigma_L / \sigma_{cr} = 1.0 + r^*$.

TIME–to–FAILURE CUMULATIVE DISTRIBUTION
from experiment and from theory

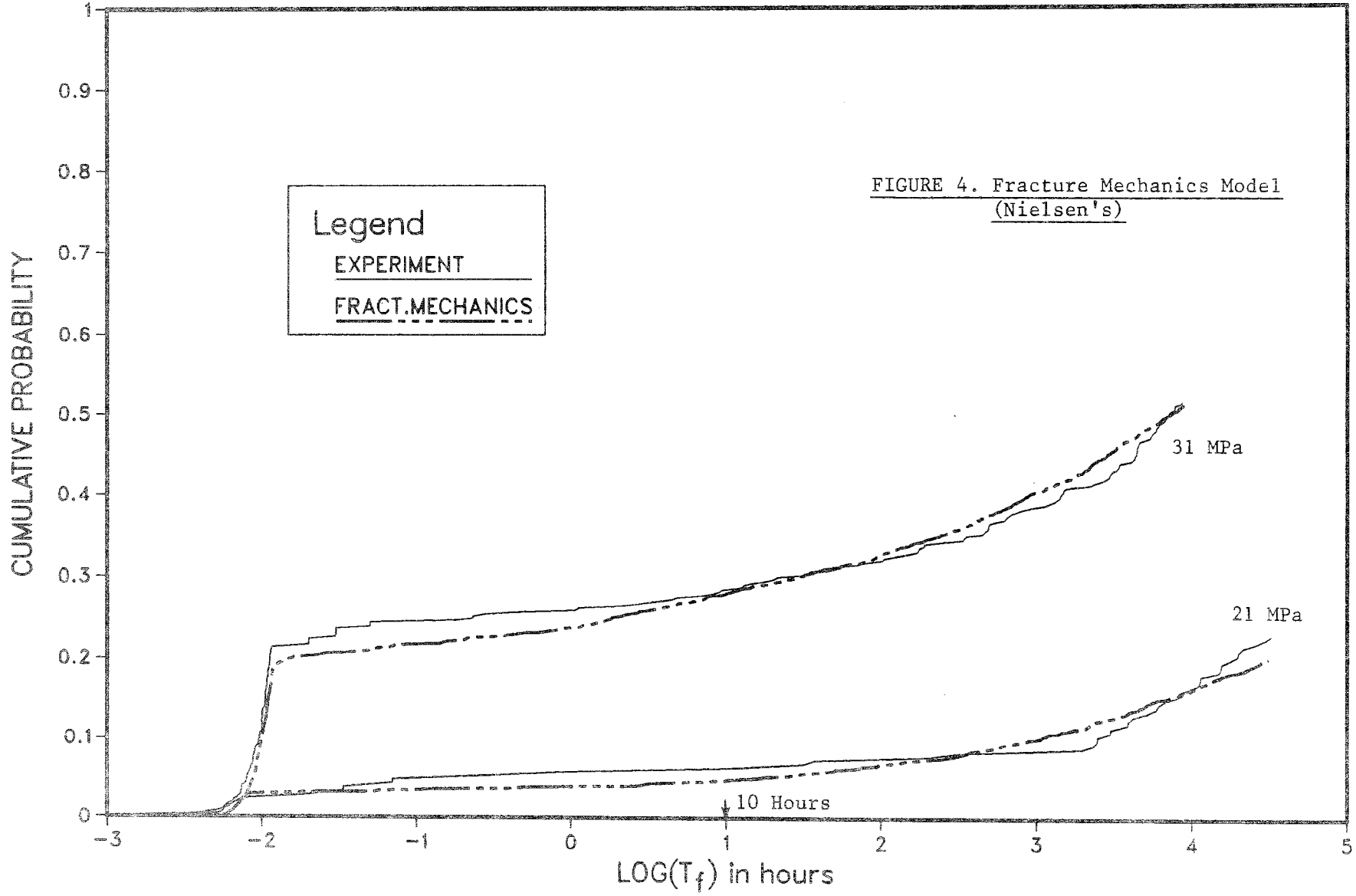


FIGURE 4. Fracture Mechanics Model
(Nielsen's)

Fig. 4 shows the corresponding fit of the test data. It is apparent that this model is capable of representing the experimental trends very well. It must be noted, however, that the expression for T_f from Eq.(12) corresponds to a step function loading, and not to the actual loading used in the experiment as shown in Fig. 1. It was assumed that the data for times-to-failure longer than 10 hours would not be affected by the manner in which the load was applied, and therefore the fit was performed including only times-to-failure longer than 10 hours.

In order to discuss the model further, let us define the quantity

$$\Theta = (\sigma_{cr}/\,\sigma(t))^2 \,/\, \kappa(t) \tag{13}$$

which initially (at $t = T_s$) takes the value $\Theta_o = (\sigma_{cr}/\,\sigma_o)^2$, where σ_o is the stress at $t = T_s$. At failure, from Eq.(11), $\Theta = 1$. Thus, this quantity behaves as a damage parameter. The rate of growth of Θ can be derived from Eq.(8),

$$d\Theta/dt + \Theta\left[2\frac{\dot{\sigma}(t)}{\sigma(t)} + \frac{\pi^2}{8\,q\,\tau}\left(\frac{\sigma_{cr}}{\sigma_L}\right)^2\left(\frac{\sigma(t)}{\sigma_{cr}}\right)^2 \frac{1}{(\Theta - 1)^{1/b}}\right] = 0 \tag{14}$$

where $\dot{\sigma}(t)$ stands for the derivative $d\sigma(t)/dt$. For the general case in which the stress varies with time, Eq.(14) is a first-order, nonlinear equation for $\Theta(t)$ with coefficients which are also functions of time. It is a very difficult problem to find closed-form solutions to this equation, and the only recourse is to utilize numerical integration procedures. This fact complicates and makes expensive the utilization of this model for simulations in calculations for reliability-based design.

It is to be noted that numerical integration must be used even to predict strength under a ramp load. The strength σ_{cr} in the model is really the strength under a very fast ramp (infinite rate of loading). The strength under a standard ramp would be lower, and due to the complications of its calculation along with the fitting procedure, the calibration of the model was performed assuming that σ_{cr} was approximately equal to the short-term strength measured in a ramp test with an average duration of 1 minute.

Only when the stress is constant, $\dot{\sigma}(t) = 0$, the variables t and Θ in Eq.(14) can be separated and the equation integrated to yield the known result for T_f.

Another interesting discussion point is the effect of strength level, or the effect of σ_{cr} in Eq.(12). For the same stress ratio τ_a/σ_{cr}, and constant values of inherent strength σ_L and creep parameters, a stronger specimen (high σ_{cr}) would result in shorter T_f. It is important in this conclusion to emphasize the role of the variables kept constant: the effect of increasing σ_{cr} alone could be completely reversed if the

creep doubling time, for example, is sufficiently increased and creep is correspondingly reduced. The correlation between σ_{cr} and the creep parameters has not been studied experimentally, and could prove difficult to do. Nevertheless, this should be the topic of further research.

It would also appear difficult to introduce creep parameters obtained from a creep test where, for example, beam deflections were monitored over time. What is needed are creep parameters for the viscoelastic behaviour around the crack tip (perhaps in tension perpendicular to the grain), and the variability in these values will depend on very localized conditions of grain deviations and density. It is the authors' opinion that the creep parameters τ and b, although "physical" in nature, cannot be easily measured and may only be obtained by calibration of the model to load duration data. To illustrate this fact, Western hemlock lumber was not observed to double its initial deflection in just 42 days, although this doubling time appears suitable for the model. A recent report by Hoyle et al. (1985) on bending creep of Douglas fir beams estimates doubling times in the order of 10^5 hours.

THE CANADIAN DAMAGE MODEL (FOSCHI)

Foschi and Barrett (1982) presented a damage accumulation model which expressed the rate of damage growth as

$$(15) \qquad d\alpha/dt = a \left[\tau(t)/ \tau_s - \sigma_o \right]^b + \lambda \alpha(t)$$

where a and λ were independent random variables lognormally distributed, b was a constant, τ_s was the short-term strength measured in a ramp test of an average duration of 1 minute, and σ_o was a constant ("threshold stress ratio") which had to be exceeded in order to have damage accumulation.

The model of Eq.(15) was fitted to the same Western hemlock data by Foschi and Barrett (1982), and the model proved to be able to represent the experimental trends very well. In particular, the constant threshold stress ratio obtained was $\sigma_o = 0.50$. This meant that in a ramp test, for example, no damage is accumulated until the stress exceeds half of the ultimate strength.

Although this model had the advantages of being successful in representing the data, and of being relatively simple to use in reliability studies (Foschi, 1984), it also offered some disadvantages. In particular, during the integration of Eq.(15), the term $\lambda\alpha(t)$ leads to an exponential growth of damage. At the beginning, this term does not control the growth process and damage increases slowly. After some point, when damage has increased substantially , the term takes over and damage increases rapidly to failure. Although this seems reasonable, there is a case in which the model leads to unreasonable results. This is when, in a random load sequence, a load has produced a substantial damage (for example, $\alpha = 0.3$) but has not failed the member, and the subsequent loads in the sequence are infinitesimally higher than the threshold. Being higher than the threshold, they will produce additional damage albeit an infinitesimally small one. Nevertheless, the damage 0.3 will grow exponentially to failure as a result of the term $\lambda\alpha(t)$. One is then

faced with the unreasonable prediction that a situation of almost no loads will lead to failure over time if the member has been sufficiently damaged.

In order to improve the model, the random variable λ was taken to be a function of the stress level as well. In this manner, when the loads are very small, the exponential growth will also be very small. The modified model expresses the rate of damage growth as follows:

$$(16) \qquad d\alpha/dt = a\,[\,\tau(t) - \sigma_o\,\tau_s\,]^b + c\,[\,\tau(t) - \sigma_o\,\tau_s\,]^n\,\alpha(t)$$

where now c and n are constants which could change from member to member in a population.

Integrating Eq.(16) for the ramp load used to obtain the short-term strength τ_s, it is found that a can be approximately obtained as a function of the other model constants:

$$(17) \qquad a = k\,(b+1)/\,[\,\tau_s\,(1-\sigma_o)\,]^{(b+1)}$$

where k is the ramp loading rate. The damage α_o done during the loading part of the stress history of Fig. 1 can also be approximately expressed as

$$(18) \qquad \alpha_o = [\,(\tau_a - \sigma_o\,\tau_s)/(\tau_s - \sigma_o\,\tau_s)\,]^{(b+1)}$$

The time-to-failure T_f for the stress history of Fig. 1 is obtained from the corresponding integration of Eq.(16):

$$(19) \qquad T_f = T_o + \frac{1}{c(\tau_a - \sigma_o \tau_s)^n} \ln\left[\frac{1 + (a/c)(\tau_a - \sigma_o \tau_s)^{(b-n)}}{\alpha_o + (a/c)(\tau_a - \sigma_o \tau_s)^{(b-n)}}\right]$$

where a is obtained from Eq.(17) and α_o from Eq.(18).

It is worthwhile comparing this model with the predictions from the fracture mechanics approach. If the stress ratio (τ_a / τ_s) is kept constant, and for the same values of c, b, n and σ_o , the time T_f will be shorter for a member with a higher short-term strength τ_s. This is in agreement with Nielsen's model, but the same comment must be made that this conclusion depends on the assumption of all other parameters remaining constant. As in the fracture mechanics model, a higher τ_s could be compensated by a lower value of c to maintain a given value for T_f. In this model, the parameter c plays the role of the creep doubling time in Nielsen's approach.

The damage model contains four parameters (b, c, n, σ_o). Each of these were assumed to be positive, independent random variables with lognormal distributions. Their means and standard deviations were taken as the unknowns in the minimization of Eq.(4) to fit the model to the Western hemlock data. The minimization was carried out with the same routine utilized for the Nielsen model. The mean and standard deviations obtained for the four parameters were:

Variable	Distribution	Mean	Standard Deviation
b	Lognormal	35.204	6.589
c	Lognormal	0.1559×10^{-6}	0.9621×10^{-7}
n	Lognormal	1.429	0.139
σ_o	Lognormal	0.578	0.163

Fig. 5 shows the fit of the model to the data. It is apparent that this damage model is capable of following the experimental trends very well. The fit is slightly better than for the fracture mechanics model, but this is mostly due to this model having only three parameters while the damage equation offers more flexibility with four.

The threshold stress ratio is no longer a constant but is lognormally distributed across members. Its mean value is still around 0.5, as in the earlier version of this model. The independence of this parameter, as well as that of c, in relation to τ_s is not proven and should be the target of future research.

COMMENTS ON MODEL CALIBRATION

The raw data from a duration of load experiment are times-to-failure under a constant stress. These data can be ranked and shown as cumulative distribution functions of the type used here for Western hemlock. It is impossible to determine simultaneously the short-term strength of the pieces loaded and, therefore, it is impossible

to determine accurately the stress ratio to which each piece has been loaded. An approximate method (Madsen and Barrett, 1976) allows the estimation of the stress ratios, and thus the representation of the data on a stress ratio vs. time-to-failure plot.

Calibration of a duration of load model could be done using either representation. Calibration to the raw data's cumulative distributions has the advantage of avoiding the uncertainty in the approximate estimation of stress ratios, and should be preferred. However, it also presents some problems. The function of Eq.(4) is relatively flat around the point corresponding to the minimum, and the fit may be quite good for rather different sets of model parameters. This may create the problem of deciding on a "good" set for the calibrated model.

A general computer program (DOLFIT) has been developed and runs in an IBM XT or AT. It can fit either the damage accumulation model or the fracture mechanics model. The procedure is as follows:

1) Given the mean and standard deviation of each parameter, and the distribution of short-term strength τ_s, generate a random sample of NREPL times-to-failure using the appropriate model;

2) Rank the sample of NREPL replicates and obtain the cumulative distribution function.

3) Compute the residual function from Eq.(4).

4) The nonlinear minimization routine requires the gradient of Eq.(4), that is, its partial derivatives with respect to each of the variables. These derivatives are computed numerically, repeating steps 1, 2 and 3 for small changes in the individual variables but with the same sequence of random numbers.

TIME–to–FAILURE CUMULATIVE DISTRIBUTION
from experiment and from theory

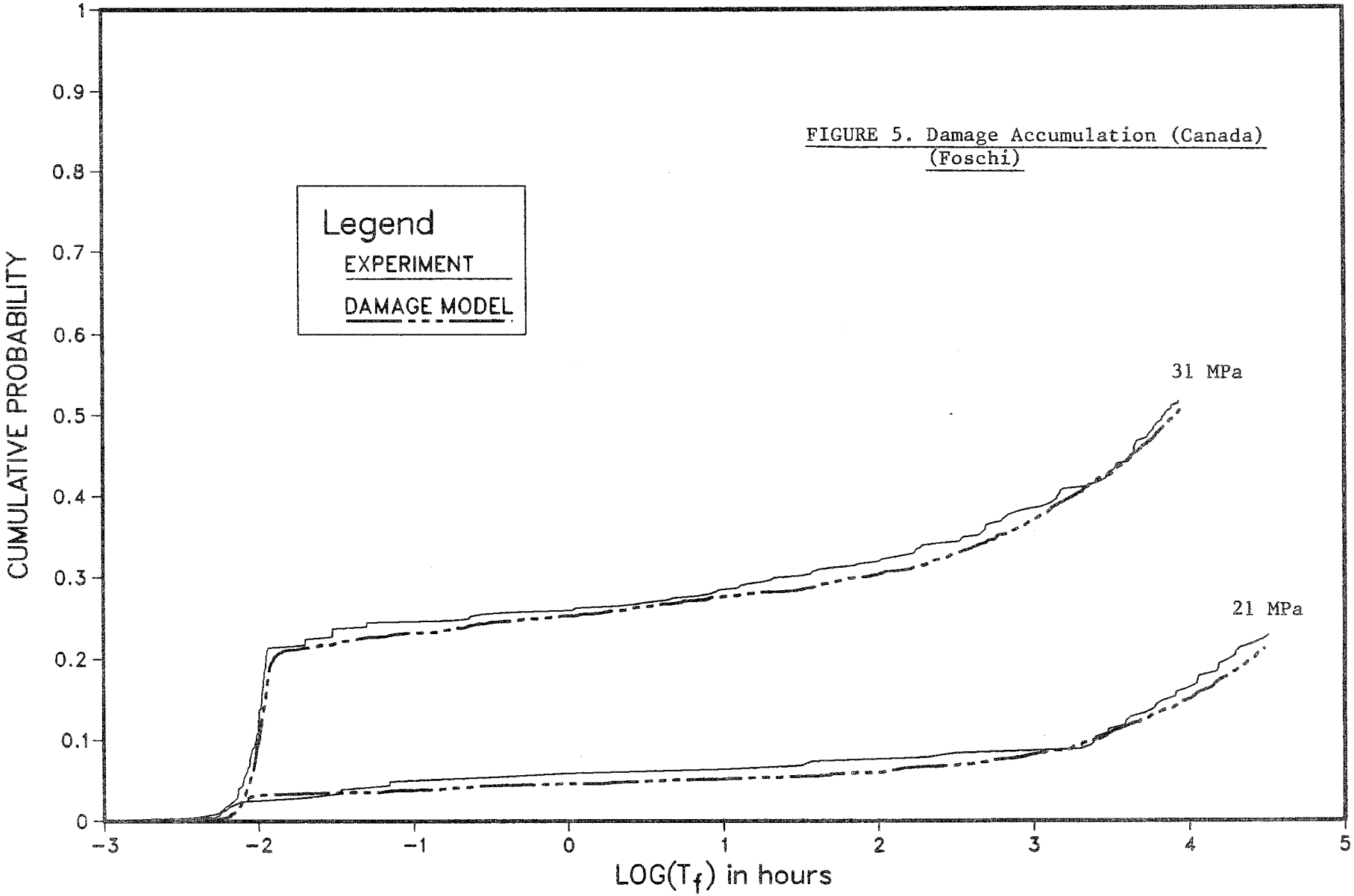


FIGURE 5. Damage Accumulation (Canada)
(Foschi)

5) The minimization routine automatically modifies the initial guesses for the variables in a search for the minimum of Eq.(4).

It was found that the sample NREPL should be sufficiently large to avoid fluctuations in the answer when the procedure is started with a different random seed. NREPL = 1000 was used in the results presented here. The derivatives were computed by changing each variable X in the amount ± 0.001 X , and computing the change in Eq.(4) over the interval 0.002 X. The procedure was stopped when the change in the variable X was less than X x 10^{-4}.

CONCLUSIONS

Three duration of load models have been considered. Two of them, the fracture mechanics approach of Nielsen and the damage accumulation model by Foschi were found suitable to represent accurately the experimental trends in Western hemlock lumber in bending. The model by Gerhards was found to be lacking in the flexibility needed to follow the experimental trends. The fracture mechanics model is not easy to use, since it requires numerical integration to obtain the time-to-failure in all cases when the applied stress varies with time. In this context, applications of these models to reliability calculations will be easier using damage accumulation. A general calibration program has been written, but fitting must be done carefully and with a degree of judgement.

REFERENCES

Fletcher, R. and Powell, M. 1963. A Rapidly Convergent Descent Method for Minimization. Comput. J.,6, pp. 163-168.

Foschi, R.O. and Barrett, J.D. 1982. Load Duration Effects in Western Hemlock Lumber. Journal of the Structural Div., ASCE, 108 (7).

Foschi, R.O. and Barrett, J.D. 1985. Duration of Load Effects, 2 x 8 Spruce Lumber in Bending: Data Analysis and Modelling. Proceedings, International Workshop on Duration of Load, Forintek Canada Corp., 6620 NW Marine Dr., Vancouver, B.C., Canada V6T 1X2

Foschi, R.O. 1984. Reliability of Wood Structural Systems. Journal of Structural Engineering, ASCE, 110 (12).

Gerhards, C.C. 1977. Effect of Duration and Rate of Loading on Strength Wood and Wood-Based Materials. USDA Forest Serv. Res. Pap. FPL 283, Forest Products Laboratory, Madison, Wisconsin, USA.

Gerhards, C.C. 1986. Effect of Loading Rate in Bending Strength of Douglas-fir 2 by 4's. Forest Products Journal, 36 (2).

Hoyle, R., Griffiths, M. and Itani, R. 1985. Primary Creep in Douglas-fir Beams of Commercial Size and Quality. Wood and Fiber Science, 17 (3).

Madsen, B. and Barrett, J.D. 1976. Time-Strength Relationship for Lumber. Struct. Res. Ser. Report No. 13, Department of Civil Engineering, University of British Columbia, Vancouver, B.C. Canada V6T 1W5.

Nielsen, L. and Kousholt, K. 1980. Stress-Strength-Lifetime Relationship for Wood. Wood Science, 12.

Nielsen, L. 1982. A Lifetime Analysis of Cracked Linear-Viscoelastic Materials - With Special Reference to Wood. Proceedings, IUFRO Wood Engineering Group Meeting, Boras, Sweden.

Nielsen, L. 1985. Wood as a Cracked Viscoelastic Material. Proceedings, International Workshop on Duration of Load, Forintek Canada Corp., 6620 NW Marine Dr., Vancouver, B.C., Canada V6T 1X2

CIB-W18/19-9-2

INTERNATIONAL COUNCIL FOR BUILDING RESEARCH STUDIES AND DOCUMENTATION

WORKING COMMISSION W18 - TIMBER STRUCTURES

DURATION OF LOAD EFFECTS FOR SPRUCE TIMBER WITH SPECIAL REFERENCE TO MOISTURE INFLUENCE - A STATUS REPORT -

by

P Hoffmeyer
Technical University of Denmark
Denmark

MEETING NINETEEN
FLORENCE
ITALY
SEPTEMBER 1986

DURATION OF LOAD EFFECTS FOR SPRUCE TIMBER WITH SPECIAL REFERENCE TO MOISTURE INFLUENCE

A STATUS REPORT

Preben Hoffmeyer
Building Materials Laboratory
Technical University of Denmark
Building 118, DK-2800 Lyngby, Denmark

1. INTRODUCTION

The present paper reports on a project which is still incomplete in terms of testing and analysis.

The paper is an interim report and presents the limited results of analysis carried out to date.

The research project is aimed in particular at an investigation of the possible influence of moisture content on the effect of duration of load on spruce timber. Such an effect was earlier found for clear wood /1/.

The project is part of a joint programme between Princes Risborough Laboratory (PRL) and The Technical University of Denmark (TUD). The Swedish Institute for Wood Technology Research (Träteknik Centrum) has supplied the test samples and carried out initial strength- and NDE-tests to ensure matching of the British and Danish samples.

2. TEST PROCEDURE

The tests are being carried out at TUD in a constant controlled environment to give either 10-11% or 19-20% moisture content. Specimens used are 45x95 mm spruce (*Picea abies*) subjected to 4-point bending.

An indication of the number of specimens in the full joint programme is given in Table 1.

Moisture Content	Constant MC = 11%		Constant MC = 19%		Cyclic 11% ⇌ 19%
Quality Level	Q_1	Q_2	Q_1	Q_2	Q_1
Short term	200	200	200*	200	-
SR_{30}	150	150	-	-	-
SR_{15}	100	100	100*	100	-
SR_{05}	100*(TUD)	-	100*	100	100
Testing Instituton	PRL		TUD		

Table 1. Number of specimens in each sample. There are 2 qualities of timber (Q_1 and Q_2) which are loaded to various percentiles (SR) of the corresponding short term strength. Only specimens from samples marked * are included in in the present report.

Each sample of specimens is composed of a number of sub-samples of 50 specimens. These sub-samples have been selected very carefully in order to secure as far as possible identical strength distributions. For further details see ref. /2/.

The results reported here are all related to the lowest (Q_1) of the two quality groups. Furthermore, only results from one half of the planned tests are old enough to be included in this status report.

Stress ratios (SR) used are the 5th- and 15th-percentiles of the short term strength (Table 2).

Moisture Content	Stress ratio(SR) Percentile	Percentage of mean short term strength	Stress MPa
11%	SR_{05}	75%	28.2
19%	SR_{05}	71%	26.5
19%	SR_{15}	84%	31.4

Table 2. Load levels for the Q_1 specimens

3. RESULTS

The number of specimens which broke on loading matched the number to be anticipated from the percentiles used. This indicates that the intended matching of strength distributions has been successful.

The true stress ratio of each specimen is estimated by assuming an equal rank between the strength of short term and constant load specimens.

Figures 1 and 2 show stress ratios against log time to failure for timber of a moisture content of 19-20% and 10-11% respectively. Results from the PRL-programme /2/ have been superimposed Figure 2.

To avoid the uncertainty of the equal rank assumption, the mean log time to failure of the four samples at the SR_{05} and SR_{15} levels are plotted against stress ratio (Figure 3). The mean value marked "3" has only been estimated from information in /2/. The other 3 mean values are very accurate , as actually 50% or more of all specimens of each sample have now failed.

Superimposed on Figure 3 are the results from tests on small clear notched specimens at different moisture content levels /1/ as well as the Madison curve.

4. CONCLUSIONS

Definite conclusions are not to be drawn on the basis of these preliminary results. However, some general trends may be seen :

- The curve for the higher stressed sample is above that for the lower stressed sample. For moist timber the effect seems to be there even for a long period of time, whilst for dry timber the effect seems to vanish after a short time. This suggests that low quality timber may be more severely weakened by load duration than high quality timber. This is opposite to the effect found by Madsen and Barrett /3/.

Although the difference may well be within experimental variability, it is suggested that the difference is real, and based on the fact that tension perpendicular to grain failure - which is the predominant failure mode for timber subjected to bending - is known to cause shorter time to failure than tension and compression parallel to grain. Gerhards and Link /4/ in a recent paper also found a duration of load effect for timber in bending in excess of that predicted by the Madison curve.

If curves for higher stressed samples are above curves for lower stressed samples , then the DOL-curves of Figure 3 will always be steeper than DOL-curves as shown in Figures 1 and 2. Based on Figure 3 it may be concluded, that the present investigation shows a duration of load effect which already during the first few months of loading is of the same order as that predicted by the Madison curve.

- The effect of moisture content on the duration of load for timber has been shown to be no less than that found for clear wood (Figure 3). The curves are shifted towards longer times, but the curves for timber runs parallel to the curves for clear wood, and the log-time difference between dry and moist states is of the same order of magnitude.

5. LITERATURE

/1/ Hoffmeyer,P., H.J.Krebs, L.Fuglsang Nielsen : "Duration of Load Tests with notched spruce beams at two moisture levels". Proceedings of the IUFRO-Wood Engineering meeting, Xalapa, Mexica, 1984.

/2/ Fewell,A.R.: "Testing and analysis carried out as part of the Princes Risborough Laboratory's programme to examine the duration of load effect on timber". Proceedings of the International Workshop on Duration of Load in Lumber and Wood Products. Forintek Canada Corp., Special Publication No. SP-27, 1986.

/3/ Madsen,B., J.D.Barrett: "Time strength relationship for lumber". Dept. of Civil. Eng., UBC, Structural Research Series, Report No. 13, 1976.

/4/ Gerhards,C.C., C.L.Link : "Use of a cumulative damage model to predict load duration characteristics of lumber", IUFRO-Wood Engineering Meeting, Madison, Wisc., 1983.

6. FIGURES

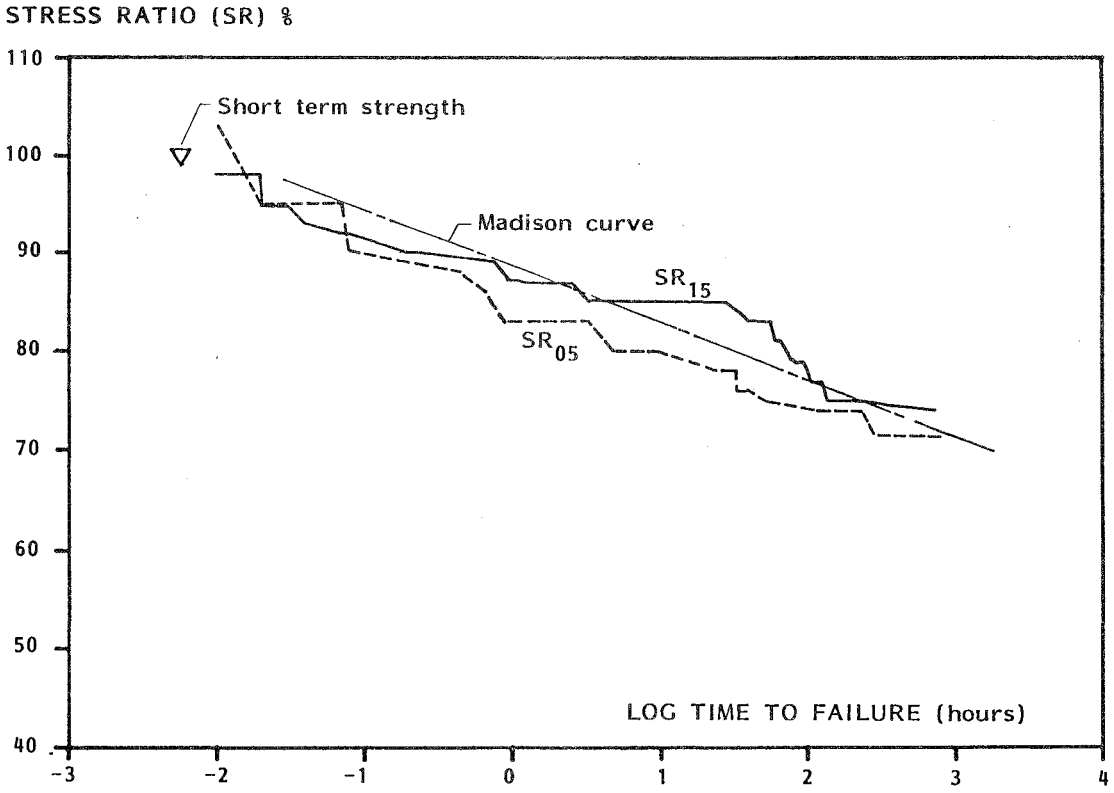


Figure 1. Stress ratio against log time to failure for spruce timber subjected to bending. Moisture content 19-20%.

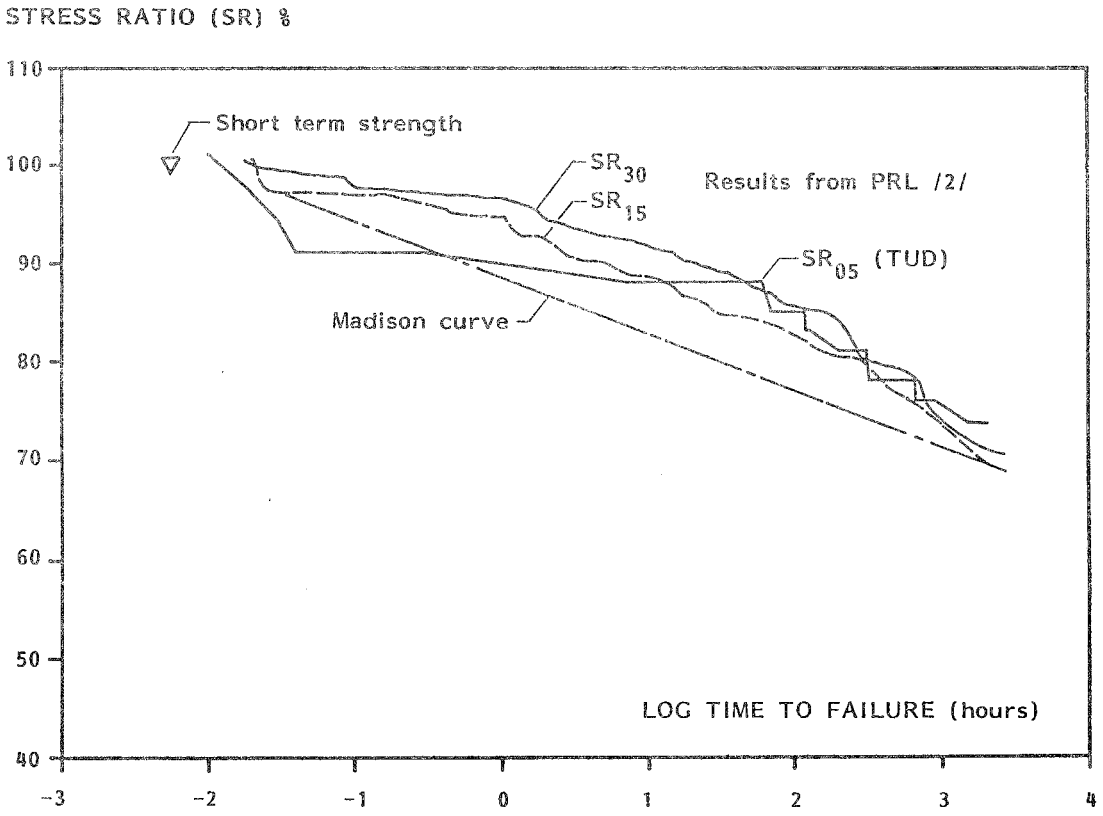
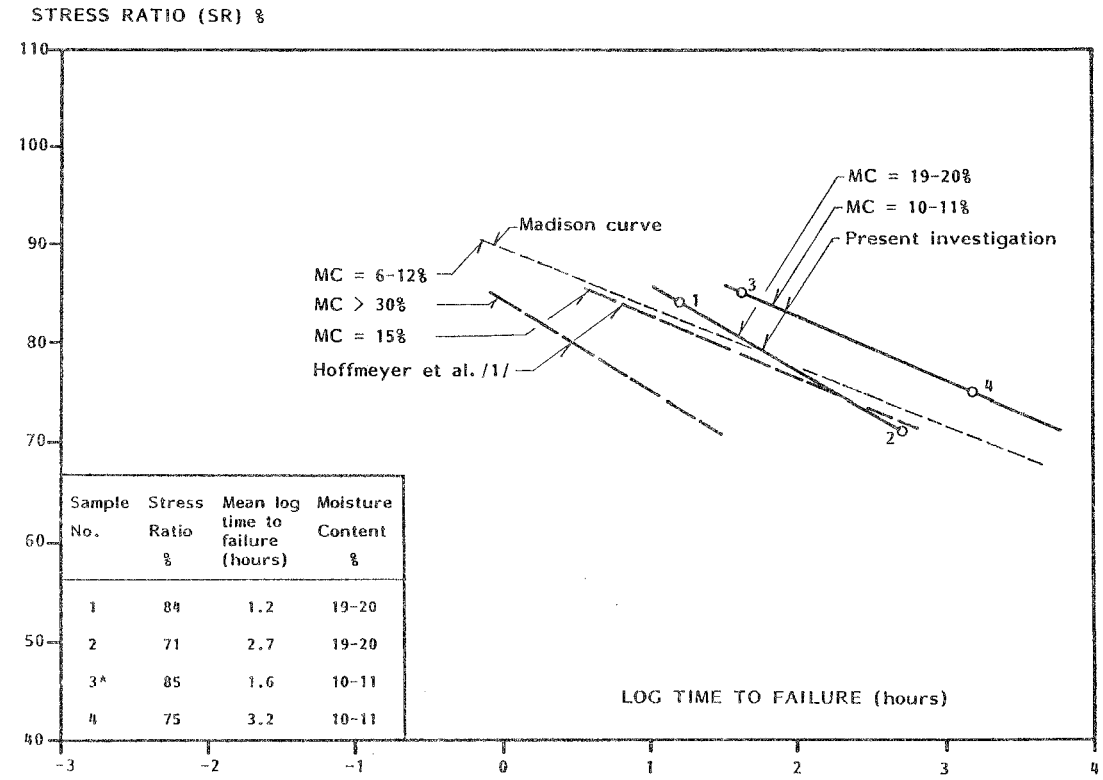


Figure 2. Stress ratio against log time to failure for spruce timber subjected to bending. Moisture content 10-11%.



Sample No.	Stress Ratio %	Mean log time to failure (hours)	Moisture Content %
1	84	1.2	19-20
2	71	2.7	19-20
3*	85	1.6	10-11
4	75	3.2	10-11

Figure 3. Mean log time to failure of the 4 SR_{05} and SR_{15} samples versus stress ratio. Included are results for small clear specimens /1/. *This result is estimated on the basis of information from /2/.

CIB-W18/19-9-3

INTERNATIONAL COUNCIL FOR BUILDING RESEARCH STUDIES AND DOCUMENTATION

WORKING COMMISSION W18 - TIMBER STRUCTURES

A MODEL OF DEFORMATION AND DAMAGE PROCESSES BASED ON THE REACTION KINETICS OF BOND EXCHANGE

by

T A C M van der Put
Delft University of Technology
Netherlands

MEETING NINETEEN
FLORENCE
ITALY
SEPTEMBER 1986

A MODEL OF DEFORMATION AND DAMAGE PROCESSES BASED ON THE REACTION KINETICS OF BOND EXCHANGE

1. Introduction

Long term creep tests during 10 to 23 years on joints, where the wood is determining for the strength, indicate that deformation- and damage-behaviour of wood is non-linear even at low loading levels and can be explained by the theory of reaction kinetics of deformation. This is confirmend by tests on clear wood, done as part of an E.E.C.-project. The basic concept of this theory of deformation kinetics is to regard plastic flow as a chemical reaction of molecular bond breaking and bond reformation. For wood this approach is complicated by the complex structure, and only an estimate of the involved processes or molecular parameters will be possible.
As long as the molecular structure and interaction is not entirely understood, every aproach will have a phenomenological character and it is at first necessary to state here a phenomenological model in a physical right form and to derive the possible simplifications to be able to find the main determining processes and to explain the behaviour. The predictions of the theory will be compaired with general experimental tendencies of the behaviour of wood known from litterature.

2. Creep and damage model

In appendix A and B the mathematical derivation of this model is given, solely based on the chemical reaction equations of plastic deformation at the deformation sites and the transmission of stresses by the surrounding elastic material. This leads to the following equations:

$$\frac{d\epsilon}{dt} = \dot{\epsilon} = \frac{\dot{\sigma}_i}{k_i} + (A_i + B_i \epsilon_i) \sinh\left(\sigma_i \phi_i (1 - C_i \epsilon_i)\right) \qquad (2.1)$$

of a parallel system of Maxwell elements, where σ_i is the stress on element i; ϵ_i is the strain of the non-linear dashpot and k_i is the spring constant. The terms with B_i and C_i give the small structural changes. As discussed in appendix B - 3, $C_i \epsilon_i$ is very small and can be neglected. Because σ_i has the form of $\sigma_i = \sigma - M\epsilon$, where M is proportional to the spring constants of the parallel elements and $M \gg C_i$, during most of the lifetime, it will hardly be possible to measure C_i.

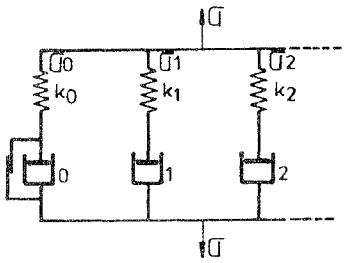


fig. 2.1 Parallel system of Maxwell units.

In most experiments, one of the processes controls the overall behaviour and only three elements (spring $k_0 + k_1$; k_2, and dashpot 2) have to be regarded (dashpots 0 and 1 are then rigid; see fig.2.1). During the deformation the loading of the springs change (transient flow) until all Maxwell elements flow. Then the behaviour can be described by a single Maxwell element.
In the following the solutions of this equation for the different loading types will be given.

3. Constant strain rate test

In fig. 3.1, a 3 - element model is given of one dominating process controlling the overall rate. For the Maxwell unit at constant strain rate $\dot{\varepsilon} = c_1$ is $\dot{\varepsilon} = \dot{\varepsilon}_e + \dot{\varepsilon}_v = c_1$ or, when the structural change can be neglected (B and C in eq.2.1):

$$\dot{\varepsilon} = \dot{\varepsilon}_e + \dot{\varepsilon}_v = \frac{\dot{\sigma}_v}{k_1} + A \sinh(\phi \sigma_v) \tag{3.1}$$

The solution of this equation is: $(\dot{\varepsilon} = c_1)$

$$\sigma_v = \frac{1}{\phi} \ln\left[\beta + \left(\sqrt{1+\beta^2}\right) \tanh\left(\frac{\sqrt{1+\beta^2}}{2} A \phi k_1 (t - c)\right)\right] \tag{3.2}$$

with: $\beta = \frac{\dot{\varepsilon}}{A} = \frac{c_1}{A}$ and $-\sqrt{1+\beta^2} \cdot \frac{A}{2} \phi k_1 c = \operatorname{arctanh}\left(\frac{1-\beta}{\sqrt{1+\beta^2}}\right)$

In fig.(3.2) the stress - time relation of the model is given. For wood k_1 and σ_v are small and the line of fig. 3.2 is approximated by a single straight line. This leads to a mean modulus of elasticity μ:

$$\mu = \frac{\sigma_m}{\varepsilon_m} = \frac{k_2 \varepsilon_m}{\varepsilon_m} + \frac{\sigma_{v\infty}}{\varepsilon_m} = k_2 + \frac{1}{\phi \varepsilon_m} \ln\left(\beta + \sqrt{1+\beta^2}\right) \approx k_2 + \frac{1}{\phi \varepsilon_m} \ln(2\beta)$$

or

$$\mu = k_2 + \frac{1}{\phi \varepsilon_m} \ln\left(\frac{2\dot{\varepsilon}}{A}\right) = k_2 + \frac{1}{\phi \varepsilon_m} \ln\left(\frac{2}{A}\right) + \frac{1}{\varepsilon_m} \ln(\dot{\varepsilon})$$

So the dependence of μ on the strain rate $\dot{\varepsilon}$ is:

$$\mu - \mu_0 = \frac{1}{\phi \varepsilon_m} \left(\ln \dot{\varepsilon} - \ln \dot{\varepsilon}_0\right)$$

or:

$$\mu = \mu_0 \left(1 + \frac{1}{\mu_0 \phi \varepsilon_m} \left(\ln \dot{\varepsilon} - \ln \dot{\varepsilon}_0\right)\right) \tag{3.3}$$

with $\mu_0 \phi \varepsilon_m = k_2 \phi \varepsilon_m + \ln(2\beta_0)$ (3.4)

Eq.(3.3) is equal to the experimental equation given in [23]
Because $k_2 \phi \varepsilon_m$ is dominating in eq.(3.4) is $k_2 \phi \varepsilon_m$ approximately constant and ϕ is inversely proportional to $k_2 \varepsilon_m$.
The increase of $1/\mu_0 \phi \varepsilon_m$ with moisture content shows that the decrease of μ_0 (k_2) dominates the increase of ϕ with moisture content at 20°C.
More probable is the existence of another Maxwell element.
Because $\mu_0 \phi \varepsilon_m \approx \sigma_m \phi = n$, a value of n = 12 applies for green wood and n = 36 at 10 % m.c. as also has be found for fracture.
It can be concluded that there is a small process in wood with a dominating constant A in eq.(2.1)

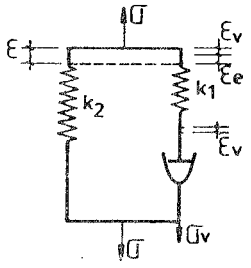


fig. 3.1 Three element model

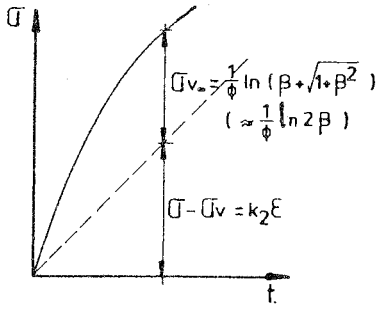


fig. 3.2 Early flow of wood

If all Maxwell elements of fig. 2.1 flow, a description by a single (dominating) Maxell element is possible (neglecting the small, almost constant, stress in k_1 in fig. 3.1). If B and C in eq.(2.1) are zero, then eq.(3.2) applies, represented by fig. 3.3.

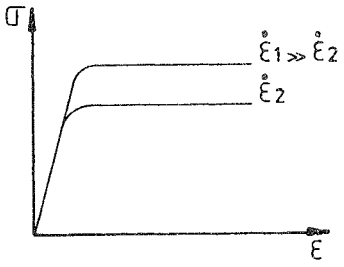


fig. 3.3 Non-linear Maxwell element

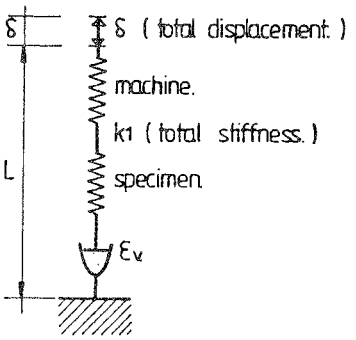


fig. 3.4 Flow of all elements

For a machine - specimen combination in a test, the crosshead displacement is (fig. 3.4):

$$\frac{\delta}{L} = \frac{\sigma}{K_1} + \varepsilon_v$$

or the constant crosshead rate $\dot{\delta} = c_1$:

$$\dot{\delta} = L\left(\frac{\dot{\sigma}}{k_1} + \dot{\varepsilon}_v\right)$$

So: $\dot{\varepsilon}_v = \frac{\dot{\delta}}{L} - \frac{\dot{\sigma}}{k_1} = \frac{\dot{\delta}}{L}\left(1 - \frac{L}{K_1}\frac{d\sigma}{d\delta}\right)$

or: $\frac{d\sigma}{d\delta} = \frac{k_1}{L} - \frac{k_1}{c_1}\dot{\varepsilon}_v = \frac{k_1}{L} - \frac{k_1}{c_1} A'T\left(\rho_0 + B'\varepsilon_v\right)\sinh\left(\sigma\phi(1 - c\varepsilon_v)\right) \rightarrow$

$$\frac{d\sigma}{d\delta} = \frac{k_1}{L} - \frac{k_1}{c_1} A'T\left(\rho_0 + B'\left(\frac{\delta}{L} - \frac{\sigma}{K_1}\right)\right)\sinh\left(\phi\sigma\left(1 - c\frac{\delta}{L} + c\frac{\sigma}{K_1}\right)\right) \qquad (3.5)$$

The analogues power equation for this case has the form:

$$\frac{d\sigma}{d\delta} = C_0 - \left(C_2 + C_3\delta - C_4\sigma\right)\left(\frac{T + C_5\varepsilon_v}{T_0}\right)^n \qquad (3.6)$$

Both equations (3.5) and (3.6) cannot be integrated to a functional form. The results of numerical integration are shown in fig. 3.5 and 3.6.

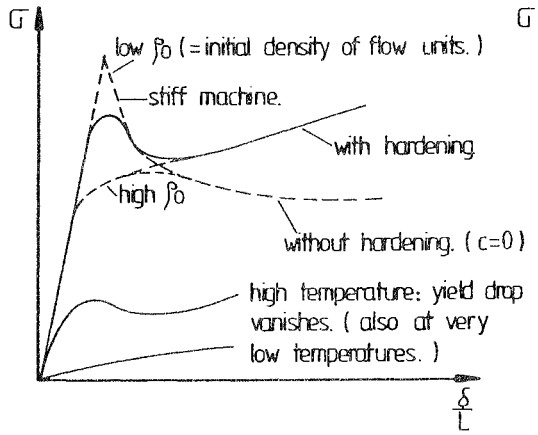


fig. 3.5 Yield drop eq.(3.5)

$A' = \nu \exp\left(-\frac{E'}{kT}\right)$ $\quad \phi = \frac{V}{kT}$

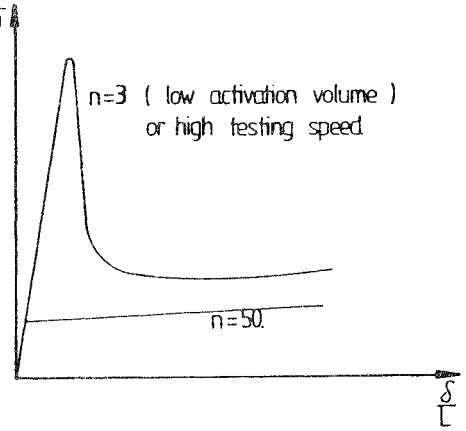


fig. 3.6 Influence of n eq.(3.6)

For wood in tension // there is a high yield drop, indicating that B' in eq.(3.5) is dominating by a low initial "dislocation" density ρ_0. This is not caused by a low value of n. ($n \approx \sigma_u \phi$)
Clear wood in compression // shows a behaviour like in fig. 3.3, indicating no hardening and no yield drop. So B' and C in eq.(3.5) may be neglected. For timber (with knots) in compression along the grain however there is a small yield drop, superposed on the behaviour of the clear wood between the knots, indicating the acting of another (tensional) maxwell element (crack propagation in grain direction at the knots). Knots act like "dislocations" with a low density.

4. Constant loading rate test

For the 3 - element model of fig. 3.1 is for this case $\dot{\sigma} = \text{constant}$ with $B_i = C_i = 0$, the integration of the differential eq.(2.1), neglecting the structural changes, gives: (like eq.(3.8))

$$\varepsilon = \frac{\dot{\sigma} t}{k_2} - \frac{1}{\phi k_2} \ln \left(\frac{1 + c_1(1+\beta) \tanh(c_2 t)}{1 + c_1(1-\beta) \tanh(c_2 t)} \right) \qquad (4.1)$$

With: $\beta = \dot{\sigma}/A k_2$; $1/c_1 = \sqrt{1+\beta^2}$; $c_2 = \frac{k_1 k_2 A \phi}{2(k_1+k_2)} \sqrt{1+\beta^2}$

Under constant loading rate the machine and specimen stiffness have no effect on the yield behaviour.
If all elements flow (fig. 3.4) the rate equation is:

$$\dot{\varepsilon}_v = A'T (\rho_0 + B' \varepsilon_v) \sinh(\phi \dot{\sigma} t) \approx \rho_0 A'T \sinh(\phi \dot{\sigma} t) \qquad (4.2)$$

or integrated: ($B' = c$)

$$\varepsilon_v = \frac{\rho_0 A'T}{\dot{\sigma} \phi} \left(\cosh(\dot{\sigma} \phi t) - 1 \right) \qquad (4.3)$$

For higher values of $\dot{\sigma} \phi t$ this is:

$$\varepsilon_v = \frac{\rho_0 A'T}{\dot{\sigma} \phi} \left(\tfrac{1}{2} \exp(\dot{\sigma} \phi t) - 1 \right) \qquad (4.4)$$

or with $\sigma = \dot{\sigma} t$:

$$\sigma = \frac{1}{\phi} \ln \left(2 + \frac{2 \dot{\sigma} \phi \varepsilon_v}{\rho_0 A'T} \right) \qquad (4.5)$$

The strength is reached for $\varepsilon_v = \varepsilon_{vu}$. So σ_1 and σ_2 at the rates $\dot{\sigma}_1$ and $\dot{\sigma}_2$ are related by:

$$\sigma_1 - \sigma_2 = \frac{1}{\phi} \ln \left(\frac{1 + \dot{\sigma}_1 c \frac{\dot{\sigma}_2}{\dot{\sigma}_1} t}{1 + \dot{\sigma}_2 c t} \right) + \frac{1}{\phi} \ln \frac{\sigma_1}{\sigma_2} - \frac{1}{\phi} \ln \frac{t_1}{t_2} \qquad (4.6)$$

or: ($c = \frac{\phi \varepsilon_{vu}}{\rho_0 A'T}$)

$$\frac{\sigma_1}{\sigma_2} = 1 + \frac{1}{\phi \sigma_2} \ln \left(\frac{1 + \dot{\sigma}_1 c t}{1 + \dot{\sigma}_2 c t} \cdot \frac{\dot{\sigma}_2}{\dot{\sigma}_1} \right) + \frac{1}{\phi \sigma_2} \ln t_2 - \frac{1}{\phi \sigma_2} \ln t_1 \qquad (4.7)$$

giving the form:

$$\frac{\sigma_1}{\sigma_2} = c_1 - c_2 \ln t \qquad (4.8)$$

This is the same relation as the experimental equation given in [24], [25] etc. where $c_1 = 1.2$ to 1.3 and $1/c_2 = n = 27$ for compression and 31 for bending. If n is aproximately linear dependent on m.c. as suggested in [23], then these values indicate a m.c. of 13 %
The same result is obtained by integration of eq.(4.9), where only the

hardening term is neglected. ($B' \neq 0$):

$$\dot{\varepsilon}_v = A'T(\sigma_0 + B'\varepsilon_v)\sinh(\phi\sigma t) \tag{4.9}$$

Only the ultimate strain ε_{vu} will have another value.
The alternative power representation becomes ($\dot{\sigma}$ = constant):

$$\dot{\varepsilon}_p = A'T(\sigma_0 + B\varepsilon_p)\left(\frac{\dot{\sigma}}{\sigma_0}\right)^n t^n \tag{4.11}$$

This is easy to integrate and the results are given in fig.(4.1).

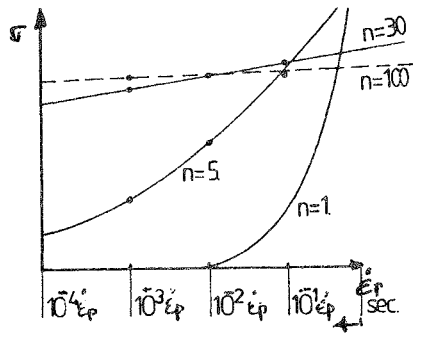


fig. 4.1 Influence of the rate of loading
or time to loading to the same strain [1]

It can be seen from this figure, that for small values of n ($n \geqslant 1$), there is a strong influence of the loading rate on the level of the flow stress. For high values of n (e.g. n = 30 as for wood), there is only a small influence and there is a linear relation between the strength and log(time to failure).
For small values of n the derivation of appendix B-4, is not general enough. From:

$$\frac{\dot{\varepsilon}}{\dot{\varepsilon}_u} = \left(\frac{\sigma}{\sigma_u}\right)^n$$

is: $\ln(\dot{\varepsilon}) = \ln(\dot{\varepsilon}_u) - \ln(\sigma_u^n) + n.\ln(\sigma)$

So: $\dfrac{d\ln\dot{\varepsilon}}{d\ln\sigma} = n$

Appliing this operation $\frac{d\ln\dot{\varepsilon}}{d\ln\sigma}$ to $\dot{\varepsilon} = A\sinh(\phi\sigma)$ gives:

$$n = \frac{\sigma\phi}{\tanh(\sigma\phi)} \tag{4.14}$$

So for small values of $\sigma\phi$ is $n \approx 1$, and for large values is $n \approx \sigma\phi$

So: $n \approx \sigma\phi \geqslant 1$
For wood there is an indication that there is an element with a small value of n. This is only noticeble at very high loading speeds (fig.4.1)

5. Creep and creep recovery

For the 3 - element model (fig.3.1), neglecting structural changes, the force on the Maxwell element is determined by eq.(3.1).
For the parallel spring k_2 is: $\dot{\varepsilon} = \frac{\dot{\sigma}_2}{k_2} = \frac{1}{k_2}\frac{d}{dt}(\sigma - \sigma_v) = \frac{1}{k_2}(\dot{\sigma} - \dot{\sigma}_v)$
Because for creep $\dot{\sigma} = 0$, is: $\dot{\varepsilon} = -\dot{\sigma}_v/k_2$
and eq.(3.1) becomes:

$$\frac{\dot{\sigma}_v}{k_1} + A\sinh(\phi\sigma_v) = -\frac{\dot{\sigma}_v}{k_2}$$

or:

$$\dot{\tau}_v + \frac{k_1 k_2}{k_1 + k_2} A \sinh(\phi \tau_v) = 0 \qquad (5.1)$$

With the boundary condition $\varepsilon_\infty = \frac{\tau}{k_2}$ is : $\tau_v = \tau - k_2 \varepsilon = k_2 (\varepsilon_\infty - \varepsilon)$
and the solution of eq.(5.1) is:

$$\frac{1}{\phi k_2} \ln\left(\tanh\left(\frac{\phi k_2}{2}(\varepsilon_\infty - \varepsilon)\right)\right) = -\frac{k_1}{k_1 + k_2} A t + \frac{1}{\phi k_2} \ln\left(\tanh\left(\frac{\phi k_2}{2}(\varepsilon_\infty - \varepsilon_0)\right)\right)$$

or, because $\operatorname{arctanh}(x) = \frac{1}{2} \ln\left(\frac{1+x}{1-x}\right)$ this can be written as:

$$\varepsilon_\infty - \varepsilon = \frac{1}{\phi k_2} \ln\left(\coth\left(-\frac{1}{2} \ln\left(\tanh\left(\frac{k_2 \phi}{2}(\varepsilon_\infty - \varepsilon_0)\right)\right) + \frac{1}{2} \frac{k_1 k_2}{k_1 + k_2} \phi A t\right)\right) \qquad (5.2)$$

In the early part of the test this reduces to the logarithmic form:

$$\varepsilon_\infty - \varepsilon \approx -\frac{1}{\phi k_2} \ln\left(-\frac{1}{2} \ln\left(\tanh\left(\phi \frac{\tau_{v0}}{2}\right)\right) + \frac{1}{2} \frac{k_1 k_2}{k_1 + k_2} \phi A t\right) \qquad (5.3)$$

or:

$$\varepsilon \approx \varepsilon_0 + \frac{1}{\phi k_2} \ln\left(1 + \frac{k_1 k_2 \phi A t}{(k_1 + k_2) \ln\left(\coth\left(\phi \frac{\tau_{v0}}{2}\right)\right)}\right) \qquad (5.4)$$

A fit of this equation is not found in literature. Our tests show however that the form of eq.(5.4) is right, also for small times. The fit is mostly done for larger times (neglecting 1 in the last term) giving:

$$\varepsilon = C_1 + C_2 \cdot \ln(t) \qquad (5.5)$$

If $\phi \tau_{v0}$ is large enough, is: $\ln(\coth(x)) = 2.\operatorname{arctanh}(e^{-2x}) \approx 2e^{-2x}$
and eq.(5.4) is:

$$\varepsilon \approx \varepsilon_0 + \frac{1}{\phi k_2} \ln\left(1 + \frac{k_1 k_2 \phi A t \exp(\phi \tau_{v0})}{2(k_1 + k_2)}\right) \qquad (5.6)$$

The shift along the time axis according to eq.(5.6) is however to small for wood and indicates a small value of $\phi \tau_{v0}$.

For very long times and high values of , eq.(5.2) can be written:

$$\varepsilon_\infty - \varepsilon = \frac{1}{\phi k_2} \ln\left(\coth\left(\frac{k_1 k_2 \phi A t}{2(k_1 + k_2)}\right)\right) \approx \frac{2}{\phi k_2} \exp\left(-\frac{k_1 k_2 \phi A t}{k_1 + k_2}\right)$$

or:

$$\varepsilon \approx \varepsilon_0 + \frac{2}{\phi k_2} \left(1 - \exp\left(-\frac{k_1 k_2 \phi A t}{k_1 + k_2}\right)\right) \qquad (5.7)$$

So the behaviour becomes quasi Newtonian after long times.
Eq.(5.1) can be expected to be quasi Newtonian for low stresses, because $\sinh(x) = x$ then. This equation then becomes:

$$\dot{\tau}_v + \frac{k_1 k_2}{k_1 + k_2} A \phi \tau_v = 0$$

with the solution: $$\varepsilon - \varepsilon_0 = (\varepsilon_\infty - \varepsilon_0)\left(1 - \exp\left(-\frac{k_1 k_2 \phi A t}{k_1 + k_2}\right)\right)$$

It is seen that test results, in not to long time ranges, can be fitted by Newtonian equations as often is done. This, however will give an underestimation of the relaxation times.

When $B_i\varepsilon_i$ dominates A_i in eq.(2.1), and A_i can be neglected, then eq.(3.1) of the 3- element model of fig. 3.1 becomes:

$$\dot{\varepsilon} = \frac{\dot{\sigma}_v}{k_1} + B\varepsilon_v \sinh(\phi\sigma_v) \tag{5.8}$$

Because: $\varepsilon = \frac{\sigma_2}{k_2} = \frac{\sigma-\sigma_1}{k_2} = \frac{\sigma}{k_2} - \frac{k_1}{k_2}(\varepsilon-\varepsilon_p)$

or: $\varepsilon_p = \frac{k_1+k_2}{k_1}\varepsilon - \frac{\sigma}{k_1}$

is: $\dot{\varepsilon}_v = \frac{k_1+k_2}{k_1}\dot{\varepsilon} - \frac{\dot{\sigma}}{k_1} = B\varepsilon_p \sinh(\phi\sigma_v) \approx \frac{B}{2}\varepsilon_p \exp(\phi\sigma_v) = \frac{B\varepsilon_v}{2}\exp(\phi(\sigma-k_2\varepsilon))$

giving: $(k_1+k_2)\dot{\varepsilon} \approx \dot{\sigma} + B\left((k_1+k_2)\frac{\varepsilon}{2} - \frac{\sigma}{2}\right)\exp(\phi(\sigma-k_2\varepsilon))$

For creep is σ= constant or $\dot{\sigma} = 0$, so: $\dot{\varepsilon} = \frac{B}{2}\left(\varepsilon - \frac{\sigma}{k_1+k_2}\right)\exp(\phi\sigma - \phi k_2\varepsilon)$

or: $\frac{d(\phi k_2\varepsilon)}{\phi k_2(\varepsilon - \frac{\sigma}{k_1+k_2})}\exp\left(\phi k_2\varepsilon - \frac{\phi k_2\sigma}{k_1+k_2}\right) = \frac{B}{2}\exp\left(\phi\sigma - \frac{\phi\sigma k_2}{k_1+k_2}\right).dt$

having the form:

$$\int_{z_0}^{z}\frac{dz}{z}\exp(z) = \int_{-\infty}^{z}\frac{dz}{z}\exp(z) - \int_{-\infty}^{z_0}\frac{dz}{z}\exp(z) = E_i(z) - E_i(z_0)$$

or:

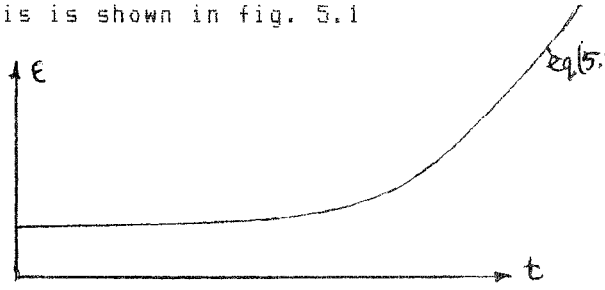
$$E_i\left(\phi k_2\left(\varepsilon - \frac{\sigma}{k_1+k_2}\right)\right) - E_i\left(\phi k_2\left(\varepsilon_0 - \frac{\sigma}{k_1+k_2}\right)\right) = \frac{B}{2}t\exp\left(\frac{\phi\sigma k_1}{k_1+k_2}\right)$$

so:

$$\phi k_2\left(\varepsilon - \frac{\sigma}{k_1+k_2}\right) = E_i^{-1}\left(\frac{B}{2}\exp\left(\frac{\phi\sigma k_1}{k_1+k_2}\right).t + E_i\left(\phi k_2\left(\varepsilon_0 - \frac{\sigma}{k_1+k_2}\right)\right)\right) \tag{5.9}$$

$$\rightarrow \quad \varepsilon = \frac{\sigma}{k_1+k_2} + \frac{1}{\phi k_2}E_i^{-1}\left(\frac{Bt}{2}\exp\left(\frac{\phi\sigma k_1}{k_1+k_2}\right) + E_i\left(\frac{k_1k_2\phi\varepsilon_{v_0}}{k_1+k_2}\right)\right) \tag{5.10}$$

This is shown in fig. 5.1



eq.(5.11): $\varepsilon \approx \frac{\sigma}{k_1+k_2} + \frac{1}{\phi k_2}\ln\left(\frac{B}{2}'\exp\left(\frac{\phi\sigma k_1}{k_1+k_2}\right)(t-t')\right)$

fig. 5.1 creep by structural change

Because $E_i(x) \approx \frac{e^x}{x}$ for larger values of x and $E_i(x) \approx 0.577 + \ln(x) \approx \ln(x)$ for small values, is eq.(5.9) approximately:

$$\text{or:} \quad \frac{\exp\left(\phi k_2\left(\varepsilon - \frac{\sigma}{k_1+k_2}\right)\right)}{\phi k_2\left(\varepsilon - \sigma/(k_1+k_2)\right)} \approx \frac{B}{2}t\exp\left(\frac{\phi\sigma k_1}{k_1+k_2}\right) + \ln\left(\phi k_2\left(\varepsilon_0 - \frac{\sigma}{k_1+k_2}\right)\right) \rightarrow$$

$$\rightarrow \quad \phi k_2\left(\varepsilon - \frac{\sigma}{k_1+k_2}\right) = \ln\left(\phi k_2\left(\varepsilon - \frac{\sigma}{k_1+k_2}\right) + \ln\left(\frac{B}{2}t\exp\left(\frac{\phi\sigma k_1}{k_1+k_2}\right) + \ln\left(\frac{\phi k_2\varepsilon_{v_0}k_1}{k_1+k_2}\right)\right)\right) \tag{5.11}$$

being a straight line on log - scale.

It will be shown that wood has a mechanism as described above.
Because this is related to the cellulose, test results of dry summerwood fibers of pine holocellulose pulp will be discussed [27].
In fig. 5.2, the average creep compliance of 50 fiber bundles is given for different initial stresses. As follows from the very different values of the initial compliances and from the not decelerating curves, flow of all Maxwell element have been occurred, without hardening (see also fig. 5.1). The kinked lines indicate two processes and a description is

possible with two Maxwell elements. Because one process will be much slower than the other, a 3- element model approach (one Maxwell element and one spring) is possible and the analysis is the same if the small plastic strain of element 2 (spring element) is subtracted from the total strain ε_b. So: $\varepsilon = \varepsilon_b - \varepsilon_{v2}$; $\varepsilon_v = \varepsilon_{v1} - \varepsilon_{v2}$
The line with the small slope is the quick process and as before, structural changes can be neglected (eq.5.1). The line with the steep slope, shows a strong delay time (see fig. 5.1) and will follow eq.(5.8). As seen in fig. 5.3, the lines can moved horizontally along the log(t) axis, to form one curve (giving the behaviour after long times at the lowest given stress).

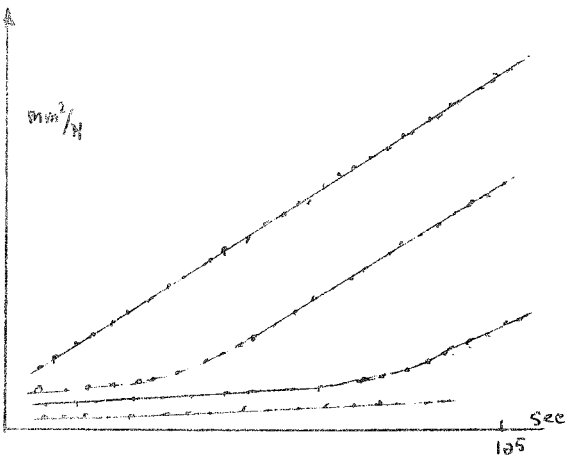


fig. 5.2 Creep compliance

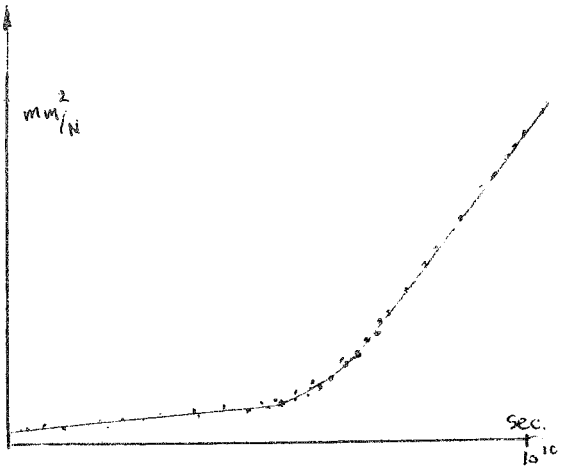


fig. 5.3 Master creep curve

The line with the small slope is accordingly to eq.(5.4) and the line with the steep slope follows eq.(5.11). Because in that equation $\ln(\phi k_2(\varepsilon - \frac{\sigma}{k_1+k_2}))$ is almost of lower order in comparison with $\phi k_2(\varepsilon - \frac{\sigma}{k_1+k_2})$ an average value of $\ln(\phi k_2(\varepsilon - \frac{\sigma}{k_1+k_2})$ can be taken leading to a corrected t' and value of B (= B'), (see the equation in fig. 5.1).
It appears that in eq.(5.4) and (5.11), $^1/_{\phi k_2}$ is approximately proportional to σ. So $\sigma \cdot \phi$ = constant, indicating that the number of relaxing mechanisms per unit area increases with increasing initial stress. An other explanation could be that the average energy of the oscillators, being: kT is equal to $c\sigma V$, or $\phi = V/kT = c'/\sigma$. Except in cellulosic materials, this property is also found in other materials, like metals and rubbers.

The compliance of eq.(5.4) is:

$$\frac{\varepsilon}{\sigma} = \frac{\varepsilon_0}{\sigma} + \frac{1}{\sigma \phi k_2} \ln\left(1 + \frac{k_1 k_2 \phi A t}{2(k_1+k_2)\,\mathrm{arccoth}(\phi \sigma v_0)}\right) \qquad (5.12)$$

where $1/\sigma\phi k_2 = c$ will be constant.
A shift of the lines along the time axis means that $\frac{\varepsilon_a}{\sigma_a}$ at t_a, has to be equal to $\frac{\varepsilon_b}{\sigma_b}$ at t_b, where the strains are the total strains: $\varepsilon_b = \varepsilon + \varepsilon_{v2}$
If this is done it appears that the shift:

$$\ln(t_a) - \ln(t_b) \approx \frac{1}{c}\left(\frac{\varepsilon_{0b}}{\sigma_b} - \frac{\varepsilon_{0a}}{\sigma_a}\right) = \frac{k_1}{c(k_1+k_2)}\left(\frac{\varepsilon_{v0b}}{\sigma_b} - \frac{\varepsilon_{v0a}}{\sigma_a}\right)$$

is mainly dependent on the difference of the relative initial plastic strains. These strains arise during the loading to the creep level (this is the part of the strain that is measured).
Because a very faint curved $\sigma - \varepsilon$ diagram can be approximated by a

parabola, the plastic strains will increase quadratic with the stress and the shift of the compliance along the time axis will roughly be proportional to the applied stress level: σ

The compliance of eq.(5.11) is:

$$\frac{\varepsilon}{\sigma} \approx \frac{1}{k_1+k_2} + \frac{1}{\phi\sigma k_2} \ln\left(\frac{B'}{2}\exp\left(\frac{\phi\sigma k_1}{k_1+k_2}\right)\cdot(t-t')\right) \qquad (5.13)$$

This equation shows hardly any shift and because it is experimentally found that the shift has to be equal to the shift of element 1, the strains have to be added and both dashpots have to be in the same Maxwell element 1.

The right form of the expression of t' in eq.(5.11) in fig. 5.1, also for wood, follows from eq.(5.9). For small values of x is $Ei(x) - Ei(x_o) = \ln(x) - \ln(x_o)$ and eq.(5.9) then becomes:

$$\ln\left(\phi k_2\left(\varepsilon - \frac{\sigma}{k_1+k_2}\right)\right) = \ln\left(\phi k_2\left(\varepsilon_o - \frac{\sigma}{k_1+k_2}\right)\right) + B't/2\,\exp\left(\frac{\phi\sigma k_1}{k_1+k_2}\right)$$

or: $$\varepsilon = \frac{\sigma}{k_1+k_2} + \frac{1}{\phi k_2}\exp\left(\frac{B't}{2}\exp\left(\frac{\phi\sigma k_1}{k_1+k_2}\right) + \ln\left(\frac{\phi\varepsilon_{vo}k_1(k_2)}{k_1+k_2}\right)\right)$$

It is seen that the strain grows exponential with time in the beginning of the creep. This behaviour is measured for wood in e.g.[28].

In the analysis above, it is assumed that the temperature is constant. To know the shift of the compliance along the time axis due to temperature differences, the same stress level has to be used in all tests at different temperatures. Then:

$$\ln(t_a) - \ln(t_b) = \ln(B'_a) - \ln(B'_b) = E'/kT_a - E'/kT_b$$

where E' is the activation energy. This is only true if $1/\sigma\phi k_2$ is independent on the temperature. Because this is unlikely, vertical shifts are also necessary to obtain the right activation energy.

If all Maxwell elements flow, one is determining for the overall rate and the power equation becomes:

$$\dot{\varepsilon} = A(\rho_o + B\varepsilon)\left(\frac{\sigma_a - M\varepsilon}{\sigma_o}\right)^n \qquad (5.14)$$

This equation cannot be integrated. Numerical solutions show that the delay time is due to "dislocation multiplication" similar to yield drop, dependent on the initial flow unit density (see fig. 5.4).

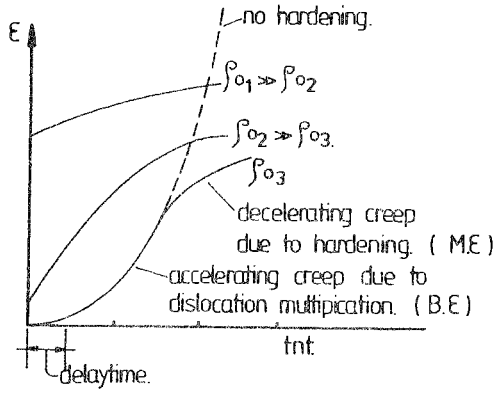


fig. 5.4 creep dependent on modelparameters.

For creep recovery, the initial conditions are $\sigma = 0$; $\varepsilon = \varepsilon_\infty$ when t = 0 leading

for the 3- element model to:

$$\varepsilon = \frac{1}{\phi k_2} \ln\left(\coth\left(-\tfrac{1}{2}\ln\left(\tanh\left(\frac{\phi\sigma_{vc}}{2}\right)\right) + \tfrac{1}{2}\,\frac{k_1 k_2}{k_1+k_2} A\phi t\right)\right) \qquad (5.15)$$

analogous to eq.(5.2).

6. Stress relaxation.

The 3- element model (fig. 3.1) loaded to σ_o, ε_c at t_o gets the stress $\sigma_o - \sigma_{vc}$ on spring 2. This remains unchanged when by relaxation stress σ_v on spring 1 decreases:
For the Maxwell element is $\dot{\varepsilon} = 0$ or: $\dot{\sigma}_v = -k_1 \dot{\varepsilon}_v$ or:

$$-\frac{\dot{\sigma}_v}{k_1} = A\sinh(\phi\sigma_v)$$

Integration gives: $\ln\left(\tanh\frac{\phi\sigma_v}{2}\right) = -A\phi k_1 t + c$
or:

$$\sigma_v = \frac{2}{\phi}\,\operatorname{arctanh}\left(\tanh\left(\frac{\phi\sigma_{vc}}{2}\right)\cdot\exp(-A\phi k_1 t)\right) \qquad (6.1)$$

This equation can be written with: $a = \tanh\left(\frac{\sigma_{vc}\phi}{2}\right)$; $b = A\phi k_1$:

$$\sigma_v = \frac{1}{\phi}\ln\frac{1 + a\exp(-bt)}{1 - a\exp(-bt)} = \frac{1}{\phi}\ln\left(\frac{\sqrt{a}\,e^{\left(\frac{bt}{2} - \ln\sqrt{a}\right)} + \sqrt{a}\,e^{\left(-\frac{bt}{2} + \ln\sqrt{a}\right)}}{\sqrt{a}\,e^{\left(\frac{bt}{2} - \ln\sqrt{a}\right)} - \sqrt{a}\,e^{\left(-\frac{bt}{2} + \ln\sqrt{a}\right)}}\right) =$$

$$= -\frac{1}{\phi}\ln\left(\tanh\left(\frac{bt}{2} - \frac{1}{2}\ln a\right)\right)$$

or:

$$\sigma_v = -\frac{1}{\phi}\ln\left(\tanh\left(\frac{A\phi k_1 t}{2} - \frac{1}{2}\ln\left(\tanh\left(\frac{\sigma_{vc}\phi}{2}\right)\right)\right)\right) \qquad (6.2)$$

For the early part of the relaxation this is:

$$\sigma_v = -\frac{1}{\phi}\ln\left(\frac{A\phi k_1 t}{2} - \frac{1}{2}\ln\left(\tanh\left(\frac{\sigma_{vo}\phi}{2}\right)\right)\right)$$

or:

$$\sigma_v = -\frac{1}{\phi}\ln\left(\frac{A\phi k_1}{2}\right) - \frac{1}{\phi}\ln\left(t + \frac{2\,\operatorname{arccoth}(\sigma_{vo}\phi)}{A\phi k_1}\right) \qquad (6.3)$$

Except for very small times this will have the empirical form:

$$\sigma_v = c_1 - c_2 \log t$$

The total stress on the specimen is: $\sigma = \sigma_o - \sigma_{vo} + \sigma_v(t)$ or:

$$\sigma = \sigma_o - \frac{1}{\phi}\ln\left(1 + \frac{A\phi k_1 t}{2\,\operatorname{arccoth}(\exp(\phi\sigma_{vo}))}\right)$$

or:

$$\frac{\sigma}{\sigma_o} = 1 - \frac{1}{\phi\sigma_o}\ln\left(1 + \frac{A\phi k_1 t}{2\cdot\operatorname{arccoth}(\exp(\phi\sigma_{vo}))}\right) \qquad (6.4)$$

in agreement with our experiments.

The shift of the relaxation lines along the time axis depend on the value of: $\operatorname{arccoth}(\exp(\phi\sigma_{vo}))$
If this is not sensitif for eq(6.4), as for creep, eq.(6.4) will show no

shift, as e.g. found in [29], for microspecimens. For larger values of $\phi\sigma_{vc}$ the shift will be:

$$\ln(t_a) - \ln(t_b) = \frac{\sigma_{vob}}{\sigma_b} - \frac{\sigma_{voa}}{\sigma_a}$$

For macrospecimens, shifts has been found [30],[31] showing greater values of $\phi\sigma_{vo}$ than for microspecimens by the high loading of the weak layers. The shift of the lines in [29], due to higher loading speed to the creep level show the existence of an element with a small value of n (see fig. 4.1), that is only noticeble at higher speeds and will quickly unload at relaxation. By this element the other elements will be lower loaded.

7. Conclusion

It is shown that the derived model is able to explain experimental phenomena, although a simplified analysis and simplified properties of the parameters where used to be able to obtain solutions in a functional form.

APPENDIX A

THEORY OF REACTION RATES FOR PLASTIC DEFORMATION IN SOLIDS

1. Introduction

In this appendix, a discussion of some aspects of the theory of deformation kinetics is given that will be used for the derivation of a simple creep and damage model, given in appendix B.
The basic concept of this theory is to regard plastic flow as a special form of a chemical reaction (like isomerization, where the composition remains constant but the bond structure of the molecules changes), because flow is a matter of molecular bond breaking and bond reformation.
A simple form of the reaction rate equation is:

$$\frac{d\rho_2}{dt} = -\frac{d\rho_1}{dt} = \rho_1 C_f - \rho_2 C_b \qquad (1)$$

where ρ is the concentration of flow units.
C= v*exp(-E/kT) (where v= a frequency factor)
E= the activation energy
k= Boltzmann's constant
T= the absolute temperature
Because there is a forward reaction into the product state and a backward reaction into the reactant state, there are two rate constants:

$$C_f = v \exp(-E_f/kT) \qquad (2)$$

$$C_b = v \exp(-E_b/kT) \qquad (3)$$

The atoms occupy equilibrium positions and are vibrating about the minimum of the free energy potential. Every position of the atoms with respect to each others determines a point of the potential energy surface. The atoms must reach an activated state on this potential surface in going from the reactant to the product state. (The thermal energy is not equally devided among the atoms and it is a matter of chance if an atom gets high enough energy to be activated and to be able to break bonds.)

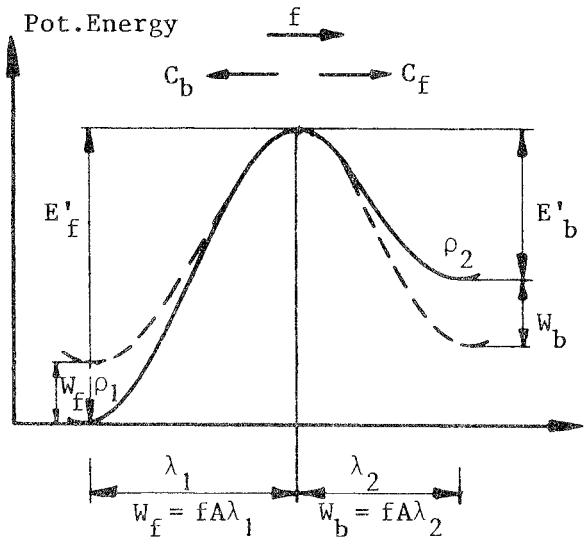


fig. 1 Potential energy change for an elementary reaction.

The explanation of the form of the rate constants C (eq.2-eq.3) is given by Bolzmann statistics.
$C = (kT/h)\exp(-E/kT)$
$\nu = kT/h$ can be approximated to the Debye frequency (about 10^{-13}) that may be regarded as the number of attempts per second of a particle to cross the barrier of height E. However, any attempt can succeed only if the energy of the particle exceeds E, and the probability of a jump per second is: $P = \nu.\exp(-E/kT)$, where kT is the mean vibrational energy of the particles.
Mostly not one group of reacting atoms is considered but a molal quantity. The molal free energy is then $E_m = N_m \cdot E$ and the Boltzmann constant is replaced by the gas constant $R = N_m \cdot k$ where N_m is Avogadro's Number. So: $E/kT = N_m E/N_m kT = E_m/RT$

$k = 8.616*10^{-5}\ eVdeg^{-1}$
$h = 4.135*10^{-15}\ eVsec$
$k/h = 2.084*10^{10}\ sec^{-1}deg^{-1}$
$R = 1.987\ cal.deg^{-1}mol^{-1}$
$N_m = 6.02*10^{23}$
1 Joule = 1Nm = $0.618*10^{19}$ eV = 0.239 cal.

2. Influence of an applied force

When the atoms are displaced from their equilibrium positions by an applied stress, the potential energy is increased. This means that the potential energy surface is changed, making the reaction more probable, decreasing the barrier height with W_f in forward direction and increasing the barrier height with W_b in backward direction, where $W = W_f + W_b$ is the work of the external constraints. So:

$$C_f = \frac{kT}{h} \exp\left(-\frac{E_f' + W_f}{kT}\right) \tag{4}$$

$$C_b = \frac{kT}{h} \exp\left(\frac{-E_b' - W_b}{kT}\right) \tag{5}$$

3. Reaction order of deformation processes

The theory is given for first order rections because nearly all materials appear to follow that law. So the slowest determining bond breaking reactions are of first order or quasi first order.
A description by higher order reactions is also possible and is p.e. given in [3] where a Taylor series expansion of the rate eq. is given for hydrogen bonded materials, leading to terms with increasing reaction order. The first term of the expansion may be of first order to explain the shown first order processes (relaxation, first moisture regain etc.) in dry cellulosic material. The disadvantage of this approach is that the rate eq. then reduces to a single forward reaction what is insufficient to describe the total behaviour of relaxation and a better approach is then possible by the first order theory (with a backward process) as done by Neredith [3]. An explanation why a first order theory can be used is given in chapter B2 where it is shown that the Eyring theory can be regarded as an expansion of the processes into first order processes. The same appears to be possible even for the complex reactions of decomposition of wood at high temperatures that can be given by pseudo-first-order reactions ($dW/dt = -\sum_i k_i(W - W_d)$; W = weight loss) [4]. Because the overall reaction has an order close to one, (at the highest rate) as follows from thermogravic experiments [5], the determining (slowest) bond breaking processes must be of first order (or quasi first order).

This can be shown by the following higher order reaction:

$$-\frac{d\rho}{dt} = C \cdot \rho^n \tag{6}$$

In the Eyring model for creep, the density of the flow units ρ is taken to be constant, as given by the last term of equation (7). This cannot be exacly true because then nothing changes and there would be no reaction. In eq.(7): $(\rho = \rho_0 + \Delta\rho)$

$$-\frac{d(\rho_0+\Delta\rho)}{dt} = -\frac{d\,\Delta\rho}{dt} = C \cdot \rho_0^n \left(1+\frac{\Delta\rho}{\rho_0}\right)^n \approx C \cdot \rho_0^n \left(1+\frac{n\Delta\rho}{\rho_0}\right) \approx C \cdot \rho_0^n \tag{7}$$

equation (6) is given, splitted in an initial value and a small change. It appears that the last two terms of eq.(7) are sufficient for the description of flow and fracture: The last term, for steady state processes, and the fore last term for severe changes in behaviour like dislocation -multiplication and -breakaway, causing yield drop in a constant strain rate test. So it appears that the theory describes small structural changes, and is linear in the variable $\Delta\rho$ being a quasi first order process. To use a higher order equation, the flow unit density has to be known. It cannot be found by indirect methods (by measuring creep etc.) As a first simplification, it is possible to regard only first order reactions.

4. Thermodynamics

The thermodynamic system is chosen to be a small volume around the dislocations (i.e. around the deformation- or fracture- site). This is surrounded by elastic material containing the external and internal stresses and the temperature dependence of the elastic constants have to be regarded separately in the model.
The variation of the Gibbs free energy at the deformation- or fracture-site, for isothermal, reversible processes (with constant: temperature T, pressure f and humidity ω) is:
$dE = d(H - TS - fc\lambda - \mu\omega) = dH - TdS - SdT - cfd\lambda - e\lambda df - \mu d\omega - \omega d\mu$
with $cf\lambda = f'\lambda_2\lambda_3\lambda = f\lambda/N$
From the first law is:
$dH = TdS + cfd\lambda + \omega d\mu$ So:
$dE = -SdT - c\lambda df - \mu d\omega = \frac{\partial G}{\partial T}dT + \frac{\partial G}{\partial f}df + \frac{\partial G}{\partial \omega}d\omega$
Because:

$$\frac{\partial^2 G}{\partial T \partial f} = -\frac{\partial S}{\partial f} = -c\frac{\partial \lambda}{\partial T}$$

and because the termal expansion $\frac{\partial \lambda}{\partial T}$ coefficient is approximate constant, between some transition temperatures, with respect to T and f, is E linear dependent on T and f . So:

$$\frac{\partial S}{\partial f} = c\frac{\partial \lambda}{\partial T} = a_1 + a_2\omega \tag{8}$$

It is also to be expected from fracture and creep tests that E may be assumed to be linear dependent on f, and may be assumed to be linear in T like for cotton and other high polymers.
In the same way, from the other partial derivatives is:

$$c\frac{\partial \lambda}{\partial \omega} = \frac{\partial \mu}{\partial f} \tag{9}$$

and:

$$\frac{\partial S}{\partial \omega} = \frac{\partial \mu}{\partial T} \tag{10}$$

Because of the linear expansion of wood with moisture content, $\frac{\partial \lambda}{\partial \omega}$ = const. and eq.(9) is:

$$\frac{\partial \mu}{\partial F} = c \frac{\partial \lambda}{\partial \omega} = a_5 + a_6 T \tag{11}$$

and E is linear in ω too, as can be expected from the following. The properties of wood follow the exp($c\omega$) - law, so the free energy may be assumed to be linear dependent on ω, as also follows from the description of sorption processes.
Eq.(10) is:

$$\frac{\partial \mu}{\partial T} = \frac{\partial S}{\partial \omega} = a_3 + a_4 F \tag{12}$$

From eq.(11) and eq.(12) μ must have the form: ($a_2 = a_4 = a_6$)

$$\mu = a_2 T F + a_3 T + a_5 F + a_7 \omega + a_8 \tag{13}$$

In the same way is:

$$S = a_1 F + a_2 \omega F + a_3 \omega + a_4 T + a_{10} \tag{14}$$

$$c\lambda = a_1 T + a_2 \omega T + a_5 \omega + a_{11} F + a_{12} \tag{15}$$

with all a's, constant.
The general form of E will be:

$$E = a_1 FT + a_2 \omega FT + a_3 T\omega + a_5 F\omega + a_{10} T + a_{12} F + a_8 \omega + a_{13} \tag{16}$$

From tests of [14], λ is constant for fracture processes, independent on T for $\omega = 0$ (see append. B). So E will be written: ($a_1 = c$)

$$E = H'' - S'T - F\lambda' \tag{17}$$

with:
$H'' = H' - c\,\omega$
$\lambda' = \lambda_0' + \omega\lambda_T'' + \omega\lambda'''$
$S' = S_0' + S''\omega$
For very quick loading, fracture is in the lignin and follows the WLF-equation around the transition temperature[22]. So a_1 is only zero below the transition temperature in that case and is constant above this temperature.

5. Parameters of the flow units

The reaction equation can be given in the dimensions of the flow units. If a segment λ_1 is moving upwards, the hole λ in fig.2 is moving downwards. The activation volume V is λ times A, and the work on one unit is: $f'.V = f'.A.\lambda$, where f' is the stress on the unit and A is the area. This can be expressed in the stress f in the material by: $f'.A.\lambda = f.\lambda/N$ where N is the number of elements per unit area.
So the force per element times A, is the force per unit area divided by the number of elements per unit area = stress / N.
λ_1 is the length of the flow unit or the distance between points of flow. So the concentration of flow units φ, being the number of activated volumes per unit volume, can be written:
$\varphi = N.\lambda.A / \lambda_1$, and for a symmetrical potential energy barrier ($E_c' = E_b'$), eq.(1) now gets the form of eq.(3.1) of appendix B.

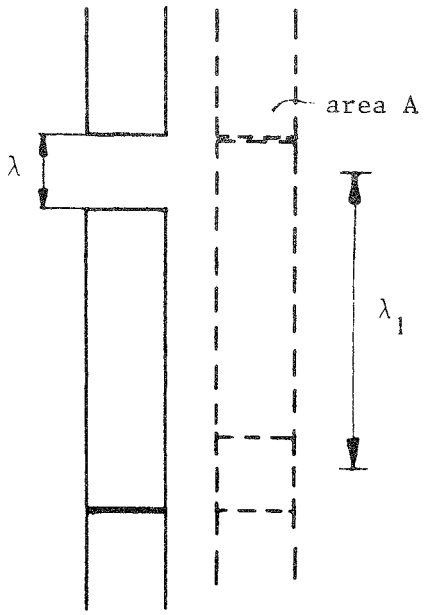


fig. 2 Moving space

APPENDIX B

DERIVATION OF A CREEP AND DAMAGE MODEL BASED ON THE THEORY OF DEFORMATION KINETICS

1. Introduction

Because the general background of the theory is not common knowledge in engineering, a short review (following [1]) is given in Appendix A.
The basic concept of this theory is to regard plastic flow as a special form of a chemical reaction, because flow is a matter of bond breaking and bond reformation.
A simple form of the reaction rate equation (for activation over a single potential energy barrier) is:

$$\text{Rate} = \frac{d\rho_2}{dt} = \rho_1 C_{1f} - \rho_2 C_{1b} \tag{1.1}$$

where $C_{1,f}$ and $C_{1,b}$ are the rate constants for forward resp. backward reactions and ρ is the concentration of flow units, that may be kinks and holes in polymers or vacancies and dislocation segments in crystalline regions.
For larger, noticible, plastic deformations, it is possible that the reaction occurs over a system of energy barriers and systems of consecutive and parallel barriers have to be regarded. There are indications that this has to be expected for the complex structure of wood.
For a two barrier system (Fig. 1) there is an intermediate stage of ρ_2 units being in steady state concentration. So:

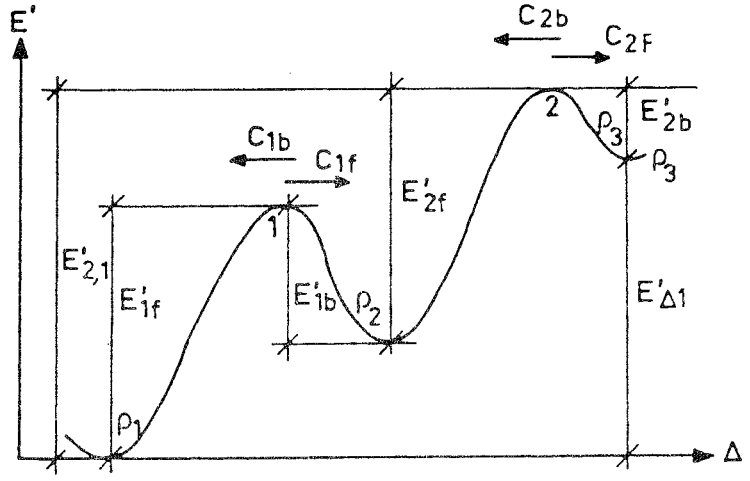


Fig. 1. Two consecutive barriers.

The net numbers of units crossing the two barrier system is:

$$\text{Rate} = \rho_2 C_{2f} - \rho_3 C_{2b} = C_{2f} \frac{\rho_1 C_{1f} + \rho_3 C_{2b}}{C_{2f} + C_{1b}} - \rho_3 C_{2b} =$$

$$= \frac{\rho_1 - \rho_3 \left(C_{1b}/C_{1f} \cdot C_{2b}/C_{2f}\right)}{1/C_{1f} + C_{1b}/C_{1f} \cdot C_{2f}} \tag{1.2}$$

For the ith obstacle is:

$$C_i = \kappa_i \frac{kT}{n} \exp\left(-\frac{E_i}{kT}\right) \tag{1.3}$$

or

$$\frac{C_{ib}}{C_{i+1,f}} = \exp\left(\frac{E_{i+1,f} - E_{i,b}}{kT}\right) \tag{1.4}$$

and

$$\frac{C_{1b}}{C_{2f} C_{1f}} = \frac{1}{\kappa} \frac{h}{kT} \exp\left(\frac{E_{2,f} - E_{1,b} + E_{1,f}}{kT}\right) = \frac{1}{\kappa} \frac{h}{kT} \exp\left(\frac{E_{2,1}}{kT}\right) = \frac{1}{C_{2,1}} \tag{1.5}$$

Similarly is:

$$\frac{C_{1b} C_{2b}}{C_{1f} C_{2f}} = \exp\left(\frac{E_{1f} - E_{1b} - E_{2b} + E_{2f}}{kT}\right) = \exp\left(\frac{E_{\Delta,1}}{kT}\right) \tag{1.6}$$

Thus the rate becomes:

$$\text{Rate} = \frac{\rho_1 - \rho_3 \exp\left(\frac{E'_{\Delta 1} - W_{\Delta 1}}{kT}\right)}{1/C_{1,1} + 1/C_{2,1}} \tag{1.7}$$

with:

$$C_{1,1} = \kappa \frac{kT}{h} \exp\left(-\frac{E'_{1,1} - W_{1,1}}{kT}\right) \tag{1.8}$$

$$C_{2,1} = \kappa \frac{kT}{h} \exp\left(-\frac{E'_{2,1} - W_{2,1}}{kT}\right) \tag{1.9}$$

and

$$E_{\Delta,1} = (E' - W)_{1f} - (E' + W)_{1b} - (E' + W)_{2b} + (E' - W)_{2f} =$$

$$= (E'_{1f} - E'_{1b} - E'_{2b} + E'_{2f}) - (W_{1b} + W_{1f} + W_{2b} + W_{2f}) = E'_{\Delta,1} - W_{\Delta,1} \tag{1.10}$$

$$E_{2,1} = E_{1f} - E_{1b} + E_{2f} = (E' - W)_{1f} - (E' + W)_{1b} + (E' - W)_{2f} =$$

$$= E'_{1f} - E'_{1b} + E'_{2f} - (W_{1f} + W_{2f} + W_{1b}) = E'_{2,1} - W_{2,1} \tag{1.11}$$

$$C_{1,1} = C_{1,f}$$

In the same way is for n obstacles in series:

$$\text{Rate}_n = \frac{\rho_1 - \rho_{n+1} \exp(E_{\Delta,1}/kT)}{\sum_{i=1}^{n} \frac{1}{C_{i,1}}} \tag{1.12}$$

with:

$$C_{i,1} = \kappa \frac{kT}{h} \exp\left(-\frac{E_{i,1}}{kT}\right) \tag{1.13}$$

For m processes parapllel is:

$$\text{Rate}_{m,n} = \sum_{j=1}^{m} \frac{\rho_1 - \rho_{n+1} \exp(E_{1,\Delta}/kT)}{\sum_{i=1}^{n} (1/C_{i,1})} \tag{1.14}$$

2. Series approximation of the rate equations

The general equations can be simplified to suitable forms for solutions of the rate equations. Because these approximations probably cannot be found in literature, the whole derivation is given here.
It is possible to expand the total potential energy curve into (Fourier-) series and regard the proces as a parallel acting system of symmetrical consecutive barriers.

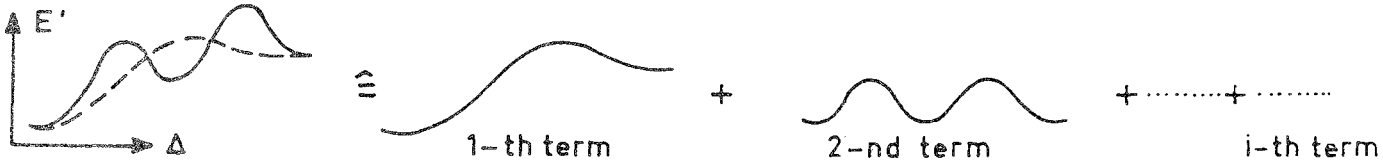


Fig. 2.1. Series approximation of E.

Except of the first term, is in all series $E'_{\Delta,1} = 0$ (see Fig. 1) and because of the symmetry of the barriers in the series, all $E_{i,j}$'s and all $W_{i,j}$'s are equal.

By eq. (1.8) is: $$C_{1,1} = \kappa \frac{kT}{h} \exp\left(-\frac{E' - W}{kT}\right) \qquad (2.1)$$

By eq. (1.9) is: $$C_{2,1} = \kappa \frac{kT}{h} \exp\left(-\frac{E' - 3W}{kT}\right) \qquad (2.2)$$

Eq. (1.13) becomes: $$C_{i,1} = \kappa \frac{kT}{h} \exp\left(-\frac{E' - (2i-1)W}{kT}\right) \qquad (2.3)$$

So:

$$\sum \frac{1}{C_{i,1}} = \frac{1}{\kappa \frac{kT}{h} \exp\left(-\frac{E'}{kT}\right)} \cdot \left(\frac{1}{\exp\left(\frac{W}{kT}\right)} + \frac{1}{\exp\left(\frac{3W}{kT}\right)} + \ldots + \frac{1}{\exp\left(\frac{(2i-1)W}{kT}\right)}\right) =$$

$$= \frac{1}{\kappa \frac{kT}{h} \exp\left(-\frac{E'}{kT}\right)} \cdot \left(\frac{1}{\exp \frac{W}{kT}} + \frac{1}{\left(\exp \frac{W}{kT}\right)^3} + \ldots + \frac{1}{\left(\exp \frac{W}{kT}\right)^{(2i-1)}}\right) =$$

$$= \frac{1}{\kappa \frac{kT}{h} \exp\left(-\frac{E'}{kT}\right)} \cdot \left(\frac{\frac{1}{\exp W/kT}\left(1 - \left(\frac{1}{\exp W/kT}\right)^{2i}\right)}{1 - 1/(\exp W/kT)^2}\right) =$$

$$= \frac{1}{\kappa \frac{kT}{h} \exp\left(-\frac{E'}{kT}\right)} \cdot \frac{1 - \exp(-2iW/kT)}{\exp \frac{W}{kT} - \left(\exp \frac{W}{kT}\right)^{-1}} =$$

$$= \frac{1 - \exp(-2iW/kT)}{2\kappa \frac{kT}{h} \exp\left(-\frac{E'}{kT}\right).\sinh\left(\frac{W}{kT}\right)} \qquad (2.4)$$

The rate is from eq. (1.10) and (1.12) with $E_{\Delta 1} = E'_{\Delta 1} - W_{\Delta,1} = -W_{\Delta,1} = -2iW$:

$$\text{Rate} = \frac{\left(\rho_1 - \rho_{n+1} \exp(-2iW/kT)\right).\left(2\kappa \frac{kT}{h} \exp\left(-\frac{E'}{kT}\right).\sinh\left(\frac{W}{kT}\right)\right)}{1 - \exp\left(-2i \frac{W}{kT}\right)} =$$

$$= 2\kappa \frac{kT}{h} \rho_1 \exp\left(-\frac{E'}{kT}\right).\sinh\left(\frac{W}{kT}\right) \qquad (2.5)$$

Equilibrium (Rate = 0) is only possible for W = 0 for these barriers and from symmetry of: $E = E_f = E_b$; ρ_1 has to be equal to ρ_{n+1}.
Calling: $1/\left((\kappa kT/h) \exp(-E'/kT)\right) = t_i$, the relaxation time of the ith expanded term, eq. (2.5) is (as chemical reaction equation):

$$\frac{d\rho_{n+1}}{dt} = -\frac{d\rho_1}{dt} = \frac{2\rho}{t_i} \sinh\left(\frac{W_i}{kT}\right) \qquad (2.6)$$

Now the work W of a flow unit with area $\lambda_2 \times \lambda_3$ moving over a barrier, over a distance λ is: $W = (f.\lambda_2.\lambda_3.\lambda)/2 = fV/2 = \sigma.\lambda/(2N)$ where V is the activation volume and N is the number of activated flow units per unit area (see Appendix A).

Because $f.\lambda_2.\lambda_3$ is the force on one element it is easy to see that: $f.\lambda_2.\lambda_3$ = force/1-element = (total force/unit area)/elements/unit area) = stress/N = σ/N. The concentration of flow units or the number of activated volumes per unit volume is: ρ = activ. volumes/unit-volume = (number-of-elements * $\lambda_2.\lambda_3.\lambda$)/(unit-area * distance $\perp$) = $(N\ \lambda_2.\lambda_3.\lambda)/\lambda_1$ where λ_1 is the length of the flow unit (or the distance between points of flow). Eq. (2.6) can now be written (with $V_i = \lambda/N_i$):

$$\frac{d}{dt}\left(\frac{N\ \lambda.\lambda_2.\lambda_3}{\lambda_1}\right) = 2\ \frac{N\ \lambda_2.\lambda_3.\lambda}{t_i\lambda_1}\ \sinh\left(\frac{\sigma_i V_i}{2kT}\right)$$

or for a constant structure $N\ \lambda_2.\lambda_3$:

$$\frac{d}{dt}\left(\frac{\lambda}{\lambda_1}\right) = \frac{2\lambda}{t_i\lambda_1}\ .\ \sinh\left(\frac{\sigma_i V_i}{2kT}\right) \qquad (2.8)$$

or

$$\frac{d\varepsilon}{dt} = \dot{\varepsilon} = \frac{\varepsilon_o}{t_i}\ \sinh\left(\frac{\sigma_i V_i}{2kT}\right) = \frac{1}{t_i'}\ \sinh\left(\frac{\sigma_i V_i}{2kT}\right)$$

with the apparant relaxation time $t_i' = t_i/\varepsilon_o$ ($\varepsilon_o \simeq 1$ for cellulosic materials). So eq. (2.6) is for no structural change:

$$\dot{\varepsilon} = \frac{1}{t_i}\ \sinh\left(\frac{\sigma_i V_i}{2kT}\right) = \frac{1}{t_i}\ \sinh\left(\phi_i\sigma_i\right) \qquad (2.9)$$

The inverse is:

$$\sigma_i = \frac{1}{\phi_i}\ \text{arc sinh}\ (t_i'\dot{\varepsilon})$$

The form of the first expanded term of the series has to be taken symmetrical for the expanded W. So from eq. (1.1) or eq. (2.5) is:

$$\text{Rate} = \kappa \frac{kT}{h} \left(\rho_1 \exp\left(-\frac{E_{1f} - W_1}{kT}\right) - \rho_{n+1} \exp\left(-\frac{E_{1,b} + W_1}{kT}\right)\right) \qquad (2.10)$$

For a creep process, it may be expected that the rate is zero for no external force (equilibrium) or $W_1 = 0$. So (2.10) becomes:

$$\rho_1 \exp\left(-\frac{E_{1,f}}{kT}\right) = \rho_{n+1} \exp\left(-\frac{E'_{1b}}{kT}\right) \qquad (2.11)$$

and eq. (2.10) can be written:

$$\text{Rate} = 2\kappa \frac{kT}{h} \rho_1 \exp\left(-\frac{E_{1,f}}{kT}\right) \sinh\left(\frac{W_1}{kT}\right)$$

or

$$\dot{\varepsilon} = \frac{1}{t_1} \sinh\left(\frac{W_1}{kT}\right) \qquad (2.12)$$

This is in agreement with creep processes in wood at low stresses where the behaviour is approximate Newtonian (then $\sinh(W_1/kT) \approx W_1/kT$).
For structural changes, as in crack propagation, the crack extension force must overcome the thermodynamic surface energy. Further energy is needed to change the material near the crack surface (the new surface contains more defects) and to fracture strong ordered areas of bonds, crossing the surface, that cannot be broken by thermal activation at normal temperatures. So calling these energies W_0, the crack is in an equilibrium state with zero velocity when $W = W_0$. Eq. (2.10) is then:

$$\rho_1 \exp\left(-\frac{E_{1,f} - W_0}{kT}\right) = \rho_{n+1} \exp\left(-\frac{E'_{1,b} + W_0}{kT}\right)$$

So eq. (2.10) can be written:

$$\text{Rate} = \kappa \frac{kT}{h} \rho_1 \exp\left(-\frac{E'_{1,f} - W_0}{kT}\right).\left(\exp\left(\frac{W_1 - W_0}{kT}\right) - \exp\left(-\frac{W_1 - W_0}{kT}\right)\right) =$$

$$= 2\kappa \frac{kT}{h} \rho_1 \exp\left(-\frac{E'_{1,f} - W_0}{kT}\right) \sinh\left(\frac{W_1 - W_0}{kT}\right) \qquad (2.13)$$

or, for a steady state process (ρ_1 = constant):

$$\dot{\varepsilon} = \frac{1}{t_1} \sinh \left(\frac{W_1 - W_0}{kT}\right) \tag{2.14}$$

with:

$$\frac{1}{t_1} = \kappa \frac{kT}{h} \exp \left(- \frac{E'_{1,f} - W_0}{kT}\right)$$

and

$$W_0 = (E'_f - E'_b)/2 - kT \ln (\nu \rho_1 / \rho_{n+1})$$

Because of the long relaxation time $t_{r,1}$, the influence of W_0 can be neglected for short term processes, even at high stress levels.
For that case is:

$$\sinh \left((W_1 - W_0)/kT\right) \approx \frac{1}{2} \exp \left((W_1 - W_0)/kT\right)$$

and

$$\dot{\varepsilon} = \kappa \frac{kT}{h} \exp \left(- \frac{E'_{1f} - W_0}{kT}\right) \sinh \left(\frac{W_1 - W_0}{kT}\right) \approx \kappa \frac{kT}{2h} \exp \left(\frac{- E_{1,f} + W_1}{kT}\right) \approx$$

$$\approx \kappa \frac{kT}{h} \exp \left(- \frac{E_{1f}}{kT}\right) . \sinh \left(\frac{W_1}{kT}\right)$$

This is done in eq. (2.16).
If there are different kinds of flow units acting together, the total applied stress is the sum of these components. So:

$$\sigma = \sum \sigma_i x_i$$

where x_i is the fraction of the stressed surface of the ith group of units.

$$\sigma = \sum_i \frac{x_i}{\phi_i} \text{ arc sinh } (t_i \dot{\varepsilon}) \tag{2.15}$$

or

$$\frac{\sigma}{\dot{\varepsilon}} = \sum_i \frac{x_i t_i}{\phi_i} \cdot \frac{\text{arc sinh } (t_i \dot{\varepsilon})}{t_i \dot{\varepsilon}}$$

For the terms with $t_i\dot{\varepsilon} \ll 1$ is: $(\text{arcsinh } (t_i\dot{\varepsilon})/t_i\dot{\varepsilon} \approx 1$,
and for terms with $t_i\dot{\varepsilon} \gg 1$ is: $(\text{arcsinh } (t_i\dot{\varepsilon})/t_i\dot{\varepsilon} \approx 0$
So there remain a limited number of terms:

$$\frac{\sigma}{\dot{\varepsilon}} = \sum \frac{x_i t_i}{\phi_i} + \sum \frac{x_i}{\phi_i \dot{\varepsilon}} \text{ arcsinh } (t_i\dot{\varepsilon}) \tag{2.16}$$

The first term of (2.16) can be expressed in a mean value:

$$\sum \frac{x_i t_i}{\phi_i} = t_1 \sum \frac{x_i}{\phi_i} = t_1 x_1 \sum \frac{1}{\phi_i} \tag{2.17}$$

and eq. (2.16) gets the form of the generalized flow theory consisting of separate symmetrical elements:

$$\frac{\sigma}{\dot{\varepsilon}} = \frac{x_1 t_1}{\phi_1} + \frac{x_2 t_2}{\phi_2} \cdot \frac{\text{arcsinh } (t_2\dot{\varepsilon})}{t_2\dot{\varepsilon}} + \frac{x_3 t_3}{\phi_3} \cdot \frac{\text{arcsinh } (t_3\dot{\varepsilon})}{t_3\dot{\varepsilon}} \tag{2.18}$$

So, by series expansion, the assumptions of this generalized flow theory have now been proven:

a. The flow unit spectrum exists (as expanded terms) and may be approximated by a limited number of elements with distinct average relaxation times. (As experimental found [2], less than 3 groups are sufficient for a description of most materials).
b. The deformation rate of all units is the same (in accordance with the observations that there are no structural changes due to rate differences during flow).

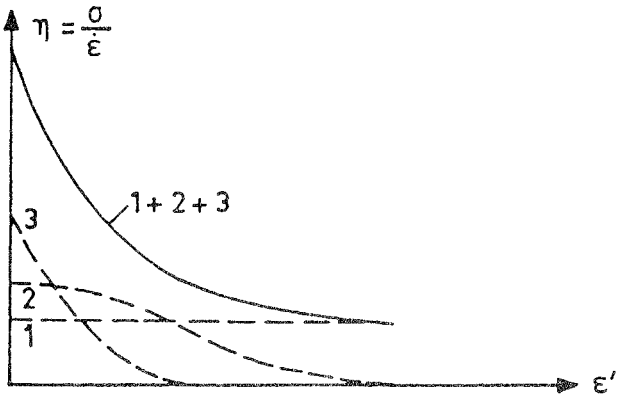


Fig. 2.2. Viscosity-strain rate relation.

The first term of eq. (2.18) represents Newtonian behaviour. The others are non-Newtonian, or Newtonian in the low strain rate range.
The fysical meaning of the expansion of the potential energy curve is, to regard the total process as a result of parallel acting simple processes. For instance, a dislocation may meet different kinds of obstacles and the waiting time at the end of the process is the mean of the waiting times at the different obstacles. At higher stresses these waiting times may change differently for the different obstacles and the apparent activation energy and volume may be stress dependent. Expansion means that groups of dislocations are supposed to meet only one type obstacle. Each group meets another type of the same obstacles in succession, resulting in a number of parallel acting simple reactions.
Hereby it is supposed that the interaction between the different mechanisms is not strong.
In elementary reactions, the activation parameters (enthalpy, entropy) are often constant (for temperature) so that a simple description of the total rate process becomes possible.
An experimental proof (by relaxation tests) of this supposition is given in [6] for metals. Those metals that where described with single barrier mechanisms, often had a stress dependent activation energy or volume. This was not the case for the metals that were described by two (so more than one) parallel symmetrical barriers. The enthalpy and entropy were also constant.
The same has be done for cotton [7] (that has a similar structure as wood). The two symmetrical barriers had constant, stress independent activation parameters.

3. Rate theory of fracture

3.1. Basic equations and fracture by constant loading

Eq. (2.18) applies for steady state processes, when the structure and bond density doesn't change.
Crack initiation and propagation occur when the rate of bond breaking exceeds the rate of bond re-establishment, leading to structural changes.
Eq. (2.8) can be written in the form:

$$\frac{d}{dt}\left(\frac{N'\lambda'}{\lambda_1}\right) = 2N\,\frac{\lambda'}{\lambda_1 t_r}\,\sinh\left(\frac{f\lambda'}{NkT}\right) \tag{3.1}$$

with $\lambda' = \lambda/2$.
If λ_1 can be regarded as a constant length of the flow unit, N or λ' may change in eq. (3.1) whether bond density change (N) or change in free volume is expected to cause fracture.
Both models give the same results because from eq. (2.6), eq. (3.1) is, for constant $\lambda' = \lambda'_o$ (and decreasing N_1):

$$-\frac{dN_1}{dt} = \frac{2N_1}{t_r}\,\sinh\left(\frac{f\lambda'_o}{N_1 kT}\right)$$

or

$$\frac{d\ 1/N_1}{dt} = \frac{1}{N_1}\,\frac{2}{t_r}\,\sinh\left(\frac{f\lambda'_o}{N_1 kT}\right) \tag{3.2}$$

For constant $N_1 = N_{n+1} = N$ and variable, increasing λ' is:

$$\frac{dN_{n+1}.\lambda'}{dt} = \frac{2N_1\lambda'}{t_r}\,\sinh\left(\frac{f\lambda'}{N_1 kT}\right)$$

or

$$\frac{d\lambda'}{dt} = \frac{2\lambda'}{t_r}\,\sinh\left(\frac{f\lambda'}{NkT}\right) \tag{3.3}$$

So eq. (3.2) in $1/N_1$ is exactly the same as eq. (3.3) in λ'.

The choise is thus possible to regard λ' as a constant (as done for crystals and metals, where λ' is taken to be equal to the Burger's vector) or to take N as constant (when slip of the chains is expected to cause fracture). A third possibility for fracture is the change of λ_1 (for instance by "dislocation" multiplication or by change in flow unit density).
Then eq. (3.1) becomes:

$$\frac{d(1/\lambda_1)}{dt} = \frac{2}{t_r \lambda_1} \sinh\left(\frac{\lambda' f}{NkT}\right) \tag{3.4}$$

It will be shown that both models eq. (3.2) and eq. (3.4) give the same results. So that the simplest equation (3.4) can be used for applications. Because fracture occurs at higher stresses eq. (3.2) can be written:

$$\frac{dN_1}{dt} = -\frac{N_1}{t_r} \exp\left(\frac{f\lambda'}{N_1 kT}\right) \tag{3.5}$$

or for constant stress f:

$$\int_{f\lambda/N_o kT}^{\infty} \left(\frac{dN_1^{-1}}{N_1^{-1}} \exp\left(\frac{\lambda' f}{kT} N_1^{-1}\right)\right) = \frac{t_f}{t_r} \tag{3.6}$$

where t_f is the lifetime of the specimen subjected to constant stress. The integral in eq. (3.6) is the exponential integral: $-E_i(-\lambda' f/NkT)$ reducing for larger values of the variable to:

$$-E_i\left(-\frac{f\lambda'}{NkT}\right) \simeq \frac{\exp\left(-\lambda' f/N_o kT\right)}{\lambda' f/N_o kT} \tag{3.7}$$

So eq. (3.6) is:

$$t_f = t_r \frac{N_o kT}{f\lambda'} \exp\left(-\frac{f\lambda'}{N_o kT}\right) = \frac{N_o h}{\kappa f\lambda'} \exp\left(\frac{E'}{kT} - \frac{f\lambda'}{N_o kT}\right) \tag{3.8}$$

or

$$\mathrm{Ln}(t_f) = \ln\left(\frac{N_o h}{\kappa\lambda' f}\right) + \frac{E'}{kT} - \frac{f\lambda'}{N_o kT} = \ln(t_o) + \frac{E'}{kT} - \frac{f\lambda'}{N_o kT} \tag{3.9}$$

In the same way eq. (3.4) can be intgrated:

$$\int_{1/\lambda_{1,0}}^{1/\lambda_{1,m}} d\ln\,(1/\lambda_1) = \frac{t_f}{t_r} \exp\left(\frac{f\lambda'}{N_o kT}\right) = \ln\left(\frac{\lambda_{1,0}}{\lambda_{1,m}}\right) \tag{3.10}$$

or

$$t_f = \frac{h}{\kappa kT} \operatorname{Ln}\left(\frac{\lambda_{1,0}}{\lambda_{1,m}}\right).\exp\left(\frac{E'}{kT} - \frac{f\lambda'}{N_o kT}\right)$$

or

$$\operatorname{Ln}(t_f) = \operatorname{Ln}\left(\frac{h}{\kappa kT} \cdot \operatorname{Ln}\left(\frac{\lambda_{1,0}}{\lambda_{1,m}}\right)\right) + \frac{E'}{kT} - \frac{f\lambda'}{N_o kT} = \operatorname{Ln}(t_o) + \frac{E'}{kT} - \frac{f\lambda'}{N_o kT} \tag{3.11}$$

giving the same form as eq. (3.9).
Eq. (3.11) gives a strain criterion for fracture:

$$t_o = \frac{h}{\kappa kT} \ln\left(\frac{\lambda_{1,0}}{\lambda_{1,m}}\right) \tag{3.12}$$

or

$$\frac{\lambda_{1,0}}{\lambda_{1,m}} = \frac{\varepsilon_m}{\varepsilon_o} = \exp\left(\frac{\kappa kT}{h}\, t_o\right) \tag{3.13}$$

From tests [8] it is found that t_o in eq. (3.11) or eq. (3.9) has a definite value for the many materials tested, being the reciprocal of the natural oscillation frequency of atoms in solids. It is seen that t_o is not constant in eq. (3.9) being the error of integrating with a constant (mean value) λ_1. This error diminishes when T approaches zero as can be seen in eq. (3.13):

$$\lambda_{1,0} \to \lambda_{1,m} \quad \text{when} \quad T \to 0$$

From eq. (3.9) it follows that when $T \to 0$, $\lambda' f/N_o \to E'$ and $t_o = N_o h/\kappa\lambda' f \to \frac{h}{\kappa E'}$ with $\kappa = 1$ is $E' \simeq \frac{h}{t_o} = h.\nu$ for $T = 0$.

It is seen that the bond breaking model, changing only the value of N only applies near ablsolute zero temperature and there will be always changes in flow unit density $1/\lambda_1$.
To show the amount of change of N and $1/\lambda_1$, eq.(3.1) can be written:

$$\frac{d}{dt}\left(\frac{1}{N\lambda_1}\right) = \frac{2\lambda}{N\lambda_1 t_r}\sinh\left(\frac{f\lambda}{kTN}\right) \approx \frac{\lambda}{N\lambda_1 t_r}\exp\left(\frac{f\lambda}{kTN}\right) \rightarrow \tag{3.14}$$

$$\frac{1}{\lambda_1}\frac{d}{dt}\left(\frac{\lambda}{N}\right) + \frac{\lambda}{N}\frac{d}{dt}\left(\frac{1}{\lambda_1}\right) = \frac{\lambda}{N\lambda_1 t_r}\exp\left(\frac{f\lambda}{NkT}\right) \rightarrow \frac{d}{dt}\left(\ln\frac{\lambda}{N}\right) + \frac{d}{dt}\left(\ln\frac{1}{\lambda_1}\right) = \frac{1}{t_r}\exp\left(\frac{f\lambda}{NkT}\right) \rightarrow \tag{3.15}$$

$$\frac{d}{dt}\left(\ln\frac{\lambda}{N}\right) + \frac{d(\ln 1/\lambda_1)}{d(\ln \lambda/N)}\cdot\frac{d(\ln \lambda/N)}{dt} = (1+A)\frac{d}{dt}\left(\ln\frac{\lambda}{N}\right) = \frac{1}{t_r}\exp\left(\frac{f\lambda}{NkT}\right) \tag{3.16}$$

with A is the mean value of $\frac{d\ln 1/\lambda_1}{dt} \Big/ \frac{d\ln \lambda/N}{dt}$; A = 0 when λ_1 = constant.

$$\int_{\lambda/N_0}^{\infty}\frac{d\ln \lambda/N}{\exp\left(f\lambda/NkT\right)} = \int_0^{t_f}\frac{dt}{(1+A)t_r} \rightarrow E_i\left(\frac{f\lambda}{N_0kT}\right) = \frac{t_f}{(1+A)t_r} \rightarrow \frac{\exp\left(-f\lambda/N_0kT\right)}{f\lambda/N_0kT} \approx \frac{t_f}{t_r}\frac{kT}{h(1+A)}\exp\left(-\frac{E'}{kT}\right) \tag{3.17}$$

or with $v = 1/t_0$:

$$\exp\left(\frac{E'}{kT} - \frac{f\lambda}{N_0kT}\right) = \frac{1}{1+A}\,\frac{t_f}{t_0}\,\frac{kT}{h\nu}\,\frac{f\lambda}{N_0kT} \rightarrow \frac{E'}{kT} - \frac{f\lambda}{N_0kT} = \ln\frac{t_f}{t_0} + \ln\left(\frac{kT}{h\nu}\frac{f\lambda}{N_0kT}\cdot\frac{1}{1+A}\right) = \tag{3.18}$$

$$= \ln\frac{t_f}{t_0}$$ (measurements, see fig.3.1) S_c

with kT/hv = 1 is: $\ln\frac{f\lambda}{N_0kT(1+A)} = 0 = \ln 1 \rightarrow 1+A = \frac{f\lambda}{N_0kT}$

Because $f\lambda/N_0kT \gg 1$, is A >> 1 and the change of $1/\lambda_1$ dominates the change of N_1 and N may be regarded as a constant.

When the plastic strain doesn't change much, it must be possible to regard a mean value of $\lambda/\lambda_1 N$. Integration then gives:

$$\frac{d}{dt}\left(\frac{\lambda}{\lambda_1 N}\right) \approx \frac{\lambda}{t_r\lambda_{1o}N_o}\exp\left(\frac{f\lambda}{N_okT}\right) \rightarrow \frac{\lambda}{\lambda_1 N} = \frac{t_f}{t_r}\frac{\lambda}{\lambda_{1o}N_o}\exp\left(\frac{f\lambda}{N_okT}\right) + \frac{\lambda}{N_o\lambda_{1o}} \rightarrow \tag{3.19}$$

$$\left(\frac{\lambda}{N\lambda_1} - \frac{\lambda}{N_o\lambda_{1o}}\right)\cdot\frac{N_o\lambda_{1o}}{\lambda} = \frac{t_f}{t_0}\cdot\frac{kT}{h\nu}\exp\left(-\frac{E'}{kT} + \frac{f\lambda}{kTN_o}\right) \rightarrow \frac{E'}{kT} - \frac{f\lambda}{kTN_o} = \ln\frac{t_f}{t_0} - \ln\left(\frac{N_o}{N_f} - 1\right) \text{ or } = \ln\frac{t_f}{t_0} - \ln\left(\frac{\varepsilon_f}{\varepsilon_0} - 1\right) \tag{3.20}$$

leading to $N_f = 0.5 \times N_o$, as experimentally found for fracture (i.e. the crack length is about the crack distance, or the intact area has reduced to 0.5 times the initial area when instable crack propagation starts). Because N/λ_1 is the strain, it is also possible to interprete this as an ultimate strain condition $\varepsilon_f/\varepsilon_0 = 2$ for this slip model, that is the same as discussed in chap. 2 of this appendix. In [10] this model was used and it was found that a maximum shear strain condition has to be applied This was compaired by other tests [11] with the bond fracture model. Both models gave almost the same results.

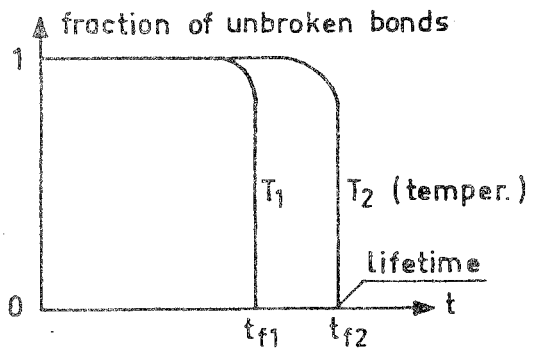


fig. 3.2

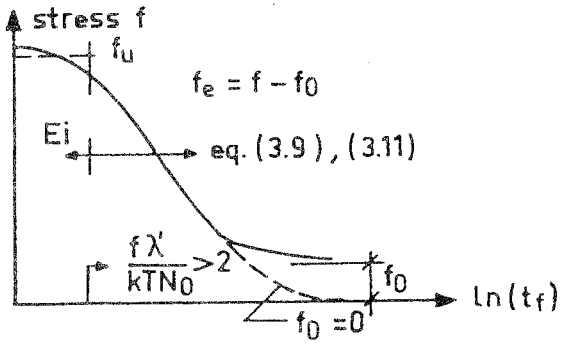


fig. 3.3

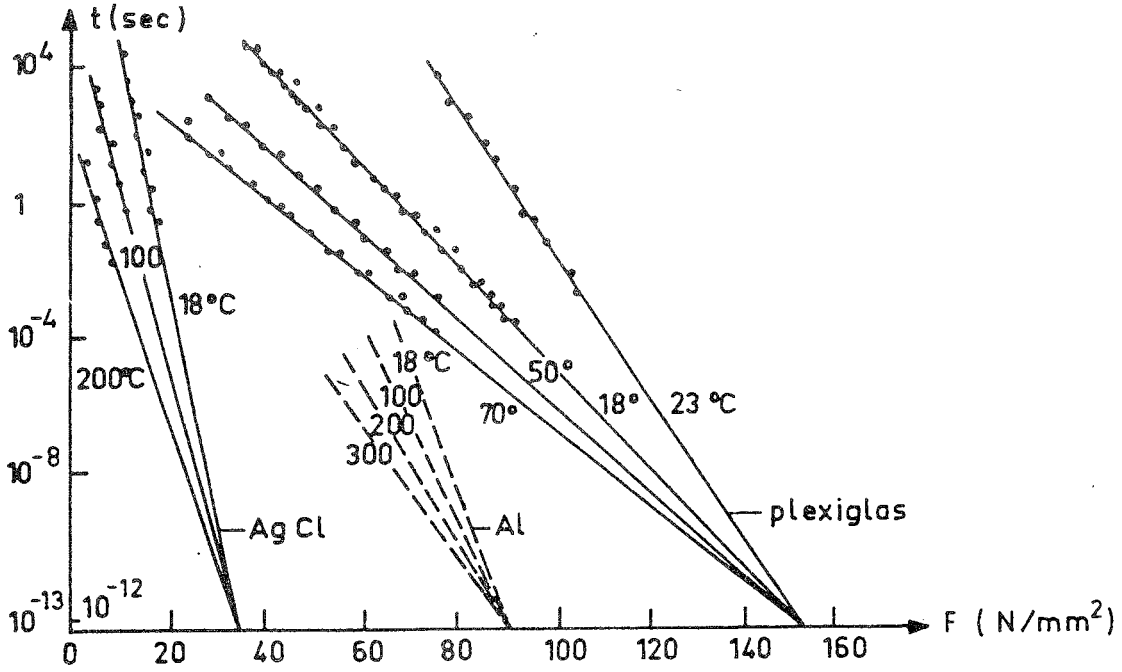


fig. 3.1 Stress and temperature dependence of the lifetime for some materials.

3.2 Fracture at constant loading rate and for creep

Numerical integration of the bond breaking eq.(3.5) [4] for constant loading rate is given in fig. 3.2, showing also the possibility of a constant value of N during the lifetime. This was also shown in par.3.1 and it is sufficient to use eq.(3.4).

For a constant loading rate $f = \dot{f}.t$ ($\dot{f}$ = constant) is eq. (3.4):

$$\frac{d}{dt}\left(\ln\left(1/\lambda_1\right)\right) = \frac{2}{t_r}\sinh\left(\frac{\lambda' \dot{f} t}{NkT}\right) \tag{3.21}$$

or

$$\ln\left(\frac{\lambda_{1,0}}{\lambda_{1,m}}\right) = \frac{2}{t_r}\frac{NkT}{\dot{f}\lambda'}\left(\cosh\left(\frac{\dot{f}\lambda' t_f}{NkT}\right) - 1\right) \simeq \frac{NkT}{t_r \dot{f}\lambda'}\exp\left(\frac{\dot{f}\lambda' t_f}{NkT}\right)$$

for higher stresses, or with $\dot{f}.t_f = f_u$:

$$Ln\left(\frac{h}{\kappa kT}\,Ln\left(\frac{\lambda_{1,0}}{\lambda_{1,m}}\right).\frac{\lambda' \dot{f}}{NkT}\right) = -\frac{E'}{kT} + \frac{f_u \lambda'}{NkT} \tag{3.22}$$

So:

$$Ln(t_f) = \ln\left(\frac{h}{\kappa kT}.\,Ln\left(\frac{\lambda_{1,0}}{\lambda_{1,m}}\right)\frac{f_u \lambda'}{NkT}\right) + \frac{E'}{kT} - \frac{\lambda' f_u}{NkT} \tag{3.23}$$

or

$$\mathrm{Ln}\left(t_f \cdot \frac{NkT}{\lambda' f_u}\right) = \ln\left(\frac{h}{\kappa kT} \ln\left(\frac{\lambda_{1,0}}{\lambda_{1,m}}\right)\right) + \frac{E'}{kT} - \frac{\lambda' f_u}{NkT} = \ln(t_o) + \frac{E'}{kT} - \frac{\lambda' f_u}{NkT} \tag{3.24}$$

This equation is the same as eq. (3.11). So the short-term failure time t_s is equivalent to a creep failure at level f_u and life-time:

$$t_c = t_s \cdot \frac{NkT}{\lambda' f_u} = \frac{NkT}{\lambda' f}$$

The normalized creep strength (creep strength divided by the short-term strength) is:

$$\frac{f}{f_s} = \frac{\frac{E'N}{\lambda'} - \frac{NkT}{\lambda'} \ln\left(\frac{t_f}{t_o}\right)}{\frac{E'N}{\lambda'} - \frac{NkT}{\lambda'} \ln\left(\frac{t_c}{t_o}\right)} = 1 - \frac{\ln(t_f/t_c)}{\frac{E'}{kT} - \ln\left(\frac{t_c}{t_o}\right)} = 1 - \frac{NkT}{f_s \lambda'} \ln\left(\frac{t_f}{t_c}\right) \tag{3.25}$$

For cellulosic polymers the same apply with $t'_o = t_o \exp(S'_o/k)$ and $\lambda' = \lambda'_o + \lambda'' \omega (T - T_m)$ giving:

$$f\lambda' = NH' - Nc\omega - S''N\omega T - kTN \ln \frac{t_f}{t_c} \tag{3.26}$$

For wood eq.(3.25) is one line (see p.e.[9]) for different wood species, moisture contents, stress states (bending, shear, compression etc.) and types of loading, indicating one common strength determining element (cellulose).
Eq.(3.25) shows that $f.\lambda'/NkT$ has to be constant, independent on moisture content. Extrapolation of eq.(3.26) to f = 0 shows that c and S'' must be zero if eq.(3.25) is independent on moisture content.
The measured value [9] of the slope of this line, for $t_c \approx 3$ sec., (and not to long lifetimes at 20° C):

$$\frac{df/f_s}{d\ \mathrm{Ln}\ t_s} = \frac{NkT}{f_s \lambda'} = \frac{1,03}{17,1\ \mathrm{Ln}\ 10} = \frac{1}{38,2}$$

so

$$n = \frac{f_s \lambda'}{NkT} = 38 \tag{3.27}$$

This is comparable with the value of [17], transformed to the 5 min. strength, giving a value of 34 then. More general eq. (3.1) can be written:

$$\frac{d}{dt}\left(\frac{\lambda'}{N\lambda_1}\right) = \frac{2}{t_r}\left(\frac{\lambda'}{N\lambda_1}\right) \sinh\left(\frac{f\lambda_1}{kT} \cdot \frac{\lambda'}{N\lambda_1}\right) \tag{3.28}$$

or

$$\frac{dL}{dt} = C_1 L \sinh\left(C_2 \lambda_1 L\right) \tag{3.29}$$

Including in L the starting value of L and the fracture of flow units with constant structure, L has the form: $L = A + BL$. In eq. (3.27) is L increasing and λ_1 decreasing, so $L.\lambda_1 = (A+BL)*(C-DL) = AC - (DA+BC\bar{L})L =$ $= \phi(1-cL)$. ($DA > BC$ because integrating with L and λ_1 constant, must give the same result as integrating in $1/\lambda_1$ alone, causing a more rapid increase in $1/\lambda_1$. Because L is proportional to the plastic strain ε, a more general form of eq. (3.27) is:

$$\dot{\varepsilon} = \left(C_1 + C_2\varepsilon\right) \sinh\left(\sigma.\phi(1 - C_3\varepsilon)\right) \tag{3.30}$$

The effect of moisture content can be regarded as a transition of mechanical properties. This can be described in this model by two parallel acting processes, one process having the fysical properties of the dry state, and the other, the properties of the wet state. At the transition point the rate of both processes is the same. For wood it is also simple to regard this effect in a single process. From Append. A (Thermodynamics) it follows that it is to be expected that the activation volume V is linear dependent on the moisture content. This is confirmed by tests in [14]. From eq. (3.26) it follows that:

$$f_a\lambda' = f_a\left(\lambda'_c + \lambda''\omega(T-T_c)\right) = NH' - kTN \ln\left(\frac{\dot{\varepsilon}_F}{\dot{\varepsilon}_c}\right) \tag{3.31}$$

In accordance with append. A - 4, and the data of [14]. See fig. 3.4 b, where the modified activation volume $V = \lambda'/N$ is given. (The deviation of the theory at 100°C indicates that more than one mechanisms are acting at higher temperatures)

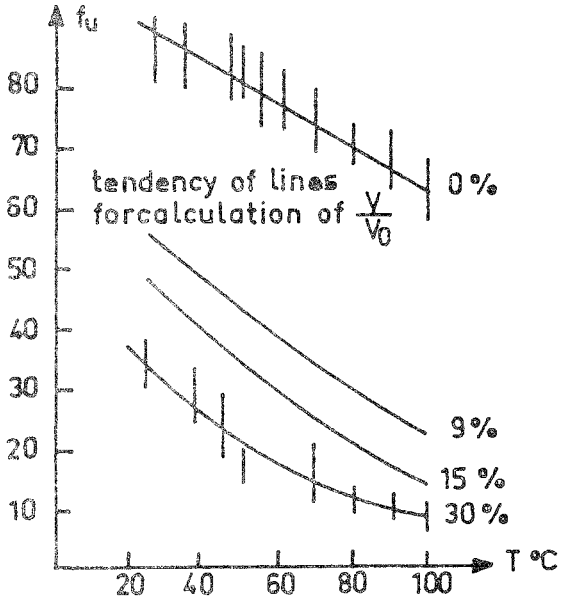
A first estimate of the numerical values of T_m and C_m/ω in:

$$\frac{V}{V_0} = 1 + C_m \frac{\omega}{\omega_m} (T - T_m)$$

are: (taken from the picture without the possibility of correction of the times to failure being probably not the same in all tests)
$T_m = 265$ and $C_m/\omega_m = 0.145$.
With these values the lines in fig. 3.4 a, given by eq.(3.31) are:

$$f_s = \frac{H' - NkT \ln(t_f/t_0')}{\lambda_0'(1 + C_m \frac{\omega}{\omega_m}(T - T_m))} = \frac{193 - 0{,}35\,T}{1 + 0{,}145\,\omega\,(T - 265)}$$

showing that the straight line for $\omega = 0$, as well as the curved line for $\omega = 0.3$, can be given by one equation. The entalphy H' is about 47 kcal.mol. (where it is assumed that the time to failure is of the order of 5 min.)



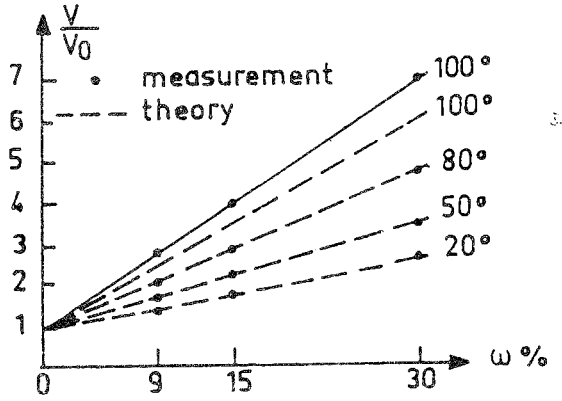


fig.3.4 Compressional strength of oak [14]

The form of the equation of $V = \lambda'/N$ indicates a transition temperature of $T_m = 265\ ^oK = -8\ ^oC$. Below this temperature $V = V_0$ is constant. Around T_m the behaviour has to be described by two mechanisms. For dry wood $\omega = 0$, this transition disappeares (and is not noticible at low m.c.). Information about this second mechanism that is determining for low temperatures can be obtained by a fit of the measured values of f.i.[15].
The smoothness of the strength curves indicate no transitions in this temperature region, so $T_m = 0$, and therefore also λ_0'/N can be neglected.
With $\lambda'/N = \omega\,\lambda''\,T/N$ is eq.(3.22): $(\omega = \omega_m)$

$$f_u = \frac{H'N}{\omega_m \lambda'' T} + \frac{Nk}{\omega_m \lambda''} \ln\left(t_0' \frac{\omega_m \lambda'' \dot{\varepsilon}}{Nk}\right)$$

or with respect to 20 °C or 293 °K (Kelvin):

$$f_u = \frac{H'N}{\omega_m \lambda'' 293} + \frac{Nk}{\omega_m \lambda''} \ln \left(t'_o \frac{\omega_m \lambda'' \dot{f}}{Nk} \right) + \frac{H'N}{\omega_m \lambda'' T} - \frac{H'N}{\omega_m \lambda'' T} =$$

$$= f_{u,20} \left(1 + \frac{H'N}{f_{u,20} \lambda'' \omega_m} \left(\frac{1}{T} - \frac{1}{293} \right) \right) \qquad (3.32)$$

From the data of [15], the compressive strength parallel-to-grain of saturated wood is: (see Fig. 3.5):

$$\frac{f_u}{f_{u20}} = 1 + 845 \left(\frac{1}{T} - \frac{1}{293} \right)$$

If the formation of ice has no influence on the strength, and the times to failure in the tests are not to far apart, then:

$$\frac{H'N}{f_{u20} \omega_m \lambda''} = 845$$

or

$$\frac{H'N}{f_{u20} \omega_m \lambda'' 293} = 2{,}88$$

Eq. (3.22) is:

$$\frac{f_u \lambda'}{NH'} = 1 + \frac{kT}{H'} \ln \left(\frac{t'_o}{t_f} \frac{\lambda' f_u}{NkT} \right) + \frac{1}{2{,}88} = 1 + \frac{2{,}0293}{H'} \ln \left(\frac{t'_o}{t_f} \frac{H'}{2.0{,}293.2{,}88} \right)$$

(and if $t_o/t_{fc} = 10^{-13}/300$ may be used) giving a value of H' of about: 30 kcal./mole. For dry wood λ'/N is constant and eq. (3.25) is nearly a straight line with respect to T because the influence of temperature of t_c is small in the ln-function (see Fig. 3.6).

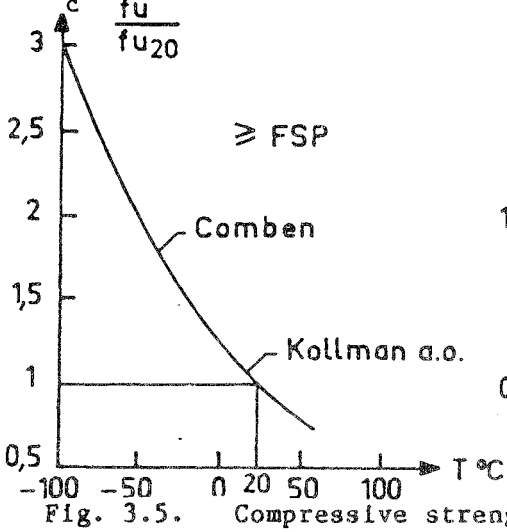


Fig. 3.5. Compressive strength //

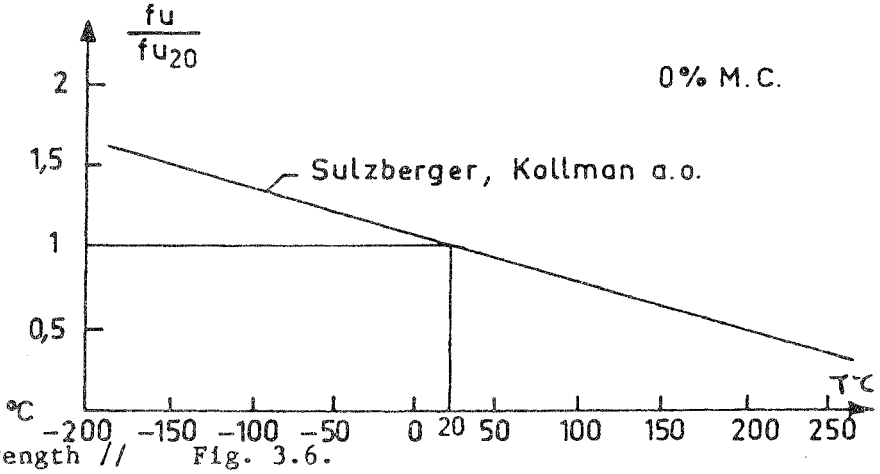


Fig. 3.6.

4. Power approximation of the rate equations

As shown in par. 2 a range of successive processes can be given by eq. (2.5):

$$\text{Rate} = 2\kappa \frac{kT}{h} \rho_1 \exp\left(\frac{-E'}{kT}\right) \sinh\left(\frac{W}{kT}\right) \tag{4.1}$$

or for higher values of W (higher stresses):

$$\dot{\varepsilon} = \dot{\varepsilon}_o \exp\left(\frac{W}{kT}\right) \rightarrow \frac{\dot{\varepsilon}}{\dot{\varepsilon}_1} = \exp\left(\frac{f\lambda'}{NkT} - f_1 \frac{\lambda}{NkT}\right) \approx 1 + \frac{f\lambda'}{NkT} - \frac{f_1\lambda'}{NkT} =$$

$$= 1 - \frac{f_1\lambda'}{NkT}\left(1 - \frac{f}{f_1}\right) \tag{4.2}$$

The experimental power equation, as used in fracture mechanics is:

$$\frac{\dot{\varepsilon}}{\dot{\varepsilon}_1} = \left(\frac{f}{f_1}\right)^n \tag{4.3}$$

This can be written for high enough stresses:

$$\frac{\dot{\varepsilon}}{\dot{\varepsilon}_1} \approx \left(1 - \frac{f_1 - f}{f_1}\right)^n \approx 1 - n\frac{f_1 - f}{f_1} = 1 - n\left(1 - \frac{f}{f_1}\right) \tag{4.4}$$

so

$$n \approx \frac{f_1\lambda'}{NkT}$$

It is shown in par. 3 that $f_1\lambda'/NkT$ is constant (for constant T), but dependent on the scaling (i.e. the choise of the 1-sec.-strength or the 5-min.-strength). It is now shown that the empirical power form of the rate equation (4.3), is identical to the theoretical expression for activation over consecutive barriers (if f is not to low).

If there is a lower bound of stress f_o where flow can be ignored: $\dot{\varepsilon} = 0$, then the effective stress $f - f_o$, has to be taken in eq. (4.3).

For the total (macroscopic) deformation rate is from Orowan's equation:

$$\dot{\varepsilon}_t = \alpha b \rho_m \lambda\dot{\varepsilon} \tag{4.5}$$

where "α" is a geometrical factor relating the active slip system to the strain direction; "b" is the Burgers vector; "ρ_m" is the mobile "dislocation" density and "$\dot{\varepsilon}\ell$" is the "dislocation velocity". For polymers the flow units take the role of dislocations in eq. (4.5).
As derived in par. 3 the structural changes can be given by adding a linear term in ε. This is also in conformity with dislocation mobility studies [21] and other experiments. So:

$$\rho_m = \rho_o + B\varepsilon_t$$

where ρ_o is the initial mobile dislocation density.
Eq. (4.5) becomes (equivalent to the damage model eq. (3.4)): (max ε_t - criterion needed)

$$\dot{\varepsilon}_t = \alpha b \left(\rho_o + B\varepsilon_t\right) \dot{\varepsilon}_n \ell \left(\frac{f - f_o}{f_1}\right)^n \tag{4.6}$$

For wood there are probably two main processes for longer times:

$$\dot{\varepsilon} = C_1 \left(1 + B_1\varepsilon\right)\left(\frac{\sigma - \sigma_o}{\sigma_1}\right)^n + C_2 \left(1 + B_2\varepsilon\right)\left(\frac{\sigma - \sigma_o}{\sigma_1}\right)^m \tag{4.7}$$

In the first process the term $B_1 \cdot C_1$, is probably small and a mean value may be taken. The second process is only noticeble at low stresses and after a long time. Here C_2 may be neglected and a mean value of the stress may be taken (because of the limited stress range where this process is dominating). So eq. (4.7) becomes:

$$\dot{\varepsilon} = C_1 \left(\frac{\sigma - \sigma_o}{\sigma_1}\right)^n + \varepsilon \left\{C_1 B_1 \left(\frac{\bar{\sigma} - \sigma_o}{\sigma_1}\right)^n + C_2 B_2 \left(\frac{\bar{\sigma} - \sigma_o}{\sigma_1}\right)^m\right\}$$

Because the damage δ is proportional to the plastic deformation this can be written:

$$\frac{d\delta}{dt} = C_1 \left(\frac{\sigma - \sigma_o}{\sigma_1}\right)^n + C_2'\delta \tag{4.8}$$

being the damage model of [16].
For creep-to-failure tests (σ = constant) is $t_s = (n + 1)/C$ and a fit of the data of [16] gives n = 36 and C = 444 hour, assuming $\sigma_o = 0$.

For $\sigma_o = 0.48\ \sigma_s$, $n = 34$ is found in [17], giving about the same value of n. This is in accordance with the previous mentioned values (eq. 3.27) confirming this interpretation of the power law.

Short term behaviour is also determined by two main processes, as follows from the experiments of [20], where two values of n are given: $n \approx 62$ for controlled crack growth tests, to $n \approx 65$ in constant strain rate tests, and $n \approx 30$ in constant load tests to failure. In other experiments also values of $n \approx 25$ to 39 are mentioned. Analysing the creep values of [18] in [19], the existence of two parallel barriers was clearly demonstrated. The quick process had a high internal stress (forward activation) and an activation energy of appr. 50 kcal/mole. The slower process was appr. symmetrical and had an activation energy of appr. 21 kcal/mole. The quick process, that was determining in the first stage of the loading may be associated with the first determining crack propagation process of [20] with $n \approx 62$. The second value of $n \approx 30$ may be associated with the slower process.

The activation energy of this process is comparable with values found in [12], where from creep tests at different temperatures for bending: $H' = 22$ kcal/mole to 24.4 kcal/mole, depending on the temperature range, have been found. From normal-to-grain relaxation tests 23 kcal/mole was reported for wet beechwood in [13]. This energy is often regarded to be the energy of cooperative hydrogen bond breaking. The activation energy of 50 kcal/mole is high enough for covalent C-C-bond rupture.

References

[1] Deformation kinetics. A.S. Krausz, H. Eyring 1975 John Wiley & Sns.

[2] Rheology, Theory and Applications. T. Ree, H. Eyring 1958 New York.

[3] Cellulose as Viscoelastic Material. A.H. Nissan, S.S. Sternstein, Dep. of Chem. Engin. Troy, N.Y., U.S.A.

[4] Influence of Heat on Creep of Dry D.-Fir. E.L. Schaffer For. Prod. Lab. Madison, Wisconsin.

[5] Thermogravimetric Analysis of Pulps. Wood Science and Techn. V10-2-1976.

[6] Kinetics of stress relaxation in metals. J.F. Wilson, N.R. Wilson, Transac. of the Soc. of Rheol. 1011, 399-418 1966.

[7] Mechanical Prop. of Textiles J.A. Lasater, E.L. Nimer, H. Eyring, Text. Res. J. 23-237-1953 [7].

[8] Kinetic Concept of the strength of Solids S.N. Zhurkov Int. J. Fract. Mech. I, 311, 1965.

[9] Bestimmung der Dauerfestigk. v. Holzkonstr. usw. J.M. Ivanov, Holztechnol. 14-1973-4.

[10] J. Polym. Sci. 20,447 1956 B. Coleman.

[11] Int. J. Fract. Mech. 6,33 1970 and J. Fract. Mech. 5,57 1969, C.B. Henderson, P.H. Graham, C.N. Robinson.

[12] Studies on Thermal Softening of Wood III O. Sawake, 1974, J. Jap. Wood Res. Soc. 20 (11): 517-522.

[13] Studies on Rheological Properties of Wood. T. Yamada et al. 1961, J. Jap Wood Res. Soc. 7 (2): 63-72.

[14] Ueber die Abhangigkeit der Festigk. D. Holzes v. d. Feuchte., J.M. Ivanov Holztechnologie 22 1981 1.

[15] Effect of Moisture Content and Temperature. Gerhards Wood and Fiber Jan. 1982 V 14 1.

[16] First Int. Confer. on Wood Fract. 1978 Banff, Alberta Canada, R.O. Foschi and J.D. Barrett.

[17] Duration of Load Test Data Analysis R.O. Foschi, J.D. Barrett, pap. G4 IUFRO-Meeting 1980 Oxford, England.

[18] Creep and Stress relaxation in Wood during Bending. P.U.A. Grossman, R.S.T. Kingston Austr. J. Appl. Sci., 1963, 14, 305-17.

[19] Time depend. Deformation of Wood etc. A. v.d. Wiel, Report 4-84-4-Ha-17, Stevin Lab. Techn. Univ. Delft.

[20] Effect of Constant Deformation Rate on Strength ⊥ grain of D.-Fir S. Mindess, Nadeau, Barrett, Wood Science 8 nr. 4 1976.

[21] Dislocation mobility studies J.J. Johnston, J.J. Gilman, J. Appl. Phys. 30, 1959; 31, 1961; 33, 1961.

[22] The significance of the glass transition of lignin in thermomechanical pulping. G. M. Irvine, Wood Science Technology 19, 1985.

[23] Predicting the effect of specific gravity, moisture content, temperature and strain rate on the elastic properties or wood. L. C. Palka, Wood Science and Technology 7, 1973.

[24] For. Prod. Lab. Report No 1767, J. A. Liska, 1950.

[25] Bulletin of A.I.J. no 32, H. Sugiyama 1953

[26] Some aspects of the rheological behaviour of wood. R. S. T. Kingston, L. N. Clarke, Australian journal of applied Science 12 no 2, 1961

[27] The creep behaviour of individual pulp fibers under tensile stress R. L. Hill, Tappi 50, no 8, Aug. 1967.

[28] Creep and strain behaviour of wood. E. G. King, Forest Prod. Journ. Oct. 1957.

[29] On the fractional stress relaxation of coniferous wood tissues. E. Kirbach, L. Bach, R. W. Wellwood, J. W. Wilson, Wood and Fiber 8, no 2, 1976.

[30] Stress relaxation of wood. P. U. A. Grossman, Nature (4392)

[31] Stress relaxation of wood at several levels of strain. H. Echenique-Manrique, U.S.N. Office of Naval Research. Techn. Rep. 37, 1967.

CIB-W18/19-9-4

INTERNATIONAL COUNCIL FOR BUILDING RESEARCH STUDIES AND DOCUMENTATION

WORKING COMMISSION W18 - TIMBER STRUCTURES

NON-LINEAR CREEP SUPERPOSITION

by

U Korin
Building Research Station, The Technion, Haifa
Israel

MEETING NINETEEN
FLORENCE
ITALY
SEPTEMBER 1986

NON-LINEAR CREEP SUPERPOSITION

Dr. Uri Korin, Building Research Station, The Technion, Haifa, Israel

1) Preface:

A method is presented for the representation of the behavior of viscoelastic materials under complex load histories (14). The method was applied during a study of the creep of glass reinforced polymers for the prediction of the creep of reinforced specimens. It was also applied to the transformation between various viscoelastic functions, like creep to relaxation, creep to stress-strain. The method is based on the basic creep superposition principle, and it was modified to treat non-linear viscoelastic materials.

It is the author's feeling that the method may be used also for analysis of creep of timber and creep superposition of timber. The paper presents the theoretical background of the proposed method and the development of the proposed superposition model.

The proposed method is programmed in computer language and may be easily applied for the analysis of creep data and for the analysis and prediction of creep superposition behavior.

2) Strain of Real Viscoelastic Materials

The strain of idealized viscoelastic materials under the action of a constant stress and at constant temperature is usually (1) divided into five parts (Figure 1).

There is the initial strain, which is the sum of the elastic and plastic components, the primary creep and the secondary steady state creep. Then follows the tertiary or terminal creep, after which a fracture occurs. All these five parts of the diagram may appear usually only in specimens loaded with high stresses. It may happen that a material will not display, for example, secondary creep. A family of creep curves under various constant strains is shown in Figure 2. This convenient description of the strain of a viscoelastic material does not necessarily correspond to any distinct molecular or time structure processes which may initiate or maintain the creep process (1).

When describing a creep law for a linear viscoelastic material, a viscoelastic representation usually but not necessarily of the springs-dashpots combination is chosen. A discrete number of Maxwell and Voigt models or a continuous spectrum may be used. Descriptions from the type

$$\frac{\varepsilon}{\sigma} = b + cxt + a \times \log t \qquad (1)$$

where b, c and a are constants for a particular experiment conditions ε - the strain, σ - the stress and t - the time, can also be used. Like for the linear viscoelastic function of the springs and dashpots combinations, the compliance is independent of the stress for this case too.

As the viscoelastic behavior of most materials is non-linear (even for small stress and short times), a stress dependent representation of viscoelastic materials creep was introduced. Many creep laws have been suggested.

A form: $\varepsilon = \varepsilon_o + m \times t^n$ (2)

where ε - strain

t - time

and ε_o, m, n, constants of materials, temperature and stress was suggested by Findley and Worley (1).

A form: $\varepsilon = S^1(\sigma) \times T^1(t)$ (3)

where ε - strain

S^1 - function of stress only

and T^1 - function of time only

was suggested by Soderberg (1).

Nadai (1) suggested dependence of the various constants on the stress of the following form:

$$C = C_o \times \sinh \frac{\sigma}{\sigma_o} \quad (4)$$

Where C - creep rate

σ - applied stress

C_o, σ_o - constant of the material and temperature.

A list of various curve fitting techniques developed for the representation of creep is given by Thorkildsen (1).

An accurate method for representation of creep is suggested by Marin et al. (2). The creep curve (Material: polymethylmethacrylate tested at 77 ± 2°F, 50 ± 2 per cent (R.H.) was split into three portions (Figure 3). The instantaneous, the retarded elasticity and flow, a process which resembles very much the superimposed creep of the four element model. They found that by plotting the primary creep on a log-log paper, a straight line was obtained, the slope of which was dependent on the stress σ by the following relation:

$$\varepsilon_p = D \times \sigma^m \times (1 - P \times e^{-p \times t}) \qquad (5)$$

Where $_p$ - primary creep

D, m, P, p - constants of the material and temperature.

The dependence of the flow on the stress σ was expressed:

$$\varepsilon_s = B \times t \times \sigma^n \qquad (6)$$

where ε_s - the secondary creep

and B and n are constants of the material and the temperature.

Apart from the curve fitting technique, attempts were made to find creep laws which will not only fit certain experimental creep results but will enable prediction of creep for longer times and different stresses. Findley (3) and Findley and Khosla (4,5) show that the hyperbolic sine law which was suggested by Nadai as a curve fitting instrument, describes also the influence of stress on the thermal activation of deformational processes in the material such as slip or rupture of atomic bonds, suggested earlier by Eyring, Kauzman and others.

It is shown (1) that the method suggested by Findley and his colleagues is the most suitable for prediction of creep and extrapolation of creep results.

The various suggestions for creep laws are summarized by Thorkildsen (1). Uniaxial creep laws are commonly separated into categories according to the mathematical form of the relationship between stress, creep strain, time and creep-strain rate. These are:

A) Time hardening - continuous decrease in the rate of strain.

B) Strain hardening - the rate of strain depends on the stress and strain of the body (the rate of strain will decrease when the strain is increased).

C) Time dependence of strain

   (1) Linear (Newtonian viscosity, secondary creep)

   (2) Non-linear

      (a) power function

      (b) logarithmic

   (3) Linear and Non-linear terms (McVetty, Marin)

D) Stress dependence of strain rate

   (1) Linear (Newtonian viscosity)

   (2) Non-linear

      (a) power function (Norton, Marin)

      (b) hyperbolic (Nadai)

3. Creep Of Viscoelastic Materials And Isochronous Curves

If a series of creep experiments at different constant stresses is performed on a viscoelastic body, it is possible to describe the stress - time - strain relations as a surface on which each point describes the strain of a body for particular stress and time. To avoid misunderstanding by over simplifying the stress - time - strain description it should be said that this surface should not be used for prediction of creep under stress which varies with time. The movement on the surface is allowed only in the direction parallel to the time axis (Figure 4). As creep is temperature dependent, different surfaces will represent the creep at different temperatures (6,7).

Sections of the surface parallel to the time - strain plane are the creep curves at constant stress from which the surface is constructed.

The sections parallel to the stress strain plane form the isochronous curves or strain at constant time for different stress. The importance of this representation is only as an aid to the understanding of the properties of the material at certain constant conditions. If the creep of the linear viscoelastic body was presented in this form all the isochronous curves would be straight lines.

4. Non-linear Superposition Of Creep

If the creep is not linear it cannot be superimposed by using Boltzman's principle. As prediction of relaxation, stress-strain relations, creep of composite materials and creep of polymers under any stress history can be done only by superposition methods. Attempts were made to find a way to enable superposition inspite of the non-linearity of the creep dependence on stress. It should be mentioned here that recovery experiments are actually superposition experiments since release of stress may be considered as applying negative stress to the body (8).

Leaderman (8) performed a number of superposition experiments on textile filaments. He found that his experiments, where the stress history was combined of cycles of loading and unloading 20 minutes each, obeyed the Boltzman superposition principle. As it will be shown later on, similar results were obtained by the author on a wide range of stepped load experiments, the duration of which was about the same. It looks as if short time experiments on a non-linear viscoelastic material cannot reveal the full non-linear creep properties.

Ratcliffe and Turner (7) suggest the stress - strain -time surface as a guide for calculation of strain when a stress is increased gradually and then maintained constant. This method, of course, is far from being a tool for prediction of strain under complex load history. In another work (9,10), Turner tests the possibility of applying the linear creep superposition principle to real polymers, and his conclusions are that the experimen-

tal results of creep under complex history of stress cannot be predicted accurately by this way even when stress increments are applied for a short time. Regarding recovery, Turner says that creep is fully recoverable provided the yield point has not been exceeded. His experiments were carried out for relatively short times and showed clear deviation form this suggestion when the creep time prior to the recovery was increased.

Sharma and Wen (11) used a non-linear creep representation suggested by Leaderman to predict creep under complex load histories. The creep expression used is:

$$\varepsilon = J(t) \times F(\sigma) \tag{7}$$

where $J(t)$ = creep compliance function for a material with non-linear response.

$F(\sigma)$ = stress function, a function of stress alone and the creep strain at time t:

$$\varepsilon(t) = \sum_{0}^{t} A\, F(\sigma) \times J(t-\tau) \tag{8}$$

However, the effect of the stress level on the creep compliance is completely ignored. If the creep started initially under stress σ_1, the expression $J(t)\ xF(\sigma)$ will continue to appear in all the expressions for the strain under further stress steps. It is possible to see that if instead of the stress σ_1 two steps of stress each $\frac{\sigma_1}{2}$ were applied, different results would be obtained.

The experimental results show considerable deviation from the suggested superposition method, even for the relatively short duration of the experiments.

Pipkin and Rogers (12) suggest criteria for extrapolation of one step creep or relaxation data to predict strain or stress response under complex load or strain history. Any extrapolation, they say, must satisfy five elementary requirements. (The requirements are given for relaxation experiment, but the creep experiment will behave in an analogous way.)

A) Time-translation invariance.

B) The nature of the rule must be independent of the particular form of $R(\varepsilon, t)$, ($R(\varepsilon, t)$ is the stress relaxation function).

C) The rule must revert to the function R in the case of a single step history.

D) If a step involving no strain change is artificially introduced, the prediction must be independent of the time at which this artificial step occurred.

E) If a step is artificially divided into two steps with the intermediate strain level maintained for only zero time, the prediction must be independent of this intermediate level.

The creep expression suggested is:

$$\varepsilon(t) = \sum_{i=1}^{i=n} [C(\sigma_i, t-t_i) - C(\sigma_{i-1}, t-t_i)] \qquad (9)$$

Although this form will comply with the requirement suggested, it seems wrong to assume that the action of a stress applied to a viscoelastic body at a particular time will remain unaffected by the later stress history of the body. According to the suggested method recovery of creep at any stress should be complete without regard to the stress level and the experiment duration. One knows perfectly well that the actual situation is different and creep may be non-recoverable.

It seems to the author that a synthesis of already established ideas may provide a solution for the subject of non-linear superposition of creep:

A. Boltzman superposition principle which says that the creep due to a certain stress, will be equal to the product of the stress and the creep compliance, and the action of one stress should not be affected by the action of other stresses on a body.

B. The activation energy of rate processes theory, suggested by Eyring, Kauzmann and others (1), adopted by Findley (3,5,13). This theory describes the influence of stress on the thermal activation of deformational processes in the material, such as slip or rupture of atomic and molecular bonds. The dependence of the compliance on the stress may be explained by this theory.

When a stress is applied to a body the body will creep under the action of this stress and a creep compliance which depends not on the applied stress, but on the total stress acting on the body.

5. Non-linear Superposition Principle

If a linear viscoelastic body is subjected to a stress σ, the strain function is:

$$\varepsilon(t,\sigma) = \sigma \times J(t) \qquad (10)$$

where ε - the strain

t - time

σ - the stress

and J - the compliance function

If the stress history comprises two stress steps where stress σ_o is applied at time t_o and is increased to σ_1 at time t_1, the strain for time $t > t_1$ is:

$$\varepsilon(t,\sigma_o,\sigma_1) = \sigma_o \times J(t-t_o) + (\sigma_1-\sigma_o) \times J(t-t_1) \qquad (11)$$

and the compliance for any time is independent of the stress level. The compliance of non-linear viscoelastic bodies does not obey this rule, and depends upon the stress as well as on the time. The strain equation for a non-linear body may be written:

$$\varepsilon(t,\sigma) = \sigma \times J(t,\sigma) \qquad (12)$$

and when one wants to find the expression for strain under complex stress action, the linear creep superposition principle does not apply.

A solution for the non-linear superposition is suggested in the following lines.

6. Non-linear Superposition Of Flow

The strain equation for the flow element, the dashpot, as a function of time and stress is:

$$\varepsilon(t, \sigma) = \sigma \times \frac{t}{\eta} \qquad (13)$$

where ε - the strain

σ - the stress

t - the time

and η - the dashpot viscosity

When a stress is applied to the dashpot it will flow at a constant rate. Upon removing the stress, the dashpot will remain in its strained position. The movement due to a new stress applied will be free of any previous stress history. The strain depends directly on the stress and the duration of the experiment. Consider a stress history of a stress σ_o applied at time t_o and increased at time t_1 to σ_1. If the flow compliance J_f is equal to $\frac{1}{\eta}$ the expression for the strain at time $t > t_1$ is:

$$\varepsilon(t,\sigma_o,\sigma_1) = \sigma_o \times J_f \times (t-t_o) +$$

$$(\sigma - \sigma_o) \times J_f \times (t-t_1) \qquad (14)$$

This equation may also be written:

$$\varepsilon(t,\sigma_o,\sigma_1) = \sigma_o \times J_f \times (t_1-t_o) +$$

$$\sigma_1 \times J_f \times (t-t_1) \qquad (15)$$

Or in other words, the total flow equals the sum of the products of the stress levels by their duration and by the flow compliance.

Assuming that instead of a linear dashpot a non-linear one is introduced. The flow compliance of which is given by the equation:

$$J_f(\sigma) = \frac{1}{\eta} \tag{16}$$

where η the dashpot viscosity is not kept constant, when a stress σ_o is applied at time t_o the strain for time $t > t_o$ is:

$$\varepsilon(t,\sigma_o) = \sigma_o \times J_f(\sigma_o) \times (t-t_o) \tag{17}$$

when the stress is changed at time t_1 from σ_o to σ_1 the strain for time $t > t_1$ will be:

$$\varepsilon(t,\sigma_o,\sigma_1) = \sigma_o \times J_f(\sigma_o) \times (t_1-t_o) + \sigma_1 \times J_f(\sigma_1) \times (t-t_1) \tag{18}$$

and for the Nth load step the total flow until time $t > t_N$ which will be marked $t_{N+1} = t$ is:

$$\varepsilon(t, \sigma_o,\sigma_1 \ldots\sigma_N) = \sum_{i=0}^{i=N} \sigma_i \times J_f(\sigma_i) \times (t_{i+1} - t_i) \tag{19}$$

7. Non-linear Superposition Of Primary Creep

When a stress is applied to a linear viscoelastic body representing retarded elasticity the creep equation is:

$$\varepsilon(t,\sigma) = \sigma \times J(t) \tag{20}$$

where J(t) is the creep compliance of the body for time t. If the stress history consists of stressing the body at time t_o by stress σ_o, the creep for time $t > t_o$ is:

$$(t,\sigma_o) = \sigma_o \times J(t-t_o) \tag{21}$$

After changing the stress at time t_1 to σ_1 the creep for time at $t > t_1$ as it was shown (Eq. 14):

$$\varepsilon(t,\sigma_o,\sigma_1) = \sigma_o \times J(t-t_o) + (\sigma_1-\sigma_o) \times J(t-t_1) \tag{14}$$

It is possible to re-write this equation in a form in which the creep at each stress level is expressed separately:

$$\varepsilon(t,\sigma_o,\sigma_1) = \sigma_o \times J(t_1-t_o) +$$

$$\sigma_o \times [J(t-t_o) - J(t_1-t_o)] +$$

$$(\sigma_1-\sigma_o) \times J(t-t_1) \tag{22}$$

The first term of the right hand side gives the creep under σ_o from t_o to t_1, and the second term gives the creep caused by σ_o and σ_1 from t_1 to t.

Another creep body obeying a creep compliance $J_o(t)$ is now assumed. The body is stressed at time t_o by a stress σ_o. At time $t_1 > t_o$ a sudden change in the creep compliance occurs and further creep will follow the new compliance $J_1(t)$. The creep for the time t_1 is expressed by:

$$\varepsilon(t_1,\sigma_o) = \sigma_o \times J_o\,(t_1-t_o) \tag{23}$$

and procedure should be found for calculation of the creep after the change.

If one assumes that the change of the compliance is not accompanied by any instantaneous change in the body configuration, it is possible to calculate the time it would take the body while under the action of the stress σ_o to creep by ε_1 according to the new compliance $J_1(t)$ (Figure 5).

This condition is expressed by:

$$\sigma_o \times J_o(t_1-t_o) = \sigma_o \times J_1(T_{o,1}) \tag{24}$$

where $T_{o,1}$ is the equivalent time of the new compliance. For time $t > t_1$ the creep is:

$$\varepsilon(t,\sigma_o) = \sigma_o \times J_o(t_1-t_o) \; +$$

$$\sigma_o \times [J_1(t-t_1 + T_{o,1}) - J_1\,(T_{o,1})] \tag{25}$$

If together with the change in the creep law at time t_o the stress σ_o was

changed to σ_1 the creep for time $t > t_1$ would be:

$$\varepsilon(t,\sigma_o,\sigma_1) = \sigma_o \times J_o(t_1-t_o) +$$

$$\sigma_o \times [J_1(t-t_1 + T_{o,1}) - J_1(T_{o,1})] +$$

$$(\sigma_1 - \sigma_o) \times J_1(t - t_1) \qquad (26)$$

$T_{o,i}$ is a dummy variable which at each new change of compliance will represent the whole strain history under the former compliances because of stress σ_o:

$$\sigma_o \times J_1 (T_{o,1}) = \sigma_o \times J_o(t_1 - t_o) \qquad (27)$$

$$\sigma_o \times J_2 (T_{o,2}) = \sigma_o \times [J_o (t_1-t_o) +$$

$$J_1 (t_2 - t_1 + T_{o,1}) - J_1 (T_{o,1})] \qquad (28)$$

$$\sigma_o \times J_N(T_{o,N}) = \sigma_o \times \sum_{i=0}^{i=N-1}$$

$$[J_i(t_{i+1} - t_i + T_{o,i}) - J_i (T_{o,i})] \qquad (29)$$

For the stress applied at time t_1, $(\sigma_1 - \sigma_o)$, the equations for calculations of the value $T_{1,i}$ are:

$$(\sigma_1-\sigma_o) \times J_2(T_{1,2}) = (\sigma_1-\sigma_o) \times J_1(t_2-t_1) \qquad (30)$$

$$(\sigma_1-\sigma_o) \times J_3(T_{1,3}) = (\sigma_1-\sigma_o) \times$$

$$[J_1 (t_2-t_1) + J_2 (t_3-t_2 + T_{1,2})$$

$$- J_2 (T_{1,2})] \qquad (31)$$

$$(\sigma_1-\sigma_o) \times J_N (T_{1,N}) = (\sigma_1 - \sigma_o) \times \sum_{i=1}^{i=N-1}$$

$$[J_i (t_{i+1} - t_i + T_{1,i}) - J_i (T_{1,i})] \qquad (32)$$

and for the stress applied at time t_{N-1}:

$$(\sigma_{N-1} - \sigma_{N-2}) \times J_N(T_{N-1,N}) =$$

$$(\sigma_{N-1}-\sigma_{N-2}) \times J_{N-1} (t_N-t_{N-1}) \qquad (33)$$

also: $T_{N,N} = 0$ and $\sigma_{-1} = 0$

The expression for the creep at time $t > t_N$ is:

$$\varepsilon_t = \sum_{i=0}^{i=N-1} (\sigma_i-\sigma_{i-1}) \times \sum_{j=i}^{j=N-1} [J_j(t_{j+1}-t_j+T_{i,j})$$

$$- J_j (T_{i,j})] \qquad (34)$$

If a body comprises an elastic part (modulus of elasticity E), a flow element and a primary creep element, the equation for the creep at time $t_{N+1} > t_N$ will be:

$$\varepsilon(t_{N+1}, \sigma_o, \sigma_1 \ldots \sigma_N) = \frac{\sigma N}{E} +$$

$$\sum_{i=0}^{i=N} \sigma_i \times J_f(\sigma_i) \times (t_{i+1} - t_i) +$$

$$\sum_{i=0}^{i=N} (\sigma_i - \sigma_{i-1}) \times \sum_{j=i}^{j=N} [J_j(t_{j+1} - t_j +$$

$$T_{i,j}) - J_j(T_{i,j})] \qquad (35)$$

Where:

ε	-	the strain
σ	-	the stress
t	-	the time
E	-	the instantaneous modulus of elasticity
J_f	-	the flow compliance
J	-	the primary creep compliance
T	-	the equivalent time

8. Non-linear Superposition Applications

The non-linear superposition method suggested above can provide the answer to some well known phenomena in the creep behavior viscoelastic materials. The first phenomenon is the so called irrecoverable creep. When a specimen is undergoing a creep experiment under a certain stress its total strain equals the sum of the instantaneous or elastic strain, the strain due to retarded elasticity, or primary creep and flow. When subjected to very

high stresses, tertiary creep leading to creep fracture is terminating the experiment. If the stresses are not high enough to cause creep fracture, the material will deform only according to the primary and the secondary creep compliances. It is quite difficult to learn about the flow from a short term creep experiment but if the duration of it is long enough to reach the stage of steady state creep, one can identify the flow function. This part of the strain is supposed to be irrecoverable. The retarded elasticity or the primary creep will continue until equilibrium is reached between the applied stress and the new configuration. As the material is non-linear viscoelastic the primary creep due to stress σ will be:

$$\varepsilon(\sigma,t) = \sigma_o \times J(\sigma,t) \tag{36}$$

Where ε - the primary creep

t - the time

σ - the stress

J - compliance

When the stress is released from the specimen at time t_1 the specimen following deformation is:

$$\varepsilon(\sigma,t) = \sigma \times J(\sigma,t_1) + \sigma[J(0,t-t_1+T) - J(0,T)]$$

$$- \sigma \times J(0,t-t_1) \tag{37}$$

where T is the equivalent compliance time.

If the compliance $J(\sigma,t_1)$ is larger than the maximum value of the compliance for zero stress, the continuous action of the initial stress will become zero and the specimen will recover according to the stress σ and the zero stress compliance. The maximum expected recovery is: $\sigma \times J(0,t^1)$

where t^1 is the time when primary creep reaches equilibrium.

Full recovery of primary creep may be expected only when the compliance for time $t_1(J(\sigma,t_1))$ is smaller or equal to the maximum recovery compliance. As this will occur usually only after very short period of stressing the amount of flow of the specimen will be very small too and one may consider polymer materials to be fully recoverable if subjected to relatively low stress for short periods. Another phenomenon is the very low primary creep rates observed sometimes if a material is stressed for the second time, after a previous long term creep experiment. Assuming the extreme case when the specimen was allowed to creep until it completed its primary creep (t^1).

For time $t > t^1$ the primary creep will remain unchanged:

$$\varepsilon(\sigma_o,t) = \sigma_o \times J(\sigma_o,t^1) \tag{38}$$

when the stress is released (stress $\sigma_1 = -\sigma_o$ is applied) and the specimen is allowed to recover its primary creep will eventually be:

$$\varepsilon(\sigma, t) = \sigma_o \times J(\sigma_o,t^1) - \sigma_o \times J(0,t^1) \tag{39}$$

when a new stress $\sigma_2 < \sigma_o$ is applied the deformation of the specimen at time t measured from the new loading moment

$$\varepsilon(\sigma_2,t) = \sigma_o \times [J(\sigma_2,t + T_{0,2}) - J(\ 2,T_{0,2})]$$

$$- \sigma_o \ x[J(\sigma_2,t + T_{1,2}) - J(\sigma_2,T_{1,2})]$$

$$+ \ \sigma_2 \times J(\sigma_2,\ t) \qquad (40)$$

As $J(\sigma_2,\ t + T_{0,2}) = J(\sigma_2,\ T_{0,2})$

we remain with the equation:

$$\varepsilon(\sigma_2,t) = \sigma_2 \times J(\sigma_2,t) -$$

$$\sigma_o \times [J(\sigma_2,t + T_{1,2}) - J(\sigma_2,T_{1,2}) \qquad (41)$$

The creep observed in the second creep experiment may be substantially smaller than creep observed of a first creep experiment on the same material.

The suggested superposition method enabled to predict very accurately the strain responses for very complex stress histories carried out by the author and by others.

REFERENCES

1. R.L. Thorkildsen,
Mechanical behavior (Engineering Design for Plastics, ed. E. Baer, Chap. 5) Reinhold 1964.

2. J. Marin, Y.H. Pao and G. Cuff,
Trans. Am. Soc. Mech. Eng. 73, 705 (1951).

3. W.N. Findley,
Creep Characteristics of Plastics, ASTM, 1944 Sympos. on Plastics, p. 18, 1944.

4. W.N. Findley, C.H. Adams and W.S. Worley,

The Effect of Tem. on the Creep of Two Laminated Plastics as Interpreted by Hyperbolic-sine law and Activation Energy Theory. Proc. ASTM, vol 48, p. 1217, 1948.

5. W.N. Findley and G. Khosla,

An Equation for Tension Creep of Three Unfilled Thermoplastics, SPE J., Dec. 1956, p. 20-25.

6. S. Turner,

Creep in Thermoplastics, Brit. Plastics, June 1964.

7. W.F. Ratcliffe and S. Turner,

Engineering design: Data required for plastic materials, Trans. J. Plastic Inst. June 1966.

8. H. Leaderman,

Elastic and Creep Properties of Filamentous Materials and Other High Polymers, The Textile Foundation, Wash., D.C., 1944.

9. W.N. Findley and G. Khosla,

Application of the superposition principle and theories of mechanical equation of state, strain and time hardening to creep of plastics under changing load, J. Appl. Phys. 26, July 1955, pp. 821-831.

10. S. Turner,

The strain response of plastics to complex stress histories. PIA 3rd Annual Conf. Nov, 1965 (Polymer Eng. Sci. 6, 306, 1966).

11. M.G. Sharma and P.R. Wren,

Non-linear viscoelastic behavior of cellulose acetate butyrate, SRE Trans., Oct. 1964, pp. 282-289.

12. A.C. Pipkin and T.G. Rogers,

A non-linear integral representation for viscoelastic behavior, J. Mech. Phys. Solids 16, pp. 59-72, 1968.

13. W.N. Findley,

Mechanism and mechanics of creep of plastics, SPE J., Jan. 1960, pp. 57-65.

14. U. Korin,

The creep superposition principle and its application to the prediction of creep of certain glass-reinforced polyester laminates, Ph.D. Thesis, Southampton University, 1969.

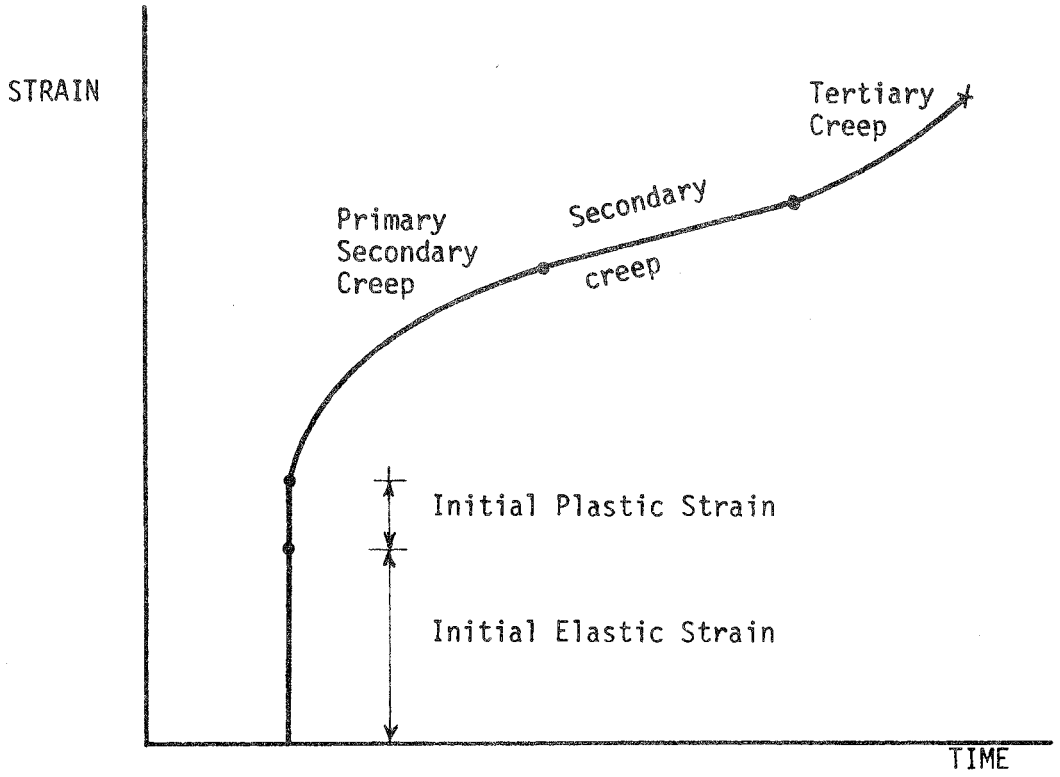


Figure 1 Idealised Constant- Stress Creep
(1)

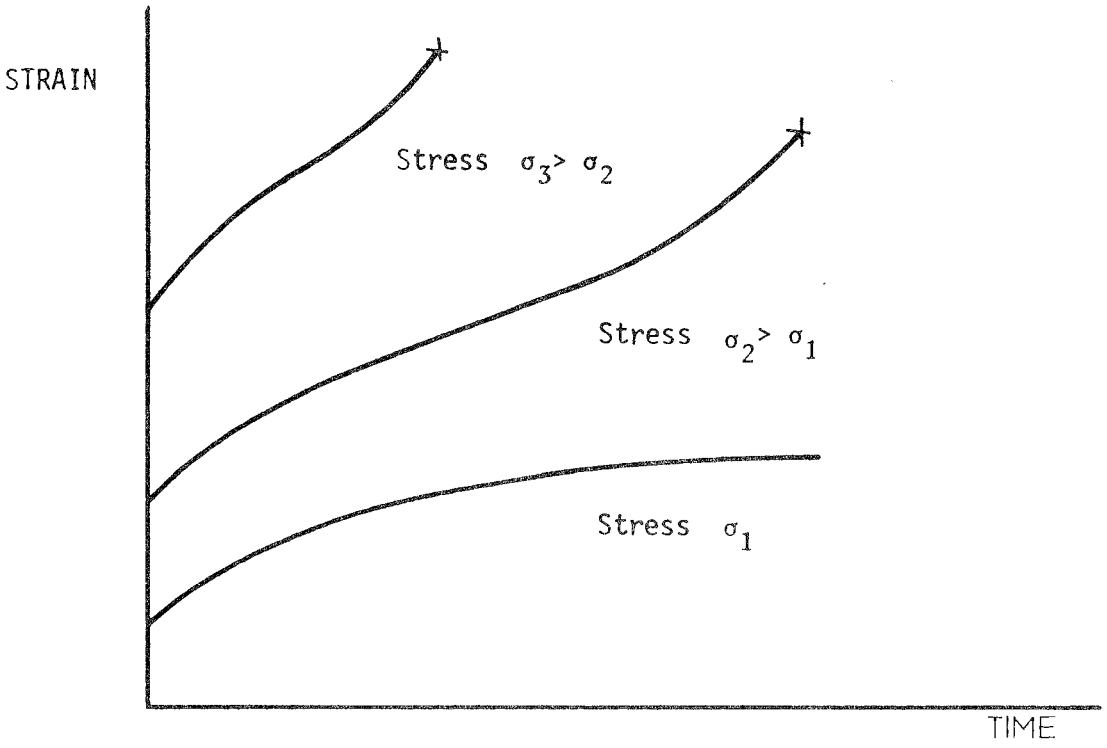


Figure 2 Family of Constant Stress Creep Curves

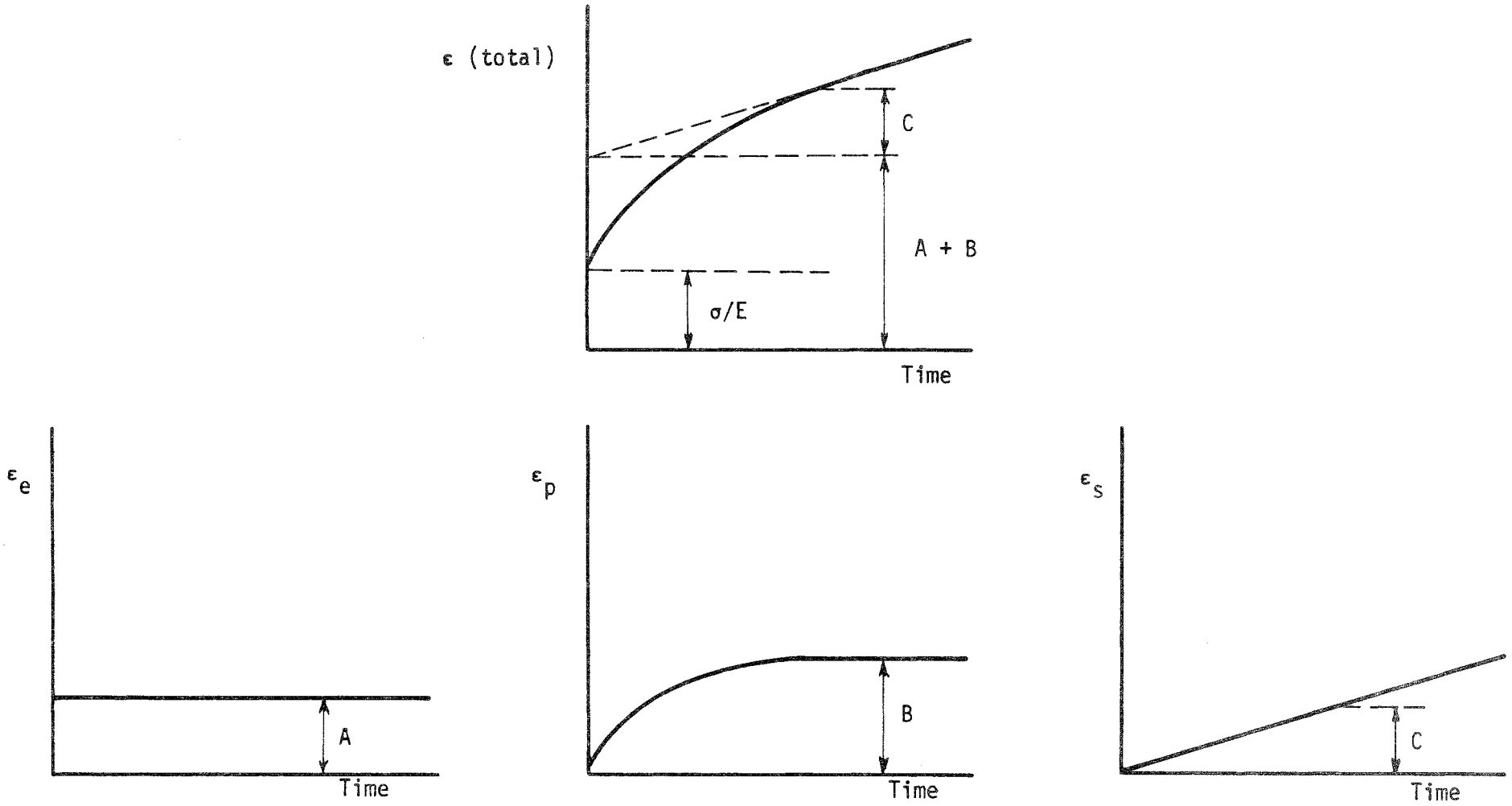


Figure 3 Division of the creep curve into three parts for improved accuracy

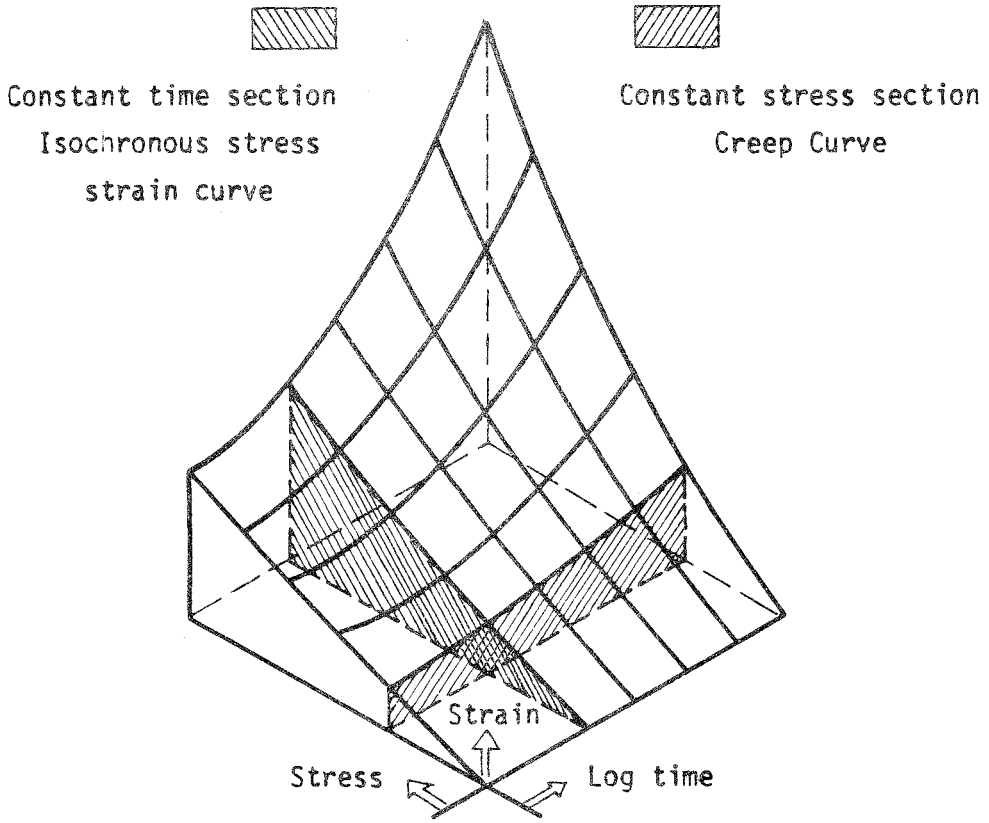


Figure 4 - stress - strain - time relationship (6)

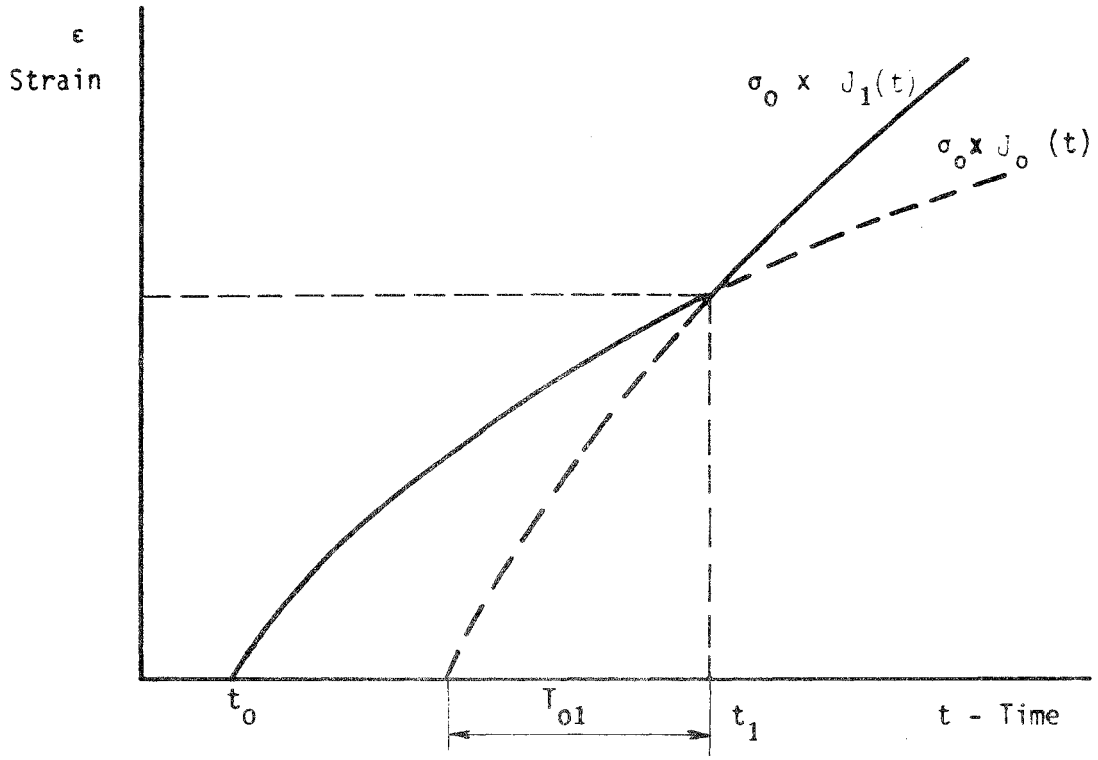


Figure 5 - The Change of Creep Compliance And
The Equivalent Time T

CIB-W18/19-9-5

INTERNATIONAL COUNCIL FOR BUILDING RESEARCH STUDIES AND DOCUMENTATION

WORKING COMMISSION W18 - TIMBER STRUCTURES

DETERMINATION OF CREEP DATA FOR THE COMPONENT PARTS OF STRESSED-SKIN PANELS

by

R Kliger
Chalmers University of Technology
Sweden

MEETING NINETEEN
FLORENCE
ITALY
SEPTEMBER 1986

DETERMINATION OF CREEP DATA FOR THE COMPONENT PARTS OF STRESSED-SKIN PANELS

by

Robert Kliger
Research assistant, Chalmers University of Technology, Dept of Structural Engineering, Div. of Steel and Timber Structures

Abstract

The main aim of this investigation has been to predict the creep characteristics of stressed-skin panels consisting of wood-based materials in the web and compression flange and a steel sheet in the tension flange. This paper describes studies of the long-term bending and shear characteristics of wood beams, the compression characteristics of particle board and the shear properties of glued joints between
(a) wood and particle board and
(b) wood and steel.
Two different rheological models are used to fit the creep data, which corresponds to the behaviour of a linearly visco-elastic material, which creeps under sustained loading. It is shown that the selection of the time for the initial measurement (after application of the load) is of great importance.

1. INTRODUCTION

Wood and wood-based products in combination with one another and in combination with non-timber materials can result in the optimal structures from a technical and economical angle. The clearly-defined creep properties in the component materials and joints should be the starting-point when studying rheological properties, such as creep in composite structures.

2. AIM AND SCOPE

The tests discussed in this paper are
(1) three series of simply-supported beams with a span of 1.2 m exposed to a constant, concentrated mid-span load,
(2) a supplementary series of 6 of the same (previously loaded) beams exposed to a constant, 4-point load,
(3) two series with 8 specimens in each, made of the same material as the beams, loaded in pure shear,
(4) three series of particle-board loaded in compression,
(5) one series of two different types of adhesive joining wood to particle board and wood to steel sheet.

All the specimens in each series were stressed for at least 4 weeks in a constant climate (21 ± 2° C and 64 ± 2% RH). The time-relative creep data was plotted for all the tested specimens and two different mathematical expressions were used to predict creep after 1,000 and 10,000 hours.
All the specimens studied here were selected to match the materials used in a number of stressed-skin panels. The long-term deformation of these panels is still continuing and another paper will be issued at a later date.

3. TESTS, SPECIMENS AND LOADING ARRANGEMENT

3.1 Wooden beams

Beams loaded in bending and wood specimens used for testing in pure shear were produced at the same time from the same materials, which was Swedish redwood (Pinus Sylvestris). The timber was virtually defect-free and had no large knots, resin deposits or cracks.

3.1.1 Specimens loaded in bending

See Table 1 for the number of simply-supported beams in each series, with a cross-section of 22 x 100 mm, the type of load, stress level and the number of weeks during which stress and recovery were measured.
The loads varied (for different series) between 0.5 and 1.0 times the design load.

3.1.2 Specimens loaded in shear

Tests to determine the long-term deformation in shear were conducted in accordance with the panel shear test-method C (in principle ASTM S2719-76), see fig.1.
The load was imposed via yokes using drawing bars attached to the floor and to a steel lever, see fig.2. Here, 8 specimens in each of two series were loaded at 1.2 and 1.5 times the design shear stress respectively.
The average stress in the shear area, which was 22 x 300 mm, was measured using 2 dial indicators, one on each side of the specimen, diagonally over a distance of 200 mm.

3.2 Particle-boards

16 prismatic specimens (2 from each plate) of UF-bonded Swedish particle board were made with a cross-section of 40 x 100 mm and a height of 200 mm. All specimens were loaded in compression with a constant load in 3 different series representing 3 stress levels, 0.75, 1.5 and 1.9 times the design load (σ_{c1}).
The loading arrangement was similar to the one used for loading in shear, where the dead weight was imposed via the steel lever, see fig.2. The average deformation was measured using 2 dial indicators, see fig.3.

3.3 Glued joints

Two different types of adhesive were used to join wood to particle board and wood to steel sheet; i.e. 4 different types of joint with 4 specimens in each were used. The adhesives were

a) Two-component PVA with isocyanate hardening agent
b) Two-component elastomeric silicone.

The wood and particle-board used was cut from specimens loaded in shear and in compression respectively. The steel sheet was completely uniform and polished, 0.6 mm thick. Both types of joint were loaded with a dead weight via a steel lever. The average deformation in the joints caused by shear was measured using 2 dial indicators, see fig.4.

3.3.1 PVA adhesive

The shear stress in the wood to steel joint was about 1.25 MPa (18% of ultimate stress level) and 0.51 MPa in the wood to particle-board (10% of ultimate stress level).

3.3.2 Silicone adhesive

In this case the stresses were much lower figure-wise but higher percentage-wise. The shear stress in the wood to steel joint was about 0.65 MPa (30% of ultimate stress level) and 0.27 MPa in the wood to particle-board (10% of ultimate stress level).

4. RESULTS

4.1 General

Two different mathematical expressions were used to predict creep after 1,000 and 10,000 hours from measurements taken during about 670 hours (4 weeks).

The power function, equation (1), is probably the most commonly used expression to fit a regression curve which represents available creep data (primary creep).

$$\Phi = \beta_o + \beta_1 t^{\beta_2} \qquad (1)$$

where relative creep $\Phi = \delta_c/\delta_o$ and δ_o is an initial deflection (deformation) obtained after one minute ± 5 seconds (after application of the load).

This equation has no theoretical justification and often produces an overestimate of creep |1|,|3|.

A 4-element model with 5 parameters is the other expression used, equation (2), to fit a regression curve and to predict creep.

$$\Phi = \beta_o + \beta_1 \left|1 - \exp(-\beta_2 t)\right| + \beta_3 t^{\beta_4} \qquad (2)$$

This model is basically Burger's model which is used to represent the visco-elastic behaviour of wood and its mechanical system contains various springs and dashpots.

In their survey of creep in chipboard Pierce et al |4| showed very good agreement between the fitted curve defined by equation (2) and measurements obtained in the tests.
The same equation (2) is used by the National Swedish Institute for Material Testing for predicting relative creep.
SAS, |5|, the Non-LINear regression computer programme was used here to fit the time-relative creep data to these two functions. The Non-LINear uses one of four iterative methods, which in this case was the Gauss-Newton method. This method regresses the residuals on the partial derivatives of the function with respect to the parameters until the convergence is reached.

4.2 Wooden beams loaded in bending

16 simply-supported beams representing the web-material in stressed-skin panels were selected and subjected to a concentrated load, see Table 1.
As the stress level was low (approx. 6% ultimate stress) in main series I, it was thought that all the beams that had been used in that series would "recover" and could then be used once again and subjected to a new concentrated load. The load and deflection cycle for beam 10 in main series I and II is shown in fig.5. The "unrecovered" deformation after series I was small and the creep rate for main series II (beams that had already been loaded) was therefore assumed to represent the creep rate in "new" beams.

In order to verify this supposition a supplementary series was run in which 6 "new" beams were loaded in exactly the same way. The relative creep and creep rate could then be compared from measurements obtained from previously loaded (series II) and newly loaded (series II A) beams.

The mean value (main series I) for relative creep after 4 weeks was 1.29 with a standard deviation of ± 0.04. For main series II (previously loaded beams) the mean value for relative creep after 4 weeks was 1.16 ± 0.016, despite the fact that the stress level was more than twice as high. Even the supplementary series IIA showed the same tendency. The relative creep value for all 6 beams was lower than the lowest value obtained in main series II. The mean value was 1.12 ± 0.012.
Another supplementary series - IIB - was conducted to compare the differences in relative creep and creep rate caused by a change in stress distribution resulting from a 4-point load. The mean relative creep values after 4 weeks happen to be exactly the same as those obtained in series IIA.

The curvefitting results show that estimated parameters do not differ significantly between the specimens in the same series using equation (1). The 5-parameter model, equation (2), produces significant differences between estimated parameters and prediction was not always successful, especially for specimens in series II, see Table 2. Almost all the values which show predicted relative creep after 10,000 hours were higher using equation (1).

Fig.6 shows the result of curvefitting using both models, equation (1) and (2).

4.3 Wooden specimens loaded in shear

The measurements of displacement and relative creep for wooden specimens loaded in shear differ significantly between the two series. The initial displacement was very small (less than 0.12 mm) and it was just possible to register the increase due to creep using dial indicators graduated to 0.001 mm. The variation between the relative creep curves is greater than that for specimens made of the same material but loaded in bending, see fig.7. Curvefitting was just possible using equation (1). The predicted relative creep after 10,000 hours varied between 1.5 and 3.4. Using equation (2) the NLIN programme failed to converge the relative creep data using 50 iterations.

4.4 Particle-board loaded in compression

A similar procedure was used here as the one for wooden beams loaded in bending. 8 specimens were loaded once at one stress level (series III). No significant findings emerged, see Table 3. Another 8 specimens were loaded twice at two different stress levels (series I and II).

Just like the wooden beams the relative creep was the highest ($\overline{\Phi} = 1.62$) for the lowest stress level, this corresponds to 0.75 times the design stress in compression. The initial deformations obtained 1 minute after loading in all three series were in agreement with the deformations calculated theoretically using the moduli of elasticity obtained during the short-term loading. Curvefitting and relative creep prediction was difficult just as it had been for the wooden specimens loaded in shear. Similar results were also obtained.

4.5 Glued joints

There was no significant difference between the relative creep curves for both types of joint with silicone adhesives, see fig.8b (despite the differences in stress level). One specimen with wood to steel joints failed after three weeks. The variation between the measurements was much greater for elastomeric joints than for PVA joints.
When comparing relative creep for joints with PVA adhesives it is significant that wood to steel joints show much higher values after a short time and then a much lower creep rate than wood to particle board joints, see fig.8a.
The relative creep data for silicone adhesives was easy to fit using both equations (1) and (2). The predicted relative creep after 60 weeks was approximately 3 times higher than the values after 4 weeks using equation (1), but about 2 times higher using equation (2). The predicted values for PVA adhesives in the wood to steel joints were almost the same as the measured values (equation (1)) and no results were obtained using equation (2). Nothing significant emerged from the wood to particle board joints.

5. DISCUSSION AND CONCLUSION

It is significant for both wooden beams loaded in bending and for particle board loaded in compression that the relative creep values were higher at the lowest stress level.

The prediction of relative creep after 10,000 hours was not confirmed by the tests, even though such a confirmation was made after 1,000 hours for the same tests. The power function, equation (1), overestimated the creep by a few percent and the 5-parameter function, equation (2), underestimated it in most cases. The difficulty involved in measuring creep in shear and compression at a low stress level is evident.

The multiple correlation value R^2 is always higher using equation (2), which indicates a better fit to the experimental data.

As mentioned before, all the relative creep data was evaluated using the initial, elastic deformation obtained 1 minute efter loading. If the initial deformation could be obtained with good precision the moment the load is applied then the results and relative creep prediction would be much different.

Table 2 shows how the estimated parameters for both functions and the actual and predicted relative creep values differ using initial readings after 1 min $\delta(1)$ and after a few seconds $\delta(0)$. This is especially noticeable in particle board and glued joint specimens. The β_o parameter (equation (1)) is higher (over 1.00) for all the compared specimens using $\delta(0)$ values. A higher stress level or more elastic material (joints with silicone adhesive) show that the initial measurement is of great importance. These types of test should be carried out with very carefully defined initial, elastic deformation. One possible way could be to use dial indicators and measure electronically the increase in stress and deformation during the first few seconds when a specimen is loaded with a constant dead weight load. The literature on this subject is extremely vague; no-one appears to have clearly defined a method for measuring initial deformation.

REFERENCES

|1| Gressel, P.: Zur Vorhersage des langfristigen Formänderungsverhaltens aus Kurz-Kriechversuchen. Holz ald Roh- und Werkstoff 42 (1984).

|2| Pierce, C. - Dinwoodie, J. - Paxton, B.: Creep in chipboard. Part 2. The use of fitted response curves for comparative and predictive purposes. Wood Sci and Techn 13, 1979.

|3| Dinwoodie, J. - Pierce, C. - Paxton, B.: Creep in chipboard. Part 4. The influence of temperature and moisture content on the creep behaviour of a range of boards at a single stress level. Wood Sci and Techn 18, 1984.

|4| Pierce, C. - Dinwoodie, J. - Paxton, B.: Creep in chipboard. Part 5. An improved model for prediction of creep deflection. Wood Sci and Techn 19, 1985.

|5| SAS, The NLIN Procedure. SAS Institute Inc. Cary, North Carolina.

|6| Nielsen, A.: Rheology of building materials. National Swedish Building Research, D6:1972.

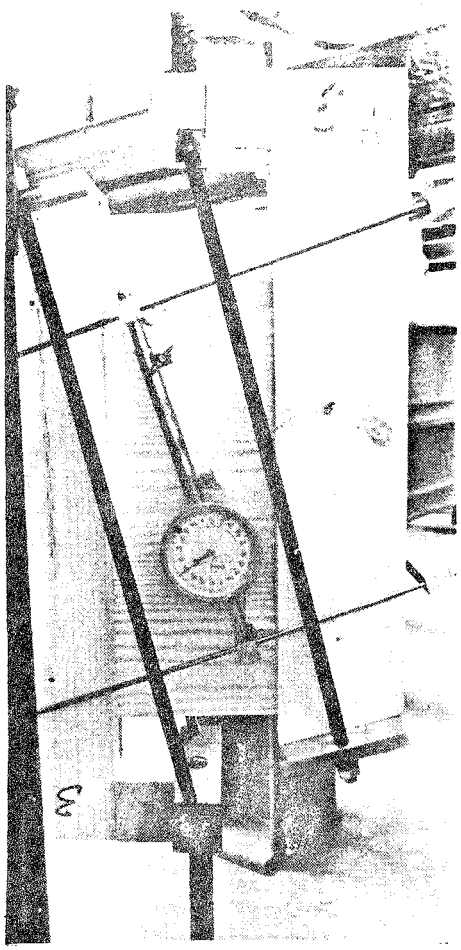


Fig.1 Specimen exposed to shear.

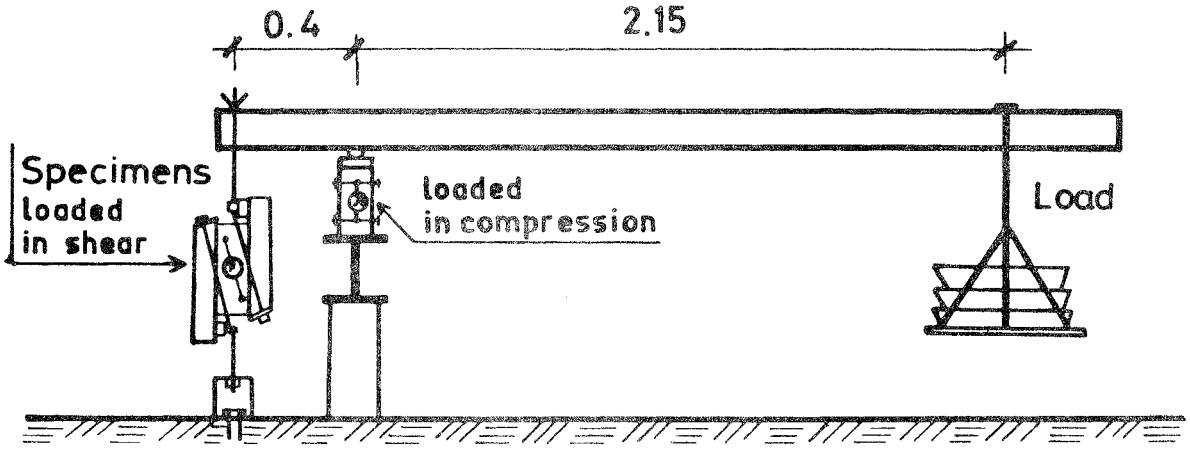


Fig.2 Loading geometry for specimens loaded in shear and in compression.

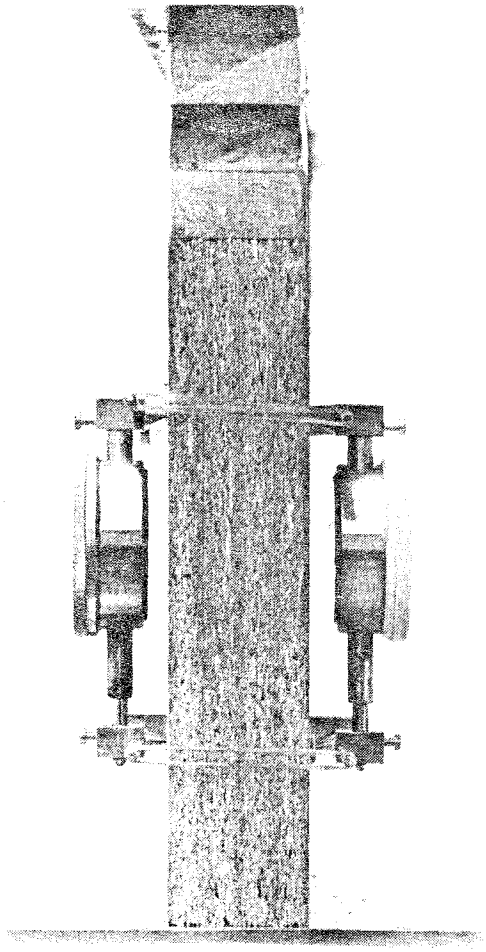


Fig.3 Particle-board specimen under constant load in compression.

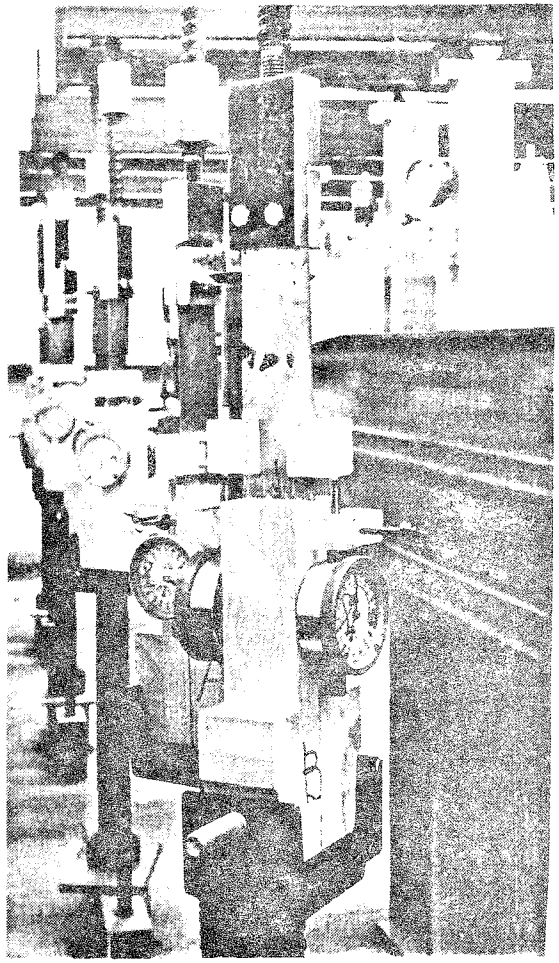


Fig.4 Tests using glued joints.

Table 1 Beams loaded in bending. No. of series, stress level and the number of weeks for stress and recovery.

	Series (No of beam)	Load P [kN]	Stresses [MPa]	Time of constant load [weeks]	Time of recovery [weeks]	Comments
Main series	I (16)	P=0.62, L=1.2	σ_b=5.1, τ=0.21, σ_b=0.5·σ_d*	4	3	
Main series	II (16)	P=1.4, L	σ_b=11.4, τ=0.48, σ_b=1.0·σ_d*	8	5	Same beams as in I
Supplementary series	IIA(6)	P=1.4, L	σ_b=11.4, τ=0.48	6	1	
Supplementary series	IIB(6) + 2 ref beams as in II	P=1.89, L/3 L/3 L/3	σ_b=10.35, τ=0.65, σ_b=0.9·σ_d*	11	—	Same beams as in I and II

* σ_d = Design stress

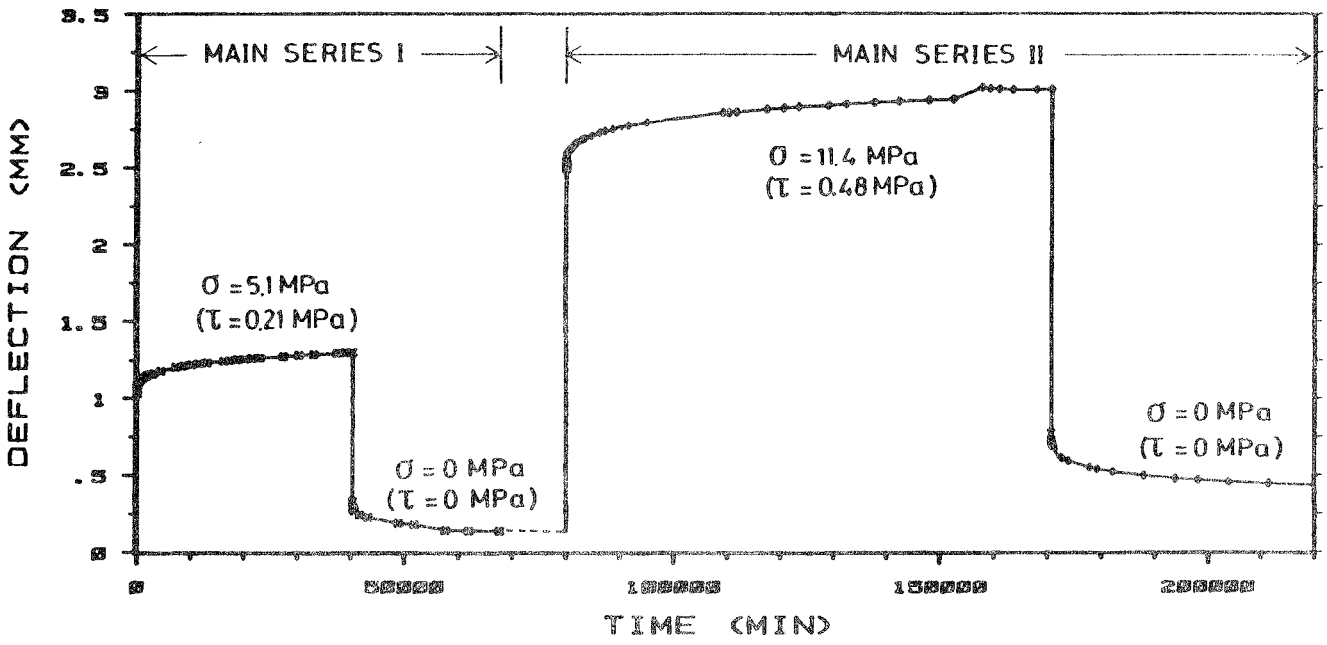
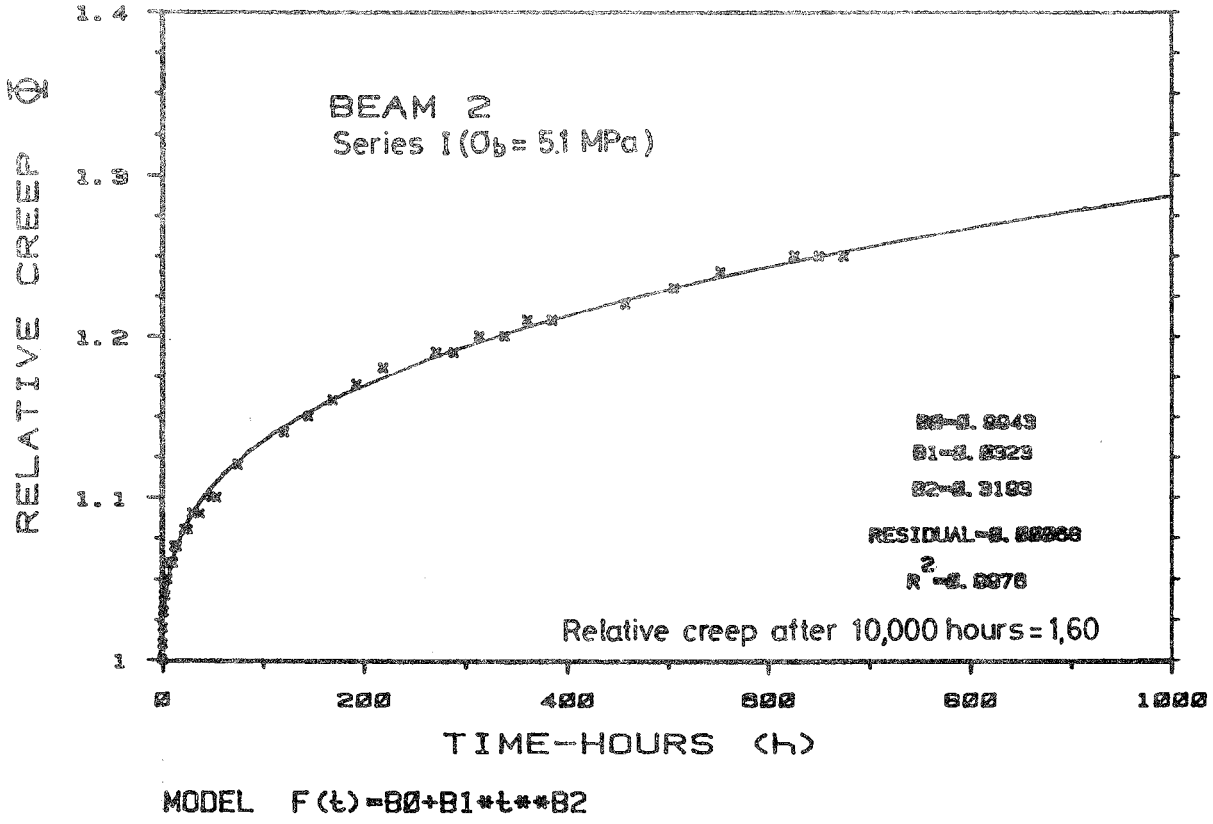


Fig.5 Load and deflection cycle for beam no.10 loaded in bending. Main series I and II.



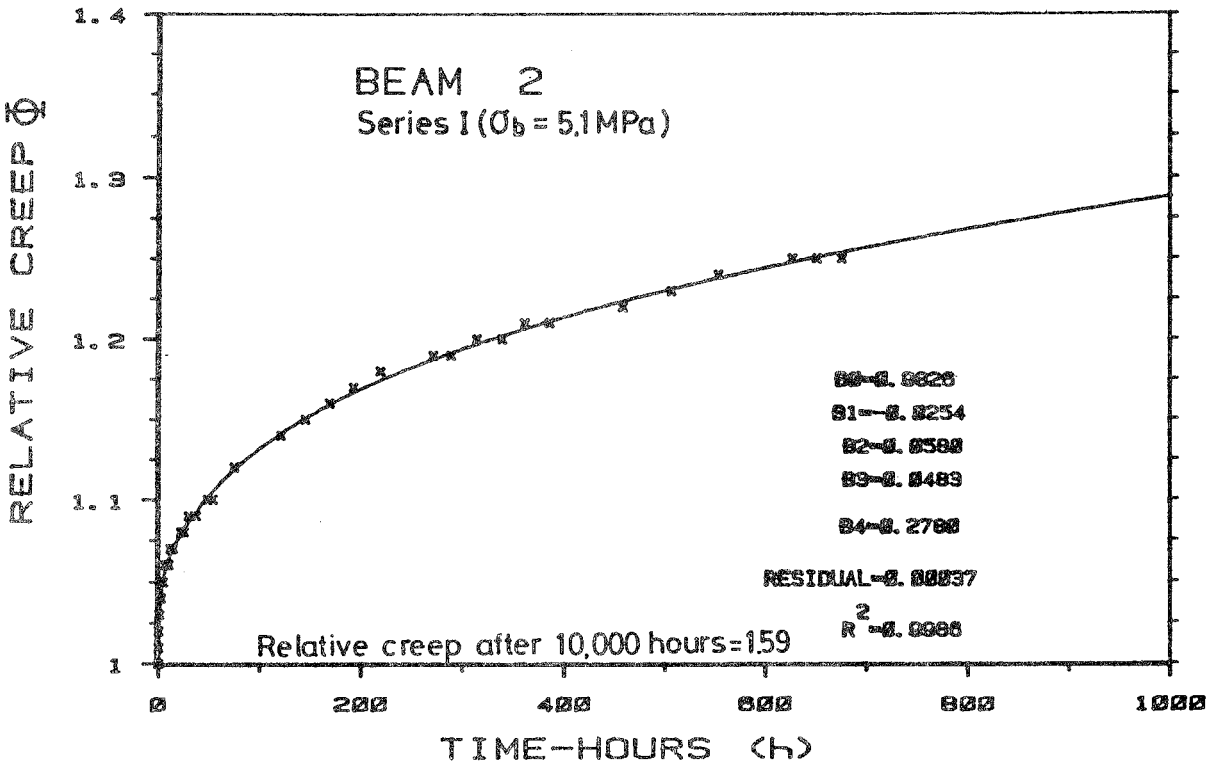


Fig.6 Curves fitted to typical creep data using equations (1) and (2).

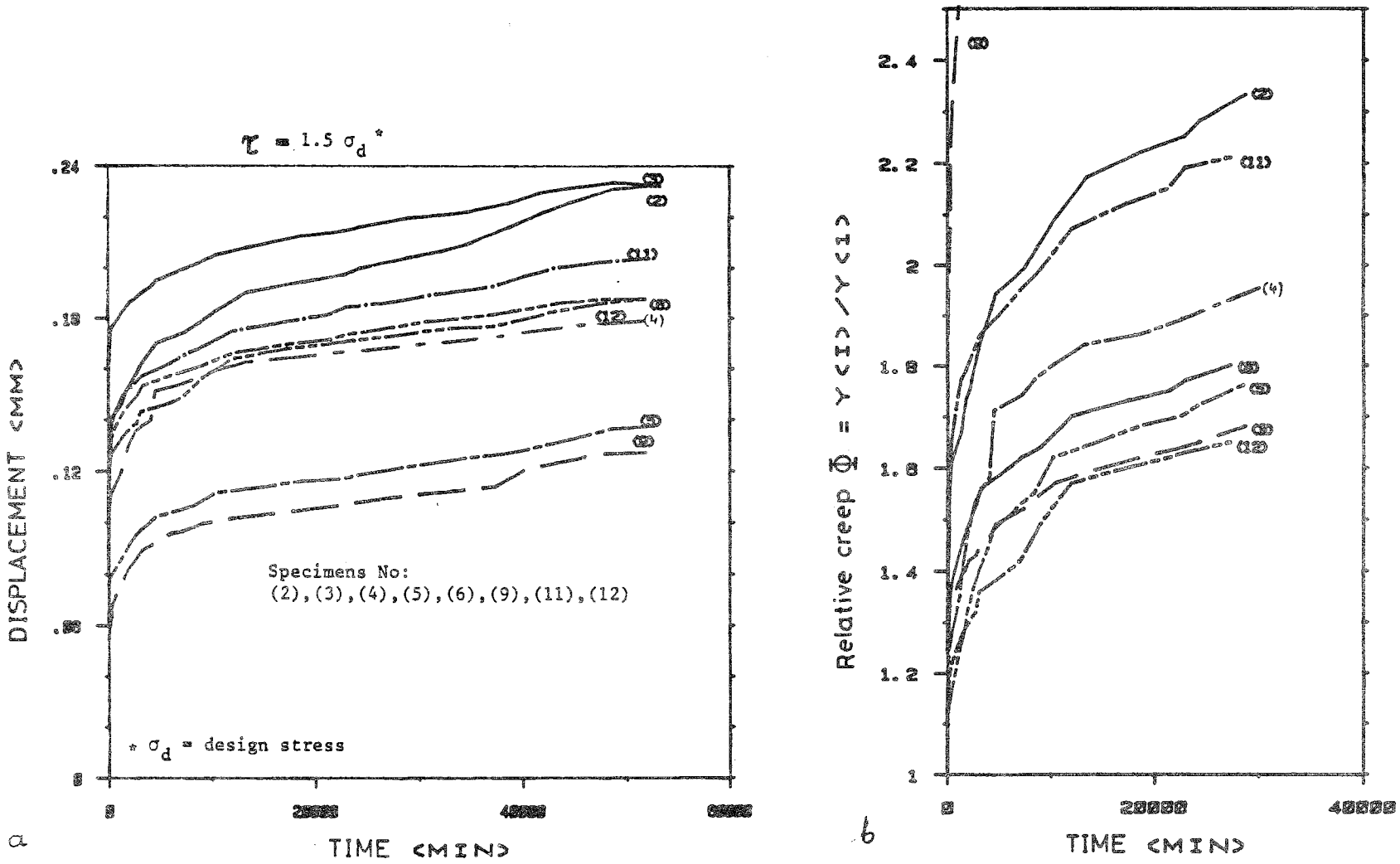
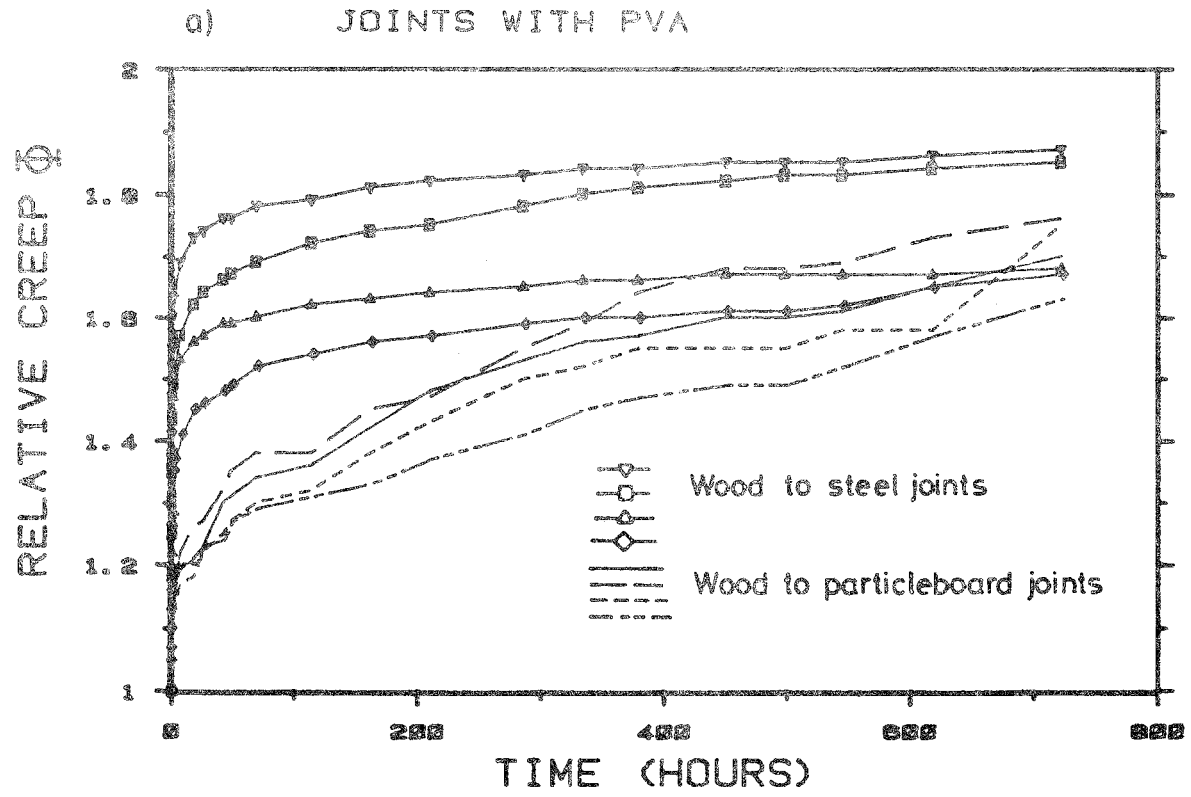


Fig.7 Creep data for specimens loaded in shear:
a) Time-displacement
b) Time-relative creep Φ.



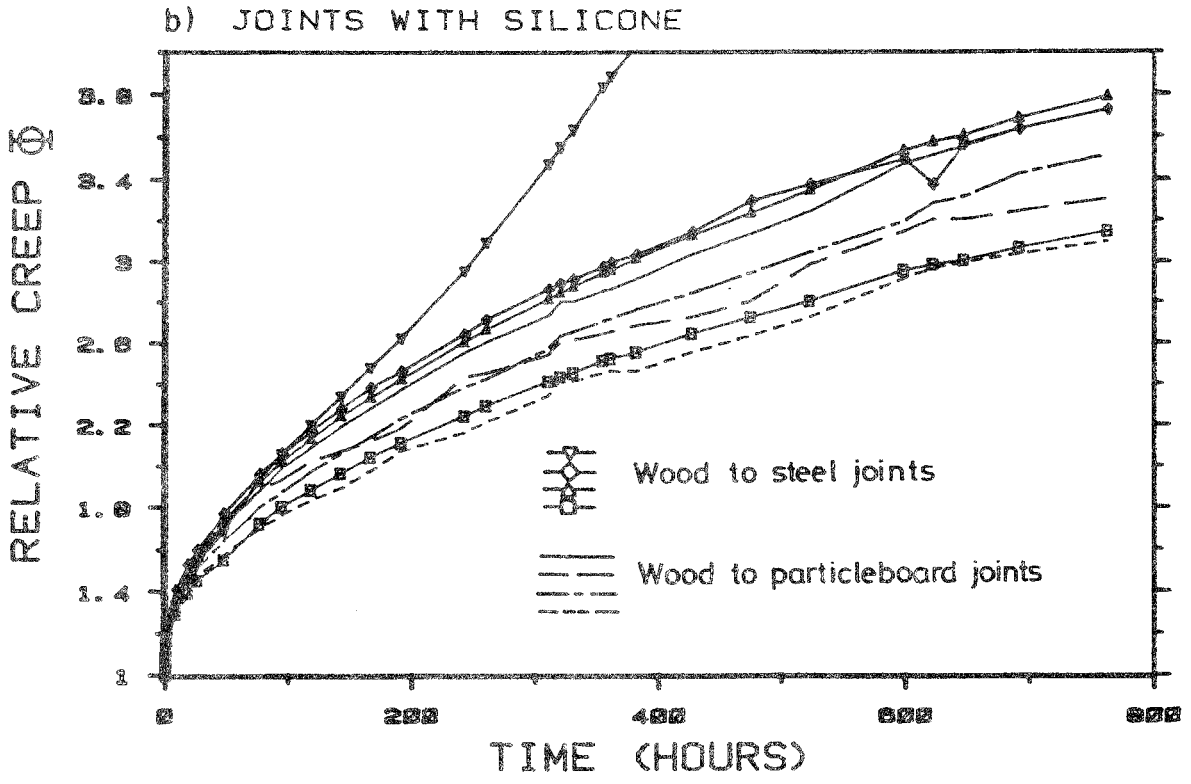


Fig.8 Creep data from test on glued joints.

Table 2 Some examples from prediction studies using equations (1) and (2). Variations seen in two different initial readings.

Specimen no.	$\Phi = \beta_o + \beta_1 \cdot t^{\beta_2}$ Estimated parameters β_o	β_1	β_2	R^2	Predicted Rel.creep Φ 60 weeks t=10,000 h	Actual Rel.creep Φ 4 weeks t=672 h	Initial readings (min)	$\Phi = \beta_o + \beta_1 \lvert 1-\exp(-\beta_2 t) \rvert + \beta_3 \cdot t^{\beta_4}$ Estimated parameters β_o	β_1	β_2	β_3	β_4	R^2	Predicted Rel.creep Φ 60 weeks t=10,000 h
Wooden beams - Series I ($\sigma_{max} = 0.5\ \sigma_d$)														
2	0.994	0.032	0.319	0.9976	1.60	1.25	$\delta(1)$	0.983	-0.025	0.059	0.048	0.278	0.9986	1.59
2	1.004	0.038	0.299	0.9956	1.60	1.27	$\delta(0)$	0.768	0.150	0.003	0.282	0.042	"	1.34
19	0.985	0.0489	0.264	0.9984	1.54	1.26	$\delta(1)$	0.989	0.082	-0.003	0.044	0.286	0.9984	1.44
19	1.005	0.0514	0.261	0.9971	1.58	1.28	$\delta(0)$	0.970	0.090	0.005	0.089	0.142	"	1.39
Wooden beams - Series II ($\sigma_{max} = 1.0\ \sigma_d$)														
2	0.996	0.028	0.262	0.9920	1.31	1.15	$\delta(1)$	0.425	0.0785	0.0033	0.6031	0.0126	0.9960	1.18
2	1.005	0.028	0.261	0.9965	1.31	1.16	$\delta(0)$	0.974	0.063	0.0015	0.0612	0.1311	0.9982	1.24
19	0.999	0.022	0.309	0.9965	1.38	1.17	$\delta(1)$	0.955	0.083	0.0032	0.0692	0.1025	0.9975	1.22
19	1.002	0.026	0.294	0.9972	1.39	1.18	$\delta(0)$	0.987	0.055	0.0024	0.042	0.189	"	1.28
Particle board ($\sigma_{c1} = 1.5\ \sigma_d$)														
SP3	1.039	0.048	0.293	0.951	1.75	1.44	$\delta(1)$							
SP3	1.181	0.112	0.205	0.938	1.92	1.63	$\delta(0)$	0.993	-0.176	0.059	0.343	0.133	0.9740	1.98
Wood to steel joints - silicone adhesive ($\tau = 0.65$ MPa)														
TS1	1.066	0,068	0.510	0.9976	8.60	2.91	$\delta(1)$	0.979	2.245	0.0007	0.1620	0.297	0.9982	5.73
TS1	1.461	0.123	0.486	0.9933	12.27	4.40	$\delta(0)$	1.320	-0.655	0.0155	0.2976	0.388	0.9963	11.27

σ_d = design stress

Table 3 Summary of results from tests using particle-board.

Chipboard No	Density [kg/m³]	Short-term load: E Modulus of elasticity [MPa] $\sigma_t = 2$	Short-term load: E Modulus of elasticity [MPa] $\sigma_t = 4$	Specimen	Long-term load: SERIES I ($\sigma_t = 0.75\ \sigma_d$) Deformation [mm] $y = \frac{NL}{EA}$	Deformation [mm] $y_{(1min)}$	Φ_{3weeks}	Predicted Rel. creep Φ(60 weeks) equation 1	SERIES II ($\sigma_t = 1.5\ \sigma_d$) Deformation [mm] $y = \frac{NL}{EA}$	Deformation [mm] $y_{(1min)}$	Φ_{3weeks}	Predicted Rel. creep Φ(60 weeks) equation 1
1	726	4000	3900	B	0.050	0.052	1.69		0.102	0.092	1.40	
				C		0.042	1.67			0.105	1.26	
2	714	4000	3900	B	0.050	0.040	1.41		0.102	0.090	1.36	
				C		0.052	1.75			0.067	1.30	
3	720	3670	3610	B	0.055	0.061*	1.70*		0.110	0.110	1.35	
				C		0.052	1.64	3.49		0.092	1.44	1.75
4	707	3920	3920	B	0.051	0.049	1.57	3.23	0.101	0.099	1.43	1.96
				C		0.050	1.57			0.075*	1.53*	
							$\bar{\Phi} = 1.62$				$\bar{\Phi} = 1.38$	
5	767	4870	4620	B					0.114	0.142	1.38	
				C						0.118	1.46	1.55 (eq.2)
6	705	4080	4050	B					0.129	0.130	1.56	1.62
				C						0.099*	1.34*	
7	714	3850	3820	B					0.139	0.062	1.72	
				C						0.149	1.37	1.66
8	712	4440	4410	B					0.118	0.138	1.43	
				C						0.068	1.47	
	$\bar{\rho}$=721	$\bar{E}$=4100	$\bar{E}$=4030								$\bar{\Phi}$=1.47	

SERIES III $\sigma_t = 1.9\ \sigma_d$

σ_d = design stress

* No mean value

CIB-W18/19-9-6

INTERNATIONAL COUNCIL FOR BUILDING RESEARCH STUDIES AND DOCUMENTATION

WORKING COMMISSION W18 - TIMBER STRUCTURES

CREEP AND LIFETIME OF TIMBER LOADED IN TENSION AND COMPRESSION

by

P Glos
University of München
Federal Republic of Germany

MEETING NINETEEN
FLORENCE
ITALY
SEPTEMBER 1986

CREEP AND LIFETIME OF TIMBER LOADED IN TENSION AND COMPRESSION

P. Glos
Institut für Holzforschung der Universität München

Summary

As a supplement to existing investigations on small, clear specimens and to full-size bending tests, long term tension and compression tests on full-size European spruce specimens (picea abies) were carried out for the first time. The material tested consisted of glulam laminates, collected as representative samples from German glulam plants. The tension and compression specimens had cross-sections of 30x120 mm and 30x 180 mm and a gauge length of 1.65 m. In 10 test series a total of 212 specimens was subjected to constant load tests (stress level 14 N/mm^2 and 21 N/mm^2; loading time 6 months) and to ramp load tests (time to failure 10 sec, 1hr and 240 or 360 hrs). All tests were carried out under constant climate conditions at 20^{0}C and 65 % r.h.

Both under tension and compression tests a pronounced duration of load effect was noticed which was clearly stronger in the lower range of strength distribution than reported in earlier bending tests carried out in Canada. The duration of load effect seems to be equally pronounced in both tension and compression despite differences in creep behaviour. Its magnitude corresponds approximately to that of the Madison curve. The test results support the assumption that unless the applied stress surpasses a threshold of roughly 50 % of the respective short term strength of timber apparently no damage or strength degradation over time is caused. A modification factor which would take into account the duration of load effect in structural timber design codes would depend not only on load history but also on strength distribution and consequently on the timber grading system.

1. INTRODUCTION

Wood is a high polymer solid-state body which, from a physics point of view, represents a compound structure of crystalline and amorphous components with statistically interspersed submicroscopic structural defects. Stress applied to this complex structure partly triggers irreversible flow processes which cause the well-known viscoelastic-plastic deformations and also a reduction in strength with increasing duration of load. In wood this phenomenon known as "creep-rupture" will already occur at normal temperatures and therefore has to be taken into account in structural uses of wood.

Structural timber design codes in many countries contain a strength reduction factor of about 0.6 for long term load. This value is based mainly on tests with small clear bending specimens (1). Up to now there is no confirmation whether this value is appropriate for full-size timber

in relation to bending and other strength properties. The existing German structural timber design codes do not explicitly mention a duration of load factor. Here, the duration of load effect is apparently covered implicitly by the allowable design stresses which are largely based on experience (2).

With regard to the envisaged transition to reliability-based structural design and to the international harmonization of structural design codes (e.g. Eurocodes) it was necessary to extend existing knowledge on the duration of load effect on the strength of structural timber. The present study aims at examining the duration of load effect in tension and compression for timber and to determine to what extent it differs from that of the much more comprehensively studied duration of load effect in bending (3). With regard to the increasing importance of glulam structures in modern timber engineering glulam laminates were chosen as test material. The test program's scope was limited by the funds available for this project.

2. TEST PLAN

The test plan with sample sizes is outlined in Table I. The test plan, both for tension and compression, comprises two constant load test series with stress levels of 14 and 21 N/mm^2 applied over a period of six months each, and three ramp load test series, each with different constant loading rates which led to failure within 10 sec, 1 hr and 240 or 360 hrs. Sample sizes for each of the 2 x 5 = 10 test series varied from 10 to 40 specimens, with a total of 212 tests. All tests were carried out under constant climate conditions at 20^0 C and 65 % r.h.

3. TEST MATERIAL

The material used was European spruce timber (picea abies), sections of glulam laminates 3 m long, collected in 1983 as representative samples from 15 out of some 40 German glulam plants. Shape and dimensions of the specimens are given in Fig. 1. After conditioning to normal climate (20^0C/ 65 % r.h.) the boards measuring 3 m in length were planed to the largest possible size of either 30 x 180 mm or 30 x 120 mm and cut to a length of 2.40 m in such a manner that the presumably weakest cross-section (biggest knot) was situated in the gauge length of 1.65 m. From each of these trimmed boards bending modulus of elasticity, knot size and density were determined. Using these characteristics and regression functions available from former test work, short term tension and compression strength were predicted for each board. The boards were then grouped into matched subsamples for the 10 test series so that each subsample exhibited equal reference strength distribution (predicted short term strength) as well as equal distribution of modulus of elasticity, knot size and density. Finally the test specimens were produced from the selected boards by nailing the shoulders to the tension specimens or cutting compression specimens at both ends down to the test length of 1.65 m.

4. TEST METHOD

In order to obtain comparable results all ramp load tests and all constant load tests were carried out in the same load frames. Test load was applied by an oil-hydraulic system. In the compression tests the load was transferred directly to specimen ends, lateral buckling of the specimens was prevented by lateral supports placed at 30 cm intervals. In the tension tests the load was transferred to the specimen via shoulders attached to each end (Fig. 1). In order to simulate the situation in a glulam beam

lateral deformation of tension specimens was also prevented by lateral supports. An electric load cell recorded the load. For each test the loading procedure including ultimate load and time to failure, where applicable, was recorded by producing a time-load diagram. For each constant load test time to failure was recorded automatically via an electric clock and a switch connected to the board. Creep deformation was measured in both constant load tension and compression tests. The gauge length for creep measurements was 1.20 m. Specimens surviving the constant load tests were subsequently subjected to a 10 sec ramp load test.

5. RESULTS

The results of all ramp load and constant load tests are shown in Figs. 2 to 5, separately for tension and compression tests.

The results of the ramp load tension tests are shown in Fig. 2 whereas those for the ramp load compression tests are given in Fig. 3, presented in ranked order. As matched subsamples with the same short term strength distribution were used the relative shifting of distribution curves can be taken as a measure for the duration of load effect. The more irregular curves in Fig. 2 representing the ramp load tension tests are due to a certain inhomogeneity of the respective subsamples on account of the bigger residual variance of the short term tensile strength estimate. However, it can be seen that both tension and compression strengths decrease with increasing time to failure. This effect is also clearly evident in the lower range of strength distribution in both tension and compression. The parallel movement of the curves indicates that the duration of load effect tends to be largely independent of wood quality.

The results of the constant load tests in tension and in compression are shown in Figs. 4 and 5 respectively, again presented in ranked order. These Figs. show the number of specimens which failed during the 6 months' constant loading period, together with their corresponding times to failure. In addition the residual short term strength (10 sec ramp load test) of those specimens which had survived the constant load test is shown. For comparison the test results of a control group (ramp load test, time to failure 10 sec) are also given.

The results of the constant load tests also indicate a significant duration of load effect. Within 6 months 2 out of 20 specimens failed under a tensile stress of 14 N/mm^2, 21 out of 30 specimens failed during the same period when a tensile stress of 21 N/mm^2 was applied. 9 out of 20 specimens failed under a compressive stress of 21 N/mm^2, while no failure was recorded under a compressive stress of 14 N/mm^2. Thus test specimens are shown to fail under a 6 months' constant tensile or compressive load under constant climate conditions when reaching or exceeding a stress level of roughly 14/24 or 21/36, i.e. approximately 0.6, related to short term strength (10 sec ramp load test). For a constant compressive stress of 14 N/mm^2 this critical stress level was not reached and therefore no failures were recorded for this test series.

For a quantitative evaluation of the duration of load effect the constant load test results were compared with the so-called Madison curve. Results for the 23 tension specimens and the 9 compression specimens which had failed during the constant load test were therefore plotted in Fig. 6 in the same manner as in Wood's report. The required but unknown short term strength of each specimen was estimated from the strength distribution of the 10 sec ramp load tests by assuming that the rank of a specimen

in the short term test is equal to its rank in the long term test.

Fig. 6 shows that the duration of load effect seems to be as strong in tension as it is in compression and its course appears similar to the Madison curve. It should be borne in mind, however, that this conclusion is based on results for no more than 23 tension and 9 compression specimens. The test results moreover support the assumption that unless the applied stress surpasses a threshold of roughly 50 % of the respective short term strength apparently no damage or strength reduction of the timber is caused.

Creep behaviour of tension and compression specimens is shown in Figs. 7 and 8, respectively. The curves show the ratio of the measured absolute deformation to initial deformation, i.e. the creep factor over time for individual specimens. Stress ratio, i.e. the ratio of stress level to the residual short term strength is given for those specimens which had survived the constant load test. Based on a loading time of 3000 hrs and a stress ratio of roughly 50 to 70 % the mean creep factor is in the order of roughly 7 % in tension and 30 % in compression. The influence of stress ratio on creep factor is more pronounced in compression than in tension.

For comparison the creep factor as reported for small clear specimens (4) is also given. Obviously the creep factor of small clear specimens is much higher than that of lumber when related to stress ratio, but roughly corresponds to that of lumber when related to applied stress level. This indicates that creep of lumber under tensile and compressive load seems to be related rather to wood structure than to strength reducing wood defects.

6. CONCLUSIONS

All test results presented here are based on a very limited number of tests on European spruce (picea abies). With this reservation the following conclusions can be drawn:

1. Structural timber exhibits a significant duration of load effect in tension and in compression under constant climate conditions. The test results indicate that this effect is more pronounced in the lower range of strength distribution than was the case for bending tests carried out in Canada (5, 6, 7). Nor were Canadian results supported by new ramp load bending tests with American Douglas-fir 2 by 4 timber. In these tests it was also found that the rate of loading affects the total distribution of bending strength (8). Whether these differences are partly due to differences between wood species or grading rules remains to be determined in current investigations in various North American and European countries.

2. The test results indicate that the duration of load effect seems to be equally strong in both tension and compression despite differences in creep behaviour. In the particularly interesting lower range of strength distribution the magnitude of the duration of load effect both for ramp load and constant load tests corresponds approximately to that of the Madison curve. A tri-linear curve as found in Canadian tests with full-size bending specimens (9, 10) could not be confirmed in the present tests.

3. The potential implications of duration of load effect on the reliability of timber structures is illustrated in Fig. 9. Several independent investigations indicate that unless the applied stress surpasses a threshold

of roughly 50 % of the respective short term strength of the timber apparently no strength degradation over time is caused (1, 2). From this follows that strength of timber will only be affected if its short term strength is less than twice the maximum applied stress. As can be seen from Fig. 9 this is the case for a small portion of the total timber population only, namaly for low strength timber around and below the population's 5th percentile. According to the present study it has to be assumed that low strength timber is also subjected to a significant duration of load effect. Therefore this effect has to be taken into account in structural timber design codes.

Only load effects within the shaded area in Fig. 9, i.e. stresses which surpass 50 % of the short term strength of the weakest component will contribute to the damage and strength reduction in structural timber. The amount and magnitude of critical stresses in that range are stochastic values and depend on the total code system, i.e. the underlying partial safety factors for load and material, load assumptions and the grading system. Therefore a modification factor which would take into account the duration of load effect in structural timber design codes cannot be derived directly from a stress ratio - time to failure diagram as done in the past. It has to be determined by means of probability analyses which include all important parameters. Studies at hand indicate that depending on partial safety factors, load assumptions and grading systems an adequate value may range from as much as 0.7 to 1.0.

REFERENCES

(1) WOOD, L.W., Relation of strength of wood to duration of load. US Dpt.of Agriculture, Report No. 1916, FPL, Madison, WI 1951, 9 pp.

(2) GRAF, O., Tragfähigkeit der Bauhölzer und der Holzverbindungen. Mitt. Fachausschuß f. Holzfragen, H. 20, Berlin 1938, 47 pp.

(3) HEIMESHOFF, B., GLOS, P. and KELLETSHOFER, W., Bestimmung des Einflußes wirklichkeitsnaher langwirkender Lasten auf das Zug- und Druckfestigkeitsverhalten von Holz sowie dessen Auswirkung auf die Zuverlässigkeit von Holzbauteilen. Technische Universität München, Lehrstuhl für Baukonstruktion und Holzbau, Abschlußbericht BOS 015 D (B) an die Kommission der Europäischen Gemeinschaften, 1986.

(4) GRESSEL, P., Kriechverhalten von Holz und Holzwerkstoffen - Auswirkungen auf den Formänderungsnachweis. In: Ingenieurholzbau in Forschung und Praxis. Hrsg. J. Ehlbeck u. G. Steck, Karlsruhe 1982: Bruderverlag pp 55- 66.

(5) MADSEN, B., Duration of load tests for dry lumber in bending. For. Prod. J. 23 (1973), No. 2, pp 21-28.

(6) MADSEN, B., Duration of load test for wet lumber in bending. For.Prod. J. 25 (1975) No. 5, pp 33-40.

(7) SPENCER, R., Rate of loading effect in bending for Douglas-fir lumber. Proc. 1st Intern. Conference on Wood Fracture, Aug. 14-16, 1978. Banff, Alberta, Canada. Forintek Canada Corp. 1979, pp 259-279.

(8) GERHARDS, C.C. and LINK, C.L., Effect of loading rate on bending strength of Douglas-fir 2 by 4's. For.Prod.J. 36 (1986) No. 2, pp 63-66.

(9) MADSEN, B. and BARRETT, J.D., Time-strength relationship for lumber. Structural Research Series, Report No. 13, Vancouver, B.C.: The University of British Columbia 1976, 181 pp.

(10) FOSCHI, R.O. and BARRETT, J.D., Load-duration effects in Western Hemlock lumber. Proc. of the ASCE, Vol.108 (1982) ST 7, pp 1494-1510.

Table I: Test plan and sample size

1.1 Ramp load tests

Property	Series no.	Time to failure	Sample size
Tension	1	30 sec	30
	2	1 h	30
	3	240 h	20
Compression	4	90 sec	20
	5	1 h	20
	6	360 h	12

1.2 Constant load tests

Property	Series no.	Stress level	Sample size
Tension	7	14 N/mm²	20
	8	21 N/mm²	30
Compression	9	14 N/mm²	10
	10	21 N/mm²	20
		Total	212

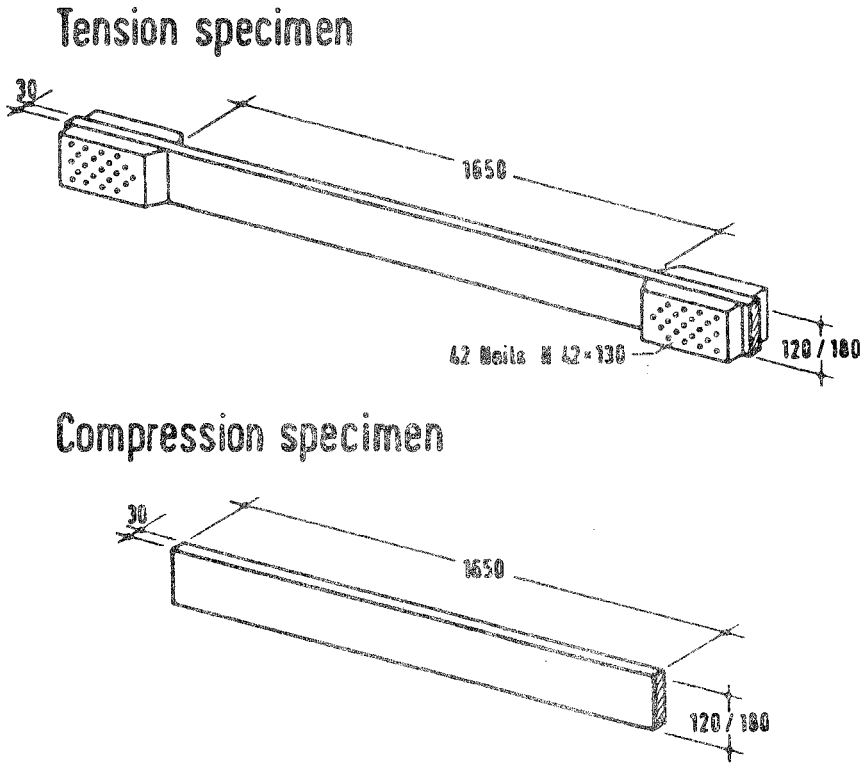


Fig. 1: Specimens for tension and compression ramp load and constant load tests

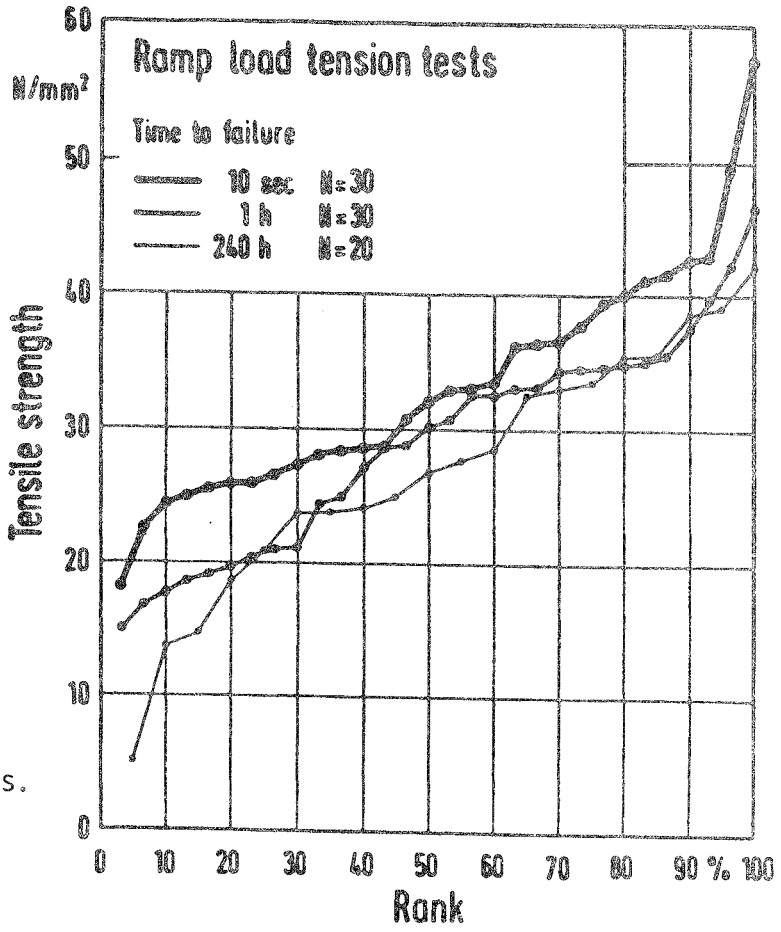


Fig. 2: Ramp load tension tests. Three different rates of loading

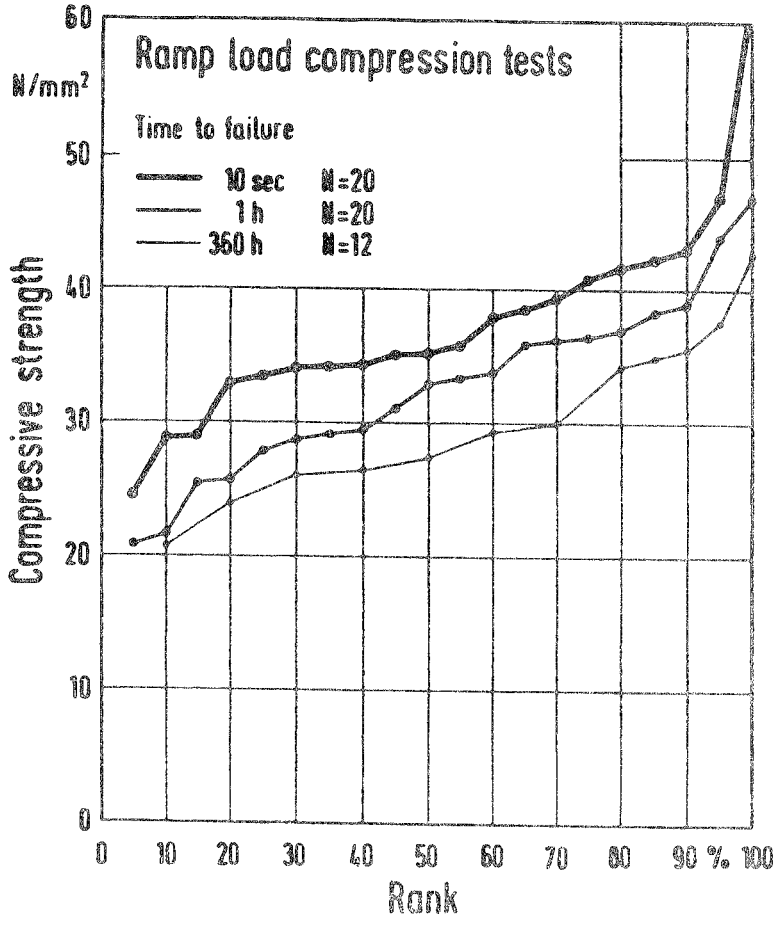


Fig. 3: Ramp load compression tests. Three different rates of loading

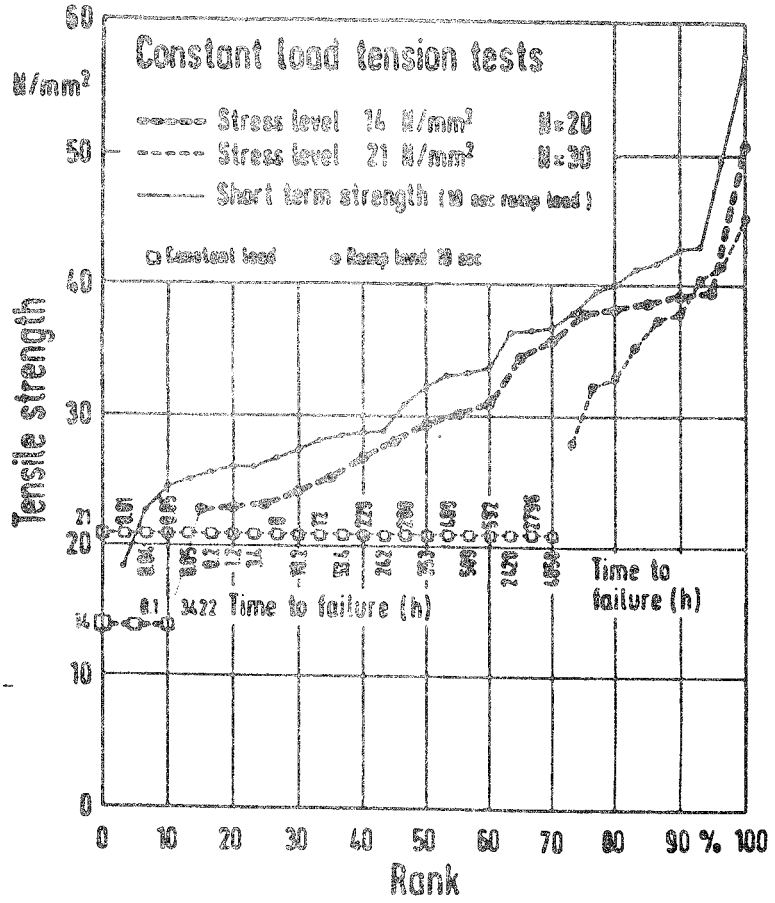


Fig. 4: Constant load tension tests (6 months), residual short term strength of unfailed specimens and short term strength of a control group

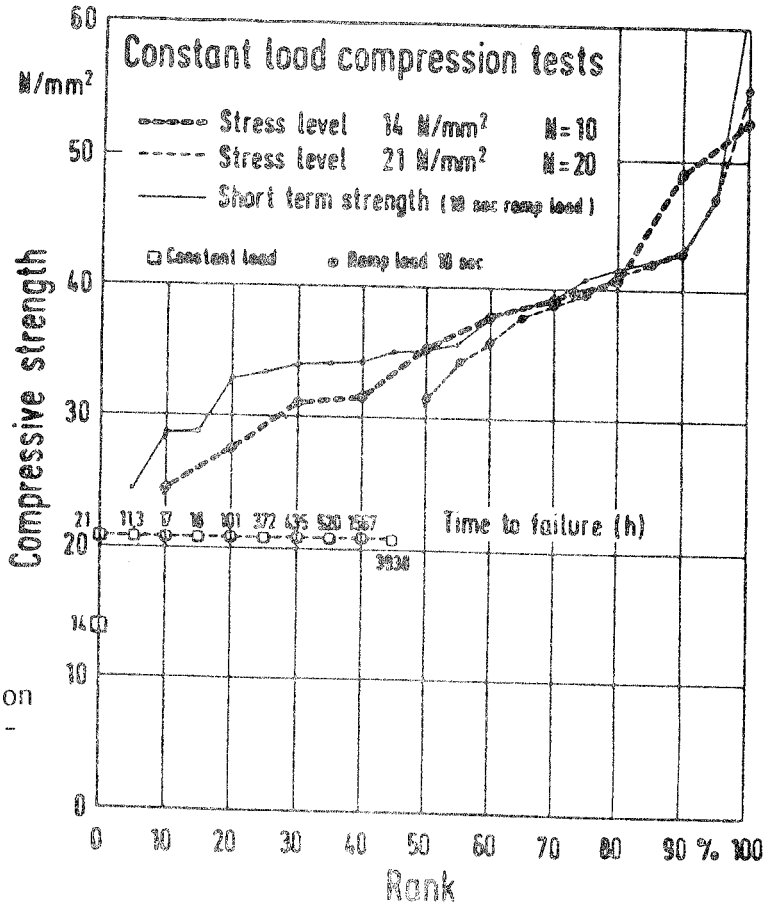


Fig. 5: Constant load compression tests (6 months), residual short term strength of unfailed specimens and short term strength of a control group

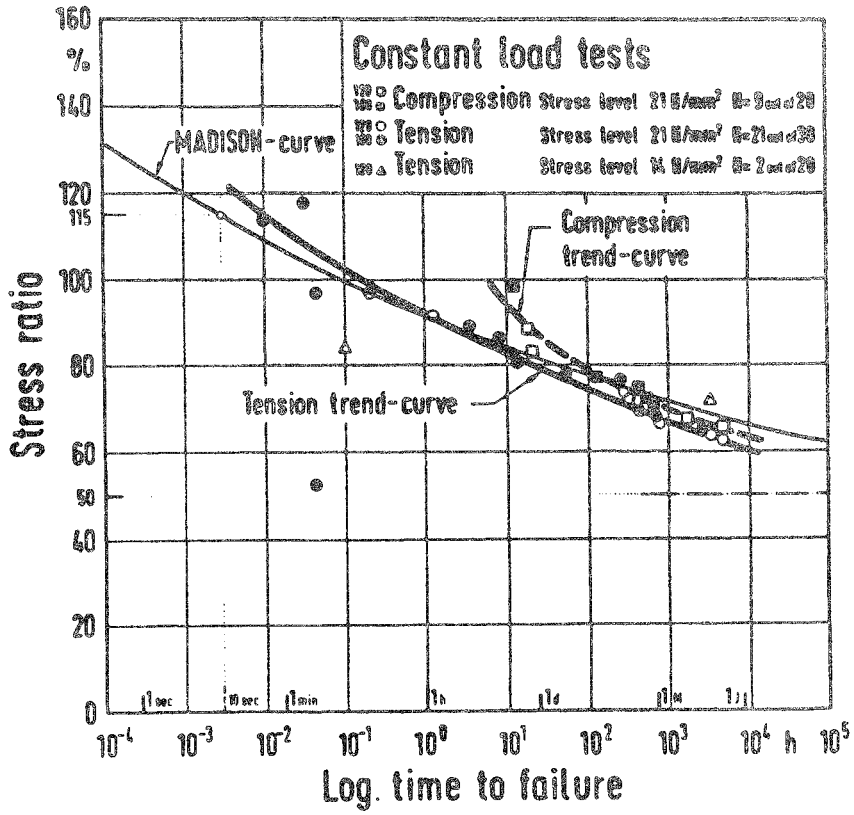


Fig. 6: Constant load tension and compression tests.
Stress ratio against log time to failure

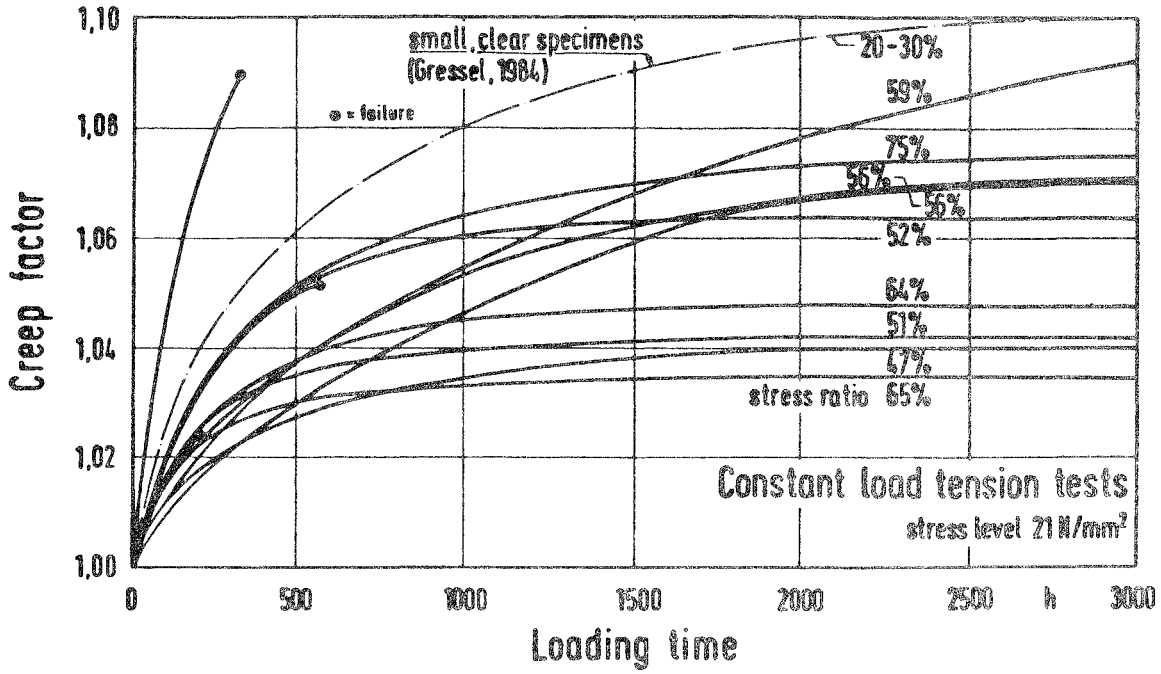


Fig. 7: Creep deformation under constant tensile load.
Stress ratio = stress level / residual short term strength of individual specimens

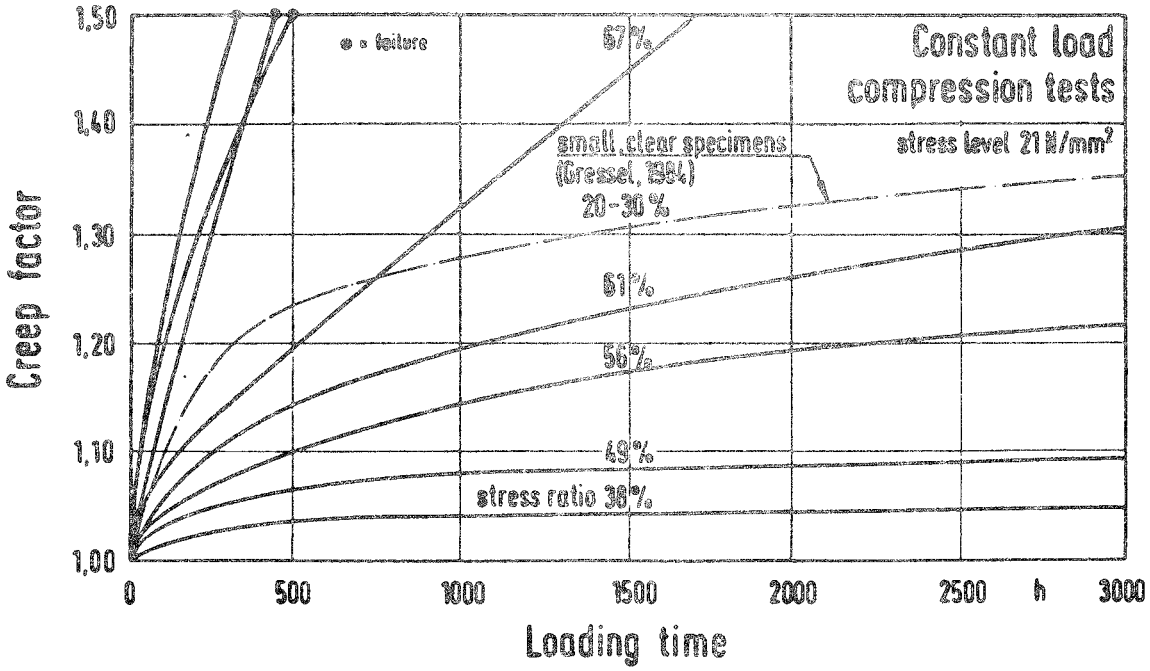


Fig. 8: Creep deformation under constant compressive load.
Stress ratio = stress level / residual short term strength of individual specimens

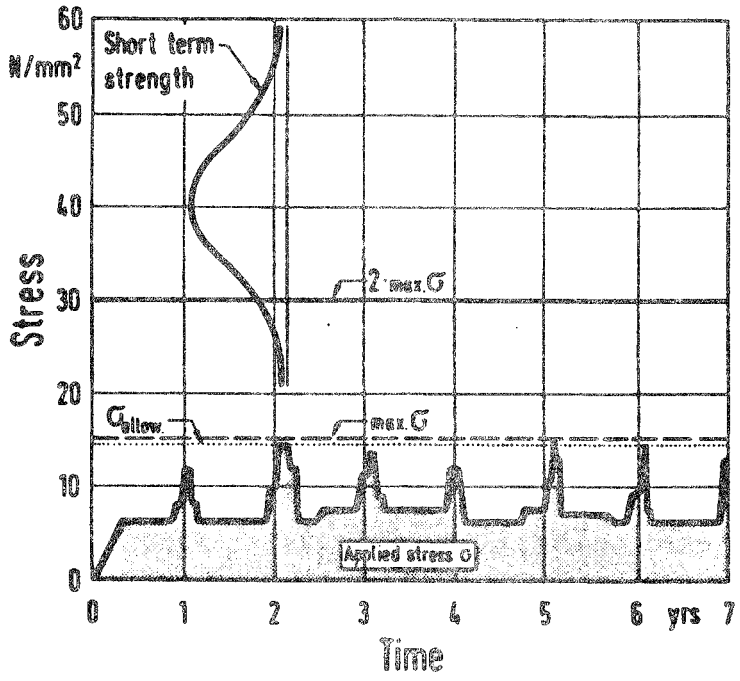


Fig. 9: Short term strength and applied stress in relation to time in a roof structure (schematic)

CIB-W18/19-10-1

INTERNATIONAL COUNCIL FOR BUILDING RESEARCH STUDIES AND DOCUMENTATION

WORKING COMMISSION W18 - TIMBER STRUCTURES

POSSIBLE CODE APPROACHES TO LATERAL BUCKLING IN BEAMS

by

H J Burgess
Timber Research and Development Association
United Kingdom

MEETING NINETEEN
FLORENCE
ITALY
SEPTEMBER 1986

C O N T E N T S

Page No.

PART 1 - CONDITIONS FOR LATERAL STABILITY OF DEEP BEAMS WITHOUT INITIAL IMPERFECTIONS WHEN IN-PLANE DEFLECTION AND INDUCED STRESSES ARE LIMITED

Introduction 1

Design for in-plane behaviour 1

Addition of the lateral buckling criterion 1

Conditions for lateral buckling to govern design 2

Bending stress critical for in-plane calculations 2

Shear stress critical for in-plane calculations 3

Conclusion for calculations assuming no initial imperfections 4

PART 2 - LATERAL BUCKLING OF RECTANGULAR SECTION DEEP TIMBER BEAMS WITH ALLOWANCE FOR INITIAL IMPERFECTIONS

Introduction 6

THEORY FOR LATERAL BUCKLING 6

Initially straight beam 6

Beam with initial twist 8

Beam with both initial twist and initial lateral curvature 9

Beam with related twist and curvature 10

Limitation of maximum combined stress 12

Exclusion of torsion term 14

Conclusion for calculation with initial imperfections 15

REFERENCES 16

POSSIBLE CODE APPROACHES TO LATERAL BUCKLING IN BEAMS

This paper is abbreviated from TRADA internal reports arising from a project partly funded by the British government Department of the Environment, with the title 'lateral stability of timber constructions'.

The paper deals with two separate topics related to the lateral buckling of timber beams with a tall rectangular section, although much of the work can be extended to other cross-sections which are symmetrical about both principal axes. The first topic links the well-known Hooley and Madsen approach with other factors which enter the design process, and is based on the theory for initially straight and untwisted beams. The second topic develops existing theory allowing for initial imperfections, to reach a result simple enough for consideration as a code of practice design formula.

PART 1 - CONDITIONS FOR LATERAL STABILITY OF DEEP BEAMS WITHOUT INITIAL IMPERFECTIONS WHEN IN-PLANE DEFLECTION AND INDUCED STRESSES ARE LIMITED.

Clause 14.8 of the British code, reproduced as Appendix 1, gives recommendations for the lateral support of solid and laminated beams of rectangular section with depth to breadth ratios ranging from 2 to 7. Increasingly stringent lateral support is required as the ratio increases.

It is recognised that this method does not allow correctly for the lateral buckling behaviour of beams as described in a 1964 report by Hooley and Madsen, which makes reference to background papers dating back to 1899. Taking proper account of this work would give prominence to the factor $\ell h/b^2$ rather than h/b, where ℓ, h and b are the span, depth and breadth of the member, and this has been done in the codes of practice of certain other countries.

The complete design procedure for a beam involves also making calculations to ensure that the in-plane deflection is acceptable and that the permissible bending and shear stresses are not exceeded. If this whole procedure is taken into account, adding the avoidance of lateral buckling as a further criterion governing the design, some different conclusions are found.

The following study will make use of formulae which are simplified by certain approximations. Only uniformly-distributed loading will be considered, and this is assumed to be applied at the level of the longitudinal axis of the beam. Somewhat different numerical results are obtained by applying the load at the top or bottom of the beam (Larsen, 1975, CIB-W18 paper 5-10-1).

Design for in-plane behaviour

The design process excluding lateral stability is illustrated by the solid lines in Figures 1 and 2, which relate to span charts of a form published by TRADA but modified to plot permissible load per unit length against span rather than against h/ℓ ratio as in the published charts. The chart uses oblique logarithmic axes to obtain a straight-line representation of the plotted values, with clear distinction between the zones where the design is governed by deflection, bending stress and shear stress.

Addition of the lateral buckling criterion

In the simplified form, the well-known expression for the critical uniform load is

$$w_{cr}\ell = \frac{28.3}{\ell^2}\sqrt{EI_y\,GJ} \qquad \text{(Timoshenko \& Gere, p.269)}$$

where w_{cr} = critical load, N/mm
E = Young's modulus
I_y = second moment of area for bending in the lateral direction
G = shear modulus, taken as E/16
J = torsion constant

$$\text{then} \quad w_{cr}\ell = \frac{28.3}{\ell^2}\sqrt{E\,\frac{hb^3}{12}\,\frac{E}{16}\,\frac{hb^3}{3}}$$

$$w_{cr} = 1.179\,E\,\frac{hb^3}{\ell^3}$$

In Figure 1 the three-part solid line gives the permissible load (N/mm) plotted against span for a particular member size b x h mm, considering only the in-plane behaviour. The top part of the solid line is the region governed by in-plane deflection, the vertical part is governed by the permissible bending stress and the bottom sloping part by shear stress.

The dashed line represents the permissible load (N/mm) governed by lateral buckling, plotted for the same size of member from the expression derived above. It is parallel to the upper part of the line, where in-plane deflection governs, and must lie below this solid line for lateral buckling to have any relevance in the design process.

The equation of the solid line for in-plane deflection is

$$w = \frac{12}{625}\,E\,\frac{bh^3}{\ell^3}$$

If the dashed line coincides with this, then inserting a load factor of 1.5 against lateral buckling,

$$\frac{12}{625}\,E\,\frac{bh^3}{\ell^3} = \frac{1.179}{1.5}\,E\,\frac{hb^3}{\ell^3}$$

$$\text{giving} \quad \frac{h}{b} = 6.4$$

as the value which must be exceeded if lateral buckling is to have any relevance.

Although obtained in a very simple manner this is a surprising result because it indicates that the h/b ratio does after all assume importance in practical design calculations, where there is generally a limitation on the in-plane deflection. The limitation incorporated in the above formula for in-plane deflection is 0.003 times the span, and the value derived for h/b would change for some other limitation. However, the result 6.4 is independent of the type of timber, so will have a wide validity where the 0.003 limitation is adopted.

CONDITIONS FOR LATERAL BUCKLING TO GOVERN DESIGN

Bending stress critical for in-plane calculations

In addition to the condition $h/b \geq 6.4$, a further condition for lateral buckling to govern is that the span must be greater than its value at the point where the dashed line of Figure 1 intersects with the vertical line.

At this point, which will be called the lateral/Bending intersection (lat/B),

$$1.179 \frac{E}{1.5} \frac{hb^3}{\ell^3} = \frac{4}{3} f_b b \frac{h^2}{\ell^2}$$

$$\text{giving} \quad \ell = 0.59 \frac{E}{f_b} \frac{b^2}{h}$$

In this expression f_b is the in-plane permissible bending stress.

Thus the two conditions for lateral buckling to govern in Figure 1 are

$$h/b > 6.4$$

$$\text{and} \quad \ell > 0.59 \frac{E}{f_b} \frac{b^2}{h}$$

Above the lat/B intersection the permissible load per mm is

$$w_{cr} = 1.179 \frac{E}{1.5} \frac{hb^3}{\ell^3}$$

Along the vertical line below the lat/B intersection, in-plane bending stress governs the design giving the permissible load per mm as

$$w = \frac{4}{3} f_b b \left(\frac{h}{\ell}\right)^2$$

Shear stress critical for in-plane calculations

For the condition shown in Figure 2 to occur, the lateral/Shear (lat/S) intersection must fall below the B/S intersection.

At the lat/S intersection,

$$1.179 \frac{Eh}{1.5} \left(\frac{b}{\ell}\right)^3 = \frac{4}{3} f_v b \left(\frac{h}{\ell}\right)$$

$$\text{yielding} \quad \ell = 0.768b \sqrt{\frac{E}{f_v}}$$

The B/S intersection is $\ell = h \frac{f_b}{f_v}$ and if this coincides with the lat/S intersection

$$h \frac{f_b}{f_v} = 0.768b \sqrt{\frac{E}{f_v}}$$

$$\frac{h}{b} = \frac{0.768}{f_b} \sqrt{Ef_v}$$

The right hand side of this expression will be a constant for the particular timber concerned, so again the h/b ratio is the factor which decides whether lateral buckling influences the design.

More extended calculations are available, dealing with cases where there is no vertical portion in the solid line, and giving numerical examples.

CONCLUSION FOR CALCULATIONS ASSUMING NO INITIAL IMPERFECTIONS

The above calculations have dealt only with the case of uniform load applied at the level of the centroidal axis in beams of rectangular section. The beams are assumed to be straight, making no allowance for the effect of initial curvature or other imperfections. However, the calculations are valid in relation to the paper by Hooley and Madsen, which also takes no account of initial imperfections. There is thus a broad indication that the type of lateral restraint recommendation appearing in the British code, i.e. based on h/b ratios as shown in Appendix 1, does after all have a rational basis.

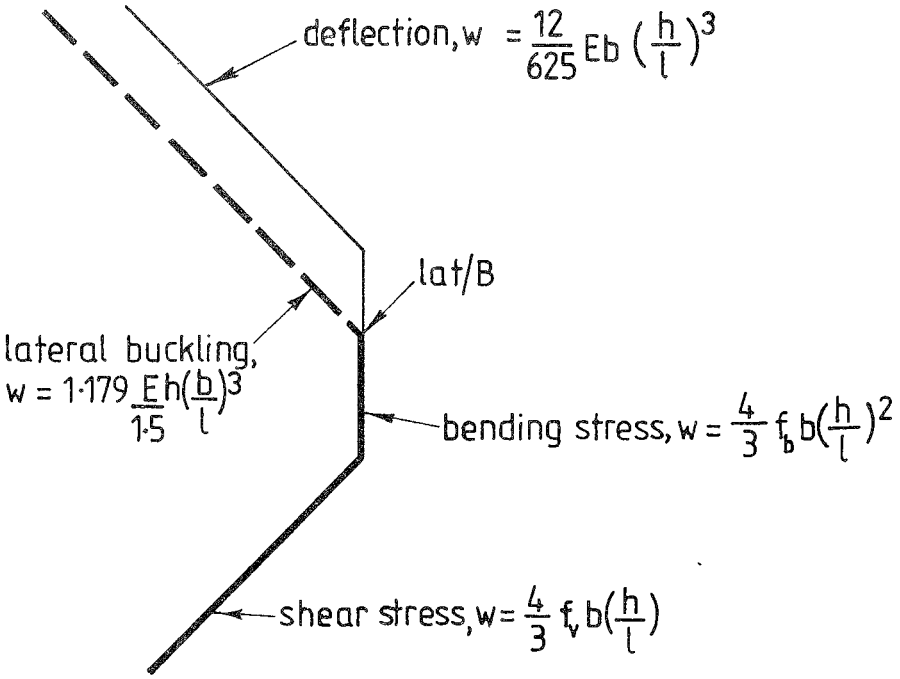


Figure 1
of Part 1

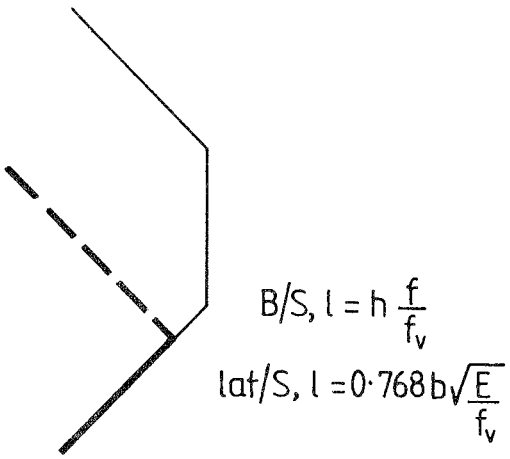


Figure 2
of Part 1

APPENDIX 1 OF PART 1

Clause 14.8 of BS 5268: Part 2: 1984

14.8 Lateral support

The depth to breadth ratio of solid and laminated beams of rectangular section should be checked to ensure that there is no risk of buckling under design load. Alternatively, the recommendations of table 17 should be followed.

Table 17. Maximum depth to breadth ratios (solid and laminated members)

Degree of lateral support	Maximum depth to breadth ratio
No lateral support	2
Ends held in position	3
Ends held in position and member held in line, as by purlins and tie-rods	4
Ends held in position and compression edge held in line, as by direct connection of sheathing, deck or joists.	5
Ends held in position and compression edge held in line, as by direct connection of sheathing, deck or joists, together with adequate bridging or blocking spaced at intervals not exceeding 6 times the depth.	6
Ends held in position and both edges held firmly in line.	7

PART 2 - LATERAL BUCKLING OF RECTANGULAR-SECTION DEEP TIMBER BEAMS WITH ALLOWANCE FOR INITIAL IMPERFECTIONS.

The basic calculations leading to the expressions presented by Hooley and Madsen take a form analogous to those made by Euler for columns, assuming the beam is perfectly straight and untwisted before loading. In later developments of column theory by Ayrton and Perry (1886), followed by experimental work by Robertson (1925), allowance was made for initial imperfections to improve the practical application of column theory, and similar proposals have been made by Flint (1950) and Larsen and Theilgaard (1979), for the application of lateral buckling theory.

Flint's paper explores the possibility of allowing for imperfections by a combination of initial twist and initial lateral curvature (both sinusoidal), although his final recommendation for practice is to simplify application of the results by adopting initial curvature alone and to represent the effect of all other anomalies by an equivalent value of the initial central deviation from straightness.

The work below develops Flint's approach in a different way to allow a much greater degree of simplification in the formation of an expression for use in practical design.

THEORY FOR LATERAL BUCKLING

As a step towards achieving simplification, it is necessary to show the work leading to the results for a beam without initial imperfections, as use will be made of these results when developing the solution for a beam with initial twist and curvature. The work will be limited to buckling under equal end moments because the introduction of initial imperfections would otherwise lead to great complication and because equal end moments will allow conservatively for other load cases. The symbol 'I' will always refer to the weak direction, and 'Z' to the stiff direction of bending.

Initially straight beam

With no initial curvature or twist the differential equations for a deep beam of rectangular section loaded by equal end moments M are

$$E\,I\,\frac{d^2v}{dz^2} - M = 0 \qquad (1)$$

$$E\,I\,\frac{d^2u}{dz^2} - \gamma M\,\phi = 0 \qquad (2)$$

$$C\,\frac{d\phi}{dz} + M\,\frac{du}{dz} = 0 \qquad (3)$$

where v and u are the vertical and lateral deflection of the centre line, z is the distance along the axis, ϕ is the twist and $\gamma = 1 - \frac{b^2}{d_2}$.

EI is the flexural rigidity in the lateral (weak) direction and C = GJ is the torsional rigidity. In later work for rectangular sections G will be taken as E/16 and the torsion constant will take the value $J = \frac{hb^3}{3}\left(1 - 0.63\,\frac{b}{h}\right)$ as given for example by Timoshenko (1934, page 249).

Differentiating (3),

$$\frac{d^2u}{dz^2} + \frac{C}{M}\frac{d^2\phi}{dz^2} = 0$$

From (2) $$\frac{d^2u}{dz^2} - \frac{\gamma M}{EI}\phi = 0$$

Subtracting to eliminate $\frac{d^2u}{dz^2}$

$$\frac{C}{M}\frac{d^2\phi}{dz^2} + \frac{\gamma M}{EI}\phi = 0$$

$$\frac{d^2\phi}{dz^2} + k^2\phi = 0 \qquad \text{where } k = M\sqrt{\frac{\gamma}{CEI}}$$

This is closely comparable with the case for a straight column and may be solved in a similar way to give

$$\phi = A \sin kz \quad = 0 \text{ when } z = \ell \text{ so that}$$

$$\sin k\ell = 0$$

$$k\ell = \pi$$

$$k = M\sqrt{\frac{\gamma}{CEI}} = \frac{\pi}{\ell}$$

$$M_{cr} = \frac{\pi}{\ell}\sqrt{\frac{CEI}{\gamma}}$$

For later use it will be convenient to know the relation between the twist ϕ and the lateral deflection u. The twist is A sin $\frac{\pi}{\ell}$ z and u may be found from (2) above, which gives with ϕ inserted

$$\frac{d^2u}{dz^2} = \gamma\frac{AM}{EI}\sin\frac{\pi}{\ell}z$$

$$\frac{du}{dz} = -\frac{\ell}{\pi}\gamma\frac{AM}{EI}\cos\frac{\pi}{\ell}z + E$$

when $z = \frac{\ell}{2}$, $\frac{du}{dz} = 0$ so $E = 0$

$$u = -\frac{\ell^2}{\pi^2} \gamma \frac{AM}{EI} \sin \frac{\pi}{\ell} z + F$$

when $z = 0$, $u = 0$ so $F = 0$

at centre, $u = -\frac{\ell^2}{\pi^2} \gamma \frac{AM}{EI}$

when $M = M_{cr}$,

$$u = -\frac{\ell^2}{\pi^2} \gamma \frac{A}{EI} \times \frac{\pi}{\ell} \sqrt{\frac{CEI}{\gamma}}$$

$$= -\frac{\ell}{\pi} A \sqrt{\frac{C\gamma}{EI}}$$

- where A is the undetermined amplitude of twist.

Beam with initial twist

As mentioned already, Flint (1950) works out the solution for a beam with initial twist and lateral deflection, but later takes the case with deflection alone as a simplification. In fact a simpler solution is obtained with initial twist alone and this is similar to the result for a column with initial curvature.

With an initial twist $\phi_o \sin \frac{\pi}{\ell} z$, if the end moments cause an additional twist ϕ_1 the differential equation given above for a straight beam becomes

$$\frac{C}{M^2} \frac{EI}{\gamma} \frac{d^2\phi_1}{dz^2} = -(\phi_o + \phi_1)$$

$$\frac{d^2\phi_1}{dz^2} + \frac{\gamma M^2}{CEI} \phi_1 = -\frac{\gamma M^2}{CEI} \phi_o \sin \frac{\pi}{\ell} z$$

$$\frac{d^2\phi_1}{dz^2} + k^2\phi_1 = -k^2\phi_o \sin \frac{\pi}{\ell} z \text{ where } k = M \sqrt{\frac{\gamma}{CEI}}$$

giving the solution

$$\phi_1 = \frac{1}{\frac{\pi^2}{\ell^2} \frac{CEI}{M^2\gamma} - 1} \phi_o \sin \frac{\pi}{\ell} z$$

$$= \frac{1}{\left(\frac{M_{cr}}{M}\right)^2 - 1} \phi \sin \frac{\pi}{\ell} z$$

writing $\alpha = \left(\frac{M}{M_{cr}}\right)^2$

$$\phi_1 = \frac{1}{\frac{1}{\alpha} - 1}\ \phi_o \sin\frac{\pi}{\ell}z = \frac{\alpha}{1-\alpha}\phi_o \sin\frac{\pi}{\ell}z$$

The total angle of twist is

$$\phi = \phi_o + \phi_1 = \phi_o \sin\frac{\pi}{\ell}z + \frac{\alpha}{1-\alpha}\phi_o \sin\frac{\pi}{\ell}z$$

$$\phi = \frac{\phi_o}{1-\alpha}\sin\frac{\pi}{\ell}z$$

The symbol $\alpha = \left(\frac{M}{M_{cr}}\right)^2$ has been used to emphasise the similarity between the results for lateral buckling of beams and those for columns where $\alpha = \frac{P}{P_e}$ has been used.

Beam with both initial twist and initial lateral curvature

With the two kinds of imperfection the differential equations become

$$EI\ \frac{d^2u_1}{dz^2} - \gamma M(\phi_1 + \phi_o) = 0 \qquad \text{(4)}$$

$$C\ \frac{d\phi_1}{dz} + M\frac{d(u_1 + u_o)}{dz} = 0 \qquad \text{(5)}$$

where the initial curvature is expressed as $u_o \sin\frac{\pi}{\ell}z$
Differentiating (5),

$$C\frac{d^2\phi_1}{dz^2} + M\frac{d^2u_1}{dz^2} + M\frac{d^2u_o}{dz^2} = 0$$

or

$$\frac{d^2u_1}{dz^2} + \frac{C}{M}\frac{d^2\phi_1}{dz^2} + \frac{d^2u_o}{dz^2} = 0$$

and from (4)

$$\frac{d^2u_1}{dz^2} - \gamma\frac{M}{EI}(\phi_1 + \phi_o) = 0$$

Subtracting,

$$\frac{C}{M}\frac{d^2\phi_1}{dz^2} + \gamma\frac{M}{EI}(\phi_1 + \phi_o) + \frac{d^2u_o}{dz^2} = 0 \qquad \text{(6)}$$

This is the same as equation (7) of Flint (1950), who then proceeds to a solution of the differential equation followed by calculations of a type shown below, to find the maximum combined stress due to in-plane bending, lateral buckling and torsion. When this expression is equated to the

permissible value, a cubic equation is obtained for σ_b, the maximum permissible value of the applied bending stress. Flint puts $\phi_o = 0$ in the cubic equation to obtain graphs for only one of the initial imperfections, i.e. u_o. With the computer it is now easy to make u iterative calculations allowing graphs to be computer-plotted for cases including either or both of the imperfections. The remainder of Flint's development and example graphs are given in an extended version of this paper, which may be obtained from the author.

Beam with related twist and curvature

In the column theory adopted as a design basis for the CIB Code, a simple solution was obtained for an initially curved column by assuming an initial curvature of the same form as the deflection after buckling in the initially straight column. It may be conjectured that an analogous result could be obtained for the lateral buckling of a beam by relating u_o and ϕ_o in the same way that u and ϕ after buckling are related in an initially straight and untwisted beam, and this possibility will now be examined.

The required relation was found at the end of the section above for a straight beam and the expression needed for u_o is

$$u_o = -\frac{\ell}{\pi}\sqrt{\frac{Cx}{EI}}\ \phi_o \sin\frac{\pi}{\ell}z$$

Differentiating this twice and inserting the result in equation (6) gives

$$\frac{d^2\phi_1}{dz^2} + \gamma\frac{M^2}{CEI}(\phi_1 + \phi_o) + \frac{\pi}{\ell}M\sqrt{\frac{\gamma}{CEI}}\,\phi_o \sin\frac{\pi}{\ell}z = 0 \qquad (7)$$

$$\frac{d^2\phi_1}{dz^2} + k^2\phi_1 = -k\left(k + \frac{\pi}{\ell}\right)\phi_o \sin\frac{\pi}{\ell}z$$

Let the particular integral be

$$\Phi = K \sin\frac{\pi}{\ell}z$$

$$\frac{d\Phi}{dz} = K\frac{\pi}{\ell}\cos\frac{\pi}{\ell}z$$

$$\frac{d^2\Phi}{dz^2} = -K\frac{\pi^2}{\ell^2}\sin\frac{\pi}{\ell}z$$

Inserting these in the differential equation,

$$-K\frac{\pi^2}{\ell^2}\sin\frac{\pi}{\ell}z + k^2K\sin\frac{\pi}{\ell}z = -k\left(k + \frac{\pi}{\ell}\right)\phi_o \sin\frac{\pi}{\ell}z$$

Equating the coefficients of $\sin \frac{\pi}{\ell} z$

$$- K \frac{\pi^2}{\ell^2} + k^2 K = -k\left(k + \frac{\pi}{\ell}\right) \phi_o$$

$$K = \frac{- k\left(k + \frac{\pi}{\ell}\right)}{\left(k + \frac{\pi}{\ell}\right)\left(k - \frac{\pi}{\ell}\right)} \phi_o$$

$$= - \frac{k\phi}{k - \frac{\pi}{\ell}} \quad \text{where } k = M \sqrt{\frac{\chi}{CEI}}$$

leading to $$K = \frac{\frac{M}{M_{cr}} \phi_o}{1 - \frac{M}{M_{cr}}}$$

so the particular integral is

$$\Phi = \frac{\frac{M}{M_{cr}} \phi_o}{1 - \frac{M}{M_{cr}}} \sin \frac{\pi}{\ell} z$$

Writing $\mu = \frac{M}{M_{cr}}$ as adopted by Flint, the solution of (7) is then

$$\phi_1 = \frac{\mu \phi_o}{1 - \mu} \sin \frac{\pi}{\ell} z$$

The total angle of twist is

$$\phi = \phi_o + \phi_1 = \phi_o \sin \frac{\pi}{\ell} z + \frac{\mu}{1 - \mu} \phi_o \sin \frac{\pi}{\ell} z$$

$$\phi = \frac{\phi_o}{1 - \mu} \sin \frac{\pi}{\ell} z$$

In the case above for initial twist alone the result similar to this which seemed a simple one contained $\alpha = \left(\frac{M}{M_{cr}}\right)^2$, so the new case with u_o and ϕ_o linked in a special way represents a major simplification even compared with the one for twist alone, and bears a remarkable resemblance to the solution for a column with initial curvature.

Limitation of maximum combined stress

Figure 1 extracted from Flint's work illustrates his calculation of the maximum fibre stress at mid span by summing the three components

(a) the stress $\frac{M}{Z}$ arising from vertical deflection

(b) the stress due to lateral deflection from position (a) to position (b) in Figure 1, given by $\frac{Eb}{2}\frac{d^2u_1}{dz^2}$

(c) the stress caused by torsion at the inside of the top flange in the I-beam he considers. The additional lateral displacement due to torsion is $\frac{h}{2}\phi_1$ where h is the height of the cross-section, and the increase in compressive stress due to this effect is

$$-\frac{Eb}{2}\left(\frac{h}{2}\frac{d^2\phi_1}{dz^2}\right)$$

Adding the three effects gives

$$\sigma_{max} = \frac{M}{Z} + \frac{Eb}{2}\left[\frac{d^2u_1}{dz^2} - \frac{h}{2}\frac{d^2\phi_1}{dz^2}\right] \qquad (8)$$

From equation (4)

$$E\,I\frac{d^2u_1}{dz^2} = \gamma M(\phi_1 + \phi_o)$$

$$= \gamma M\frac{\phi_o}{1-\mu}\sin\frac{\pi}{\ell}z$$

For $\frac{d^2\phi_1}{dz^2}$ where ϕ_1 is the additional rotation

$$\phi_1 = \frac{\mu\phi_o}{1-\mu}\sin\frac{\pi}{\ell}z$$

$$\frac{d\phi_1}{dz} = \frac{\pi}{\ell}\frac{\mu\phi_o}{1-\mu}\cos\frac{\pi}{\ell}z$$

$$\frac{d^2\phi_1}{dz^2} = -\frac{\pi^2}{\ell^2}\frac{\mu\phi_o}{1-\mu}\sin\frac{\pi}{\ell}z$$

Inserting the central values in (8),

$$\sigma_{max} = \frac{M}{Z} + \frac{Eb}{2}\left[\frac{\gamma M}{EI}\,\frac{\phi_o}{(1-\mu)} + \frac{h}{2}\,\frac{\pi^2}{\ell^2}\,\frac{\mu\phi_o}{(1-\mu)}\right]$$

For a rectangular cross-section this can be manipulated into the form

$$\sigma_{max} = \frac{M}{Z} + \frac{\phi_o}{1-\mu}\,\frac{h}{b}\left[\gamma\frac{M}{Z} + E\,\frac{\pi^2}{4}\,\left(\frac{b}{\ell}\right)^2\mu\right]$$

and if σ_{max} is limited to the permissible bending stress f_b

$$f_b = \sigma_b + \frac{\phi_o}{1-\mu}\,\frac{h}{b}\left[\gamma\sigma_b + \frac{2}{4}E\,\left(\frac{b}{\ell}\right)^2\mu\right]$$

Dividing through by f_b and using the symbol f_{cr} rather than σ_{crit} for the critical stress

$$1 = \frac{\sigma_b}{f_b} + \frac{\phi_o}{1-\frac{\sigma_b}{f_{cr}}}\,\frac{h}{b}\left[\gamma\frac{\sigma_b}{f_b} + \frac{\pi^2}{4}\,\frac{E}{f_b}\,\left(\frac{b}{\ell}\right)^2\frac{\sigma_b}{f_{cr}}\right] \qquad \text{(9)}$$

Although this is only a quadratic in σ_b instead of a cubic equation, it is still convenient to solve iteratively in a simple computer program, and the computer-plotted results are shown in Figure 2 for $\phi_o = 0.0001\,\ell/b$, with of course the related value of u_o incorporated in the behaviour. It is seen that the curves have a shape similar to Perry-Robertson column curves, but meet the vertical axis slightly below $\sigma_b/f_b = 1.0$.

The curves are drawn for the single value of $h/b = 8$, and for E/f_b values of 400, 800 and 1200. Corresponding curves are shown for a beam without initial imperfections.

Computed relationships

The complete set of relationships included in the computer program is as follows for a tall rectangular cross-section of depth h and breadth b.

$$h/b = 8$$

$$\phi_o = 0.0001\,\ell/b$$

$$M_{cr} = \frac{\pi}{\ell}\sqrt{\frac{EIGJ}{\gamma}} = \frac{\pi}{\ell}\sqrt{\frac{E}{\gamma} \times \frac{hb^3}{12} \times \frac{E}{16} \times \frac{hb^3}{3}\left(1 - 0.63\,\frac{b}{h}\right)}$$

$$= \frac{\pi}{\ell} E \frac{hb^3}{24} \sqrt{\frac{1 - 0.63\,\frac{b}{h}}{1 - \left(\frac{b}{h}\right)^2}}$$

$$f_{cr} = \frac{M_{cr}}{Z} = \frac{\pi}{\ell} E \frac{hb^3}{24} \frac{6}{bh^2} \sqrt{\frac{1 - 0.63\frac{b}{h}}{1 - \left(\frac{b}{d}\right)^2}}$$

$$\frac{f_{cr}}{f_b} = \frac{\pi}{4} \frac{b}{\ell} \frac{b}{h} \frac{E}{f_p} \sqrt{\frac{1 - 0.63\,\frac{b}{h}}{1 - \left(\frac{b}{h}\right)^2}}$$

$$\mu = \frac{M}{M_{cr}} = \frac{\sigma_b}{f_{cr}} = \frac{\sigma_b}{f_b} \frac{f_b}{f_{cr}}$$

To plot the permissible values of $\frac{\sigma_b}{f_b}$ against $\frac{\ell}{b}$ from (11), the computer program sets values for $\frac{E}{f_b}$ and $\frac{\ell}{b}$, increments $\frac{\sigma_b}{f_b}$ in fine steps until the expression on the right hand side exceeds unity and then by interpolation calculates the value of $\frac{\sigma_b}{f_b}$ making the expression equal to unity.

Exclusion of torsion term

For the particular ratio h/b = 8, the second term in the square bracket of (9) has only a small effect on the graphs of Figure 2. This can be seen from the fact that eliminating this torsion term has the effect of making the curves terminate at $\sigma_b/f_b = 1.0$ instead of slightly below this point.

Leaving out the torsion term gives

$$1 = \frac{\sigma_b}{f_b}\left[1 + \frac{\eta'}{1 - \frac{\sigma_b}{f_{cr}}}\right] \qquad \text{(10)}$$

where $\eta' = \frac{h}{b}\phi_o$

In the case for which Figure 2 is plotted $\phi_0 = 0.0001\,\ell/b$ and

$$\eta' = 0.0001\,\gamma\frac{h\ell}{b^2}$$

so the factor $h\ell/b^2$ retains the same importance as in the theory without initial imperfections. For Figure 2, $h/b = 8$ and $\gamma = 1 - b^2/h^2 = 0.9844$.

$$\text{so } \eta' = 0.0008 \frac{\ell}{b} \text{ in Figure 2.}$$

These expressions correspond very closely with those for columns. A formula similar to the Perry-Robertson expression is found by solving (10) for σ_b to give

$$\sigma_b = \frac{f_b}{2} + \tfrac{1}{2}(1 + \eta')f_{cr} - \sqrt{\left\{\frac{f_b}{2} + \tfrac{1}{2}(1 + \eta')f_{cr}\right\}^2 - f_b f_{cr}} \qquad (11)$$

or

$$\frac{\sigma_b}{f_b} = \tfrac{1}{2} + \tfrac{1}{2}(1 + \eta')\frac{f_{cr}}{f_b} - \sqrt{\left\{\tfrac{1}{2} + \tfrac{1}{2}(1 + \eta')\frac{f_{cr}}{f_b}\right\}^2 - \frac{f_{cr}}{f_b}}$$

$$\text{with } f_{cr} = \frac{\pi}{Z\ell}\sqrt{\frac{EIGJ}{\gamma}} \quad \text{and} \quad \eta' = \gamma\frac{h}{b}\phi_o$$

Conclusion for calculation with initial imperfections

A proposal was made some years ago for the British code (Ozelton, 1973) in which expression (11) was put forward without the theoretical background given above, with the idea that it would be beneficial if the presentation of formulae for beam buckling could show a consistency of form with the Perry-Robertson formula for struts.

Where approaches similar to that of Hooley and Madsen have been adopted in codes, it has been necessary to apply a transition curve over the range of smaller ℓ/b values, to approach the value $\frac{\sigma_b}{f_b} = 1.0$. Different artificial curves have been adopted as described by Larsen (1975, CIB-W18 paper 5-10-1). With the background theory now provided it seems greatly preferable to adopt code rules based on (11) in harmony with the theory for solid columns. It would be especially meaningful to do so in the centenary year of the article that led to the Perry-Robertson formula (Ayrton and Perry, 1886).

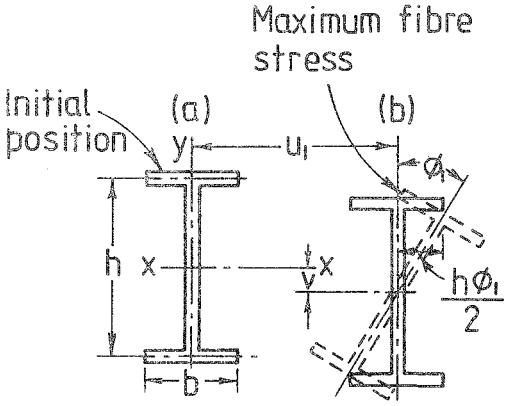


Figure 1
of Part 2

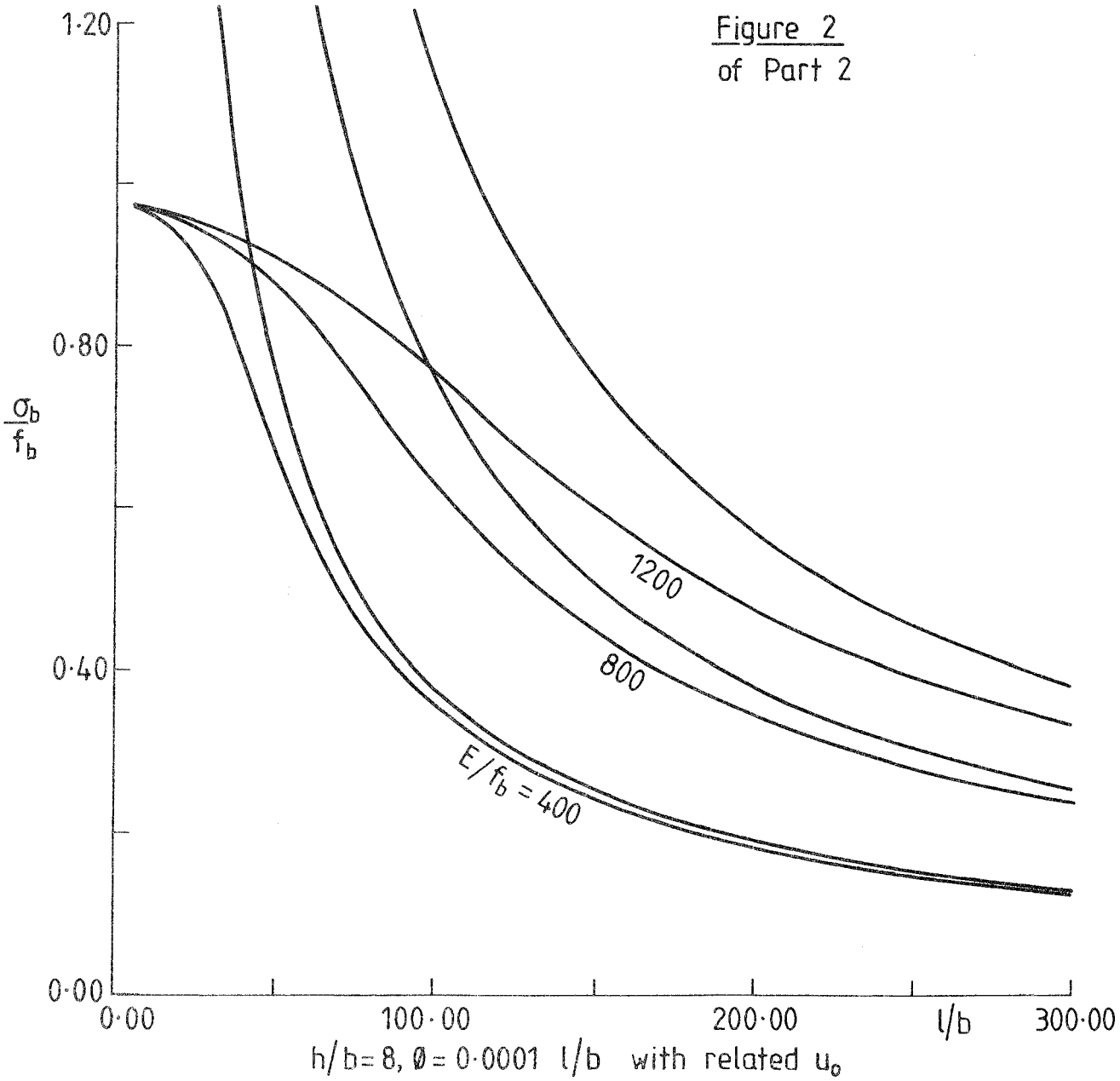


Figure 2
of Part 2

REFERENCES

Ayrton, W E and Perry, J (1886) - On struts. The Engineer, 10 and 24 December 1886, Vol 62 (1886), pp 464-5 and 513-5.

Burgess, H J (1971) - Further applications of TRADA span charts, TRADA technical brochure TBL42, 1971.

Burgess, H J and Masters, M A (1976) - Span charts for solid timber beams (revised edition 1976). TRADA technical brochure TBL34.

Flint, A R (1950) - The stability and strength of slender beams. Engineering, 22 December 1950.

Hooley, R F and Madsen, B (1964) - Lateral stability of glued laminated beams. J l. Structural Div. ASCE, Vol 90 No. ST3, June 1964.

Larsen, H J (1975) - The design of timber beams. International Council for Building Research Studies and Documentation. Paper No. CIB-W18 5-10-1, Karlsrühe, October 1975.

Larsen, H J and Theilgaard, E (1979) - Laterally loaded timber columns. J l. Structural Div. ASCE, Vol 105 No. ST7, July 1979.

Ozelton, E C (1973) - The buckling of timber beams. Paper for working group on stability, BS5268 working stresses sub-committee, May 1973.

Robertson, A (1925) - The strength of struts. ICE selected engineering papers No. 28.

Timoshenko, S (1934) - Theory of Elasticity, 1st edition, McGraw-Hill, London 1934.

Timoshenko, S P and Gere J M (1961) - Theory of elastic stability, 2nd edition, McGraw-Hill, London 1961.

CIB-W18/19-11-1

INTERNATIONAL COUNCIL FOR BUILDING RESEARCH STUDIES AND DOCUMENTATION

WORKING COMMISSION W18 - TIMBER STRUCTURES

EXPERIMENTAL ANALYSIS ON ANCIENT DOWNGRADED TIMBER STRUCTURES

by

B Leggeri and L Paolini
University of Florence
Italy

MEETING NINETEEN
FLORENCE
ITALY
SEPTEMBER 1986

1. INTRODUCTION

The following analysis arose because the Department of Constructions of Florence University was commissioned by the Public Works Department of the borough of Jesi to carry out a set of experimental tests on some of the wooden floor-boards in the G.B. Pergolesi theatre.

This theatre shows, within the boundary of the masonry structures, a complex wooden structural organism with horizontal and vertical elements which constitute the structures of the different stall levels, of the ceiling and the roof. A big part of the overall wooden structure of the theatre shows, paricularly in its horizontal structures which are made with a white regional fir tree, a considerable deterioration caused by the Hilotrupes Baiolus, a xylophage insect able to produce holes 4-6 mm wide.

The several treatments tried on the test pieces,obtained from the samples taken "in situ", have shown the possibility of restoring in the deteriorated wood the original mechanical properties. In this way it is possible to avoid those replacements, usual in the practice of restoration, which sometimes cause the distruction of some types of constructions which are of great interest and the lost of a unique heritage.

2. EXPERIMENTAL CAMPAIGN

2.1. Samples

Four pieces of beam, about 1 m long, were selected and removed from the horizontal structures of the ceiling above the first stalls.These samples, which appeared considerably deteriorated by the xylophage insect mentioned above, were considered particularly suitable to a comparative analysis betwen test pieces before and after consolidation (Fig.I).

2.2. Test Pieces

The test pieces were obtained from the four semples, denoted

by the letters A,B,C,D, the cuts done during their preparation showed tha the insect of the Hilotrupes Bajolus, in this particular case, was concentrated in the boundary region (sapwood) of the transversal section of the beam, whereas the central nucleus (heartwood) of it appeared compact and intact. The test pieces obtained from the four samples were divided into four groups:

- first group:test pieces at the original (not treated) state;
- second group: test pieces treated with an anti-parasitic made with poisonous products in oily suspension and volatile diluting substances and applied to the surface until they were completely imbued;
- third group: treated with Silicate of Sodium (20 Bé)in water solution, applied to the surface up to the total imbuition;
- fourth group: treated with fluid epoxydic resins Araldite-Ciba and corresponding hardening (hardening resins BY 158; hardening HY 2996) applied to the surface up to the total imbuition.

The aim of the experimental tests was to measure the parameters useful to the definition of a possible consolidation of the deteriorated material; with this purpose in mind two different sets of tests were carried out:

O) ordinary tests
physical tests for the definition of:
level of dampness
specific weight
mechanical tests of:
axial compression (Figs. IIa, IIb)
static tangential bending (Figs. IIIa, IIIb, IIIc)

S) special tests
mechanical tests of:
tension test (Figs. IVa, IVb)
definition of the Elasticity Modulus in Com

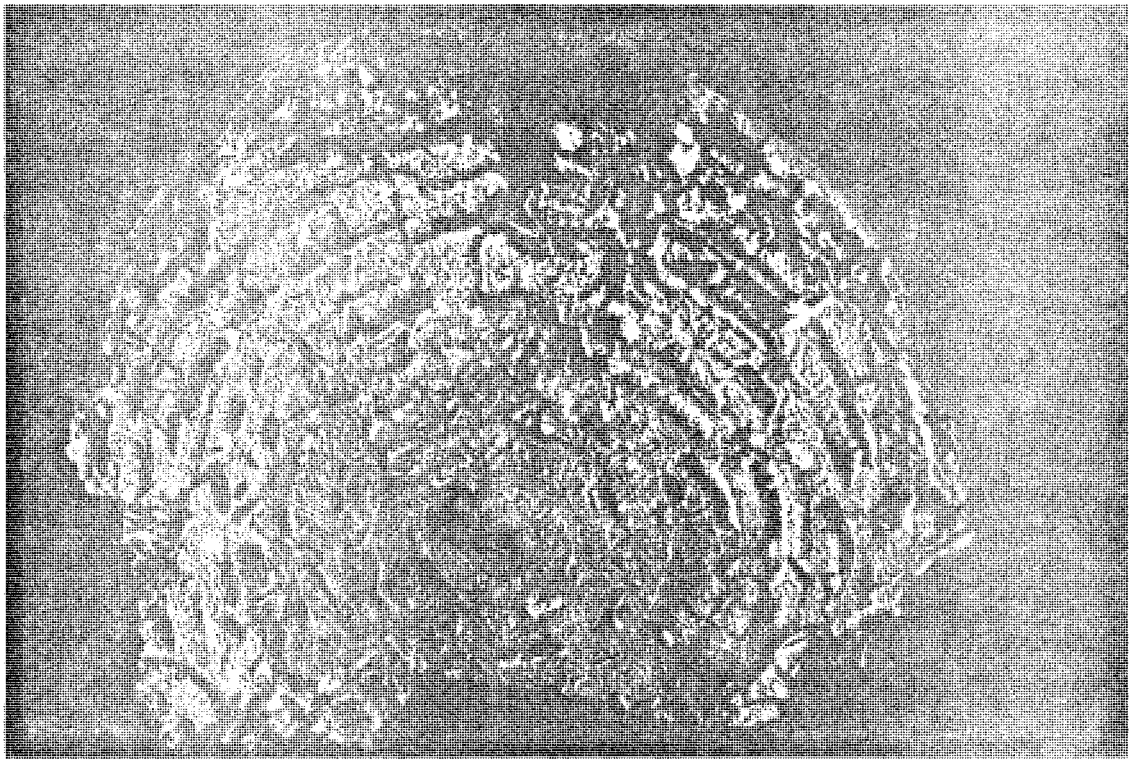
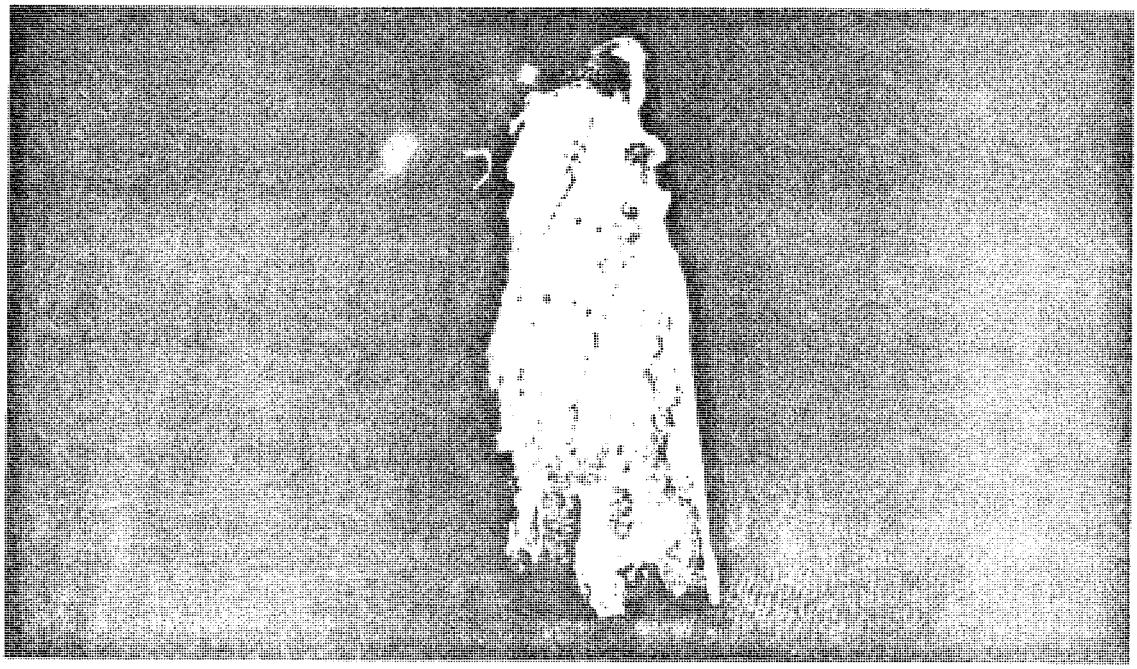
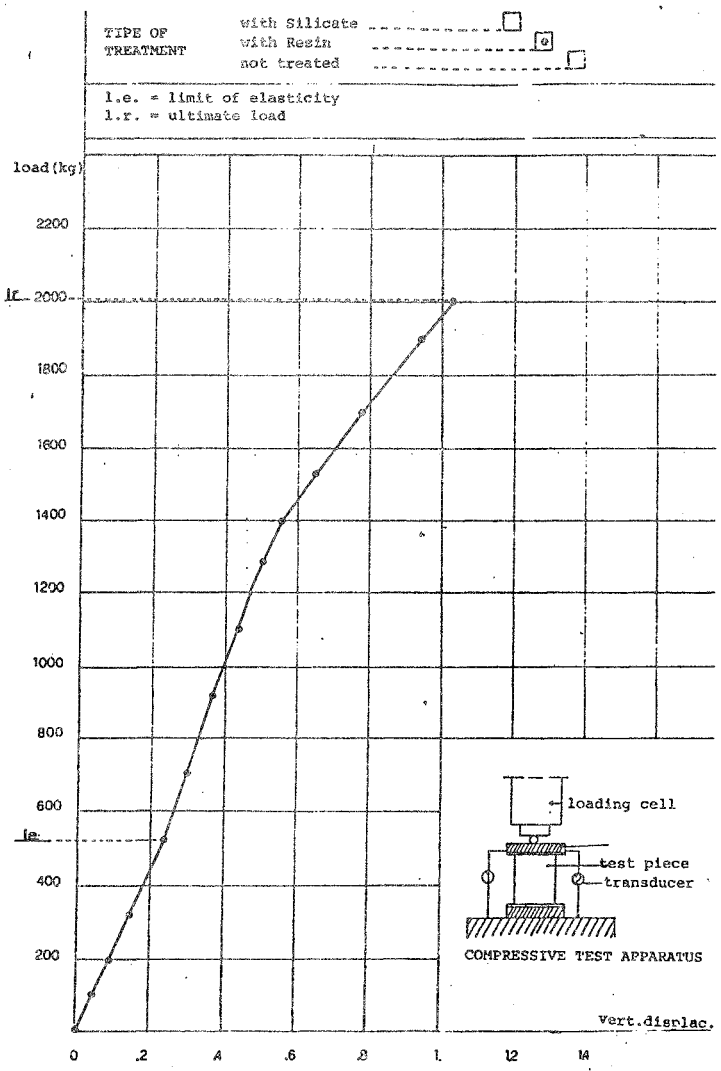


Fig. I

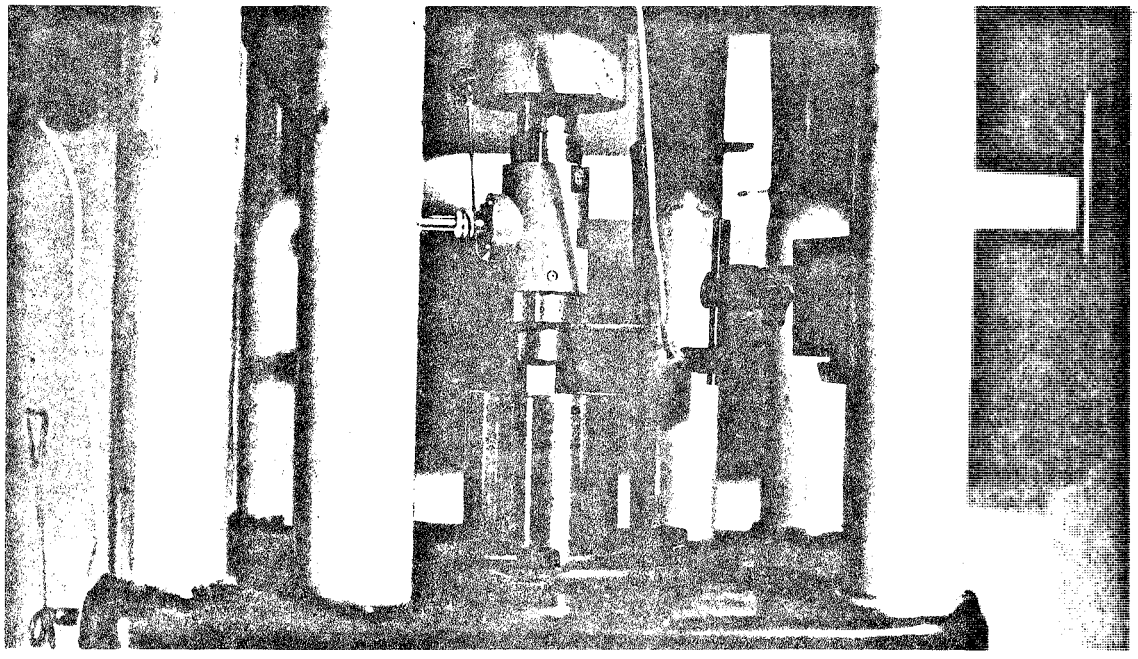


Same load-displacement diagrams are presented in order to show the following figs.

Fig.11 a)



b)



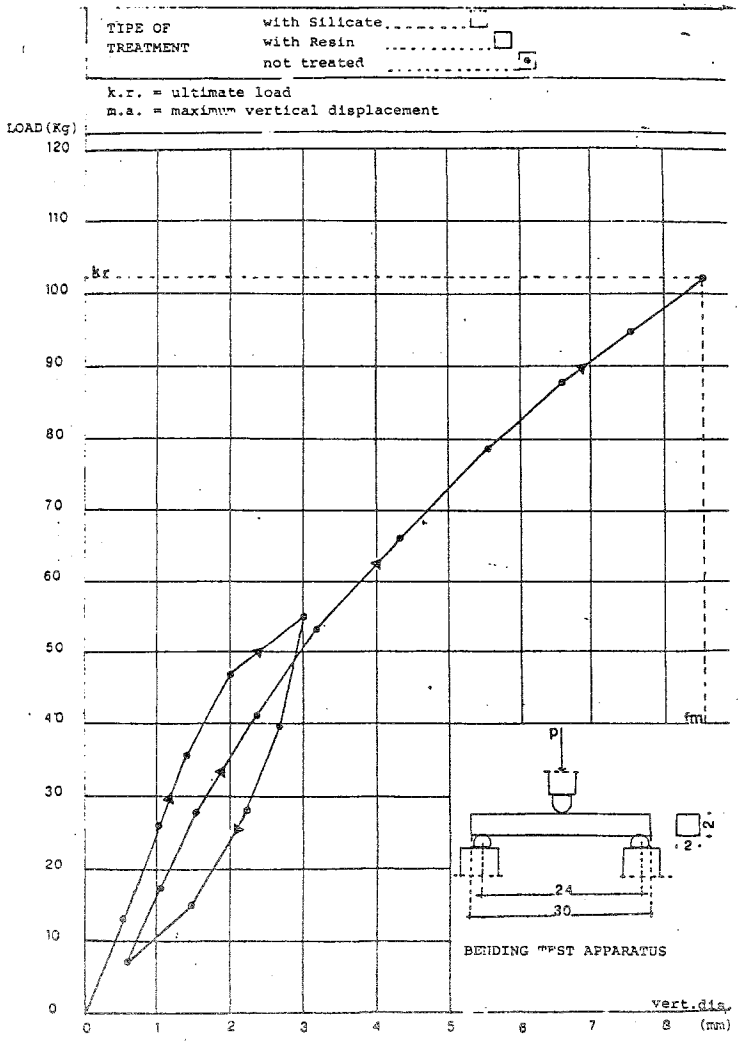

TIPE OF TREATMENT
with Silicate
with Resin
not treated
k.r. = ultimate load
m.a. = maximum vertical displacement
LOAD (Kg)
120
110
100
90
80
70
60
50
40
30
20
10
0
kr
fmi
P
2
2
24
30
BENDING TEST APPARATUS
vert.dis.
0
1
2
3
4
5
6
7
8
(mm)

Fig. III

a)

b)

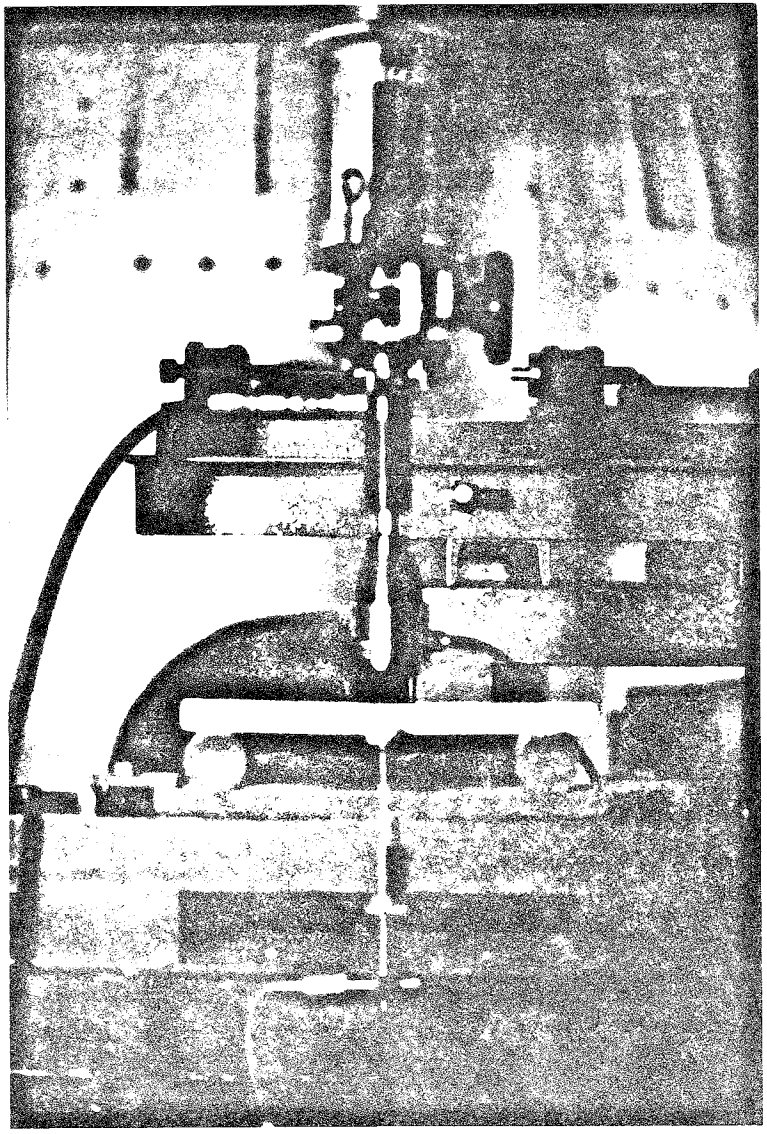
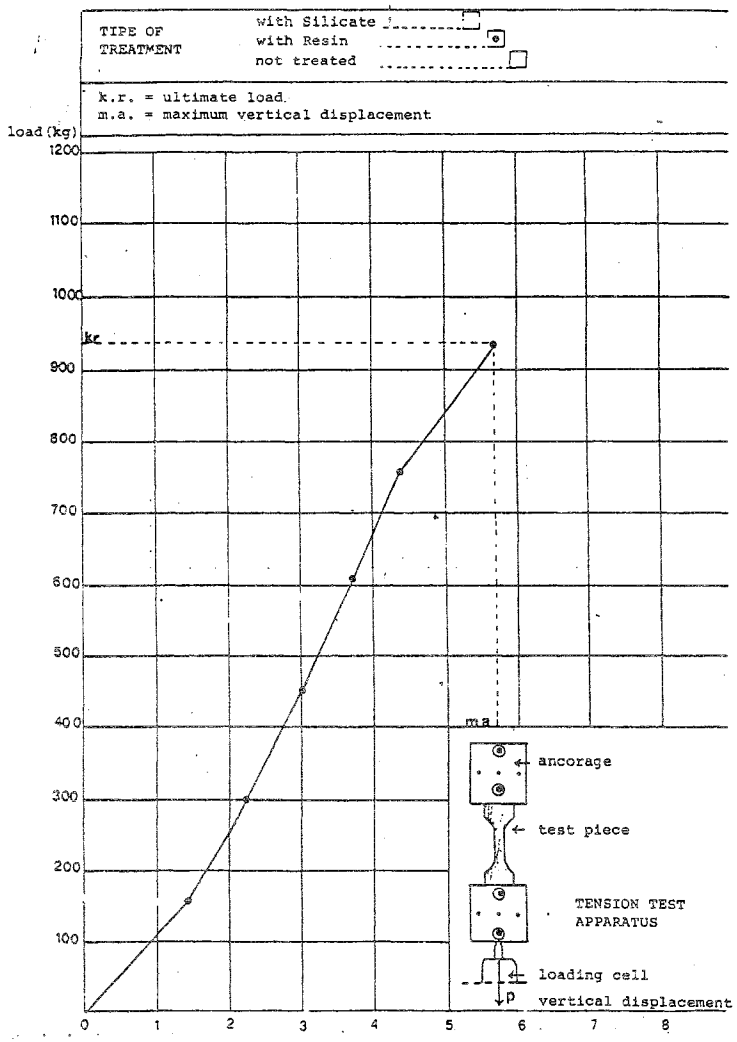
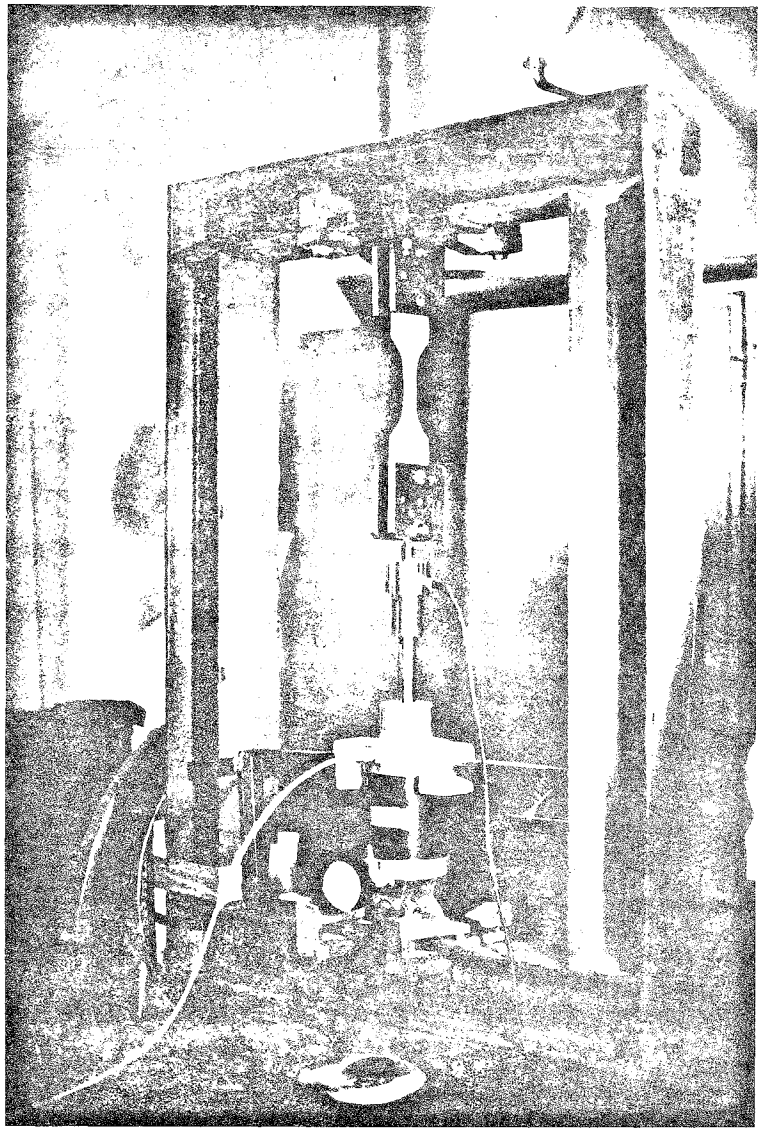


Fig. IV


TIPE OF TREATMENT
with Silicate
with Resin
not treated
k.r. = ultimate load.
m.a. = maximum vertical displacement
load (kg)
1200
1100
1000
900
800
700
600
500
400
300
200
100
kr
ma
0
1
2
3
4
5
6
7
8
ancorage
test piece
TENSION TEST APPARATUS
loading cell
P
vertical displacement

a)

b)



pression, bending and tension
hardness test

As far as it possible, all the best pieces were dimensioned according to the UNI Codes; even the test procedure is in accordance with these Codes.

2.3. Test apparatus

An air circulating oven, with an approximation of $\pm$ 1°C and a BOSCH electronic scale with an approximation of 1/100 of of mm were used for the definition of the dampness level; the same scale was used to define the specific weight.
For both the ordinary mechanical tests (axial compression and tangential elastic bending) and the special tests (definition of the Elasticity Modulus in compression and bending) a fixed metallic frame was used as a support of the test piece and to react to the actions induced by the hydraulic loading apparatus.
The displacements were measured by means of inductive transducers with an approximation of 1/100 of mm and recorded by a portable TDS-301 data logger.
In both the ordinary tensile test and the test for the definition of the Elasticity Modulus in tension, two strain-gauges EA-06-500Gb-120 were applied to each test piece in order to measure the strains, the values of which were recorded by a portable data logger TDS.301 (ASW-30 A/50A).
For the Brinnel test the instrument of the Galileo Laboratory in Milan was used.

3. EXPERIMENTAL RESULTS

The ordinary test for the definition of the dampness level and the specific weight provided the following average values:

- dampness level "u" :

$$11,97\% \leq u \leq 12,05\%$$

- specific weight "D_a" :

$$D_a = 0,49$$

The special test for the definition of the hardness "B_j" in the axial direction provides "B_j"

$$B_j = 426 \text{ Kg}$$

This test was preceded by the definition of the average number of yearly rings on each squared centimeter of radius.
From the mechanical tests carried out in the dampness conditions mentioned above, with a room temperature of 18°C (± 1), the following results were obtained:

(Kg/cm^2)	a	b	c	d
N -axial compression	108	105	119	137
" -tangential bending	185	178	209	273
S -tangential compression	60	61	66	69
" -tension	235	216	242	287

Elasticity Modulus (Kg/cm^2)	a	b	c	d
in axial compression	63	62	78	82
in bending	74	72	86	90
in tension	64	65	74	81

N = ordinary test

S = special test

a = original untreated test piece

b = test piece treated with anti-parasitic

c = test piece treated with Silicate of Sodium

d = test piece treated with epoxydic resin

By comparing the experimental results concerning the original and treated test pieces, one can notice the following changes in percentage in the Elasticity Modulus.

Elasticity Modulus (t /cm^2)	b	c	d
in compression	-	24	30
in bending	-	16	22
in tension	2	16	27

4. CONCLUSIONS AND COMPARISIONS

From the obtained results one can see that the three different kinds of treatment, one can apply to deteriorated wood, are extremely useful. In fact it is possible to say that, after each treatment, wood reverts to the original mechanical strength properties. However, treatment with resins needs a further wood preservative treatment, expecially against fire and parasites. The treatment with Silicate of Sodium in water solution has the double effect of restoring in the material the physical and mechanical properties (Fig. V) and preserving wood against the onset of fire and parasites.Moreover it does not alter its exterior characteristics.

REFERENCES

1) GIORDANO, G.: "Tecnologia del legno" vol. I,II. - Torino, 1981.

2) TAMPONE, G.: "Restauro delle strutture in legno".- In "Legno nel restauro e restauro del legno" Atti del Convegno Nazionale, Firenze 30 nov.-3 dic. 1983, p. 129-158. - Milano, 1983.

3) CECCOTTI, A.: "Le strutture di legno nell'edilizia". - In "L'impiego del legno nell'edilizia: aspetti tradizionali e nuove tecnologie" Atti del Convegno, Bologna 23 marzo 1983, suppl. Inarcos n. 441(1983), p. 6-8.

4) DE VITTORIO, L.; HAJO, S.: "Il recupero delle strutture in legno: indagini sperimentali per il consolidamento del materiale". - Doctoral Dissertation, University of Florence, 1986.

CIB-W18/19-12-1

INTERNATIONAL COUNCIL FOR BUILDING RESEARCH STUDIES AND DOCUMENTATION

WORKING COMMISSION W18 - TIMBER STRUCTURES

STRENGTH OF GLUED LAMINATED TIMBER

by

J Ehlbeck and F Colling
University of Karlsruhe
Federal Republic of Germany

MEETING NINETEEN
FLORENCE
ITALY
SEPTEMBER 1986

STRENGTH OF GLUED LAMINATED TIMBER

1 Introduction

Strength and stiffness values of glued laminated timber are dependent of the design of glulam beams, i.e. the properties of the outer and inner laminations as well as the quality of the finger joints. On principle, the outer laminations are of better or at least the same quality as the inner laminations. The extreme sixth of the depth or at least two laminations on either side of the beam are defined as outer laminations. It is necessary to differentiate in that way because the outer laminations decide essentially the bending strength of the glulam beam, whereas the tension perpendicular to grain and the shear strengths are in most cases controlled by the properties of the inner laminations.

2 Bending strength

The bending strength of glulam beams depends especially on the tensile strength of the outer laminations. The tensile strength of a lamination is defined and tested according to ISO Standard 8375, clause 3.1.1. The strength of a lamination in a glulam beam differs, however, in two ways from that in a regular ISO 8375 tension test (strength increasing effects):

a) Lateral displacements of the laminations, occuring in a regular tension test, are prevented when the laminations are part of a glulam beam; this effect can be taken into account by a modification factor k_1.

b) Longitudinal strains of a weak zone of the lamination (i.e. zones with knots and low modulus of elasticity) are hindered by the adjacent laminations; let this be taken into account by a modification factor k_2.

Due to these effects it is explicable that outer laminations of a rather low characteristic tensile strength produce glulam beams of a rather high bending strength. In case of finger joints with a modulus of elasticity in the range of that of clear wood the second strength increasing effect does not exist.

Thus, the bending strength of a glulam beam can be derived by the following two basic equations:

$$f_{m,Glulam} = k_1 \cdot k_2 \cdot f_{t,o} \qquad (1)$$

$$f_{m,Glulam} = k_{1,fj} \cdot f_{t,o,fj} \qquad (2)$$

where

$f_{m,Glulam}$ mean bending strength of a glulam beam
$f_{t,o}$ mean tensile strength of a lamination parallel to grain
$f_{t,o,fj}$ mean tensile strength of a finger joint

The characteristic strength is defined as a fractile, normally the 5-percentile, and can be written as

$$f_k = f\,(1 - k \cdot v) \qquad (3)$$

where

f_k characteristic strength
f mean strength
v coefficient of variation
k constant of a statistical distribution for calculating the 5-percentile.

k may roughly be assumed to be 1.7 or in accordance with the Gauß-distribution, k = 1.645.

From equ. (3) follows:

$$f_{m,k,Glulam} = k_1 \cdot k_2 \cdot f_{t,o,k} \cdot \frac{1-k \cdot v_{m,Glulam}}{1-k \cdot v_{t,o}} \qquad (4)$$

and

$$f_{m,k,Glulam} = k_{1,fj} \cdot f_{t,o,k,fj} \cdot \frac{1-k \cdot v_{m,Glulam}}{1-k \cdot v_{t,o,fj}} \qquad (5)$$

With

$$k_{v,1} = \frac{1-k \cdot v_{m,Glulam}}{1-k \cdot v_{t,o}}$$

and (6a, b)

$$k_{v,2} = \frac{1-k \cdot v_{m,Glulam}}{1-k \cdot v_{t,o,fj}}$$

equs. (4 and 5) read

$$\boxed{f_{m,k,Glulam} = k_1 \cdot k_2 \cdot k_{v,1} \cdot f_{t,o,k}} \qquad (7)$$

$$\boxed{f_{m,k,Glulam} = k_{1,fj} \cdot k_{v,2} \cdot f_{t,o,k,fj}} \qquad (8)$$

The factors $k_{v,1}$ and $k_{v,2}$ depend on the variability of the test data and will be discussed later.

A current quality control of the tensile strength of the finger joints, $f_{t,o,fj}$ is difficult to perform in glulam factories. The bending strength of the finger joints, $f_{m,fj}$, is, however, in many countries under permanent quality control according to a stipulated test method. If the relationship between the tensile strength and the bending strength of the finger joint is sufficiently known, i.e.

$$f_{t,o,fj} = k_3 \cdot f_{m,fj} \tag{9}$$

and

$$f_{t,o,k,fj} = k_3 \cdot f_{m,k,fj} \cdot \frac{1-k \cdot v_{t,o,fj}}{1-k \cdot v_{m,fj}} \tag{10}$$

then equ. (8) can be replaced by

$$\boxed{f_{m,k,Glulam} = k_{1,fj} \cdot k_3 \cdot k_{v,2} \cdot k_{v,3} \cdot f_{m,k,fj}} \tag{11}$$

with

$$k_{v,3} = \frac{1-k \cdot v_{t,o,fj}}{1-k \cdot v_{m,fj}} \tag{12}$$

LARSEN [1] performed tests to find the relationship between the tensile strength of the laminations, $f_{t,o}$, and the bending strength of the glulam beams, f_m. The ratios given in table 1 correspond to the product $k_1 \cdot k_2$ - see equ. (1) - and to the factor $k_{1,fj}$, respectively - see equ. (2).

Table 1: Relationship between bending strength of glulam beams and tensile strength of lamination or finger joint (LARSEN, 1982)

Quality of outer lamination[1]	$\frac{f_m}{f_{t,o}}$	$\frac{\sigma_o}{f_{t,o}}$ [2]	equivalent to
Ucl T 300 T 400	1.34 to 2.05 1.20 to 1.73 1.02 to 1.17	1.18 to 1.66 1.28 to 1.52 1.24 to 1.36	$k_1 \cdot k_2$
finger joint	1.36 to 1.71	1.43 to 1.89	$k_{1,fj}$

1) according to the Nordic grading system;

2) σ_o is the bending stress when the transformed section of the glulam beam is taken into account.

The data in table 1 show a rather high variability, but the following points should be noticed:

- the lateral displacements measured during the tension tests of the laminations varied extremely; therefore, the modification factor k_1 is difficult to determine; the tension test according to ISO 8375 is suitable to test the tensile strength of solid timber in structural sizes. If the laminations of glulam beams are tested in this way, then the deduction of the glulam bending strength becomes problematic.

- the ratio $f_m/f_{t,o}$ in table 1 depends on the building-up of the beams. For example, a high MOE of the outer lamination and a low MOE of the second lamination causes an effective bending stress in the outer lamination which is higher than calculated by using the ordinary formula $f_m = M/W$, where M is the bending moment, and W is the section modulus of the full cross-section. Therefore the ratio $\sigma_o/f_{t,o}$ is also given in table 1.

- the depth of the beams tested was in all cases 233 mm. This comparatively small depth and consequently unequal stress distribution in the outer laminations raise the question if these ratios are of the same level in beams of high depths.

- the ratios for finger joints ($k_{1,fj}$), found by LARSEN, are high compared with those of the laminations themselves ($k_1 \cdot k_2$) because the effect of hindered longitudinal strains of weak zones does not exist in finger joints. On the other hand, finger joints may be more sensible to lateral displacements due to higher brittleness.

For establishing the factors $k_{v,1}$ and $k_{v,2}$ as well as $k_{v,3}$ the relevant coefficients of variation are needed. Therefore, a big number of tests is desirable to obtain reliable data. In table 2, these factors are listed on the basis of $k \approx 1.7$.

Table 2: Factors $k_{v,i} = \dfrac{1 - k \cdot v_1}{1 - k \cdot v_2}$

v_2 \ v_1	0.10	0.15	0.20	0.25	0.30
0.10	1.0	0.90	0.80	0.69	0.59
0.15	1.11	1.0	0.89	0.77	0.66
0.20	1.26	1.13	1.0	0.87	0.74
0.25	1.44	1.30	1.15	1.0	0.85
0.30	1.69	1.52	1.34	1.17	1.0

LARSEN showed that the coefficient of variation depends on the grade and the method of grading of the laminations. The grading systems should therefore reduce the variability of the tensile strength. This will also lead to a smaller coefficient of variation of the glulam bending strength.

Assuming coefficients of variation of 0.10 to 0.15 for the glulam bending strength and of 0.15 to 0.30 for the lamination tensile strength, respectively, the factor $k_{v,1}$ will range from 1.11 to 1.52 (see table 2).

Thus, from table 1 and 2, and equ. (7) can be derived:

$$f_{m,k,Glulam} = (1.18 \text{ to } 1.66) \cdot (1.11 \text{ to } 1.52) \cdot f_{t,o,k}$$

$$\boxed{f_{m,k,Glulam} = (1.31 \text{ to } 2.52) \cdot f_{t,o,k}} \qquad (13)$$

Assuming that the coefficients of variation, $v_{m,Glulam}$ and $v_{m,fj}$ are equal, then

$$k_{v,2} \cdot k_{v,3} = \frac{1 - k \cdot v_{m,Glulam}}{1 - k \cdot v_{m,fj}} \approx 1.0 \quad . \qquad (14)$$

LARSEN |2| found, that

$$k_3 = \frac{f_{t,o,fj}}{f_{m,fj}} \approx 0.6 \quad . \qquad (15)$$

Then from table 1 and equ. (11) follows:

$$f_{m,k,Glulam} = (1.43 \text{ to } 1.89) \cdot 0.6 \cdot 1.0 \cdot f_{m,k,fj}$$

$$\boxed{f_{m,k,Glulam} = (0.86 \text{ to } 1.13) \cdot f_{m,k,fj}} \qquad (16)$$

Any possible volume effects are not taken into account, because the numerical values are derived from glulam bending test with a constant depth of 233 mm. Therefore, it cannot be excluded that further reductions of the coefficients in equs. (13 and 16) are necessary. Tests by EHLBECK, COLLING, GÖRLACHER |3| verified, however, equ. (16). The tensile strength of finger joints, with 239 replications, turned out to be approximately

$$f_{t,o,fj} \approx 35 \text{ N/mm}^2$$

with $v_{t,o,fj} \approx 0.24$. It is essential to point out that these tests were not performed according to ISO 8375, but with a test set-up which excluded any lateral displacement of the test length of about 150 mm. Hence, using these data the modification factor $k_{1,fj}$ is unity.

Bending tests with finger joints taken from the same production period as those for the tension tests proved a bending strength of

$$f_{m,fj} \approx 44.5 \text{ N/mm}^2$$

with $v_{m,fj} \approx 0.14$. From this follows that

$$k_3 = \frac{f_{t,o,fj}}{f_{m,fj}} = 0.79 \quad . \tag{17}$$

Then from equ. (11) follows:

$$f_{m,k,Glulam} \approx 1{,}0 \cdot 0{,}79 \cdot 1.0 \cdot f_{m,k,fj}$$

$$\boxed{f_{m,k,Glulam} \approx 0.80 \cdot f_{m,k,fj}} \tag{18}$$

Recent bending tests from EHLBECK and COLLING |4| with glulam beams of different depth between 330 and 1250 mm and with or without finger joints in the outer tensile laminations confirmed the assumptions that

- the bending strength of glulam beams depends on the tensile strength of the outer laminations and their finger joints,

- longitudinal strains of zones with finger joints can not be inhibited by adjacent laminations because of the higher stiffness of finger joints compared with the timber,

- there is no depth effect influencing the bending strength of glulam beams (with depths $\geq$ 330 mm) as long as the strength of the finger joints controls the ultimate load-carrying capacity.

The interrelations described by the equations (13, 16 and 18) are the basis for establishing in EUROCODE 5 |5| characteristic bending strength values depending on the strength classes of the laminations and the bending strength (in flatwise bending) of the finger joints.

3 Other strength properties

In case of tension parallel to grain high stresses are distributed across the total cross-section. Therefore, the tensile strength is dependent on the strength properties of all laminations, and to a certain degree the weakest laminations control the strength. By gluing together all laminations, the strength of the total cross-section increases, however, considerably because of the redistribution of forces corresponding to the individual elasticity of the laminations. Due to this effect the variation of the strength decreases. Hence, the characteristic tensile strength of a glulam cross-section is higher than that of the weakest individual lamination.

In curved and cambered glulam beams the highest tensile stresses perpendicular to grain occur generally in the zone of the inner laminations. A melioration effect by gluing together different laminations does not exist. Hence, the characteristic tensile strength perpendicular to grain is in accordance with that of the individual inner laminations.

In case of compression parallel to grain the gluing effect is similar to that under tensile stresses. Therefore, an increased characteristic compressive strength of glulam members is ascertained in comparison to the individual laminations.

In case of compression perpendicular to grain the outer laminations, where the loads are directly imposed, control the characteristic strength, with no substantial variation-reducing effect.

12

The same effect as for tension perpendicular to grain applies when shear stresses are induced by shear forces (in bending members).

The modulus of elasticity is correlated to several physical properties of the wood (such as density and knot area ratio). Hence, the mean value of the modulus of elasticity increases when individual laminations of different physical properties are composed by adhesives. The characteristic modulus of elasticity is approximately 80 % of the mean value, based on the assumption of a coefficient of variation of 12 %.

References

|1| Larsen, H.J., 1982: Strength of glued laminated beams, Part 5. Inst. of Build.Techn. and Struct. Eng., Report No. 8201, Aalborg University, Denmark.

|2| Larsen, H.J., 1980: Strength of finger joints. Inst. of Build. Techn. and Struct. Eng., Rep. No. 8002, Aalborg University, Denmark.

|3| Ehlbeck, J., Colling, F., Görlacher, R., 1984: Einfluß keilgezinkter Lamellen auf die Biegefestigkeit von Brettschichtholzträgern. Forschungsbericht der Versuchsanstalt für Stahl, Holz und Steine, Abt. Ingenieurholzbau, Universität Karlsruhe.

|4| Ehlbeck, J., Colling, F., 1986: Biegefestigkeit von Brettschichtholz in Abhängigkeit von Rohdichte, Elastizitätsmodul, Ästigkeit und Keilzinkung der Lamellen, der Lage der Keilzinkung sowie von der Trägerhöhe. Forschungsbericht der Versuchsanstalt für Stahl, Holz und Steine, Abt. Ingenieurholzbau, Universität Karlsruhe (in preparation).

|5| Brüninghoff, H., Crubilé, P., Ehlbeck, J., Larsen, H.J., Sunley, J., 1985: EUROCODE 5, Common unified rules for timber structures. 1st report prepared for the European communities.

CIB-W18/19-12-2

INTERNATIONAL COUNCIL FOR BUILDING RESEARCH STUDIES AND DOCUMENTATION

WORKING COMMISSION W18 -TIMBER STRUCTURES

STRENGTH MODEL FOR GLULAM COLUMNS

by

H J BLASS
University of Karlsruhe
Federal Republic of Germany

MEETING NINETEEN
FLORENCE
ITALY
SEPTEMBER 1986

STRENGTH MODEL FOR GLULAM COLUMNS

by
Hans Joachim Blaß
Lehrstuhl für Ingenieurholzbau und Baukonstruktionen
Universität Karlsruhe, W. Germany

INTRODUCTION

The design specifications for compression members of the current standard DIN 1052 "Holzbauwerke, Berechnung und Ausführung" (timber structures, design and construction) are based on a second order elastic analysis, which underlies the ultimate loads for timber compression members given by Möhler /1/. In the CIB Structural Timber Design Code, Publication 66 and in EUROCODE 5 "Common Unified Rules for Timber Structures" the verification of the compression member is also founded on the elastic theory.

More accurate methods of calculation for timber structural members under compressive stress - particularly a second order plastic analysis - could not lead to a more efficient utilization of timber as a building material, until the stochastic scatter of the dominant influencing variables entered into the calculation, since the advantage of a more realistic mechanical model had so far been compensated by uncertainties concerning the assumed basic material properties. The introduction of the concept of reliability in connection with a probabilistic safety principle then made it possible to develop a mechanical model giving an accurate description of the member behaviour in the limit state, taking account of the statistic distribution functions of the basic variables. Whether a given level of reliability can be attained in an economical manner, depends on how exactly the mechanical model describes the loadbearing behaviour and on how well the stochastic model of the basic variables is known.

Generally, the failure probability p_f can be determined as a function of the random variables 'resistance R' (e.g. loadbearing capacity of a column) and 'load effect S', as decribed in the following (Fig. 1).

$$p_f = \int_0^\infty f_S(s) \; F_R(s) \, ds$$

$$p_f = \int_0^\infty \int_0^x f_S(s) \; f_R(r) \, dr \, ds$$

The literature provides comprehensive information on the load distribution /2/,/3/,/4/,/5/,/6/, whereas the resistance has been investigated only to some extent /7/,/8/,/9/. The object of this work is to determine the resistance of glued laminated compression members taking account of the geometrically and physically non-linear behaviour of the structural components. A mechanical model of the timber compression member is obtained by a second order plastic analysis, which directly yields the loadbearing capacity of a structural member. The stochastic model of the basic variables covers the distribution functions of all governing characteristic quantities including the respective parameters of the distribution.

DESCRIPTION OF THE DOMINANT INFLUENCING VARIABLES:

Information on the loadbearing capacity of glued laminated columns is obtained on the basis of the statistic distribution functions of the important parameters. On the one hand, structural imperfections affecting the strength and strain properties of the material and, on the other hand, geometric imperfections having a direct effect on the ultimate loads of timber compression members have to be taken into account.

Structural imperfections

Among the most important structure parameters of wood which affect the strength of laminations for glued laminated structural members, the dominant variables having a significant influence on the shape of the stress-strain relationship and thus on the strength and strain properties of the laminations are, according to /10/, the oven-dry density ρ_o, the knot area ratio KAR, the pressure wood content d and the moisture content u. Besides these parameters, the presence of a finger joint also has an effect on the strength and strain properties of a member under tensile or compressive stresses.

Figs. 2 and 4 show the histograms of oven-dry density and pressure wood content according to /10/. The best fit curve of a theoretical probability density, which in both cases was found to be a logarithmic normal distribution, is also presented and forms a basis of the subsequent simulation. The frequency distribution of the KAR value (Fig. 3) of more than 7000 board sections 150 mm in lengths of grade II laminations determined at Karlsruhe University in the course of two research projects /11/,/12/ also entered into the simulation as a representative of the statistical population. The histogram of the moisture content (Fig. 5) is based on measurements on glued laminated columns of accomplished structures. The logarithmic normal distribution was found to be the best fit curve of the measured values and is used, like the distributions of oven-dry density, knot area ratio and pressure wood content, for modelling the structure of glued laminated columns. For the distance between the finger joints in the board, /13/ assumes a Gaussian distribution with the mean value μ_x = 4,30 m and the standard deviation σ_x = 0,71 m.

Geometric imperfections

The dominant geometric imperfections were determined in a series of measurements on accomplished structures and are shown in Figs. 6 to 8 in the form of frequency distributions. The best fit curves of theoretical probability distributions were found to be a logarithmic normal distribution for the ratio of section width to nominal width, a Gaussian distribu-

tion for the amplitude of a sinusoidal member axis and a Gaussian distribution for the angle of inclination of the member axis.

SIMULATION OF THE COLUMN STRUCTURE

Simulating the column structure has the purpose of reproducing the manufacturing process of glued laminated structural components on the basis of the statistic distribution functions of all dominant influencing variables. It is then possible to model a great number of compression members with given dimensions, the ultimate loads of which can be used in a Monte-Carlo simulation program to determine the probability distribution of the strength of glued laminated columns. The random numbers required for the simulation are generated by means of a pseudo-random number generator. Fig. 9 shows a glued laminated structural member made from an endless board, the laminations of which were divided in sections 150 mm in length. For the arithmetical model, the fortuitous location of the finger joints must be displaced to the nearest section boundary.

Allocation of parameters

We allocate to each lamination in equidistant cross-sections a parameter vector of oven-dry density ρ_0, knot area ratio KAR, pressure wood content d and moisture content u, from which we obtain the expected values of the characteristic quantities of the stress-strain relation. For a realistic description, the autocorrelation of the parameters along the board is of great importance. The correlation of the oven-dry density within a board is such that the density can approximately be considered to be constant. Knot area ratio KAR and pressure wood content d are allocated individually to each lamination cross section from the respective frequency distributions, whereas the moisture content is assumed to be constant over the whole member. By means of regression equations according to /10/, the allocated parameters can be used to determine characteristic values of the stress-strain diagram for compressive stress and tensile stress (Fig. 10), which have to be corrected by fortuitous portions, the so-called residues, since the characteristic values are not completely explained by the parameters

ρ_o, KAR, d and u. These residues are also autocorrelated, i.e. the variation of the residual scatter, e.g. of the elastic modulus E_d, within a board is less than between different boards. The allocated parameter vector and the residues R (...) yield the characteristic values of the stress-strain diagram of a lamination cross section /10/,/11/:

$$E_d = -4690 + 51{,}1 \cdot \rho_o - 0{,}59 \cdot \rho_o \cdot u - 0{,}225 \cdot \rho_o \cdot KAR - 20{,}1 \cdot u \cdot d + 0{,}771 \cdot u^2 \cdot d + R\,(E_d) \quad |N/mm^2|$$

$$\sigma_{dB} = -1{,}9 - 2{,}23 \cdot u + 0{,}224 \cdot \rho_o - 0{,}713 \cdot KAR + 0{,}109 \cdot u^2 - 0{,}00741 \cdot u \cdot \rho_o + 0{,}09 \cdot u \cdot KAR - 0{,}000773 \cdot \rho_o \cdot KAR - 0{,}000645 \cdot \rho_o \cdot d - 0{,}00248 \cdot u^2 \cdot KAR + 0{,}00064 \cdot u^2 \cdot d + R\,(\sigma_{dB}) \quad |N/mm^2|$$

$$\sigma_{dBA} = 7{,}8 - 1{,}46 \cdot u + 0{,}141 \cdot \rho_o - 0{,}265 \cdot KAR + 0{,}0588 \cdot u^2 - 0{,}00442 \cdot u \cdot \rho_o + 0{,}0076 \cdot u \cdot KAR + R\,(\sigma_{dBA}) \leq \sigma_{dB} - 1 \quad |N/mm^2|$$

$$\varepsilon_{dB} = 6{,}47 - 0{,}326 \cdot u + 0{,}022 \cdot KAR + 0{,}067 \cdot d + 0{,}0072 \cdot u^2 - 0{,}00011 \cdot u^2 \cdot d + R\,(\varepsilon_{dB}) \geq \frac{7 \cdot \sigma_{dB}}{6\,E_d} \cdot 10^3 \quad |‰|$$

$$E_z = \exp\,(8{,}2 + 0{,}00313 \cdot \rho_o - 0{,}0117\,KAR + R\,(E_z)) \quad |N/mm^2|$$

$$\sigma_{zB} = \exp\,(-4{,}22 + 0{,}876 \cdot \ell n\,(E_z) - 0{,}00093 \cdot KAR \cdot \ell n\,(E_z) + R\,(\sigma_{zB})) \quad |N/mm^2|$$

If a finger joint in the lamination cross section has to be taken into account, the material properties of the lamination with finger joint can be derived, for the compressive stress range, from those of the lamination without finger joint:

$$E_d^{KZV} = E_d$$

$$\sigma_{dB}^{KZV} = -2{,}13 + 0{,}849 \cdot \sigma_{dB}$$

$$\sigma_{dBA}^{KZV} = \sigma_{dBA}$$

$$\sigma_{dB}^{KZV} = 1{,}50 + 0{,}586 \cdot \sigma_{dB}$$

For tensile stress the following regression equations apply:

$$E_z^{KZV} = \exp\,(8{,}459 + 0{,}002517 \cdot \rho_o + R\,(E_z^{KZV}))$$

$$\sigma_{zB}^{KZV} = \exp\,(2{,}716 + 5{,}905 \cdot 10^{-5} \cdot E_z^{KZV} + R\,(\sigma_{zB}^{KZV}))$$

Now we know the shape of the stress-strain function for tensile and compressive stress of each lamination cross section and we conclude modelling the column structure by simulating the geometric imperfections eccentricity of the member axis and deviation of the cross-sectional dimensions from the nominal values.

MECHANICAL MODEL

The purpose of the mechanical model is to describe the behaviour of glued laminated compressive members subjected to normal forces and transverse loads. For the calculation of the ultimate load we make the following restrictive assumptions:

a) For compressive stress, the stress-strain behaviour of timber corresponds to the stress-deformation diagram according to /10/, whereas for tensile stress the underlying behaviour is linear-elastic/brittle. It is presumed that the stress-strain relationships determined for uniform, plane deformation of the cross-section also apply to other conditions of deformation.
b) The member cross section is symmetrical with the load acting in the plane of symmetry only. Lateral deflection is excluded.
c) The Bernoulli hypothesis applies even if plastic deformations occur in the cross section.
d) The deflections are small, and the linearized differential equation of the elastic line can be used.
e) Calculating the shear deformations we assume the shearing angle and the shear modulus G to be constant over the cross-sectional depth and the relationship between shear stress and deformation to come under Hooke's Law.
   The influence of the shear force on the moment-curvature relation is not taken into account.
f) The stress-strain relation for compressive stress also applies in the case of local removal of the load, i.e. the removal of the load of the plastic range on a straight line is neglected.

Relations

In the Federal Republic of Germany, glued laminated members are generally made from whitewood boards. Columns are mostly made of members with rectangular cross sections, although it is possible to fabricate more complex sections. The arithmetical model is based on a rectangular section of

boards 30 mm in thickness with element properties being independent of each other.

Based on the notations of Fig. 11, we obtain the internal normal force as the integral of the direct stresses over the cross-sectional area:

$$N_i = \frac{h}{\Delta\varepsilon} \cdot \sum_{j=1}^{M} \int_{\varepsilon_{aj}}^{\varepsilon_{ij}} \sigma_j(\varepsilon) \cdot d\varepsilon$$

The momentary position of the centre of gravity, which is a function of the stress distribution, can be determined by means of the secant modulus method /14/,/15/, if the edge strains ε_a and ε_i are known:

$$\varepsilon_s = \frac{\sum_{j=1}^{M} \int_{\varepsilon_{aj}}^{\varepsilon_{ij}} E_j(\varepsilon) \cdot \varepsilon \cdot d\varepsilon}{\sum_{j=1}^{M} \int_{\varepsilon_{aj}}^{\varepsilon_{ij}} E_j(\varepsilon) \cdot d\varepsilon}$$

Hence, the internal moment referred to the respective position of the centre of gravity is:

$$M_i = \frac{h^2}{\Delta\varepsilon^2} \cdot \sum_{j=1}^{M} \int_{\varepsilon_{aj}}^{\varepsilon_{ij}} \sigma_j(\varepsilon) \cdot (\varepsilon - \varepsilon_s) \cdot d\varepsilon$$

Bending stiffness EI and strain stiffness EA of the glued laminated section are calculated using the internal section parameters M_i and N_i:

$$E\,I = \left| \frac{M_i \cdot h}{\Delta\varepsilon} \right|$$

$$E\,A = \frac{N_i}{\varepsilon_s}$$

Loadbearing behaviour of a glued laminated section

Compressive strength of section:

The compressive strength of a glued laminated section is defined as the maximum value of the stress-strain relationship of the section under compressive stress. The stress-strain diagram of the section results from the independent, randomly distributed stress-strain diagrams of the individual laminations, the shapes of which also depend on several randomly distributed input quantities. Fig. 12 shows an example of a stress-strain diagram of a section under compressive stress and the respective stress-strain diagrams of the laminations. The section ultimate strain lies between the minimum and maximum ultimate strains of the laminations, and the compressive strength is characterized by the stress value corresponding to the section ultimate strain of the section stress-strain diagram.

Moment-curvature relation:

The moment-curvature function yields for a given normal force the moment capacity of the section as a function of the curvature or, respectively, the different strains in the extreme fibres. Fig. 13 shows for a glued laminated section of 10 lamellas the moment-curvature relations for various normal forces with the moment referred to the geometric centre of gravity. Due to the variable location of the centre of gravity, the functions generally do not run through the point of origin and are not symmetrical. The discontinuities in the curve are due to abrupt changes of the section

bending stiffness as a result of tensile failure of individual laminations, whereas the maxima for high normal forces depend on the special shape of the lamination stress-strain diagrams. We can now explain two failure modes of glued laminated sections: In the case of a high M/N ratio, the section fails by bending tension fracture, which is mostly initiated by rupture of the extreme tension lamination. At a small M/N ratio, the curvatures increase infinitely after exceeding a limit load, i.e. the section is fully plasticized and forms a plastic hinge. In the calculation of the ultimate load of glued laminated columns, failure of slender members is characterized by bending tension fracture, whereas short deep members form a plastic hinge in the cross section.

Ultimate bearing capacity of a glued laminated section

In current standards for timber structures, the verification for bending with longitudinal force is based on a linear interaction of moment and normal force . This linear relationship does not take account of the plastic behaviour of the material in the compressive stress range. The member is assumed to fail when an elastic limit stress has been reached at the strained edge. A more realistic description of the ultimate bearing capacity takes account of the non-linear relation between compressive stress and compressive strain and does not ignore the possibility of bending tension failure under the combined action of compressive force and bending moment. Entering the moments and axial forces at failure of a moment-curvature relation in an interaction diagram of moment and normal force yields the curve of the ultimate bearing capacity of the section. Results of simulating calculations of glued laminated sections are shown in Figs. 14 to 16. For sections of 7, 15 and 30 laminations, the M-N interaction curves were calculated for every 1000 sections and evaluated for given eccentricities e = M/N. The individual sections were modelled, analogous to the simulation of the column structure, by choosing for each lamination random values of the parameters oven-dry density ρ_0, knot area ratio KAR and pressure wood content d from the frequency distributions and by assuming the moisture content u to be constant over the whole cross section. The statistical evaluation of the random tests showed that for each eccentric-

ity e the values of the ultimate bearing capacity can be assumed to have a Gaussian distribution along the line M = e N.

CALCULATION OF THE ULTIMATE LOAD

The ultimate load of a structure is the load at which deformations grow infinitely without further load increase and cause failure of the structure /16/. For glued laminated compressive members this is the case, when the section stiffness decreases with increasing curvature of the member axis, but does not reach a limit value characterizing a stable state of equilibrium. If the load is above the ultimate load, deformation increments diverge in the course of the calculation, whereas below the ultimate load they asymptotically tend towards zero. Since the ultimate load of a given structure can be determined by iteration only, each assumed load has to be studied as to whether it is above or below the ultimate load. Thus, we have two iterative cycles for calculating the ultimate loads: the inner cycle which varies the stiffnesses for an assumed load until either a stable state of equilibrium has been found and the end deformation of the member under this load is known or the deformations are found to diverge with the assumed load being above the ultimate load; and the outer cycle yielding the maximum load carried by the member. Fig. 17 shows the flow of the inner cycle of iteration of stiffnesses and deformations, in which the forces and moments of the structure are calculated for the respective state of stiffness according to a finite element analysis in matrix notation. This method can be used to study structures with any conditions of support, even statically indeterminate structures, taking account of the rearrangement of static forces due to varied stiffness distribution.

The load iteration has the function of improving estimated values of the ultimate loads such that the ultimate load is localized more and more exactly and can finally be determined with given precision. By the Monte Carlo simulation, the ultimate loads of the simulated columns are calculated to 1 % precisely.

Example of calculation

For a simulated column hinged at both ends, Fig. 18 shows the moment curve immediately before the ultimate load is reached, referred to the geometric (1) and to the effective centre of gravity (2). Fig. 19 shows the increasing deformations or moments, respectively, of the critical cross section as the normal force increases, as well as the decreasing bending stiffness EI. The distribution of the longitudinal stresses in the critical cross section (Fig. 20) for the three load steps shows clearly that the compressive stresses are quasi-linear even at 90 % of the ultimate load and that plastic deformations occur only immediately before the ultimate load has been reached, which then, however, cause rapid failure of the structural member.

ULTIMATE LOAD STRESSES OF GLUED LAMINATED COMPRESSION MEMBERS

The ultimate loads determined in several hundred runs of the simulation and calculation represent a random test which can be evaluated statistically. Fig. 21 shows the results of such Monte Carlo simulations for slenderness ratios between 10 and 200 with step size 10, i.e. the curves of the mean values and the 5th percentiles of the ultimate load stresses for axially loaded grade II glued laminated compression members hinged at both ends. By means of the modified graphical method according to /17/ a three-parameter Weibull distribution was fit to each random sample with a given slenderness. For comparison, the ultimate load stresses according to /18/ are plotted, which underlie the ω-values according to the draft DIN 1052, 8/84, as well as the stresses derived for grade II glued laminated compression members.

It can be concluded that the diffusion of the allowable stresses agrees well with the path of the 5th percentiles of the simulation calculation. The ratio of 5th percentile to allowable stress is about 2,9 for $\lambda = 10$ and increases to about 3,4 for $\lambda = 200$.

References

/1/ Möhler, K.: Tragkraft und Querkraft von ein- und mehrteiligen Holzdruckstäben nach Versuch und Rechnung. Dissertation Universität Karlsruhe 1942.

/2/ ICSS: Basic Notes on Actions. Third draft 1976.

/3/ DIN 1055: Lastannahmen für Bauten
Teil 1, Ausgabe Mai 1978
Teil 4, Ausgabe Mai 1977
Teil 5, Ausgabe Juni 1975

/4/ Prückner, R.; Rackwitz, R.: Zur Neudefinition der Nennwerte von Schneelasten. Arbeitsberichte zur Zuverlässigkeitstheorie der Bauwerke, SFB 96, Heft 3/1973.

/5/ Luy, H.; Rackwitz, R.: Darstellung und Auswertung von Schneehöhenmessungen in der BRD. Arbeitsberichte zur Zuverlässigkeitstheorie der Bauwerke, SFB 96, Heft 31/1978.

/6/ König, G.; Zilch, K.: Untersuchung zur Schaffung von Unterlagen für wirtschaftliche und sichere Annahmen über Windlasten - Windgeschwindigkeitskarte Deutschland. Schlußbericht eines mit Förderung des BMBau durchgeführten Forschungsvorhabens, 1973.

/7/ Steck, G.: Die Zuverlässigkeit des Vollholzbalkens unter reiner Biegung. Dissertation Universität Karlsruhe 1982.

/8/ Kersken-Bradley, M.: Beanspruchung von Bauteilquerschnitten bei streuenden Kenngrößen des Kraftverformungsverhaltens innerhalb des Querschnittes. Arbeitsberichte zur Zuverlässigkeitstheorie der Bauwerke, SFB 96, Heft 56/1981.

/9/ Maier, W.: Beitrag zu einem Zuverlässigkeitsmodell für Dachbalken aus Brettschichtholz unter besonderer Berücksichtigung seines Festigkeitsverhaltens. Arbeitsberichte zur Zuverlässigkeitstheorie der Bauwerke, SFB 96, Heft 30/1978.

/10/ Glos, P.: Zur Bestimmung des Festigkeitsverhaltens von Brettschichtholz bei Druckbeanspruchung aus Werkstoff- und Einwirkungskenngrößen. Arbeitsberichte zur Zuverlässigkeitstheorie der Bauwerke, SFB 96, Heft 35/1978.

/11/ Ehlbeck, J.; Colling, F.; Görlacher, R.: Einfluß keilgezinkter Lamellen auf die Biegefestigkeit von Brettschichtholzträgern. Forschungsbericht im Auftrag der EGH in der DGfH 1984.

/12/ Ehlbeck, J.; Colling, F.: Biegefestigkeit von Brettschichtholz. Forschungsbericht im Auftrag der EGH in der DGfH 1986, bisher unveröffentlicht.

/13/ Larsen, H.J.: Strength of Glued Laminated Beams, Part 2. Institute of Building Technology and Structural Engineering, Report No. 8004, Aalborg University, Danmark, 1980.

/14/ Heil, W.: Traglastermittlung von räumlich belasteten Durchlaufträgern mit offenem, dünnwandigem Querschnitt bei beliebigem Werkstoffgesetz. Dissertation Universität Karlsruhe 1979.

/15/ Ackermann, T.: Traglastberechnung räumlicher Rahmen aus Stahl- oder Leichtmetallprofilen mit dünnwandigen offenen Querschnitten. Dissertation Universität Karlsruhe 1981.

/16/ Vogel, U.: Die Traglastberechnung stählerner Rahmentragwerke nach der Plastizitätstheorie II. Ordnung. Forschungshefte aus dem Gebiete des Stahlbaues 15 (1965), Stahlbau-Verlag Köln.

/17/ Pierce, C.B.: The Weibull Distribution and the Determination of its Parameters for Application to Timber Strength Data. Building Research Establishment, Princes Risborough, 1976,

/18/ Möhler, K.; Scheer, C.: Knickzahlen für Voll-, Brettschichtholz und Holzwerkstoffe. Holzbau Statik Aktuell, Folge 7, 1983.

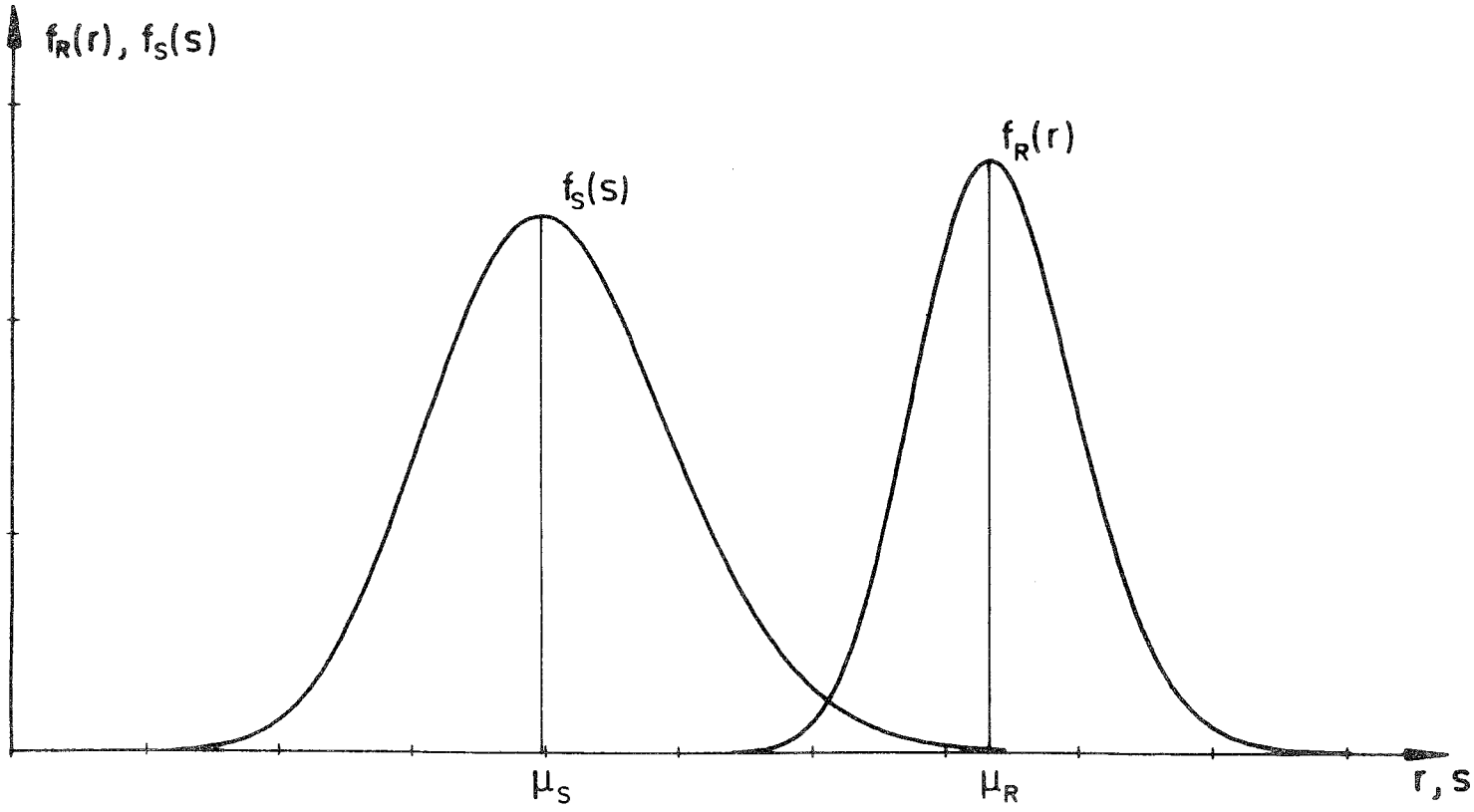


Figure 1: Density functions of load effect S and resistance R

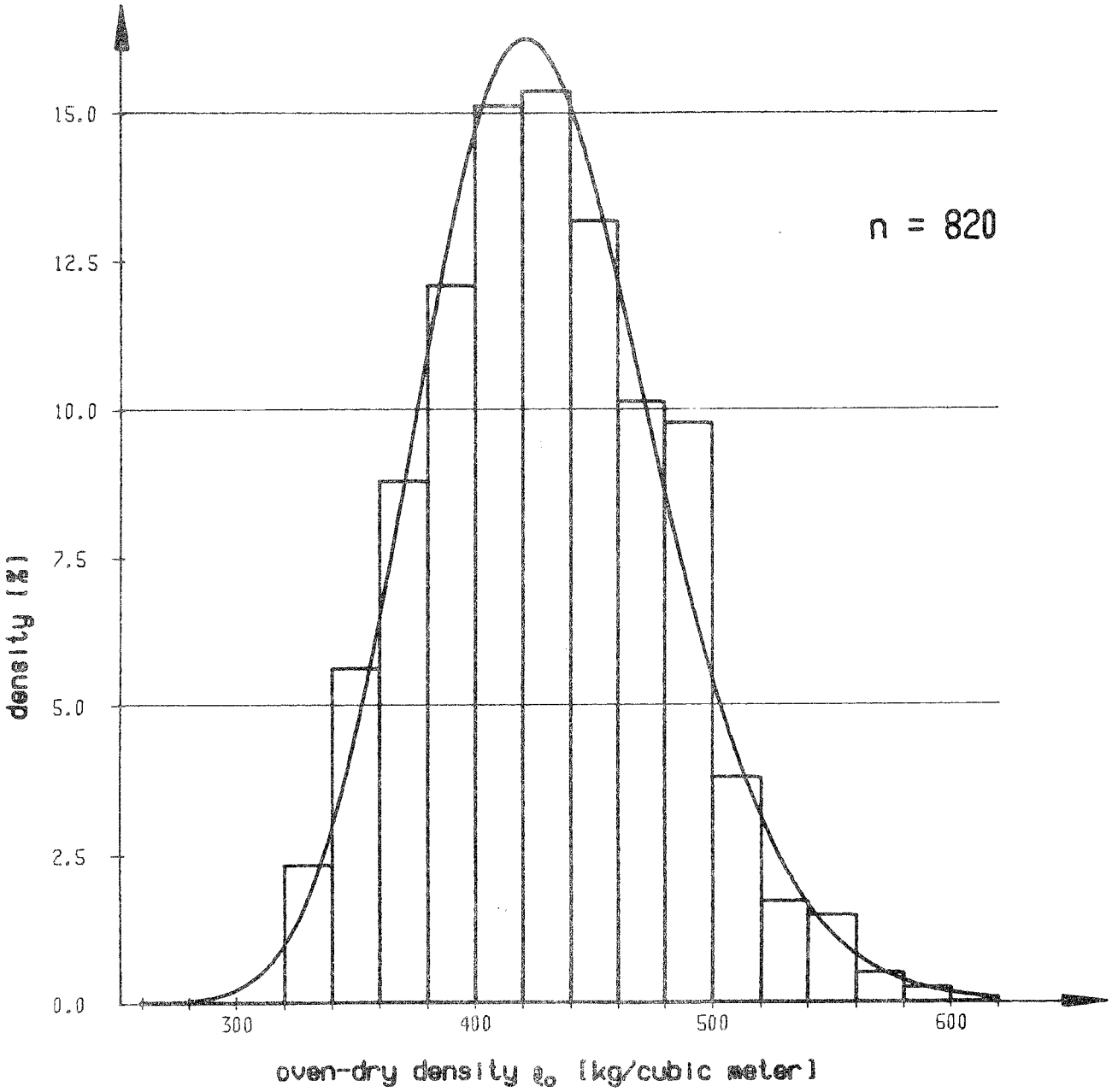


Figure 2: Distribution of oven-dry density according to GLOS [10]

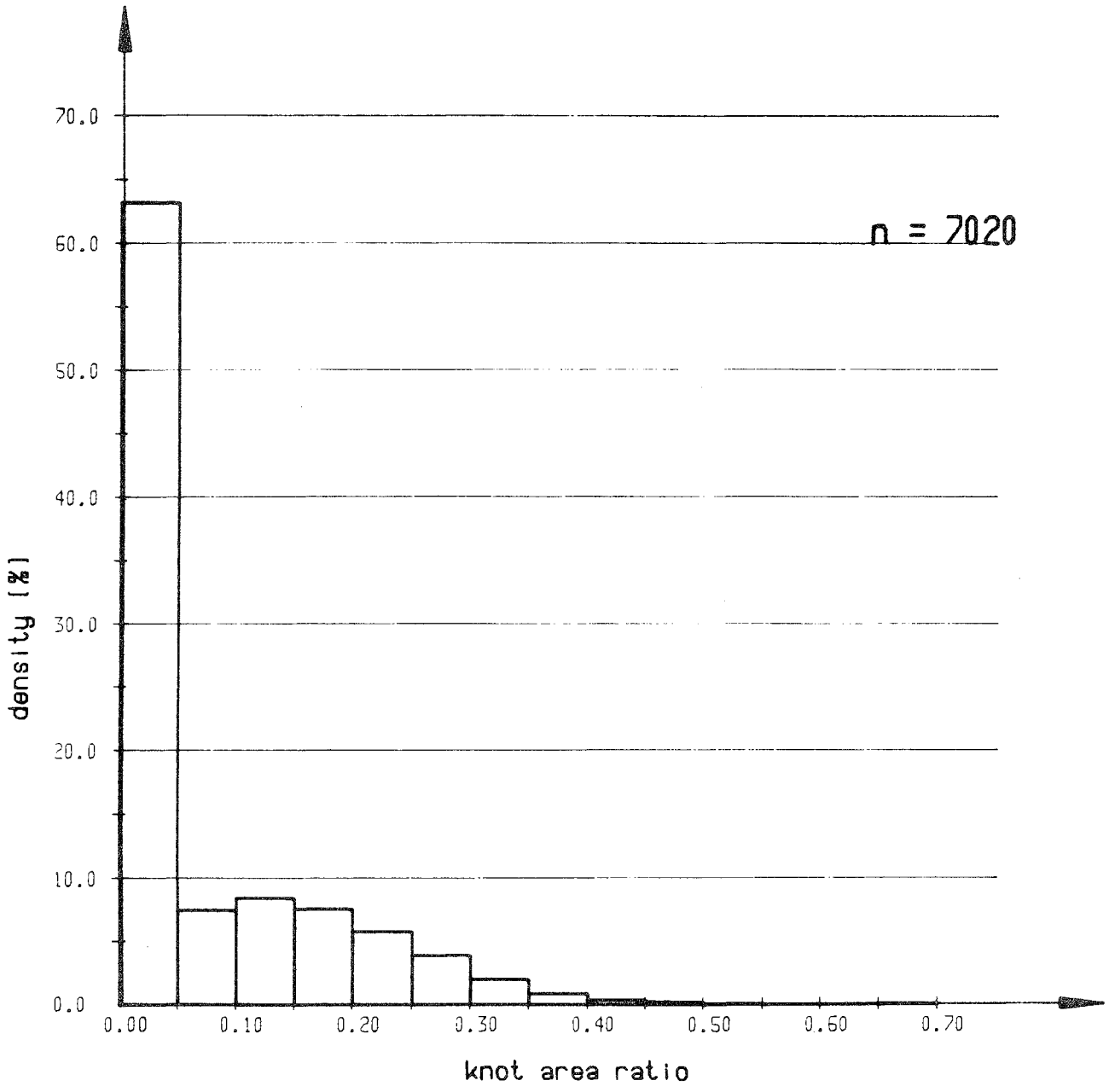


Figure 3: Distribution of knot area ratio of 150 mm specimen according to |11|, |12|

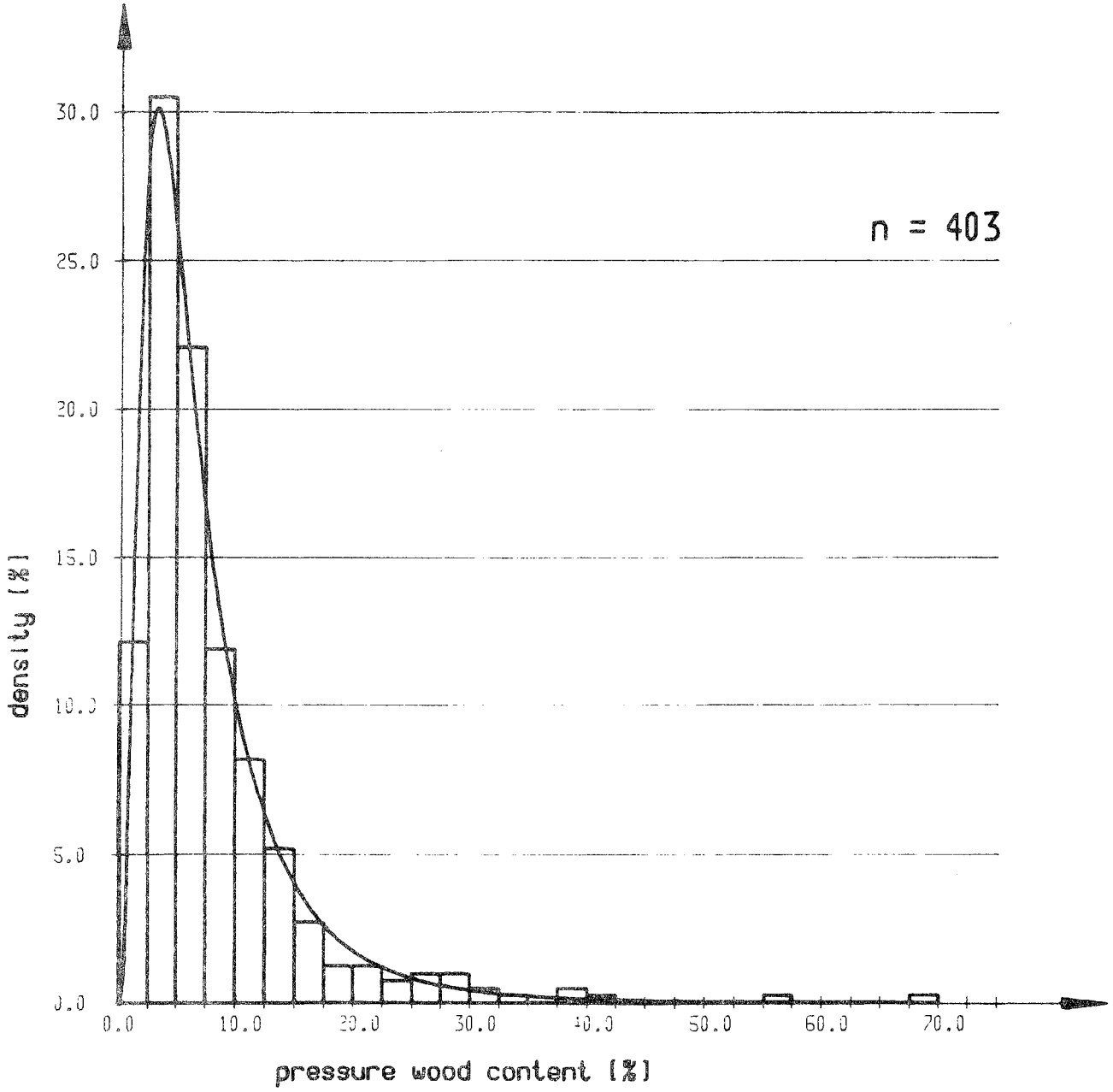


Figure 4: Distribution of pressure wood content according to GLOS |10|

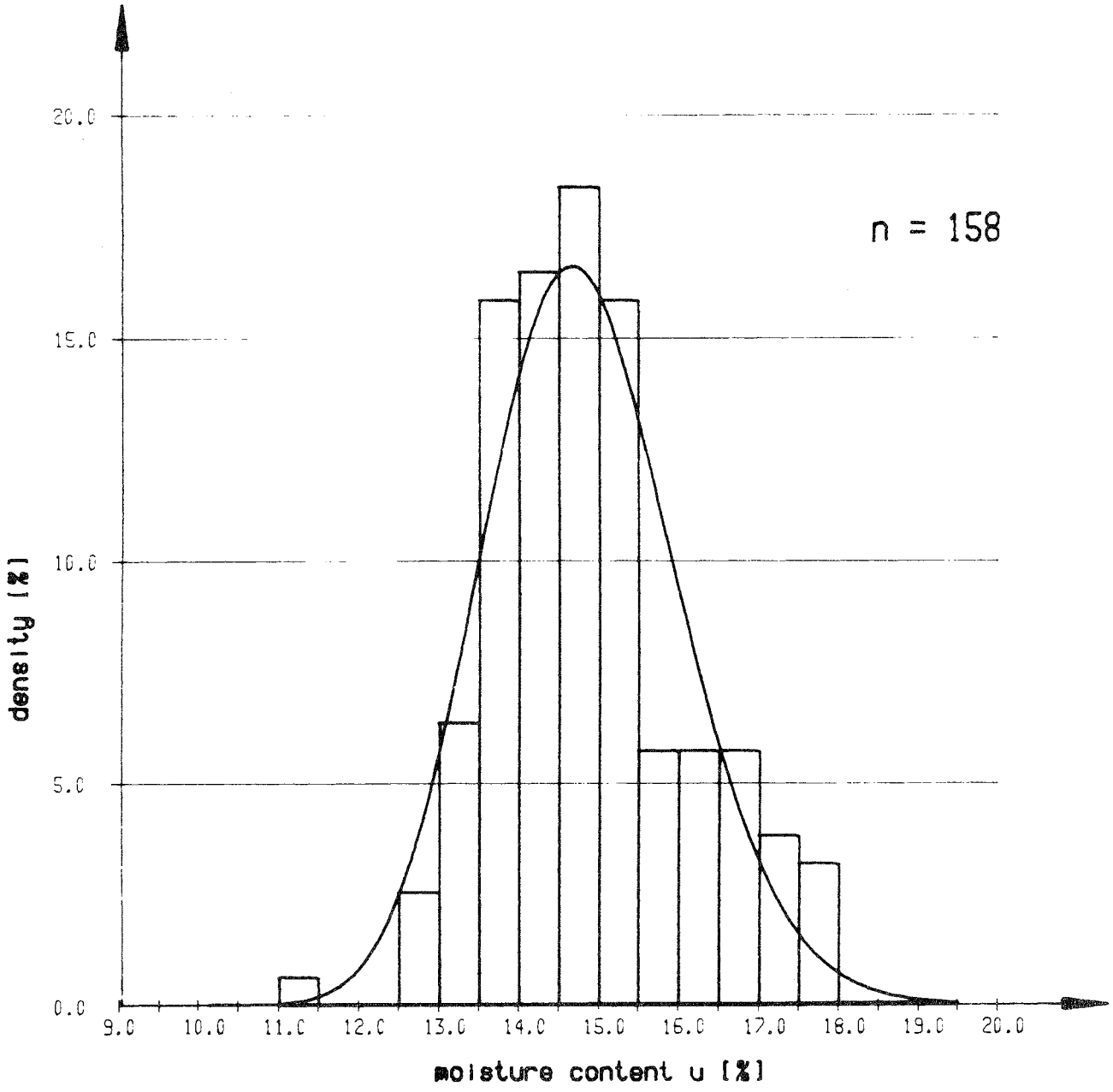


Figure 5: Distribution of moisture content of glulam columns

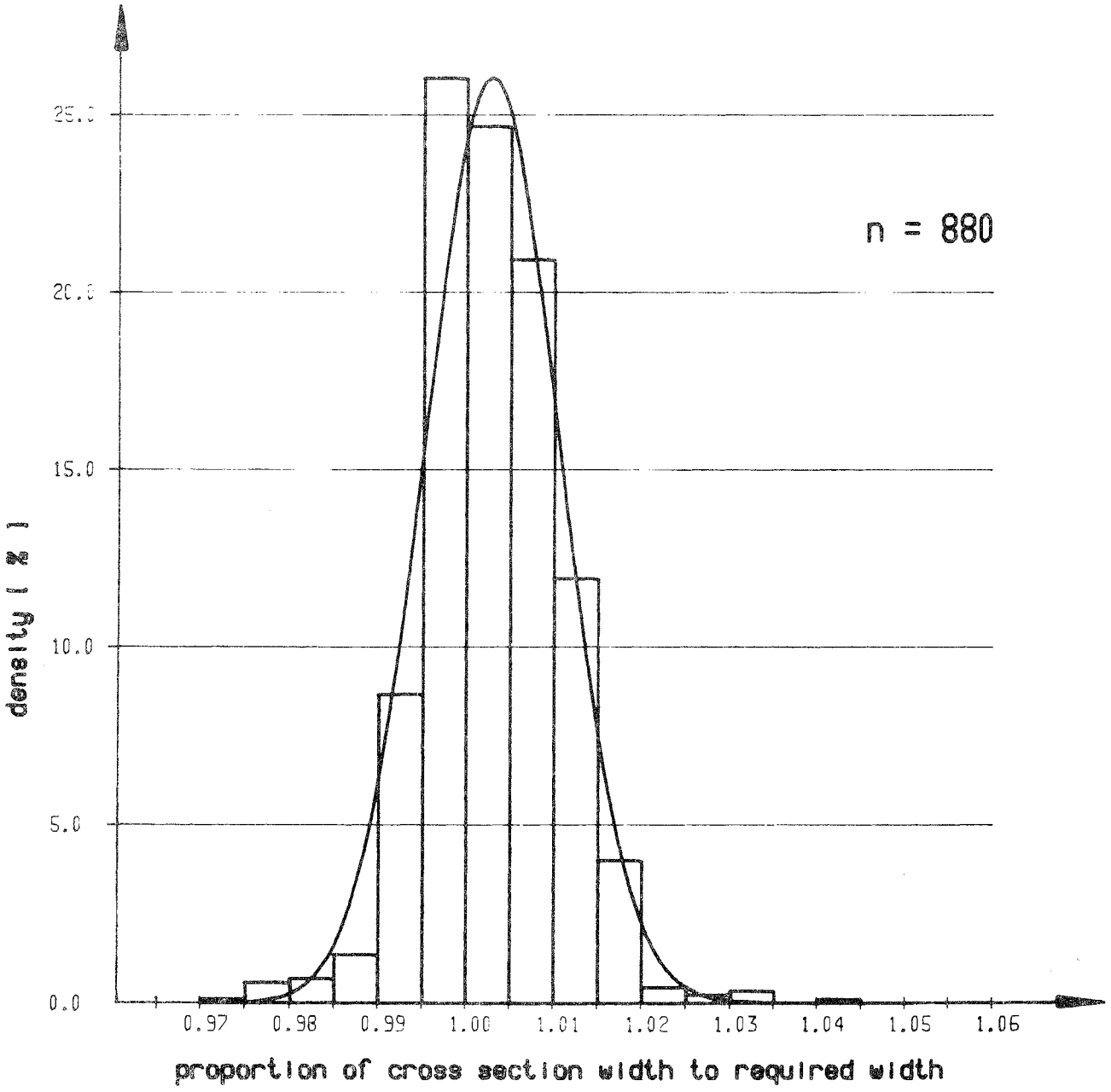


Figure 6: Distribution of the geometric imperfection cross section width

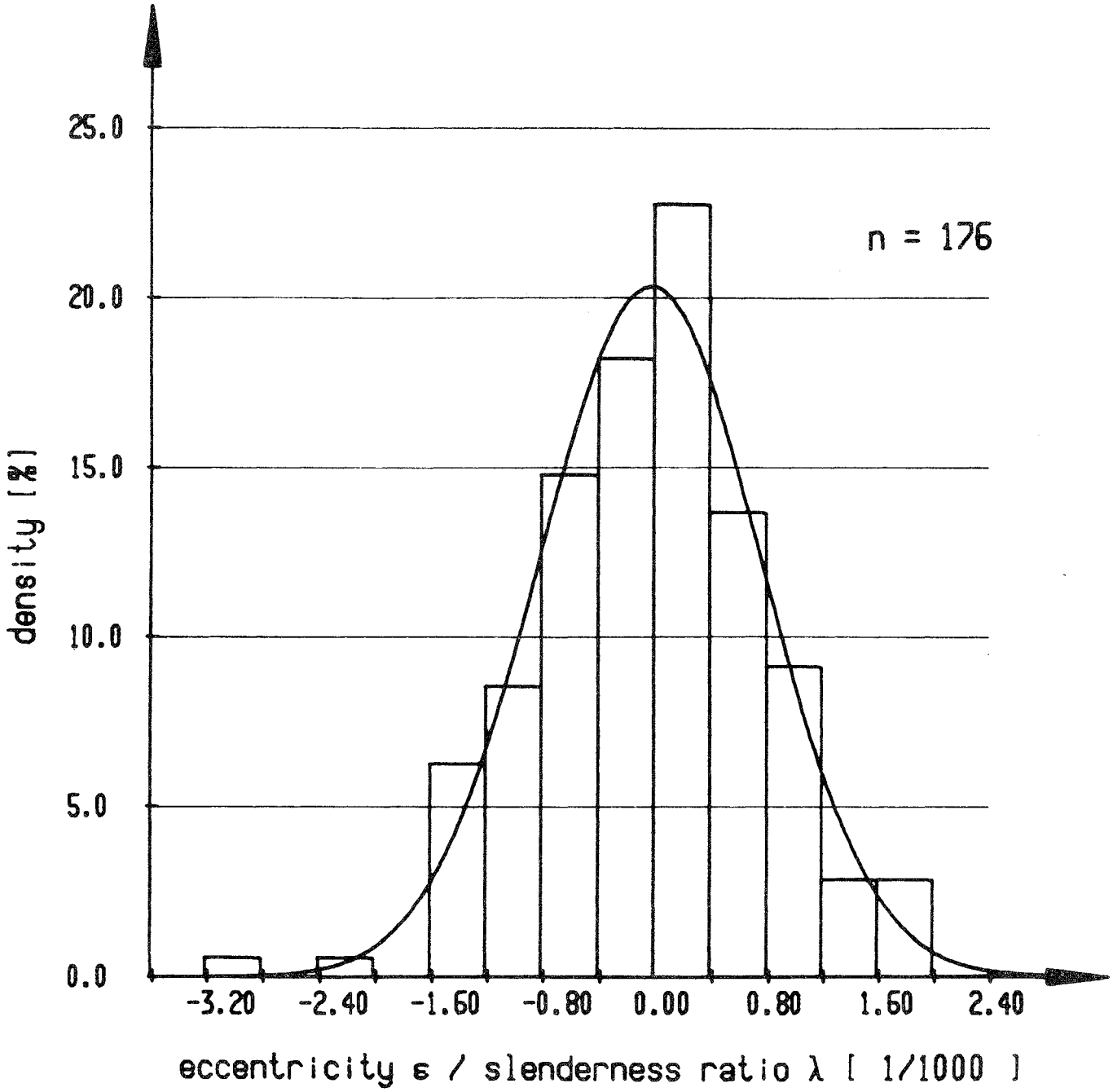


Figure 7: Distribution of the geometric imperfection column eccentricity

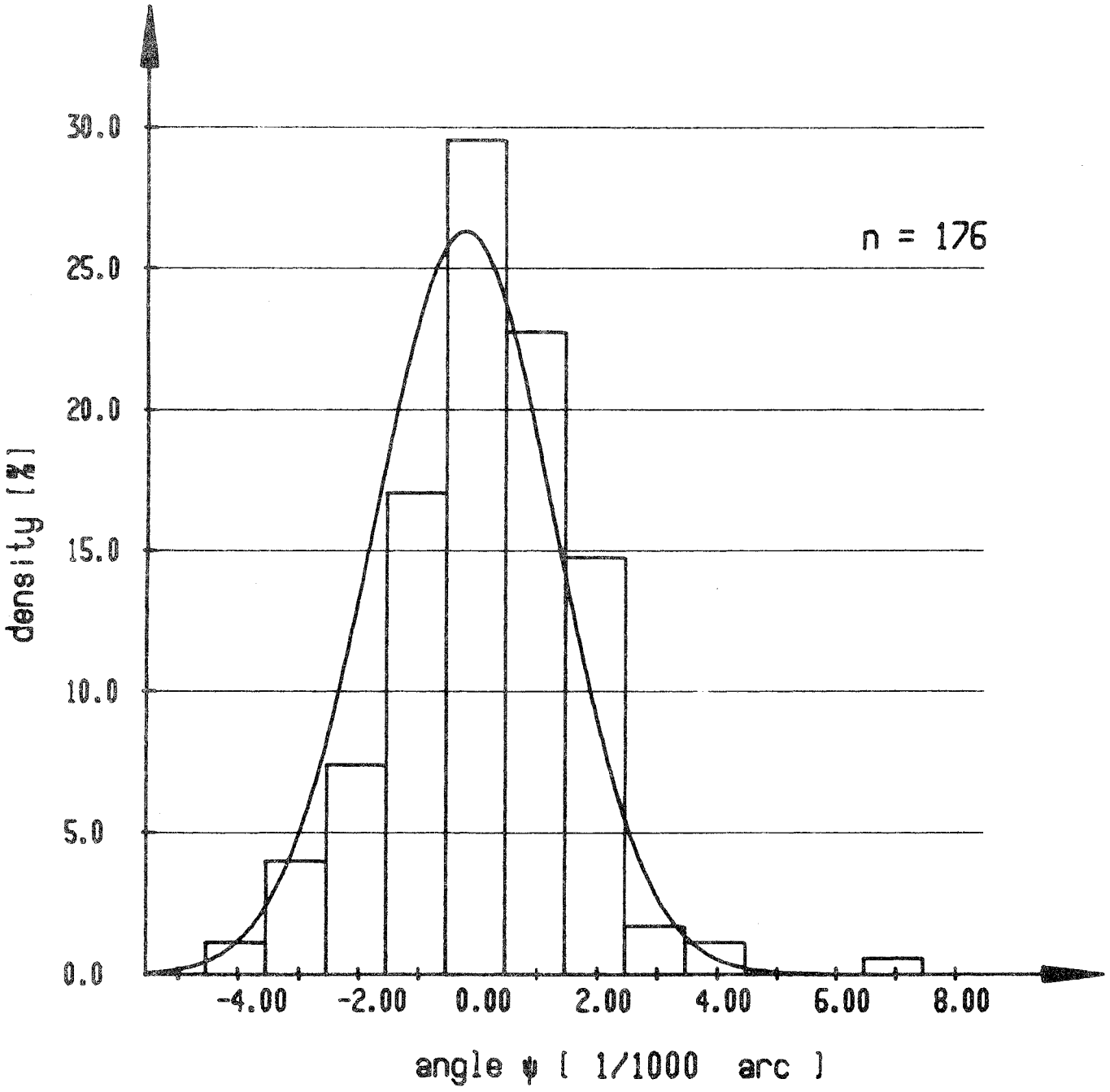


Figure 8: Distribution of the geometric imperfection angle of inclination

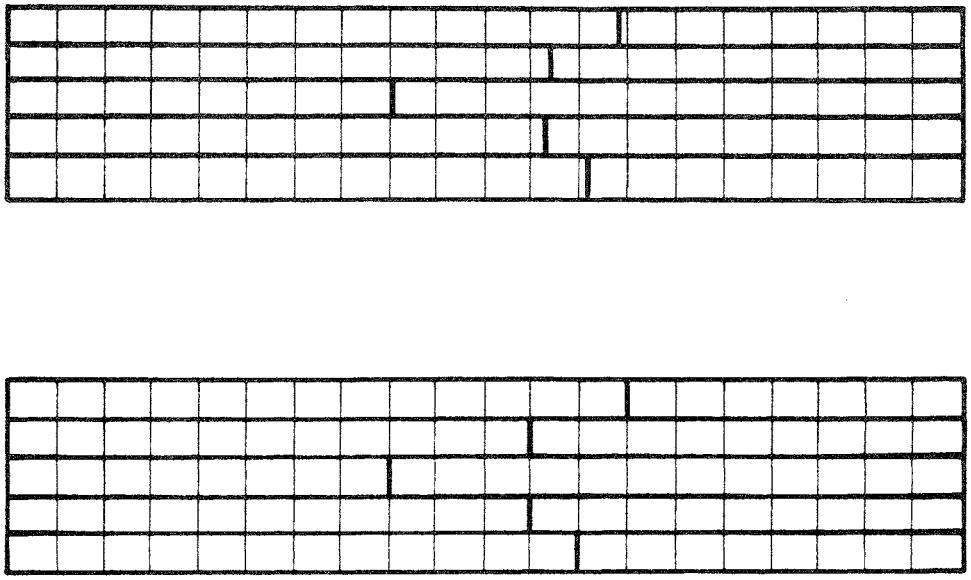


Figure 9: Glulam column with simulated finger joints (a.) and displaced finger joints (b.)

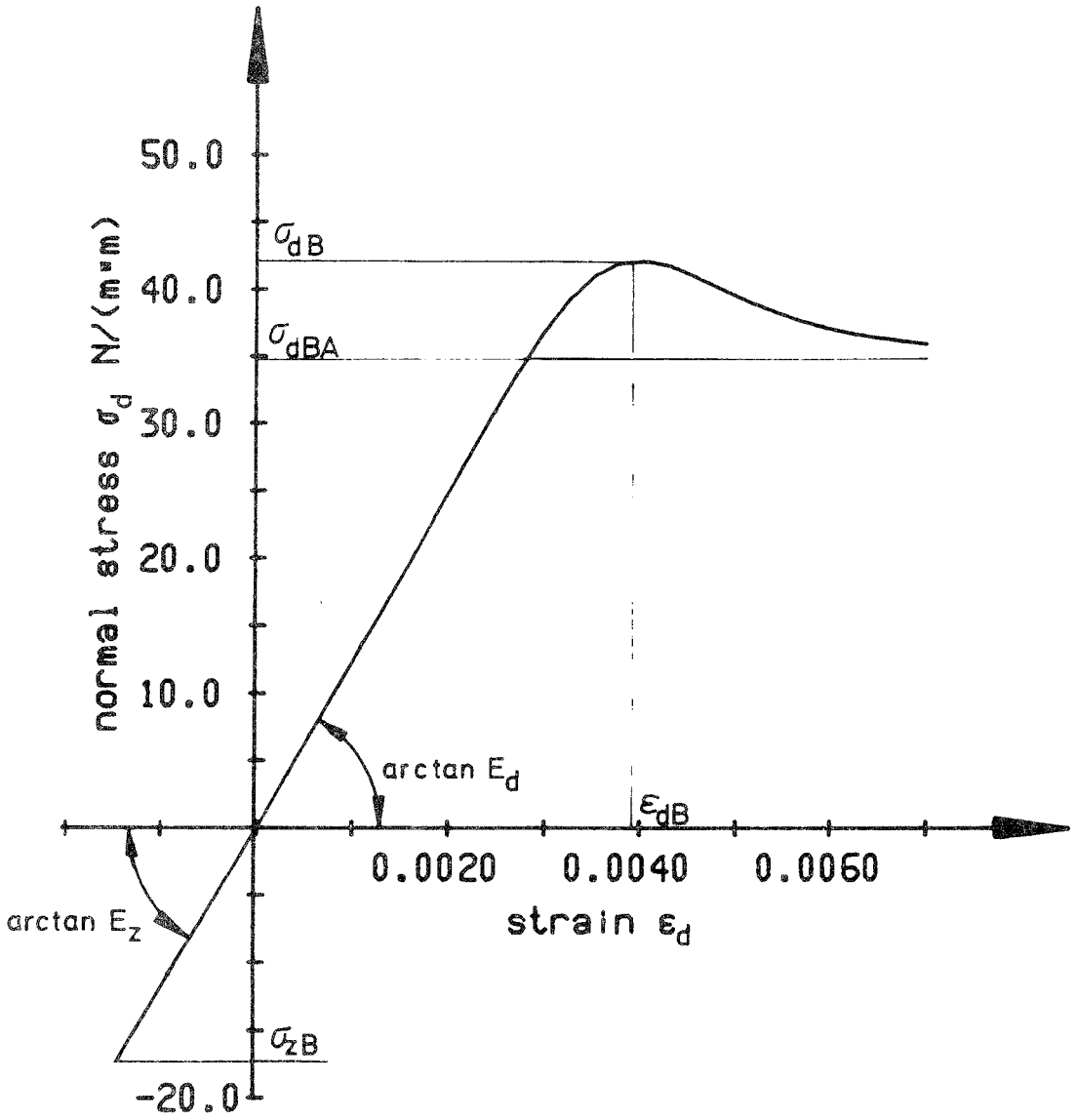


Figure 10: Stress-strain relationship of a lamination cross section

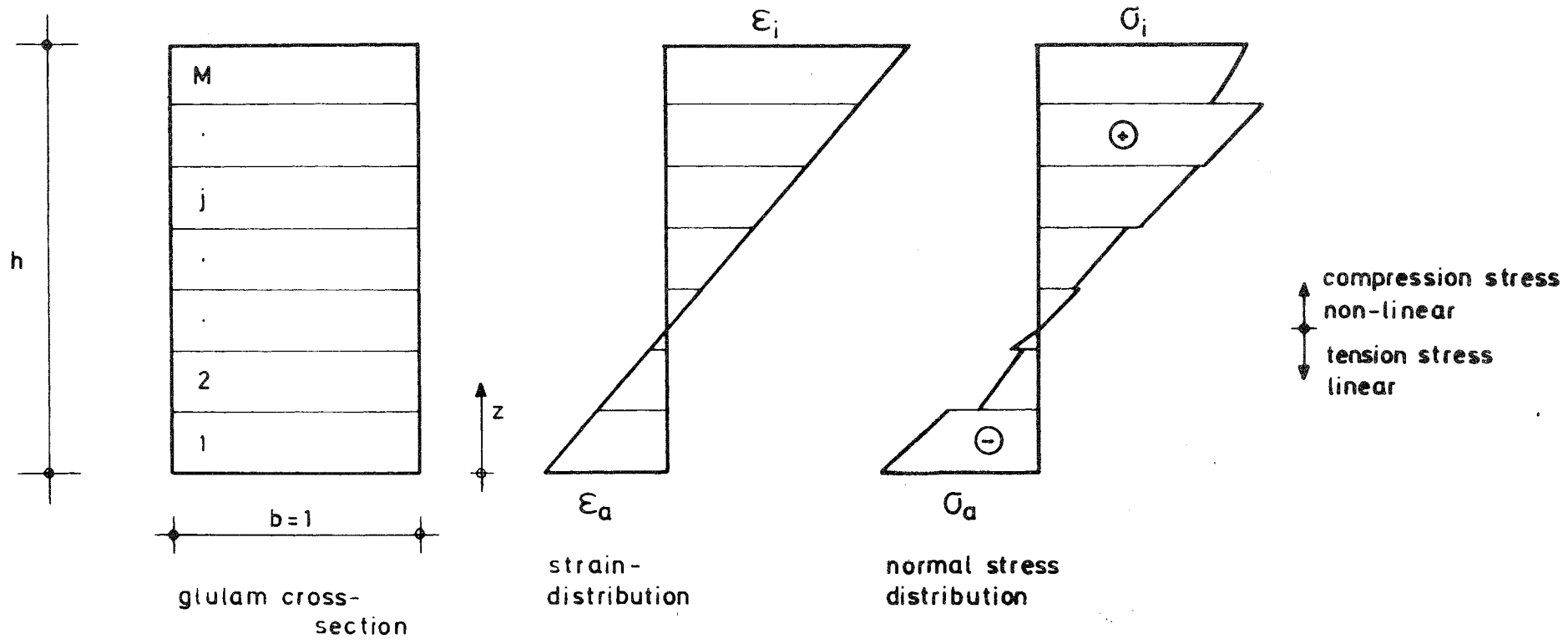


Figure 11: Strain distribution and stress distribution of a glulam cross section

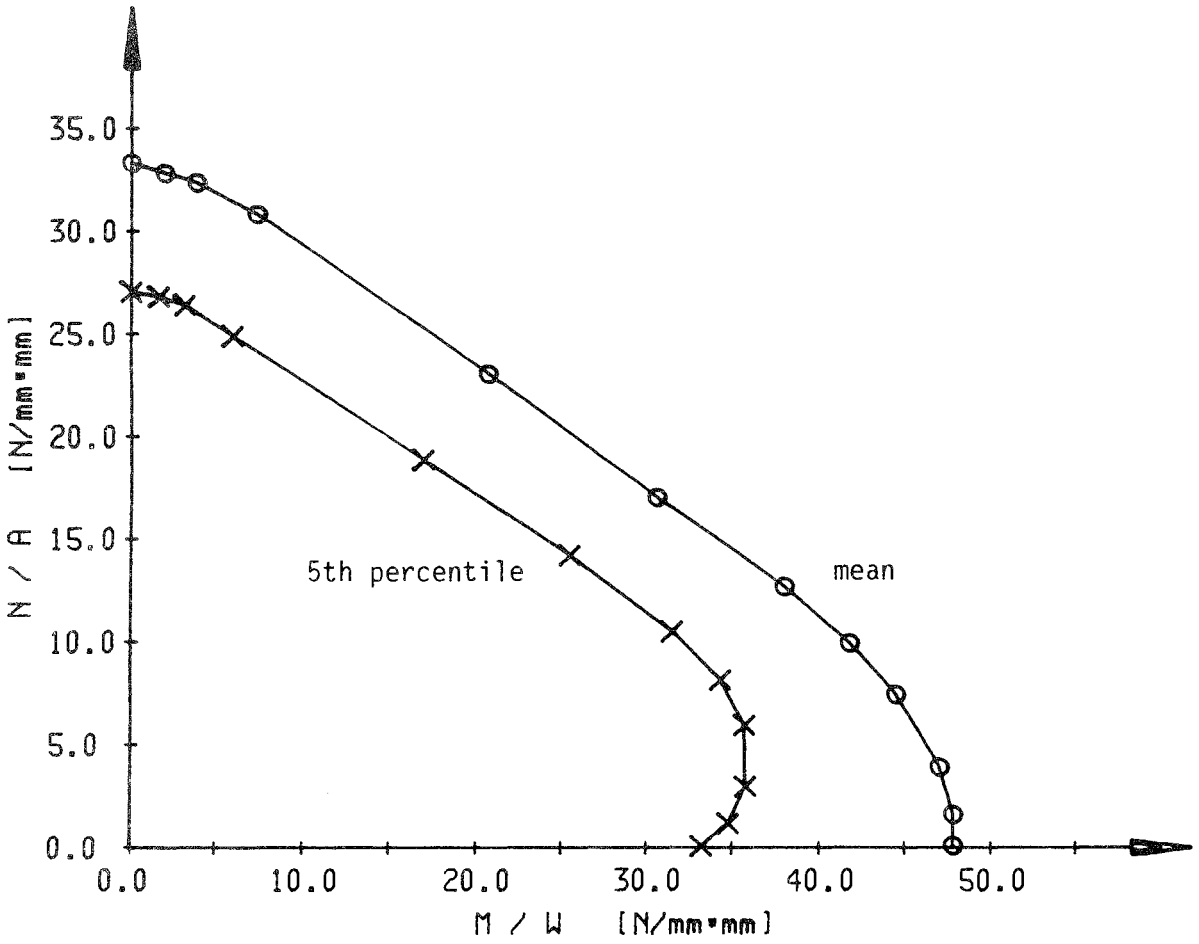


Figure 14: Function of cross section failure for glulam cross sections with 7 laminations

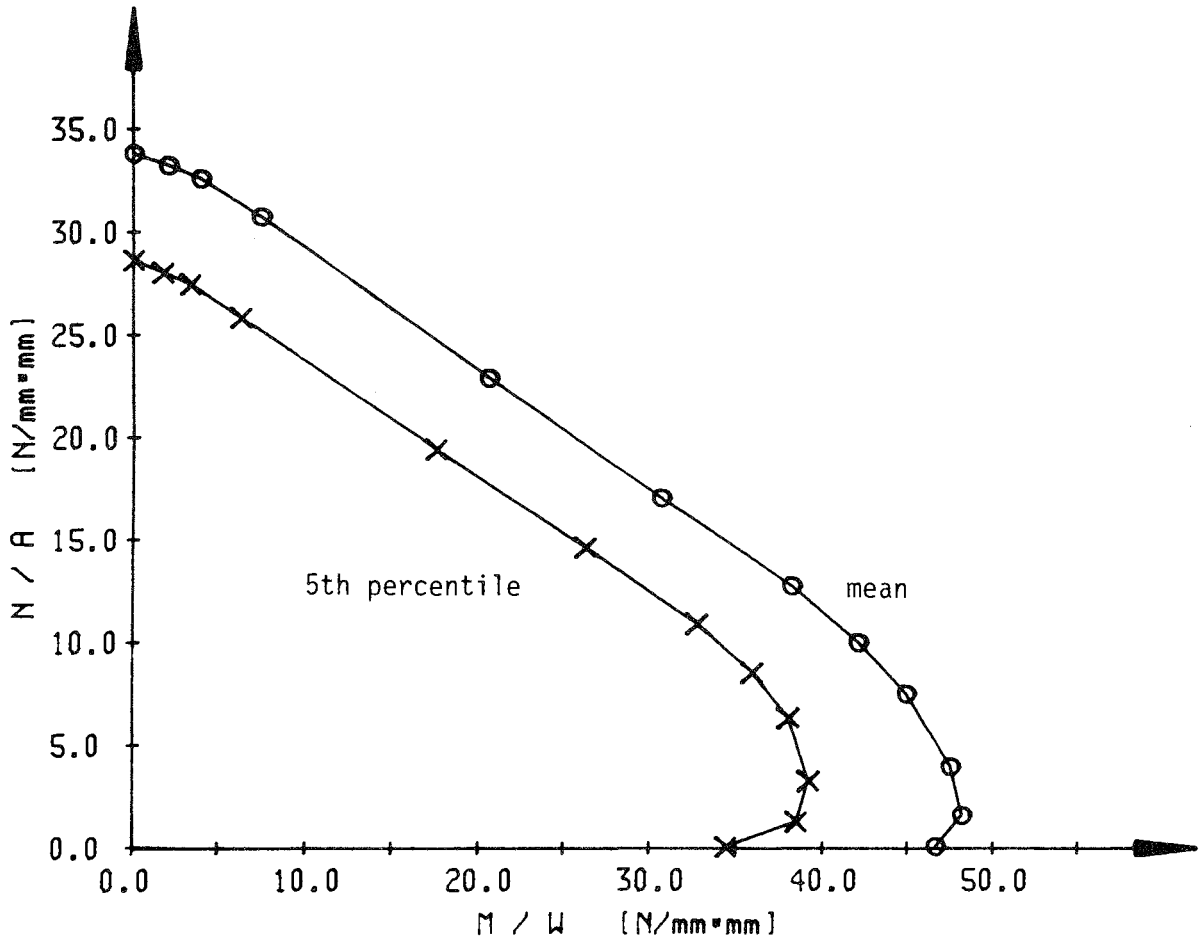


Figure 15: Function of cross section failure for glulam cross sections with 15 laminations

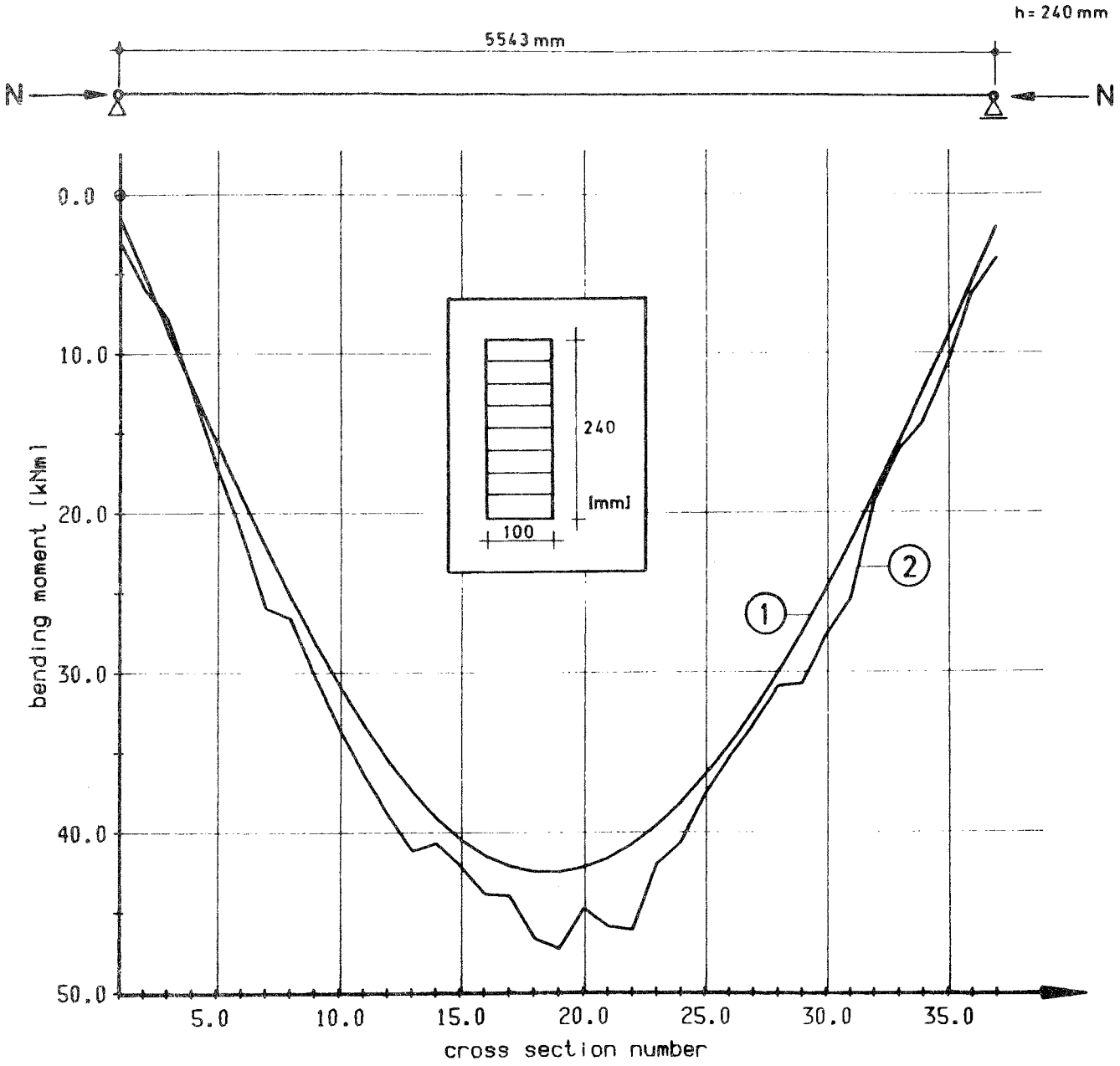


Figure 18: Bending moment under $N = N_{max}$ for a column with a slenderness ratio $\lambda = 80$

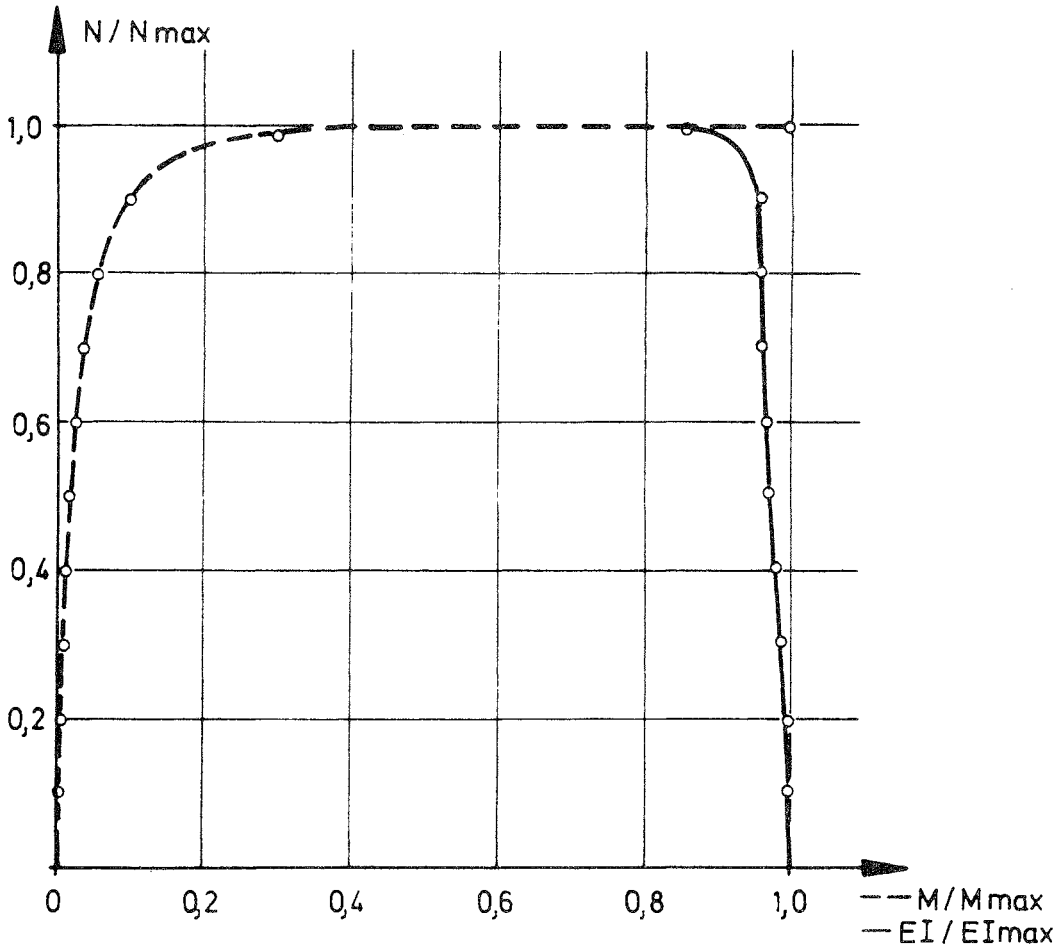


Figure 19: Increase of bending moment and deflection and decrease of stiffness of the critical cross section

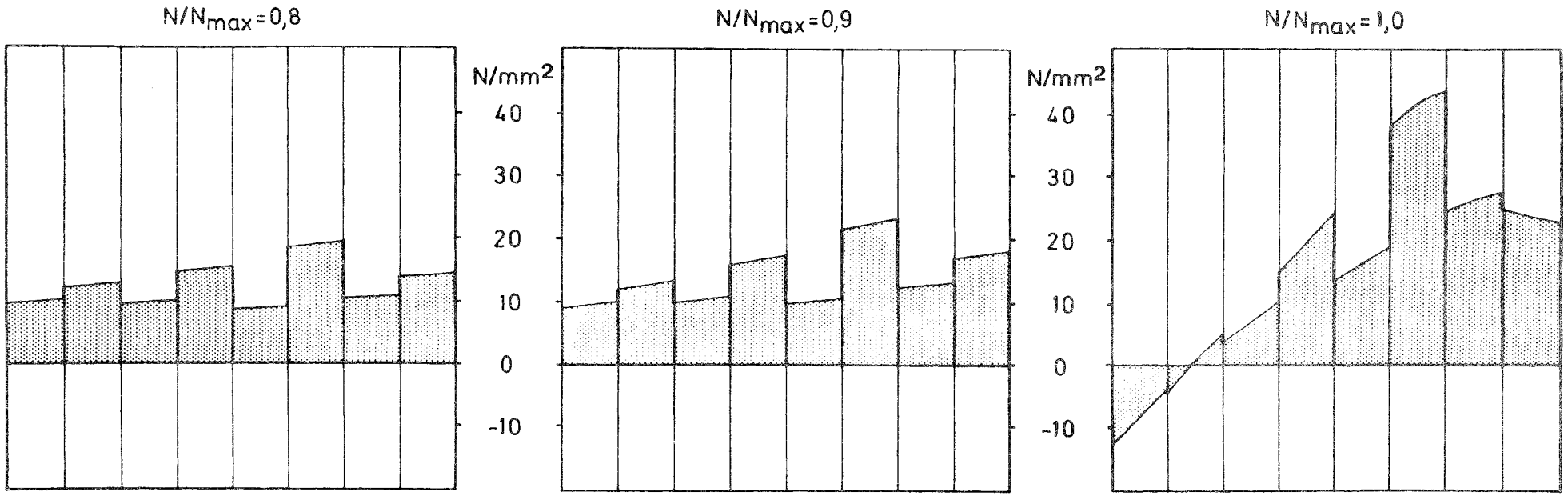


Figure 20: Stress distribution in the critical cross section for 3 load increments

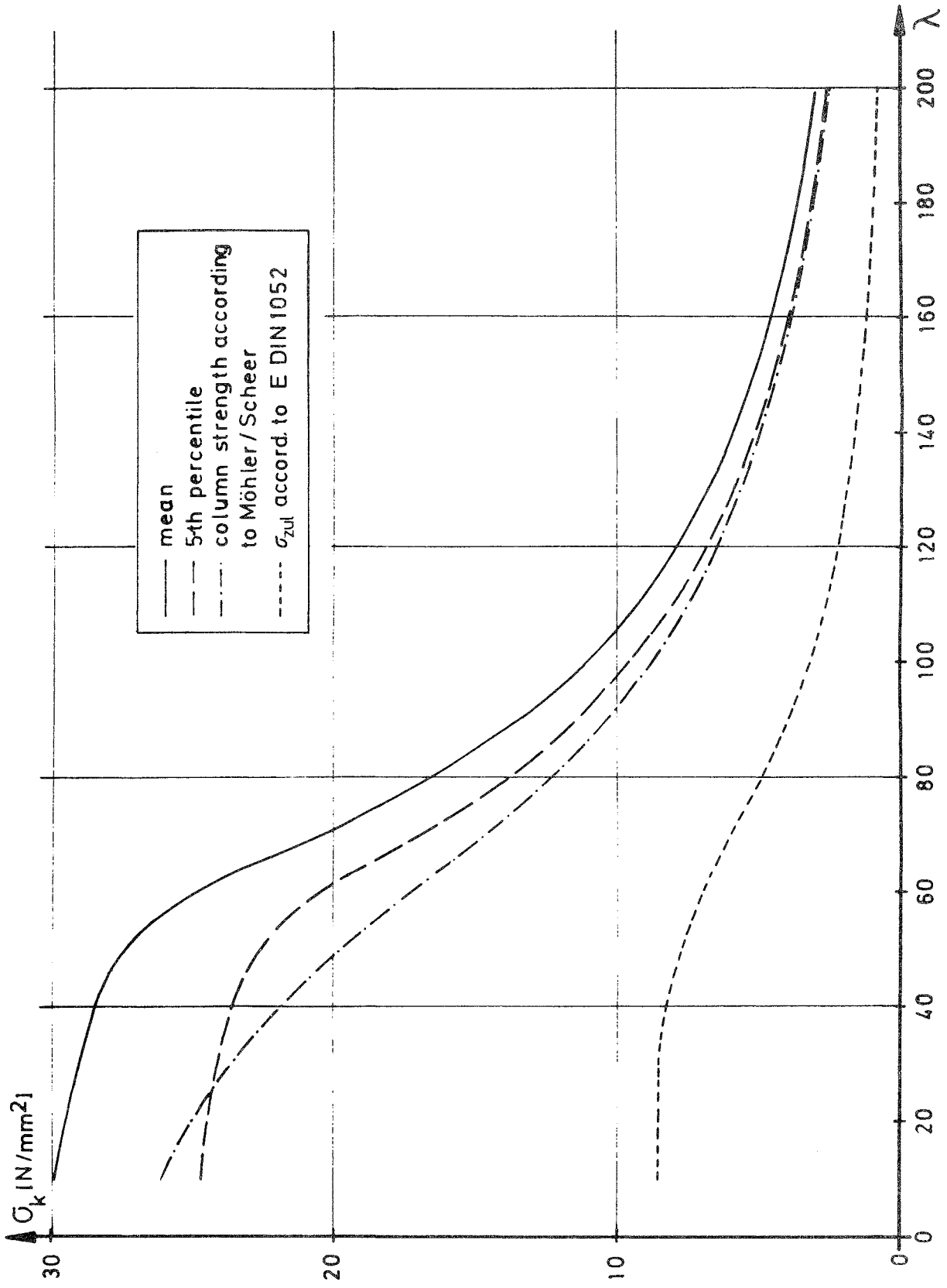


Figure 21: Column strengths from the strength model (mean and 5th percentile), according to Möhler/Scheer and allowable stress according to E DIN 1052

CIB-W18/19-12-3

INTERNATIONAL COUNCIL FOR BUILDING RESEARCH STUDIES AND DOCUMENTATION

WORKING COMMISSION W18 - TIMBER STRUCTURES

INFLUENCE OF VOLUME AND STRESS DISTRIBUTION ON THE SHEAR STRENGTH AND TENSILE STRENGTH PERPENDICULAR TO GRAIN

by

F Colling
University of Karlsruhe
Federal Republic of Germany

MEETING NINETEEN
FLORENCE
ITALY
SEPTEMBER 1986

INFLUENCE OF VOLUME AND STRESS DISTRIBUTION ON THE SHEAR STRENGTH AND TENSILE STRENGTH PERPENDICULAR TO GRAIN

by

François Colling

Lehrstuhl für Ingenieurholzbau und Baukonstruktionen

Universität Karlsruhe

W. Germany

1. ABSTRACT

In 1939 WEIBULL [1] developed a theory, which allows to estimate the influence of the size of the stressed volume and the stress-distribution over this volume on the strength of homogeneous, isotropic materials with brittle fracture behaviour. Although wood as material is neither homogeneous nor isotropic, it has been shown, that the application of Weibull's theory is possible. Weibull's theory has even entered several design codes (CIB-structural timber design code, Euro-Code 5, Canadian code ...). It is used especially in the case of shear and tension perpendicular to the grain, not least because of the existing brittle fracture behaviour.

In this paper, the application of Weibull's theory in the case of shear and tension perpendicular to the grain is discussed.

2. GENERAL

To estimate the influence of the stress-distribution and the size of the stressed volume on the strength, the two-parameter Weibull-distribution is used. The cumulative frequency is defined by:

$$S = 1 - \exp\left[-\int_V \left(\frac{\sigma}{\sigma_1}\right)^k dV\right] \qquad (1)$$

where σ' and k are the parameters of the Weibull-distribution, and $\sigma = \sigma(x,y,z)$ is the stress distribution over the volume V.

The (constant) width W of a beam with rectangular cross section is assumed not to influence its strength, so that the integral in eq (1) may be written [2]

$$\int_V \left(\frac{\sigma}{\sigma'}\right)^k dV = W \cdot \int_{x=0}^{L} \int_{y=0}^{D(x)} \left(\frac{\sigma(x,y)}{\sigma'}\right)^k dy\, dx \qquad (2)$$

For a beam with constant depth (D(x) = D) eq. (2) may be written:

$$\int_V \left(\frac{\sigma}{\sigma'}\right)^k dV = W \cdot \left(\frac{\max \sigma}{\sigma'}\right)^k \cdot L \cdot \underbrace{\int_{\varepsilon=0}^{1} f^k(\varepsilon)\, d\varepsilon}_{\lambda_L^k} \cdot D \cdot \underbrace{\int_{\xi=0}^{1} f^k(\xi)\, d\xi}_{\lambda_D^k} \qquad (3)$$

or

$$\int_V \left(\frac{\sigma}{\sigma'}\right)^k dV = V \cdot \left(\left(\frac{\max \sigma}{\sigma'}\right) \cdot \lambda_L \cdot \lambda_D\right)^k \qquad (4)$$

where V = stressed volume

max σ = maximum stress occuring over the volume V

$f(\varepsilon)$, $f(\xi)$ = dimensionless stress-distribution over the length and depth resp. related to max σ

λ_L, λ_D = "fullness-parameters" to describe the fullness of the stress-distribution.

λ_L and λ_D are dependant on the stress-distribution and the exponent k of the 2-parameter Weibull-distribution. A value of λ near 1 stands for a nearly constant stress distribution.

In fig.1 equations for the determination of the fullness-parameters λ are given as a function of the exponent k (see also [3]). The equation for the parabolic stress distribution ((6)) is only an approximation, because the integral can not be solved directly with a quadratic stress distribution. The exponent k only depends on the variation of the distribution and may approximately be determined by the following equation [2]:

$$k \cong \frac{1{,}15}{v} \tag{5}$$

where v is the coefficient of variation.
In the case of shear and tension perpendicular to the grain, a value of $k \sim 5$ may be assumed, corresponding to a coefficient of variation of $v \sim 0{,}23$. For $k = 5$ the values of the fullness-parameters λ are shown in fig. 2 and fig. 3 for any parabolic stress distribution. Fig. 2 is used when the maximum stress occurs at an edge, whereas fig. 3 is used, when the maximum stress occurs along the span.

If the fullness-parameter λ_L can not be determined directly by fig. 1-3, due to the kind of loading or support, it is possible to divide the given stress distribution in several fields (with the length l_i), for which the fullness-parameters λ_i can be determined according to fig. 1-3. The fullness-parameter λ_L of the beam may then be determined by:

$$\boxed{\lambda_L^5 = \Sigma \frac{l_i}{L} \cdot \left(\frac{\max \sigma_i}{\max \sigma} \cdot \lambda_{L,i}\right)^5} \tag{6}$$

where

l_i = length of the i-th field

$\max \sigma_i$ = maximum stress occuring along l_i

L = length of the beam

$\max \sigma$ = maximum stress occuring along L

$\lambda_{L,i}$ = fullness-parameter of the i-th field

Eq. (8) may therefore be written as

$$\boxed{\frac{\max \tau_2}{\max \tau_1} = \frac{k_{L/D,1}}{k_{L/D,2}} \cdot \frac{\lambda_{L,1}}{\lambda_{L,2}} \cdot \frac{\lambda_{D,1}}{\lambda_{D,2}} \cdot \left(\frac{V_1}{V_2}\right)^{0,2}} \qquad (10)$$

This relationship is valid for beams with rectangular cross section and constant depth.

3.2 Shear stress in tapered beams

In the case of a tapered beam, the depth D is not a constant (cf.eq.(2) and eq.(3)).

With the substitution $\xi = y/D(x)$ eq. (2) may be written

$$\int \left(\frac{\tau}{\tau'}\right)^k dV = W \cdot \left(\frac{\max \tau}{\tau'}\right)^k \cdot L \cdot \underbrace{\int_{\varepsilon=0}^{1} f^k(\varepsilon) \cdot h(\varepsilon) d\varepsilon}_{\lambda^k_{L,tap}} \cdot D_{max\tau} \cdot \underbrace{\int_{\xi=0}^{1} f^k(\xi)\, d\xi}_{\lambda^k_D} \qquad (11)$$

or

$$\int \left(\frac{\tau}{\tau'}\right)^k dV = W \cdot L \cdot D_{max\tau} \cdot \left(\frac{max\tau}{\tau'} \cdot \lambda_{L,tap} \cdot \lambda_D\right)^k \qquad (12)$$

where

$D_{max\tau}$ = depth of the beam where $max\tau$ occurs

$\lambda_{L,tap}$ = fullness-parameter of the stress distribution over the length L, taking into account the variable depth

$h(\varepsilon)$ = dimensionless function of the depth related to $D_{max\tau}$

In the case of a uniformly distributed load i.e. a linear distribution of the shearforce, the values of $\lambda_{L,tap}$ are given in fig. 6, assuming a value of k = 5 for the exponent of the Weibull-distribution.

According to eq.(6) of section 2, the fullness-parameter $\lambda_{L,tap}$ may be calculated knowing the $\lambda_{L,tap,i}$-values of each field of the beam (with the length l_i):

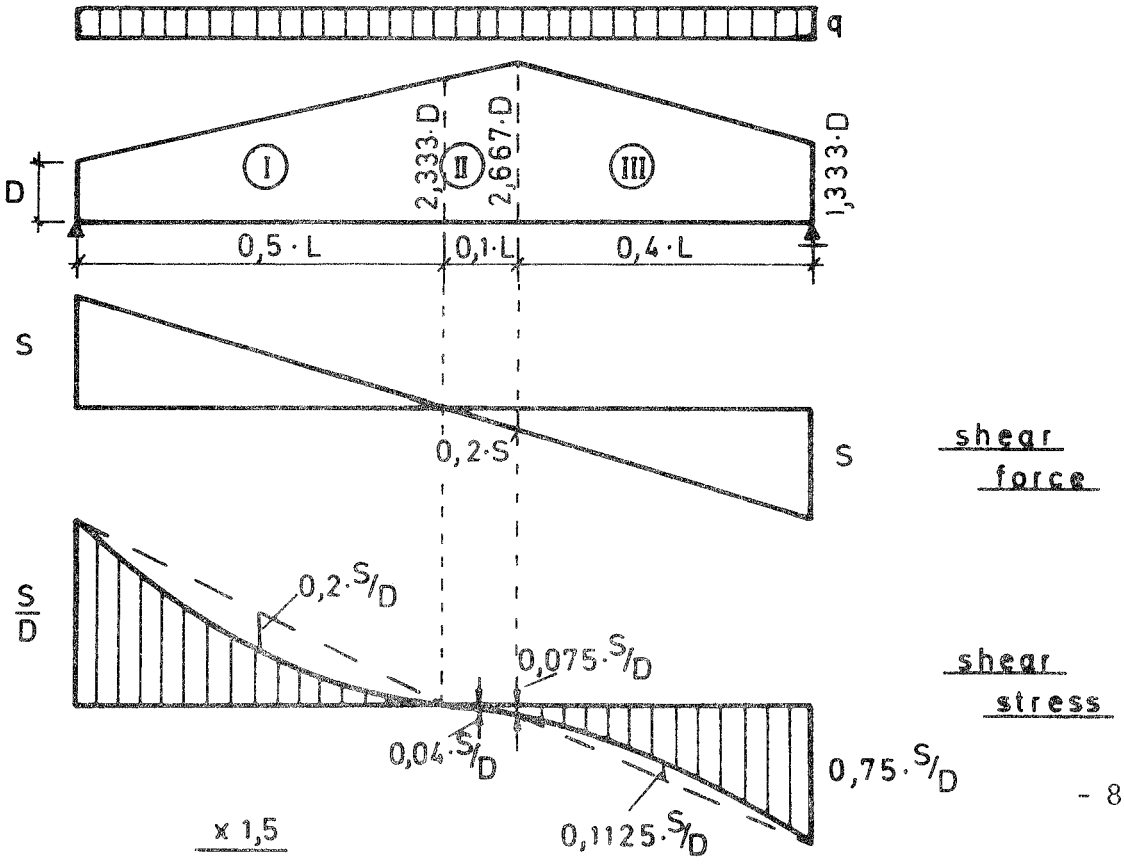
$$\lambda^5_{L,tap} = \Sigma \frac{l_i}{L} \cdot \frac{D_{max\tau_i}}{D_{max\tau}} \cdot \left(\frac{max\tau_i}{max\tau} \cdot \lambda_{L,tap,i}\right)^5 \qquad (13)$$

where

$D_{max\tau_i}$ = depth of the beam in the i-th field , where the maximum shear stress max τ_i occurs

$D_{max\tau}$ = depth of the beam, where the maximum shear stress max τ occurs

Example



field	S_1/S_2 ($S_1<S_2$)	D_1/D_2	$\lambda_{L,tap,i}$ see fig. 6
(I)	0	2,33	0,625
(II)	0	0,875	0,710
(III)	0,2	2,0	0,658

with eq. (13):

$$\lambda^5_{L,tap} = 0,5\cdot\frac{1}{1}\cdot\left(\frac{1}{1}\cdot 0,625\right)^5 + 0,1\cdot\frac{2,667}{1}\left(\frac{0,075}{1}\cdot 0,710\right)^5 + 0,4\cdot\frac{1,333}{1}\left(\frac{0,75}{1}\cdot 0,658\right)^5$$

$$= 0,0633$$

$$\lambda_{L,tap} = 0,576 \qquad \text{and } V = W \cdot D \cdot L$$

An approximation of this value for $\lambda_{L,tap}$ may be obtained with eq. (6): this calculation is based on the stress-distribution of the tapered beam, where the variable depth is considered in contrast with the distribution of the shear force. This approximation is determined with the help of fig. 2 and eq. (6):

field	τ_1/τ_2	τ_o/τ_2	$\lambda_{L,i}$
(I)	0	- 0,2	0,63
(II)	0	0,033	0,71
(III)	0,1	- 0,15	0,66

$$\lambda_L^5 = 0{,}5\cdot\left(\frac{1}{1}\cdot 0{,}63\right)^5 + 0{,}1\left(\frac{0{,}075}{1}\cdot 0{,}71\right)^5 + 0{,}4\cdot\left(\frac{0{,}75}{1}\,0{,}66\right)^5$$

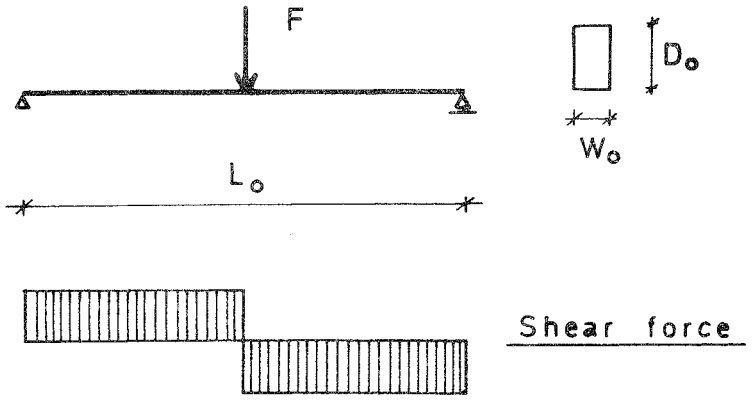
$$= 0{,}0615$$

$$\lambda_L = 0{,}573 \cong 0{,}576 = \lambda_{L,tap}$$

Therefore the fullness-parameters for tapered beams may be calculated in good approximation according to section 2 and section 3.1 resp., based on the distribution of the shear stress, whereas in the case of beams with rectangular cross section and constant depth the fullness-parameters may be calculated on the basis of the distribution of the shear force.

3.3 Design

If the characteristic shear strength $\tau_{0,k}$ is determined using the following test specimen



we have: $\lambda_{L_o} = 1{,}0$ (constant stress distribution)

$\lambda_{D_o} = 0{,}82$ (parabolic stress distribution)

k_{L_o/D_o} according to eq. (9)

and $V_o = W_o \cdot D_o \cdot L_o$.

Assuming a parabolic stress distribution over the depth for all beams, the characteristic shear strength of any beam may be determined by:

$$\tau_k = \frac{1}{\lambda_L} \cdot \frac{k_{L_o/D_o}}{k_{L/D}} \cdot \left(\frac{V_o}{V}\right)^{0,2} \cdot \tau_{o,k} \qquad (14)$$

where λ_L = fullness-parameter according to section 2 (fig. 1-3)

$k_{L/D}$ = determined according to section 3.1 (eq. 9)

$V = W \cdot L \cdot D_{max\tau}$

W = Width of the beam

L = length of the beam

$D_{max\tau}$ = depth of the beam where maxτ occurs

12

4. Tension perpendicular to the grain

4.1 Comparison of the theory with test results [6]

Kolb/Frech [6] tested three types of beams:
curved beams (type I), cambered beams (type II) and tapered cambered beams (type III). The beam configurations, test set-up and test results are given in fig. 7.

The maximum tensile stress perpendicular to the grain is calculated according to the following equations [7]:

$$\max \sigma_{\perp} = \kappa \cdot \frac{6\,M}{W \cdot D_{ap}^2} \qquad (15)$$

$$\kappa = A + B \cdot \left(\frac{D_{ap}}{R_{ap}}\right) + C \cdot \left(\frac{D_{ap}}{R_{ap}}\right)^2 \qquad (16)$$

with

$$A = 0{,}2 \cdot \tan\gamma$$

$$B = 0{,}25 - 1{,}5 \cdot \tan\gamma + 2{,}6 \cdot \tan^2\gamma$$

$$C = 2{,}1 \cdot \tan\gamma - 4 \cdot \tan^2\gamma$$

γ = slope of the beam (upper border) at the apex (for type I : $\gamma = 0$)

D_{ap} = depth of the beam at the apex

$$R_{ap} = R_1 + D_{ap}/2 = 6{,}0 \text{ m} + \frac{D_{ap}}{2}$$

The tensile strength perpendicular to the grain is shown for all beams in fig. 8. This fig. clearly shows the decrease of the tensile strength perpendicular to the grain within each type with increasing slope γ and the different bearing capacity between the three types of beams: the tensile strength perpendicular to the grain of type I is on average 0,75 times the strength of type II and 0,625 times the strength of type III. It shall now be shown how far these different bearing capacities can be explained by Weibull's theory.

The distribution of the tensile stress perpendicular to the grain was investigated with the method of finite elements. The following beams were considered:

beam I.3
II.3 } to investigate the differences between the beam types
III.3
III.2 } to investigate the differences within one beam type
III.1

In table 1 the κ-values of eq. (16) are compared with the κ-values, determined by the method of finite elements.

Table 1:

Beam	D_{ap} mm	R_{ap} mm	κ eq.(16)	κ FE
I.3	1000	6500	0,0385	0,0394
II.3	1450	6725	0,0942	0,0934
III.3	1450	6725	0,0942	0,0935
III.2	1250	6625	0,0700	0,0705
III.1	1110	6555	0,0535	0,0534

This comparison shows a good agreement (also for the tapered cambered beams, if the slope of the upper border is used in eq. (16)). The fullness parameters were determined by

$$\lambda_L \cdot \lambda_D = \left[\frac{\Sigma(\frac{\sigma_{i\perp}}{\max \sigma_\perp})^5 \cdot V_i}{V_{tot}}\right]^{0,2} \qquad (17)$$

where

V_i = volume of a finite element with tensile stress perp. to grain

$\sigma_{i\perp}$ = tensile stress perp. to grain of a finite element with volume V_i

$V_{tot} = \Sigma V_i$ = stressed volume

$\max \sigma_\perp$ = maximum tensile stress perp. to grain in the volume V_{tot}

These values are given in table 2.

Table 2:

Beam	V_{tot} m^3	$\Sigma(\frac{\sigma_{i\perp}}{max\sigma_\perp})^5 \cdot V_i$ m^3	$\lambda_L \cdot \lambda_D$
I.3	0,922	0,05547	0,570
II.3	0,835	0,05715	0,585
III.3	0,420	0,05880	0,675
III.2	0,310	0,04800	0,689
III.1	0,246	0,03320	0,670

In design calculations the volume V_c of the curved part of the beam(between the points of tangency)is used. This volume corresponds to the shaded area in fig. 7.

According to eq. (7) and eq. (8) resp., the fullness-parameters $(\lambda_L \cdot \lambda_D)_c$ corresponding to the volume V_c are calculated by

$$(\lambda_L \cdot \lambda_D)_c = \lambda_L \cdot \lambda_D \cdot (\frac{V_{tot}}{V_c})^{0,2} \qquad (18)$$

and given in table 3.

Table 3:

Beam	V_c m^3	$(\lambda_L \cdot \lambda_D)_c$
I.3	0,545	0,633
II.3	0,667	0,612
III.3	0,446	0,667
III.2	0,287	0,700
III.1	0,147	0,743

The higher fullness-parameters of beam-type III may be explained by the fact, that the whole volume V_c of type III is located between the loading points (constant bending moment) whereas a part of the volumes V_c of type I and II is located outside the loading points (i.e. the stress in this part is lower). Another factor that might explain the higher values of $(\lambda_L \cdot \lambda_D)_c$ for type III is the influence of the loading points: in case of beam type I and II a greater part of the volume V_c is strained by a compressive stress perpendicular to the grain.

For the investigation of the bearing capacity within beam type III, the expected $\frac{\max\sigma_{i\perp}}{\max\sigma_{j\perp}}$ -values were calculated according to eq.(8) and compared with the test-values (see table 4).

Table 4:

	$\frac{\sigma_{i\perp}}{\sigma_{j\perp}}$					
i / j	III.1		III.2		III.3	
	eq(8)	test	eq(8)	test	eq(8)	test
III.1	1,0	1,0	0,928	0,914	0,892	0,864
III.2	1,077	1,094	1,0	1,0	0,961	0,945
III.3	1,121	1,158	1,041	1,058	1,0	1,0

This comparison shows a good agreement between the theoretical values according to Weibull's theory and the test values.

The decrease of the bearing capacity with increasing slope γ can thus be explained and numerically evaluated with the help of Weibull's theory.

The expected ratios of the tensile strength perpendicular to the grain for the different beam types are given in table 5 and are again compared with the test results.

Table 5:

$\frac{\sigma_{i\perp}}{\sigma_{j\perp}}$

i / j	I.3 eq(8)	I.3 test	II.3 eq(8)	II.3 test	III.3 eq.(8)	III.3 test
I.3	1,0	1,0	0,994	1,471	0,988	1,770
II.3	1,006	0,680	1,0	1,0	0,994	1,204
III.3	1,012	0,565	1,006	0,831	1,0	1,0

According to Weibull's theory (eq.(8)) all types would have the same tensile strength perp. to the grain: the value $(\lambda_L \cdot \lambda_D)_c \cdot (V)^{0,2}$ (cf. table 3) is nearly a constant for all beam types. The oppositely oriented influences of a greater volume and a lower fullness-parameter counteract, so that the expected strength is the same for all three beam types.

The tests however showed a clear tendency, that the tensile strength perp. to the grain of the cambered beams is higher than the strength of the curved beams with constant depth, and that the strength of the tapered cambered beams is even higher than the strength of the other two beam types.

As too little is known about the tests described in [6], no explanation could be found concerning the contradiction between the theoretical and the test-values.

Therefore further (theoretical and experimental) investigation in this field is required.

4.2 Design

The characteristic tensile strength perpendicular to the grain $\sigma_{0\perp}$ is determined by a pure tension test (i.e. $\lambda_L \cdot \lambda_D = 1,0$) with a test specimen of volume V_0.

The characteristic strength of any beam can be calculated according to eq. (8):

$$\sigma_{k}^{\perp} = \frac{1}{\lambda_L \cdot \lambda_D} \cdot \left(\frac{V_o}{V}\right)^{0,2} \cdot \sigma_{o,k}^{\perp} \qquad (19)$$

According to the draft of Eurocode V (October 1985), the characteristic tensile strength perp. to grain of the strength class C3 (determined with a test specimen of volume $V_o = 0,02\ m^3$) is:

$$\sigma_{k}^{\perp} = 0,4 \quad N/mm^2$$

In the case of beam I.3 we could expect (according to eq. 19 and table 3) a characteristic strength:

$$\sigma_{k}^{\perp} = \frac{1}{0,633} \cdot \left(\frac{0,02}{0,545}\right)^{0,2} \cdot 0,4 \approx 0,33\ N/mm^2$$

Assuming a coefficient of variation of about 25%, the mean strength may be calculated approximately to

$$\sigma^{\perp} \cong 0,33 \cdot \frac{1}{1-1,645 \cdot 0,25} \cong 0,56\ N/mm^2$$

(Gauss-distribution)

This value is approximately reached by beam I.3 (mean strength ~ 0,65 N/mm^2).

With the assumption, that the decrease of strength with increasing slope γ within one beam type can be explained by Weibull's theory (see section 4.1), eq. (19) may be used for beam type I (curved beam with constant depth).

Theoretically, eq. (19) is also valid for beam type II and III, but the higher bearing capacities of these beams (c.f. fig 8) might be taken into account in the following way:

$$\sigma_{k}^{\perp} = 1,3 \cdot \frac{1}{\lambda_L \cdot \lambda_D} \cdot \left(\frac{V_o}{V}\right)^{0,2} \cdot \sigma_{o,k}^{\perp} \qquad (20)$$

for beam type II (cambered beams)

and

$$\sigma_{k\perp} = 1{,}6 \cdot \frac{1}{\lambda_L \cdot \lambda_D} \cdot \left(\frac{V_0}{V}\right)^{0{,}2} \cdot \sigma_{0,k\perp} \qquad (21)$$

for beam type III (tapered cambered beams).

5. SUMMARY AND CONCLUSIONS

Weibull's theory of brittle fracture is used to describe the influence of the stress distribution and the size of the stressed volume on the strength of a beam.

The determination of the so called fullness-parameters λ (which stand for the fullness of the stress-distribution) is shown. Also a mathematical relationship between the expected ratio of the strength of two beams and their fullness-parameters and their stressed volume has been deducted.

The application of this theory and a possible design method has been shown in the case of shear stress and tensile stress perpendicular to the grain.

Because of the differences between the theoretical and the experimental results in the case of tensile stress perpendicular to the grain, further investigations are required. The application of a modified weakest link theory (with weighted influences of the beam-length and depth) as well as the further dependency of the strength on the wood-properties (density, growth rings, knots ...) will probably be investigated in a proposed research program in Karlsruhe.

References

[1] Weibull, W. 1939: A statistical theory of the strength of materials. Ing. Vetensk. Akad. Handb. No. 151

[2] Colling, F. 1986: Einfluß des Volumens und der Spannungsverteilung auf die Festigkeit eines Rechteckträgers. Herleitung einer allgemeinen Beziehung mit Hilfe der 2-parametrigen Weibull-Verteilung. Holz als Roh- und Werkstoff 44, S. 121 - 125 .

[3] Colling, F. 1986: Einfluß des Volumens und der Spannugnsverteilung auf die Festigkeit eines Rechteckträgers. Bestimmung der Völligkeitsbeiwerte . Anwendungsbeispiele. Holz als Roh- und Werkstoff 44, S. 179 - 183

[4] Foschi, R.O.; Barrett, J.D. 1976: Longitudinal shear strength of Douglas-fir.
Can. J. Civ. Eng., Vol. 3, p. 198-208

[5] Foschi, R.O.; Barrett, J.D. 1977: Longitudinal shear in wood beams: a design method.
Can. J. Civ. Eng., Vol. 4, p. 363-370

[6] Kolb, H; Frech, P. 1975: Biegeversuch zur Ermittlung der Querzugfestigkeit von gekrümmten Trägern aus Brettschichtholz.
Prüfungsbericht Nr. 30667, FMPA Stuttgart, Germany

[7] Blumer, H. 1972/79: Spannungsberechnungen an anisotropen Kreisbogenscheiben und Satelträgern konstanter Dicke. Veröffentlichung des Lehrstuhls für Ingenieurholzbau und Baukonstruktionen, Universität Karlsruhe, Germany.

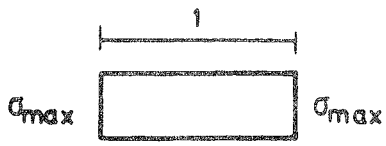
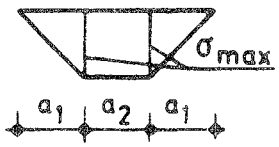
	stress - distribution	$\lambda = \left[\int_{\varepsilon=0}^{1} f^k(\varepsilon)\, d\varepsilon \right]^{1/k}$
①		1,0
②		$\left(\frac{1}{k+1}\right)^{1/k}$
③		$\left(\frac{1}{k+1} \cdot \frac{1-\eta^{k+1}}{1-\eta}\right)^{1/k}$
④		$\left(\frac{1}{k+1} \cdot \frac{1+\lvert\eta\rvert^{k+1}}{1+\lvert\eta\rvert}\right)^{1/k}$
⑤		$\left[\frac{1}{k+1}\left(1+a_2 \cdot k\right)\right]^{1/k}$
⑥		$\left[\frac{1}{k+1}\left(1+0{,}345\ k - 0{,}027 \cdot k^2 + 0{,}0013 \cdot k^3\right)\right]^{1/k}$

fig.1: fullness-parameter λ as a function of the exponent k of the two-parameter Weibull-distribution

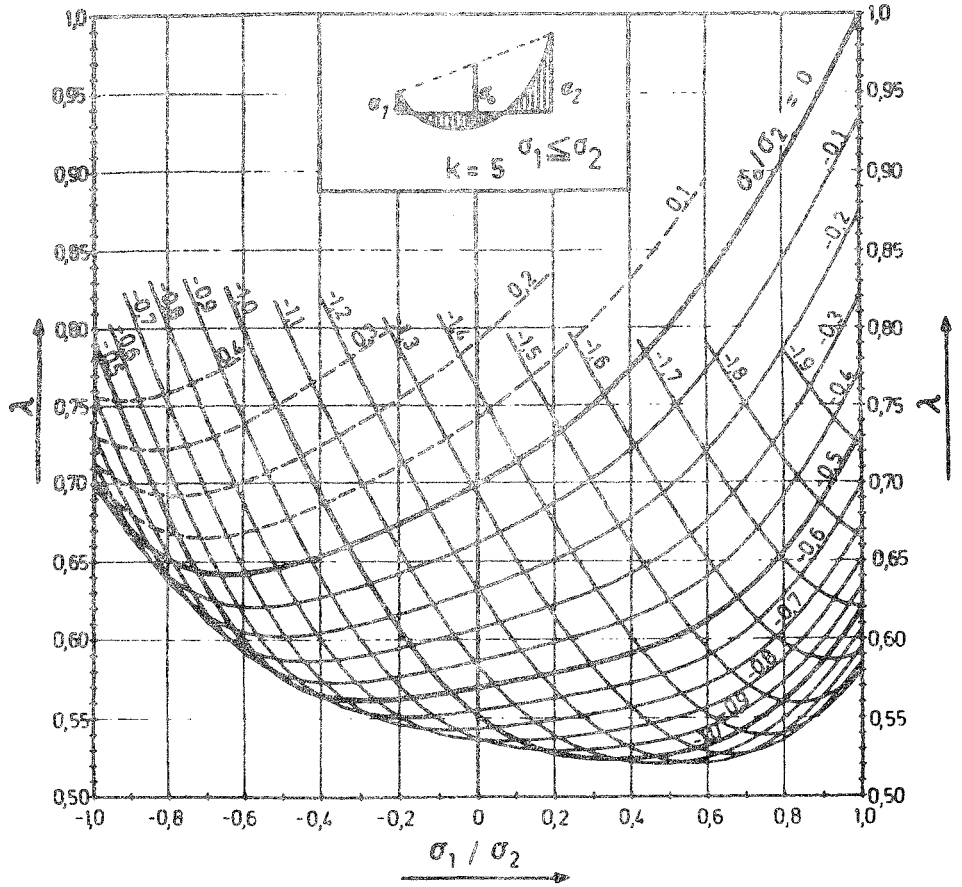


fig.2: fullness-parameter λ for a parabolic stress distribution, with the maximum stress occuring at the edge

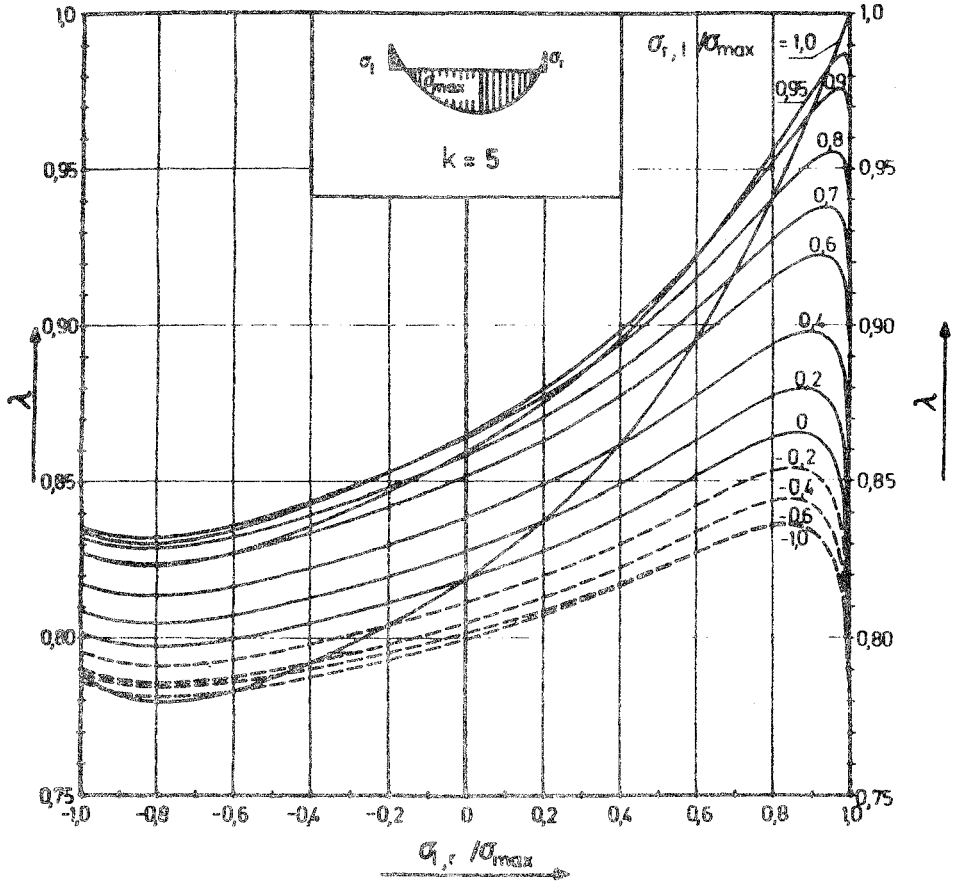


fig.3: fullness-parameter λ for a parabolic stess distribution, with the maximum stress occuring along the span

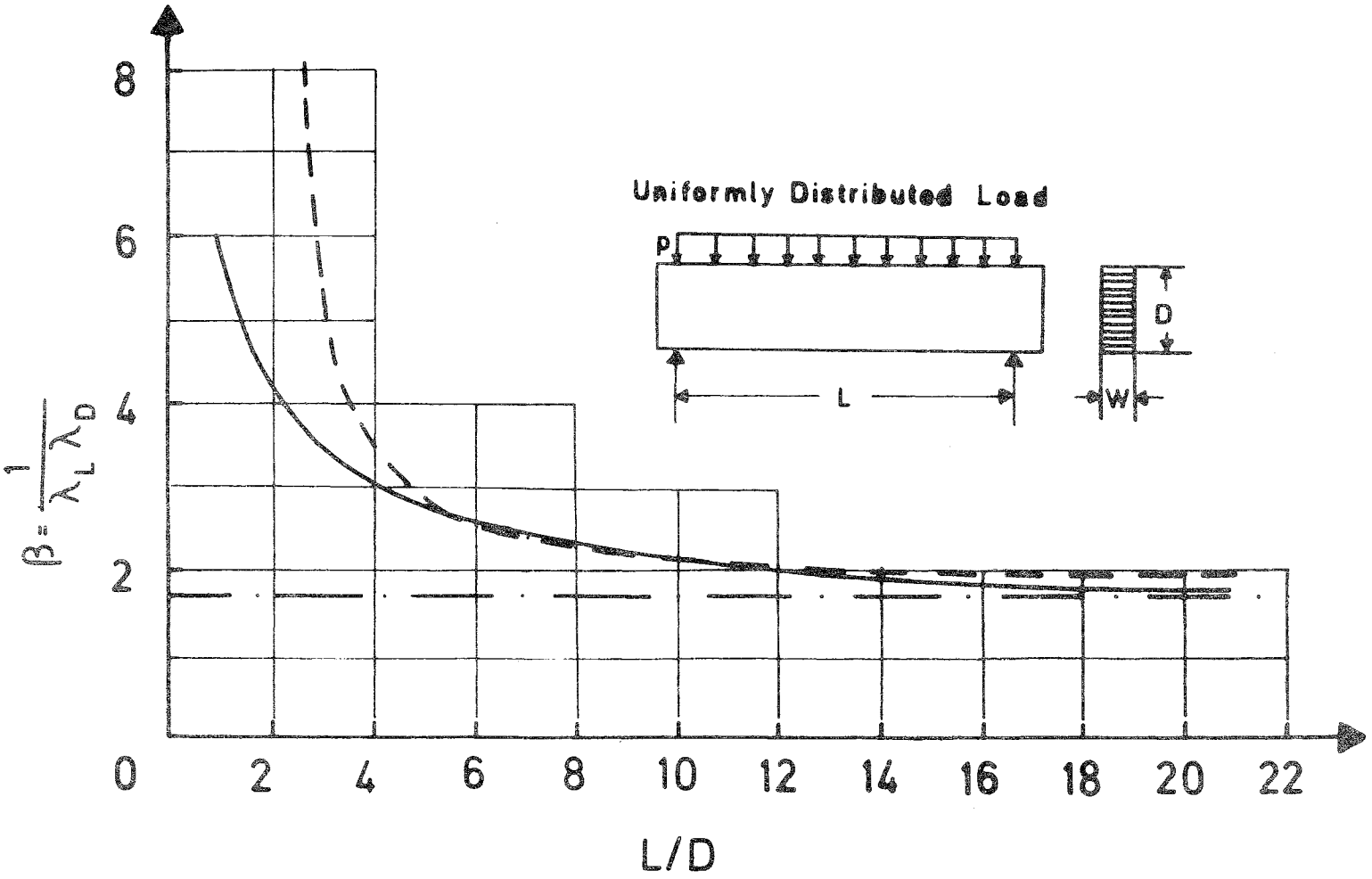


fig.4: β-values for uniformly distributed load

——— according to Foschi/Barrett [4]

—·— according to section 2 ($\frac{1}{\lambda_L \cdot \lambda_D} = \frac{1}{\lambda_{\Delta} \cdot \lambda_D} = \frac{1}{0,70 \cdot 0,82} = 1,742$)

----- $1,742 \cdot \frac{L/D}{L/D-2}$

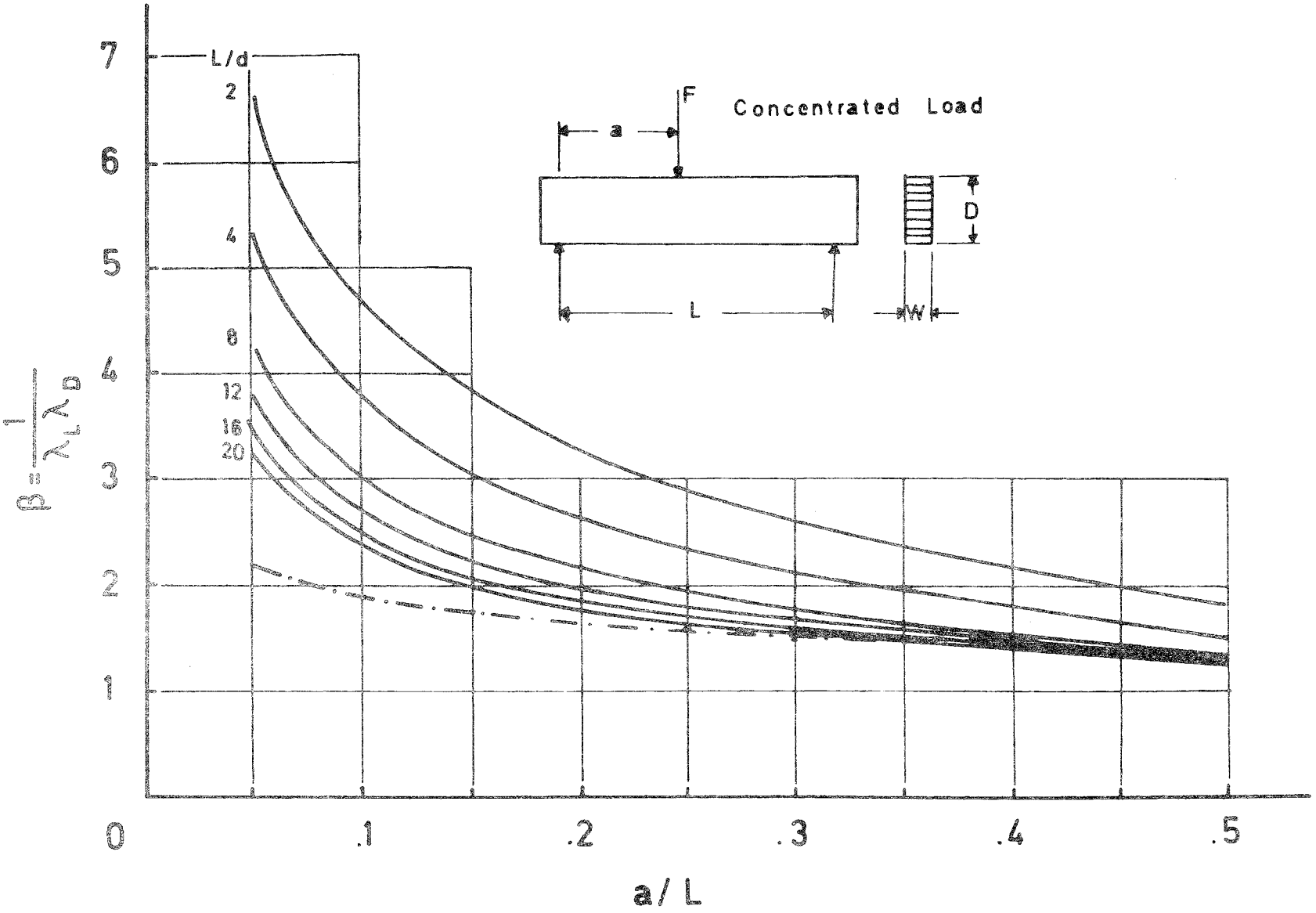


fig.5: β-values for concentrated load

——— according to Foschi/Barrett [4]

—·— according to section 2

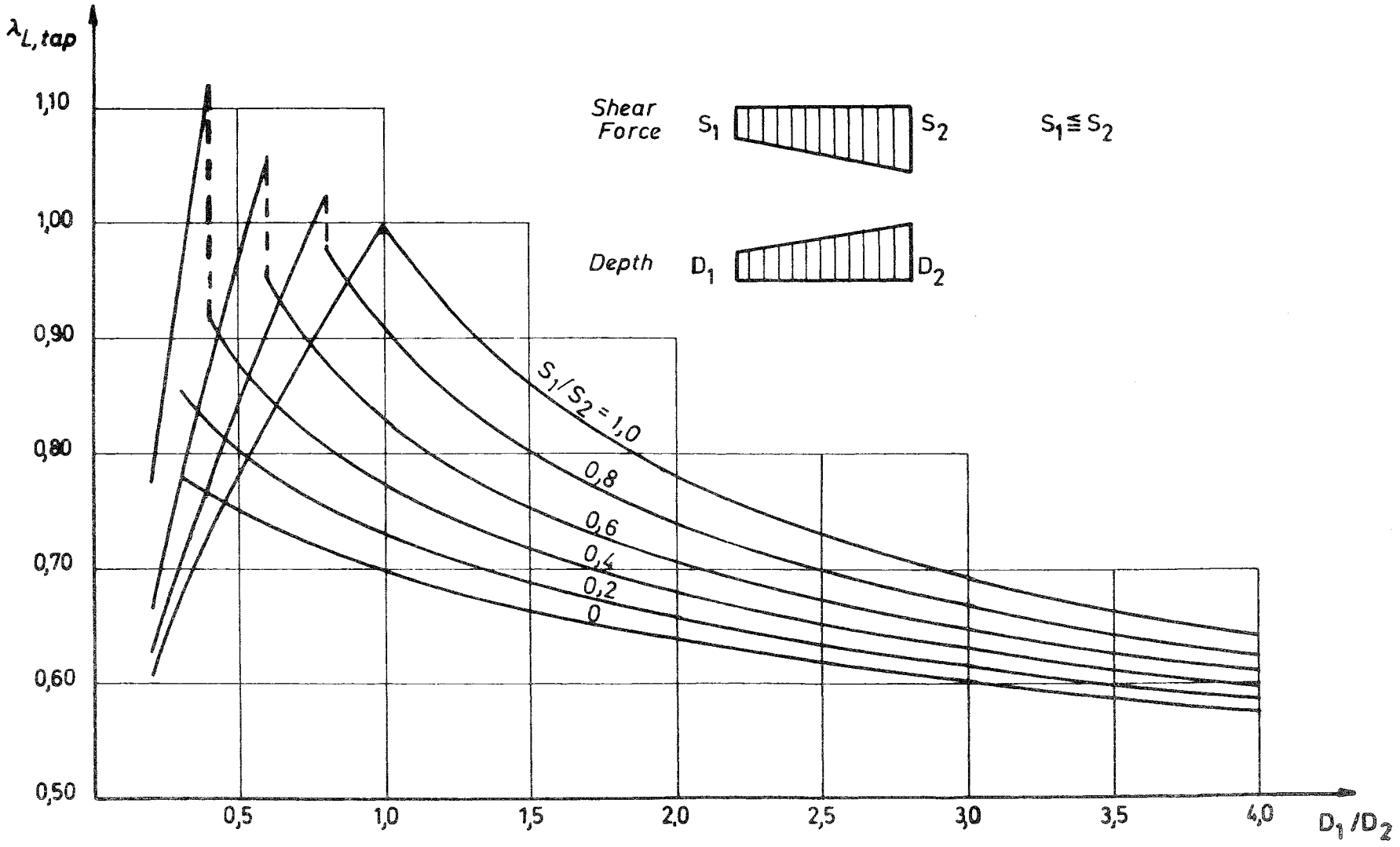


fig.6: fullness-parameter $\lambda_{L,tap}$ for tapered beams

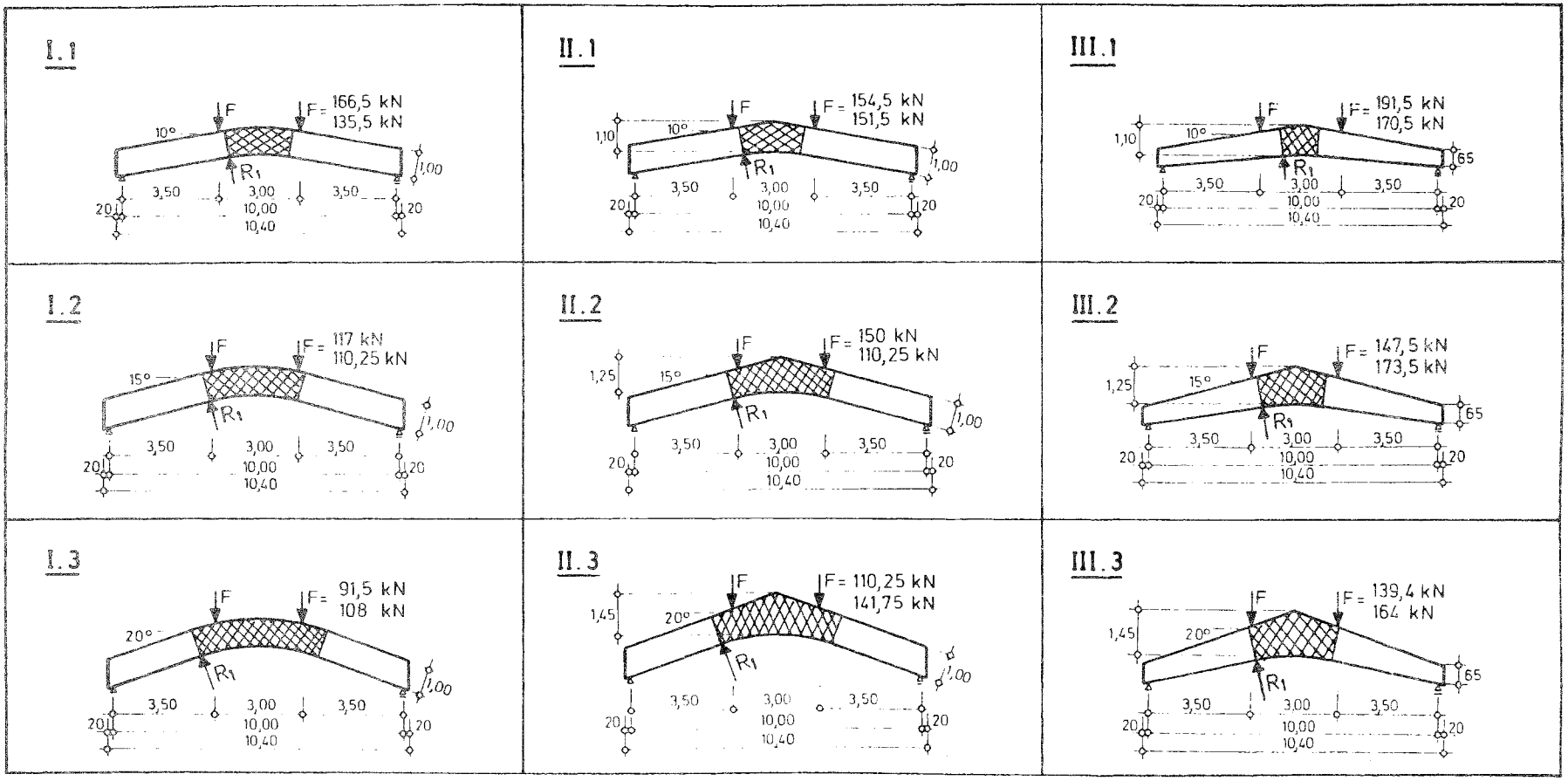


fig.7: beam configuration, test set-up and test results [6]

radius of curvature R_1 = 6,0 m
width of the beam W = 120 mm } for all beams

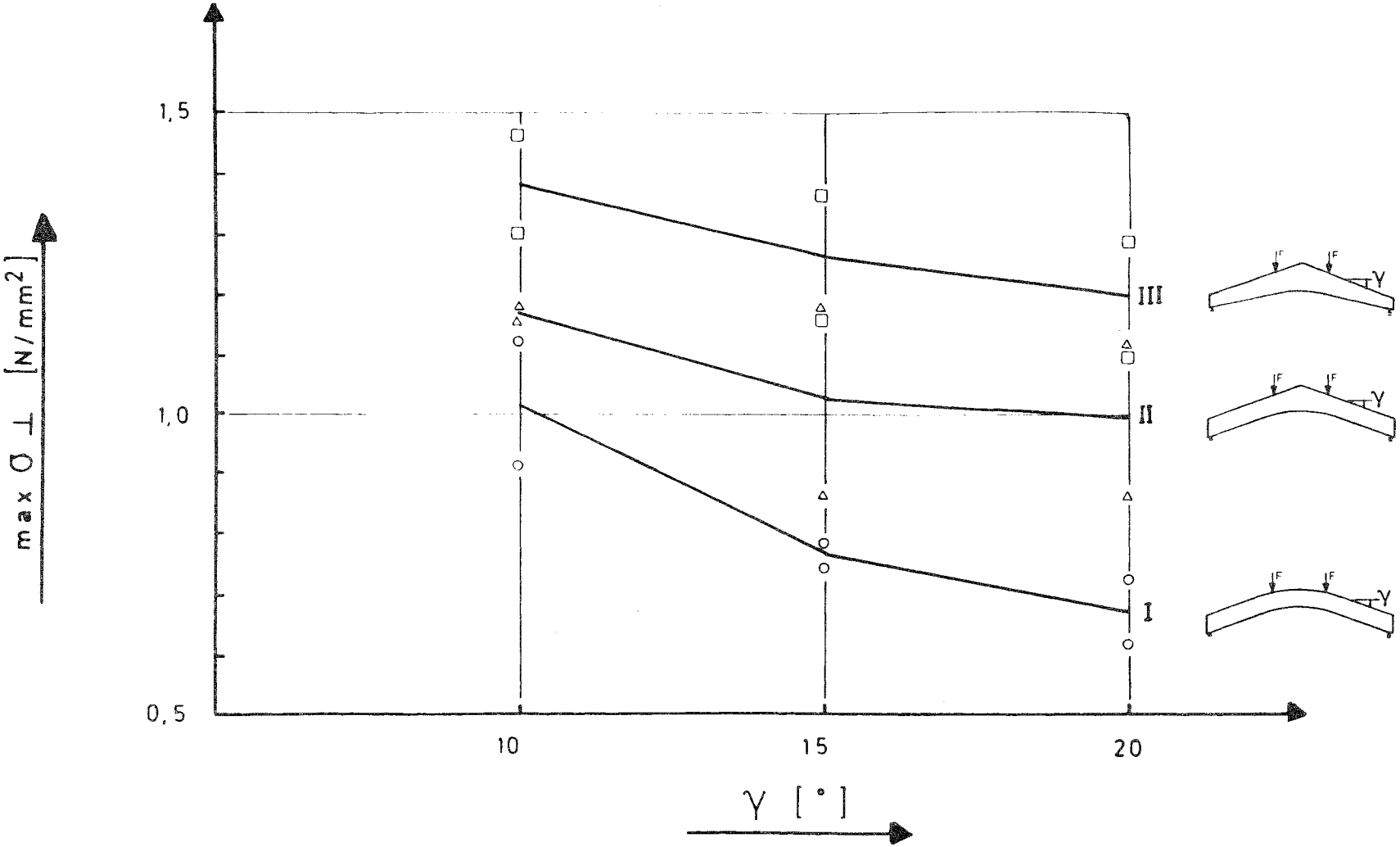


fig.8: tensile strength perpendicular to the grain $\sigma_{\perp}$

- ○ type I (curved beam with constant depth)
- △ type II (curved cambered beam)
- □ type III (curved tapered cambered beam)

CIB-W18/19-12-4

INTERNATIONAL COUNCIL FOR BUILDING RESEARCH STUDIES AND DOCUMENTATION

WORKING COMMISSION W18 - TIMBER STRUCTURES

TIME-DEPENDENT BEHAVIOUR OF GLUED-LAMINATED BEAMS

by

F Zaupa
University of Padua
Italy

MEETING NINETEEN
FLORENCE
ITALY
SEPTEMBER 1986

C.I.B. W18 - I.U.F.R.O. S 5.02
JOINT MEETING 1st - 5th September 1986
Dipartimento di Ingegneria Civile, Università degli Studi di Firenze, Italy

TIME-DEPENDENT BEHAVIOUR OF GLUED-LAMINATED BEAMS

F.ZAUPA
Istituto di Scienza e Tecnica delle Costruzioni,
Università di Padova, Via Marzolo, 9, Italy.

ABSTRACT (*)

The long-term deformation and failure of inflected glued-laminated spruce beams subjected to various levels of stress were studied over a three year period.

For the beams subjected to lower stress (30% of the short-term ultimate load), after three years the total viscous deformation was found to be equal to 55% of the initial elastic deformation; however, the phenomenon had not yet ceased. The beams subjected to greater stress (60% of the short-term ultimate load), failed after between 8 and 28 months. The time-dependent deformation developed up to the onset of failure was, after eight months, 30%, and after twenty-eight months, 55% of the initial elastic deformation.

The study revealed the dependence of the creep strain on the level and duration of loading. Observations on the mechanisms of the onset of the self-accelerating process of failure were formulated.

1. INTRODUCTION

The present study is part of a wider on-going programme of experimental and theoretical research at the Istituto di Scienza e Tecnica delle Costruzioni in the University of Padova. The aim of the programme is

(*) This study was made possible thanks to the kind collaboration of Federlegno and especially HOLZBAU S.p.A., Bressanone - Brixen (BZ) who supplied the beams at no cost. It was then developed with research funding from the Ministero della Pubblica Istruzione, "40% Fund".

to develop the study of the behaviour of glued laminated structural members in conditions of long-term, high intensity stress.

Presented in this paper is the work carried out to date, with specific reference to the time dependent behaviour of beams in bending under various levels of constant loading.

In a previous report, dedicated to a wider field of experimentation [1], the results of a short-term bending test, carried out on two glued-laminated beams, taken to failure, were illustrated. This time, on four other beams from the same batch, bending tests were carried out using long-term loading equal to 30%, for two of the beams, and for the remaining two, 60% of the average short-term ultimate load obtained for the first two beams of the batch.

The experiment, developed over about three years, highlighted the dependence of the viscous behaviour of the members on the load applied, and saw the failure of the more stressed beams.

2. OBJECTIVES AND SCOPE OF THE PRESENT WORK

Starting with the general aim of acquiring experimental data of the mechanical characteristics of glued-laminated structural elements, as they are commercially available, this study falls into the field of research into the rheological behaviour of wood based materials and structures [3] - [19]. It has the specific objective of investigating the time-dependent behaviour of members in bending subjected to long-term, high intensity stress, in order to be able to evaluate, among other things, the possibility of manufacturing major mixed structures of glued-laminated wood and reinforced concrete.

Deflected beams of the usual shape and dimensions, subjected to two different load levels have been investigated. The first load level corresponds to general working conditions, and the second to a level (twice the first) that resulted critical for the structural elements examined. The characteristics of progressive failure, which was manifested in the more stressed beams, were revealed in detail. After the onset of the failure, the beams were unloaded and kept in this condition until the end of the strain recovery period. The decay of short-term strength was then measured.

To date, the research may be considered concluded as concerns the experimental observation of the time-dependent deformation.

The study will continue extending to include dif-

ferent stresses, small samples of base and composite wood materials, and also the analysis of creep in the glue layers of the laminae, and in finger joints under the action of long-term loading.

3. EXPERIMENTAL INSTALLATION

The group of beams comprised six equal members of 2nd grade laminated wood all taken from the same batch, manufactured using sawn boards of Alpine spruce and Aerodux 185 glue. The elements had dimensions of 139x290x4000 mm^3, made up of 9 laminae of average thickness 32 mm. The moisture content, determined from four samples of the batch, was found to be 11%.

In the preliminary phase the short-term bending strength of two sample beams (no. 1 and no. 2) was determined using the loading scheme shown in figure 1. The following results were obtained:

beam 1 : ultimate load P_u = 66.0 kN.
beam 2 : ultimate load P_u = 62.5 kN.

The load levels to be employed in the long-term tests were determined as fraction of the average short-term strength thus found. Beams 3 and 6 were loaded to a level (30%) corresponding approximately to the maximum working load conditions (the maximum stress was, in fact, 14 MPa). Beams 4 and 5 were loaded to a higher level (60%) which was chosen so as to be likely to be greater than the "creep limit" [11], [12], of the outermost fibres.

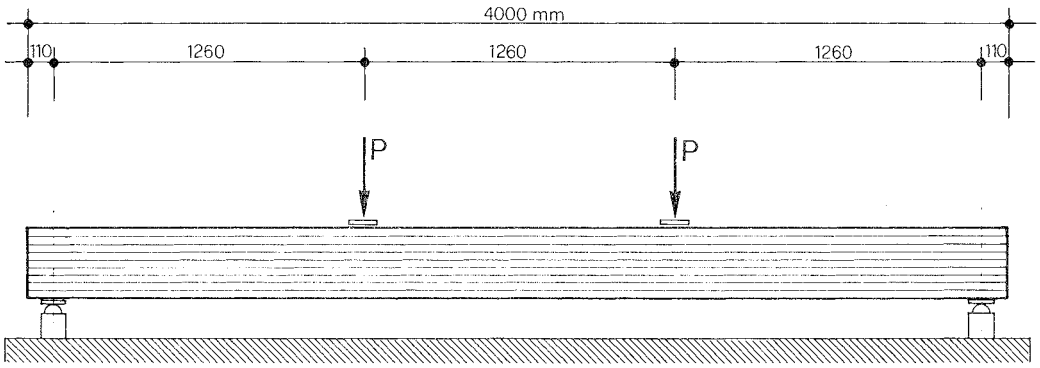


Fig. 1 - Loading scheme employed in the short-term and long-term tests.

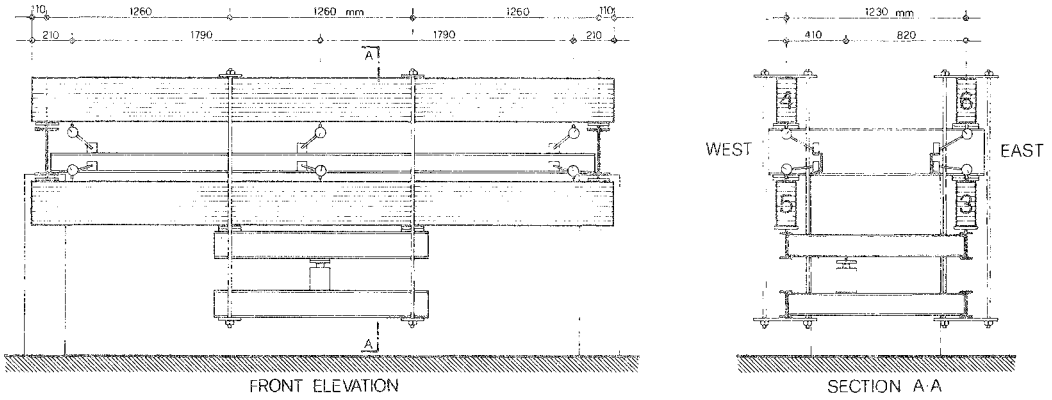


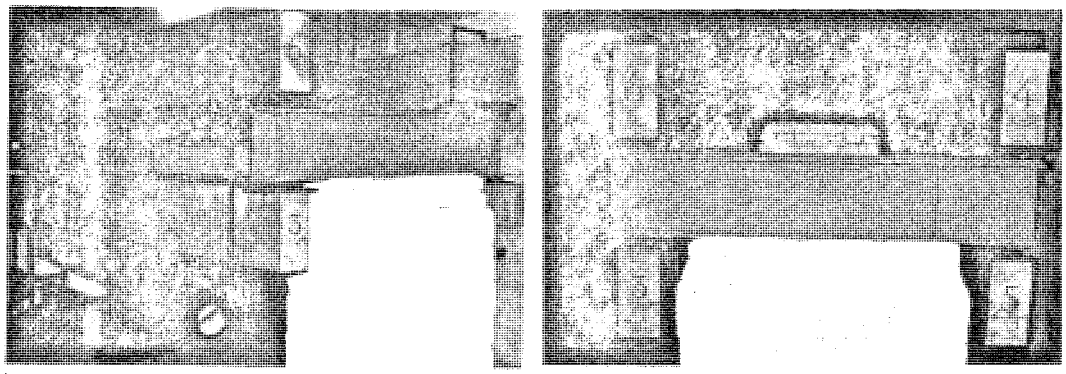
Fig. 2 - Test apparatus.

Special testing equipment was constructed to apply the different loadings to the four beams simultaneously, for a prolonged period, in a relatively restricted space. It consisted of two equal, parallel, self-balancing systems. Each comprised two hangers so positioned as to apply the loading at third points of the span of the two beams which were centered vertically one above the other. Thus the loading could be transmitted reciprocally between the beams. The whole apparatus rested on two steel cantilevers mounted on two concrete walls (figs. 2,3,4).

The forces were generated using a single hydraulic jack. The jack was fed by a constant pressure circuit activated by a calibrated piston, balance and weights. The piston was kept constantly rotating back and forth about its vertical axis in order to avoid any sliding friction which might alter the oil pressure in the circuit. The jack acted between two transmission beams which transmitted the load to the parallel systems.It was positioned so that the ratio of its distance from the symmetrical vertical mid-plane of the two pairs of beams was 1 to 2. Steel distribution plates and sliding hinges, with guides and safety stops, were constructed into the supports at the ends of the beams.

Three centesimal dial gauges per beam were used to measure the deflections. They were positioned along the edge in tension: two near the supports, and the third at the midspan of the beams. In this way any cross-sectional thermal or hygrothermal expansion, affecting uniformly the whole length of the beam, was eliminated from the measurements. The dial guages were attached to two longitudinal steel beams which were welded at their ends to the same cantilevers that supported the entire apparatus. Each of these longitudinal beams constituted the reference plane for the deflection measurements of the pairs of test beams.

The test was carried out in a thermically insulated,



Figs. 3,4 - Photographs of test apparatus.

underground room. The environmental conditions were regularly measured concomitantly with the deflection measurements.

The following is a list of basic characteristics of the loading and measuring apparatus.

a) Loading apparatus:

. actuator piston diameter : 12.5 mm;
. gravitational load on the piston : 1110 N;
. oil pressure in circuit : 9.05 MPa;
. effective area of jack : 124 cm^2;
. total force generated by jack : 112.20 kN;
. forces applied to beams 3 and 6 : 2x18.70 kN;
. forces applied to beams 4 and 5 : 2x37.40 kN.

b) Oil-pressure control instrumentation:

. 2 no. manometers: with a sensitivity of 0.1 MPa and 0.5% precision; one placed at the beginning of the circuit, the other on the jack.

c) Deflection measurement instrumentation:

. Borletti centesimal dial gauges with a range from 0 to 50 mm.

4. OBSERVATIONS AND RESULTS

The test started with the application of the pre-established force; this took place progressively over a period of about 40 minutes. The corresponding deflections confirmed the correct load distribution and functioning of the apparatus. The deflections measured 5 minutes after this loading operation were taken as corresponding to the initial elastic deformations and as the reference zeros for the time-dependent strain. Observations of the deflections and the environmental conditions were then made twice a day for the first 15 days and once a day thereafter.

The variations in the total deflection of the four beams are shown in figure 5 together with the varia-

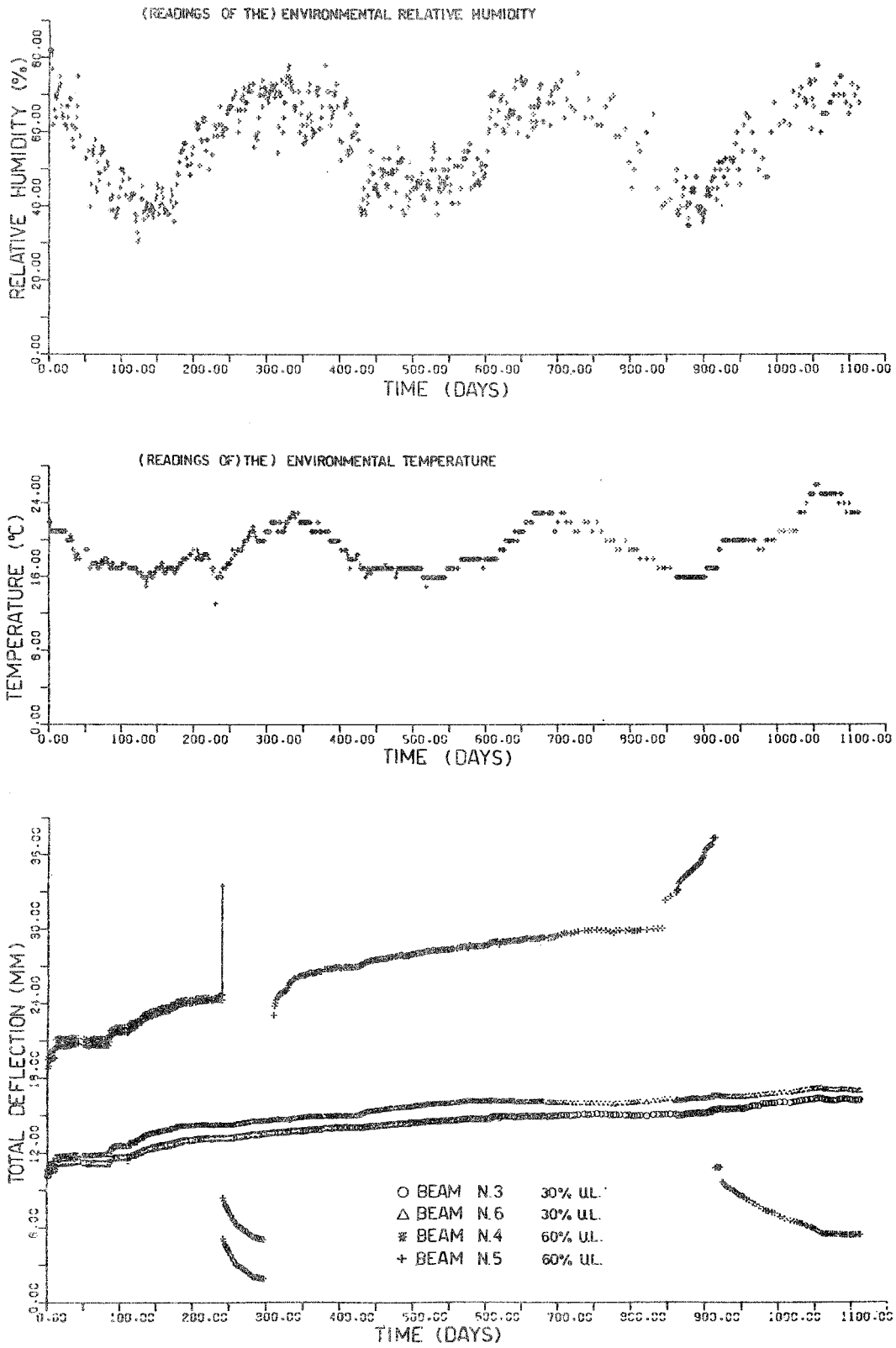


Fig. 5 - Evolution of the deflections of the test beams and the distribution of the relative humidity and temperature.

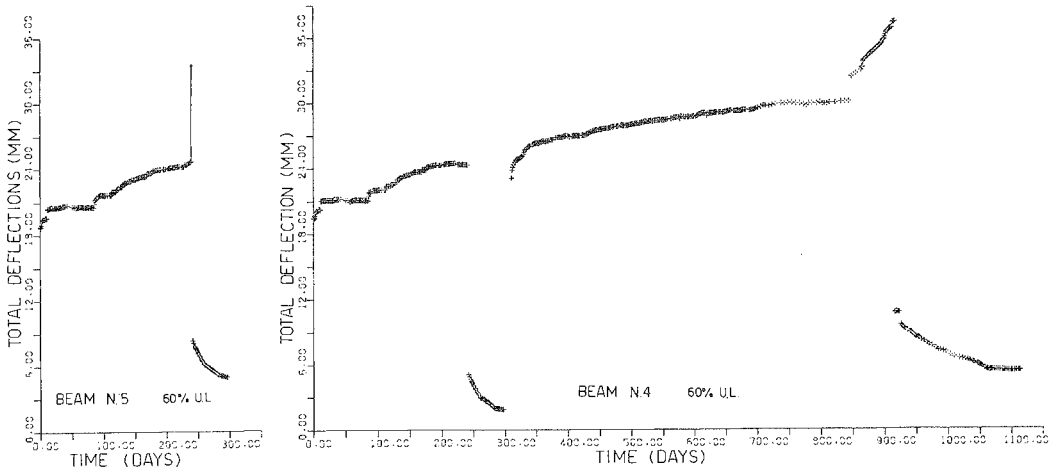


Fig. 6 - Evolution of the total deflection of beams 5 and 4.

tions in the temperature and relative humidity of the environment. In figure 6 are the individual curves of the total deflection of beams 5 and 4. Some irregularities, approximately proportional to the extent of the initial elastic deformation, can be seen in the deflection curves of all four beams for the first three months of testing. They can be attributed to the formation of frictional forces between the piston and the cylinder liner, due to a fault in the rotary oscillation generating device of the piston itself. Once this was repaired, on the 85th day, the total deflection curves for each of the four beams assumed a regular shape with optimum correspondence between the beams under the same loading and a substantial similarity between the beams subjected to different loading. This can be seen from figure 7 which shows, for each of the beams, the results normalized according to the corresponding initial elastic deflection.

After about eight months of testing, beam 5, which had been subjected to 60% of its estimated short-term strength, showed the first signs of failure. This seems to have been preceded, during the previous twenty days, by an increase in the rate of deformation with respect to the antecedent period. This increase can be estimated to be in the order of 60%, the rate passing from:

$$f = 7.34 \times 10^{-8} \text{ mm s}^{-1} \quad \text{to:} \quad f = 44.0 \times 10^{-8} \text{ mm s}^{-1}$$

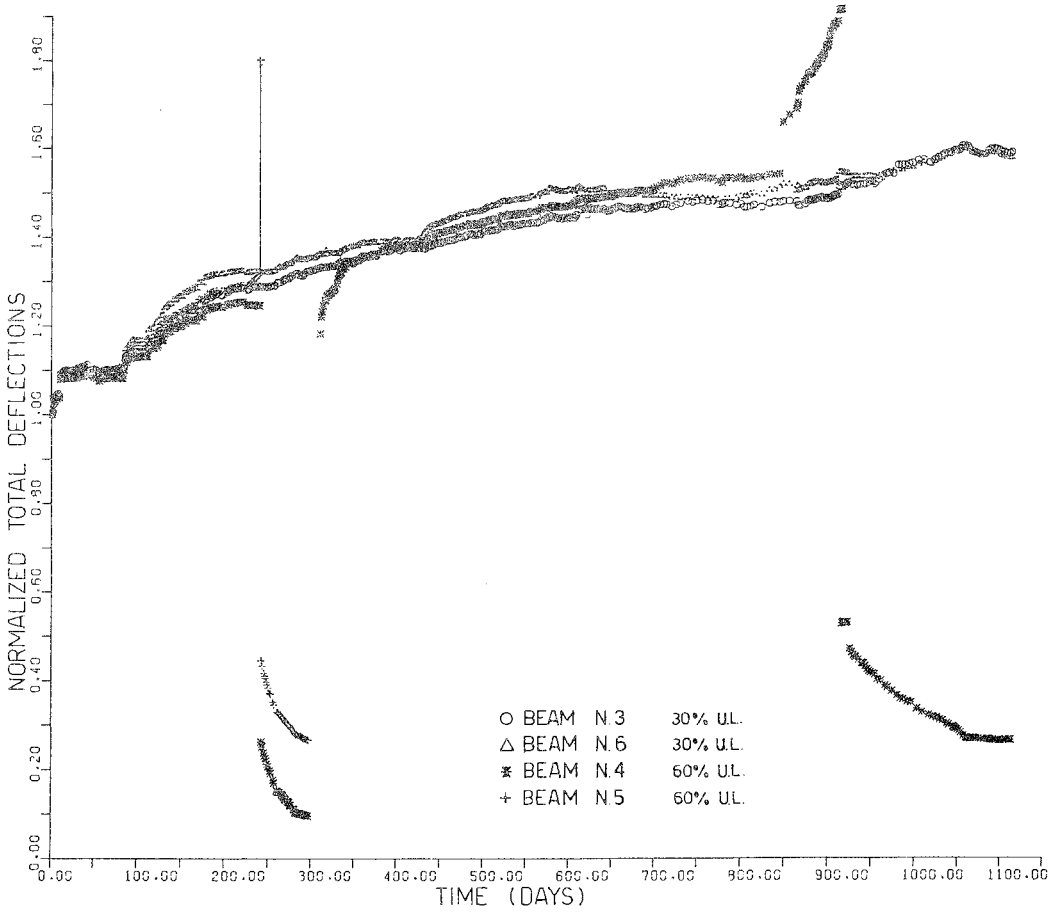


Fig. 7 - Evolution of the total deflection normalized to the initial deflection.

On the 241st day, this phenomenon then culminated in a sharp increase in deflection accompanied by fracturing of the outermost fibres in tension in the central zone, which was subject to the maximum bending moment. These cracks, irregular in shape, affected the whole width of the beam to a vertical depth of 32 mm, the thickness of the external lamina. The crack originated at the site of two knots in the lamina, which were longitudinally about 30cm apart, on opposite edges, and crossed this lamina obliquely from the lower face to the sides. The fracture line ran between these two knots (fig. 8), developing tranversally along the edge of a very slight damage mark, received during transportation, which had nevertheless weakened the fibres.

The test apparatus was then unloaded. Beams 5 and 4 were left unloaded, while the other two were loaded again to the previous level (30% U.L.). This operation took about an hour.

Later, beam 5 was subjected to a short-term bending

Fig. 8 - Detail of the fracture system on the edge in tension of beam 5.



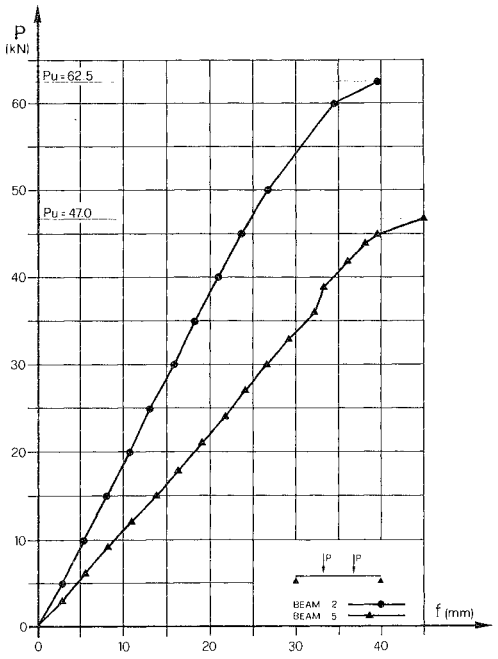


Fig. 9 - Load-deflection diagrams of beam 5 (after the onset of failure in the long-term test) and beam 2.

strength test, applying the loading at the same points as for the long-term test, to reveal the decay in stiffness and strength produced after the initial fracturing. The results, as shown in figure 9, were:

global tangent stiffness modulus : P/f = 1.11 kN/mm
ultimate load : Pu = 47.0 kN

This is equal to 60% and 73% respectively of the average values found for test beams 1 and 2. Figures 10 -13 document the salient phases of the test and the characteristics of the break-slippage fracture system developed at failure.

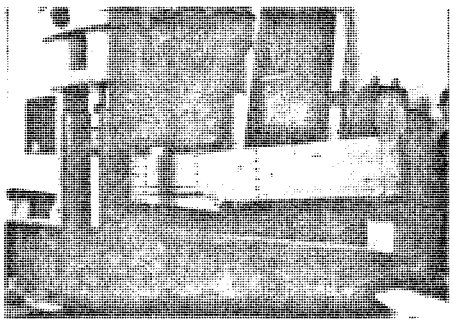
On the 30th day unloaded, beam 4 was reloaded to the original level (60% of the short-term estimated strength), restoring the system to two reciprocally contrasting pairs of beams by means of a steel substitute for the beam which had failed.

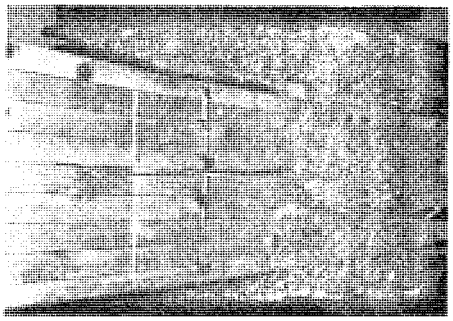
For the three remaining test beams the experiment continued, under these conditions, until the 842nd day, when the onset of failure was noted in the second of the beams loaded at 60% U.L. A sharp increase in deflection was recorded, along with the appearance of a cracking in the lamina in tension. The crack had initiated along the glued surface of a finger joint then spread along the beam, the first part limited to the depth of the lamina, the rest following the glue layer between the first and second laminae (figs. 14 -17). The beam was kept loaded for a further 70 days during which the behaviour in the post-critical phase (after the first appearance of the cracking) was analyzed. This was characterized by an average deflection rate of about 9 times that of the immediately preceding period. The splitting also continued to spread in both directions, starting from the finger joint, for 120cm towards the midspan, and 30 cm towards the support, slanting slightly towards the neutral axis. The cracks also crossed the fibres of the second lamina passing the second glue layer. Figure 18b shows the progress of the fracture system.

Tests on this beam were suspended on the 915th day, because of the extent of the accumulated deformation. As in the first case, unloading this beam involved a temporary reduction (for about an hour) in the loading applied to beams 3 and 6. Once unloaded, beam 4 was kept under observation for a further period of about 200 days during which the delayed elastic recovery was able to take place to completion. In this case, too, the beam was then subjected to a short-term bending strength test, to determine the reduction in stiffness and strength compared to its original state. The following results were obtained:

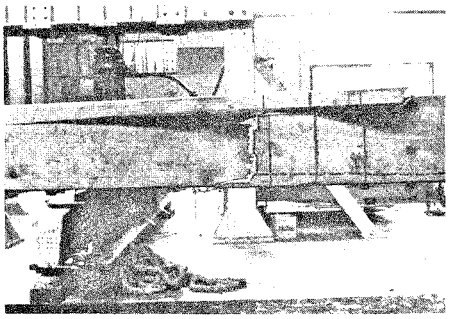
. global tangent stiffness modulus: P/f = 1.35 kN/mm
. ultimate load : Pu = 51.5 kN

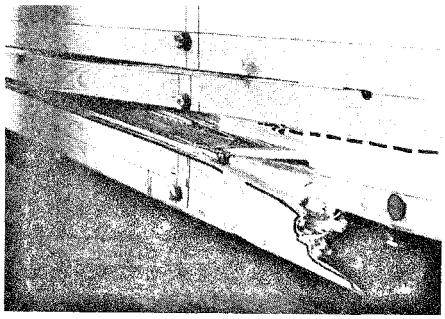
These represent 73% and 80% respectively of the average values found for test beams 1 and 2.





Figs. 10,11 - Salient phases in the short-term bending strength test taken to the collapse of beam 5, after the long-term test.





Figs. 12,13 - Details of the fracture system at the collapse of beam 5.

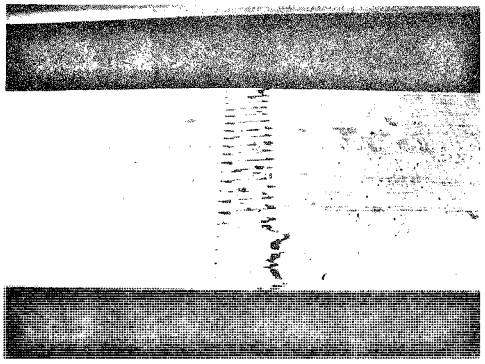
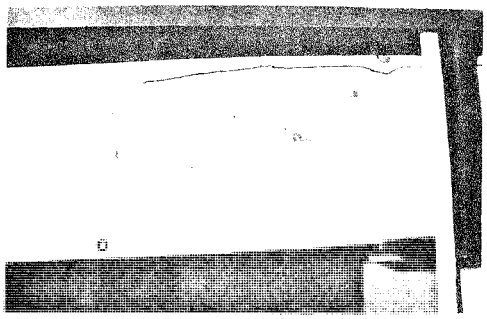




Fig. 14,15 - Details of the first fracture on the edge under tension and on the west side of beam 4.



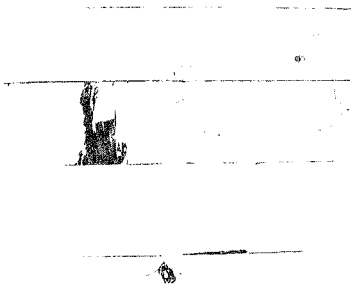


Fig. 16 - Detail of the fracture on the east side of beam 4.

Fig. 17 - Details of the final phases of longitudinal propagation of the fracture on the west side of beam 4 before unloading. The zone around a class 4 knot in the third lamina from the edge in tension.

5. DISCUSSION OF THE RESULTS

5.1 General behaviour of the beams.

The observations carried out seem to permit a sufficiently precise description of the phenomenon and a first interpretation of the results, which are shown in table 1. Note that at present the tests are continuing on beams 3 and 6 subjected to 30% U.L. of the ultimate loading.

It can be seen that all the beams, independently of the intensity of bending stress, behave in a similar way during their lifespan. Thus, with sufficient accuracy even for stresses large enough to introduce, in the outer fibres, states of tension which go beyond the creep limit,it seems possible to represent the viscous behaviour of beams in bending as a linear function with respect to the loading (fig. 7). This is due to the particular type of distribution of normal bending stresses, parallel to the grain of the beam, with values decreasing from the maximum to zero from the outer edges to the neutral axis: thus, the different behaviour of the external fibres has a limited influence on the global response of the beam. As was shown by the failure of beams 5 and 4, these fibres can be characterized by local viscoplastic behaviour, but with a time dependent law of the increase in deformation influenced by their congruence with the inner fibres, which remain in a linear viscoelastic state.

The most obvious difference in behaviour between the two groups of beams is the fact that those loaded to 60% U.L. showed signs of failing after some time. This phenomenon occurred with fracturing that affected the outermost fibres, which were in substantially uniaxial stress conditions in the middle-third of the free span. The cracks originated at points weakened by intrinsic defects (for example, knots, or deficient glued joints), or by even very slight fortuitous damage (such as punch marks, denting of the surface fibres caused by knocks or binding during transportation, or hammering). They then spread to the remaining band of undamaged fibres for the whole width of the member. So, it seems possible to extend the creep limit theory, which has been developed and verified for base material without defects, also to actual structural elements, with standard dimensions, which have limited, uniformly distributed defects as is the case of glued-laminated members.

From the results gathered so far, despite the fact that the tests are still in progress for beams 3 and 6, it seems already possible to deduce that the creep limit for the inflected beams under test falls between

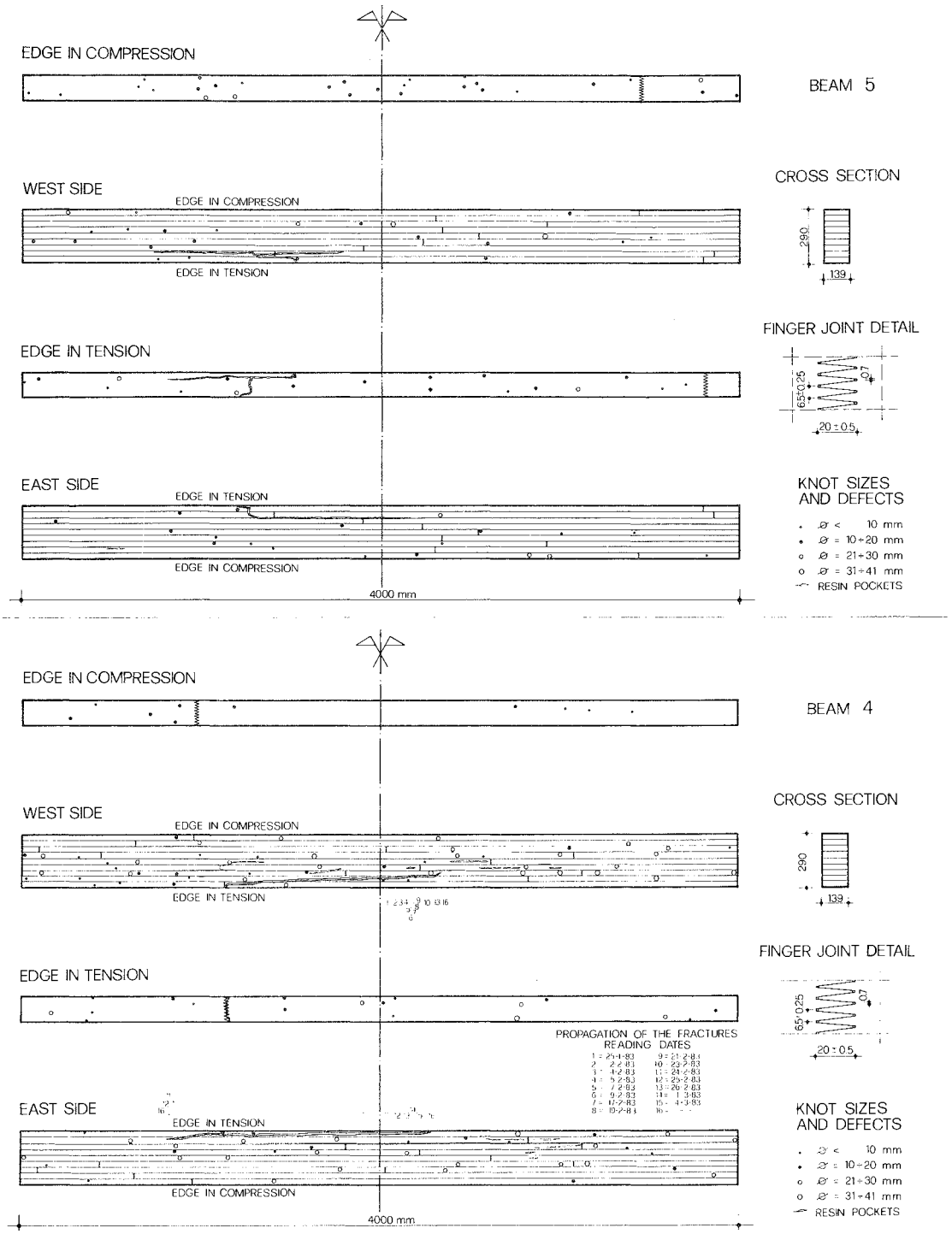


Fig. 18 - Survey of the fracture system at the end of the long-term tests.
a) Beam 5; b) Beam 4.

TABLE I: TEST RESULTS

	LOAD				STRESS		DEFLECTION		MODULUS OF ELAST.	LONG-TERM DEFLECTION					
										AFTER 220 DAYS		AFTER 842 DAYS		AFTER 1112 DAYS	
BEAM N.	P_o [kN]	P [kN]	G [kN]	g [kN/m]	$\bar{M}$ [kN/m]	M_o [kN/m]	f_o [mm]	f_o/M_o [mm/kNm]	E^o_f [kN/cm^2]	f-f_o [mm]	$\frac{f-f_o}{\bar{M}}\frac{M_o}{f_o}$ [0]	f-f_o [mm]	$\frac{f-f_o}{\bar{M}}\frac{M_o}{f_o}$ [0]	f-f_o [mm]	$\frac{f-f_o}{\bar{M}}\frac{M_o}{f}$ [0]
3	0.52	18.70	-0.22	-0.20	22.94	22.91	10.13	$442.2\cdot10^{-3}$	1218.0	2.995	0.227	4.935	0.487	6.090	0.600
6	0.52	18.70	+0.82	+0.20	24.94	22.91	10.66	$465.3\cdot10^{-3}$	1157.4	3.53	0.304	5.545	0.478	6.255	0.539
4	1.03	37.40	+0.82	+0.20	48.50	45.83	19.46	$424.6\cdot10^{-3}$	1268.3	5.03	0.244				
			-0.22	-0.20	46.50							10.629	0.538	/	/
5	1.03	37.40	-0.22	-0.20	46.50	45.83	18.69	$407.8\cdot10^{-3}$	1320.6	5.60	0.295	/	/	/	/

Key:
P_o : initial pre-loading
P : permanent loading applied by the test apparatus
G : weight of the test apparatus
g : weight of the beams
M : average total bending moment in the midspan of the test beam (reference stress for the long-term deflection)
f : total deflection after time t
M_o, f_o: amplitude of the bending moment and corresponding immediate elastic deflection measured at loading
E^o_f : longitudinal modulus of elasticity in bending

$$(E^o_f = -\frac{23}{213}\frac{Ml^2}{f\ J})$$

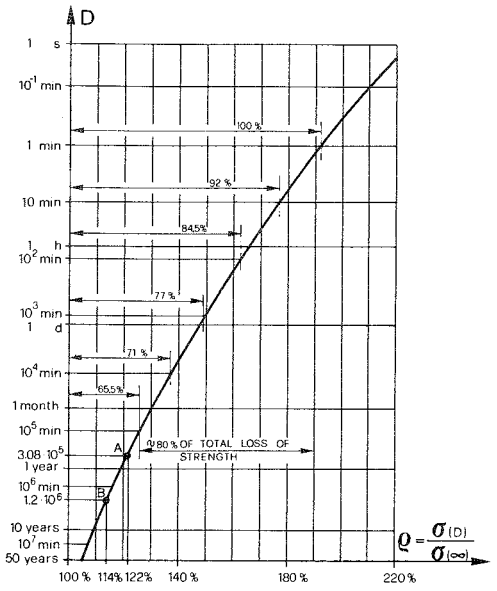


Fig. 19 - Duration of the strength at working stress Vs. the ratio of working stress and creep limit.

30% and 60% of the short-term ultimate loading: close to 50%, the value generally attributed to the creep limit for the base material [14], [15], [17].

Notice also that by substituting the relative data for beams 5 and 4 into Wood's [4] curve (points A and B in figure 19) it is possible to make a retrospective estimate of the ultimate loading applied for 1 minute:

. beam 5 : $Pu = \frac{192\%}{122\%} \times 36.91 = 58$ kN,

. beam 4 : $Pu = \frac{192\%}{114\%} \times 36.91 = 62$ kN,

An optimal approximation of the values obtained in the preliminary short-term tests carried out on the beams 1 and 2 (66 kN and 62.5 kN respectively), is obtained.

As far as the extent of the time dependent deformation reached by the various members is concerned, it can be seen that just before the onset of failure in beam 5, after eight months of permanent loading, an increase in deflection of 5.6 mm, which is 29% of the

initial elastic deflection, was noted. The accelerated increase in deflection during the following twenty days' progressive failure, which culminated in the sharp variation already mentioned, was 9.26 mm (fig. 6). The time dependent deflection produced in the same period in the corresponding still sound beam 4, was 5 mm, which is 24% of the respective initial elastic deflection. Beams 3 and 6, at 30% U.L., developed time dependent deflections of 3 and 3.5 mm during the same period; this represents 23% and 30% of the respective initial elastic deflections.

Regular observations of beams 5 and 4, which were kept unloaded from the 215th day, for about 70 days starting after the onset of failure of beam 5, made it possible to follow the evolution of the strain recovery phase. The deflection immediately recovered by beam 5, when unloaded, was 25 mm, starting from the configuration reached after the appearance of the first cracks; this is 134% of the initial elastic deflection. The delayed elastic recovery was 18% of the immediate elastic recovery, and 21% of the initial deflection, the residual deflection being 15% of the total deflection developed before unloading. For beam 4, which had not yet failed, the immediate elastic recovery was 97% of the initial deformation at loading. The delayed elastic recovery, substantially complete after about two and a half months, was 17% of the immediate elastic recovery; the residual deflection, which corresponds to the unrecoverable viscous creep developed during eight months' loading, was 9% of the initial elastic deflection.

With reference to the longer lifespan of beam 4, (28 months) the total time dependent deformation was found to be 54% of the initial elastic deformation. The increase in deflection during the following 70 days characterized by the onset of the progressive failure of the beam, was 7.3 mm. During the unloaded phase there was an immediate recovery of 26.6 mm deflection, which is 135% of the initial elastic deflection. A delayed recovery of 5.3 mm, which is 20% of the immediate elastic recovery, was noted, the residual deflection being 5.2 mm which is 14% of the total deflection developed before unloading (fig. 6).

After 28 months of permanent loading, the time dependent deformation of beams 3 and 6, at 30% of the ultimate load, was found to be 48% and 49% respectively of the initial elastic deflection. Still later after 1112 days of permanent loading, values of 60% and 54% were recorded.

5.2 Failure mechanism of beams 5 and 4.

As already mentioned, the failure of beams 5 and 4

was marked, macroscopically, by the localized breaking of fibres of the external lamina in tension, around a part of the beam characterized by local defects. In the case of beam 5, the fracture line ran between two knots at opposite edges of the lamina and longitudinally about 30 cm apart. It followed the edge of a very slight damage mark that ran across the lamina, was about a tenth of a millimeter deep, and had been caused accidentally during transportation. For beam 4, the local weakening which determined the site and the shape of the fracture was the loss of strength of a glued finger joint between two boards on the external lamina. Once the fractures had opened across the whole width of the beam to a depth that was generally not more than the external lamina, they propagated along the member following slippage surfaces which were rather irregular but substantially parallel to the longitudinal axis, extending in parts through the glue layers, or splitting the wood, and showing a tendency to slant slightly towards the neutral axis (fig. 18).

Another interesting aspect of the mechanism of failure concerns the fact that the failure, in both cases, came about in a substantially sudden way, without premonitory signs. The jump in the rate of deflection is a warning of the formation of the cracking;the jumps the deflection correspond to successive macroscopic slippage that characterize the evolution of the longitudinal splitting. The onset of failure under long-term loading is thus accompanied by an apparent fragility, even if the subsequent accelerating process of progressive failure seems have completion times of the order of months, at least for loading comparable to those examined (60% of the short-term ultimate load). Correspondingly, also the strength relative to short-term loading is not suddenly lost, with the onset of failure, but reduces progressively, being able to exploit the reserves associated with the non uniform distribution of bending stresses on the cross section. The inner layers, in fact, under lower stress than the outermost ones until the moment of fracturing, present a consistent margin of strength over time.

In a previous paper [2], the author formulated an approximate evaluation of the complex "transverse fracturing - longitudinal splitting" phenomenon, considering only conditions of equilibrium, and retaining the hypothesis of linear behaviour up to failure, as schematically represented in fig. 20. The results appeared in good accordance with the observations.

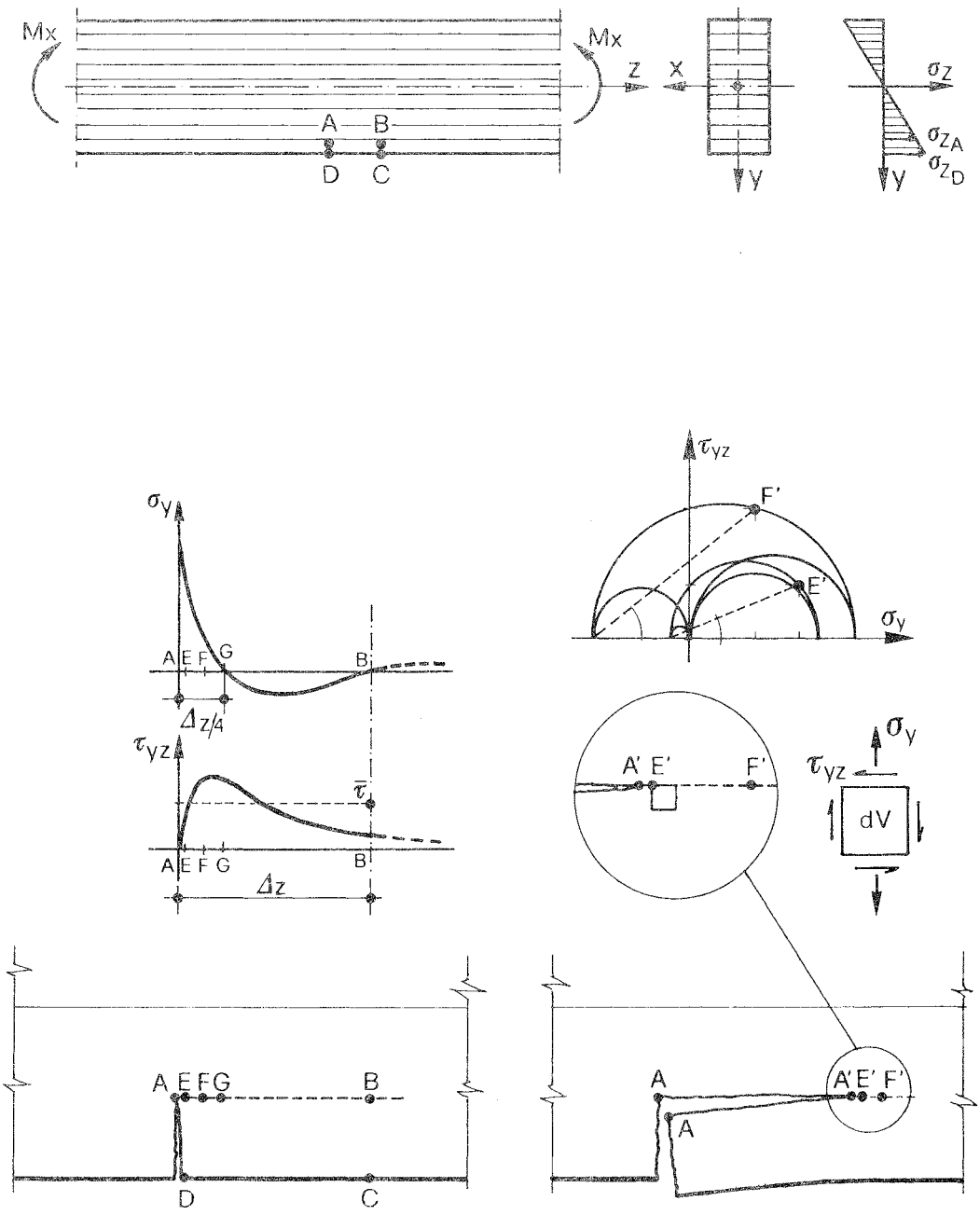


Fig. 20 - Representation of a simplified model of the fracture mechanism.

6. CONCLUSIONS

The results of the experiments carried out so far in this first, direct analysis make it possible to draw some conclusions.

The rheological behaviour of glued-laminated beam, subjected to long-term bending loads appears to fit the linear visco-elasticity of solids.

The time dependent delayed elastic deformation which, in the case of beam 4, was also measured in the unloaded and reloaded phases, was well evident: of the order of 17% of the initial elastic deformation, which represents about 65% of the total time dependent deformation. It reached completion in a period of some months.

There is, then, at least in the presence of high stresses, also an appreciable degree of irreversible creep, which indicates a viscoplastic deformation component. These values of delayed plastic strain are, however, of the order of 10% of the initial elastic deformation and 50% of the delayed elastic deformation.

In many ways, behaviour of this type appears comparable to that of concrete, and confirms the possibility of producing interesting mixed structures of glued laminated wood and reinforced concrete, even if the various initial elastic, delayed elastic and unrecoverable strain components have different impacts on the total deformation in these materials. The substantial differences seem to be reducible to the critical phases in the lifespan of the two materials. For concrete the first phase is critical because of the improvement with age of its rheological characteristics and its mechanical properties. With wood, because it has no analogous age dependent characteristics, later phases of its lifespan are critical: after a certain period of time a process of accelerating progressive failure may be manifested, if the permanent loads exceed about 50% of the short-term ultimate load.

The latter phenomenon comes about suddenly, without apparent premonitory signs, following a loss of resistance to tensile stress in the outermost fibres. The failure of the member, however, reaches completion after a period long enough to allow corrective measures, if the situation is recognized immediately. The site of the first fracturing corresponds to defects in the structural member, such as knots, weak joints, even slight damage to the fibres, and other types of local dishomogeneity, to which the wood proves to be rather sensitive.

Regarding this particular aspect, it is evident that, because of the limited degree of heterogeneity that characterizes accurately manufactured composite laminated elements, chosen on the basis of high quality

control criteria, they may offer decisively more favourable conditions than the corresponding solid wood elements.

To the extraordinary ease of manufacture, transportation and installation of these elements there corresponds a high vulnerability, to errors and carelessness, that should not be underestimated.

REFERENCES

1. MODENA C., ZAUPA F.: "Ricerca sperimentale sulle caratteristiche meccaniche di travi in legno lamellare incollato. Prima serie di risultati." Istituto di Scienza delle Costruzioni, Università di Padova, Mar. 1981.

2. ZAUPA F.,MODENA C.: "Indagine sperimentale sul comportamento viscoso di travi inflesse di legno lamellare incollato." Istituto di Scienza delle Costruzioni, Università di Padova, Aug.1983.

3. WOOD L.W. : "Bahavior of Wood Under Continued Loading", Engineering News-Record, Dec. 11, 1947.

4. WOOD L.W. : "relation of strength of wood to durtion of load", F.P.L. Rpt 1916, USDA Forest service, Forest Products Laboratory, Madison, Wis, 1951.

5. WLINEN A. : "Uber den Einfluss der Verformungsgeschwindigkeit auf die Bruchfestigkeit des Holzes", Holz als Rohr-und Werkstoff Juni 1959, Heft 6.

6. KING E.G. : "Time-Dependent Strain Behavior of Wood in Tension Parallel to the Grain", Forest Products Journal, March 1961.

7. KOLLMANNF. :"Rheologie und Strukturfestigkeit von Holz", Holz als Roh-und Werkstoff, marz 1961, Heft 3.

8. YLINEN A. : "Uber die Bestimmung der zeitbedingten elastischen und Festigkeitseigenschaften des Holzes mit Hilfe eines allegemeinen nichtlinear visko-elastischen rheologischen Modelles," Holz als Roh-und Werkstoff, Mai 1965, Heft 5.

9. KOLLMANNF. : "Kriechen von Holz und Holzwerkstoffen", Holztechnologie 1972 (2).

10. MADSEN B. : "Duration of Load Test for Dry Lumber in Bending", Forest Products Journal, Vol. 23, N. 2, Feb. 1973.

11. REINHARDT H.W. : "Zur Beschrebung des rheologischen Verhaltens von Holz", Holz als Rohr-und Werkstoff, Vol. 28, 1973, S.352-355.

12. SUGIYAMA H. : "On the effect of the loading time on the strength properties of wood", Wood Science, Vol. 1, 1968.

13. KUFNER M. : "Das Kriechen von Holzspanplatte bei langzeitiger Biegebeansprunchung", Holz als Rohr- und Werkstoff 1970 (11).

14. BHATNAGAR N.S. : "Kriechen von Holz bei Zugbeanspruchung in Faserrichtung", Holz als Rohr-und Werkstoff, Sep. 1964, Heft 9.

15. YLINEN A. : "Zur theorie der Dauerfestigkeit des Holzes", Holz als Rohr-und Werkstoff, mai 1957, Heft 5.

16. KALINA M. : "Zerstörungsfreie Bestimmung der Dauerfestigkeit von Trägern aus dem rheologischen Verhalten unter Dauerlast", Holztechnologie, 1971 (4).

17. CIZEK L. : "Dauerfestigkeit und rheologische Eingenschaften von Holz und Holzwerkstoffen", Holz als Rohr-und Werkstoff, Marz 1961 Heft 3.

18. LITTLEFORD J. : "Performance of glued-laminated beams under prolonged loading", For. canada Corp., For. Prod. Lab., Inf. Report., vancouver, 1967.

19. PEDROTTTI P. :"Indagine sul comportamento meccanico del larice lamellare sollecitato a flessione pura", Contributi scientifico-pratici per una migliore conoscenza e utilizzazione del legno Vol. XXV, C.N.R., Roma 1979.

20. DIN 4074, teil 1: "Gütebedingungen für Bauscnittholz (Nadelholz)" Ausgabe Dezember 1958.

21. KOLLMANN F.: "Technologie des Holzes", Voll. I,II, Springer Verlag, Berlin, 1951-55.

22. GIORDANO G.: "La Moderna technica delle costruzioni in legno", U. Hoepli, Milano, 1964.

CIB-W18/19-14-1

INTERNATIONAL COUNCIL FOR BUILDING RESEARCH STUDIES AND DOCUMENTATION

WORKING COMMISSION W18 - TIMBER STRUCTURES

ANNEX ON SIMPLIFIED DESIGN OF W-TRUSSES

by

H J Larsen
Danish Building Research Institute
Denmark

MEETING NINETEEN
FLORENCE
ITALY
SEPTEMBER 1986

ANNEX 3 SIMPLIFIED DESIGN OF W-TRUSSES

A 3.1 Scope

This annex gives a simplified method for determining the forces in symmetrical W-trusses.

A 3.2 Notation and assumption

The special notation used in this annex is given below, together with the assumptions for the validity of the method.

A 3.2.1 General geometry

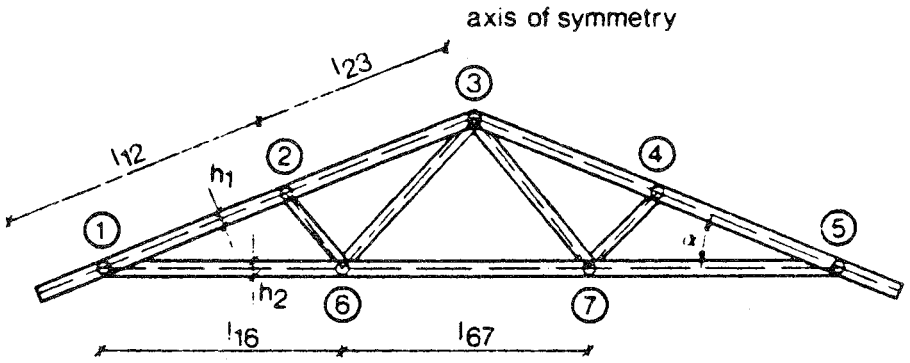


Figure A 3.2.1

It is assumed that

- $\alpha \geq$ about 14^0 (1:4)
- $l_{12} \sim l_{23}$
- $l_{16} \sim l_{67}$

A 3.2.2 Support geometry

A 3.2.2.1 Small eccentricity.

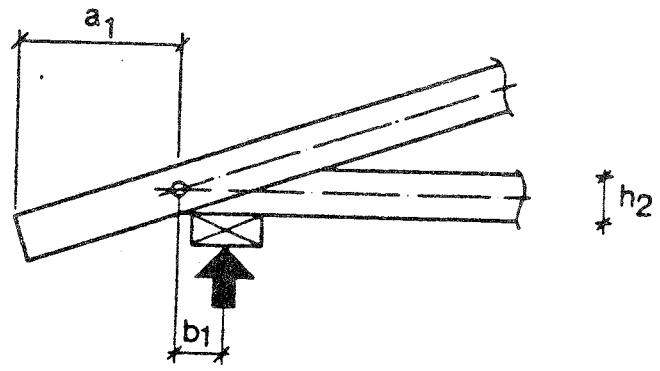


Figure A 3.2.2 a. Support geometry, small eccentricity

It is assumed that

$b_1 \leq 200$ mm and $b_1 \leq 2h_2$

A 3.2.2.2 Big eccentricity.

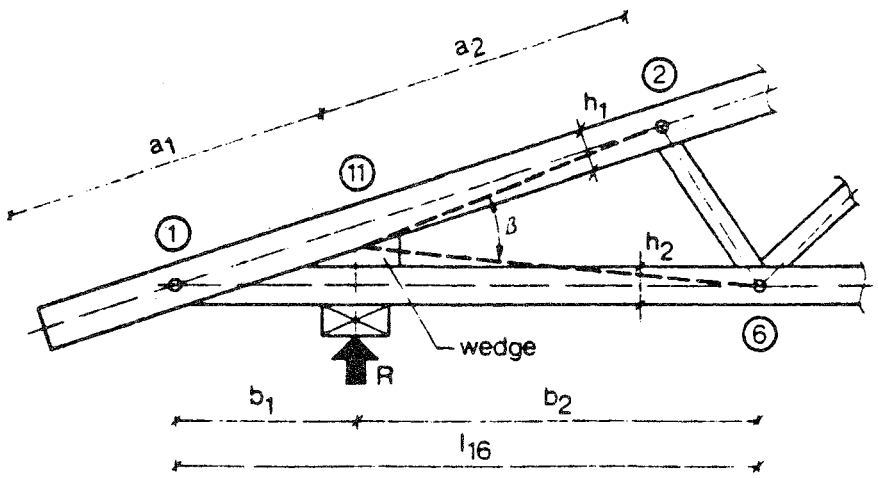


Figure A 3.2.2 b. Support geometry, big eccentricity

It is assumed that there is a wedge in the space between the top and bottom chord covering the whole support area.

A 3.2.2 Nodal point geometry

A 3.2.3.1 Centric connections.

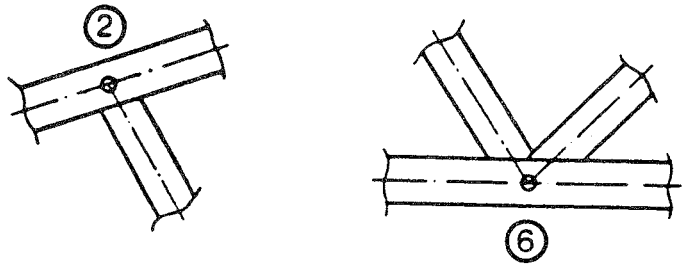


Figure A 3.2.3 a. Centric connections

A 3.2.3.2 Eccentric connections.

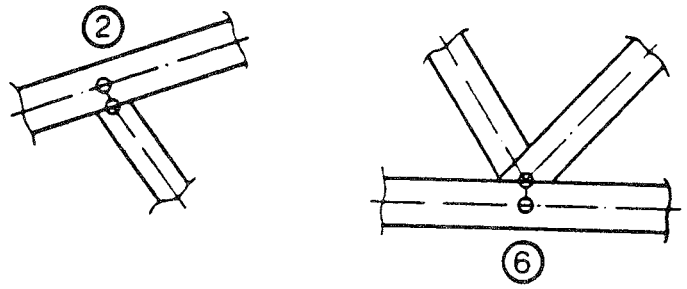


Figure A 3.2.3 b. Eccentric connections

A 3.2.4 Actions

A 3.2.4.1 General.

The following actions are taken into account:

- concentrated forces acting in the nodal points
- uniformly distributed loads acting on the upper chords, see A 3.2.4.2
- uniformly distributed loads acting on the lower chord, see A 3.2.4.3.

A 3.2.4.2 Uniformly distributed loads on the upper chord. It is assumed that the load is constant between node 1 and 3 and between 3 and 5.

The loads are described either by their vertical (q_v) and horizontal (q_h) components, see figure A 3.2.4 a; or by their components perpendicular (q_{per}) and parallel (q_{par}) to the chords, see figure A 3.2.4 b.

All loads are given per unit length of the chords, i.e. the total vertical load on the chord from 1 to 3 is $q_{v,13}(l_{12} + l_{23})$ and $q_{per} = q_v\cos\alpha + q_h\sin\alpha$.

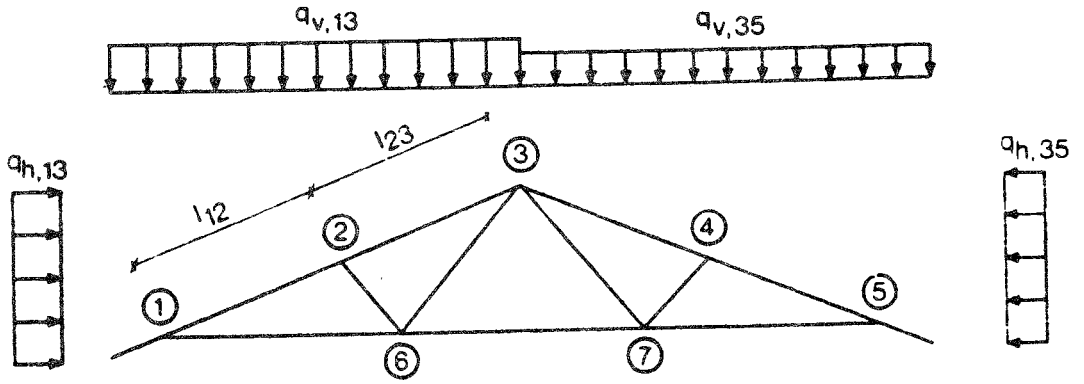


Figure A 3.2.4 a. Uniformly distributed vertical and horizontal loads on the upper chords

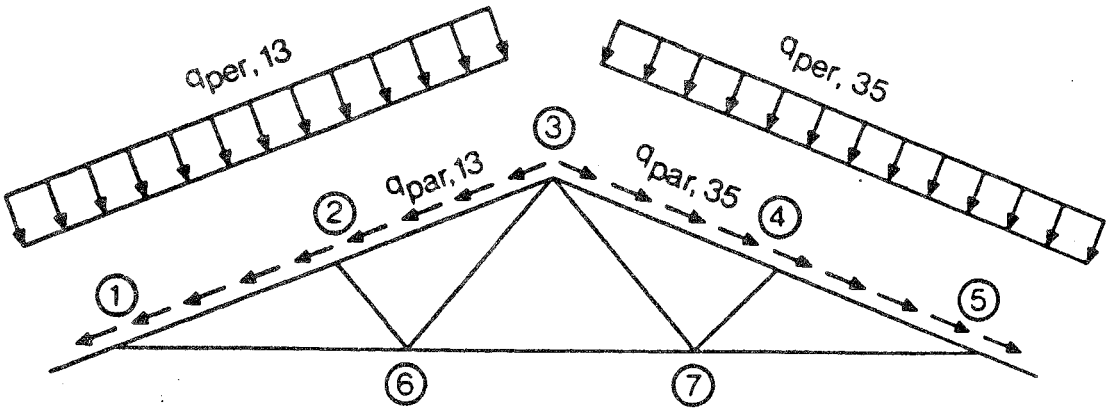


Figure A 3.2.4 b. Uniformly distributed perpendicular and parallel loads on the upper chords

A 3.2.4.3 Uniformly distributed loads on the bottom chord. It is assumed that the main load is a vertical constant load (q_{15} per unit length) between 1 and 5. There can further be partial vertical loads (q_b per unit length) acting on limited lengths b_3 of the chord. See figure A 3.2.4 c.

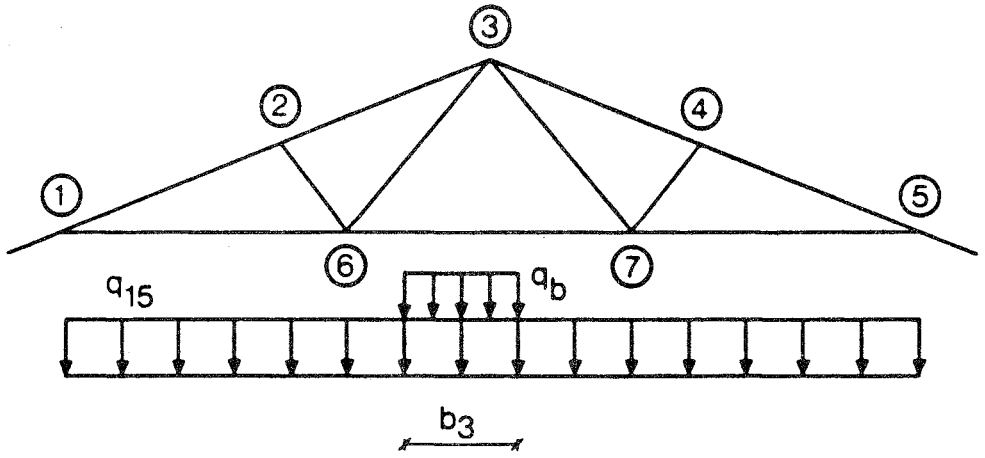


Figure A 3.2.4 c. Uniformly distributed loads on the bottom chord

A 3.2.5 Joint types

Three joint types are considered:

Type A Punched metal integral nail plates

Type B Joints with nails driven directly through thin steel plate gussets

Type C Joints with nails in gusset plates of plywood or of thin steel plates with prebored holes.

A 3.3 Axial forces

The axial forces can be found under the following assumptions:

- all members are connected by pin joints at the nodes
- uniformly distributed loads are transformed to nodal forces by simple equilibrium requirements, e.g. in node 2 a vertical load

$$F_{v,2} = (q_{v,13} (l_{12} + l_{23}))/2$$

and a horizontal load

$$F_{h,2} = q_{h,13} (l_{12} + l_{23})/2$$

A 3.4 Moments

A 3.4.1 Concentrated loads at the nodes

The moments can be disregarded.

A 3.4.2 Uniformly distributed constant loads

The moments in node 2 can be found by

$$M_2 = k_{m,2}\ q_{per,13}\ l_{12}^2$$

The moments in node 6 can be found by

$$M_6 = k_{m,6}\ q_{15}\ l_{16}^2$$

The moments correspond in most cases to tension in the bottom fibres but may, especially for joints of type C, correspond to compression.

The moments in the spans can be found by

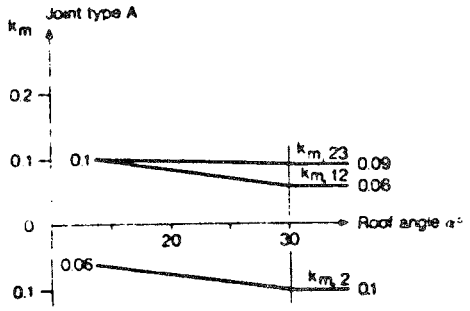
$$M_{12} = k_{m,12}\ q_{per,13}\ l_{12}^2$$

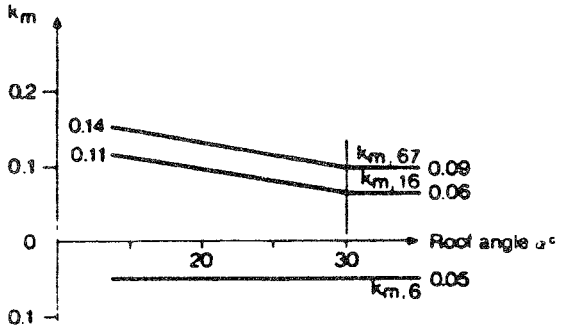
$$M_{23} = k_{m,23}\ q_{per,13}\ l_{23}^2$$

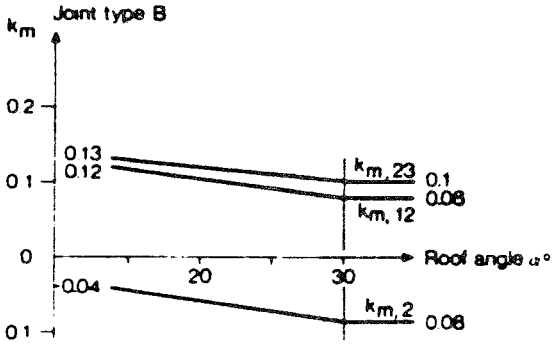
$$M_{16} = k_{m,16}\ q_{15}\ l_{16}^2$$

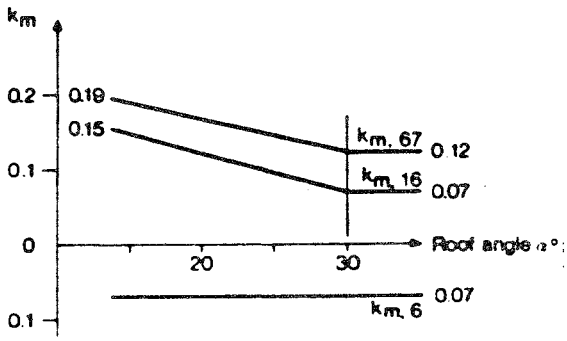
$$M_{67} = k_{m,67}\ q_{15}\ l_{67}^2$$

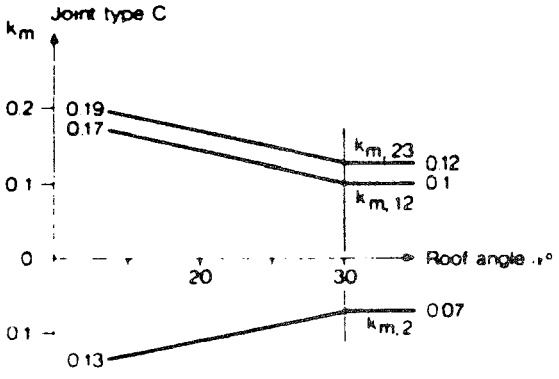
The moment coefficients k_m are given in figure A 3.4 a for centric nodal point geometry, and in figure A 3.4 b for eccentric nodal point geometry (see A 3.2.3). For intermediate nodal point geometry linear interpolation can be used.











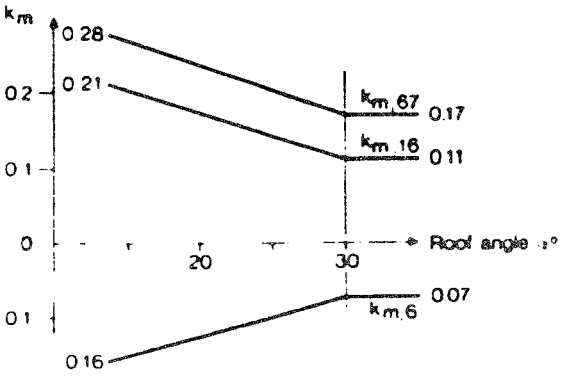


Figure 3.4 a. Moment coefficients for central connections between chords and diagonals

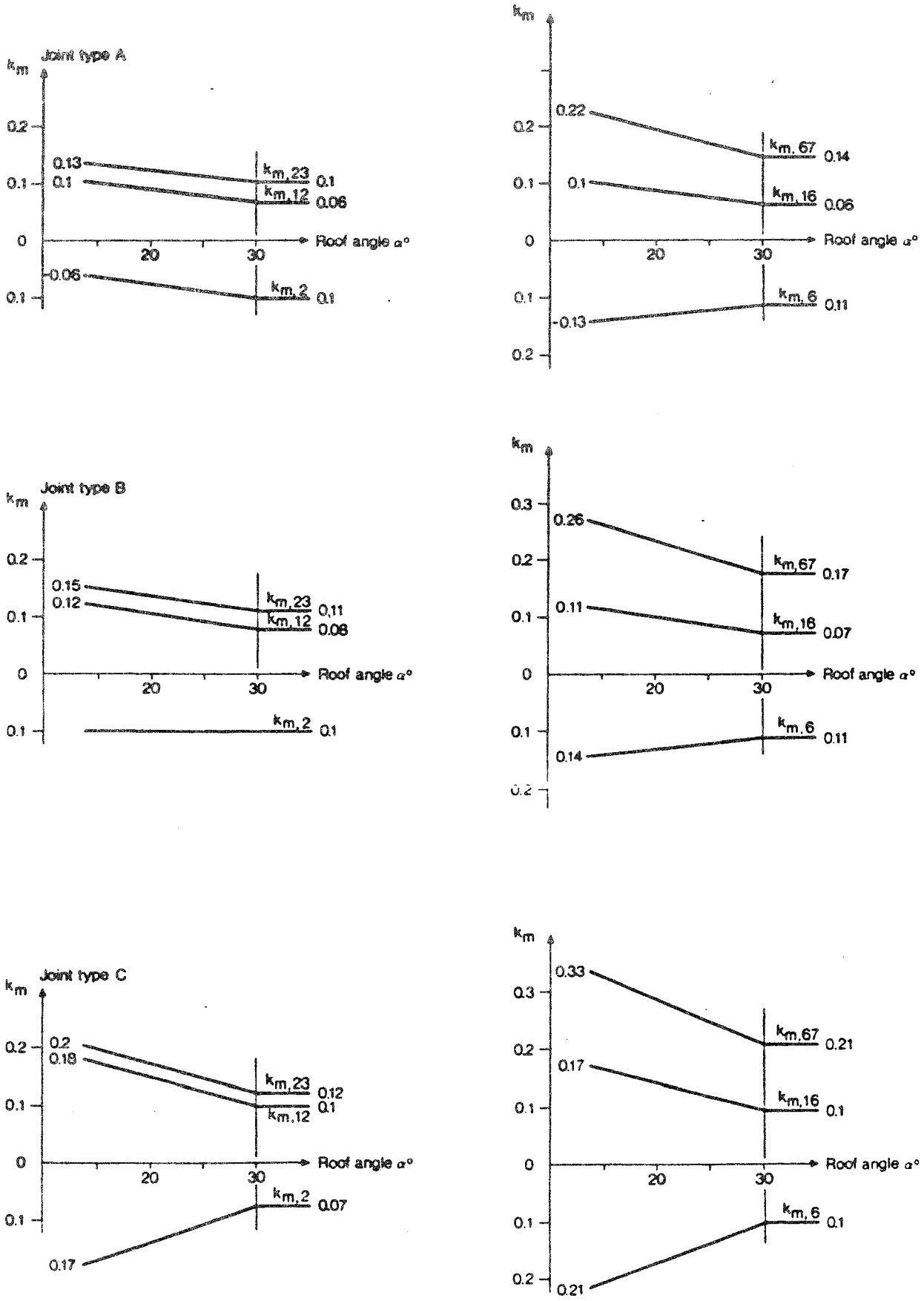


Figure 3.4 b. Moment coefficients for eccentric connections where the diagonals are connected to the inner side of the chords

A 3.4.3 Partial vertical loads on the bottom chord

The moments can be found as follows:

- determine the moments M_6 and M_7 at points 6 and 7 from the partial loads assuming a continous beam supported at points 1, 6, 7 and 5
- reduce these moments by a factor of 0.8
- calculate the moment distribution using these reduced moments.

A 3.5 Special calculation of trusses with large support eccentricity

For trusses with large support eccentricity a supplementary calculation should be made of the sections in the bottom and top chord just outside the wedge, see A 3.2.2.2.

The axial forces can be found by the following formulae:

$$F_{16} \sim (R - F_{11}) \cot\beta \qquad \text{(tension)}$$

$$F_{12} \sim -F_{16}/\cos\beta \qquad \text{(- = compression)}$$

where

$$F_{11} = q_{v,13}(a_1 + a_2)^2/(2a_2) + q_{15}(b_1 + b_2)^2/(2b_2)$$

The moments (numerical values) are

$$M_{12} \sim M_o \frac{h_1^2}{h_1^2 + h_2^2}$$

$$M_{16} \sim M_o \frac{h_2^2}{h_1^2 + h_2^2}$$

where

$$M_o = F_{16}b_1 \tan\alpha + 1/2\ q_{v,13}a_1^2 + 1/2\ q_{15}h_1^2$$

A 3.6 Failure condition

For the sections at the nodes, inclusive of the sections investigated in A 3.5, the usual failure conditions can be replaced by

$$\frac{\sigma_{t,o}}{f_{t,o}} + \frac{\sigma_m}{k_f f_m} \leq 1$$

$$\frac{\sigma_{c,o}}{f_{c,o}} + \frac{\sigma_m}{k_f f_m} \leq 1$$

where $k_f = \boxed{1.4}$ takes into account the reduced probability of failure because of the short length with high stresses.

CIB-W18/19-14-2

INTERNATIONAL COUNCIL FOR BUILDING RESEARCH STUDIES AND DOCUMENTATION

WORKING COMMISSION W18 - TIMBER STRUCTURES

SIMPLIFIED STATIC ANALYSIS AND DIMENSIONING OF TRUSSED RAFTERS
- PART 2 -

by

H Riberholt
Technical University of Denmark
Denmark

MEETING NINETEEN
FLORENCE
ITALY
SEPTEMBER 1986

PREFACE

During the analyses of the trusses I have received valuable comments and points of view from T. Feldborg, SBI, Denmark, for which I thank.

CONTENT

1. INTRODUCTION

In /Riberholt, 1984/ a simple calculation method is forwarded for the determination of the internal forces and moments in a W-truss. This paper continues along the same line for WW-trusses, scissor trusses, King post trusses and pulpit trusses.

This paper has been written at the same time as the parameter studies have been performed. So the different sections contain some repetitions, which could have been avoided if there had been time enough.

2. DISCRIPTION OF THE MOMENT COEFFICIENT METHOD

The description is given in /Riberholt, 1984/. Briefly summarized this states that the normal forces may be calculated from a pinned joint truss model, where the distributed loads are concentrated to nodal forces.

The moments in the chords are determined taking their continuity in consideration.

For distributed loads over several bays this may be done by means of moment coefficients k_{mom}. These are found by calibration with the results of a frame program.

For a minor distributed load over a part of a bay or for a concentrated force in a bay the moment distribution in the chords may be found by modelling them as continuous beams over several spans. Meanwhile the nodal moments from this analysis must be reduced in order to take into account the effect of the deflection of the truss nodes.

3. CALIBRATION OF MOMENT COEFFICIENTS. ASSUMPTIONS

Due to the fact that trusses are designed and produced so that they are internal statically indeterminate, the moments in the chords will increase when the slip in the joints are increased or when the bending stiffness (cross sectional height) of the chords are increased.

The values of the slip in the joints employed in this analysis are given in subsection 3.1.

The width of the cross sections was always put to 50 mm. The height was chosen so that the stresses were of such a magnitude that ordinary timber (relatively weak timber) would have sufficient strength. With stronger timber the cross sections would be more slender so the secondary moment-causing effects would be of less importance.

3.1. Regarded phenomena, review

By analysing the trusses it was found that the moment distribution did depend on the following. It was sensitive to some of the parameters and relatively insensitive to others.

I: Slope of the roof. The following have been analysed, 1:4, 1:3, 1:2.

II: Slip in the connections. The following values have been used. They are chosen from those given in /Feldborg & Johansen, 1981/ for long term loaded trusses.

TABLE 3.1 Slip emploied for the stress analysis

Connections Characterizing:	Slip in mm. 0	1	2	4	6
Heel joint slip in the direction of the top chord	0	1	2	4	6
Splice in the bottom chord	0	0.5	1.5	3	6
Ridge connection. Slip in the direction of the chord, each side	0	0.5	1	1	2
Vertical web member under the ridge of a scissor truss	0	0.5	1	2	3

III: Eccentricities in the connections between the diagonals and the chords. The diagonals were connected to the chords by pinned joints positioned either at the centre line or the inner periphery of the chord.

IV: Eccentric support of the heel joint. The eccentricities corresponded to what may occur in praxis.

V: The dimensions of the bottom and top chord, including the stiffness of the chords.

VI: The span of the truss.

VII: The load on the top chord in proportion to the load on the bottom chord, e.g. heavy or light roof.

VIII: Attic load over a part of the bottom chord.

IX: Continuous or pinned jointed chords.

In all trusses with a ridge the eccentricity at the top e_{top} was put equal to $h_{top}/6$. This takes into account that the compression force is transferred at the bottom most part of the contact zone between the two top chords.

All analyses have been done with a linear elastic frame program. In those where the internal static redundancy caused large moments in the chords separate analyses with a lower E-modulus for the chords were carried out.

4. WW-TRUSS

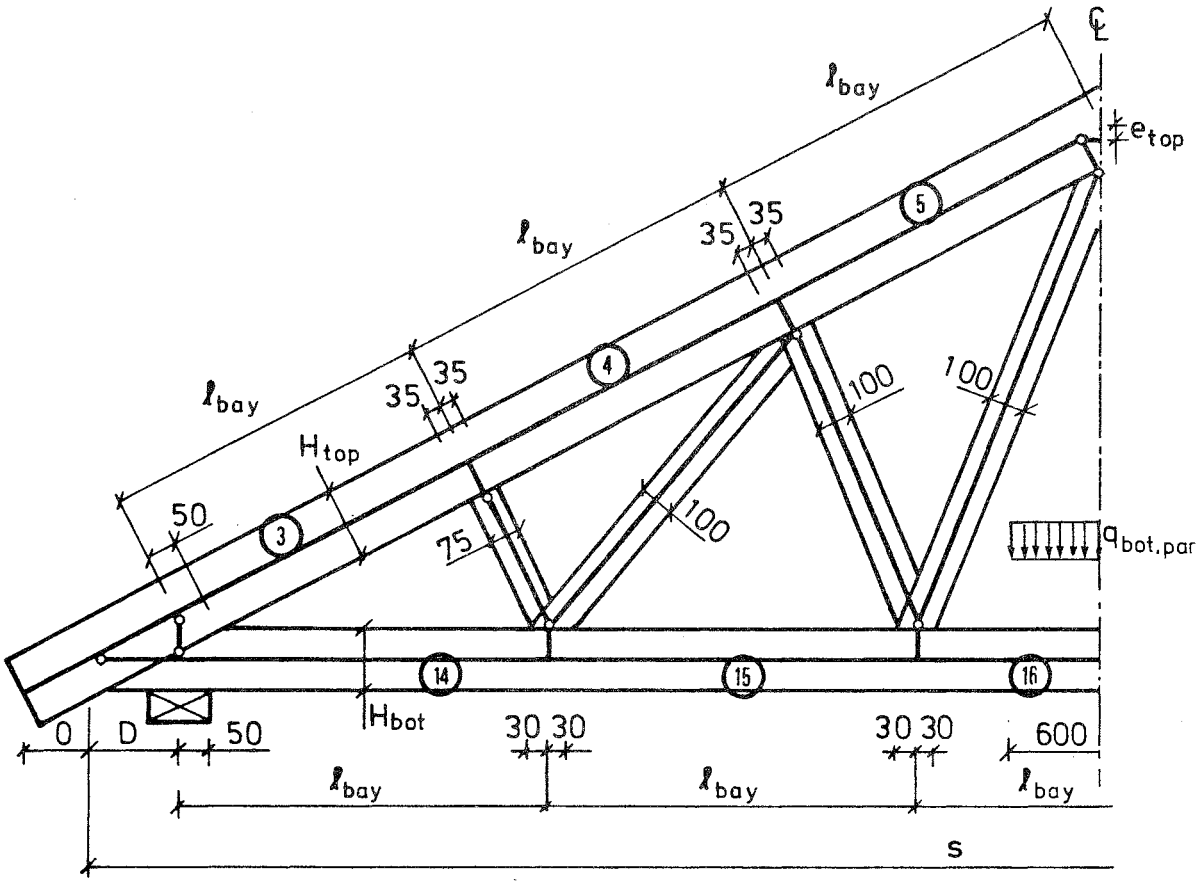
All the phenomena regarded have been analysed.

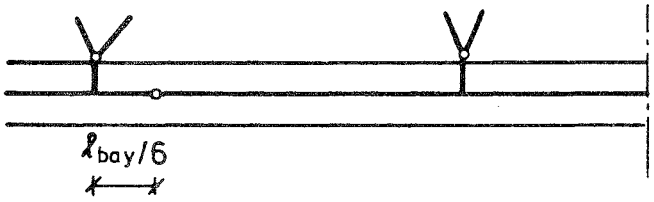
The deformations enforced due to the slip in the connections have special influence on the moment distribution in the chords close to the heel joint. So for WW-trusses the stiffness (dimension) and the continuity of the chords are of special importance.

A reference truss configuration has been selected. It has the following parameter values. The other configurations analysed have been selected with this as reference and so that only a few parameters have been altered for each configuration analysed.

Reference WW-truss

I Slope of the roof: 1:3
II The five slip categories have all been analysed.
III Centric connections.
IV Support eccentricity D = 70 mm
V H_{top} = 150 mm, H_{bottom} = 125 mm, Width = 50 mm, E_{chord} = 8,400 MPa, E_{dia} = 7,200 MPa
VI Span S = 12.0 m
VII Heavy roof q_{top} = 1.61 N/mm, q_{bottom} = 0.3 N/mm
VIII No partial attic load.
XI Continuous chords.





Position of the pinned joint in the bottom chord.

Figure 4.1 Frame model, geometry parameters, bay numbers and lengths. The pinned joint at the ridge can be shifted downwards in order to model that the compression-force between the top chords is transferred in the lower part of the joint. The truss is shown with eccentric diagonal-chord connections. Centric connections are similar to those shown in figure 5.1.

The position of the joints were chosen so that the bay lengths were of almost equal size in the top chord and in the bottom chord.

4.1. Centric connections between diagonals and chords.

Because of the influence of the enforced deformations from the slip in the connections both trusses with continuous chords and trusses with two symmetrically positioned pinned joints in the bottom chord were analysed. The position of a pinned joint is shown in figure 4.1.

4.1.1. Continuous chords

In figure 4.2 the calibrated moment coefficients for 3 trusses are shown all equal except for the roof slope.

It can be seen that the moment coefficients k_{mom} approximately depend linearly on the characterizing slip at the heel joint. This is also to be expected due to the linear elasticity of the wood and the proportional values of the slip in the different joints. It is thus acceptable to interpolate linearly between two k_{mom} values for two different joint slips.

In table 4.1 and 4.2 moment coefficients are given for two limit values of the heel joint slip. Several truss configurations have been analysed covering a relevant parameter space for the phenomena regarded.

For selected trusses the stresses have been calculated. It can be seen that these are in a range where ordinary lumber has sufficient strength.

For the trusses with partial attic load the moment coefficients for the bottom chords have been calculated as described in section 3.3.7 in /Riberholt, 1984/. Briefly described the approximate moment distribution from the partial attic load has been subtracted from the moment determined by the frame model. The approximate moment distribution is equal to that for a continuous beam loaded with the partial attic load and with the "support moments" reduced by a factor of 0.8. These reduced frame model moments have been emploied to calibrate the moment coefficients.

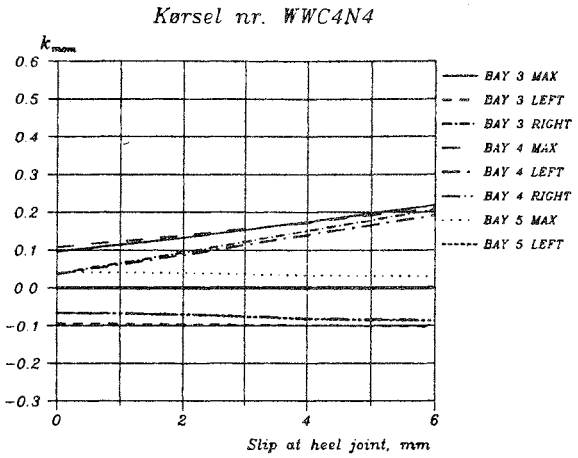
It was found that the moment coefficients did depend on the stiffness of the chords. The stiffness is here expressed in EI/l_{bay}^2. The examples cover stiffnesses up to

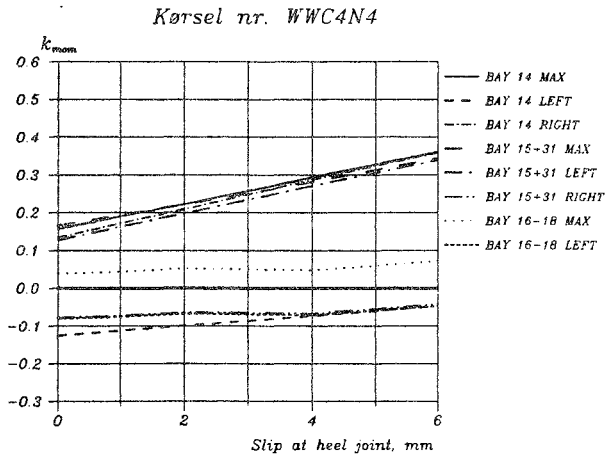
40 kN mm²/mm² for the top chords, for width = b = 50 mm
20 kN mm²/mm² for the bottom chords

TOP CHORD:

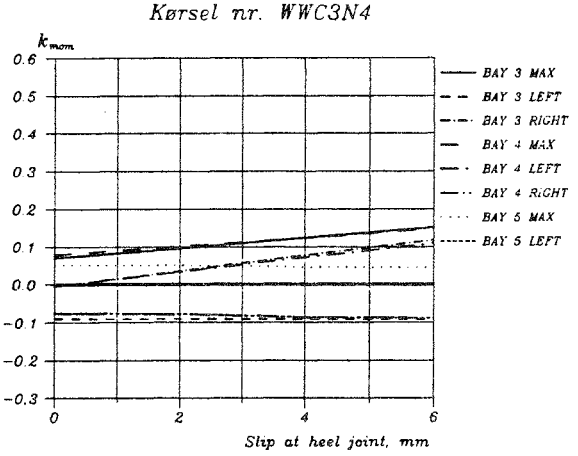
BOTTOM CHORD:

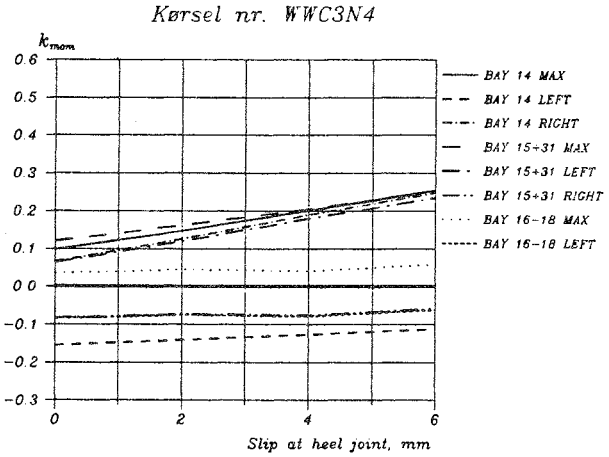
Roof slope 1:4



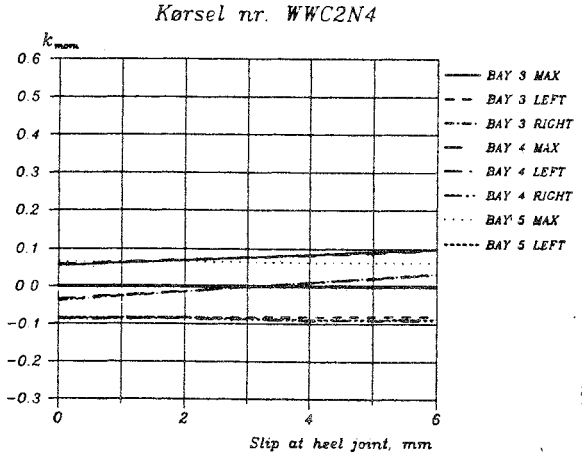


Roof slope 1:3





Roof slope 1:2



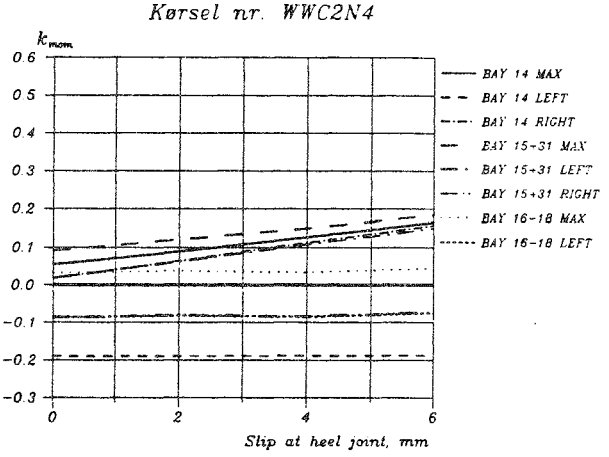


Figure 4.2 Moment coefficients for different roof slops and slips in the connections. Run "WWC3N4" is a reference truss. All similar except for the roof slope.

Table 4.1 Moment coefficients for the top chord of WW-trusses. Continuous chords. Centric connections. Values: 100 · k_{mom}. Stresses in MPa.

Roof slope	Span m	H_{chord} mm	Bay 3 max		Bay 3 right		Max k_{mom}, typical bay		Max k_{mom}, typical node		
			Slip at heel joint, mm: 1	4	1	4		1	4	*	1	4
WWC2N4												
1:2	12	150	6.2	8.4	-2.7	1.0	5/4	6.5	8.2	5L	-8.6	-9.1
WWC3N4. Reference												
1:3	12	150	8.3	12.3	1.5	7.7	4	9.0	12.3	5L	-7.6	-8.6
		σ_c =		3.8				3.6			2.8	
		σ_m =	2.6	3.9	0.4	2.2		3.1	4.2		-3.0	-3.3
WWC4N4												
1:4	12	150	11.4	17.4	6.5	15.1	4	12.3	17.3	5L	-6.8	-8.3
WWC3GBN4, partial attic load												
1:3	12	150	8.4	12.5	1.7	8.0	4	9.2	12.5	5L	-7.4	-8.4
WWC2N6												
1:2	16	175	6.4	-7.4	-4.8	-3.0	4	6.7	6.7	5L	-8.8	-9.1
WWC3N6												
1:3	16	175	7.7	9.4	-1.9	1.2	4	7.2	8.7	5L	-8.1	-8.6
		σ_c =		4.4				4.2			3.2	
		σ_m =	3.2	3.9	-1.0	0.3		2.5	2.4		-3.9	-4.1
WWC4N6												
1:4	16	175	9.6	12.2	1.9	6.1	4	9.6	11.8	5L	-7.2	-8.0
WWC3GBN6, partial attic load												
1:3	16	175	7.8	9.5	-1.8	1.3	4	7.3	8.8	5L	-7.7	-8.3
WWC3N7LI Light roof 1.31 kN/m												
1:3	12	150	8.7	13.8	2.1	9.8	4	9.4	13.5	5L	-7.5	-8.8
WWC3N7H Very heavy roof 3.0 kN/m												
1:3	12	150	7.4	9.5	0.1	3.5	4	8.2	9.8	5L	-7.7	-8.3
WWC3N7												
1:3	12	125	6.5	8.7	-1.1	2.6	4	7.4	9.2	5L	-8.1	-8.7
		σ_c =		5.8				5.5			4.3	
		σ_m =	1.9	4.0	0.8	0.9		3.6	4.5		-4.5	-4.8

* L signifies the left end of the bay.

4.1.2. Two pinned joints in the bottom chord

In order to reduce the effect on the chord moments from the enforced slip deformations two pinned joints have been introduced

in the bottom chord. The position of the joints is shown in figure 4.1, and in figure 4.3 the frame model is shown in principle together with the deformed truss chords.

Table 4.2 Moment coefficients for the bottom chord of WW-trusses. Continuous chords. Centric connections. Values: 100 · k_{mom}. Stresses in MPa.

Roof slope	Span m	H_{chord} mm	Bay 14 max		Bay 14 right		Max k_{mom}, typical bay			Max k_{mom}, typical node		
			Slip at heel joint, mm: 1	4	1	4		1	4	*	1	4
WWC2N4												
1:2	12	125	7.1	12.7	4.1	11.3	15	10.5	15.0	16L	-8.6	-8.5
WWC3N4. Reference												
1:3	12	125	12.2	20.2	9.6	19.0	15	14.0	20.5	16L	-8.0	-7.9
			σ_t =		4.3			3.6			2.7	
			σ_m = 1.5	2.5	1.2	2.3		1.9	2.7		-1.1	-1.1
WWC4N4												
1:4	12	125	19.0	29.4	17.2	28.8	15	19.3	28.1	16L	-7.5	-7.1
WWC3GBN4, partial attic load												
1:3	12	125	14.6	22.9	13.0	22.4	15	14.0	21.6	16L	-10.6	-10.4
							16	1.9	2.1			
WWC2N6												
1:2	16	150	6.5	9.0	0.5	4.3	15	8.5	10.8	16L	-8.4	-8.5
WWC3N6												
1:3	16	150	10.4	14.2	4.9	10.0	15	11.2	14.5	16L	-8.2	-8.1
			σ_t =		4.9			4.1			3.0	
			σ_m = 1.6	2.2	0.7	1.5		1.8	2.4		-1.4	-1.4
WWC4N6												
1:4	16	150	15.6	20.7	11.2	17.6	15	15.3	19.8	16L	-7.9	-7.7
WWC3GBN6, partial attic load												
1:3	16	150	11.8	15.8	7.4	12.5	15	10.5	14.2	16L	-9.8	-9.8
							16	0.9	1.0			
WWC3N7LI Light roof 1.31 kN/m												
1:3	12	125	10.9	18.5	7.2	16.6	15	12.6	18.8	16L	-7.9	-7.5
WWC3N7H Very heavy roof 3.0 kN/m												
1:3	12	125	20.7	30	20.6	30	15	21.7	29.1	16L	-8.6	-8.4
WWC3N7												
1:3	12	100	7.9	11.7	3.0	7.8	15	10.0	12.9	16L	-8.0	-8.0
			σ_t =		5.4			4.5			3.3	
			σ_m = 1.5	2.3	0.5	1.5		2.1	2.7		-1.8	-1.8

* L signifies the left end of the bay.

It is thus a precondition for the moment coefficients mentioned in this section that the splice which constitute the pinned joint has sufficient tensile capacity and plastic deformation capacity.

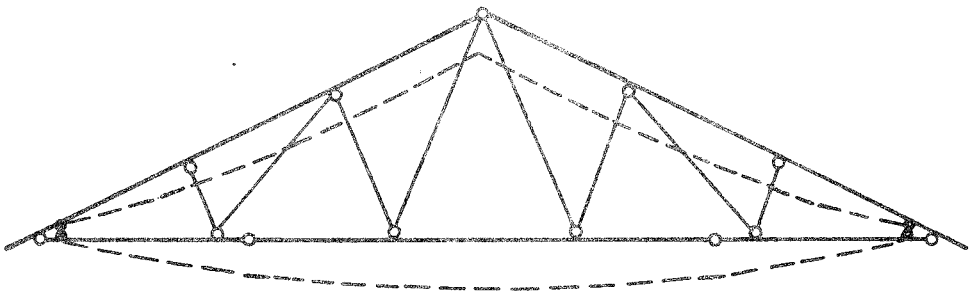


Figure 4.3 Frame model in principle for a truss with two pinned joints in the bottom chord. Deformed chords are shown with dotted lines.

Table 4.3 and 4.4 show the calculated moment coefficients. By comparison with table 4.1 and 4.2 respectively it can be seen that for the top the differences are small while for the bottom chord the moment coefficients are smaller in this case.

Table 4.3 Moment coefficients for the top chord of WW-trusses. Centric connections. Two pinned joints in the bottom chord. Values: $100 \cdot k_{mom}$.

Roof slope	Span m	H_{chord} mm	Bay 3 max Slip at heel joint, mm: 1	4	right 1	4	Max k_{mom}, typical bay	1	4	node	1	4
WWC2N3												
1:2	12	150	5.9	7.8	-2.5	1.1	5/4	6.8	8.9	5L	-8.1	-7.1
WWC3N3												
1:3	12	150	8.0	11.6	1.8	7.7	4	9.3	13.3	5L	-7.2	-5.8
WWC4N3												
1:4	12	150	11.1	16.9	7.2	15.2	4	12.8	18.5	5L	-6.3	-4.5
WWC3N5L												
1:3	15	175	7.8	9.8	-0.5	3.3	4	8.1	10.6	5L	-7.5	-6.6
WWC3N5H	Very heavy roof 3.0 kN/m											
1:3	12	175	8.9	12.0	3.0	8.0	4	10.2	13.5	5L	-6.8	-5.6

Table 4.4 Moment coefficients for the bottom chord of WW-trusses. Centric connections. Two pinned joints in the bottom chord. Values: $100 \cdot k_{mom}$.

Roof slope	Span m	H_{chord} mm	Bay 14 max		Bay 14 right		Max k_{mom}, typical bay			Max k_{mom}, typical node		
			Slip at heel joint, mm: 1	4	1	4		1	4		1	4
WWC2N3												
1:2	12	125	0.7	1.1	-6.6	-7.0	15/16	5.0	6.0	16L	-7.6	-6.4
WWC3N3												
1:3	12	125	3.1	5.0	-6.7	-7.3	15/16	5.4	8.0	16L	-6.8	-4.0
WWC4N3												
1:4	12	125	6.0	9.5	-6.8	-7.6	16	6.1	10.1	16L	-5.8	-1.8
WWC3N5L												
1:3	15	150	4.5	5.8	-6.6	-7.0	15/16	5.3	6.8	16L	-7.2	-5.2
WWC3N5H	Very heavy roof 3.0 kN/m											
1:3	12	150	0	2.4	-7.0	-7.9	16	5.8	10.8	16L	-6.0	-1.1

4.2. The support eccentricity at the heel joint

From figure 4.4 it can be seen that the moment coefficients depend on the support eccenticity at the heel joint. This is of course due to the fact that the support eccentricity introduces a large moment in the chords.

The figure shows that there is a substantial change in the moment coefficients when the eccentricity D is altered from 100 mm to 150 mm. This means that the moment coefficients only are applicable for a support eccentricity less than 100 mm.

For larger eccentricities it is the chord moments at the heel joint which are dimensioning. It is suggested that these moments are determined and the dimensioning is carried out in a similar way as described in section 4.2 of /Riberholt, 1984/.

4.3. Diagonal-chord connections at the inner chord periphery.

Both trusses with continuous chords and with 2 pinned joints in the bottom chord (positioned as described in section 4.) were analysed. A comparison revealed that the differences in k_{mom} were relatively small for the top chord while there were essential differences for the bottom chord. The values of k_{mom} are for continuous chords given in figure 4.5, and for a pinned jointed bottom chord in figure 4.6 but only for a selected configuration.

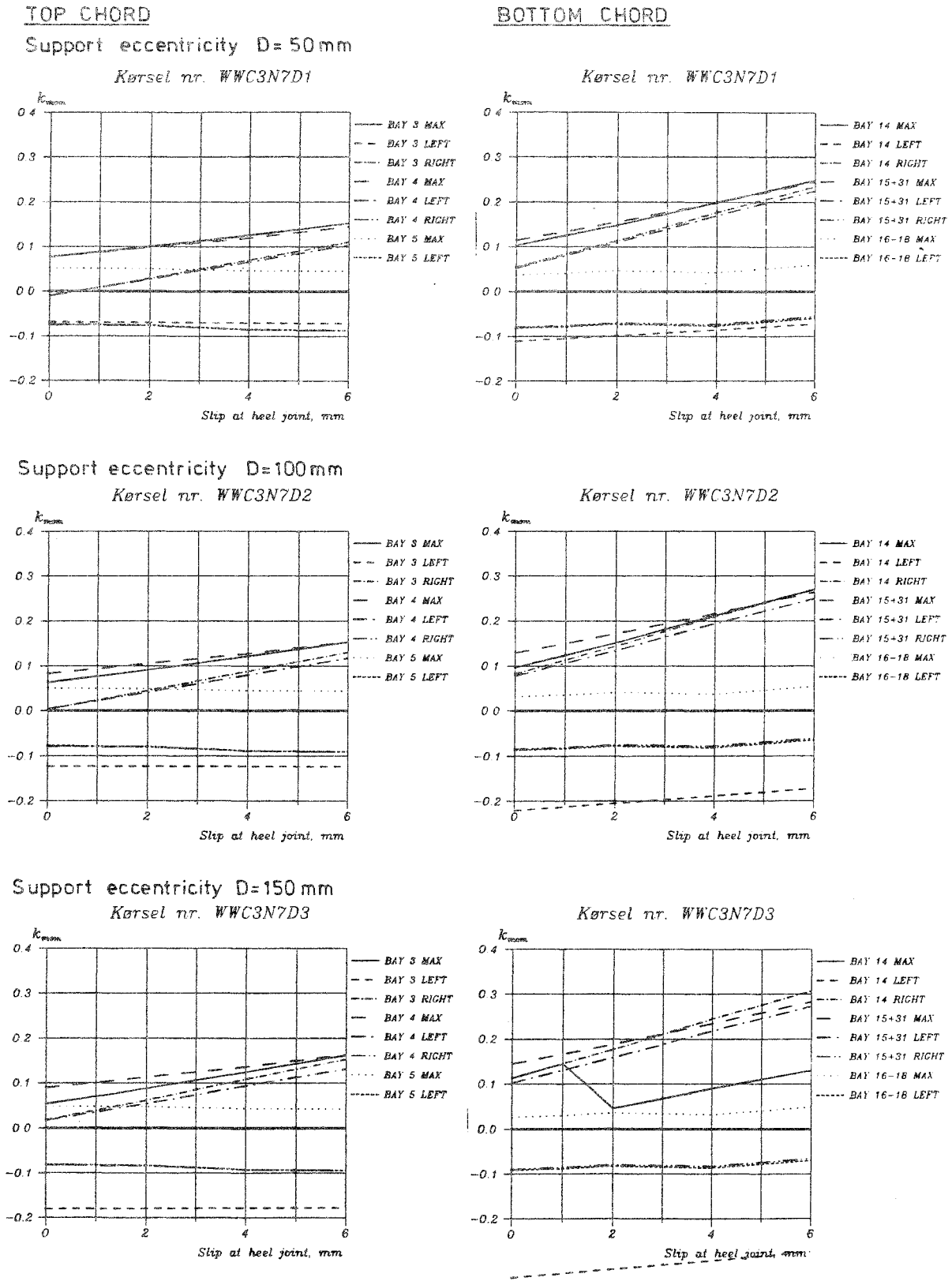
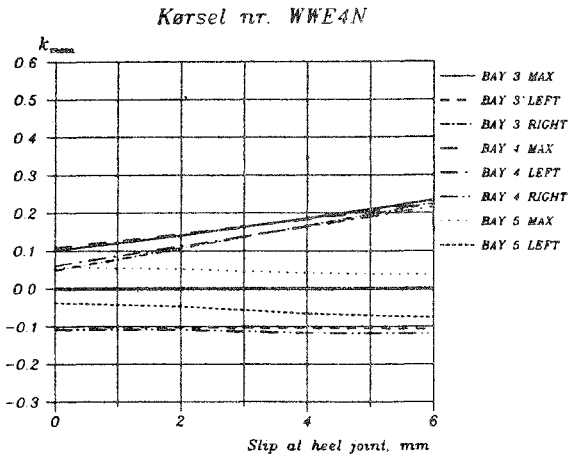


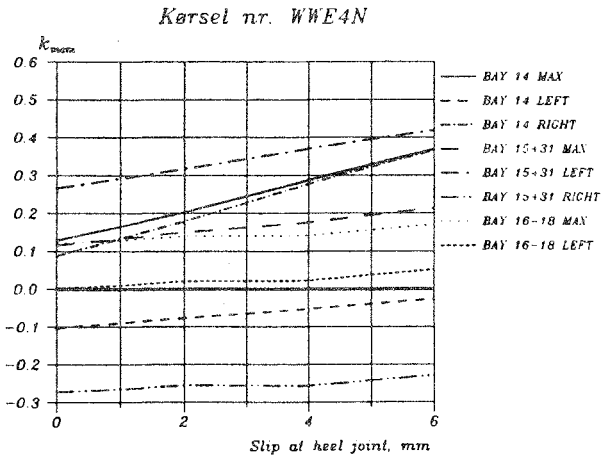
Figure 4.4 Moment coefficients for a roof slope of 1:3, span = 12.0 m and different support eccentricities D . Centric connections.

TOP CHORD

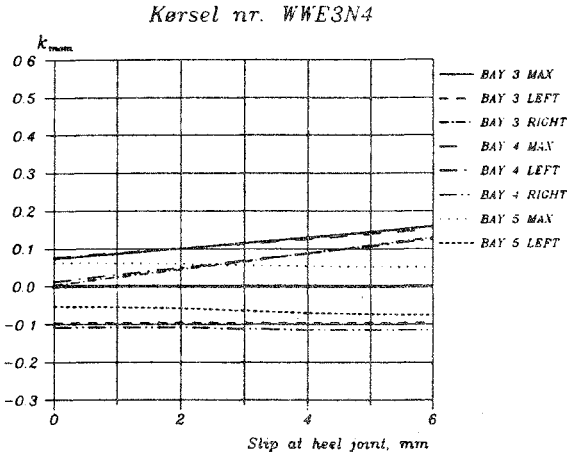
Roof slope 1:4

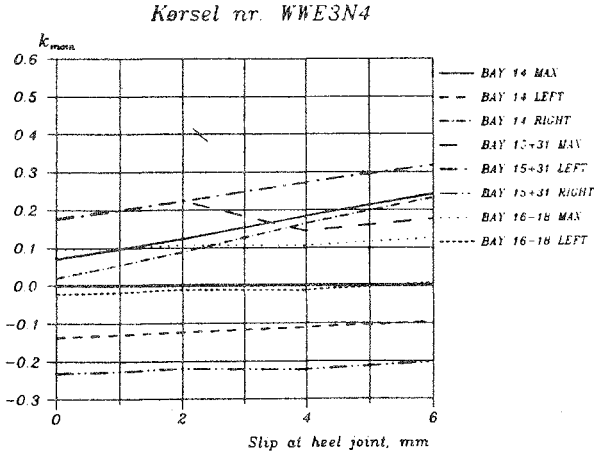


BOTTOM CHORD

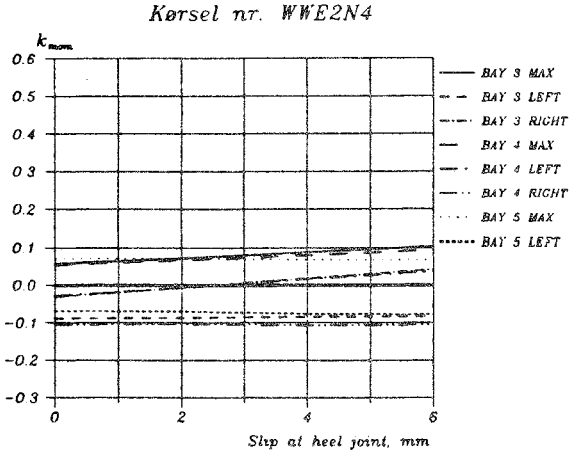


Roof slope 1:3





Roof slope 1:2



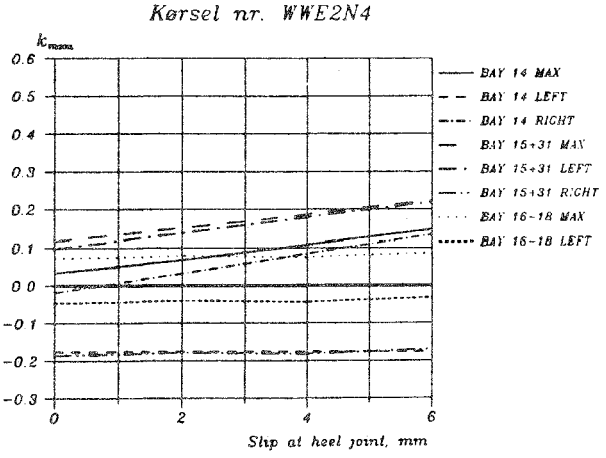


Figure 4.5 Moment coefficients for different roof slops and slips in the connections. Run "WWC3N4" is a reference truss except for the eccentric connections. All chords are continuous.

As noticed in section 4.1 the moment coefficients approximately vary linearly with the characterizing slip at the heel joint. It is thus acceptable to interpolate linearly in the heel joint slip.

In table 4.5 og 4.6 moment coefficients are given for two limit values of the heel joint slip. It has been investigated that the stresses belong to a range where ordinary lumber has sufficient strength.

Table 4.5 Moment coefficients for the top chord of WW-trusses. Eccentric connections. Continuous chords. Values: 100 · k_{mom}.

Roof slope	Span m	H_{chord} mm	Bay 3 max Slip at heel joint, mm: 1	4	right 1	4	Max k_{mom}, typical bay 1	4	node 1	4
WWC2N4										
1:2	12	150	6.5	8.8	-1.9	1.8	5	7.1	6.8	4R -10.4 -10.7
WWC3N4	Reference									
1:3	12	150	8.7	12.9	2.4	8.8	4	8.8	12.5	4R -10.8 -11.4
WWC4N4										
1:4	12	150	12.0	18.6	7.7	16.6	4	12.6	18.3	4R -10.8 -11.7
WWE2N6										
1:3	16	175	6.6	7.7	-4.1	-2.3	5	7.3	7.2	4R -10.6 -10.7
WWE3N6										
1:3	16	175	7.9	9.7	-1.1	2.1	4	6.8	8.5	4R -11.1 -11.4
WWE4N6										
1:4	16	175	10.0	12.7	2.9	7.3	4	9.5	12.1	4R -11.2 -11.8

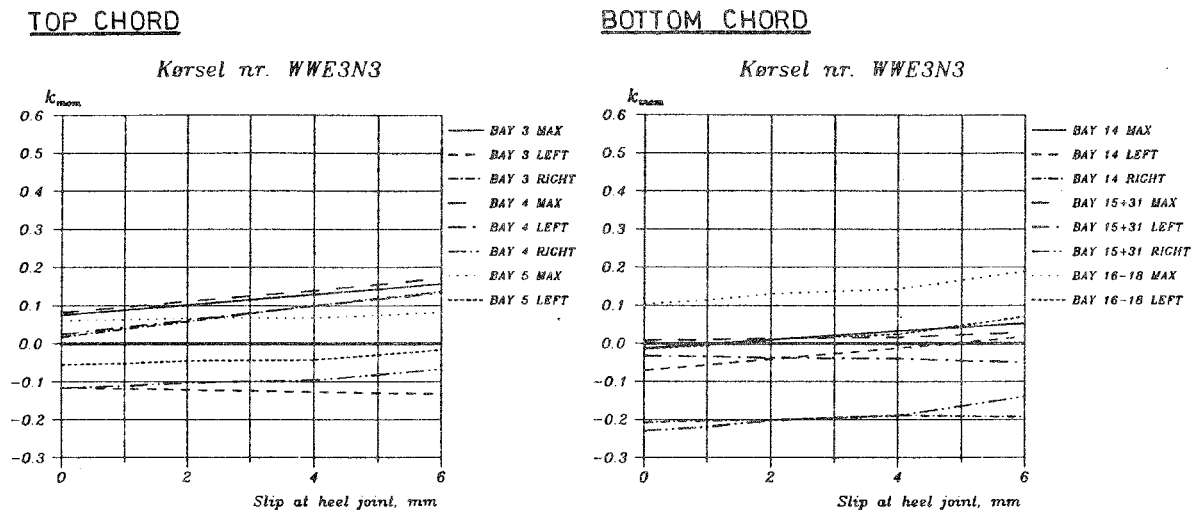


Figure 4.6 Moment coefficients for a truss similar to a reference truss except for eccentric connections and 2 pinned joints in the bottom chord.

Table 4.6 Moment coefficients for the bottom chord of WW-trusses. Eccentric connections. Continuous chords. Values: 100 * k_{mom}.

Roof slope	Span m	H_{chord} mm	Bay 14 max Slip at heel joint, mm: 1	4	right 1	4	Max k_{mom}, typical bay	1	4	node *	1	4
WWE2N4												
1:2	12	125	5.0	10.8	.7	8.5	15	13.4	18.7	15R	-18.3	-18.2
							16	7.5	7.6	16L	-4.4	-4.3
WWE3N4	Reference											
1:3	12	125	9.7	18.4	5.4	16.4	15	20.1	14.4	15R	-22.6	-22.2
							16	10.0	10.6	16L	-1.9	-1.3
WWE4N4												
1:4	12	125	16.5	28.8	13.3	27.8	15	13.2	17.6	15R	-26.6	-25.7
							16	12.8	14.1	16L	0.9	2.2
WWE2N6												
1:2	16	150	4.8	7.3	-3.0	1.1	15	10.7	13.4	15R	-17.6	-17.6
							16	7.2	7.2	16L	-4.8	-4.8
WWE3N6												
1:3	16	150	8.2	12.2	0.3	6.2	15	16.2	20.1	15R	-21.9	-21.7
							16	9.3	9.5	16L	-2.8	-2.5
WWE4N6												
1:4	16	150	13.0	18.7	6.2	7.3	15	11.3	13.8	15R	-25.8	-25.4
							16	11.5	12.0	16L	-0.6	0

* L and R signify the left and right end of the bay respectively.

It has been investigated whether the equation (4.1) gives a reasonable estimate of the maximum moments at the nodes.

$$M_{ecc.} = M_{cen} + k_M |M_e| \qquad (4.1)$$

$$= k_{mom,cen}\, q_{90}\, l_{bay}^2 + k_M\, e |F_{par}|$$

where

$M_{ecc.}$ Node moment in a truss with eccentric diagonal-chord connections.

M_{cen} Node moment in a truss with centric diagonal-chord connections. Is calculated by means of moment coefficients for trusses with centric connections.

M_e Eccentricity moment arising from the eccentric connected diagonals. It can be calculated from the eccentricity e and the resulting force of the diagonal forces parallel to the chord. See figure 4.7.

k_M A factor, which takes into account that M_e is distributed to both bays.

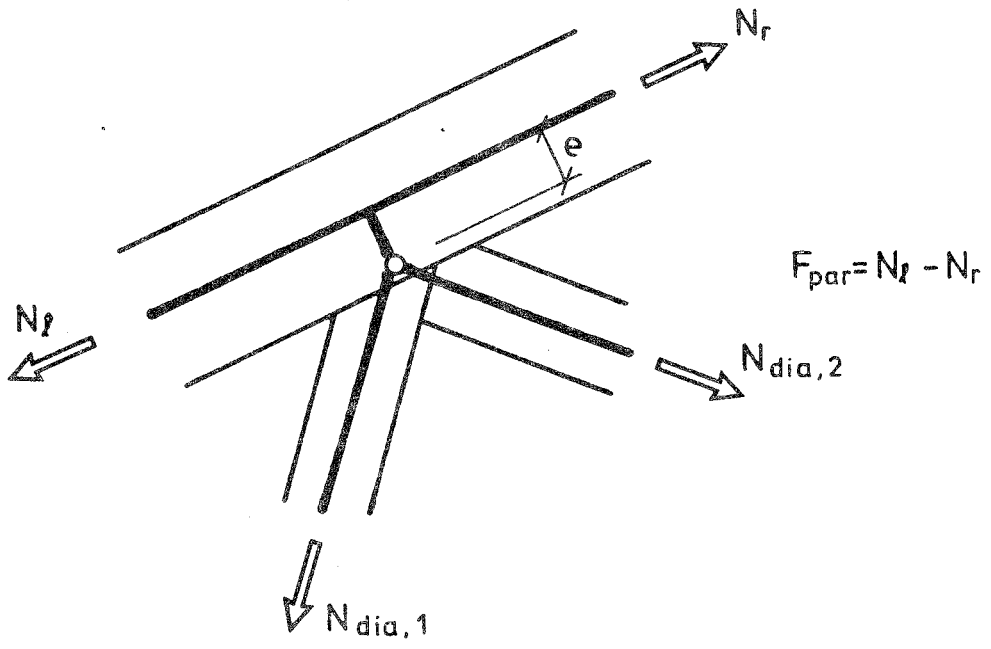


Figure 4.7 Eccentric diagonal-chord connection. Definition of the eccentricity e and the chord parallel force F_{par}.

The factor k_M has been found by calibration of equation (4.1). Three truss configurations have been emploied of which the run WWC3N4 is an analysis of the reference truss. The other were similar except for the roof slope. The results are given in table 4.7.

The table 4.7 shows also values of k_M determined by applying the eccentricity moments M_e to the nodes of a continuous beam over three and five bays and thereby modelling the top chord and the bottom chord respectively. M_e is found from a normal force analysis and the geometry. In this case e was equal to $0.5 \cdot h_{chord}$.

Table 4.7 Values of k_M. Found partly by calibration of the frame models, partly by an analysis of a continuous beam, values in brackets.

Chord	Node between bay	Char. heel slip	Roof slope and computer runs: 1:2 WWC2N4+WWE2N4	1:3 WWC3N4+WWE3N4	1:4 WWC4N4+WWE4N4
TOP	3-4	1	0.47 (0.85)	0.90 (0.93)	1.2 (0.90)
	4-5	1	-0.55 (-0.59)	-0.56 (-0.58)	-0.70 (-0.58)
	3-4	4		0.88	
	4-5	4		-0.51	
BOT-TOM	14-15	1	0.71 (0.73)	0.74 (0.74)	0.75 (0.77)
	15-16	1	-0.73 (-0.72)	-0.77 (-0.71)	0.72 (-0.70)
	14-15	4		0.64	
	15-16	4		-0.71)	

Since the eccentricity moments contribute only with a minor part to the stresses in a cross section it is proposed that the distribution factor is put to a constant valid for each node in the truss. As an alternative the distribution of the node eccentricity moments can be found from an analysis of a continuous beam, see figure 4.8.

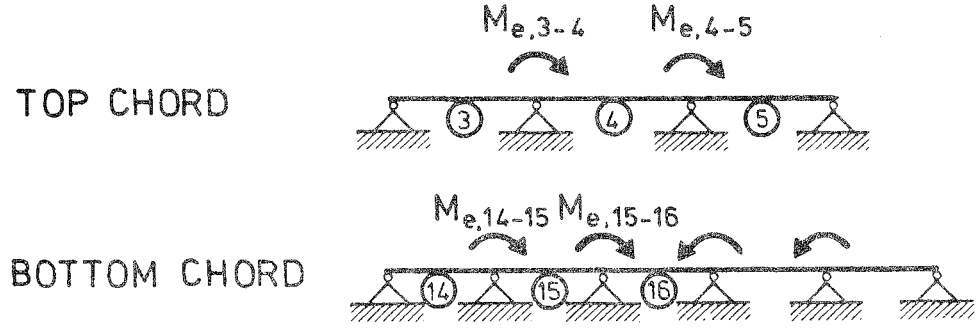


Figure 4.8 Eccentricity moments on continuous beams for an approximate analysis of the chords.

4.4. A simple stress analysis for a WW-truss

The normal forces and internal chord moments are calculated as described in section 4.4.1 and 4.4.2/4.4.3 respectively. It is assumed that the connections are designed so that the diagonals only are subjected to normal forces, not to moments.

4.4.1. Normal forces

The normal forces can be found under the assumption that all the connections in the WW-truss act as pinned joints loaded with nodal forces. These are found by means of some approximate equilibrium requirements for the adjacent chord bays. See for example section 2 in /Riberholt, 1984/ and figure 4.9.

For trusses with a support eccentricity D larger than 100 mm this influences the normal forces in the top and bottom chord at the heel joint. See section 4.4.3 and section 4.2 in /Riberholt, 1984/.

4.4.2. Chord moments for a WW-truss with a little support eccentricity

The chord moments can be calculated in the way described here provided that:

The support eccentricity D is less than
  100 mm.
  2 · height of the bottom chord.
Almost equal bay lengths in the top chord. The same requirement to the bottom chord.
The slope of the roof is larger than 1:4.
The stiffness per crosssectional width $EI/(bl_{bay}^2)$ is less than
  Top chord 0.8 kN mm²/mm³
  Bottom chord 0.4 kN mm²/mm³
The constant distributed load on the bottom chord is larger than 0.1 times the top chord load.

4.4.2.1. Uniformly distributed loads

The moments in the nodes and in the bays can be calculated from equation (4.2)

$$M = k_{mom}\, q_{90}\, l_{bay}^2 \qquad (4.2)$$

where

k_{mom} Moment coefficient in figure 4.10-4.12 whichever is applicable to the case.

q_{90} Distributed constant load perpendicular to the chord.

l_{bay} Bay length

The moment coefficients depend on the slip in the joints. They are given for two cases characterized by the slip in the heel joint. A heel joint slip of 1 mm is applicable for nail plates with long teeth and a heel joint slip of 4 mm is applicable for nailed plywood, wood gussets or for connectors with teeth pressed into the wood. For intermediate heel joint slips a linear interpolation may be used.

For WW-trusses with eccentric diagonal-chord connections the moments in the nodes and bays may alternatively be calculated from the equations (4.3) and (4.4).

At a node

$$M = M_{centric} + M_{eccentric}$$
$$= k_{mom,cen}\, q_{90}\, l_{bay}^2 + k_M\, e\, |F_{par}| \qquad (4.3)$$

In a bay

$$M = M_{centric} + M_{eccentric}$$
$$= k_{mom,cen}\, q_{90}\, l_{bay}^2 + 1/2(k_M\, e\, |F_{par}|)_{left} + 1/2(k_M\, e |F_{par}|)_{right} \qquad (4.4)$$

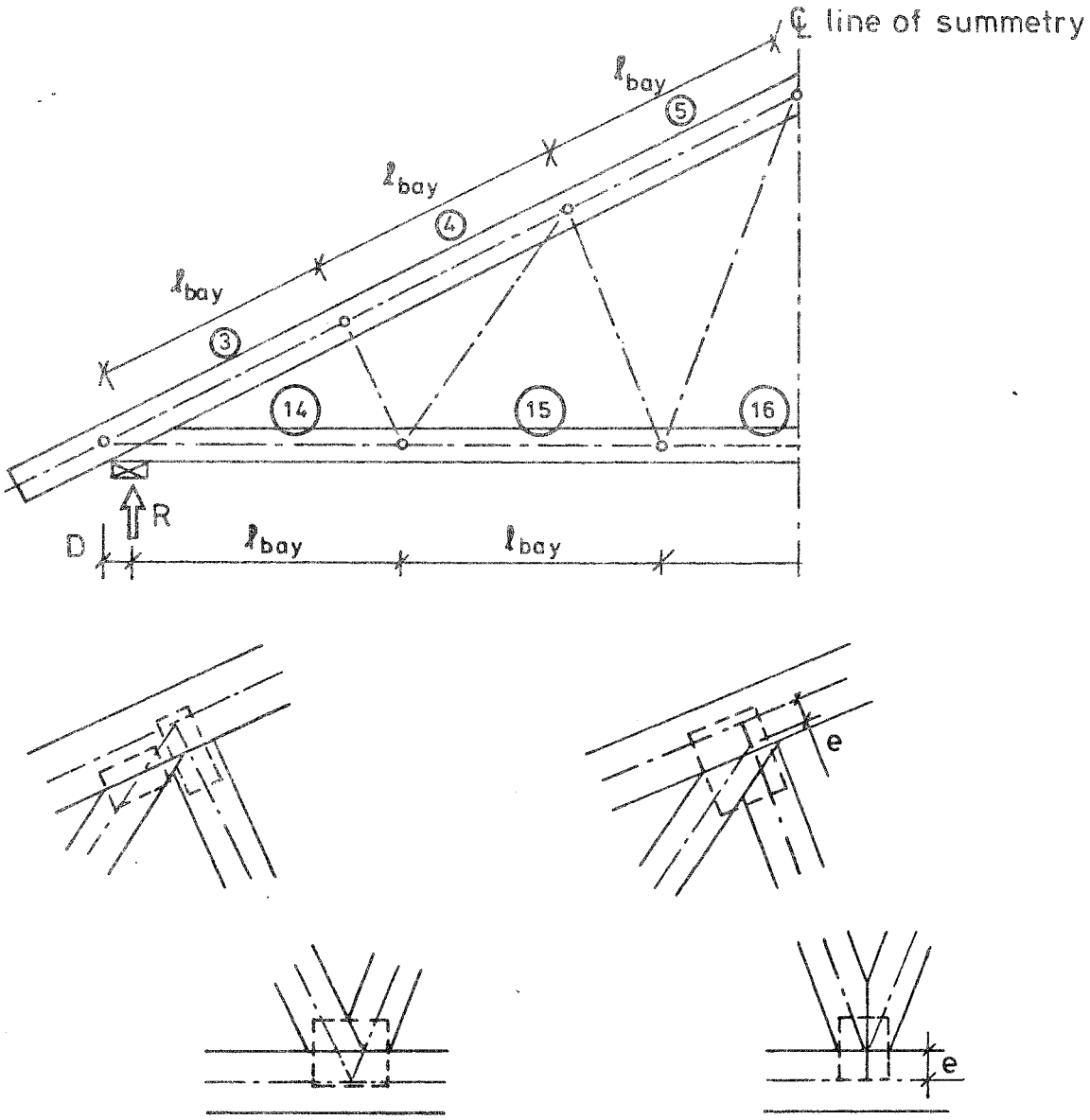
where the first terms are the moments in an equivalent truss with centric diagonal-chord connections. The last term(s) are due to the eccentric connections and the notation is

k_M Moment distribution factor, see table 4.8

e Connection eccentricity, see figure 4.7

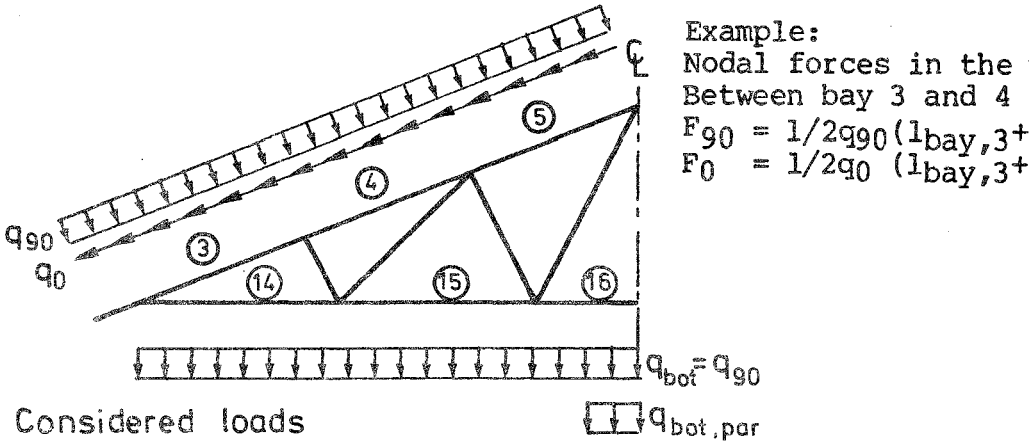
F_{par} Resulting force of the diagonal forces parallel to the chord, see figure 4.7.

The term $M_{eccentric}$ may also be determined by analysing a continuous beam subjected to node moments equal to the eccentricity moments $e\, F_{par}$, see figure 4.8.



Centric connections

Eccentric connections



Considered loads

Example:
Nodal forces in the mode
Between bay 3 and 4

$F_{90} = 1/2 q_{90} (l_{bay,3}+l_{bay,4})$

$F_0 = 1/2 q_0 (l_{bay,3}+l_{bay,4})$

Figure 4.9 Geometry of and loads on a WW-truss.

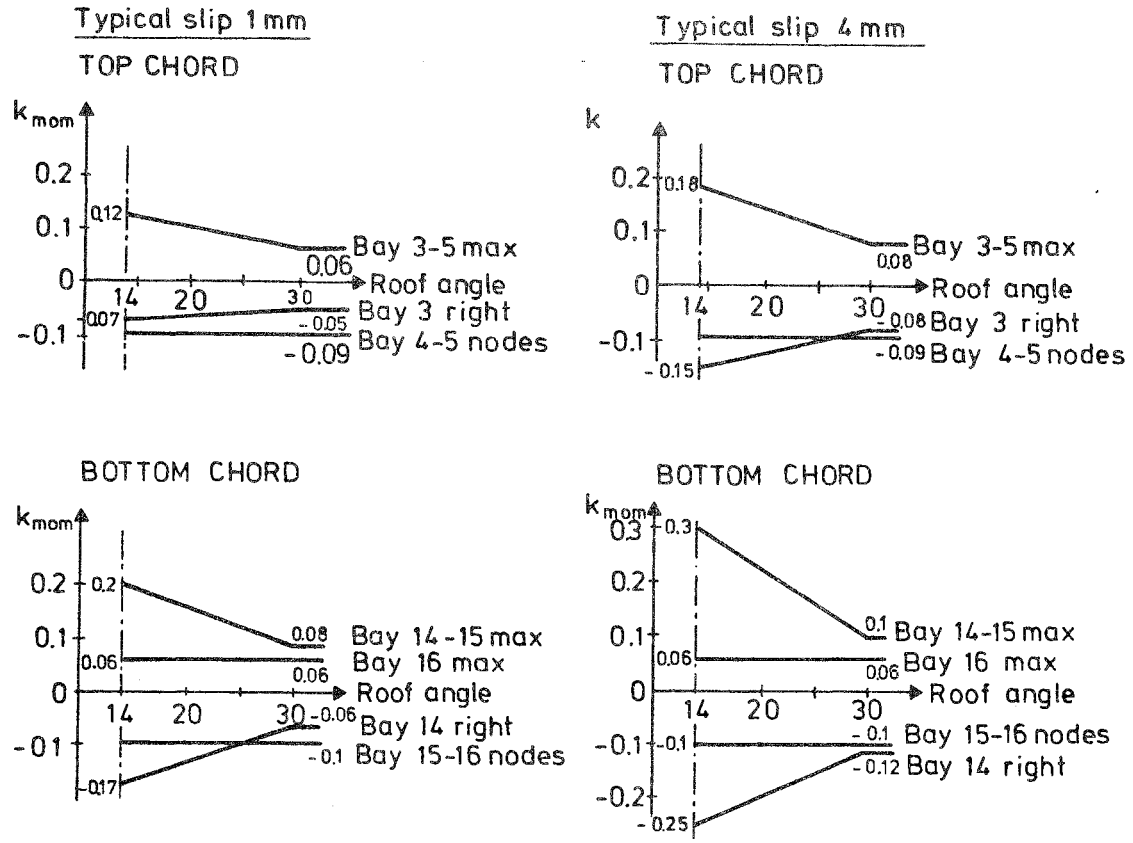


Figure 4.10 Moment coefficients for a WW-truss with centric diagonal-chord connections and continuous chords.

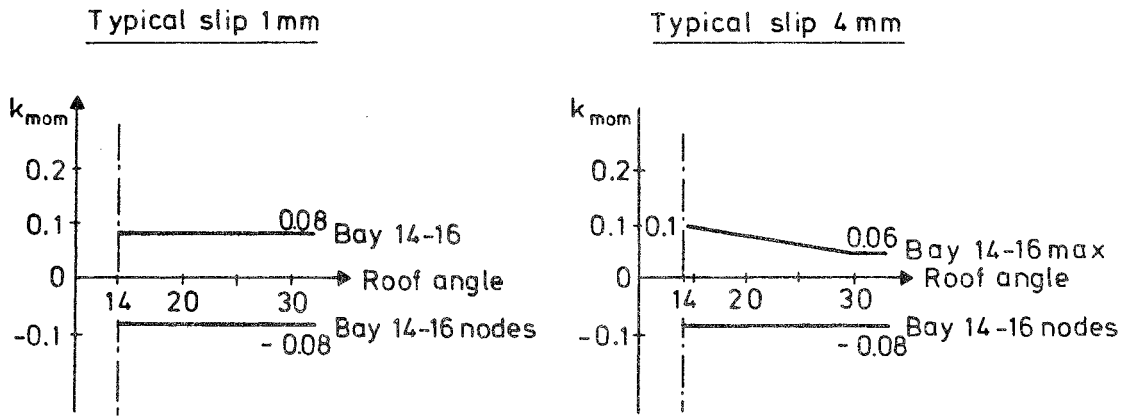


Figure 4.11 Moment coefficients for the bottom chord of a WW-truss with centric diagonal-chord connections and 2 pinned joints in the bottom chord positioned as shown in figure 4.1. For this case k_{mom} for the top chord may be taken from figure 4.10.

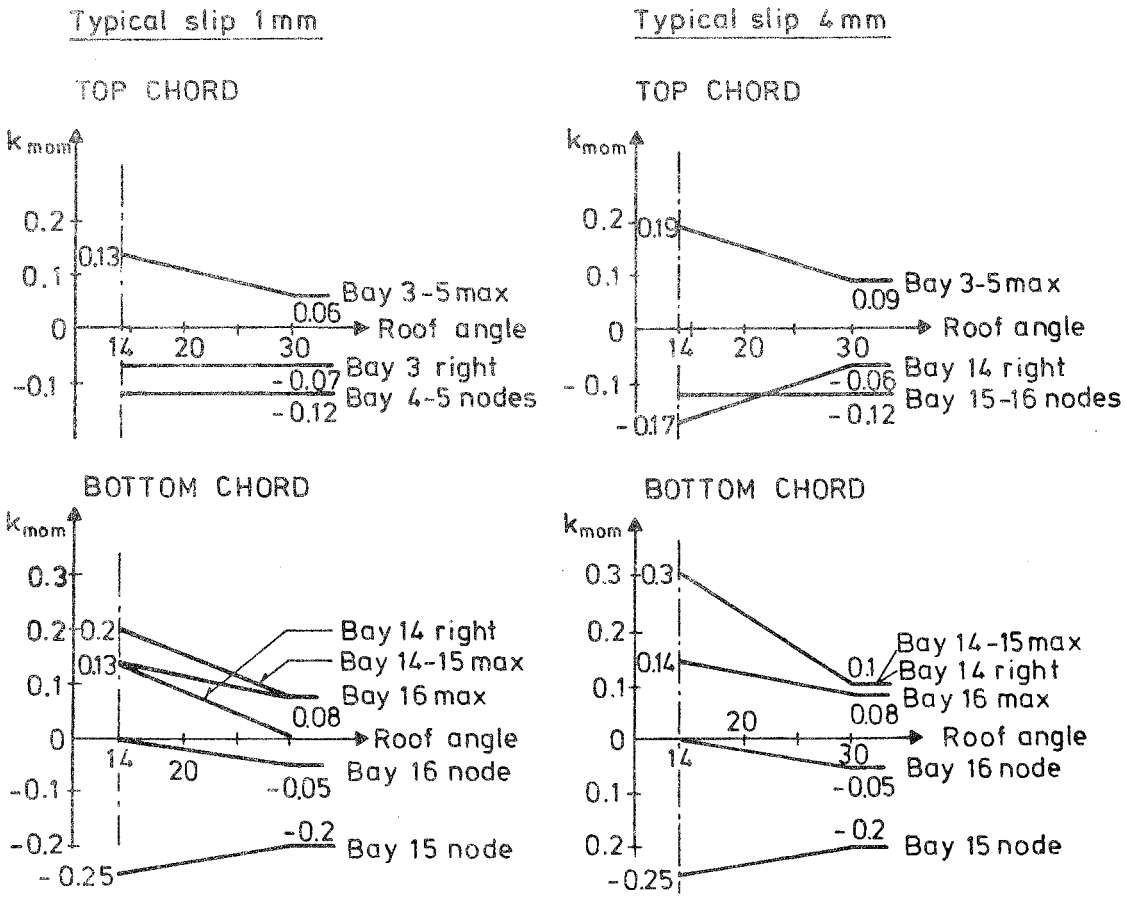


Figure 4.12 Moment coefficients for a WW-truss with eccentric diagonal-chord connections and continuous chords. The diagonals are assumed connected to the inner periphery of the chords.

Table 4.8 Values of the moment distribution factor k_M

Node between bay	3-4	4-5	14-15	15-16
k_M	1.0	-0.6	0.75	-0.75

4.4.2.2. Partial distributed uniform load

The chord moments can be found by first determining the node moments in a fictitious continuous beam with span lengths equal to bay length of the straight and continuous chord. The beam shall be subjected to the same loads as the chord.

These node moments must be reduced by a factor of 0.8, and with the reduced node moments the moment in any cross section may be calculated.

4.4.3. Chord moments for a WW-truss with a large support eccentricity.

For a support eccentricity D larger than assumed in subsection 4.4.2 the moments in the chords can approximately be found as described in that subsection, except for the cross sections at the support. Here a special investigation of the chord moments at the heel joint must be carried out in a similar way as described in subsection 4.2 of /Riberholt, 1984/.

5. SCISSOR-TRUSS

All the phenomena mentioned in chapter 3 have been analysed.

Scissor trusses are dealt with as the WW-trusses. So the comments to the results are reduced.

Scissor trusses may be produced with 2x2, 2x3, 2x4... bays in the top chord and bottom chord. Only for trusses with 2x2 bays a simple stress analysis method has been proposed. For trusses with more bays the internal static redundancy leads to that a simple method is not reasonable and suitable except for trusses with 2x3 bays and with connections as stiff as nail plates.

Reference truss configurations have been selected for trusses with 2x2 and 2x3 bays. The other configurations have been selected with this as reference and so that only a few parameters have been altered for each configuration analysed.

Reference Scissor-trusses with 2x2 or 2x3 bays.

I Slope of the roof and ceiling 22 and 8 degrees respectively.

II The five slip categories have all been analysed.

III Centric connections

IV Support eccentricity D = 70 mm.

V E_{chord} = 8,400 MPa, E_{dia} = 7,200 MPa, Width = 50 mm
2x2 bays: H_{top} = 125 mm, H_{bot} = 100 mm
2x3 bays: H_{top} = 150 mm, H_{bot} = 125 mm

VI 2x3 bays: Span = S = 8.0 m
2x3 bays: Span = S = 12.0 m

VII Light roof q_{top} = 1.31 N/mm, q_{bottom} = 0.3 N/mm.

VIII No partial attic load.

IX Continuous chords.

The position of the joints were chosen so that the bay lengths were of almost equal size in the top chord and in the bottom chord.

It is typical for scissor trusses that the construction height is little. So the deflections are larger and therefore the internal redundancy causes larger extra moments.

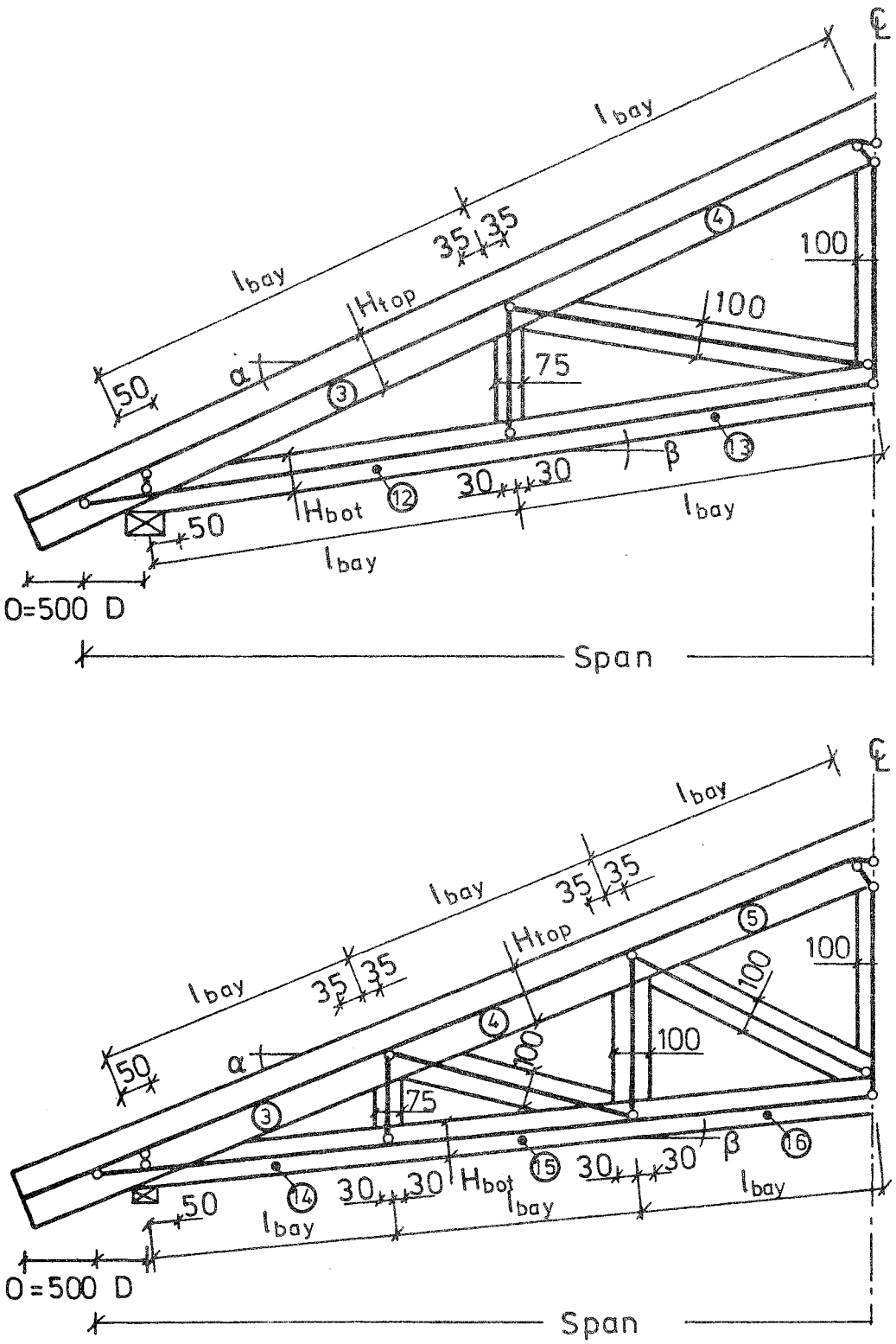


Figure 5.1 Frame model, geometry parameters, bay numbers and lengths. The pinned joint at the ridge has been shifted downwards $H_{top}/6$ in order to model that the compression force between the top chords is transfered in the lower part of the joint. The truss is shown with centric diagonal-chord connections. Eccentric connections are similar to those shown in figure 4.1.

Scissor trusses may have an other web configuration, which results in the fact that the chord has one bay more than the bottom chord. This type has not been analysed since it has a static behaviour similar to that of W- or WW-trusses. But this type is more suitable - specially for large top chord loads - because the secondary moment causing effects are not so significant as for the type analysed. This better type is suggested analysed by means of moment coefficients valid for a W- or WW-truss with a similar configuration.

5.1. Centric connections between diagonals and chords

Scissor trusses with 2x2 and 2x3 bays are dealt with. To avoid repetition of comments the results for trusses with 2x3 bays are only commented when they deviate from those for 2x2 bays trusses.

5.1.1. Scissor truss with 2x2 bays.

In figure 5.2 the calibrated moment coefficients for 2 trusses are shown both equal except for the slope of the roof and the ceiling.

As for the WW-trusses it can be seen that the moment coefficients vary linearly with the characterizing heel joint slip. One exception is bay 12 of the bottom chord, where there for a heel joint slip of 6 mm exist no maximum in the bay. So linear interpolation in the joint slip is acceptable for a heel joint slip less than 4 mm.

It has been found that for the above mentioned truss types that it is the construction height, which to a high degree controls the values of the moment coefficients. The construction height is given by the difference between the roof slope and the ceiling slope. For pairs of roof and ceiling slopes between (14^o, 0^o) and (30^o, 16^o) and between (18^o, o^o) and (30^o, 12^o) a difference in k_{mom} of 10 percent has been observed.

A comparison with moment coefficients for W-trusses with the same construction height shows that the values of k_{mom} are approximately equal.

In table 5.1 and 5.2 moment coefficients are given for two limit values of the heel joint slip. Several truss configurations have been analysed covering a relevant parameter space for the phenomena regarded.

For selected trusses the stresses have been calculated. It can be seen that these are in a range where ordinary lumber has sufficient strength.

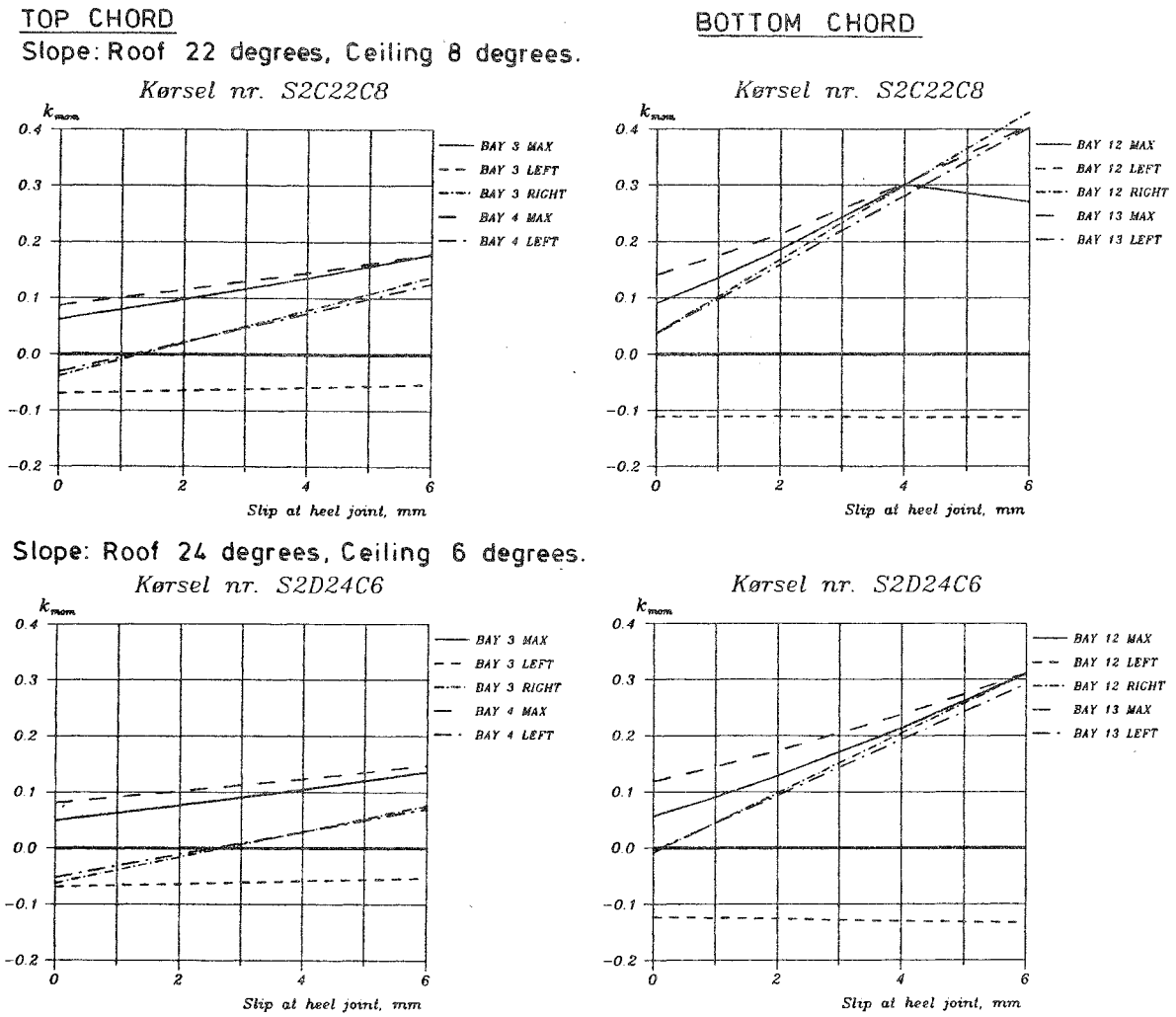


Figure 5.2 Moment coefficients for different roof and ceiling slopes and for different slips in the connections. Run "S2C22C8 is a reference truss, the other is similar except for the slopes.

It was found that the moment coefficients did depend on the stiffness of the chords. The stiffness is here expressed in EI/l_{bay}^2. The examples cover stiffnesses up to

25 kN mm²/mm² for the top chords, width = b = 50 mm

17 kN mm²/mm² for the bottom chords

From the tables 5.1 and 5.2 it can be seen that for the bottom chord the k_{mom} values are sensitive to the top chord load when the construction height is little. See run "S2F22CC". The effect is essential.

Table 5.1 Moment coefficients for the top chord of 2x2 bay scissor trusses. Centric connections. Values: 100 · k_{mom}. Stresses in MPa.

Roof/ Ceiling slope	Span	H_{top}	Bay 3				Max k_{mom}, typical					
			max		right		bay			node		
degree	m	mm	Slip at heel joint, mm: 1	4	1	4		1	4	*	1	4
S2C22C8 Reference												
22/8	8	125	7.9	13.5	-0.9	7.8	4	10.0	14.5	4L	-0.5	7.3
			σ_c =		2.9			2.0			2.0	
			σ_m = 2.9	5.0	-0.6	2.7		4.1	5.9		-0.6	2.7
S2C24C6												
24/6	8	125	6.3	10.5	-3.9	2.9	4	9.1	12.3	4L	-3.2	2.9
S2B22C8 Higher chords												
22/8	8	150	10.8	21.2	3.5	18.3	4	11.9	20.3	4L	3.4	16.4
S2F24CA												
24/6	8	150	8.3	16.0	-0.8	11.0	4	10.3	16.3	4L	-0.4	9.9
S2F22CC Very Heavy roof 3.0 kN/m												
22/8	8	125	6.5	8.8	-3.3	0.5	4	9.3	11.1	4L	-2.6	0.8
S2F24CB												
24/6	8	125	5.3	7.0	-5.7	-2.7	4	8.5	9.8	4L	-4.7	-2.1
S2F22CE Longer span												
22/8	9.6	150	8.2	12.6	-1.8	5.3	4	9.6	13.2	4L	-1.4	5.0

* L signifies the left end of the bay.

Table 5.2 Moment coefficients for the bottom chord of 2x2 bay scissor trusses. Centric connections. Values: 100 · k_{mom}. Stresses in MPa.

Roof/ Ceiling	Span	H_{top}	Bay 12				Max k_{mom}, typical					
slope			max		right		bay			node		
degree	m	mm	Slip at heel joint, mm: 1	4	1	4		1	4		1	4
S2C22C8 Reference												
22/8	8	100	13.5	30.1	10.2	30.0	13	17.5	30.3	13L	9.8	28.2
		σ_t =		3.4					3.4			3.4
		σ_m =	2.9	4.0	1.3	4.0		2.5	4.4		1.3	4.0
S2C24C6												
24/6	8	100	9.1	21.3	4.5	20.5	13	14.4	23.7	13L	4.4	19.3
S2B22C8 Higher chords												
22/8	8	125	24.4	-*	23.9	61.3	13	26.0	-*	13L	22.5	57.3
S2F24CA												
24/6	8	125	16.2	-*	14.6	45.2	13	20.1	42.6	13L	13.9	42.4
S2F22CC Very Heavy roof 3.0 kN/m												
22/8	8	100	25.6	-*	25.6	45.3	13	27.2	42.8	13L	24.2	42.6
S2F24CB												
24/6	8	100	15.6	-*	15.2	31.1	13	20.5	31.3	13L	14.5	29.4
S2F22CE Longer span												
22/8	9.6	125	14.8	29.5	10.7	29.0	13	17.8	29.8	13L	10.2	27.5

* No maximum in the bay

5.1.2. Scissor truss with 2 x 3 bays.

The comments to this truss configuration are the same as those for scissor trusses with 2 x 2 bays.

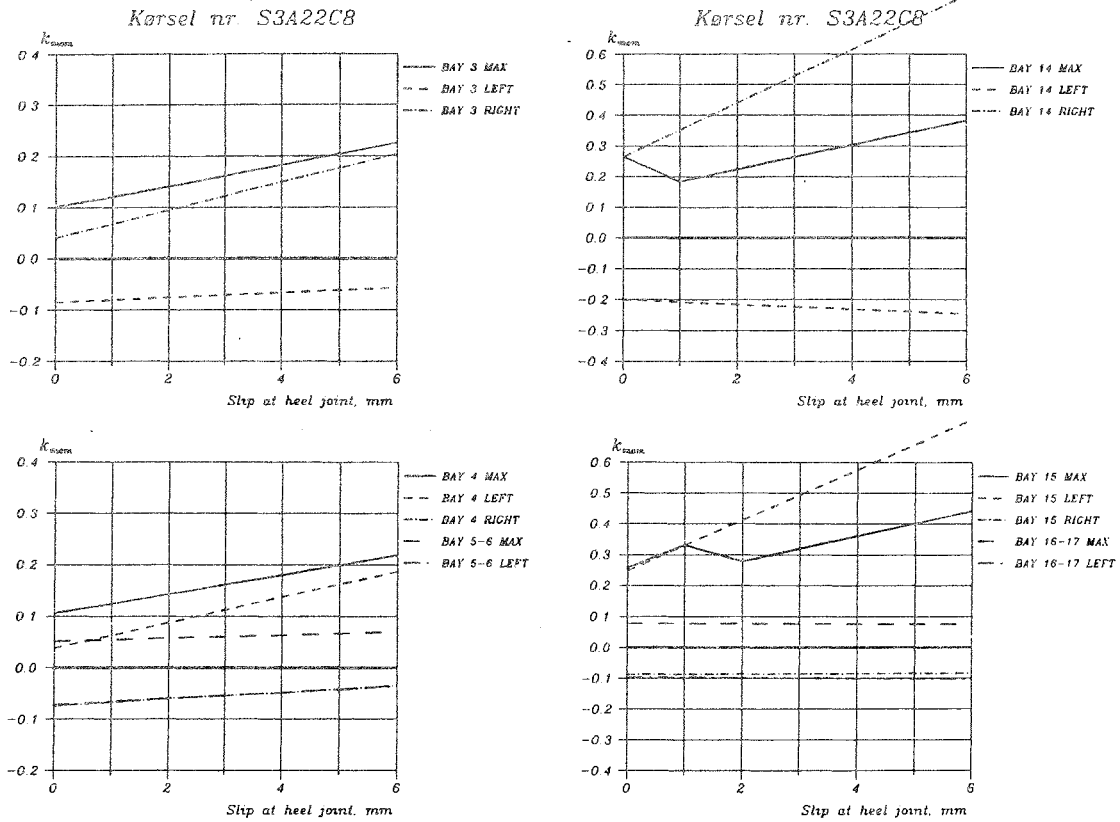
The range of the stiffness number EI/l^2_{bay} went up to the following values. But the moment coefficient method is apparently applicable with sense only for stiffness values as those for trusses with 2 x 2 bays.

40 kNmm²/mm² for the top chords, width = b = 50 mm

29 kNmm²/mm² for the bottom chords.

TOP CHORD BOTTOM CHORD

Slope: Roof 22 degrees, Ceiling 8 degrees.



Slope: Roof 24 degrees, Ceiling 6 degrees.

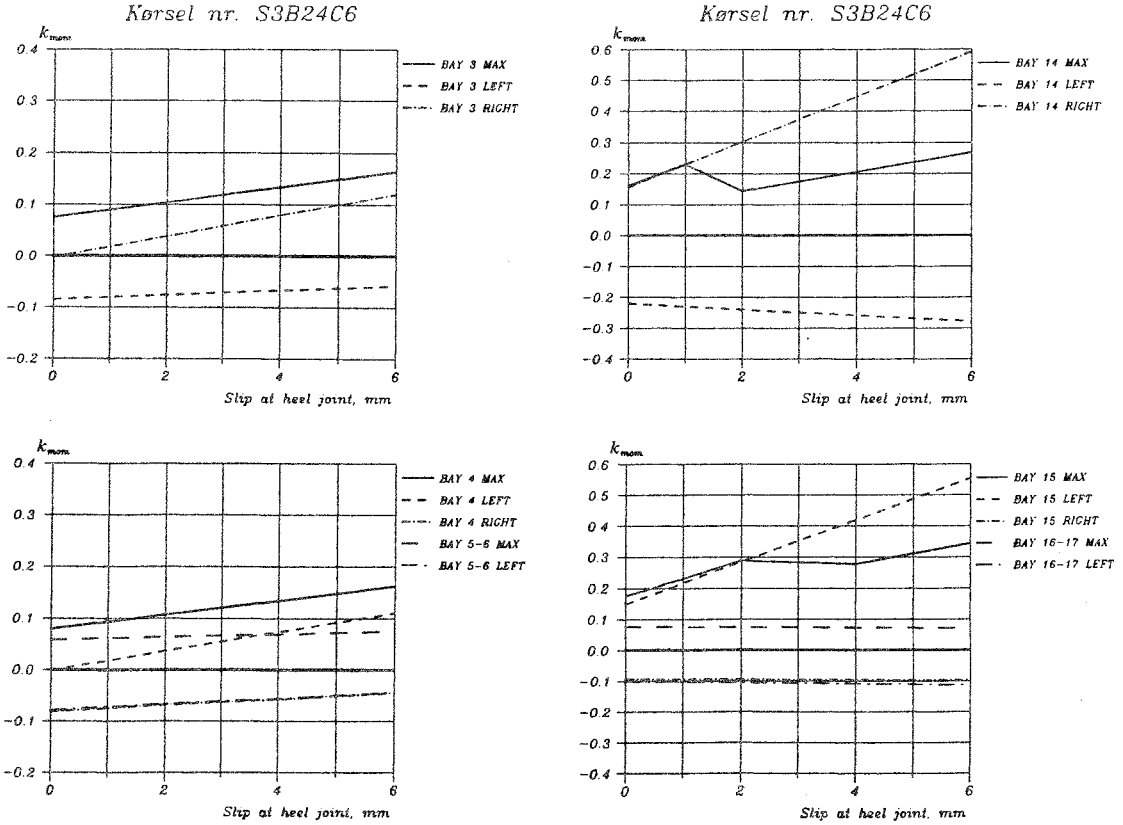


Figure 5.3 Moment coefficients for different roof and ceiling slopes and for different slips in the connections. Run "S3A22C8 is a reference truss, the other is similar except for the slopes.

Table 5.3 Moment coefficients for the top chord of 2x3 bay scissor trusses. Centric connections. Values: 100 · k_{mom}. Stresses in MPa.

Roof/ Ceiling slope	Span	H_{top}	Bay 3				Max k_{mom}, typical				
			max		right		bay		node		
degree	m	mm	Slip at heel joint, mm: 1	4	1	4		1	4	*	1	4
S3A22C8 Reference												
22/8	12	150	12.1	18.2	6.7	15.0	4	12.4	18.0	4R	-6.6	-5.0
			σ_c =		4.8			3.5			3.5	
			σ_m = 3.0	4.6	1.6	3.7		3.5	5.0		-2.1	1.6
S3B24C6												
24/6	12	150	8.9	13.3	1.7	7.9	4	9.3	13.4	4R	-7.5	-5.8
S3D22CH Higher chords												
22/8	12	175	15.7	25.8	11.5	24.1	4	15.7	24.7	4R	-5.3	-2.2
S3D24CH												
24/6	12	175	18.5	11.4	14.6	4.9	4	18.1	11.5	4R	-6.3	-3.6
S3D22C8 Very Heavy roof												
22/8	12	150	10.2	12.8	4.0	7.6	4	10.6	13.0	4R	-7.4	-6.6
S3D24C6												
24/6	12	150	7.7	9.6	-0.1	2.5	4	8.1	9.8	4R	-8.0	-7.3

* R signifies the right end of the bay.

Table 5.4 Moment coefficients for the bottom chord of 2x3 bay scissor trusses. Centric connections. Values: 100 · k_{mom}. Stresses in MPa.

Roof/ Ceiling slope	Span	H_{bot}	Bay 14				Max k_{mom}, typical					
			max		right		bay			node		
degree	m	mm	Slip at heel joint, mm: 1	4	1	4		1	4		1	4
S3A22C8 Reference												
22/8	12	125	-*	-*	35.2	61.6	15	33.2	-*	16L	-9.7	-10.0
		σ_t =			4.4				4.5			3.8
		σ_m =			3.0	5.4		3.1			-1.0	-1.0
S3B24C6												
24/6	12	125	23.0	-*	23.0	44.7	15	22.9	-*	16L	-10.3	-10.9
S3D22CH Higher chords												
22/8	12	150	-*	-*	54.5	98.1	15	-*	-*	16L	-8.7	-8.5
S3D24CH												
24/6	12	150	-*	-*	37.2	73.6	15	35.0	-*	16L	-9.8	-10.4
S3D22C8 Very Heavy roof												
22/8	12	125	-*	-*	71.2	97.6	15	-*	-*	16L	-9.7	-10.0
S3D24C6												
24/6	12	125	-*	-*	47.9	69.6	15	-*	-*	16L	-10.8	-11.4

* No maximum in the bay.

5.2. The support eccentricity at the heel joint

From plots similar to those in figure 4.4 it has been found that a substantial change in the moment coefficients takes place for support eccentricities D above the following values

Scissor truss 2 x 2 bays D = 150 mm

2 x 3 bays D = 120 mm

5.3. Diagonal-chord connections at the inner periphery

TOP CHORD

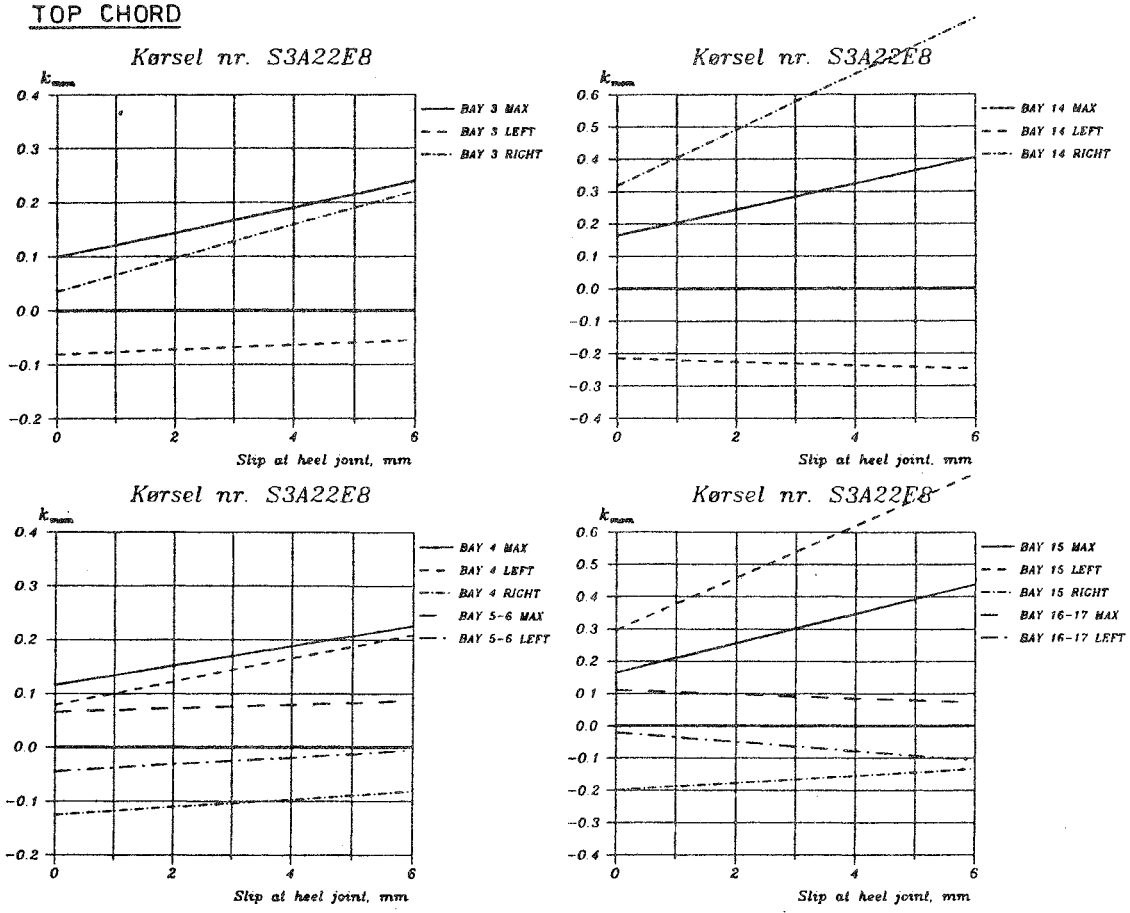


Figure 5.4 Moment coefficients for different slips in the connections. The example is a reference truss with 2 x 3 bays except for the eccentric connections.

Table 5.5 Moment coefficients for the top chord of scissor trusses. Eccentric connections. Values: 100 · k_{mom}.

Roof/ Ceiling slope	Span	H_{bot}	Bay 3 max		Bay 3 right		Max k_{mom}, typical bay			node		
degree	m	mm	Slip at heel joint, mm: 1	4	1	4		1	4		1	4
2 x 2 BAYS												
S2E22E8 Reference												
22/8	8.0	125	6.7	12.8	-3.5	6.4	4	12.1	16.6	4L	3.0	10.5
S2E24E6												
24/6	8.0	125	5.3	9.7	-6.2	1.3	4	10.4	13.6	4L	-0.6	5.2
2 x 3 BAYS												
S3A22E8 Reference												
22/8	8.0	150	12.1	19.0	6.6	15.9	4	13.4	18.8	4R	-11.8	-9.7
S3B24E6												
24/6	8.0	150	8.6	13.4	1.0	7.9	4	9.9	13.9	4R	-11.2	-9.3

Table 5.6 Moment coefficients for the bottom chord of scissor trusses. Eccentric connections. Values: $100 \cdot k_{mom}$.

Roof/ Ceiling slope	Span	H_{bot}	Bay 12 or 14				Max k_{mom}, typical					
			max		right		bay			node		
degree	m	mm	Slip at heel joint, mm: 1	4	1	4	1	4		1	4	
2 x 2 BAYS												
S2E22E8 Reference												
22/8	8.0	100	14.9	33.2	12.9	33.2	13	19.0	32.8	13L	12.2	31.2
S2E24E6												
24/6	8.0	100	9.6	22.9	6.2	22.5	13	15.3	25.0	13L	6.0	21.2
2 x 3 BAYS												
S3A22E8 Reference												
22/8	8.0	125	-*	-*	40.5	66.4	15	-*	-*	15R	-18.8	-15.5
S3B24E6												
24/6	8.0	125	-*	-*	27.1	48.8	15	25.4	-*	15R	-18.7	-17.2

* No maximum in the bay.

It has been investigated whether the equation (4.1) gives a reasonable estimate of the maximum moments at the nodes. With the same arguments as stated in subsection 4.3 it is found that the moment caused by the nodal moment $e \cdot F_{par}$ can be found from the node moment distribution factor k_F given in table 5.6. Or the moment distribution can be found from an analysis of a continuous beam loaded with nodal moments equal to $e \cdot F_{par}$, see figure 4.7.

Table 5.7 Suggested values of k_M

	Scissor truss with 2 x 2 bays	2 x 3 bays
Top chord	0.5	0.6
Bottom chord	0.5	0.6

5.4. A simple stress analysis for scissor trusses

5.4.1. Scissor trusses with a little support eccentricity

The internal forces can be calculated as described in subsection 4.4 provided that:

The suppport eccentricity D is less than
150 mm for a truss with 2 x 2 bays
120 mm - - - - 2 x 3 bays
2 • height of the bottom chord

Almost equal bay lengths in the top chord. The same requirement to the bottom chord.

The difference in the slope of the top chord and the bottom chord must be larger than 1:4.

The stiffness per crosssectional width $EI/(b\ l_{bay}^2)$ is less than

Top chord 0.5 kNmm²/mm³
Bottom chord 0.35 kNmm²/mm³

The constant distributed load on the bottom chord is larger than 0.1 times the top chord load.

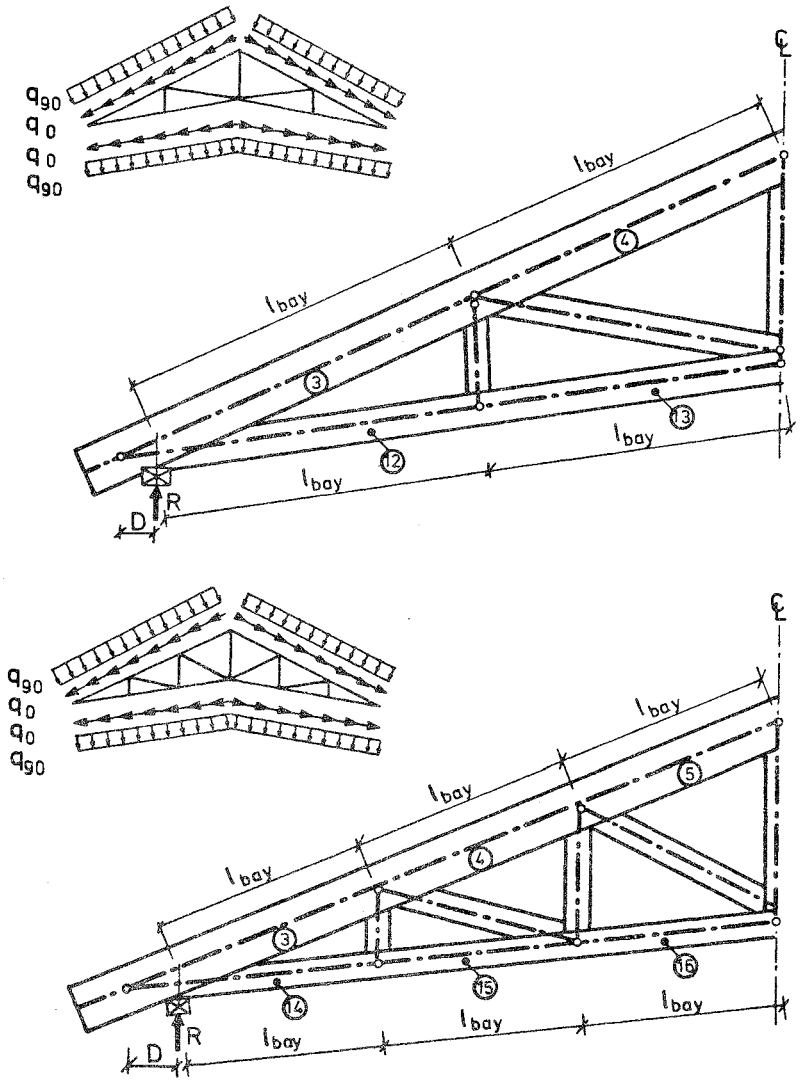
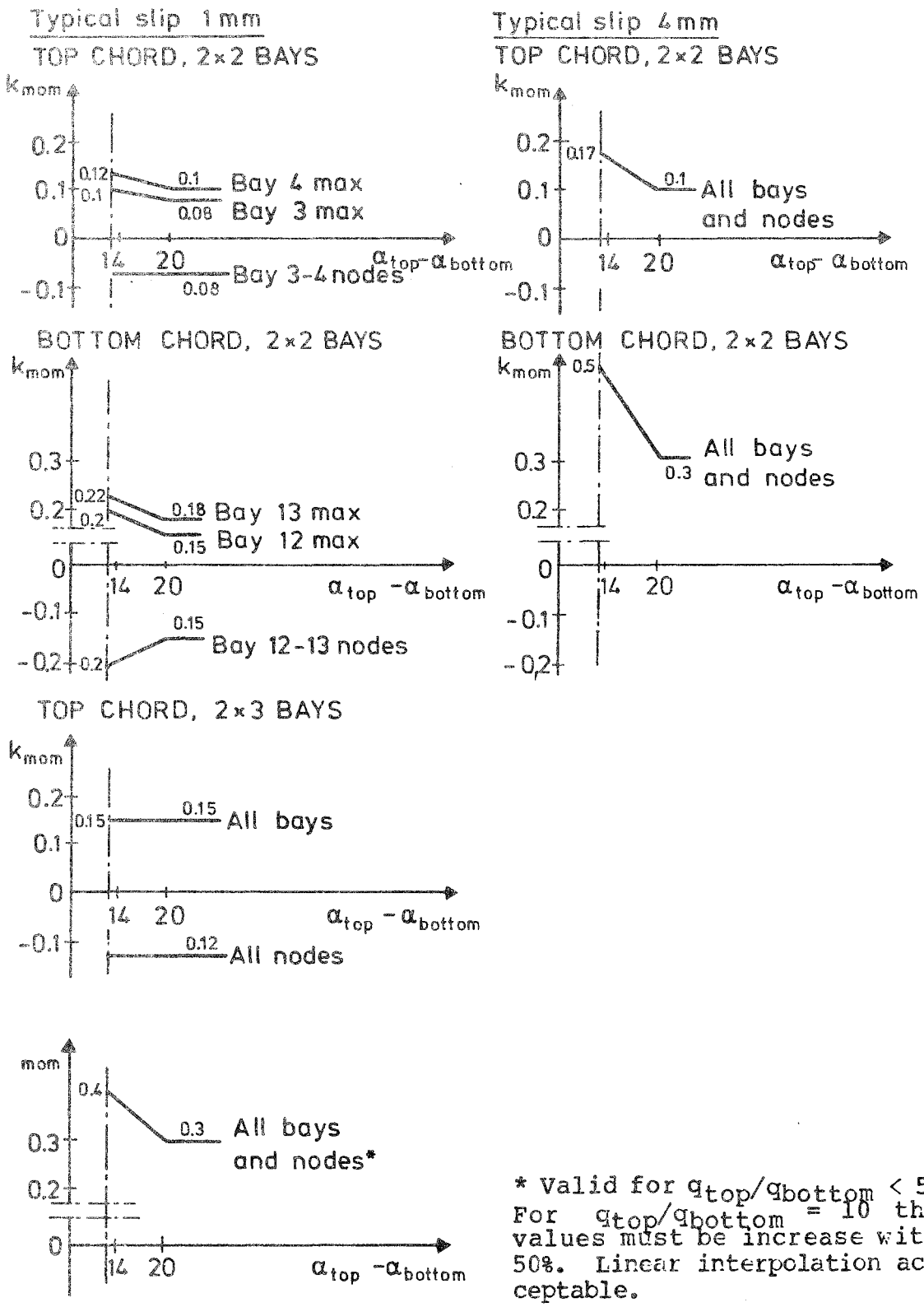


Figure 5.5 Geometry of and loads on scissor trusses.



* Valid for $q_{top}/q_{bottom} < 5$. For $q_{top}/q_{bottom} = 10$ the values must be increase with 50%. Linear interpolation acceptable.

Figure 5.6 Moment coefficients for a scissor truss with 2 x 2 and 2 x 3 bays with centric diagonal-chord connections or with these connections at the inner periphery of the chords.

Table 5.7 Values of the node moment distribution factor k_M for scissor trusses.

	Number of bays: 2 x 2	2 x 3
Top or bottom chord	0.5	0.6

6. KING POST TRUSS

King post trusses have been dealt with as the previous truss types. So the comments to the results are short.

Reference King post truss

I Slope of the roof: 1:3
II The five slip categories have all been analysed.
III Centric connections
IV Support eccentricity D = 70 mm
V H_{top} = 150 mm, H_{bottom} = 100 mm, Width = 50 mm E_{chord} = 8,400 MPa, E_{dia} = 7,200 MPa
VI Span S = 6.0 m
VII Heavy roof q_{top} = 1.61 N/mm, q_{bottom} = 0.3 N/mm
VIII No partial attic load

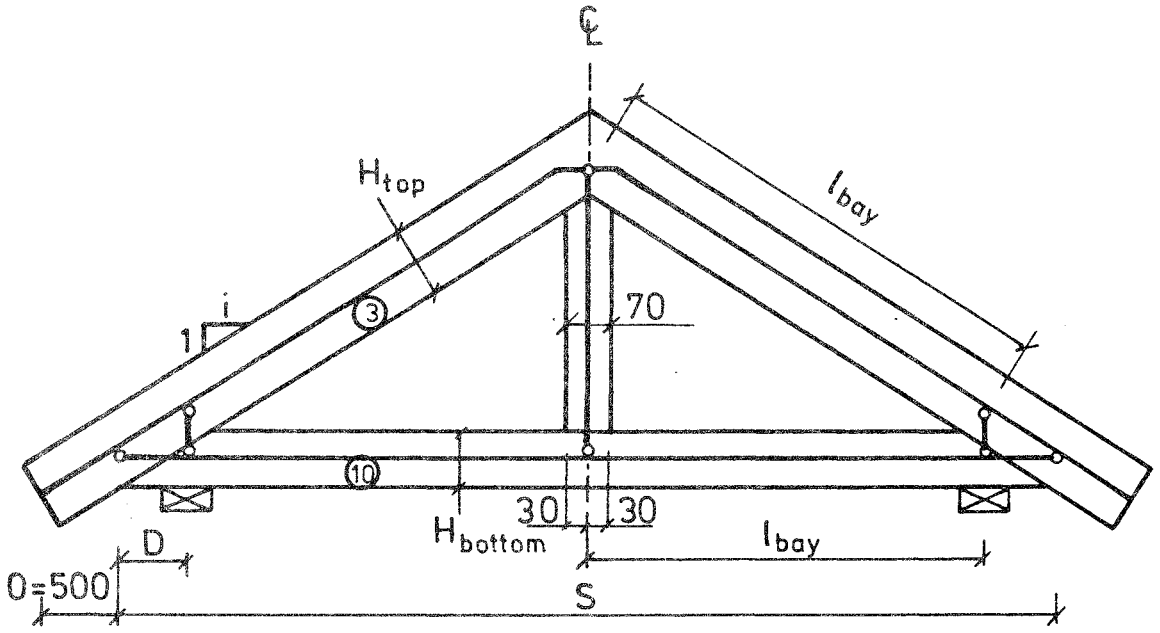


Figure 6.1 Frame model, geometry parameters, bay members and lengths. The pinned joint at the ridge is shifted downwards ($H_{top}/6$) in order to model that the compression force between the top chords is transfered in the lower part of the joint.

It is assumed that the bottom chord is continuous.

6.1. Calibration of moment coefficients

From figure 6.2 it can be seen that the moment coefficients for the top chord are relatively insensitive to the characterizing slip. This is also the case for the maximum moment in the bottom chord. The negative node moment in the bottom chord vanish (changes sign) for large slip values.

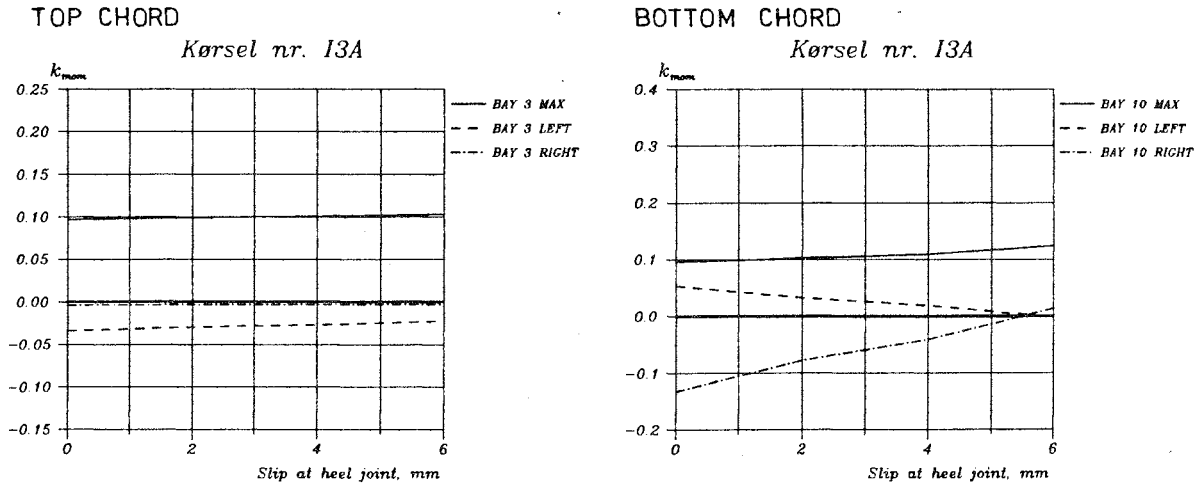


Figure 6.2 Moment coefficients for the reference truss.

From table 6.1 it can be seen that the values of k_{mom} for the top chord are in a reasonable and constant range for all examples. For the bottom this is not the case for run I3ASH, Short span, where the stiffness measure EI/l_{bay}^2 is special large. For the run I3AH this stiffness measure is

8,0 kNmm²/mm² for the bottom chord, width = b = 50 mm

Table 6.1 Moment coefficients for the top and bottom chords of King post trusses. Values: $100 \cdot k_{mom}$. Stresses in MPa.

Roof slope	Span	Cros.sec. heights		Top chord max		Bottom chord max		Bottom chord middle node	
		Top	Bot.	Slip at the heel joint, mm:					
	m	mm	mm	1	4	1	4	1	4
I2A									
1:2	6.0	150	100	10.0	10.2	9.8	10.1	-12.2	-7.6
I3A Reference									
1:3	6.0	150	100	9.8	10.1	9.9	10.9	-10.5	-4.1
			σ_c =		1.2		σ_t = 1.7		1.7
			σ_m =	7.2	7.4	3.0	3.4	- 3.5	-1.4
I4A									
1:4	6.0	150	100	9.6	9.9	10.1	12.0	- 8.3	0.0
I3AH Higher chords									
1:3	6.0	175	125	9.7	10.2	10.7	14.3	- 7.4	4.8
I3ALI Light roof, q_t = 1.31									
1:3	6.0	150	100	9.9	10.2	8.9	10.2	- 9.7	-3.2
I3AHE Very heavy roof, q_t = 3.00									
1:3	6.0	150	100	9.6	9.8	15.4	15.2	-14.5	-8.1
I3ALD Long span									
1:3	9.0	150	100	10.3	10.4	11.8	11.7	-15.6	-14.4
I3ASH Short span									
1:3	4.0	150	100	9.2	10.5	12.5	22.0	6.6	39.6

Only for a support eccentricity D > 500 mm, the heel joint moment becomes dimensioning for the top chord. For the bottom chord this is the case for D > 400 mm

6.2. A simple stress analysis for King post trusses

For King post trusses the internal forces can be calculated as described in subsection 4.4 provided that:

The support eccentricity D is less than 400 mm.
The slope of the roof must be larger than 1:4.
The stiffness of the bottom chord per cross sectional width $EI/(bl_{bay}^2)$ is less than 0.16 kNmm²/mm³.
The constant distributed load on the bottom chord is larger than 0.1 times the top chord load.

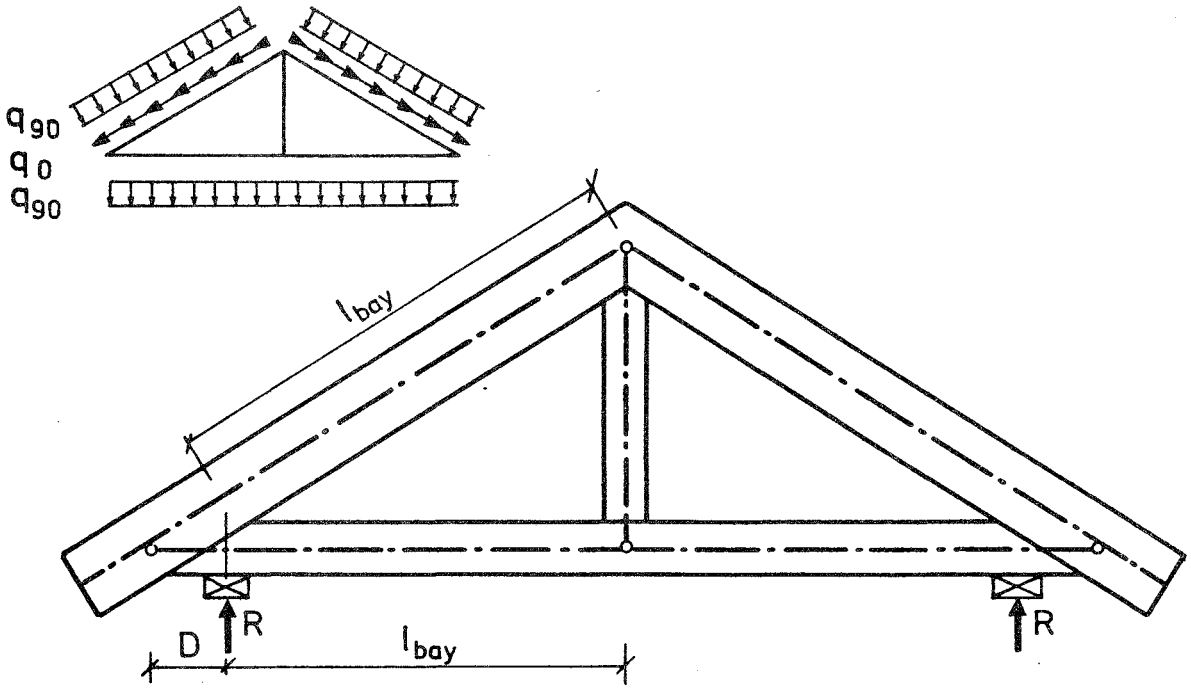
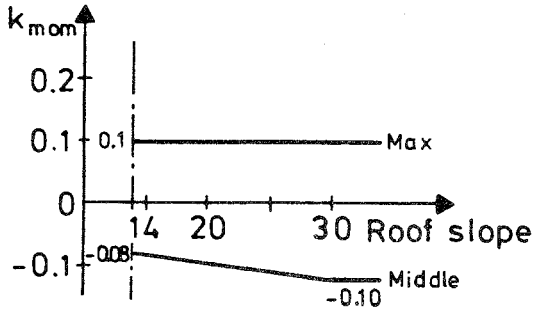


Figure 6.3 Geometry of and loads on a King post truss.

TOP CHORD: $k_{mom} = 0.10$

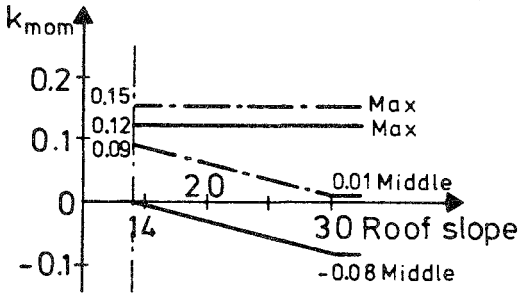
BOTTOM CHORD:

Typical slip 1 mm



All stiffness values

Typical slip 4 mm



Valid for $EI/(bl^2_{bay})$

—— 0.08 kNmm²/mm³
---- 0.16 kNmm²/mm³

Figure 6.4 Moment coefficients for a King post truss. For the bottom chord the moment coefficients are valid for $q_{top}/q_{bottom} < 5$. For $q_{top}/q_{bottom} = 10$ the values must be increased with 50%.

7. PULPIT TRUSSES

Pulpit trusses have been dealt with as the previous truss types. So the comments to the results are short.

Trusses with 3 or 4 bays in the top chord have been analysed. For the type with 3 bays there has been calculated with a slip in a splice in the bottom chord. For the type with 4 bays there has been calculated with a splice slip both in the top and bottom chord. The slip in the top chord has been put equal to the values in table 3.1 for the ridge connection.

Reference pulpit trusses

I Slope of the roof: 1:3
II The five slip categories have all been analysed.
III Centric connections.
IV Support eccentricity D = 70 mm.
V E_{chord} = 8,400 MPa, E_{dia} = 7,200 MPa, Width = 50 mm
3 Bays: H_{top} = 125 mm, H_{bot} = 125 mm
4 Bays: H_{top} = 150 mm, H_{bot} = 125 mm
VI 3 Bays: Span = S = 7.0 m
4 Bays: Span = S = 10.0 m
VII Heavy roof q_{top} = 1.61 N/mm, q_{bot} = 0.3 N/mm
VIII No partial attic load.

It is typical for the pulpit trusses that the moment coefficients are not so sensitive to the slip in the joints. This is caused partly by the large construction height, partly by the slender cross sections.

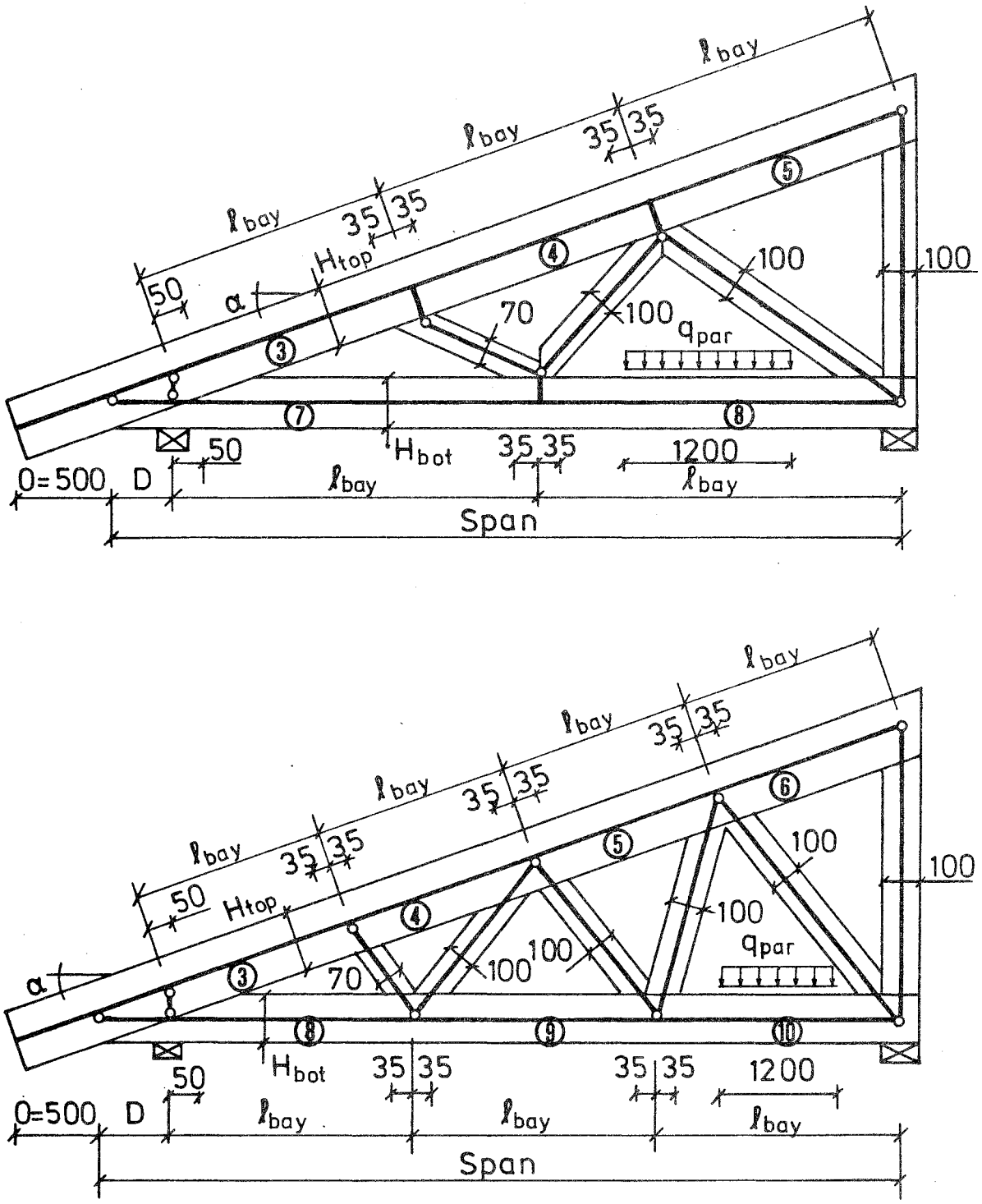
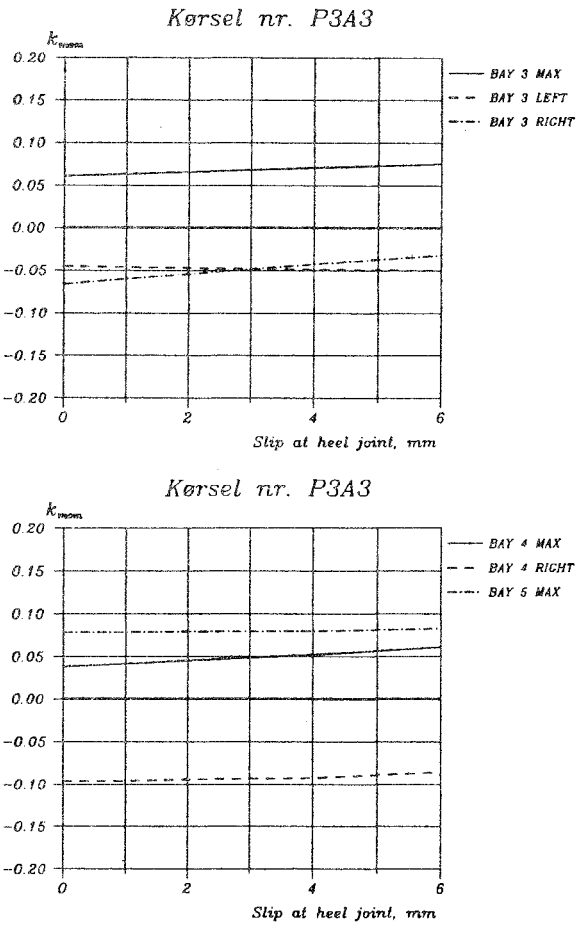


Figure 7.1 Frame model, geometry parameters, bay numbers and lengths. The 2 truss types are shown with diagonal-chord connections which are partly centric, partly eccentric i.e. akt the inner periphery of the chords.

7.1. Centric connections between diagonals and chords

7.1.1. Pulpit truss with 3 bays in the top chord

TOP CHORD



BOTTOM CHORD

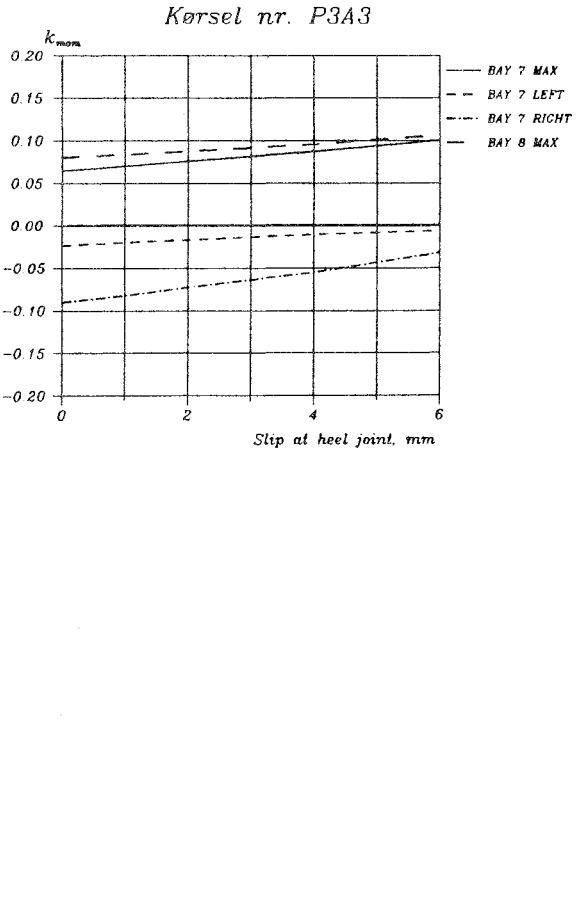


Figure 7.2 Moment coefficients for the reference truss.

Table 7.1 Moment coefficients for the top chord of 3 bay pulpit trusses. Centric connections. Values: 100 · k_{mom}. Stresses in MPa.

Roof slope	Span	H_{top}	Bay 3 max		right		Max k_{mom}, typical bay			node		
degree	m	mm	Slip at heel joint, mm: 1	4	1	4		1	4		1	4
P3A2												
26.6	7.0	125	6.1	6.5	-7.0	-6.0	5	7.8	7.9	4R	-9.7	-9.4
P3A3 Reference												
18.4	7.0	125	6.3	7.1	-6.0	-4.3	5	7.9	8.0	4R	-9.6	-9.2
			σ_c =		2.3				0			1.6
			σ_m = 4.1	4.6	-4.4	-3.2		5.2	5.3		-6.9	-6.7
P3A4												
14.0	7.0	125	6.7	7.8	-4.8	-2.4	5	7.9	8.0	4R	-9.5	-9.1
P3A3H2 Higher chords												
18.4	7.0	150	6.9	8.2	-5.0	-2.0	5	7.9	8.1	4R	-9.5	-8.9
P3A3GB Partial attic load												
18.4	7.0	125	6.0	6.7	-5.6	-3.9	5	7.8	8.0	4R	-9.7	-9.3
P3A3HE Very Heavy roof 3.0 kN/m												
18.4	7.0	125	5.9	6.3	-6.2	-5.3	5	7.8	7.9	4R	-9.7	-9.5

The stiffness measures EI/l^2 are in $kNmm^2/mm^2$ and for a cross section width of 50 mm.

Run	P3A3	P3A3HI (high chords)
Top chord	13	22
Bottom chord	5.6	9.6

Table 7.2 Moment coefficients for the bottom chord of 3 bay pulpit trusses. Centric connections. Values: 100 · k_{mom}. Stresses in MPa.

Roof slope	Span	H_{bot}	Bay 7 max		Bay 7 right		Max k_{mom}, typical bay			Max k_{mom}, typical node		
degree	m	mm	Slip at heel joint, mm: 1	4	1	4		1	4		1	4
P33A2												
26.6	7.0	125	6.1	7.1	-9.1	-7.1	8	8.0	8.8	8L	-9.5	-7.4
P3A3 Reference												
18.4	7.0	125	7.0	8.7	-8.2	-5.5	8	8.3	9.5	8L	-8.5	-5.7
			σ_t =		2.1			1.1			1.1	
			σ_m = 2.0	2.5	-2.5	-1.7		2.3	2.6		-2.5	-1.7
P3A4												
14.0	7.0	125	8.1	10.5	-7.0	-3.5	8	8.9	10.5	8L	-7.3	-3.7
P3A3HI Higher chords												
18.4	7.0	150	7.7	10.7	-6.6	-2.0	8	9.0	11.3	8L	-6.9	-2.0
P3A3GB Partial attic load												
18.4	7.0	125	5.2	6.8	-11.6	-8.9	8	6.9	8.2	8L	-11.2	-9.2
P3A3HE Very Heavy roof 3.0 kN/m												
18.4	7.0	125	8.1	9.9	-7.1	-4.4	8	8.8	10.1	8L	-7.4	-4.6

7.1.2. Pulpit truss with 4 bays in the top chord

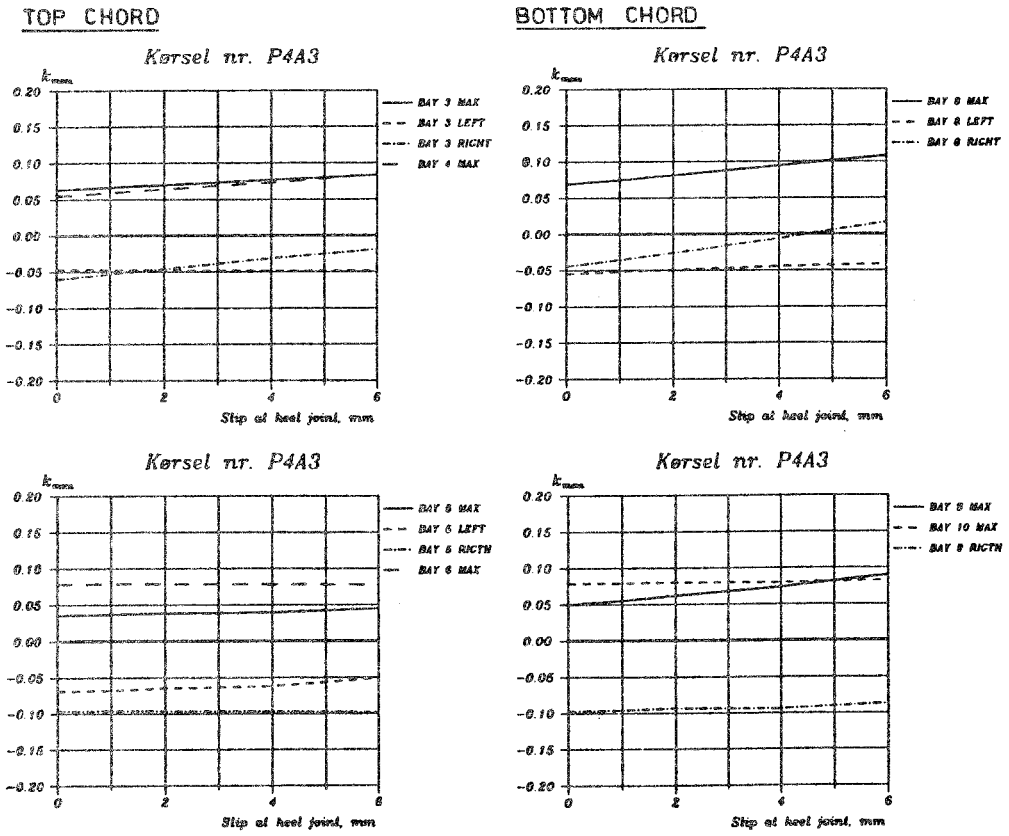


Figure 7.3 Moment coefficients for the reference truss.

Table 7.3 Moment coefficients for the top chord of 4 bay pulpit trusses. Centric connections. Values: 100 · k_{mom}. Stresses in MPa.

Roof slope	Span	H_{top}	Bay 3				Max k_{mom}, typical					
			max		right		bay			node		
degree	m	mm	Slip at heel joint, mm: 1	4	1	4		1	4		1	4
P4A2												
26.6	10	150	6.0	6.6	-7.1	-5.8	6	7.8	7.7	5R	-10.0	-10.0
P4A3 Reference												
18.4	10	150	6.6	7.7	-5.3	-3.2	6	7.9	7.8	5R	-9.7	-9.7
			σ_c =		2.9				0			1.3
			σ_m = 3.4	4.0	-3.1	-2.0		4.2	4.2		-5.5	-5.6
P4A4												
14.0	10	150	7.6	9.1	-3.2	-0.1	6/4	8.0	8.9	5R	-9.3	-9.4
P4A3HI Higher chords												
18.4	10	175	7.4	9.1	-4.0	-0.6	6/4	7.9	8.9	5R	-9.6	-9.7
P4A3GB Partial attic load												
18.4	10	150	6.7	7.8	-5.3	-3.2	6	7.9	7.8	5R	-9.6	-9.7
P4A3HE Very Heavy roof 3.0 kN/m												
18.4	10	150	6.2	6.7	-5.7	-4.5	6	7.9	7.8	5R	-9.7	-9.7

The stiffness measures EI/l^2_{bay} are in kNmm/mm² and for a cross section width of 50 mm

Run	P4A3	P4A3HI (high chords)
Top chord	19	30
Bottom chord	6.3	11

Table 7.4 Moment coefficients for the bottom chord of 4 bay pulpit trusses. Centric connections. Values: 100 · k_{mom}. Stresses in MPa.

Roof slope	Span	H_{bot}	Bay 8 max		Bay 8 right		Max k_{mom}, typical bay			Max k_{mom}, typical node		
degree	m	mm	Slip at heel joint, mm: 1	4	1	4		1	4		1	4
P4A2												
26.5	10	125	6.1	7.3	-5.0	-2.8	10	7.9	7.9	9R	-9.6	-9.5
P4A3 Reference												
18.4	10	125	7.5	9.4	-3.6	-0.6	10	7.9	8.0	9R	-9.6	-9.4
			σ_t =		3.4			1.2			2.3	
			σ_m = 1.9	2.4	-1.0	-0.3		2.0	2.0		-2.6	-2.5
P4A4												
14.0	10	125	9.2	11.8	-1.6	2.2	10/9	7.9	9.1	9R	-9.6	-9.3
P4A3HI Higher chords												
18.4	10	150	8.6	12.0	-1.3	3.9	10/9	8.0	10.3	9R	-9.4	-9.1
P4A3GB Partial attic load												
18.4	10	125	7.5	7.5	-2.6	-0.4	10	7.8	7.9	9R	-11.9	-11.8
P4A3HE Very Heavy roof 3.0 kN/m												
18.4	10	125	8.7	10.7	-1.1	1.9	10/9	7.9	8.9	9R	-9.6	-9.4

7.2. The support eccentricity at the heel joint

From plots similar to those in figure 7.2 and 7.3 it has been found that a substantial change in the moment coefficients takes place for support eccentricities D above the following values.

Pulpit truss	3 top chord bays	D = 200 mm
	4 top chord bays	D = 150 mm

7.3. Diagonal-chord connections at the inner periphery

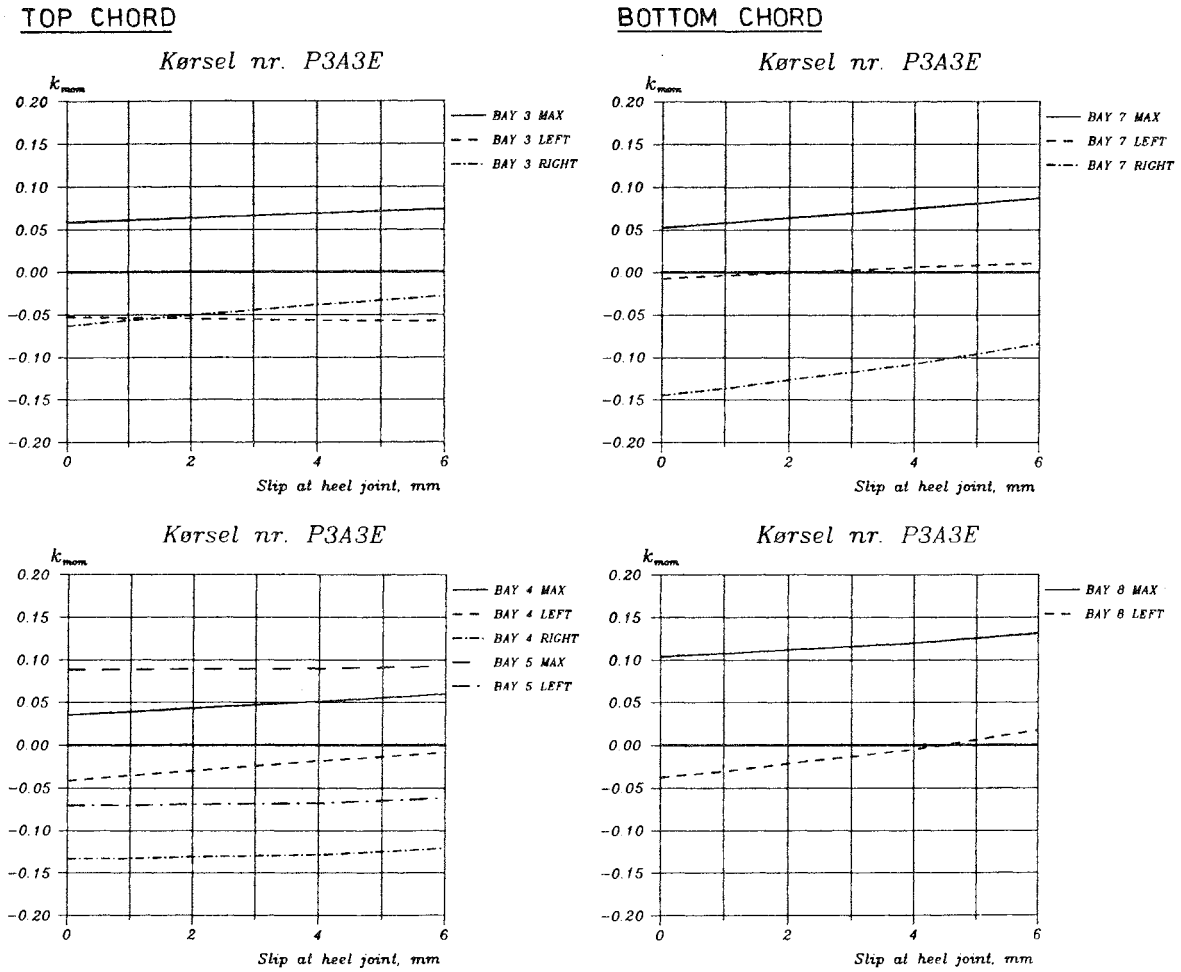


Figure 7.4 Moment coefficients for a pulpit truss with 3 top chord bays and similar to the reference truss except for the diagonal-chord connections at the inner periphery.

Table 7.5 Moment coefficients for the top chord of pulpit trusses. Eccentric connections. Values: 100 · k_{mom}. Stresses in MPa.

Roof slope	Span	H_{top}	Bay 3 max		Bay 3 right		Max k_{mom}, typical bay			Max k_{mom}, typical node		
degree	m	mm	Slip at heel joint, mm: 1	4	1	4		1	4		1	4
3 Top chord bays												
P4A2E												
14.0	7.0	125	6.0	6.4	-6.7	-5.6	5	8.5	8.6	4R	-11.8	-11.6
P3A3E Reference												
18.4	7.0	125	6.1	6.9	-5.7	-3.9	5	8.9	9.0	4R	-13.3	-12.9
P3A3HEE Very heavy roof 3.0 kN/m												
18.4	7.0	125	5.7	6.1	-6.0	-5.0	5	8.7	8.8	4R	-13.0	-12.8
4 Top chord bays												
P4A2E												
14.0	10	150	6.0	6.6	-6.8	-5.6	6	8.3	8.2	5R	-12.3	-12.3
P4A3E Reference												
18.4	10	150	6.4	7.5	-5.2	-3.0	6	8.8	8.8	5R	-13.6	-13.6
P4A3HEE Very heavy roof 3.0 kN/m												
18.4	10	150	5.9	6.5	-5.7		6	8.7	8.7	5R	-13.2	-13.2

Table 7.5 Moment coefficients for the bottom chord of pulpit trusses. Eccentric connections. Values: 100 · k_{mom}. Stresses in MPa.

Roof slope	Span	H_{bot}	Bay 7 or 8 max		Bay 7 or 8 right		Max k_{mom}, typical bay			Max k_{mom}, typical node		
degree	m	mm	Slip at heel joint, mm: 1	4	1	4		1	4		1	4
3 Top chord bays												
P3A2E												
14.0	7.0	125	5.2	6.2	-12.8	-10.8	8	9.5	10.4	8L	-5.8	-3.8
P3A3E Reference												
18.4	7.0	125	5.8	7.5	-13.6	-10.8	8	10.8	12.0	8L	-3.1	-0.5
P3A3HEE Very heavy roof 3.0 kN/m												
18.4	7.0	125	6.4	7.9	-16.5	-13.6	8	13.4	14.7	8L	2.2	4.7
4 Top chord bays												
P4A2E												
14.0	10	125	5.0	6.1	-8.3	-6.0	10	9.1	9.2	9R	-15.3	-15.1
P4A3E Reference												
18.4	10	125	6.0	7.9	-8.2	-5.0	10	9.8	9.9	9L	-18.0	-17.7
P4A3HEE Very heavy roof 3.0 kN/m												
18.4	10	125	6.0	7.9	-9.1	-6.0	9	13.9	16.3	9R	-24.2	-23.9

Equation (4.1) can give a reasonable estimate of the maximum moments at the nodes if the values suggested in table 7.6 are employed.

Table 7.6 Suggested values of the node moment distribution factor k_M

No. of top chord bays	Node between bay:	Top chord 3-4	4-5	5-6	Bottom chord 7-8	8-9	9-10
3		0	0.6		0.5		
4		0	0.4	0.6		0.4	0.7

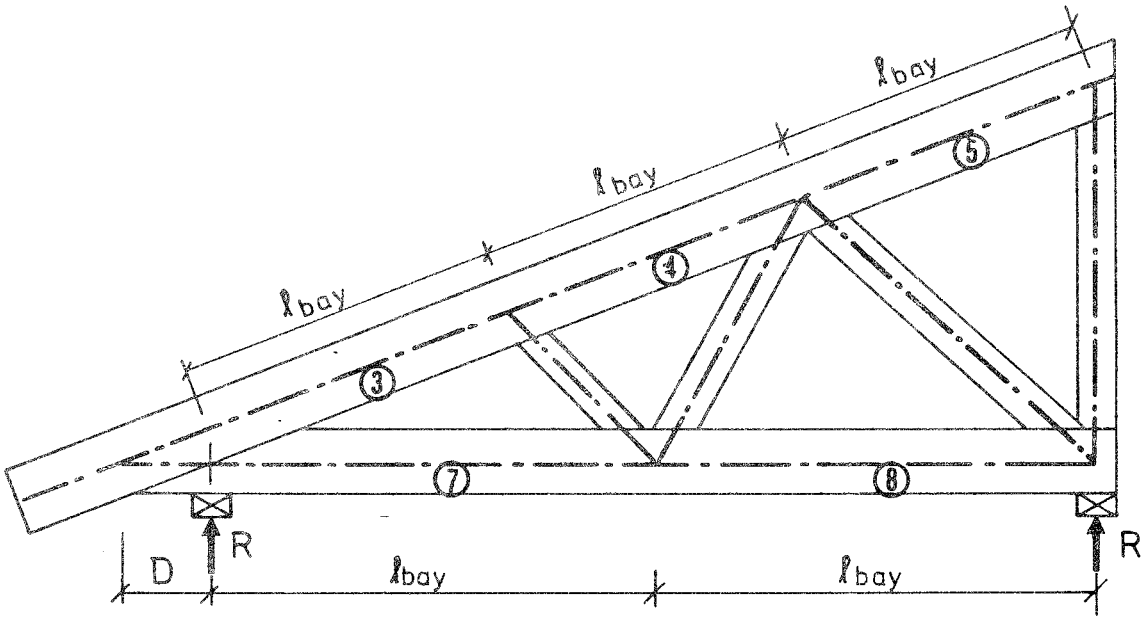
7.4. A simple stress analysis for pulpit trusses

The internal forces can be calculated as described in subsection 4.4 provided that:

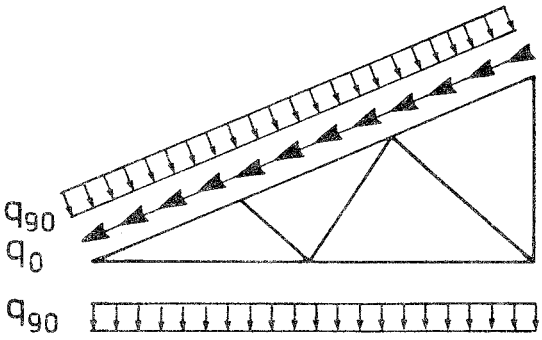
The suppport eccentricity D is less than
200 mm for a truss with 3 top chord bays
150 mm - - - - 4 - - -
2 · height of the bottom chord
Almost equal bay lengths in the top chord. The same requirement to the bottom chord.

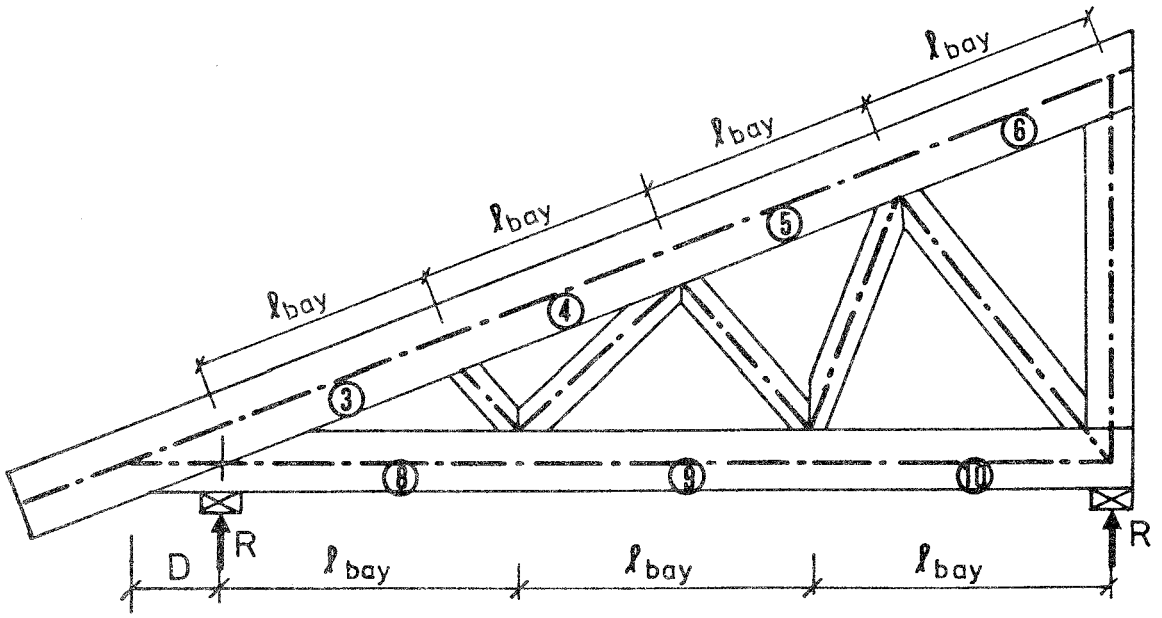
The stiffness per crosssectional width $EI/(b\ l_{bay}^2)$ is less than
Top chord 0.4 kNmm²/mm³
Bottom chord 0.15 kNmm²/mm³

The constant distributed load on the bottom chord is larger than 0.1 times the top chord load.



Centric connections





Eccentric connections at the inner periphery

Figure 7.5 Geometry of and loads on pulpit trusses.

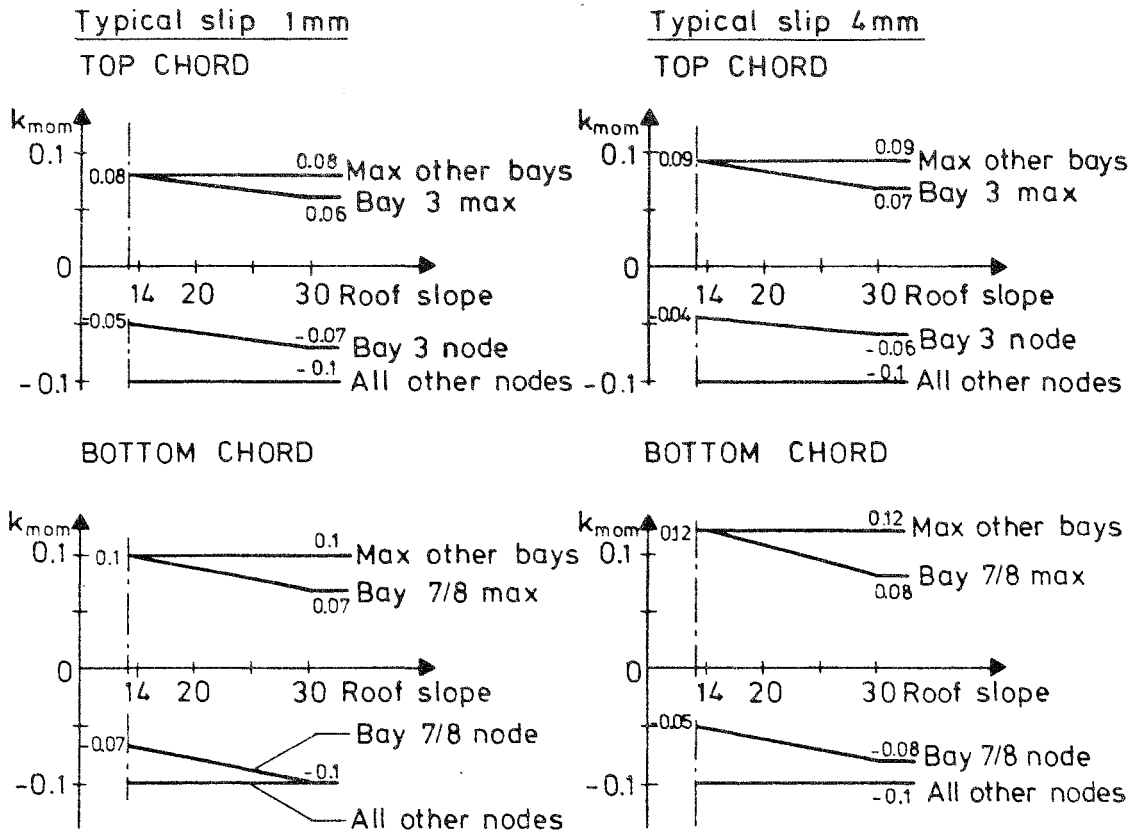


Figure 7.6 Moment coefficients for pulpit trusses with 3 or 4 bays in the top chord. Centric diagonal-chord connections. For the bottom chord 7/8 signifies the bays closest to the support at the low end.

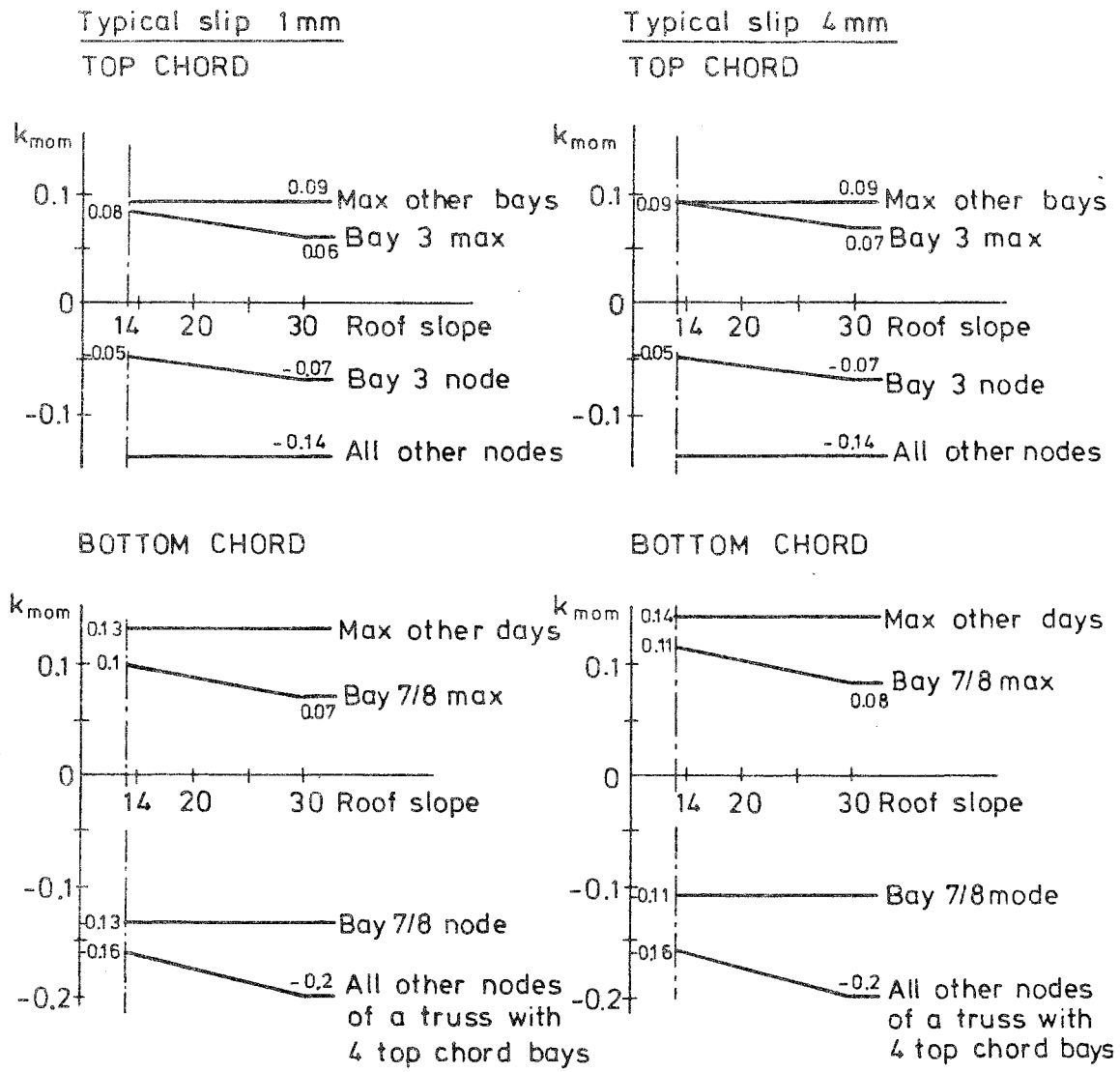


Figure 7.7 Moment coefficients for pulpit trusses with 3 or 4 bays in the top chord. Diagonal-chord connections at the inner periphery of the chords. For the bottom chord 7/8 signifies the bay closest to the support at the low end.

Table 7.6 contains the suggested values of the node moment distribution factor k_M .

Litterature

Riberholt, H. 1984. Simplified static analysis and dimensioning of trussed rafters. CIB 17-14-2. Rapperswil, Switzerland, May 1984.

CIB-W18/19-14-3

INTERNATIONAL COUNCIL FOR BUILDING RESEARCH STUDIES AND DOCUMENTATION

WORKING COMMISSION W18 - TIMBER STRUCTURES

JOINT ECCENTRICITY IN TRUSSED RAFTERS

by

T Poutanen
Tampere
Finland

MEETING NINETEEN
FLORENCE
ITALY
SEPTEMBER 1986

Joint eccentricity in trussed rafters

by

Tuomo Poutanen
M.Sc. (dipl.eng.), Director, Insinööritoimisto Tuomo Poutanen Ky, Omenapolku 3A,
SF-33270 TAMPERE
Specialist lecturer, Tampere Technical University

Abstract

Connection eccentricity may create large moments in trussed rafters with nail plate joints. This paper describes one model for eccentricity calculation, demonstrates it with simple examples and makes comparison with test results. Some topics concerning truss design are discussed.

Contents:

1. Introduction	2
2. Model	2
3. Eccentricity calculation	6
4. Example 1	7
5. Example 2	9
6. Comparison with test results	10
7. Discussion	12
8. Further developments	12
9. Conclusions	13
10. Aknowledgements	13
11. References	13

1. Introduction

The author has described the basic model in /1/. The model (computer program) is constantly under development. This paper describes the development level reached by August 1, 1986.

2. Model

The basic idea of the model is shortly described:

a. The model is based on 2-dimensional frame theory which is linear (with some exceptions).

b. A structural model is created assuming that forces have two alternative paths over the connection: nail plate and contact. Contact force is not necessarily perpendicular to contact surface, which means that friction is considered and its maximum size is limited by friction coefficient. Both paths can transfer moment. Nail plate can transfer moment via eccentrically located plate and/or spring behaviour of plate (i.e. moment is created when timber and plate rotate relative to each other). Contact can transfer moment by eccentricity and/or nonuniformally distributed contact stresses. If connection is under tension contact does not usually exist but may occur in some cases (especially in cases with large moment).

c. Buckling is taken into consideration using geometric nonlinear (physically linear) analysis.

d. It is assumed that force is transferred via nail plate in the following way (fig. 1): A force (with moment) comes to the connection through the center line of a timber beam. When the force reaches the connection boundary line it makes a curve to the center of the anchorage area of the plate and timber. This curve represents the eccentricity between timber center line and and center of anchorage area. In the center of the anchorage area force is transferred from timber to the plate via a spring which represents the slip between the plate and timber. Finally having reached the plate the force continues to the center of the nail plate. This last path represents the

eccentricity between the nail plate center and the center of the anchorage area. From this point the force is transferred to other timber parts in opposite path order.

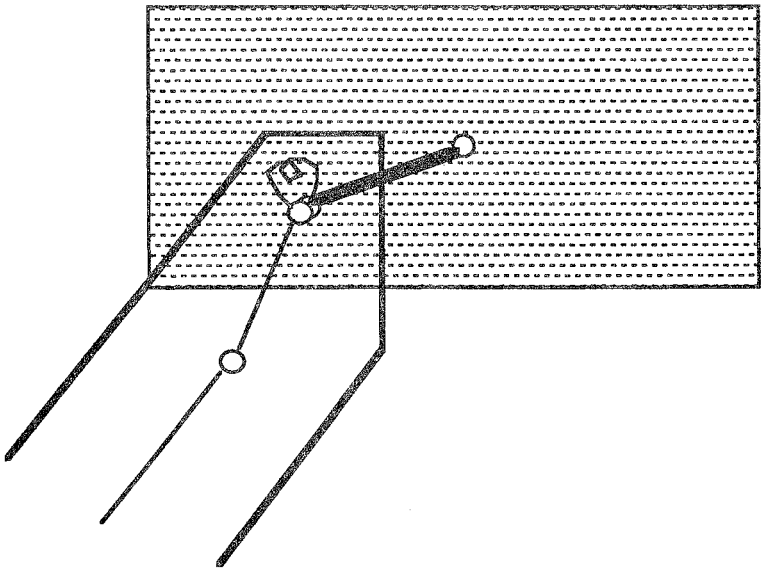


Fig. 1, Force path from timber to plate: timber center line - boundary line of the plate - center of anchorage area - spring - center of the plate. Circles represent nodes in the frame program. One plate may connect any number of timber parts, each of them having a similar force path. However, if timber does not end under the plate, nodes are created slightly differently but the basic principle is the same.

All this means that each connection of nail plate and timber has two eccentricities: eccentricity between timber center line and center of anchorage area and eccentricity between center of anchorage area and nail plate center. It is shown later that both eccentricities must be considered separately and it is not possible to handle them with one eccentricity (in general cases). It is also shown that the slip between timber and nail plate is essential in eccentricity calculation.

e. The contact force is calculated in the following way: Calculation uses an iterative process. Firstly analysis is made without contact. It is assumed that all connections have a small gap in unloaded state. Check is made whether timber parts get into each other, if so, a contact force is created, (fig. 2). It is assumed that the contact stress is linearly the larger the more timber beams get into each other. Contact stiffness is found partly by experimental tests, partly by theoretical calibration /3/. Friction force is created if timber surfaces move relative to each other.

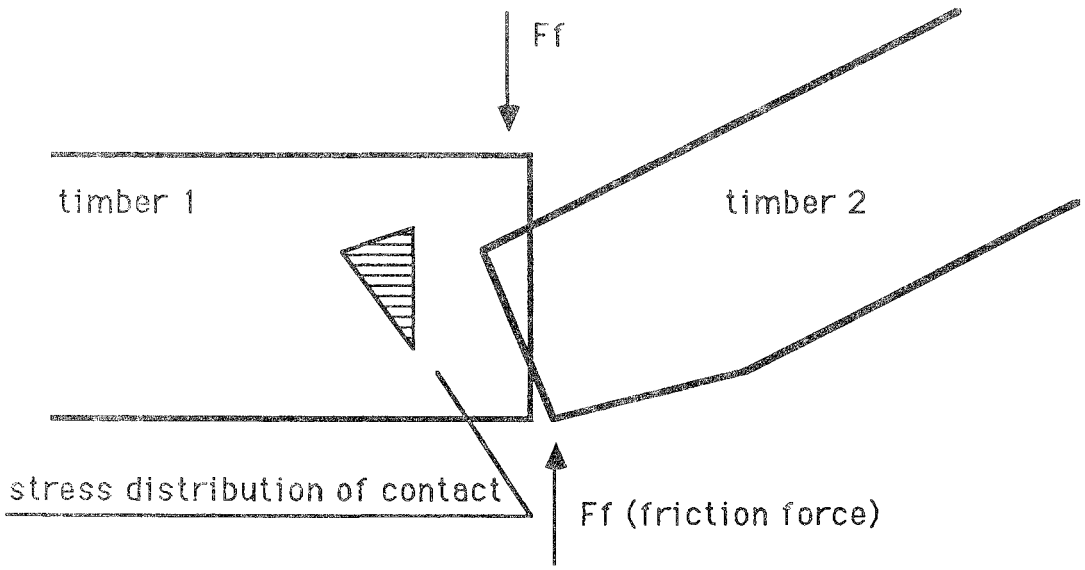


Fig. 2, Principle for contact calculation. Friction and contact eccentricity are considered.

This process converges slowly and needs appr. 6 iteration cycles. According to experience all heavy contacts are then balanced but some small contacts may still be unbalanced. Anyhow, they do not have much effect on stress distribution.
Moment distribution calculated with and without contact does not usually differ much (but may in some cases differ a lot).
However, there are several reasons why contact is considered:
- Contact occurs in real trusses. Nail plates cannot transfer all contact forces due to plate buckling. Present nail plates are 1-1.5 mm thick and they can carry only 20...40% of the compression forces which may exist in 38...48 mm thick timber. Contact improves truss economy because nail plates can be thinner and smaller in compressed connections.
- When contact is considered in the analysis a more correct moment distribution is achieved.
- Contact calculation is useful because it tends to smoothen stresses and reduce stress peaks.
- Plate design would otherwise be very approximative.
- Plate design is far simpler when contact is considered in the analysis. There are some joints with complicated force paths, which would not be possible to analyze otherwise. Fig. 3 shows an example of this.

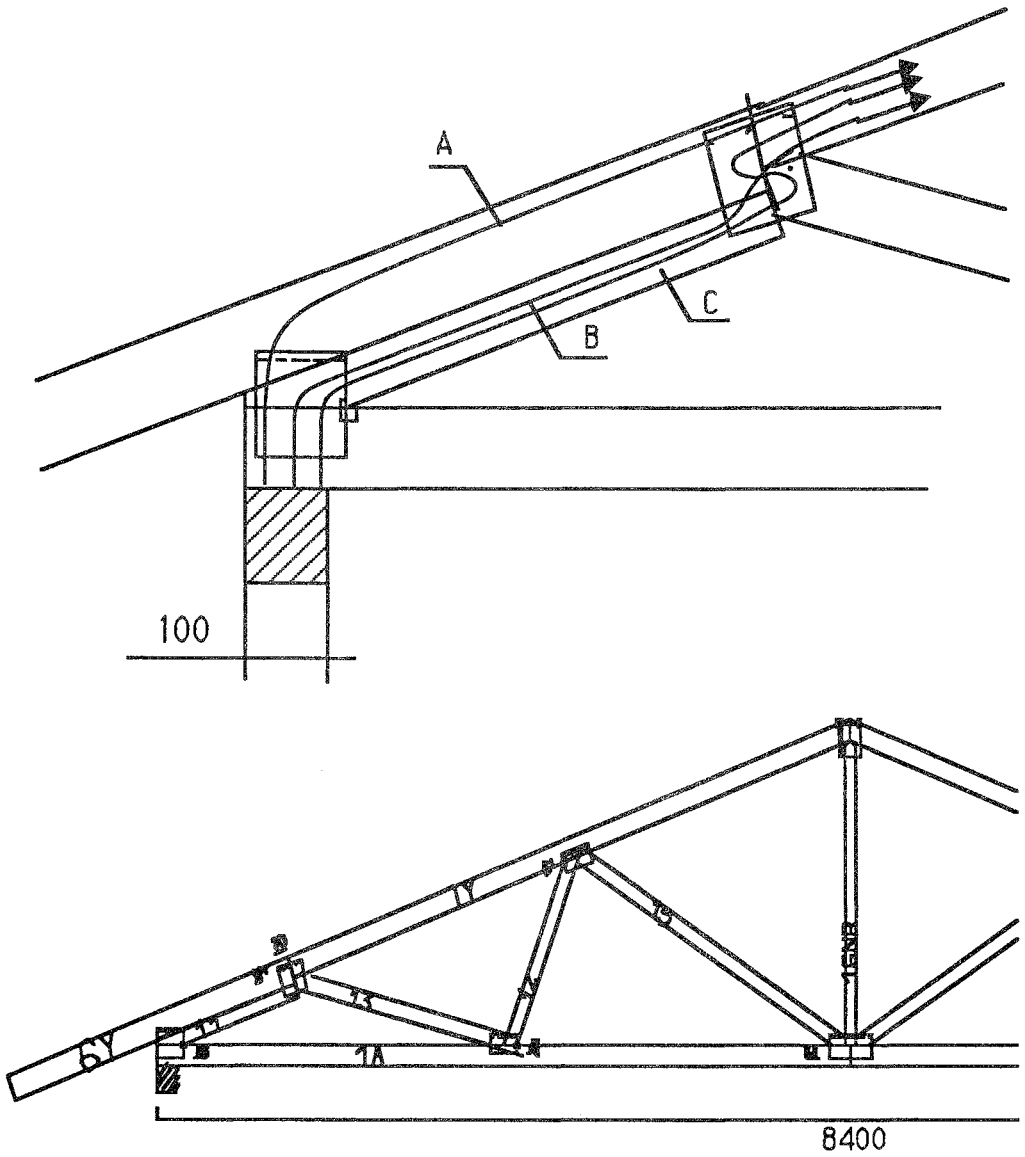


Fig.3 Example of a truss which has complicated force paths

When we study the truss we find that there are 3 force paths A,B,C from support to chord 7Y shown in the figure:
A: Support - chord 6Y - chord 7Y
B: Support - wedge 11 - chord 7Y
C: Support - wedge 11 - diagonal 13 - chord 6Y - chord 7Y
The model defines the force size in each path and calculates the side effects (contact, eccentricity) in each path. Path C is especially interesting. This can be seen in fig. 4 showing the iteration process. Arrows represent forces acting from timber to plate and contact force between timber parts in each iteration cycle.

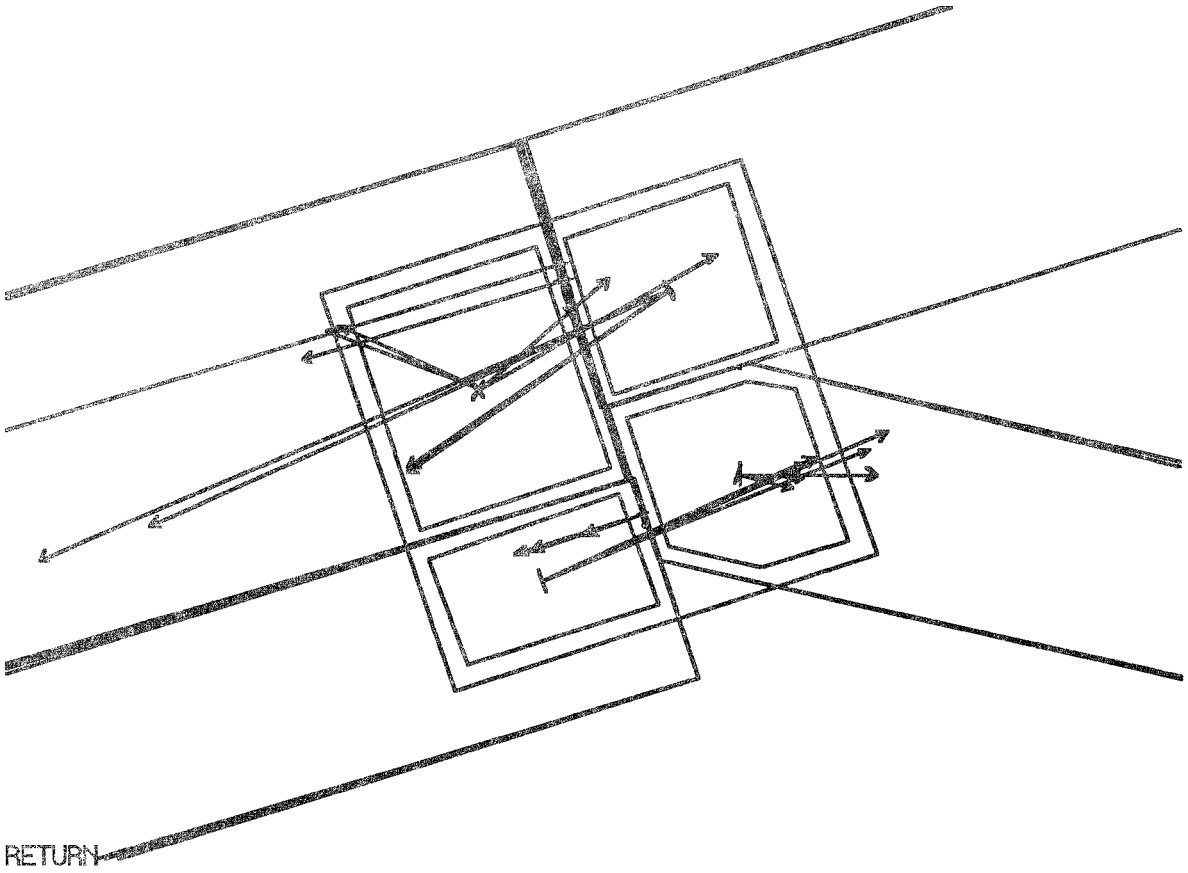


Fig. 4, Example of contact iteration showing forces acting from timber to plate and timber to timber on each itration cycle

3. Eccentricity calculation

Joint eccentricity has usually been calculated in 2 alternative ways /2/:

a. It is assumed that forces are transferred through center lines of timber parts.

b. It is assumed that forces are transferred to chords through hinges located in chord edges.

In both cases it is assumed that plate location and stiffness have no effect on eccentricity. It is also assumed that eccentricity moments are distributed to chord beams only.
Both methods are approximative and they give correct results only in special cases. This is shown by 2 examples and 1 comparison to full scale tests.

It must be emphasized that eccentricity can create large stresses. This can be demonstrated by the following example: Assume we have timber cross section b*h which is loaded by tension force 1*b*h. Assume the force has eccentricity e=0, h/6, h/3, h/2 (cases A, B, C and D). Then the cross section edges have stresses shown in fig. 5.

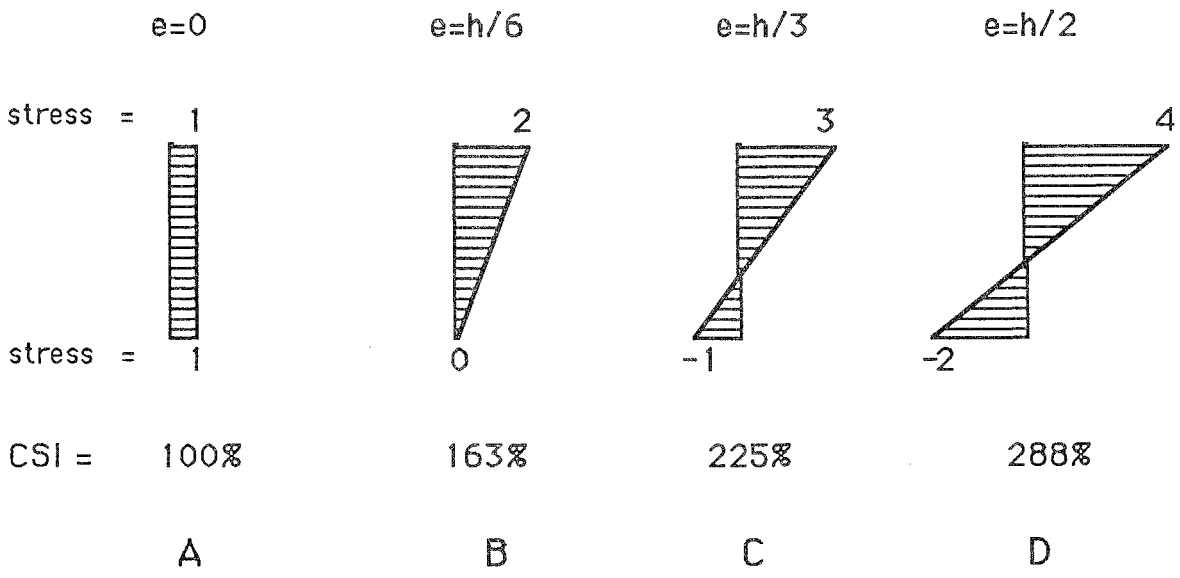


Fig. 5, Stresses of a cross section with the same tension force and different eccentricity e.

Some designers think that eccentricity is not an important factor in timber structures. Some even follow the principle that eccentricity need not be considered if it is less than half a chord in depth. This means e.g. that cases A and D of fig. 5 are considered equal. The figure shows the csi (compound stress index) based on assumption $f_b=1.6*f_t$. We see that the principle may create an error larger than safety factor.

In common trusses eccentricity is often h/6...h/3. We can see from the figure that eccentricity moment may be of the same magnitude as the moment created by other factors.

One may think that eccentricity is a bad thing always increasing stresses. In fact, appr. in half of the cases eccentricity increases stresses and in half it decreases them. When eccentricity is properly mastered it can be used as a design tool to achieve economical structures. This is done by designing eccentric joints creating a balanced stress distribution.

4. Example 1

Assume we have 3 beams 1,2 and 3 (fig. 6,7,8) which are made of 3 timber parts A,B and C. These parts are connected to each other with 2 splices 1 and 2:

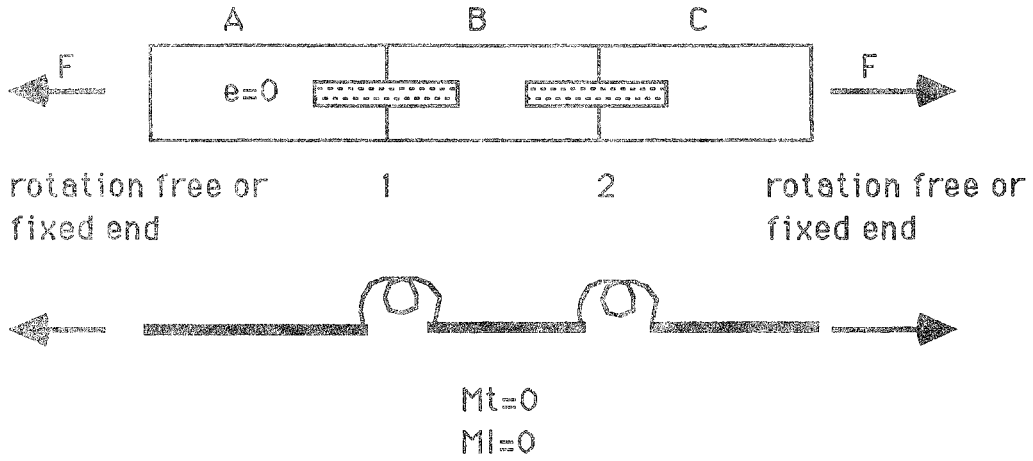


Fig. 6 Beam 1 has centric splices and ends are fixed or free to rotate, there is no eccentricity

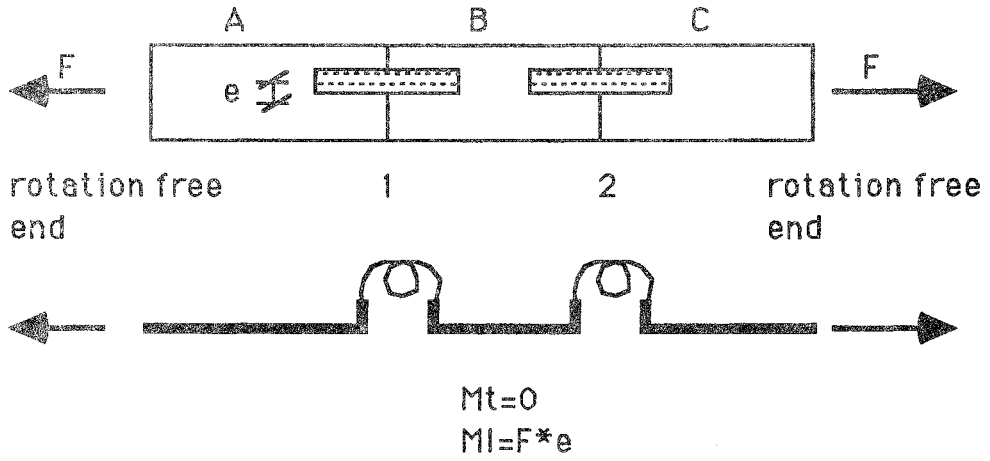


Fig.7 Beam 2 has eccentric splices and ends are free to rotate, timber eccentricity is 0, plate eccentricity is F*e

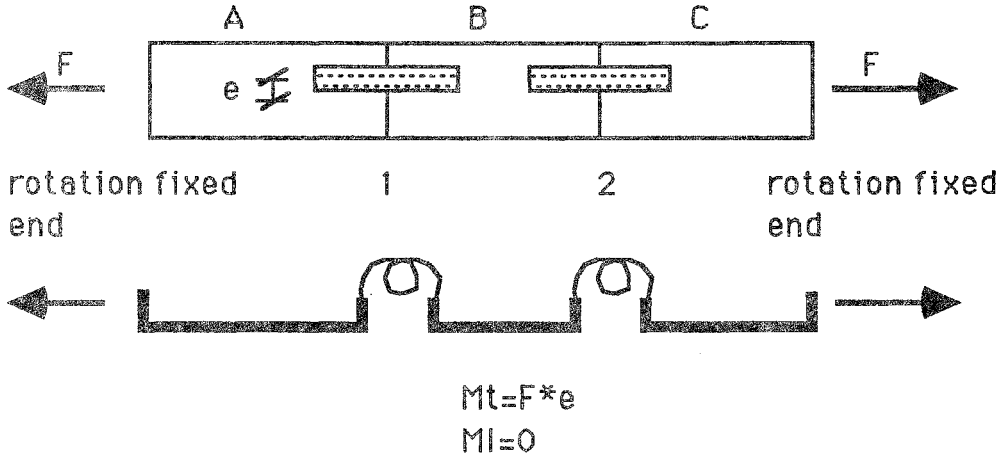


Fig. 8 Beam 3 has eccentric splices and ends are rotation fixed, timber eccentricity is F*e, plate eccentricity is 0.

To make thinking easier we assume that plate and timber stiffness is ∞, (numerical analysis made with real geometry and stiffness values gives appr. the same results).When we apply center line eccentricity calculation to these cases we find that they are all equal. According to the principle there is no eccentricity in any beam, because the force is located on the center line of the timber beam.
However, when we study these beams, we find that beam 1 obviously has no plate and no timber moment and it has 0 eccentricity. In beam 2 all timber parts have 0 moment but both splice plates must carry moment M=F*e which can be seen from the structural model. In this case timber eccentricity is 0 but plate eccentricity is e.
In beam 3 all timber parts have moment M=F*e and both splice plates have 0 moment. This is obvious

because the ends are rotation fixed which creates support moments M=F*e. This is equal to moment free load at distance e as shown in the structural model.
We find that beams 2 and 3 have an eccentricity moment which exists either in plate or in timber depending upon the end stiffness of the beam.
Now, we may assume that beam parts A and C represent chords of a truss and beam part B represents a diagonal or vertical. Analogy is complete and we find that eccentricity cannot be calculated without considering end stiffnesses.

5. Example 2

Eccentricity can be studied by a truss shown in fig. 9. The truss is loaded by a force of 10 kN and supported at joint centers at either end. All timber members have cross section — 50*100. When we study the bottom chord 1A we find that the possible moment is with large accuracy caused by joint eccentricity.

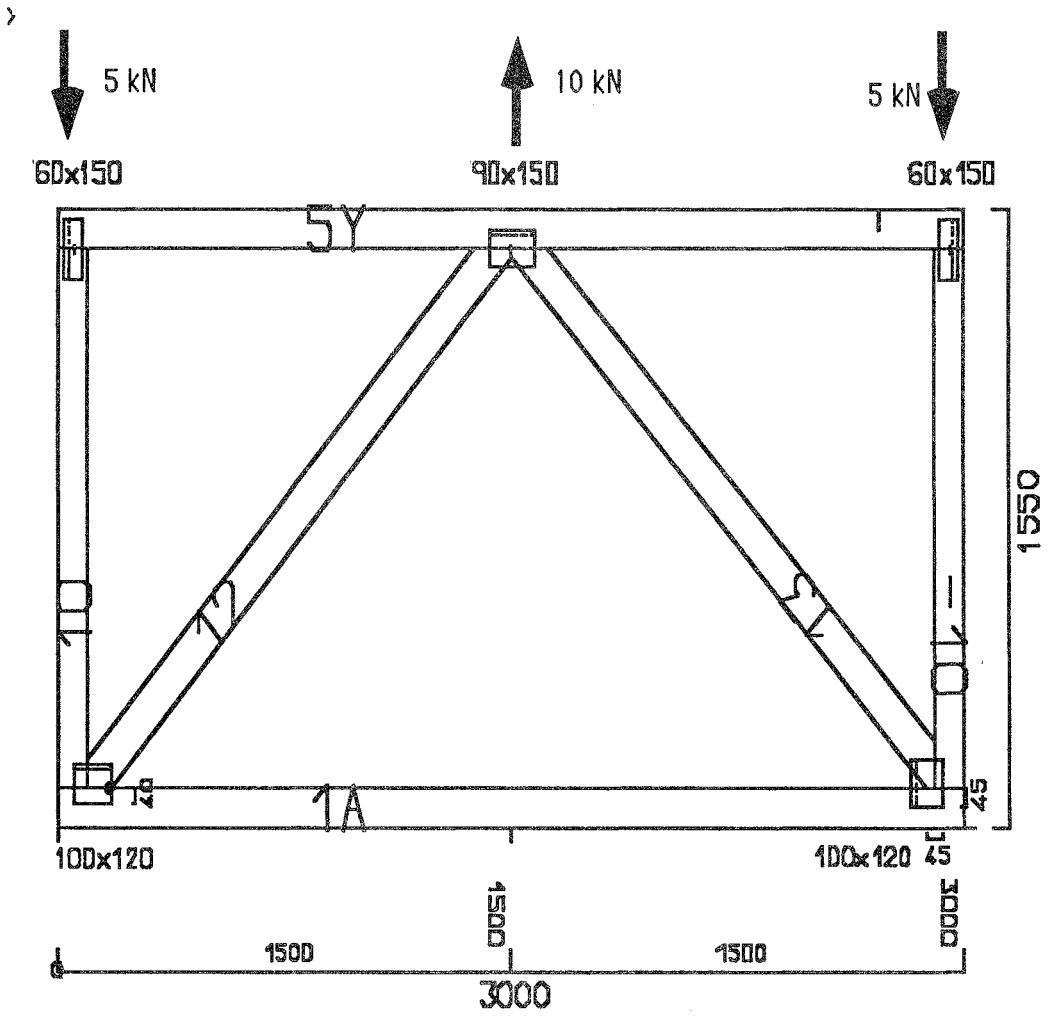


Fig.9. A truss for eccentricity demonstration

We do the following calculations with the model:

A. We study first a truss which is symmetrical with the left part of fig. 9 having all joints centric according to the center line principle. We assume that there is no contact between the timber parts. We define nail plate size and location appr. according to present usual design methods. We find that chord 1A has an eccentricity of 23 mm. We also notice that small changes of plate size or location create essential changes in eccentricity. These can be even 50 mm =h/2 (though then the connection does not fulfill the strength requirement).

We find that changing plate size or location can change eccentricity 0...h/2.

B. If we select a large plate e.g. 200*200 mm^2 and locate it so that the plate has a large anchorage area in each timber part, we find that eccentricity disappears, e=3 mm and we do not find any essential eccentricity if plate size or location is slightly changed. We can notice the same effect if we use the original small plate and a large stiffness value of the plate.

C. If we assume that contact may occur between timber parts and use the original plate size 100*120 mm^2, eccentricity disappears, e=2 mm. This is partly a coincidence because change in plate size or location changes the eccentricity but far less than in case A. Effect B can be noticed if a large plate or stiffness is used.

D. Assume that diagonal 12 is cut creating eccentricity 50 mm=h/2, shown on the right side in fig. 9. If we assume no contact, eccentricity is 44 mm and it varies largely if the plate is changed.

E. If we assume the same as in D but contact may occur, eccentricity is 12 mm.

F. If we assume the same as in E but plate size or plate stiffness is large eccentricity is 16 mm.

If the center line principle were correct, cases A,B and C should show no eccentricity and cases D,E and F should show eccentricity h/2=50 mm.
The calculation shows completely different results and we can draw the following conclutions.
A nail plate connection has 2 ultimate behaviour types:
Type 1: The nail plate is small and there is no contact. Eccentricity has to be calculated considering separately timber and plate eccentricity. Eccentricity moment must be divided considering plate and timber stiffness. Plate size and location has an essential effect on eccentricity.
Type 2: The nail plate is large. Eccentricity can be calculated assuming that the connection is completely stiff. Fictitious eccentricity elements are created with the center line principle. Eccentricity moment is distributed to all connecting timber parts (not only chords but also diagonals and verticals) proportional to their stiffness. The plate size or location has no effect on eccentricity assuming the plate has a large anchorage area in every connecting timber part.
If the nail plate has large stiffness it has the same effect as a larger plate with a lower stiffness and the connection tends to behave closer to type 2.
If contact occurs between timber parts, the connection tends to behave far closer to type 2. Contact creates eccentricity which has to be considered separately.

6. Comparison with test results

Fig. 10 shows a truss which has been tested in full scale with top chord uniform load. Moment has been measured in 12 cross sections and moment distribution has been analyzed with the model. Fig. 10 shows also the moment distribution, circles represent moment measurements, circle size has been defined according to maximum cumulative measurement error, so the true moment value should lie inside the circle.

We study the joint between support diagonal and top chord (joint connecting diagonals 18 and 16 and chord 6Y). We study the first top chord bay after support diagonal (bay B). It is obvious that this is the most interesting top chord bay because this bay has full compression force and the joint eccentricity is large. We apply the two methods for eccentricity calculation:
Method 1: eccentricity is calculated according to the center line principle.
Method 2: eccentricity is calculated assuming it equal to half chord depth.
Assume we have a load level which creates support reaction 9.9 kN. Then resultant force from diagonals 18 and 16 parallel to top chord is F=19 kN.
Eccentricity calculated according to method 1 is e=120 mm. The appr. dimensioning moment in bay B is 1100 Nm (=F*e/2). The model and test shows that the dimensioning moment is only 170 Nm. Method 1 leads to a moment which is more than 6 times too big.
If method 2 is applied the dimensioning force is appr. 500 Nm and appr. 3 times too big.
Both methods are more than safe where bay B is concerned. However, when we study diagonal 18, both methods give the diagonal 0 moment. The model and test shows that the diagonal has a moment of appr. 1200 Nm. 25 % of the diagonal strength is spent on compression force (16 kN). Eccentricity moment needs 70 % of timber

strength capacity if we assume no size effect. We find that both methods 1 and 2 underestimate the csi of diagonal 18 appr. 3 times. If size effect is considered methods 1 and 2 underestimate the csi of diagonal 18 more than twice.
When we look at the moment distribution in fig. 10 we find that eccentricity is shared mainly by diagonal 18 and chord bay A. When small changes of plate size or location are made we find no practical change in moment distribution. This means that the plate (120*300 mm^2) is large enough to give stiff connection behaviour.

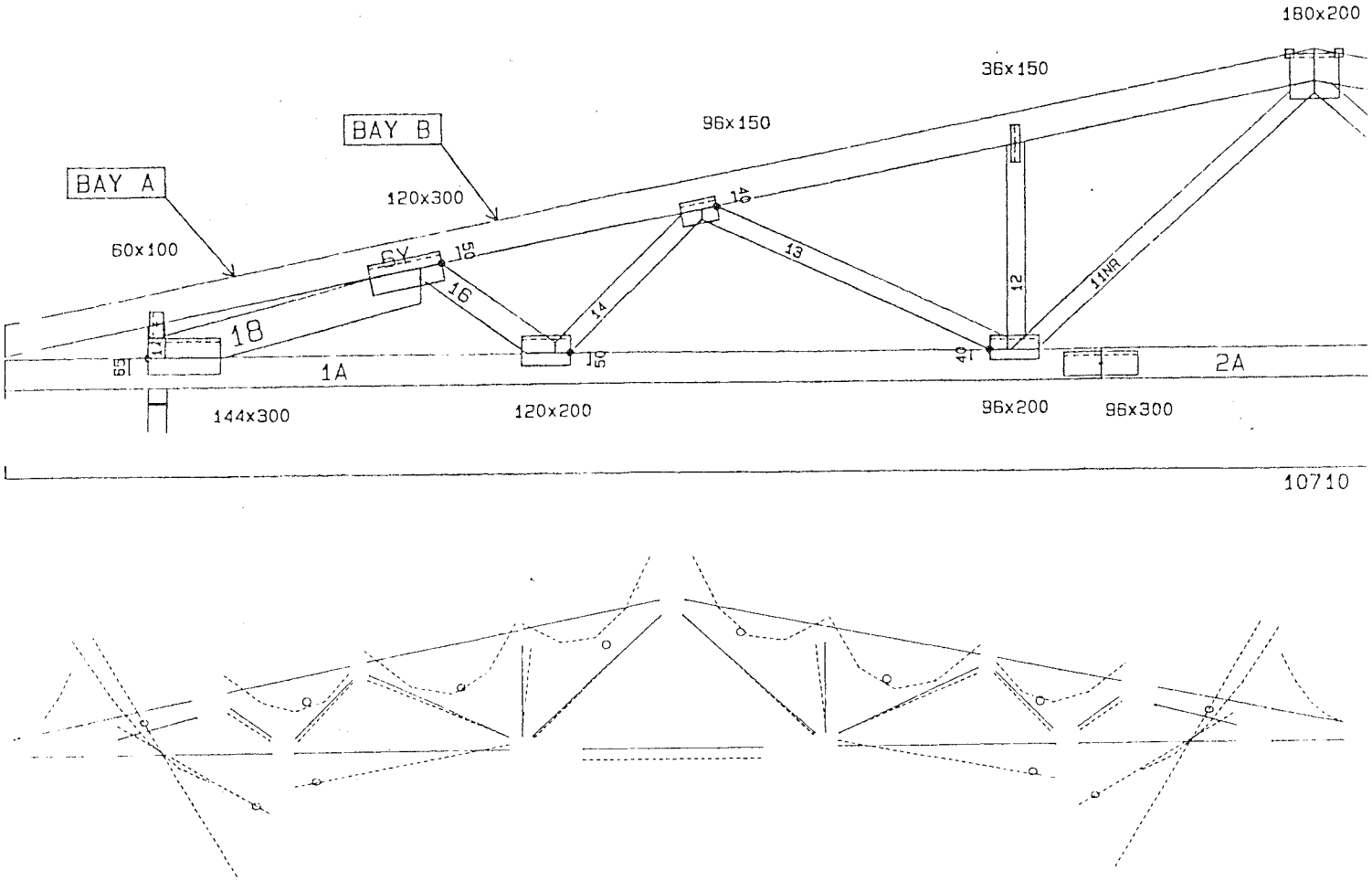


Fig. 10, Test truss and its moment curve calculated with the model. Circles represent moment measurements

7. Discussion

We can see from fig. 10 that the moment curve calculated with the model does not always go through the circles got from measurements. This means that the match between the model and measurement is not complete though it is very good. Differences can be explained (either completely or at least mainly) with contact eccentricity. The truss test was a part of quality control procedure and the truss was randomly selected at plant. No special attention was paid to connection gaps. The analysis made with the model is based on average gaps,

contact and plate stiffnesses found from joint behaviour calibration. Differences in contact may create the differences in moment distribution.
Tests have been made with 10 other trusses of different types, all of them measured at 3 load levels. Usually the model has a complete match with measurements (calculated moment is inside measuring accuracy limits). Sometimes differences are larger but it seems that the model can predict the dimensioning moment (largest moment in each bay) with appr. 20 % accuracy.
The model may look complicated and better suited to theoretical studies. However it is used in everyday truss design. Appr. 50 % of the trusses with nail plate joints manufactured in Finland are designed with the model. This means appr. 10000 designs/year.
There are many reasons which make the use of the model justified:
- It is believed that the model gives more reliable structures and the safety factor deviates less.
  Trusses designed with the model have proved to be economical.
- The model can analyze and design any kind of structure made out of timber and nail plates.

8. Further developments

There are many effects which should be considered in truss design. We should have some criterion to decide whether some effect is included or excluded.
The author suggests the following criterion: If some matter in an average case has an effect greater than the difference between standard timber size, timber grade or plate size, this matter should be included in the design. (Meaning roughly e.g.: if some matter affects the csi more than 10...15%, it should be included.)
According this criterion there are many things not yet included in the model such as:
- Size effect
- Physical nonlinearity
- Connection moment design
- Calibration of the model with joint and truss tests

It is well known that moments affecting only small timber lengths are not as serious as moments affecting long lengths. It is also known that long timber can resist smaller tension forces than short timber. Both effects can be explained with simple statistical probability analysis. Size effect can be included in the model because the model is able to define the moment distribution reliably.
It is known that timber has plastic behaviour in compression. This thing has turned out to be so complicated that including general plasticity has not yet been successful. However there are two simple effects which will be included shortly:
- Plate stiffness is smaller at high load levels than low ones.
- Contact has elasto-plastic behaviour.

Both these effects are essential e.g. in apex analysis. When the present model is used in apex analysis at different load levels it is found that when load is increased relative apex moment is increased. This happens because a larger share of the force is transferred from plate to contact. Contact has larger eccentricity which leads to larger relative apex moment. Tests show clearly the opposite: increased load leads to decreased relative apex moment. The reason is lower plate stiffness which leads to smaller plate moment and contact plasticity which leads to smaller contact eccentricity.

It is shown clearly in this paper that nail plate carries moment. This means that moment has to be considered in anchorage and steel failure analysis. The model gives a good starting point for considering both effects because it includes plate eccentricity. We must note that the external moment is not necessarily the same as the moment which affects the plate. In fig. 8 we see that there is external moment in the connection but the plate moment is 0. The opposite may also be true as seen in fig.7. Another example of this is shear connection: Assume we select 4 equal timber parts and 4 equal plates and make two joints as shown in fig. 11. Assume the plate is small enough (appr. 80*120 mm^2) to lead to anchorage failure and the gap between timber parts is large enough for there to be no friction. When we test the joints we can find that joint A carries an appr. 40 % larger force than joint B. Neither joint has external moment but joint B has internal plate eccentricity moment which is the reason for reduced strength. This has been found in full scale tests and it can also be predicted with the model.

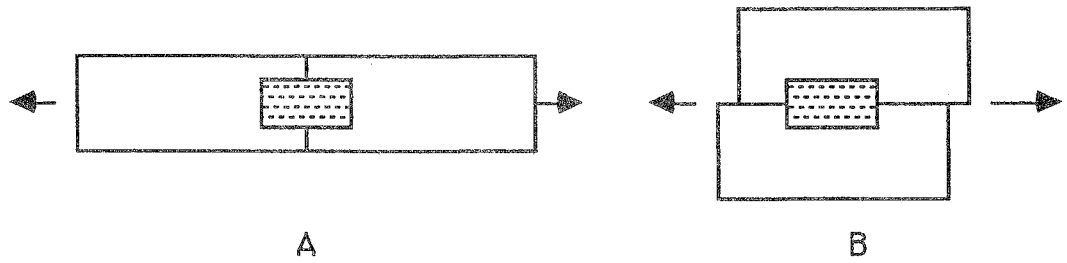


Fig. 11. Joints with no external moment but different internal plate moment.

The model has to be calibrated with real structures. This is done in the following way: A test truss is loaded, moments and deflections are measured at several points. Moments are measured in the way explained in /1/. The model is used to find calculative moments and deflections at these same points.
It is found that the same procedure can be used in nail plate tests. In this way many interpretations and approximations can be avoided. In this way the model becomes "self-calibrating".

9. Conclusion

- Joint eccentricity in nail plate connection has to be calculated considering both timber and plate eccentricity.
- Contact between timber parts may have an essential effect on eccentricity.
- If nail plate is large or very stiff, eccentricity can be calculated assuming that the connection in completely stiff.

10. Aknowledgements

Mika Leivo, Kalevi Kantojärvi and Mauri Laasonen, all working in the Technical Research Center of Finland, have carried out the truss test with great care and accuracy. The staff in the author's office has helped in the preparation of this paper.

11. References

1. Poutanen Tuomo, Model for Trussed Rafter Design, CIB-W18/18-14-2, Beit Oren, 1985
2. Riberholt H., Guidelines for Static Models of Trussed Rafters, CIB-W18/15-14-1, Karlsruhe, 1982
3. Poutanen Tuomo, Stiffness of Contact and Plate in Nail Plate Joints; (to be published shortly)

CIB-W18/19-15-1

INTERNATIONAL COUNCIL FOR BUILDING RESEARCH STUDIES AND DOCUMENTATION

WORKING COMMISSION W18 - TIMBER STRUCTURES

CONNECTIONS DEFORMABILITY IN TIMBER STRUCTURES: A THEORETICAL EVALUATION OF ITS INFLUENCE ON SEISMIC EFFECTS

by

A Ceccotti and A Vignoli
University of Florence
Italy

MEETING NINETEEN
FLORENCE
ITALY
SEPTEMBER 1986

CONNECTIONS DEFORMABILITY IN TIMBER STRUCTURES: A THEORETICAL EVALUATION OF ITS INFLUENCE ON SEISMIC EFFECTS

by Ario CECCOTTI and Andrea VIGNOLI

Department of Civil Engineering, University of Florence

1. Object and scope

Timber construction plays an important role in many areas throughout the world, and finds a wide application in low-cost residential dwellings and public buildings.
Many of the areas where wooden structures proved to be very feasible are highly seismic regions; indeed, as earthquake experiences have taught, they provide a very good response to seismic waves (refs. 1, 2, 3).

Recently, the European Community Commission has issued a draft of Eurocode 8 "Common Unified Rules for Structures in Seismic Zones" (ref. 4).
By these rules, the assessment of seismic loads is based on the frequency and intensity of the seismic events, the quantity and distribution of masses, structural geometry; behaviour is assumed to be elastic. The nature of material and the type of structure are taken into account by introducing a modifying factor (in order to reduce seismic action, the so-called behavioural factor "q"), determined by the structure's capacity of dissipating energy through its hysteretical ductility and resisting severe earthquakes by reaching domains of non-elastic behaviour.

In the draft of Eurocode 8, values ranging from 1 to 6 were suggested for the different materials (e.g. 6 for steel), so reducing the seismic design action considerably, down to 16% of the expected theoretical peak for a structure with indefinitely elastic behaviour. Since structural timber shows usually an elasto-linear behaviour before yielding (with a brittle failure) (refs. 5, 6, 7), a factor q=1 was proposed for timber structures, which apparently makes it very difficult to obtain cost-effective dimensioning.
That choice does not come from poor performance of timber structures under earthquakes (experience showed just the opposite); rather it was felt by the members of the draft panel that what is presently known about sections and joints behaviour, especially under cyclic loads, is not enough to allow detailed structural analysis as required by Eurocode 8, and by any updated design code.

A recent proposal for new Italian seismic design codes (ref. 8), regarding all building materials, does acknowledge the brittle behaviour of timber sections; still, it points at structures capacity of dissipating energy at connections, and the need for further wide and detailed investigations to this effect.
A behavioural factor q=2 is suggested, to take into account that

dissipating capacity at thousands of nailed connections between plywood panels and timber frame elements.

However referred to a very simple example, this study is aimed as a preliminary contribution to the quantitative assessment of the effect of connections deformability on peak stress conditions that a timber structure could undergo during an earthquake.

2. Method

Two simple portal frames of glue-laminated timber (dimensions are shown in fig.1) were selected, one fixed at the base (A) and the other hinged (B); both were subjected to a 1000 daN/m total load on the beam.

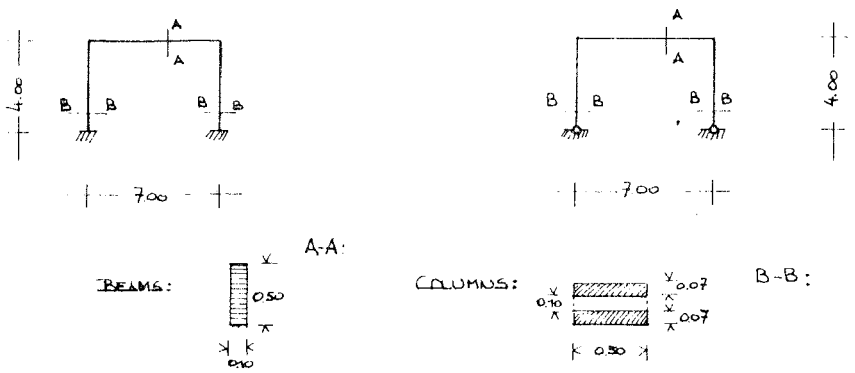


Fig. 1: dimensions of studied structures

Connections were assumed to be sometimes rigid (such as glued joints), sometimes semi-rigid (such as bolted joints), as shown in fig. 2.

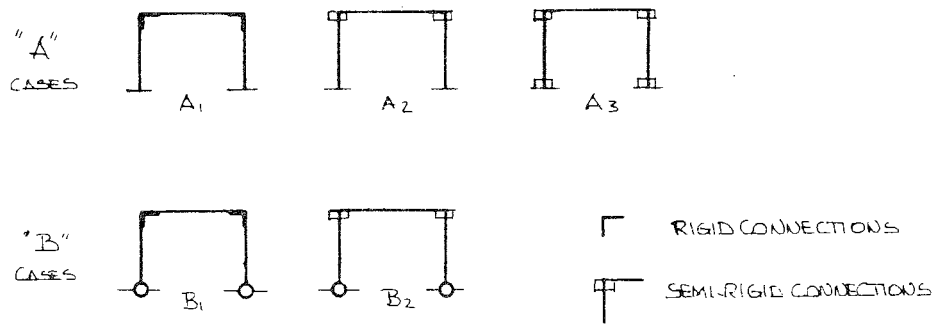


Fig. 2: selected cases

For the semi-rigid joint, a moment-rotation behaviour was assumed which was derived from test histories (ref. 10) and idealized by a bilinear law (fig. 3).
The behaviour law under cyclic load was assumed to follow the type shown in fig. 4.

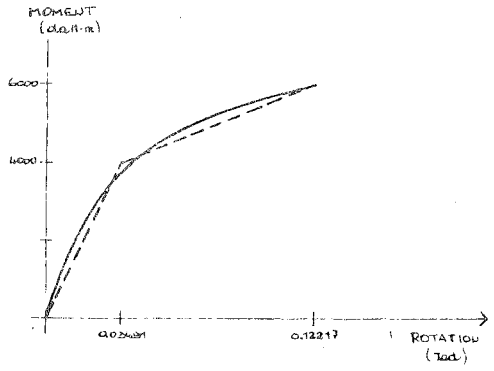


Fig. 3: connections behaviour under static loading

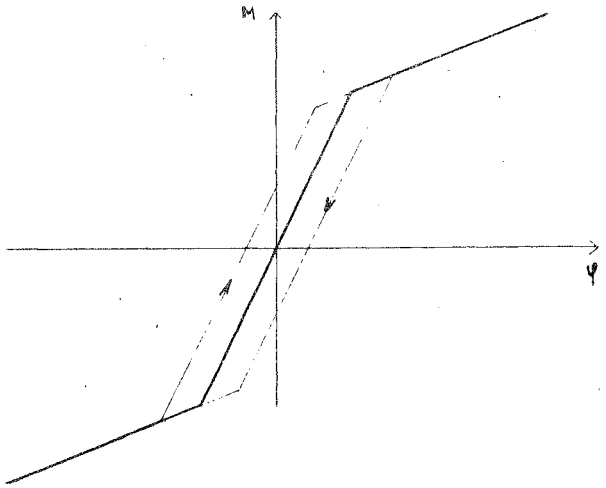
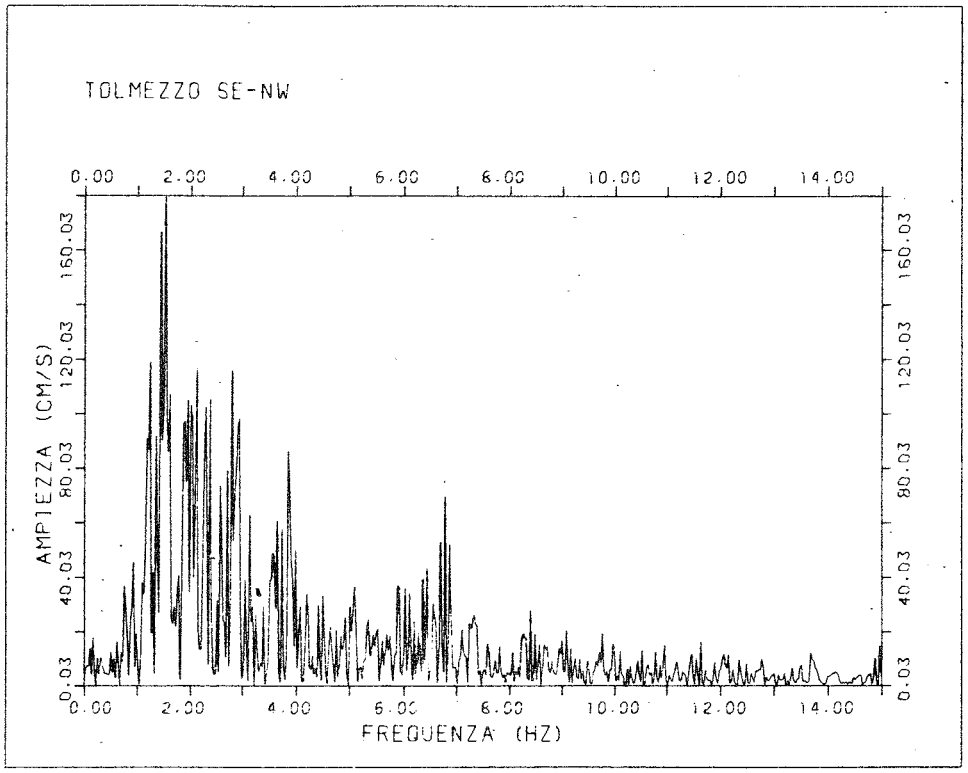


Fig. 4: connections behaviour under cyclic loading (idealized)

Timber behaviour was assumed to keep elastic till strength characteristics values (under instantaneous loading) were reached: 30 MPa for bending, tension, compression and 2.4 MPa for shear.
The modulus of elasticity of timber was considered to keep on higher values than what is the case for static loads, i.e. at about 15,000 MPa (ref. 11). Overall damping factor was prudentially assumed to be 5% of critical damping.
Using a so-called direct-integration non-linear analysis program (DRAIN 2D; ref. 12), two accelerograms were applied at the base, one from Tolmezzo (Friuli, Italy, 1976) SE-NW component, and another from El Centro (California, USA, 1940) NS component; their Fourier spectra are shown in fig. 5. In order to focus on semi-rigid connections contributing to plastic behaviour, in some cases the analysis was carried further by amplifying accelerograms by a factor 2.
So doing, the actual behaviour could be recorded moment by moment in terms of beam displacements and forces at sections. The analysis takes into account both mechanical and geometrical non-linearity.

3. Results

Most significant results are synoptically reported in figg. 6A-6B in terms of beam maximum displacement (δ) and maximum inertial force at beam (F), along with exact time of their occurring. The figure also shows whether and when sections characteristic values or connections elastic threshold were reached.



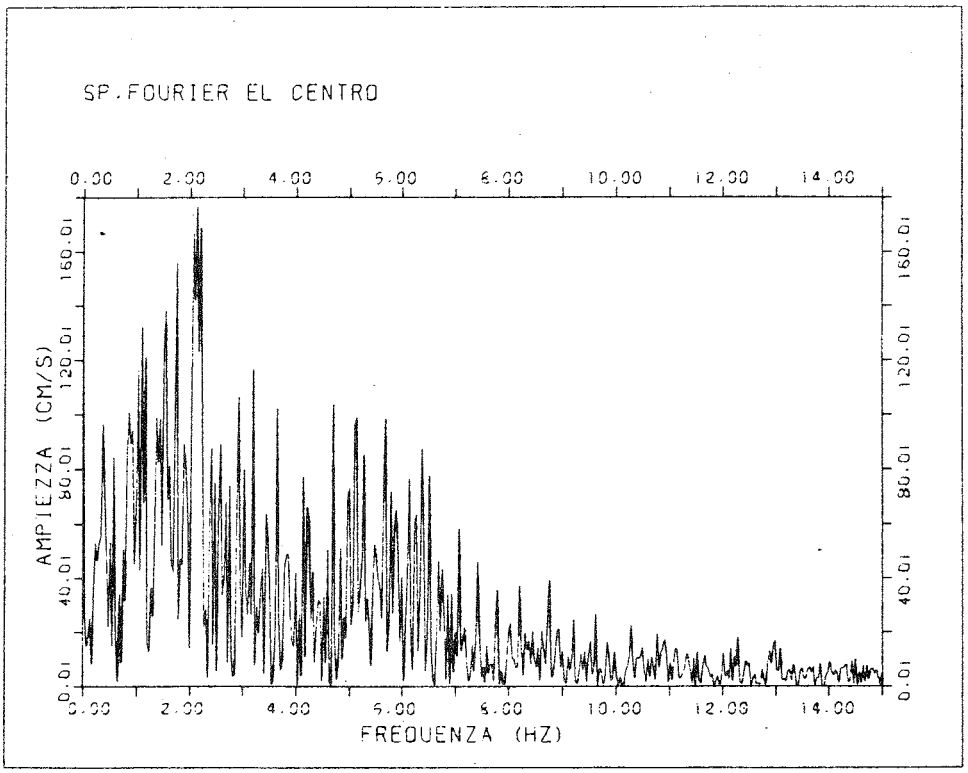


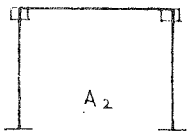
fig. 5: Selected Earthquakes, Fourier spectra

INPUT: TOLMEZZO EARTHQUAKE

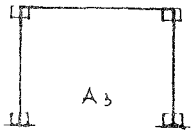
AMPLIFICATION FACTOR: [×1]



$\delta(5.36) = 1.62$ cm
$F(5.36) = 6795$ daN

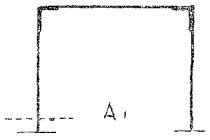


$\delta(4.22) = 3.54$ cm
$F(4.22) = 7723$ daN

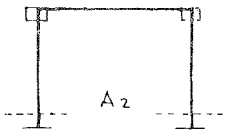


$\delta(4.54) = 9.50$ cm
$F(4.54) = 2541$ daN

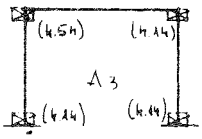
AMPLIFICATION FACTOR: [×2]



$\delta(4.18) = 3.04$ cm
$F(4.18) = 12533$ daN



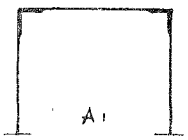
$\delta(4.24) = 7.76$ cm
$F(4.24) = 10317$ daN



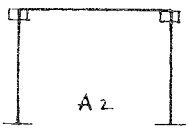
$\delta(4.54) = 16.35$ cm
$F(4.54) = 4157$ daN

INPUT: EL CENTRO EARTHQUAKE

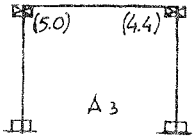
AMPLIFICATION FACTOR: [×1]



$\delta(2.52) = 1.45$ cm
$F(2.52) = 6092$ daN

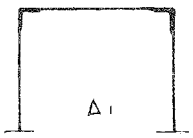


$\delta(2.64) = 2.41$ cm
$F(2.64) = 5275$ daN

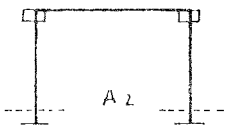


$\delta(4.48) = 14.508$ cm
$F(4.48) = 3741$ daN

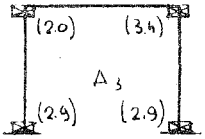
AMPLIFICATION FACTOR: [×2]



$\delta(2.52) = 2.91$ cm
$F(2.52) = 12185$ daN



$\delta(2.44) = 4.57$ cm
$F(2.44) = 9180$ daN

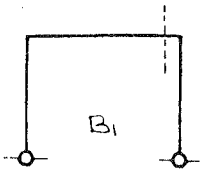


$\delta(4.50) = 24.31$ cm
$F(4.38) = 4604$ daN

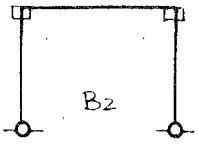
fig. 6A: Results for fixed portal frames.

INPUT: TOLMEZZO EARTHQUAKE

AMPLIFICATION FACTOR: ×1

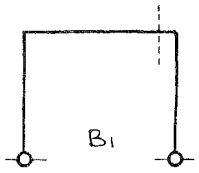


$\delta(6.62) = 6.88$ cm.
$F(6.62) = 6250$ daN

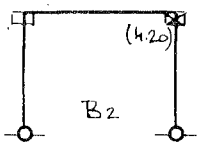


$\delta(4.20) = 8.09$ cm.
$F(4.20) = 1026$ daN

AMPLIFICATION FACTOR: ×2



$\delta(4.08) = 6.88$ cm.
$F(4.08) = 5958$ daN



$\delta(4.20) = 16.24$ cm.
$F(4.20) = 1858$ daN

LEGENDA :

- ⌐ RIGID CONNECTIONS
- □ SEMI-RIGID CONNECTIONS
- $\delta(t)$ PEAK DISPLACEMENTS (AT t TIME, SECONDS)
- $F(t)$ PEAK INERTIA FORCES (AT t TIME, SECONDS)
- ----- SECTION COLLAPSE
- ⊠ (t) SEMI-RIGID CONNECTIONS PLASTIC RANGE WITHOUT COLLAPSE (SINCE t TIME, SECONDS)

NOTE : THE TIME t IS COMPUTED FROM EARTHQUAKE BEGINNING

fig. 6B: Results for hinged portal frames.

3.1

Results suggested that connections deformability does contribute to actions reduction: its effect was most relevant in B, where semi-rigid connections were placed so to be subjected to maximum bending action (Fmax at beam reduces to 15% !).
The same effect, albeit slightly reduced, occurred in A in passing from A1 to A2, while the transition from A1 to A3 involves a much stronger reduction (Fmax at beam down to an average 35%).

3.2

It was also noted that for A1, A2, A3 neither sections collapse nor connections enter plastic domain under the effect of a non-amplified earthquake, while for B collapse is obtained in beam end sections.
By increasing seismic intensity twice, collapse is reached in a greater number of cases; still, the influence of connections semi-rigidity on stress reduction remains just as effective.

4. Conclusions and further investigations

The authors are well aware of the following limits in their research: the geometry and shape of the structure; just two input accelerograms; the cyclic behaviour model not fully reflecting actual joint behaviour - cyclic behaviour laws were in fact derived from a model implemented for steel structures. Moreover, hysteretic damping could not be considered directly; rather, the type of analysis involved assuming damping at generic time as depending on the stiffness matrix: such assumption should be confirmed or rejected through tests on full-scale models, along with damping value at time t=0; in our study, this was prudentially assumed to be 5%, and constant for all structures.
However, they think that such method, once extended and refined by means of both improved analysis programs and a greater wealth of experimental data, could help effectively in studying seismic effects on timber structures and allow a more exact assessment of the values required by Eurocode 8 draft panel.

REFERENCES

[1] F.J. KEENAN, 1980: "The Earthquake resistance of timber construction". In: International Conference on Engineering for Protection from Natural Disaster (January: Bangkok) Proceedings, pp. 273-285.

[2] A. CECCOTTI, 1983: "Seismic upgrading of timber structures of ancient buildings: design and operative problems"*. In: Symposium "Il legno nel restauro e il

restauro del legno" (30 Nov. - 3 Dic.: Florence) Proceedings, Vol. I, pp. 193-220.

[3] I. SAKAMOTO; Y. OHASHI; M. SHIBATA, 1984: "Some problems and considerations on aseismic design of wooden dwallings houses in Japan" In: 8.th World Conf. Earthquake Engineering (23-28 July: San Francisco) Proceedings, Vol. V, pp. 669-676.

[4] BRUSSELS, 1984: "Common Unified Rules for Structures in Seismic Zones", (Eurocode 8, part. III), Preliminary Draft proposal.

[5] B. MADSEN, 1985: "Timber engineering in the past, present and future" In: Symposium on Forest Products Researche International-Achievements and future (22-26 April: Pretoria) Proceedings, Vol. IV, pp. 3-1, 1/7.

[6] A. CECCOTTI, 1983: "Timber structures in house-building"*. INARCOS, Vol. 38, n. 441 (suppl), pp. 6-22.

[7] A. CECCOTTI; P. SPINELLI; L. UZIELLI, 1983: "Behaviour under static and dynamic loads of spruce fir and poplar glue-laminated beams"*. La PREFABBRICAZIONE, Vol. 19, n. 6, pp. 401-416.

[8] ROMA 1985: "Draft proposal of technical rules for construction in seismic zones"*. INGEGNERIA SISMICA, Vol. 2, n. 1 (Annex).

[9] G. AUGUSTI; A. CECCOTTI, 1985: "Antiseismic rules for timber structures: an Italian proposal". In: Symposium on Forest Products Research International-Achievements and future (22-26 April: Pretoria) Proceedings, Vol. IV, pp. 3-21, 1/15. CIB-W18/18-102-1.

[10] F. LANER, 1982: "Experimental tests an connections of glue-laminated portal frames"*. In: 4.th CTE Symposium "Su la industializzazione edilizia"(11-14 Novembre: Verona) Proceedings, pp. C 27-C 34.

[11] A. CECCOTTI; A. VIGNOLI, 1985: " Full-scale structures in glued laminated timber, dynamic test: theoretical and experimental studies". In: International Council for Building Research Studies and Documentation, Working Commission W18, Timber Structures. Meeting Eighteen (4-6

June: Haifa), Proceedings, n. 18-15-1.

[12] G.H. POWELL, 1975: "DRAIN-2D User's Guide", Earthquake Engineering Researche Center, Report n. UCB/EERC 73-22, University of California, Berkeley.

Refereces marked [*] are in Italian.

CIB-W18/19-15-2

INTERNATIONAL COUNCIL FOR BUILDING RESEARCH STUDIES AND DOCUMENTATION

WORKING COMMISSION W18 - TIMBER STRUCTURES

THE BRACING OF TRUSSED BEAMS

by

M H Kessel and J Natterer
École Polytechnique Fédérale de Lausanne
Switzerland

MEETING NINETEEN
FLORENCE
ITALY
SEPTEMBER 1986

1 Introduction

The top chord of trussed beams vertically loaded normally works in compression. The bracing system has to stabilize the chord against lateral buckling. The subject of this paper is to determine the lateral loads which act between the chord and the bracing. Before investigating the complete 3 dimensional problem, we shall start with the simple bar to show some basic effects.

2 Bar laterally stabilized

The first investigation into this problem was carried out by Engesser / 1 / in 1884. He treated the top chord of a low-truss bridge as a simple bar as shown in figure 1. Furthermore he assumed a sinusoidal distribution of the lateral load, which is true only, as we know and as is proved in / 2 /, for a constant internal force in the chord. Therefore Engesser already used the mean value of the internal forces of the members of the top chord as a basis for calculating the lateral load.

To find the real distribution of the lateral load q(x) due to an arbitrary axial loading p(x) in figure 2 we have to solve simultaneously the differential equations

$$-p + N' = 0 \qquad (1.a)$$

$$-q - (N\bar{v}')' - M'' = 0 \qquad (1.b)$$

with N as the internal axial force, M as the bending moment and $\bar{v} = v_o + v$ as deflection (v_o: initial deflection). For an axial loading of figure 3

$$p(x) = \frac{40\pi}{L} \cos \frac{\pi}{L} x \,, \qquad (2)$$

which leads to a sinusoidal distribution of the internal axial force N (in accordance with N of the top chord in fig.1), the diff.equ.s (1) are solved by the finite element method. You find the results in figure 4.a. The

distribution of the system DA32VF is found for a bar with laterally fixed ends, whereas in the case of DA32V the ends are free, that means they are supported only by the bracing system. By way of comparison you find in figure 4.a the sinusoidal distribution of DA32CF for constant N as the mean value of sinusoidal N. Finally figure 4.b shows the corresponding shear forces.

The differences between the three curves of both figures are important and we can conclude that the lateral load due to the constant N can no longer be interpreted as an approximation but as an estimation for the lateral load due to sinusoidal N.

3 Parallel chord truss

Since in the preceding chapter we have cut off the top chord of the truss and interpreted as a simple bar, we shall now investigate a complete 3 dimensional structure as shown in figure 5.

For end loads P = 25.5 kN, representing couples at both ends, the sinusoidal distribution of figure 6 follows by again using geometrically nonlinear finite elements. The results coincide with those of system DA32CF in figure 4, which means that for end couples the top chord can in fact be treated as a simple bar.

For the same truss a uniformly distributed vertical load p = 2.42 kN/m approximately causes in the top chord a sinusoidal axial force with the mean value 25.5 kN as in the case of figure 3. The corresponding lateral loads and shear forces are given in figure 7.a and 7.b for two different elastic lateral deflections f_z^o of the top chord. Although the initial deformations are considerably smaller, the lateral load q and the shear force Q are considerably larger in comparison with q and Q of system DA32VF in

figure 4.a and 4.b. In explanation of this behaviour we find out that the bottom chord is deflected in the opposite direction of z with respect to the top chord. Since the bottom chord is stressed in tension, this leads to additional loads in the bracing.

As a result of figure 7.a we can conclude that for a uniformly distributed vertical load, a uniformly distributed lateral load as is supposed in the design codes is not even an approximation of the real loads. Also the assumption of a sinusoidal lateral load which corresponds to a constant axial force does not fit in much better with q of figure 7.a.

As an approximation derived from the potential energy functional we can give, however, for a sinusoidal vertical load

$$p(x) = p_o \sin \frac{\pi}{L} x \qquad (3)$$

the formulae

$$q(x) = 2p_o(t_o + t) \cos \frac{2\pi}{L} x \qquad (4.a)$$

$$Q(x) = p_o(t_o + t) \frac{L}{\pi} \sin \frac{2\pi}{L} x \qquad (4.b)$$

where t_o and t are the initial and elastic twists of the truss. These approximations are shown in figure 7.a and 7.b by way of comparison.

4 Roof trusses

We now have seen the discrepancy in determining the lateral loads of a 3 dimensional parallel chord system with the aid of a simple bar. So it is evident that we can treat the roof truss system of figure 8 only as a completely 3 dimensional one. Roof trusses are distinguished by their triangular geometry. Hence it follows that the bracing consists of two halves and hence the problem arises of determining their transitional loads at the apex.

For this purpose we look at one half of a three-hinged frame in figure 9.a as a more general system which is subjected to a symetrical load P. It can readily be found by statics

$$O_1 = O_2 = \frac{PL}{4b}\,\frac{h}{s} \,. \qquad (5)$$

The transition to the roof truss is now given by h = 0 as shown in figure 9.b and, therefore, we obtain

$$O_1 = O_2 = 0.$$

Hence it follows that each half of the bracing works like a cantilever beam due to the clamping caused by the tensile force in the bottom chords. The effect of a laterally restraining moment at the heel joint is also discussed in / 3 /. From the practical point of view this is a very important result, for it simplifies the bracing details considerably.

To give a clear idea of the distribution of the lateral loads due to a uniformly distributed vertical load for roof trusses, we shall first describe the transition from the parallel chord truss (d = 0) to the roof truss (d = 50 cm) for the forces induced in the top chord. The parameter d is explained in figure 10 and figure 11 shows the variation of the forces in the top chord with a = L/32 as the distance between the struts. Figure 11, which is again a result of finite element calculations, calls back to mind that for roof trusses the maximum of the chord forces is displaced near the supports. This leads, of course, to the differences in the distribution of the lateral loads as shown in figure 12.a and 12.b. Since the truss systems of figures 11 and 12 are of no practical interest, they have been chosen only for illustration and we have calculated simultaneously conventional W-trusses. The finite element results are given in figure 13.a and 13.b and labelled SD08V. In fact, q becomes a zero value at the

middle of the span, as we have derived previously from equ. (5). Again the differences in the distribution in relationship to parallel chord trusses (PCO8V) become remarkable, because for them q becomes a maximum at the middle of the span.

For more details and results of full scale tests see at / 4 /.

5 Conclusions

The distribution of the lateral load for the bracing of trusses is much more complex than is assumed in the design codes. However, from the practical point of view it seems to be too expansive always to take the real distribution of q into account when dimensioning the bracing. Therefore two strategies for dimensioning are left. The first is to determine the lateral loads by at least geometrically nonlinear finite elements, which is valid for large scale systems only. The second is to use the code formulae and to bear in mind that a uniformly and even a sinusoidal distributed lateral load merely gives an estimation of the loads which are really applied to the bracing system.

References

/ 1 / Engesser, F. : Die Sicherung offener Brücken gegen Ausknicken. Zentralblatt der Bauverwaltung 40(1884)415-417

/ 2 / Gerold, W. : Zur Frage der Beanspruchung von stabilisierenden Verbänden und Trägern. Stahlbau 32(1963)278-281

/ 3 / Pienaar F R P: The bracing of timber roof trusses. CSIR special report HOUT 311 October 1983

/ 4 / Natterer, J. Kessel, M.H. : Theoretische und experimentelle Untersuchungen zur seitlichen Stabilisierung von Biegeträgern. Forschungsbericht KFWF Nr.1075 EPF Lausanne März 1985

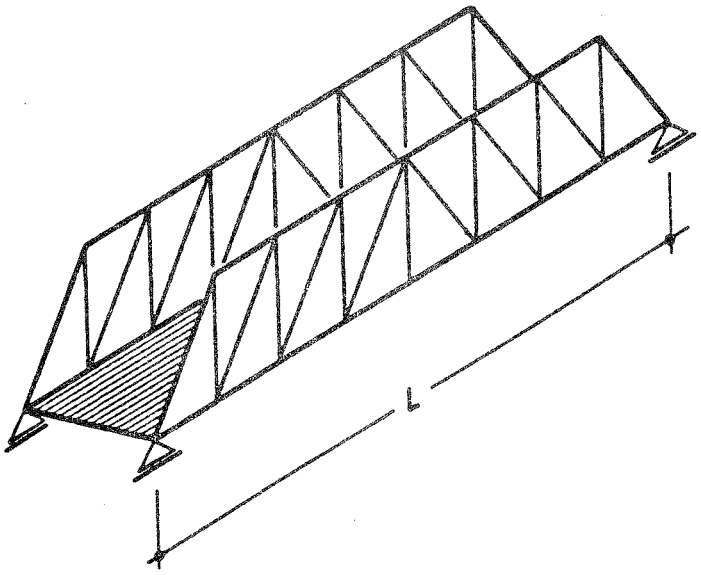


Figure 1 Low-truss bridge

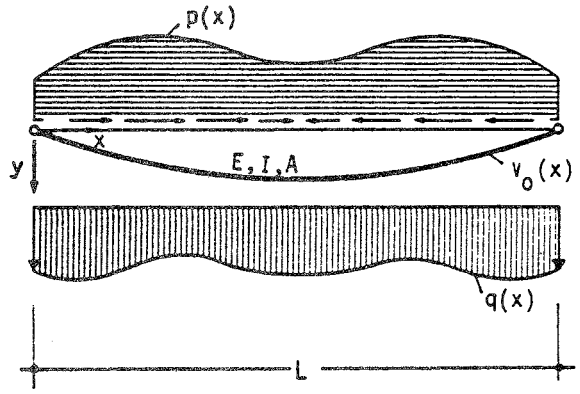


Figure 2 Bar on elastic foundation under distributed axial load

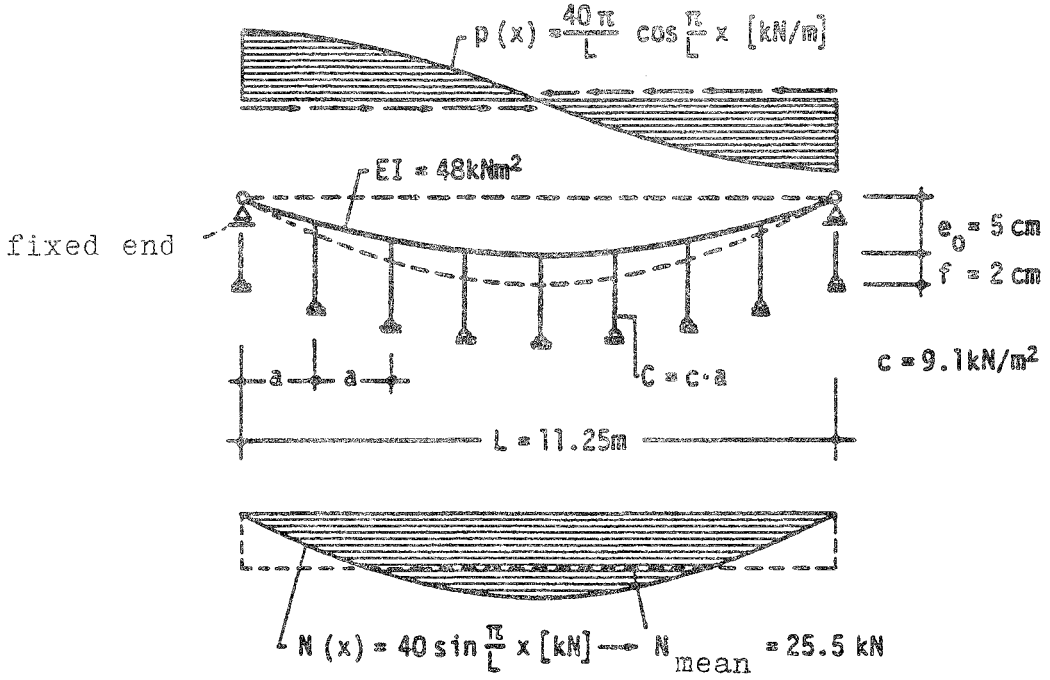


Figure 3 System DA08VF (a=L/8) with sinusoidal internal force N

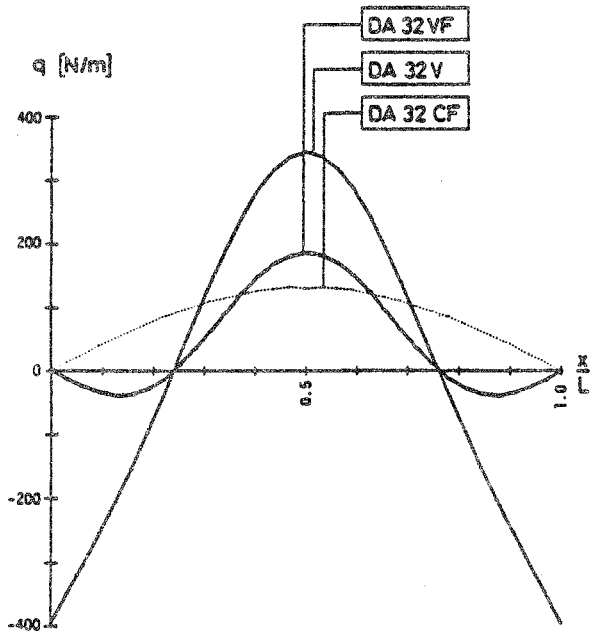


Figure 4.a Lateral load q

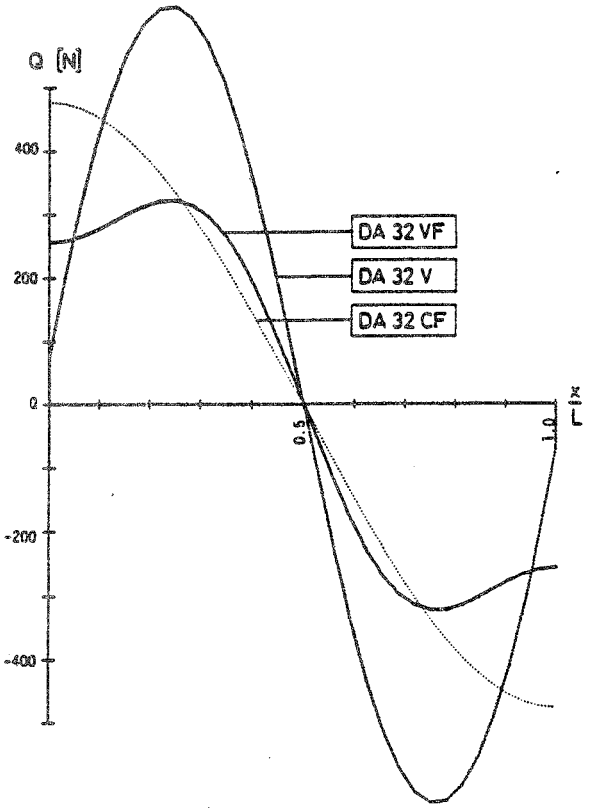
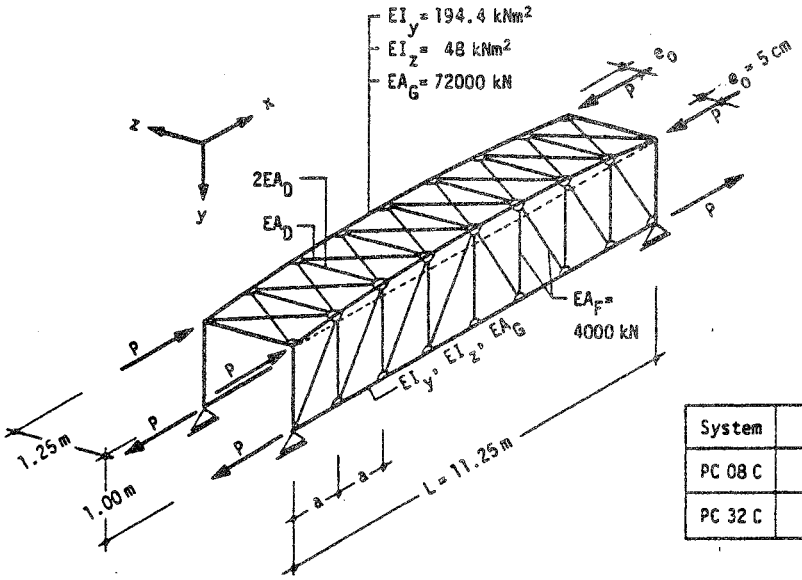


Figure 4.b Corresponding shear force Q

DA32VF: a=L/32, sinusoidal N (fig.3), fixed ends
DA32V : a=L/32, sinusoidal N (fig.3), free ends
DA32CF: a=L/32, constant N=25.5 kN , fixed ends



System	a	EA_D	f_z^o
PC 08 C	L/8	274 kN	2 cm
PC 32 C	L/32	356 kN	2 cm

f_z^o: lateral elastic deflection of top chord

Figure 5 Parallel chord system

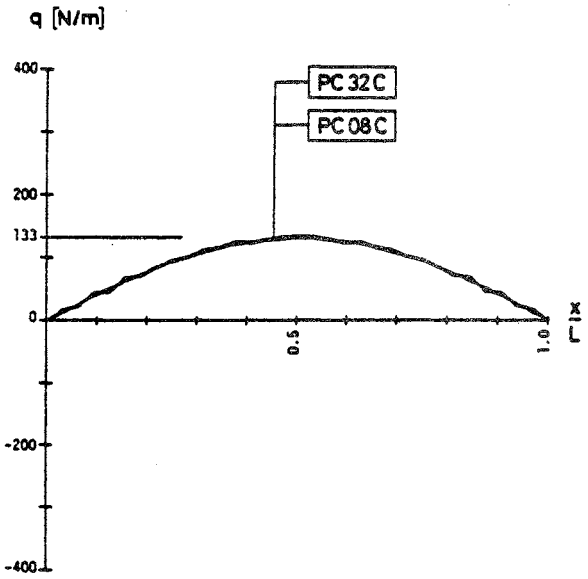


Figure 6.a Lateral load q

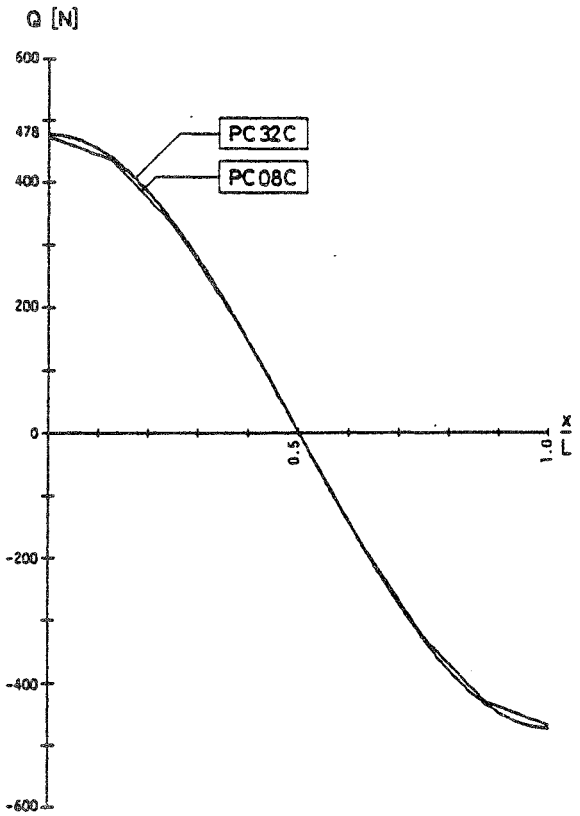


Figure 6.b Corresponding shear force Q

PC08C : a=L/8 , constant N=25.5 kN
PC32C : a=L/32, constant N=25.5 kN

t: elastic twist of truss

f_z^o: lateral elastic deflection of top chord

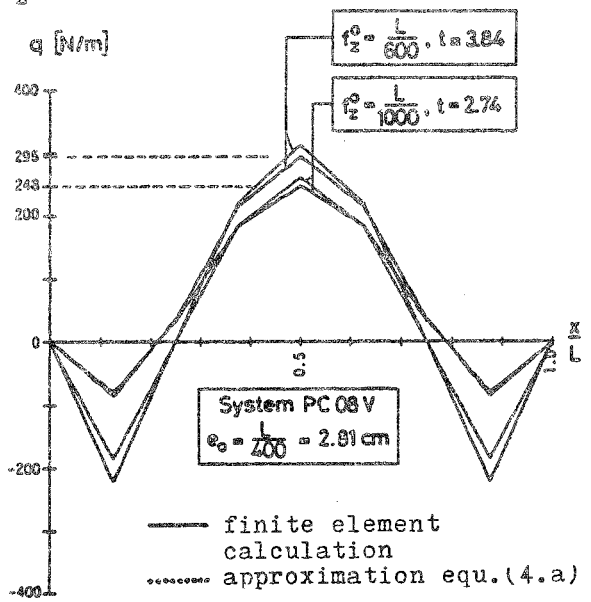


Figure 7.a Lateral load q

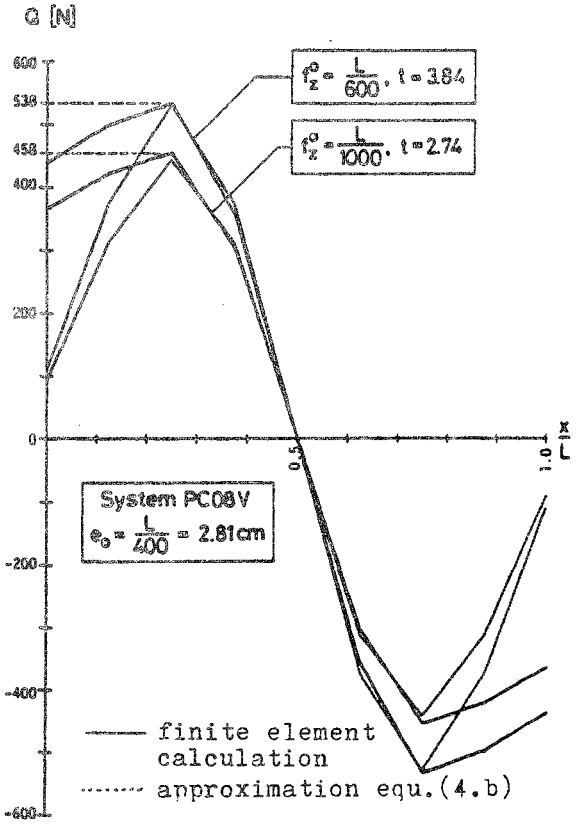


Figure 7.b Corresponding shear force Q

PC08V : a=L/8, quasi sinusoidal N

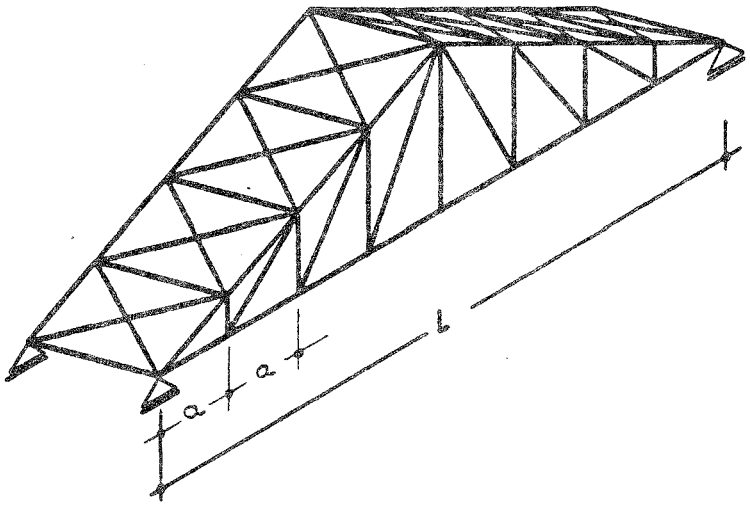


Figure 8 Roof truss (SC08..)

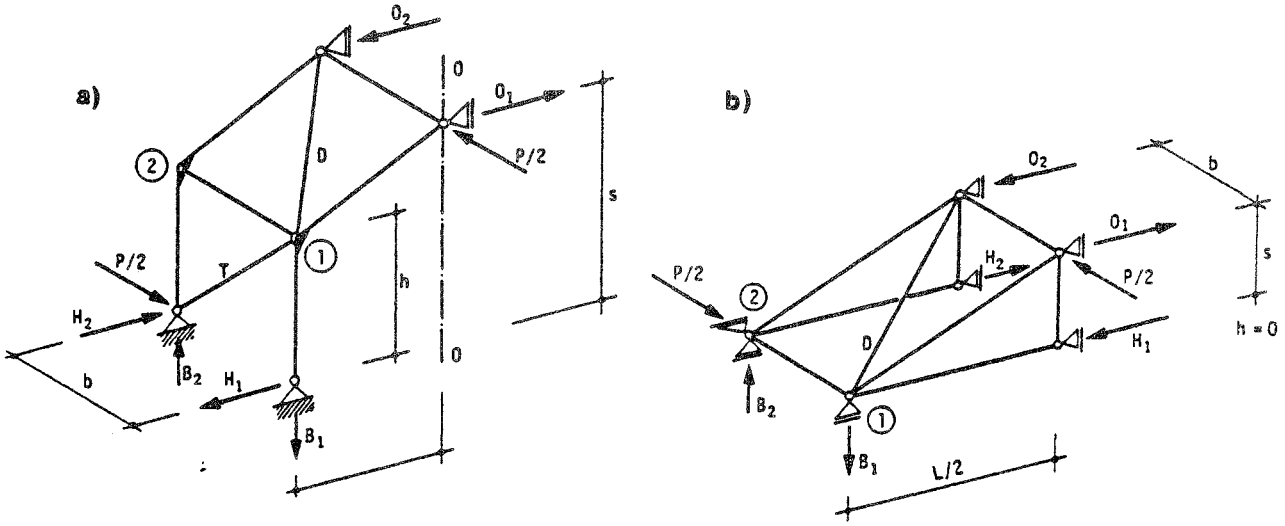


Figure 9 Equilibrium of the forces acting on one half of
a a braced three-hinged frame (symetrical load P)
b a braced roof truss

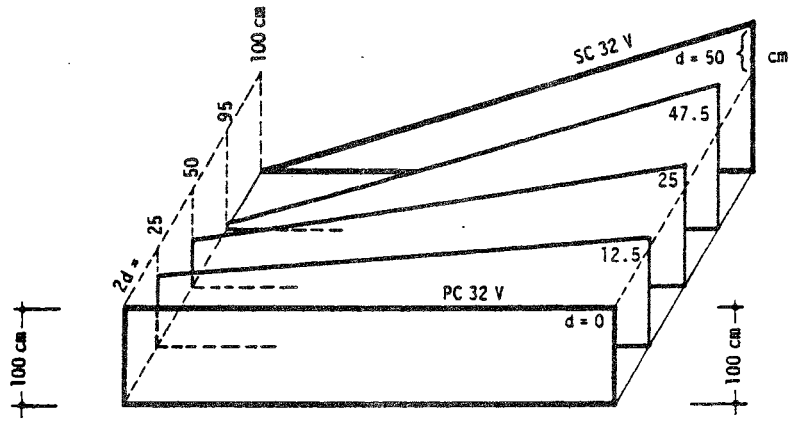


Figure 10 Transition from the parallel chord truss to the roof truss described by the parameter d

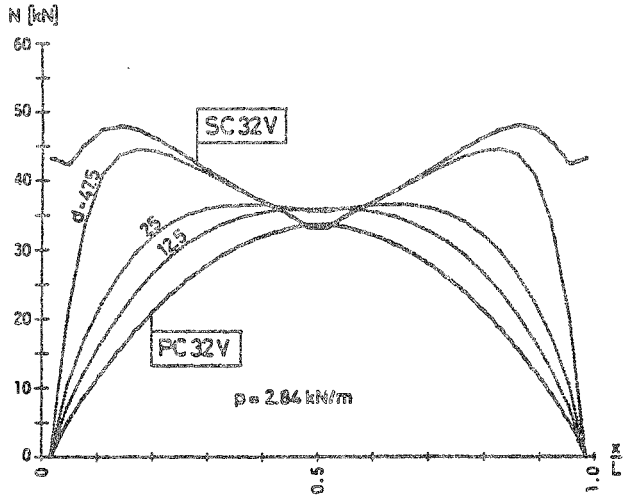


Figure 11 Variation in compressive force in the top chord

SC32V : roof truss, a=L/32, uniformly distributed vertical load p

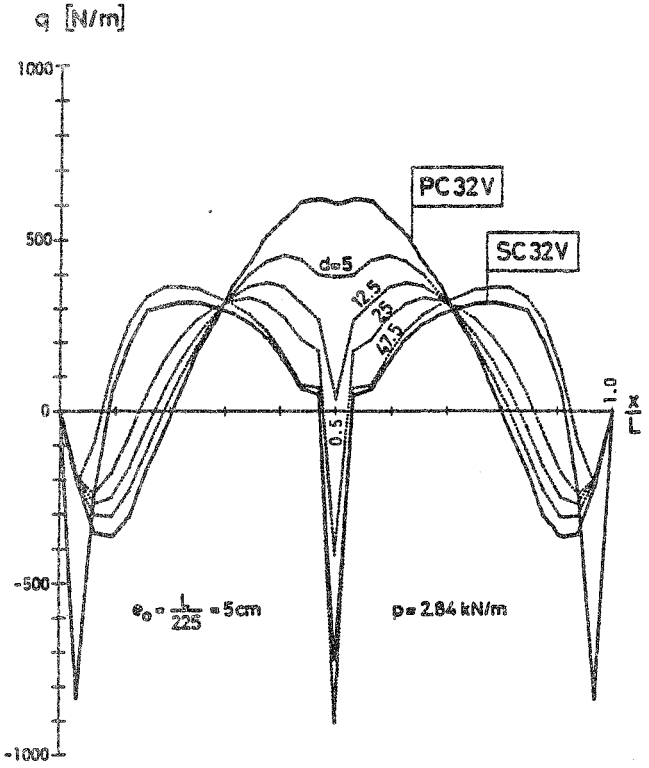


Figure 12.a Variation of lateral load q

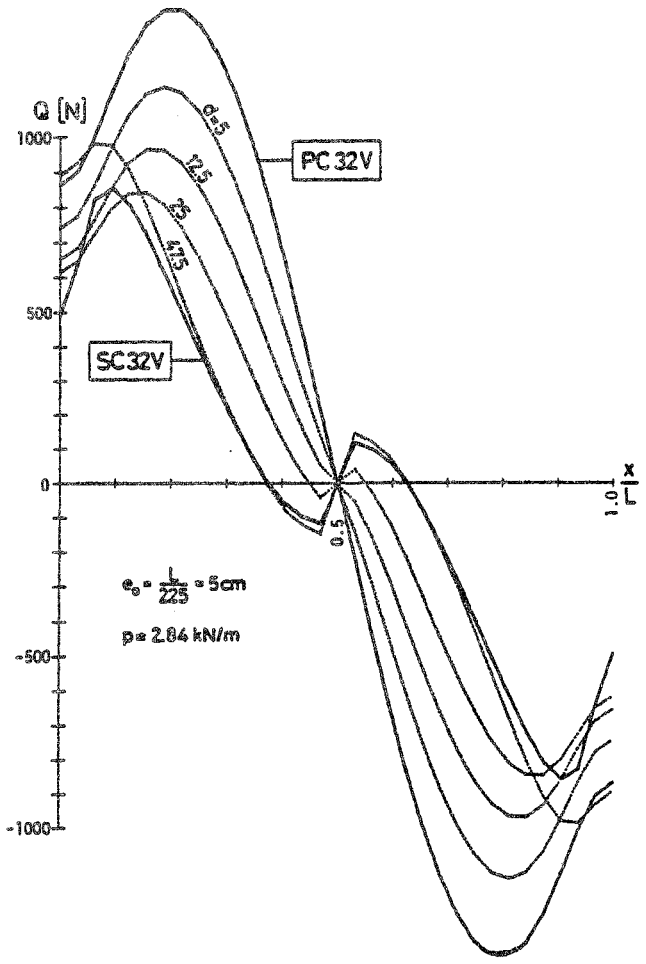


Figure 12.b Variation of corr. shear force Q

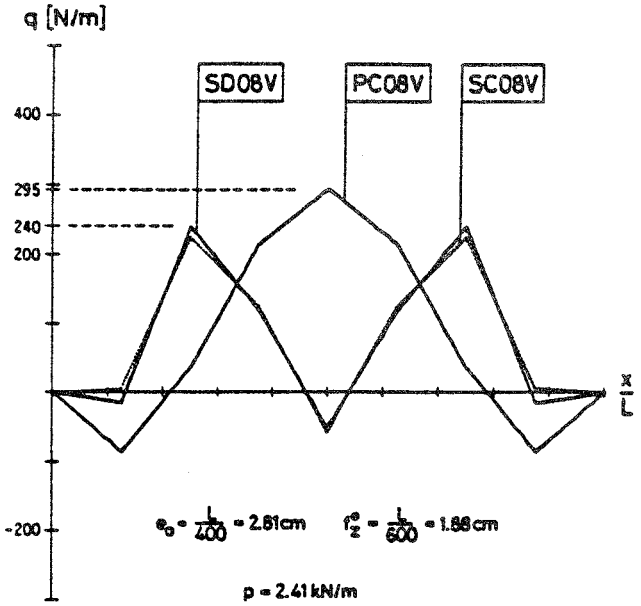


Figure 13.a Lateral load q

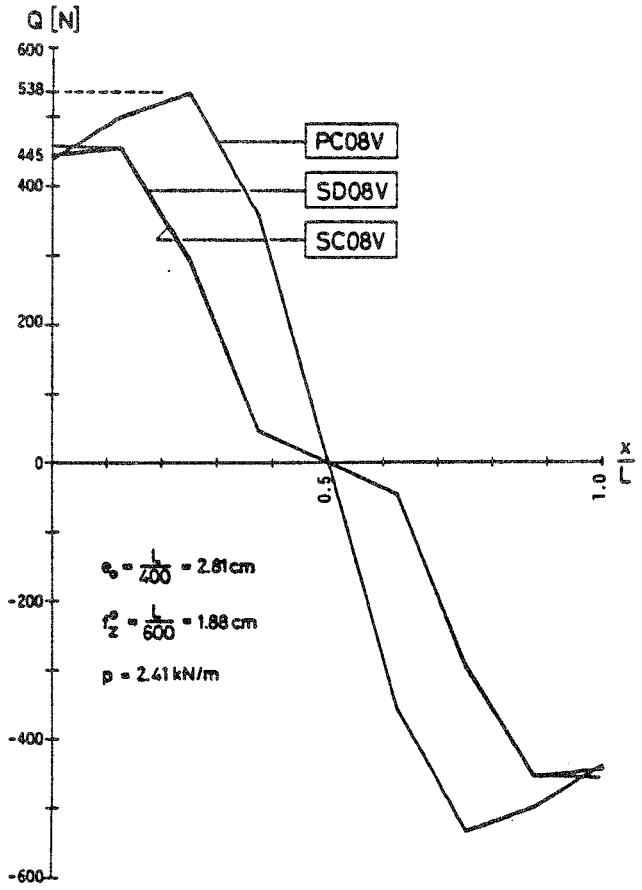


Figure 13.b Corresponding shear force Q

PC08V : par.chord truss, a=L/8, uniformly distributed vertical load p with quasi sinusoidal N

SC08V : roof truss of fig. 8, a=L/8, uniformly distributed vertical load p

SD08V : W-truss, a=L/8 (only valid for bracing), uniformly distributed vertical load p

CIB-W18/19-15-3

INTERNATIONAL COUNCIL FOR BUILDING RESEARCH STUDIES AND DOCUMENTATION

WORKING COMMISSION W18 - TIMBER STRUCTURES

RACKING RESISTANCE OF WOODEN FRAME WALLS WITH VARIOUS OPENINGS

by

M Yasumura
Building Research Institute
Ministry of Construction
Japan

MEETING NINETEEN
FLORENCE
ITALY
SEPTEMBER 1986

RACKING RESISTANCE OF WOODEN FRAME WALLS WITH VARIOUS OPENINGS

by Motoi YASUNURA
B.R.I.,Japan

INTRODUCTION

Wooden frame construction, practically used for only small dwellings in Japan, can be applied to various uses for a building if the rational design procedure on the basis of structural calculation is developed. Although several theoretical studies have been done on the racking strength of wooden frame wall panels [2][3][4][5], they are based on the analysis of blind walls and do not explain the mechanical properties of the entire wall panel with openings. A purpose of this study is to present the useful data for calculating the lateral resistance of wooden frame construction. Twelve full-sized plywood-sheathed wall panels with various openings were subjected to the racking loads, and the influence of openings on the shear stiffness and strength was observed [6]. Experimental results were compared with the calculated values on the basis of non-linear load-slip relation of a nail, and comparatively good agreement between experimental and calculated values was obtained.

CURRENT DESIGN PROCEDURE

Building Standard Law [1] requires that the effective length of the bearing walls which is the sum of the actual length of each bearing wall multiplied by the racking resistant ratio given in Table 1 shall conform to the values given in Table 2 per square meter of each floor area and to the values given in Table 3 per square meter of each story projected area, both in span direction and lateral direction of the buildings.

This procedure is based on the assumption that two thirds of the lateral load are supported by the sum of the racking resistance of the blind walls which are arranged in the relevant direction and whose length is greater than ninety centimeters,

and the remaining one third is supported by the non-bearing members like small walls, perpendicular walls, etc. This procedure is simple and efficient to check the approximate lateral resistance of small dwellings, however more accurate calculation is necessary to design larger-scale buildings. Disregarding the effects of the amount of the shear resistance of small walls, this procedure has a tendency to underestimate the racking strength of a wall panel having small openings and to overestimate that of a wall panel consisting of slender blind walls and large openings.

DESCRIPTION OF WALL PANELS

Twelve wall panels of 7.28 meters in length with various openings were constructed with kiln dried S-P-F lumbers of nominal size of 2-by 4 inches and 9.5 millimeters thick Douglas-Fir plywood. Studs, spaced on 45.5 centimeters on center, were connected to bottom plate and to double top plates with end nailing of CN90-E wire nails, and plywood sheets of 3-by 8 feet were fastened to the frame with CN50 wire nails which were spaced 10 centimeters around the perimeters of a plywood sheet and 20 centimeters along the intermediate support (See Fig.2).

Six types of wall panels are shown in Fig.4. Each specimen except for F-1 and 2 includes three bearing walls of ninety-one centimeters in length at the both ends and in the center of a panel, and F-1 and 2 include two bearing walls at the both ends of a panel.

TEST METHODS

Fig.1 shows the test setup for racking test. Double top plates were bolted to a 15-by 30 centimeters glulam timber with seven bolts of 16 millimeters in diameter, and bottom plate was anchored to a 9-by 9 centimeters wooden sill and to a steel member with seven bolts of 16 millimeters in diameter. End studs were connected with a steel member with three bolts of 16 millimeters in diameter and steel plates as shown in Fig.3. The horizontal cyclic force was applied at the end of wooden girder. For each type of wall panel, two specimens whose way of apprica-

tion of plywood sheets was different were tested.

EXPERIMENTAL RESULTS

Fig.5 shows the relation between the racking load and apparent shear strain in each specimen, and Table 4 shows the racking load for apparent shear strain of 1/300,1/200,1/120 and 1/60, the maximum load and shear strain at the point of the maximum loading. The allowable racking load of each panel estimated by the current design procedure is also compared with the maximum racking load of the specimens in Table 4. The allowable racking load of a wall panel with openings was estimated from the allowable racking load of blind walls of 1.82 meters in length which was obtained as follows:

$$\text{Allowable racking load per length} = \min. \begin{cases} P_{1/300} \\ 2/3\ P_{max} \end{cases} \times 3/4 \div 1.82$$

where $P_{1/300}$ and P_{max} are respectively the racking load for actual shear strain of 1/300 and the maximum load obtained from racking test of blind walls of 1.82 meters in length.

The allowable racking load of a wall panel with openings was obtained by multiplying the allowable racking load per length by the sum of the length of the blind walls whose length was greater than ninety centimeters according to the current design procedure. As the Building Standard Law allows that two thirds of the seismic load and wind load are supported by the blind walls whose length is greater than ninety centimeters and the remaining one third is supported by the non-bearing members like small walls etc., the allowable racking load was multiplied by 1.5.

The maximum load of specimens A-1 and 2 was almost the same as the allowable racking load, and that of specimens B-1 and 2 was approximately 60% greater than the allowable racking load. This indicates that the current design procedure may overestimate the racking resistance of a wall panel which consists of only slender blind walls and contains no small walls, while lintel walls contribute to increase the racking resistance of a wall panel having comparatively large openings. The maximum load of

specimens C-1 and 2 to F-1 and 2 was 3.1 to 5.3 times greater than the allowable racking load. This indicates that the current design procedure underestimates considerably the racking resistance of a wall panel which contains only small openings, and some rational design procedure is necessary to evaluate more precisely the racking resistance of wall panels.

THEORETICAL ANALYSIS

FUNDAMENTAL EXPRESSIONS. - For a shear element which consists of a frame and a single sheet of sheathing shown as in Fig.6, the horizontal load P_X, the vertical load P_y and the equilibrium expressions are :

$$P_X = \Sigma F_X(i) \cdot Y(i)/h \qquad (1)$$

$$P_y = \Sigma F_y(i) \cdot X(i)/a \qquad (2)$$

$$\Sigma F_X(i) = 0 \qquad (3)$$

$$\Sigma F_y(i) = 0 \qquad (4)$$

$$\Sigma F_X(i) \cdot Y(i) - \Sigma F_y(i) \cdot X(i) = 0 \qquad (5)$$

where $F_X(i)$ and $F_y(i)$ = X- and Y-component of a force acting along the surface of a sheathing sheet by the i-th nail, X(i) and Y(i) = the coordinate of the i-th nail along the X and Y- axis, a= the width of the element, and h= the height of the element (not always equal to the height of a sheathing sheet).

RACKING MODEL. - Tuomi's racking model for a light-frame wall [4] was applied to unsymmetrical deformation of a frame. The racking model is based on the assumptions that (1) all the fastenings between frame members are a pin, (2) bending deformations of a frame members are neglected, (3) deformation of a shear element was obtained by the sum of the shear deformation of a frame and that of a sheathing sheet and (4) each element is independent. Different from Tuomi's racking model, unsymmetrical deformation of a frame shown as in Fig.7 was assumed. Assuming

the sheet does not deform, X- and Y-components of the displacement of the i-th nail $\Delta X(i)$ and $\Delta Y(i)$ are :

$$\Delta X(i) = d_1 \cdot (1+t_1) \cdot Y(i)/h - d_1 t_1 \qquad (6)$$

$$\Delta Y(i) = d_2 \cdot (1+t_2) \cdot X(i)/a - d_2 t_2 \qquad (7)$$

where d_1 = the horizontal displacement of top plate, d_2 = the vertical displacement of right stud, t_1 = ratio of the horizontal displacement of bottom plate to that of top plate and t_2 = ratio of the vertical displacement of left stud to that of right stud.

LINEAR ANALYSIS. - Assuming the load-slip relation of a nail is linear, $F_x(i)$ and $F_y(i)$ are :

$$F_x(i) = k \cdot \Delta X(i) \qquad (8)$$

$$F_y(i) = k \cdot \Delta Y(i) \qquad (9)$$

where k= shear stiffness of a nail.

Substituting equations (6) to (9) into equations (1) to (4), P_x and P_y are expressed as the function of d_1 and d_2 .

$$P_x = A \cdot k \cdot d_1 \qquad (10)$$

$$P_y = B \cdot k \cdot d_2 \qquad (11)$$

in which

$$A = \frac{N \cdot \Sigma (Y(i)/h)^2 - (\Sigma Y(i)/h)^2}{N - \Sigma Y(i)/h} \qquad (12)$$

$$B = \frac{N \cdot \Sigma (X(i)/a)^2 - (\Sigma X(i)/a)^2}{N - \Sigma X(i)/a} \qquad (13)$$

$$t_1 = \frac{\Sigma Y(i)/h}{N - \Sigma Y(i)/h} \qquad (14)$$

$$t_2 = \frac{\Sigma X(i)/a}{N - \Sigma X(i)/a} \qquad (15)$$

where N= total number of nails.

Substituting equations (10) and (11) into equation (5), d_2 is expressed by d_1.

$$d_2 = d_1 \cdot A \cdot h/(B \cdot a) \qquad (16)$$

Shear strain of the element γ is obtained as the sum of the shear deformation of a frame γ_f and that of a sheathing sheet γ_s.

$$\gamma = \gamma_f + \gamma_s \qquad (17)$$

$$\gamma_f = d_1 \cdot (1+t_1)/h + d_2 \cdot (1+t_2) / a \qquad (18)$$

$$\gamma_s = P_x \cdot r_0 / (G \cdot a \cdot t_0) \qquad (19)$$

where G= shear modulus of elasticity of a sheathing sheet, t_0 = the thickness of a sheathing sheet, r_0 = ratio of the area of the element (a x h) to that of a sheathing sheet.

Rearranging equations (17) to (19) by substituting equations (10) and (16) into, P_x is :

$$P_x = K \cdot \gamma \qquad (20)$$

where

$$\frac{1}{K} = \frac{1+t_1}{A \cdot k \cdot h} + \frac{(1+t_2) \cdot h}{B \cdot k \cdot a^2} + \frac{r_0}{G \cdot t_0 \cdot a}$$

NON-LINEAR ANALYSIS. - If we express a force of the i-th nail F(i) by radical expression of the nail slip Δ (i), it becomes :

$$F(i) = \alpha \cdot \Delta (i)^{\beta} \qquad (21)$$

$$\Delta (i) = C_0(i) \cdot d_1 \qquad (22)$$

where

$$C_0(i) = \{ (1+t_1)Y(i)/h - t_1 \}^2 + \{ (1+t_2)X(i)/a - t_2 \}^2 (Ah/Ba)^2 \qquad (23)$$

$F_x(i)$ and Fy(i) are expressed as follows :

$$F_x(i) = F(i) \cdot \Delta X(i)/\Delta (i) \qquad (24)$$

$$F_y(i) = F(i) \cdot \Delta Y(i)/\Delta (i) \qquad (25)$$

Substituting equations (6)(7)(24) and (25) into, simultaneous equations (1) to (5) can be solved numerically by using iterative calculations. However this method usually requires tedious calculations. Then linear deformation of a frame was assumed instead of solving these non-linear equations. First the value of d_1 was fixed, and then d_2, t_1 and t_2 were calculated from equations (12) to (16). The internal energy absorbed by the nails I is :

$$I = \Sigma \int_0^{\Delta (i)} \alpha \cdot X^{\beta} \, dX$$

$$= \frac{\alpha \cdot C \cdot \gamma_f^{\beta+1}}{(\beta+1) \cdot D^{\beta+1}} \qquad (26)$$

where

$$C = \Sigma C_0(i)^{\beta+1}$$

$$D = (1+t_1)/h + (1+t_2) \cdot A \cdot h / (B \cdot a^2)$$

Assuming P_x is also obtained by radical expression of γ_f, the racking load P_x and the external energy E are :

$$P_x = \alpha' \cdot (h \cdot \gamma_f)^{\beta'} \qquad (27)$$

$$E = \alpha' \cdot h^{\beta'+1} \cdot \gamma^{\beta'+1} / (\beta'+1) \qquad (28)$$

Comparing equation (28) with equation (26), α' and β' are :

$$\alpha' = \alpha \cdot C / (D \cdot h)^{\beta+1}, \quad \beta' = \beta \qquad (29)$$

Consequently,

$$P_x = \frac{\alpha \cdot C \cdot \gamma_f^{\beta}}{h \cdot D^{\beta+1}} \qquad (30)$$

$$\text{or } \gamma = \left(\frac{h \cdot D^{\beta+1}}{\alpha \cdot C} \right)^{1/\beta} \cdot P_x^{1/\beta} + \frac{P_x}{G \cdot a \cdot t_0} \qquad (31)$$

CALCULATION OF RACKING RESISTANCE

The load-slip relation of a nail subjected to a shear force was estimated from racking test of blind wall panels whose length were 1.82 meters (See Fig. 10). The relation between the lacking load and actual shear strain was approximated by use of a least squares method as follows:

$$P_x = 1235 \cdot (\gamma / \gamma_{max})^{0.235} \qquad (32)$$

where $\gamma_{max} = 0.025$

Comparing equation (30) to equation (32), the load-slip relation of a nail was obtained as follows:

$$F = 119 \cdot (\delta / \delta_{max})^{0.235} \qquad (33)$$

where $\delta_{max} = 1.08$ (cm)

Fig. 11 shows the comparison of the load-slip relation obtained from single shear test of nail fastenings. The shear stiffness and strength of a nail estimated from racking test of blind wall panels were approximately 10 to 20 percent smaller in average than those obtained from single shear test of nail fastenings. It is considered the effects of the angle of the direction of a nail force to that of the fibers of plywood veneer and frame members, bending deformation of frame members and the slip of fasteners connecting them appeared sensitively. However the load-slip relation of a nail obtained from racking test of blind wall panels seems to represent more adequately the load-slip relation which connects a sheathing sheet to a frame of a wall panel than that obtained from single shear test of nail fastenings. Then the former was applied to computing the racking resistance of wall panels with openings.

The racking resistance of twelve wall panels were calculated as the sum of the shear resistance of each shear element (see Fig.8). The relation between P_x and γ was computed by changing the value of d_1. If the slip of certain nail exceeded δ_{max}, expression (32) was replaced with F=0 . Vertical force acting on each stud was obtained by the sum of Y-componete of shear force of a nail which connected a sheathing sheet to the stud.

Two models were assumed to compute the racking resistance of wall panels. Model(1) was based on the assumption that all the fastenings between frame members were a pin and there were no slips between frame members, and Model(2) allowed the pulling out of studs which were arranged at the end of blind panels or door openings and were not connected tightly to the foundation and horizontal members. For Model(2) the nails connecting a sheathing sheet to the studs arranged at the end of a door opening were neglected as shown in Fig.9 . Shear modulus of elasticity of the plywood sheathing was assumed to be 5,000 kgf/cm^2.

COMPARISON OF THEORY WITH EXPERIMENTAL DATA

The solution developed previously was compared with the experimental results in Tables 5 and 6 . The racking load for apparent shear strain of 1/200 of specimens A to F calculated from Model(1) was 5 to 80 percent greater than the experimental

results, and that calculated from Model(2) showed comparatively good agreement with the experimental results except for B-2. The tendency that the calculated values for specimens B-1 and 2 were greater than the experimental results would be caused by the assumption that frame members were rigid, and it seems to be necessary to consider the effect of bending of frame members to compute more precisely the shear deformation of a wall panel having large openings of door type[7]. The ultimate load calculated from Model(2) agreed however well with the experimental results within the maximum error of thirteen percent.

Fig.12 shows measured vertical displacements of studs and vertical force calculated from Model(1) for the specimens B-1 to F-1. It seems that the calculated vertical forces acting on the studs represent well the vertical displacements of the studs. Both calculated forces and measured displacements indicate that large vertical forces were concentrated at the studs arranged at the end of a panel or door openings, and they should be connected tightly to the foundation and horizontal members when full nail action is expected. Otherwise shear force of the nails which connect a sheathing sheet to the studs subjected to a large drawing force should be neglected in case of the computation of the racking resistance.

CONCLUSIONS

The results of this study lead to the following concluding statements:

1. The current design procedure is apt to overestimate the racking resistance of a wall panel which consists of only slender blind walls and contains no small walls, and underestimate considerably the racking resistance of wall panels which contains only small openings.
2. Large vertical forces were concentrated at the studs arranged at the end of a wall panel or door openings. These studs should be connected tightly to the foundation and horizontal members when full nail action is expected. Otherwise shear force of the nails which connect a sheathing sheet to the studs subjected to large drawing force should be neglected when the racking resis-

tance of a wall panel is computed.

3. The shear stiffness and strength of a nail fastening estimated from racking test of blind wall panels were approximately 10 to 20 percent smaller than those obtained from single shear test of nail fastenings. The effects of the angle of the fibers of sheathing material and frame members on the shear stiffness and strength of nail fasteners and those of bending deformation of frame members and the slip of the fastenings on the shear properties of wall panels should be studied more precisely to apply the load-slip relation of a nail obtained from single shear test of nail fastenings directly to the computation of the racking resistance of wall panels.

4. The solution developed previously agreed comparatively well with the experimental results. However this method has the tendency to overestimate slightly shear stiffness of wall panels having large openings of door type. This indicates that the effects of bending deformation of frame members should be considered to compute more precisely the shear stiffness of a wall panel having this type of openings. The ultimate load calculated from this solution however agreed well with the experimental results.

ACKNOWLEDGMENT

The writer should like to express his grateful thanks to JAPAN 2× 4 Homebuilders Association who supported this research and extended him their kind assistance.

REFERENCES

1. Building Standard Law, Enforcement Order No.56, Ministry of Construction, January 1982.
2. HIRASHIMA,Y., " Derivation of Racking Deformation Formula of Nailed Frame Panel" , Journal of the Japan Wood Research Society 27-2, February 1981.
3. KAMIYA,F., " Theoretical Studies on Racking Stiffness and Strength of Wooden Sheathed Walls" , Transactions of the Architectural Institute of Japan No.309, November 1981.
4. TUOMI,R.L. and McCUTCHEON,W.J., " Predicting Racking Strength of Light-frame Walls" , Preprint for ASCE Meeting,October 1977.
5. YASUMURA,M., " Influence of Opening on the Shear Properties of Plywood-sheathed Wall Panels" , Doctoral Dissertation Presented to Department of Forest Products, the University of Tokyo,1981.
6. YASUMURA,M.and SAKAI,H., " Racking Test of Wooden Frame Wall Panel with Various Openings" , Summary of Technical Paper of Annual Meeting 1985, the Architectural Institute of Japan, October 1985.
7. YASUMURA,M. and SUGIYAMA,H., "Shear Properties of Plywood-sheathed Wall Panels with opening",Transactions of the Architectural Institute of Japan No.338, April 1984

NOTATION

The following symbols are used in this paper:

a = the width of a shear element

d_1, d_2 = the horizontal displacement of top plate and the vertical displacement of right stud

E = the external energy

$F_x(i), F_y(i)$ = X- and Y-component of a force acting along the surface of a sheathing sheet by the i-th nail

$F(i)$ = a force acting on the i-th nail

G = shear modulous of elasticity

h = the height of a shear element

I = the internal energy

k = shear stiffness of a nail fastening

N = number of nails

P_x, P_y = the horizontal and vertical loads

r_0 = ratio of the area of the element to that of a sheathing sheet

t_1, t_2 = ratio of the horizontal displacement of bottom plate to that of top plate and ratio of vertical displacement of left stud to that of right stud

t_0 = the thickness of sheathing sheet

$X(i), Y(i)$ = the coordinate of the i-th nail along the X and Y-axis

α, β = constant

γ_f, γ_s = shear deformation of a frame and that of a sheathing sheet

γ = shear strain of a panel

δ = slip of a nail fastening

Table 1

	Type of Stress Bearing Wall	Multiplying Factor
(1)	Stress bearing wall nailed with 1st Class of structural plywood of not less than 9mm thickness on one side	3.5
(2)	Stress bearing wall nailed with 1st Class of structural plywood of not less than 7.5mm but less than 9mm thickness, 2nd Class of structural plywood of not less than 9mm thickness, hardboard of not less than 7mm thickness or particleboard of not less than 12mm thickness on one side	3
(3)	Stress bearing wall nailed with 2nd Class of structural plywood of not less than 7.5mm but less than 9mm thickness, hardboard of not less than 5mm but less than 7mm thickness or cemented wooden chip board of not less than 12mm thickness on one side	2.5
(4)	Stress bearing wall nailed with flexible board of not less than 6mm thickness, asbest parlite board of not less than 12mm thickness, cemented pulp board of not less than 8mm thickness, asbest silica calcium board of not less than 8mm thickness or magnesium carbonate board of not less than 12mm thickness on one side	2
(5)	Stress bearing wall nailed with gypsum board of not less than 12mm thickness or lumber of not less than 13mm thickness and not less than 21mm width to be placed diagonally on one side	1.5
(6)	Stress bearing wall nailed with sheathing fiberboard of not less than 12mm thickness or metal lathing sheet on one side (zinc coated metal sheet shall be 0.4mm thick or more and other metal lathing sheet shall be 0.6mm thick or more)	1
(7)	Stress bearing wall nailed with lumber of not less than 13mm thick and not less than 21cm wide to be placed horizontally on one side	0.5
(8)	Stress bearing wall nailed with the materials other than the (1) through (7) above on one side and when the Minister of Construction deems that it has same or more figure of factor as specified in (1) through (7) above	As decided by the Minister
(9)	Stress bearing wall nailed with the materials as specified in (1) through (8) on both sides	Factors to be added However, in no case factor can be more than 5.
(10)	Stress bearing wall with brace of not less than 18mm thickness and not less than 89mm width	0.5
(11)	Stress bearing wall as specified in (1) through (9) above with addition of brace per (10) above	Factors to be added However, in no case factor can be more than 5.

Table 2

	Building	Factor to be multiplied by floor space(Unit: cm per square meter)				
		One Story Building	Two Story Building		Three Story Building	
			First Floor	Second Floor	First Floor	Second Floor
(1)	The roof thatched with light materials like metal sheet,slate, asbesto slate, wood or the like	11	29	15	38	25
	The roof thatched with the materials other than above	15	33	21	42	30
(2)	District with maximum snowload of 1m	25	43	33	52	42
	District with maximum snowload of 1m and more but up to 2m (Interpolated factor between)	25 and 39	43 and 57	33 and 51	52 and 66	42 and 60
	District with maximum snowload of 2m	39	57	51	66	60

(1) Building in a district other than the heavy snow area (which is to be specified by the Executive Administrative Office in accordance with Article 86 of the Ordinance).
(2) Building in heavy snow area

Table 3

	District	Multiplying Factor to Plumb Measure Size (Unit: cm per square meter)
(1)	District as specified by the Executive Administrative Office as the strong wind area in accordance with Item 3, Article 46 of the Ordinance	More than 50 up to 75 as specified by the Executive Administrative Office in accordance with Item 3, Article 46 of the Ordinance
(2)	Other district than above	50

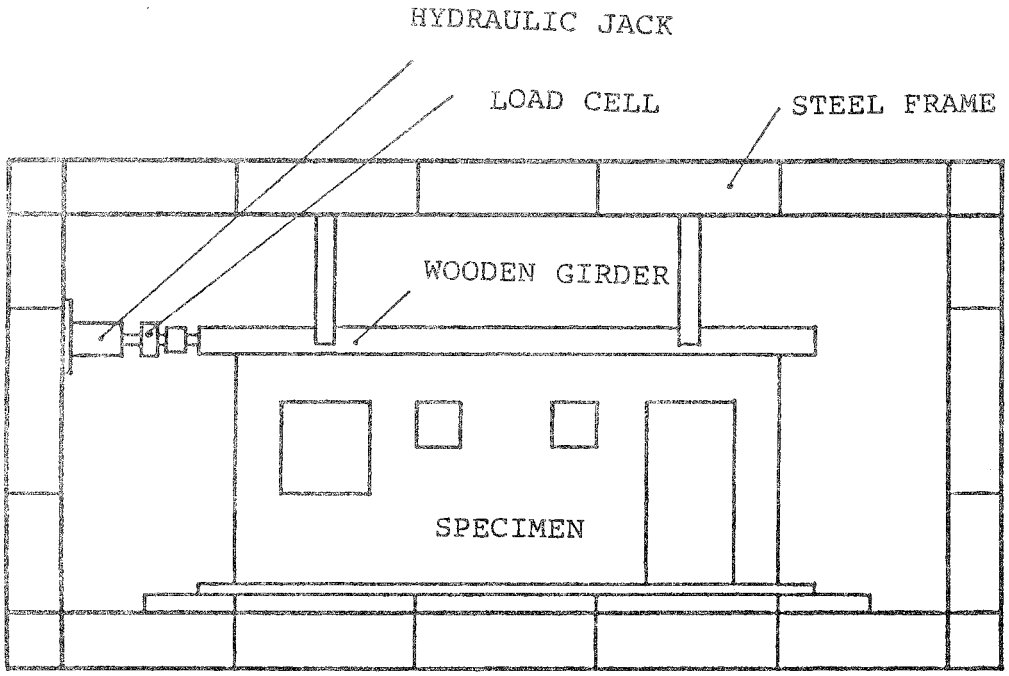


Fig.1 Apparatus for a racking test

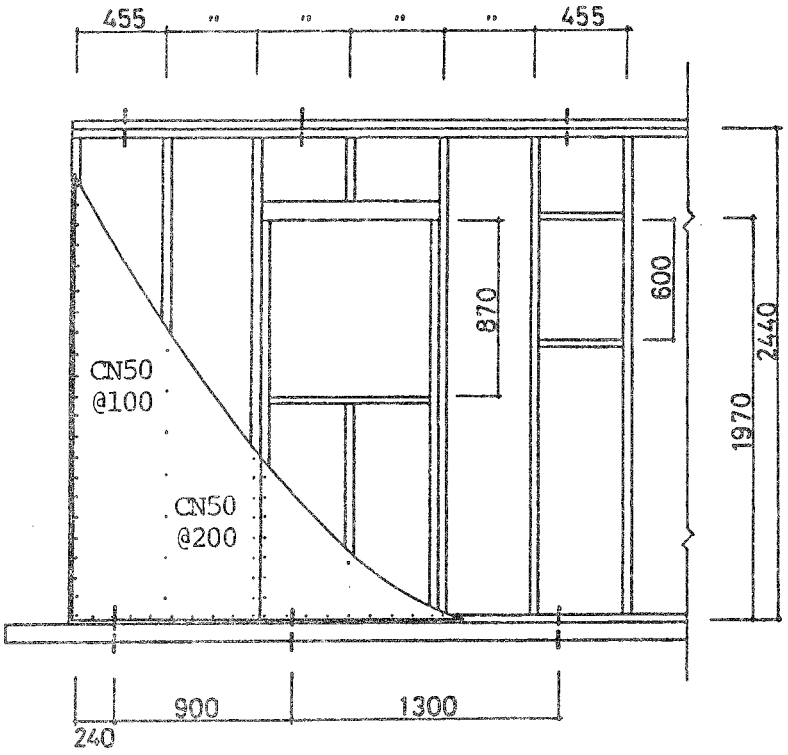


Fig.2 Structure of wooden frame wall

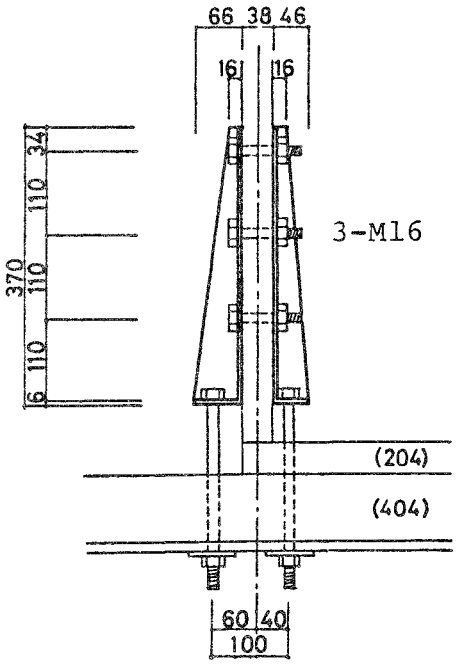


Fig.3 Connection of end studs to a steel frame

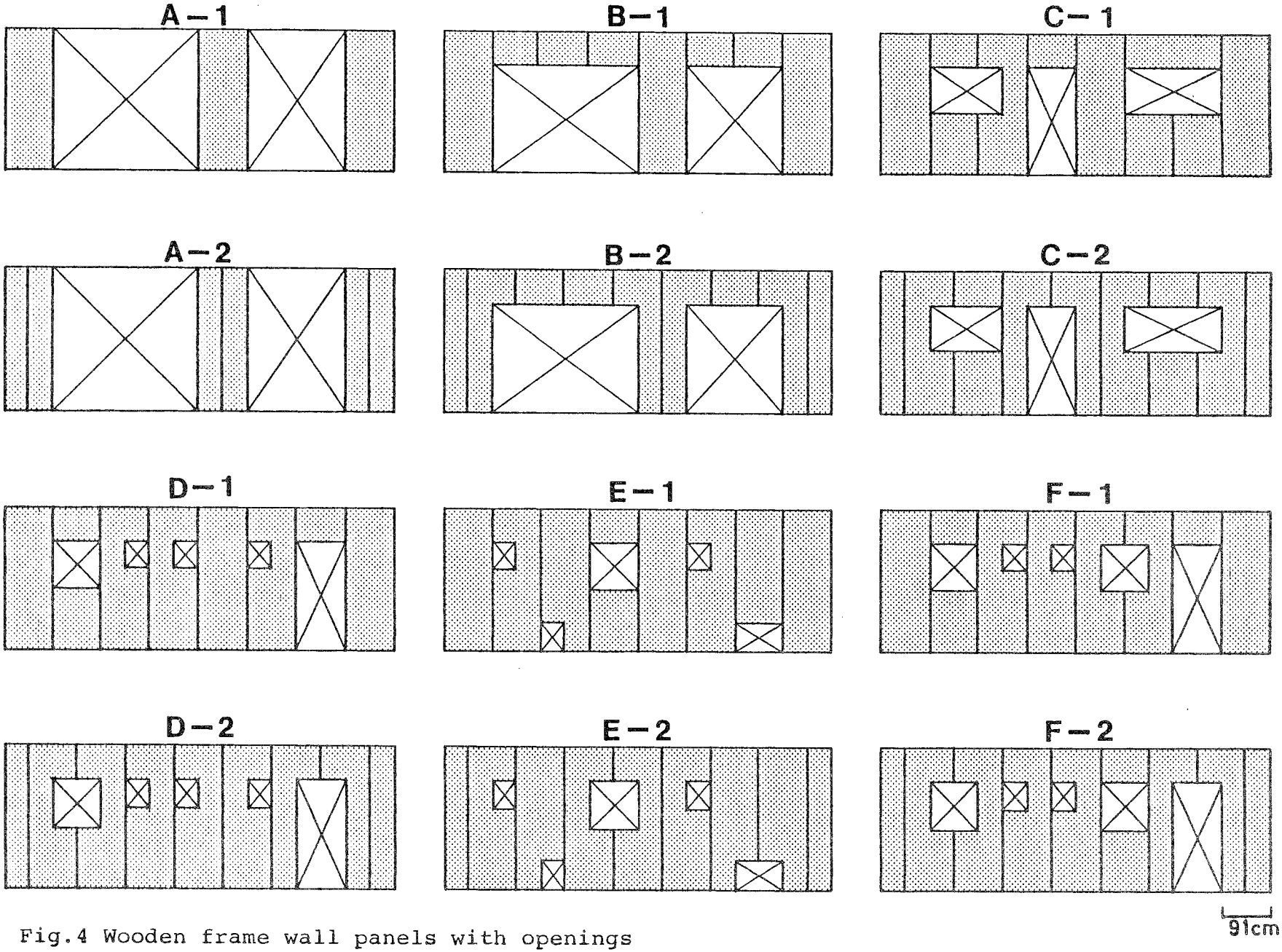


Fig.4 Wooden frame wall panels with openings

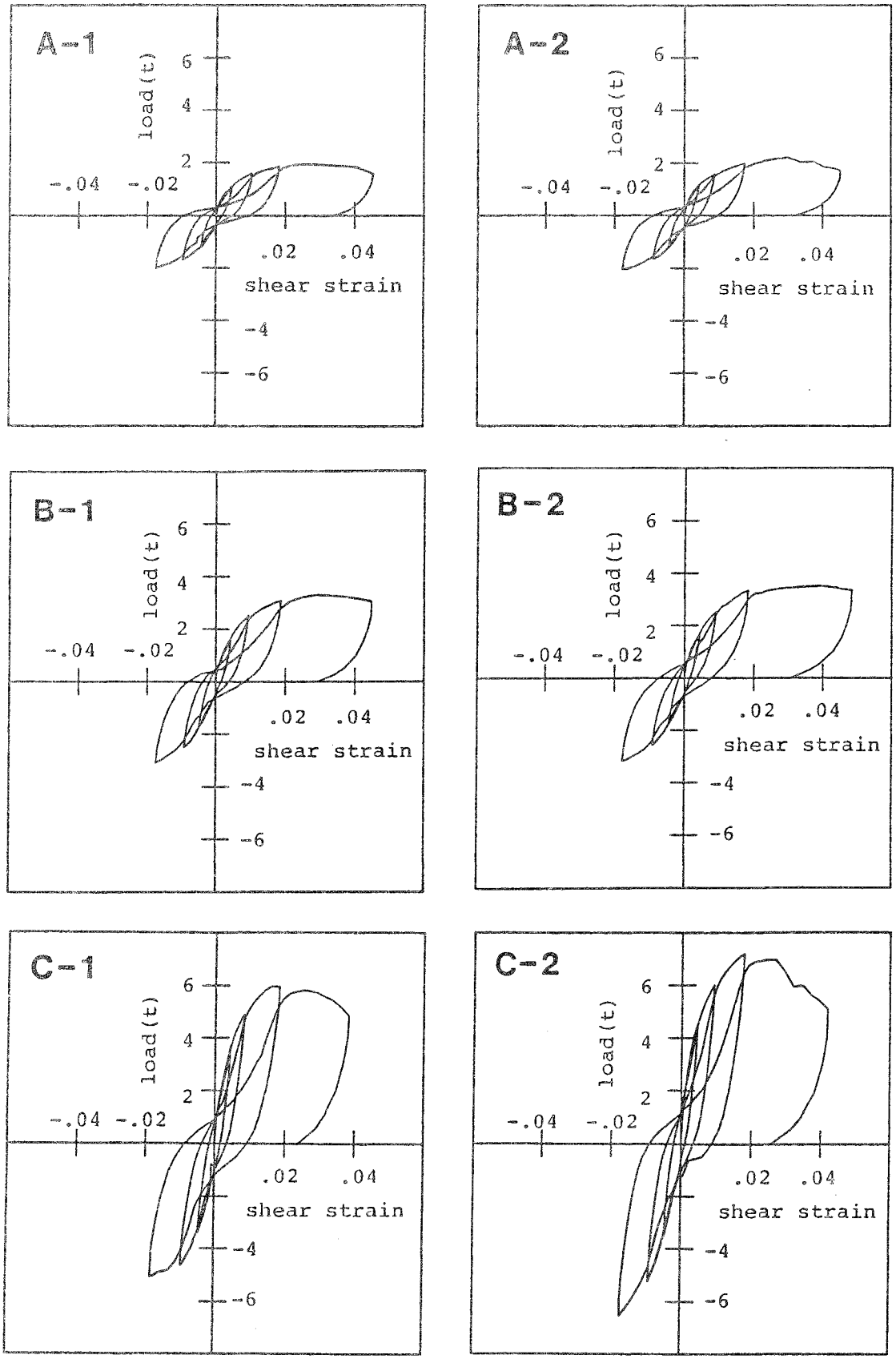


Fig.5 The relation between the racking load and apparent shear strain in specimens A,B and C.

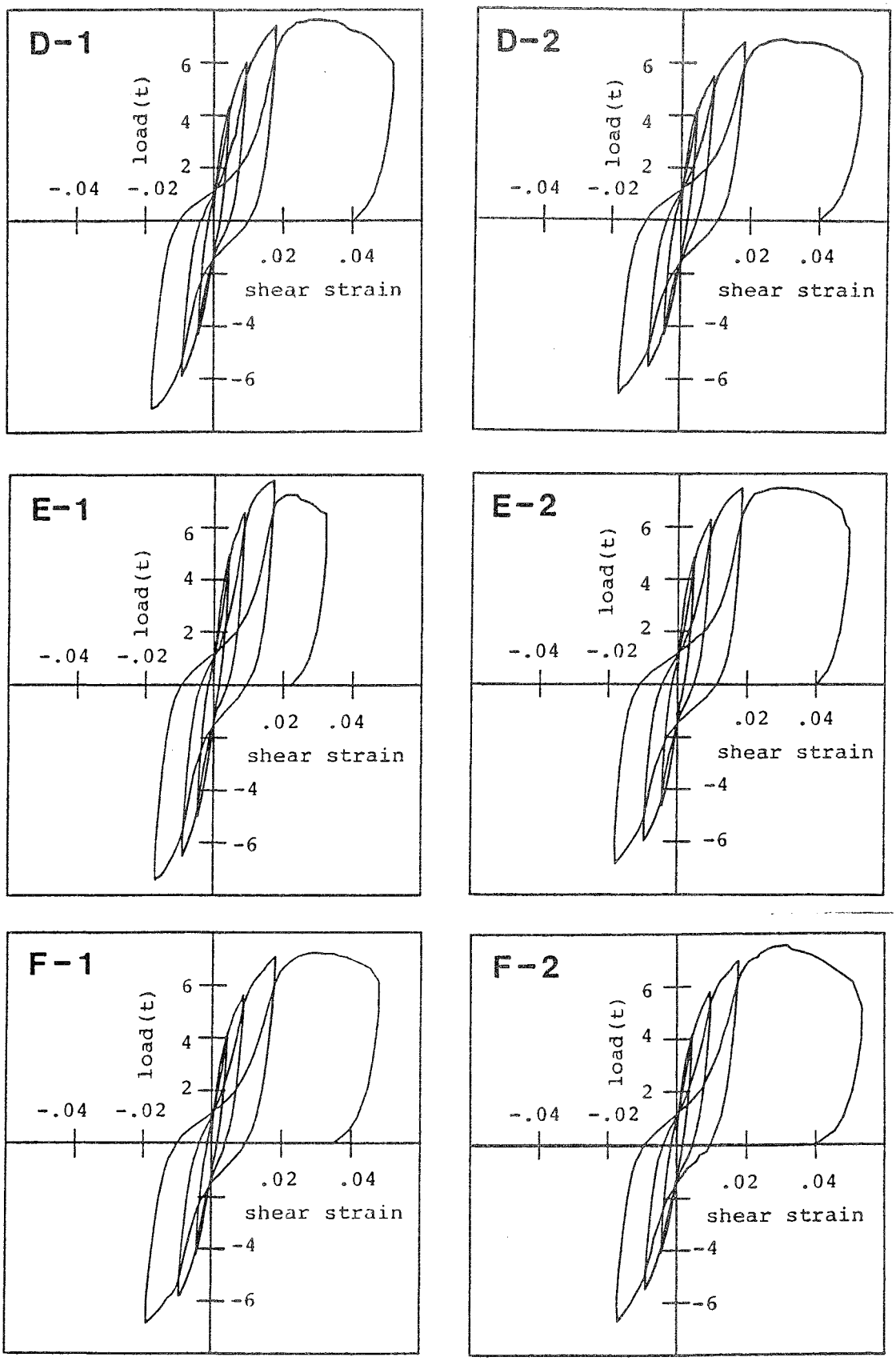


Fig.5 The relation between the racking load and apparent shear strain in specimens D,E and F.

Table 4. Racking test results of wall panels with openings

Specimen	Racking load for apparent shear strain of 1/300 (kgf)	1/200 (kgf)	1/120 (kgf)	1/60 (kgf)	Maximum load(2) (kgf)	Shear strain for maximum load	Total length of bearing walls(m)	Allowable racking load(1)(kgf)	Ratio (2)/(1)
A-1	1001	1220	1543	1897	2024	0.0174			
A-2	1049	1280	1593	1993	2204	0.0298	2.73	2099	1.0
av.	1025	1250	1568	1945	2114	-			
B-1	1444	1805	2386	3008	3280	0.0283			
B-2	1486	1874	2441	3172	3496	0.0366	2.73	2099	1.6
av.	1465	1840	2414	3039	3388	-			
C-1	2984	3648	4659	5465	5972	0.0159			
C-2	3405	4132	5380	6775	7196	0.0178	2.73	2099	3.1
av.	3195	3890	5020	6120	6584	-			
D-1	3705	4359	5655	7110	7632	0.0272			
D-2	3764	4338	5337	6531	6912	0.0286	2.73	2099	3.5
av.	3730	4349	5496	6821	7272	-			
E-1	4329	5075	6404	7582	7804	0.0172			
E-2	4115	4695	5843	6975	7472	0.0290	2.73	2099	3.6
av.	4222	4885	6124	7279	7638	-			
F-1	3637	4363	5517	6738	7228	0.0288			
F-2	3579	4214	5296	6762	7568	0.0313	1.82	1400	5.3
av.	3608	4289	5457	6750	7398	-			

(1) Obtained from the test results of blind walls of 1.82 meters in length as shown in Fig. 10 as follows:

$$Pa = \min \begin{cases} P1/300 \\ 2/3\ Pmax \end{cases} \times 3/4 \div 1.82 \times 1.5 \times (\text{The sum of the length of bearing walls of a wall panel with openings})$$

where, P1/300 and Pmax: the racking load for actual shear strain of 1/300 and the maximum load in blind wall panels

Table 5. Comparison of the experimental and calculated racking load for apparent shear strain of 1/200 (unit:kgf)

Specimen	Experiment	Calculated Model(1)	Ratio	Model(2)	Ratio
A-1	1220	2229	1.82	1534	1.25
A-2	1280	1826	1.43	1377	1.08
B-1	1805	2903	1.61	2207	1.22
B-2	1874	2927	1.56	2696	1.44
C-1	3648	4336	1.19	3988	1.09
C-2	4132	4454	1.08	4337	1.05
D-1	4359	4933	1.13	4586	1.05
D-2	4338	5051	1.16	4934	1.14
E-1	5075	5304	1.05	-	-
E-2	4695	5368	1.14	-	-
F-1	4363	4826	1.11	4479	1.03
F-2	4214	4771	1.13	4577	1.09

Table 6. Comparison of the experimental and calcurated ultimate racking load (unit:kgf)

Specimen	Experiment	Calculated Model(1)	Ratio	Model(2)	Ratio
A-1	2024	3589	1.77	2161	1.07
A-2	2204	3368	1.53	2392	1.09
B-1	3280	4660	1.42	3223	0.98
B-2	3496	4435	1.27	3934	1.13
C-1	5972	6905	1.16	6205	1.04
C-2	7196	6833	0.95	6518	0.91
D-1	7632	7936	1.04	7212	0.94
D-2	6912	7779	1.13	7496	1.08
E-1	7804	8473	1.09	-	-
E-2	7472	8548	1.14	-	-
F-1	7228	7715	1.07	7014	0.97
F-2	7568	7334	0.97	7006	0.93

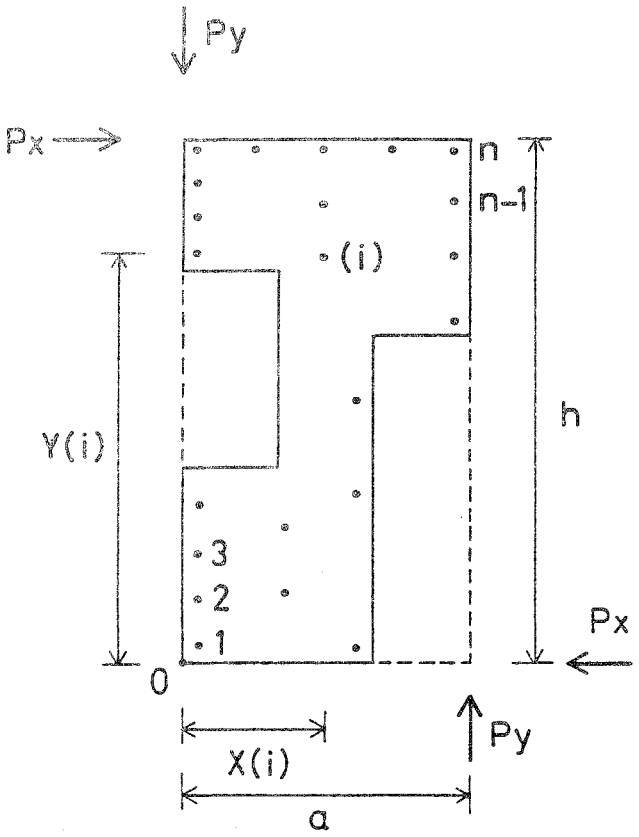


Fig.6 Shear element consisting of a single sheet of sheathing and a frame

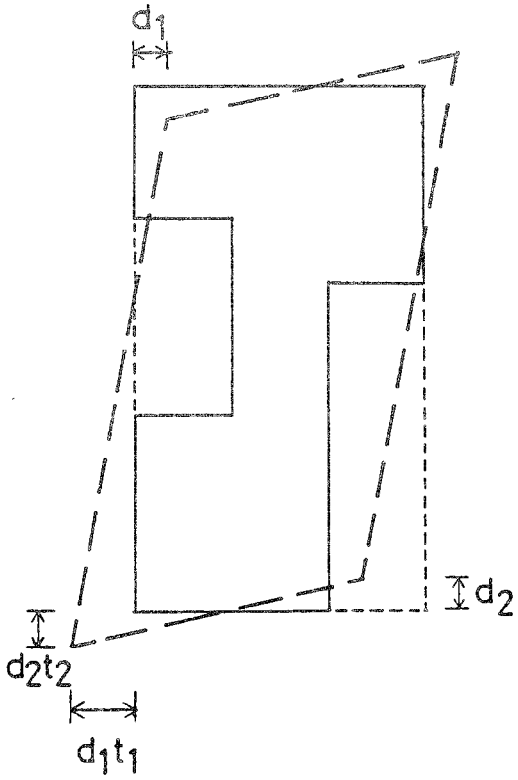


Fig.7 Racking model in which the frame distorts like a parallelogram, while the sheet retains the original form

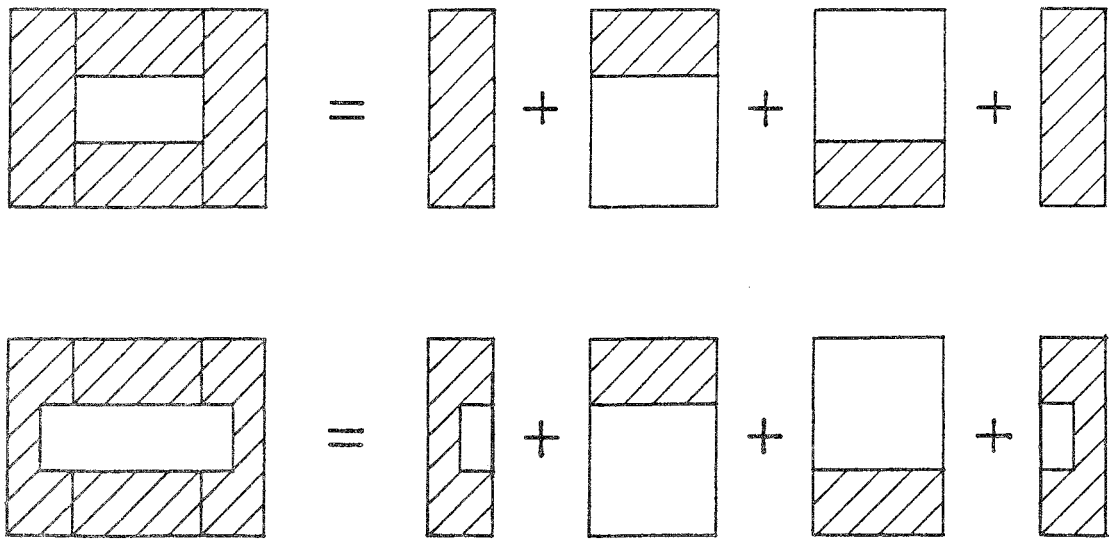
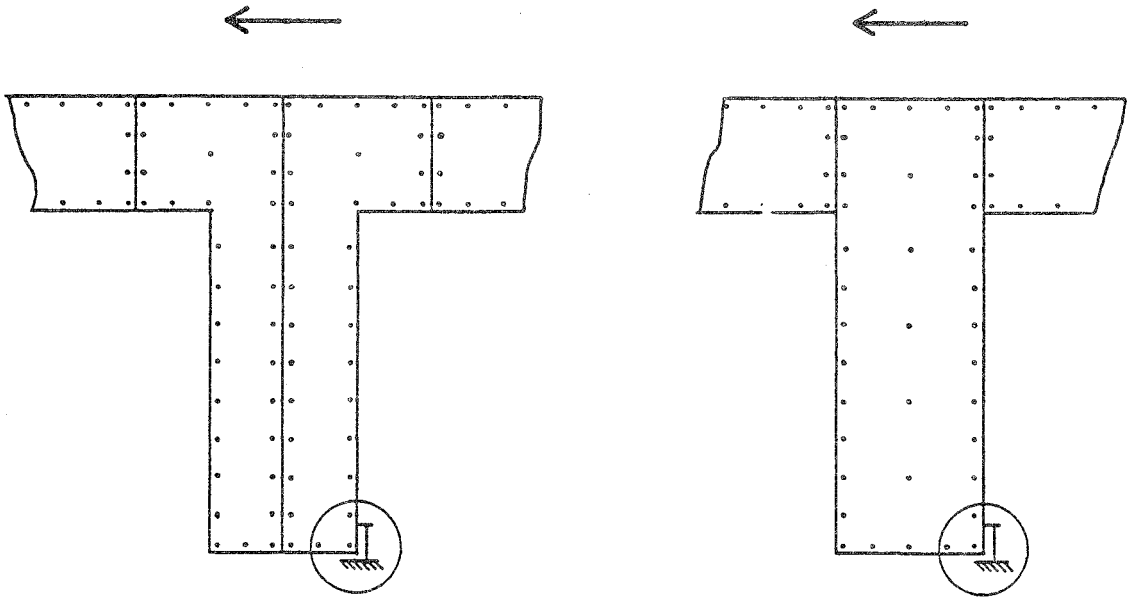
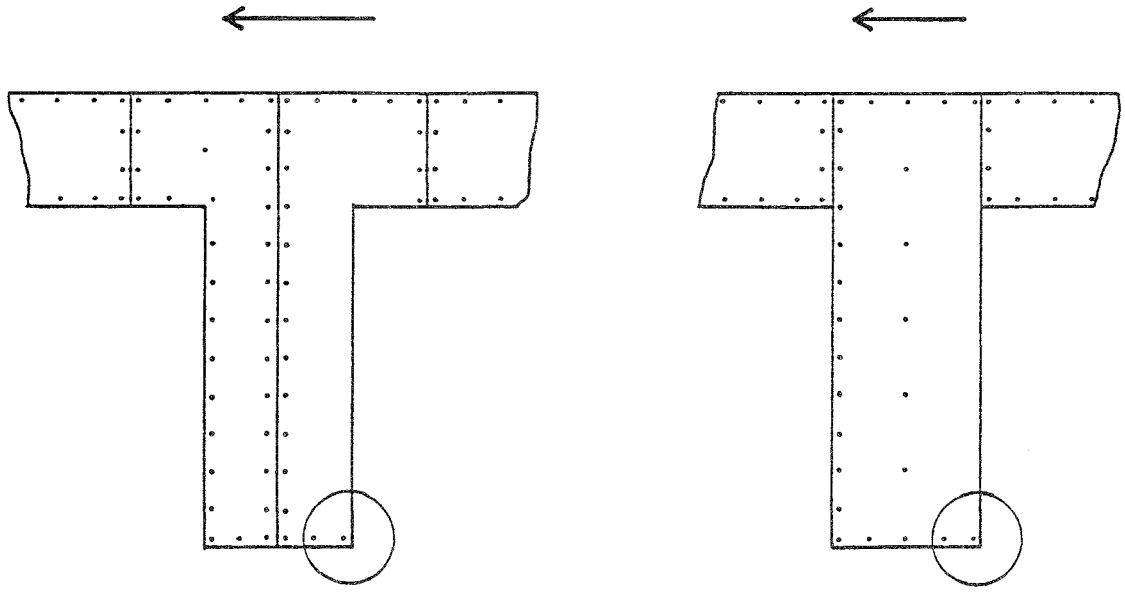


Fig.8 Racking resistance of a panel is obtained as the sum of the shear resistance of shear elements which are independant one another.



Model(1): all the fastenings between frame members are assumed to be a pin, and there is no slip between frame members.



Model(2): the nails connecting a sheathing sheet to the studs which are arranged at the end of a blind panel or a door opening and which are not connected tightly to the foundation and a horizontal member are neglected.

Fig.9 The asummption of the nail arrangement according to the fastening condition of the end studs.

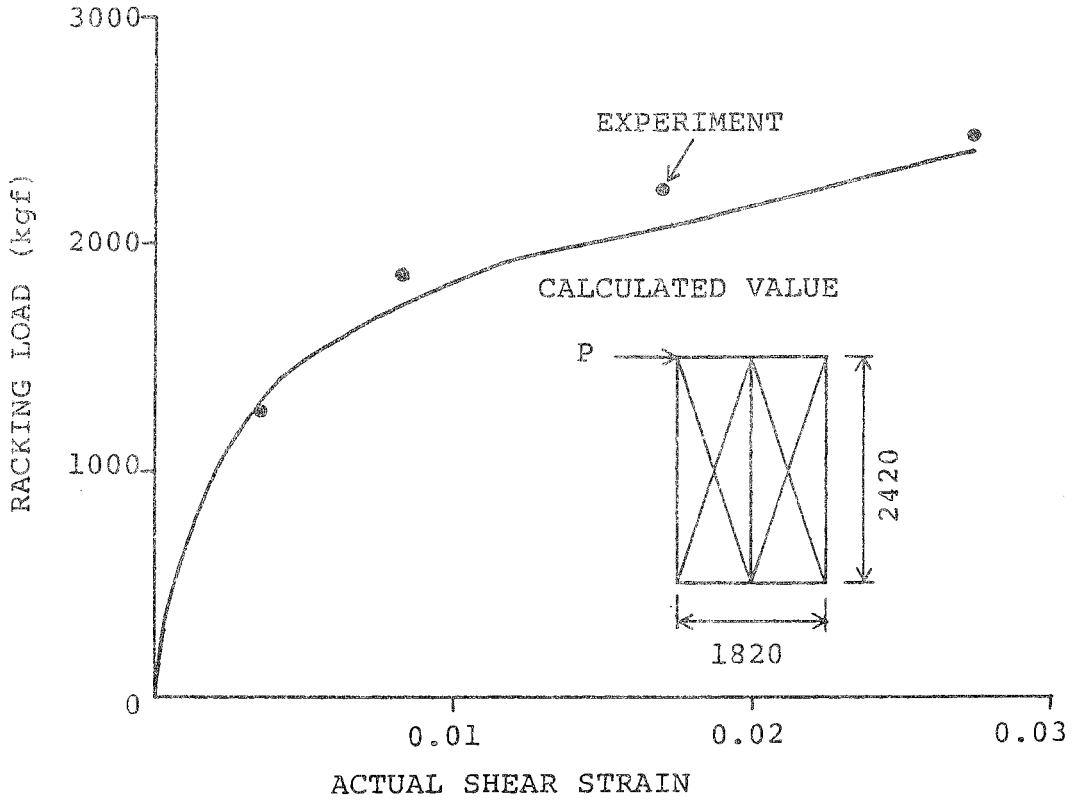


Fig.10 Comparison of the calculated and experimental load-shear strain relations.

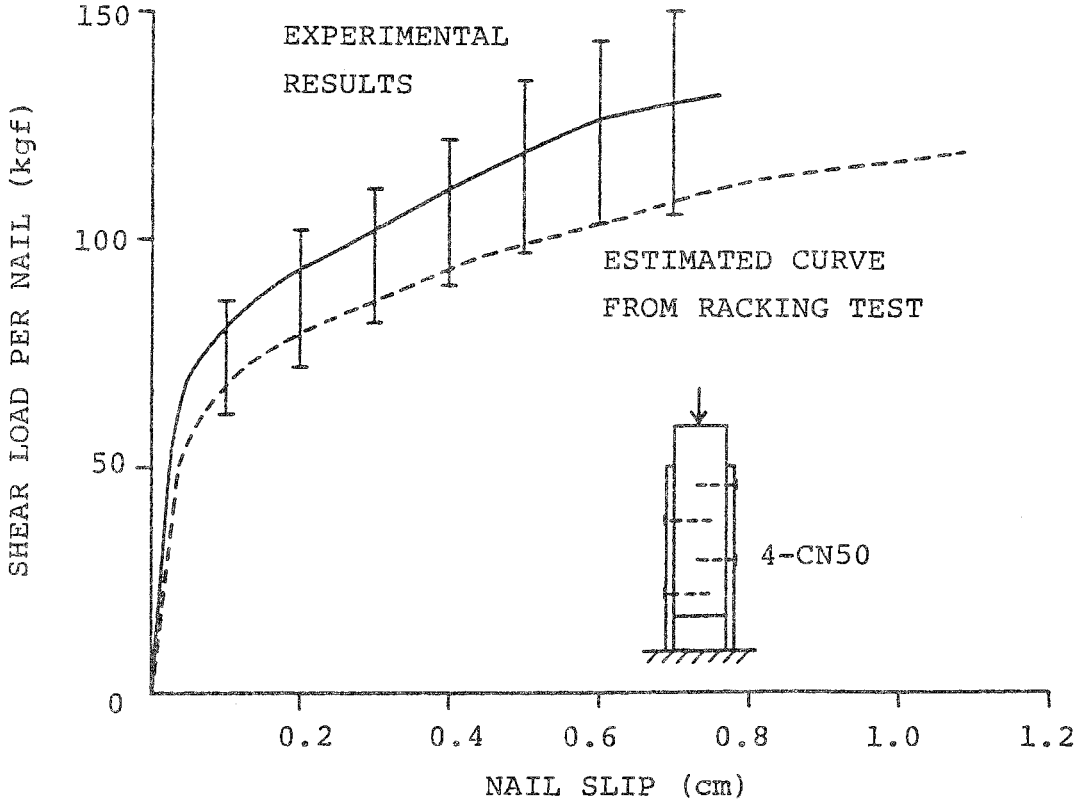


Fig.11 Comparison of the load-slip relation estimated from a racking test of panels as shown in Fig.10 with experimental results.

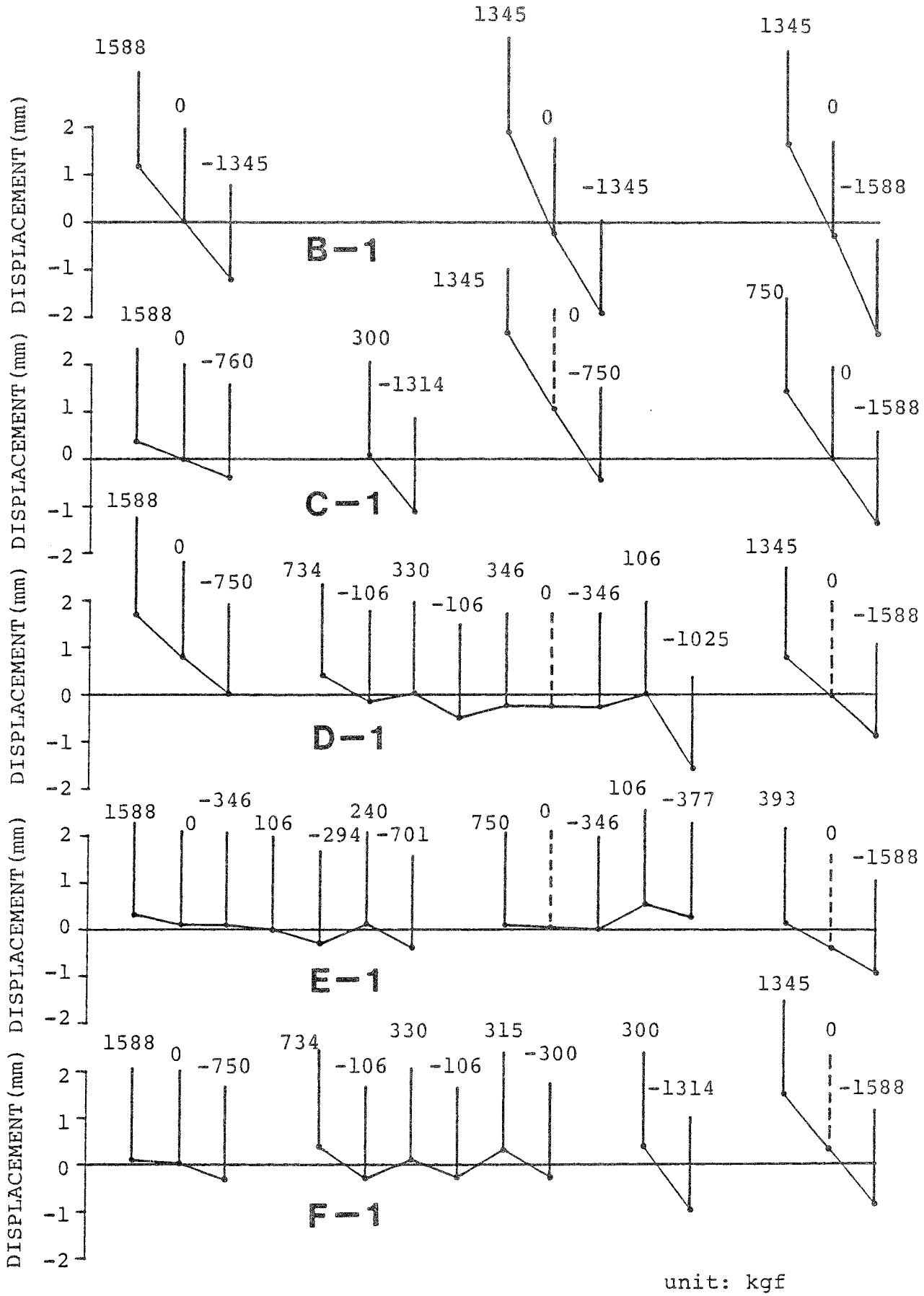


Fig.12 Measured vertical displacements of studs and vertical forces calculated from Model(1).

CIB-W18/19-15-4

INTERNATIONAL COUNCIL FOR BUILDING RESEARCH STUDIES AND DOCUMENTATION

WORKING COMMISSION W18 - TIMBER STRUCTURES

SOME EXPERIENCES OF RESTORATION OF TIMBER STRUCTURES FOR COUNTRY BUILDINGS

by

G Cardinale
Civil Engineering Consultants Florence
Italy
P Spinelli
University of Florence
Italy

MEETING NINETEEN
FLORENCE
ITALY
SEPTEMBER 1986

SUMMARY

A restoration work on the timber structures of a country building in Tuscany is here presented. Some recurrent details are illustrated, particularly regarding the connection between timber horizontal structures and vertical masonry structures. The operations tend to improve the safety of the structural assessment in seismic region, recovering the structural function of timber and avoiding its substitution with other material.

1. INTRODUCTION

The present work deals with some restoration works, particularly on timber structures of some old country building in Tuscany. The peculiarity of such buildings is that timber is utilized essentially for horizontal structures whilst vertical structures are made by stone or masonry, so that the structure is really a "composite type" structure. Thus in the restoration work the main problem is to study an efficient structural connection assessment between ancient and recent structural components and between stone masonry concrete and timber. Besides as the buildings are in seismic risk region another problem is to give improvement to the structural safety from this point of view.
The restoration work is also focused on the aim to leave to the timber structures the "dignity" of really resisting structures and not to relegate it to simple ornamental fitting. To arrive at this scope it is necessary to activate a structural collaboration between old timber beams and recent concrete slab through steel connectors fitted with epoxy resins to the timber beams and inserted in the concrete slab just like the connectors in steel concrete composite structures; on the other hand at the boundary of roofs reinforced concrete beams are inserted as in the following described, to connect effectively stone, masonry and timber.
The description of the works done represents a "case history" that can show some recurrent problems that are met in many restorations of buildings in Tuscany. The analysis of some simple but recurrent structural connections can constitute an useful suggestion to the designer of timber restoration, with the aim, as just said, of leaving to the timber full structural dignity.

2. DESCRIPTION OF THE BUILDINGS AND OF THE STRUCTURES

The most important building to restore is a complex, named "Vaccherecia" farm (see fig. 1, 2), whose probable construction date is around the half of 18th century. It was at first property of Caselli Count and presents the classic architectural disposition of a country residence. So near the main villa, many other rooms are present like a chapel, farm houses and a spinning

mills factory. During more recent years the property of "Vaccherecia" farm passes to an agricultural society which changes some rooms use to the storage of cereals or similar products. In the last years the property of this building togheter with other 15 country buildings passes to the Tuscany region administration. The aim of the new owner is to transform the buildings in popular houses mainly, to satisfy the high demand of residences. So instead of build new reinforced concrete houses and to leave to ruin these ancient buildings, the choice was to restore these and to adapt to the new use.
The structural assessment of the building is constituted by vertical structures all in stone and masonry walls with thickness 0.40-0.50 mt., and by horizontal structures all in timber.
The composition of horizontal structures is described in fig.3, 4, and can be described like follows.
For the floor structure:
-Main beams in chestnut wood (span 5-8.00 mt., distance 3-3.50 mt.)
-Secondary beams in fir wood (span 3-3.5 mt., distance 0.33 mt.)
-Bricks under pavement (flat pieces of dimensions 0.12x0.28x0.02mt.)
-Filling in sand
-Pavement (usually in brick)

For the roof structures:
-Main beams (or sometime timber trusses of king-post type - see fig.5) in chestnut or fir wood (span 5-8.00 mt., distance 2.8-3.2 mt.)
-Secondary beams in fir wood (span 2.8-3.00 m, distance 0.33 mt.)
-Bricks under roof covering (as in floor structures)
-Roof covering in flat and curved brick tiles.

It is to underline also some peculiar timber structure false ceilings called "cannicciati" with timber structure of span up to 8.00 mt. supporting a cane mat with superimposed plaster (see fig.6).

The analysis of the building deterioration made evident the following structural incoveniences:
-The timber structures of floors have deterioration levels very high with serious deflections expecially for secondary beams and in some cases also for main beams. The causes of such behaviours can be sumed in the following way:
a)-insufficient timber sections (span to height ratio up to 60);
b)-support conditions in masonry structures not accurately achieved;
c)-presence of up to three successive floor layers done each upon the preceding one;
d)-too high live loads one the floor zones used for cereals storage.

-The timber structures of roofs show the same incoveniences of the floor structures together with marked absence of maintenance. Besides also the edge masonry structures present a number of

vertical cracks consequently to the horizontal thrust of the roof structures due to inaccurate support execution.

Finally on a great part of timber structures for main and secondary beams it was evident the fungi and parasite attack which reduced also up to 50 % the resistant section of some beams.

3.RESTORATION OPERATIONS

The phases of restoration works concerning roof timber structures are the following:
- at first the dismounting of the old timber structure of the roofs, followed by the accurated analysis of the deterioration state of single components. The secondary beams are scarsely reutilized due to the high deterioration level, whilst the main beams have reached up to the 60 % of reutilization level;
- in the case of timber structures reutilized appropriate treatment against parasite attack has been done (Bayer Xilamon) and it is put attention in the omogeneus absorption of the product by the wood. To be noted that this prevention treatment is used also for the new wood which substitute the irrecoverable timber beams;
- a particular attention is paid in the assuring proper support conditions to the beams and contemporaneusly in the accurate connection between horizontal and vertical structures. At this scope a boundary reinforced concrete beam is constituted which collects all the ends of timber main beams of the roof. To reach a proper connection between reinforced concrete and timber, the ends of each beam is furnised whith a couple of steel flanges connected with timber through bolts in holes filled with epoxy resin, and with reinforced concrete beam through stirrups welded to the flanges. The details of such connections are shown in fig.7a, b, c, d;
- the secondary beams of the roof are almost generally substituted by chestnut wood timber beams three years seasoned. Over the brick pieces under covering, a concrete slab 0.04 is poured, and the reinforcement in electrically welded net is connected with the secondary timber beams through nails 0.04 mt. diameter.
- for the roof also a functional improvement is reached through the insertion of an insulation layer between the roof tiles and the timber structure (see fig.8);

Of different type is the restoration operations on the floor slabs:
- it is impossible to achieve an edge reinforced concrete beam as in the roof, so that it is necessary to operate in the reconstitution of the support for every beam end. The support is reconstituted inserting steel plates under the timber beam and contemporaneusly making concrete iniections in the masonry zones at the support. In some cases are inserted tie steel bars through

the separation wall to connect two contiguous floor slabs.
- it is created a composite wood concrete section through insertion of steel connectors fixed in holes of timber structures through epoxy resin expecially for secondary beams. This operation is achieved for three reasons: first for limiting the deflection of the secondary beams; second to guarantee the effective connection between concrete and timber due to variation of humidity and fluage effects; third to reach infinite stiffness in its own plane of the floor slab to improve resistance to seismic effects of the structural complex. The secondary beams are verified through the technique outlined in (ref.1,2) tacking into account in the specific case no sliding between the timber beam and the concrete slab, i.e. in the hypothesis that the entire section remains plane after the deformation. The fluage effects are took into account with the fictitious E modulus technique used also for steel concrete composite beams (ref.3,4).

4. CONCLUSIONS

Often in restauration work of simple timber structures a hurried operation is roughly to substitute timber beams with steel or reinforced concrete beams. This work tends to demonstrate that with simple connection details it is possible to restore timber with timber, without reduction of structural safety. It is hopeful that more experimental and theoretical work will be developed in the field of the behaviour of composite timber concrete beams so that these techniques will be applied currently in engineering practice.

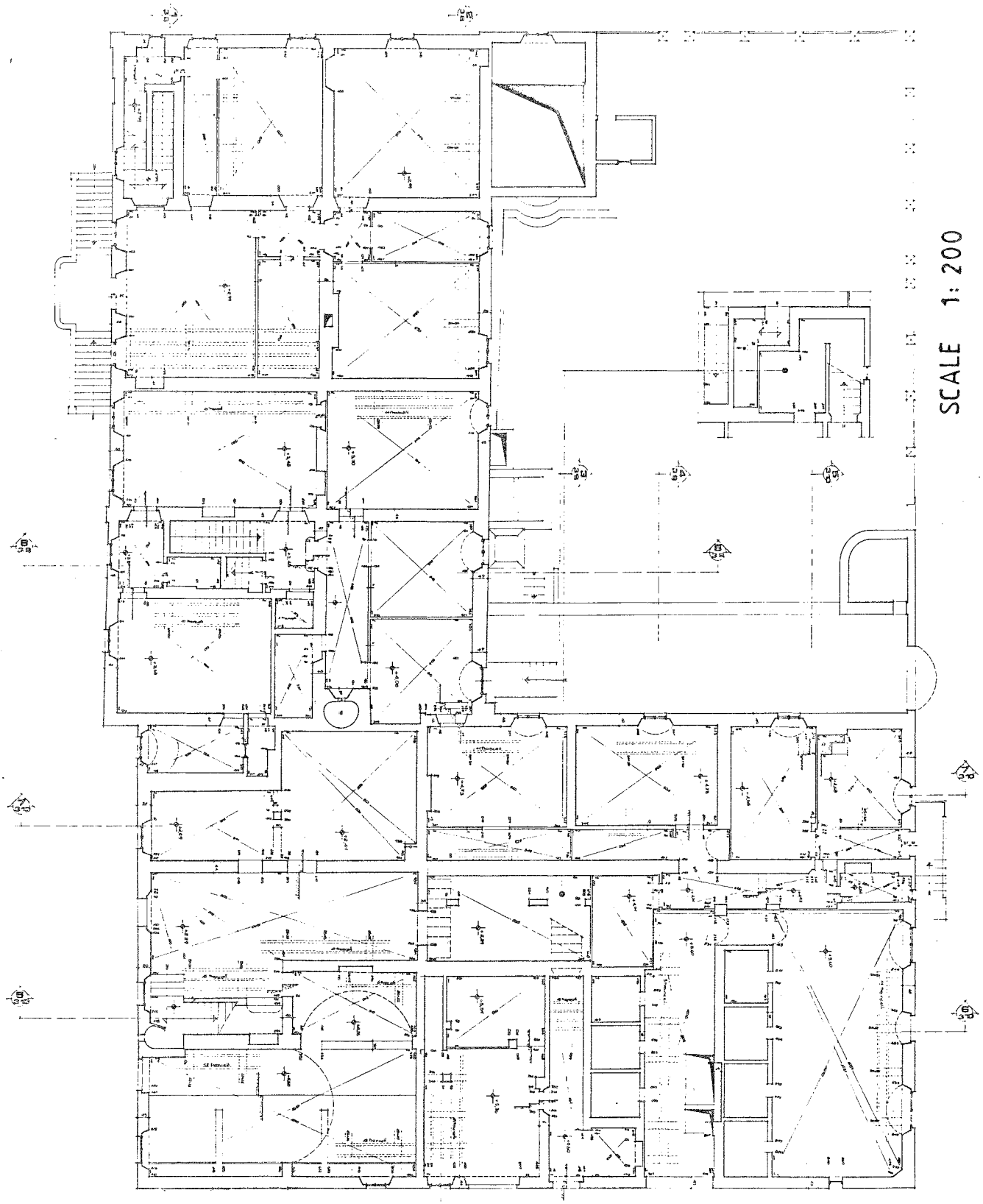
5. REFERENCES

1. G.TURRINI, M.PIAZZA "Il recupero dei solai in legno", RECUPERARE n.5-6-7, 1983
2. P.SPINELLI "Recupero e verifica delle strutture in legno: problemi strutturali e normativi", INARCOS, n.451, 1984
3. P.MATILDI, M.MELE "Impalcati a piastra ortotropa ed in sistema misto acciaio-calcestruzzo", CISIA, 1972
4. "Regles de calcul et de conception des charpentes en bois", Regles C.B. 71, mod. 1975, Eyrolles, Paris

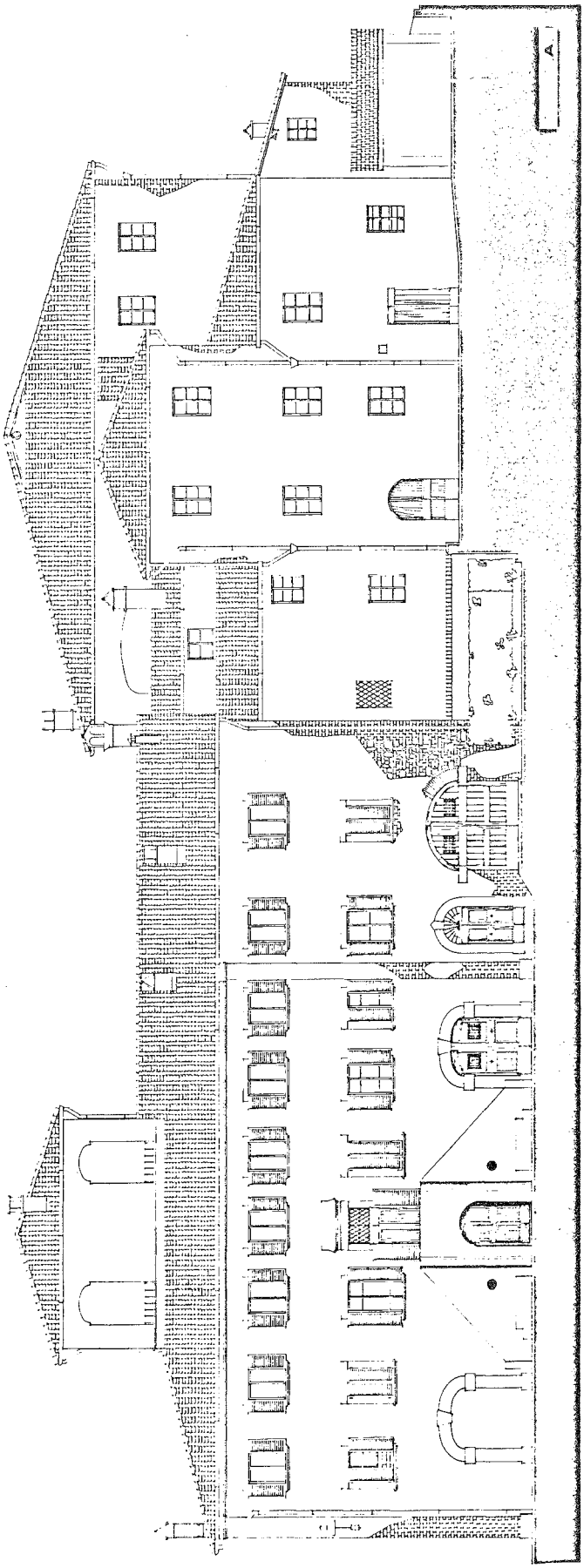
The "Vaccherecia farm" restoration design is conducted by G.Cardinale and P.Spinelli engineers, and by L.De Filla and G.Merlini architects. The property is of Tuscany Region. Director of the works executed by "La Poggio" srl firm is G.Cardinale engineer.

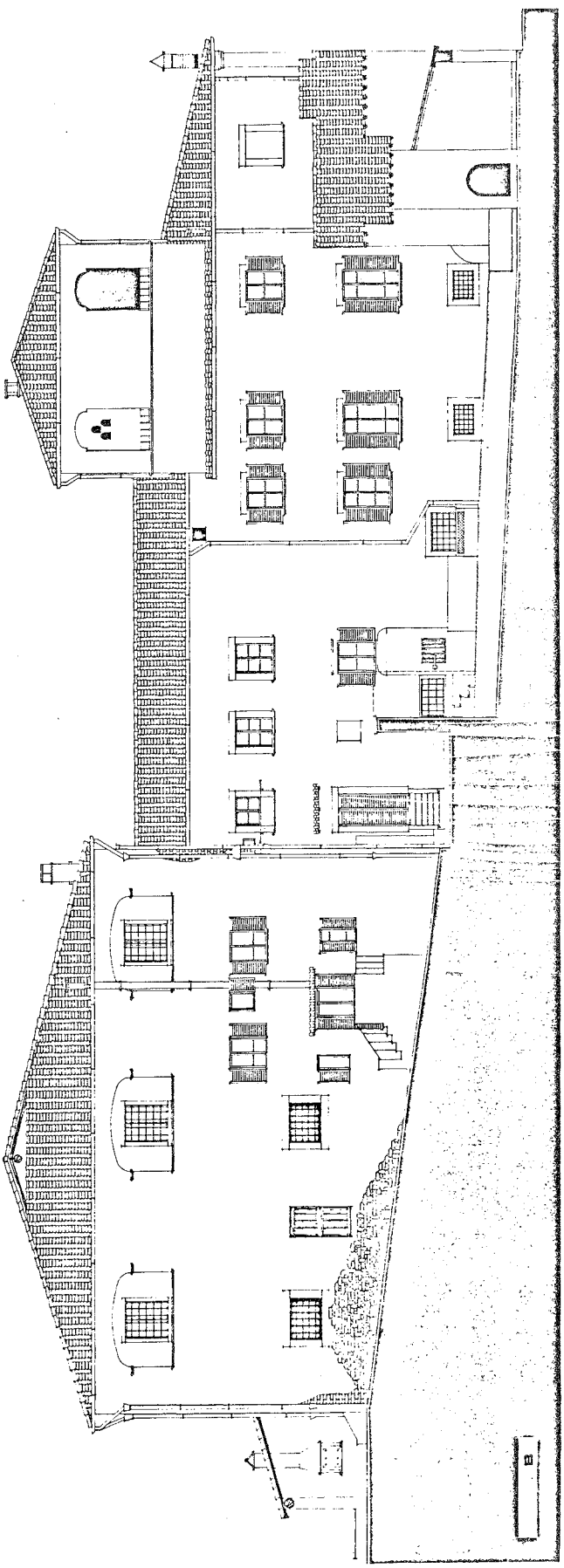
CAPTIONS OF FIGURES

FIG. 1 - Plan of "Vaccherecia farm".
FIG. 2 - Elevation of "Vaccherecia farm".
FIG. 3 - Detail of floor structure.
FIG. 4 - Detail of roof structure.
FIG. 5 - King-post type truss.
FIG. 6 - False ceiling structure callled "cannicciati".
FIG. 7a,b,c,d - Connections with steel flanges between roof beams and trusses reinforced concrete edge beam.
FIG. 8 - Detail of roof insulation.

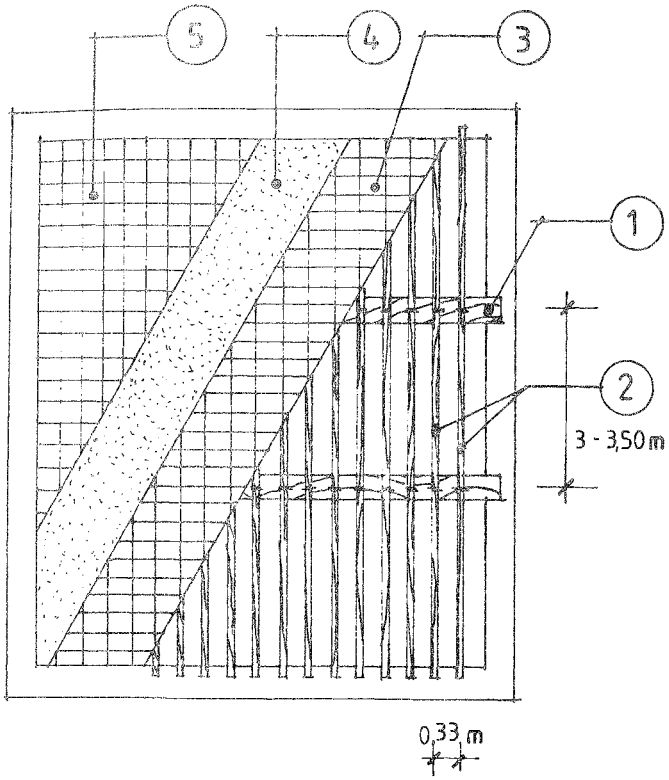


- FIG. 1 -

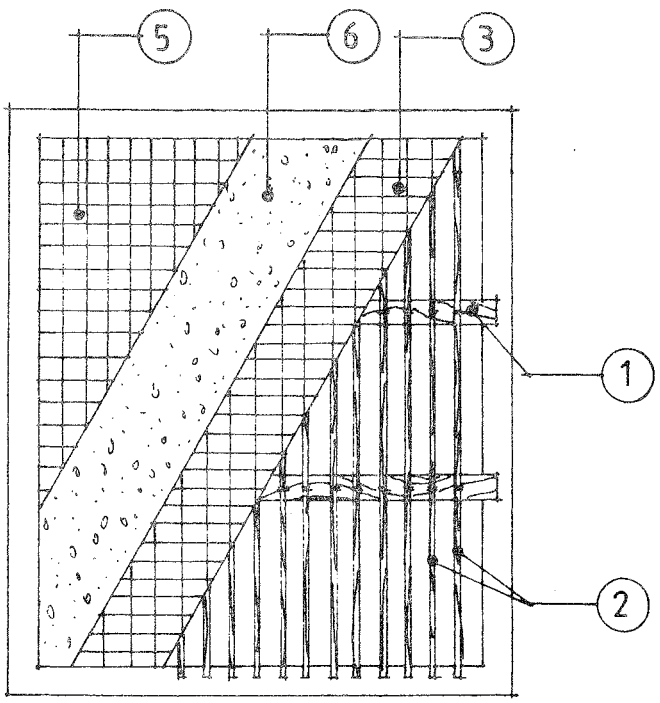




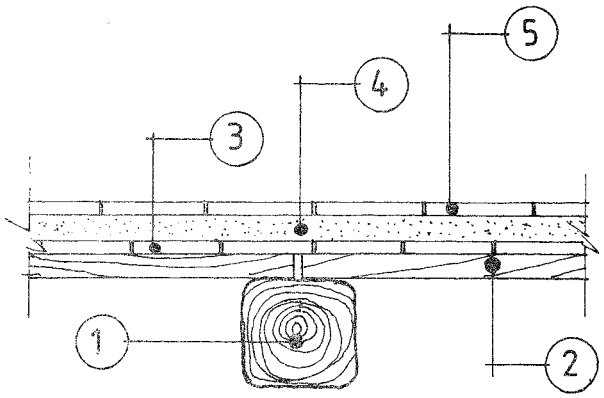
- FIG. 2 -

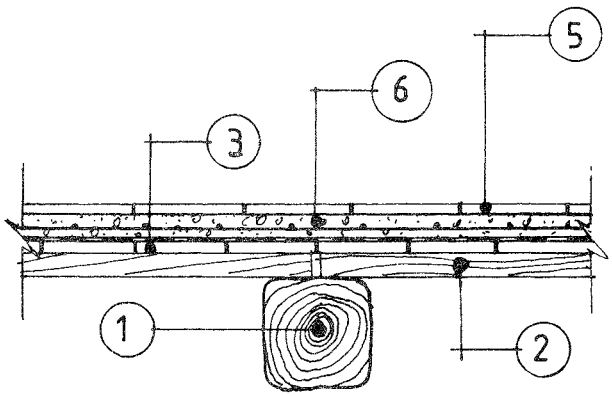


ORIGINAL SITUATION



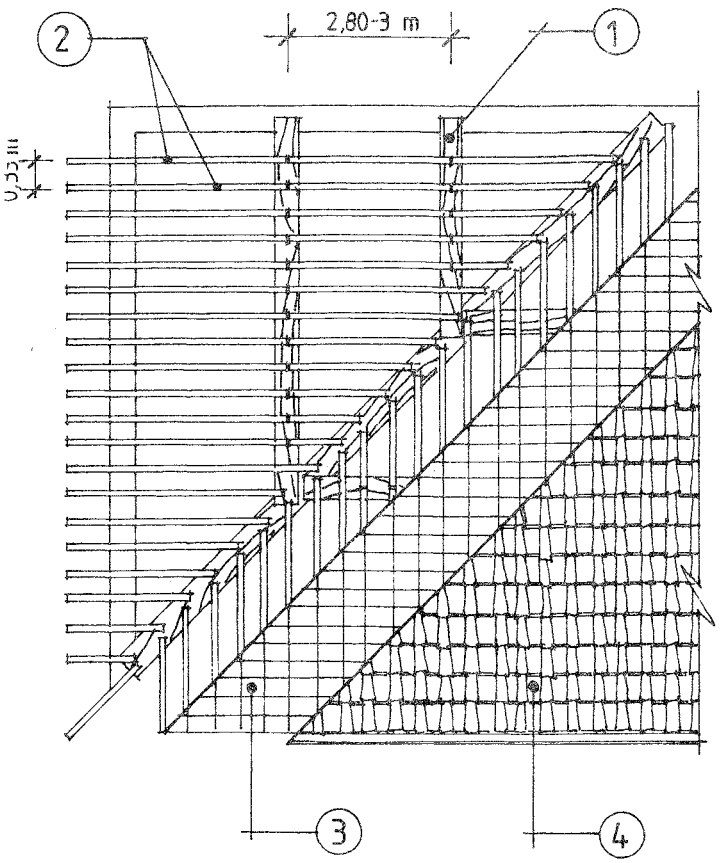
RESTORED SITUATION

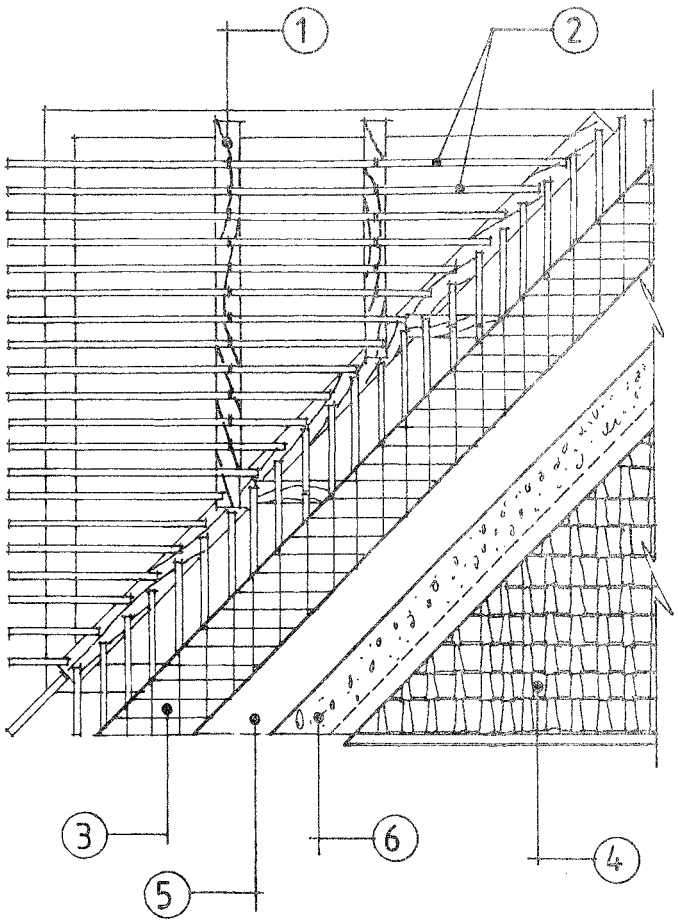




1. MAIN BEAMS IN CHESTNUT WOOD
2. SECONDARY BEAMS IN FIR WOOD
3. BRICKS UNDER PAVEMENT
4. FILLING WITH SAND
5. PAVEMENT
6. CONCRETE SLAB WITH E.W. NET

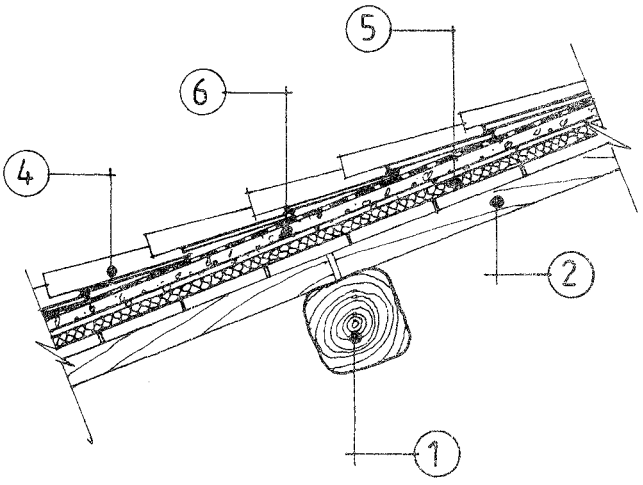
-FIG. 3-

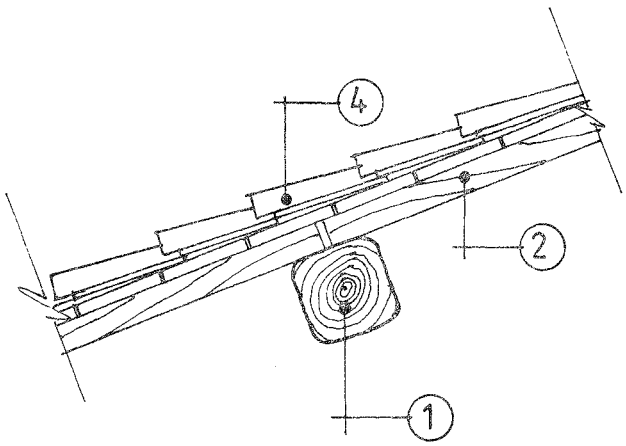




ORIGINAL SITUATION

RESTORED SITUATION





(1) MAIN BEAMS IN CHESTNUT WOOD

(2) SECONDARY BEAMS IN FIR WOOD

(3) BRICKS UNDER COVERING

(4) BRICK TILES

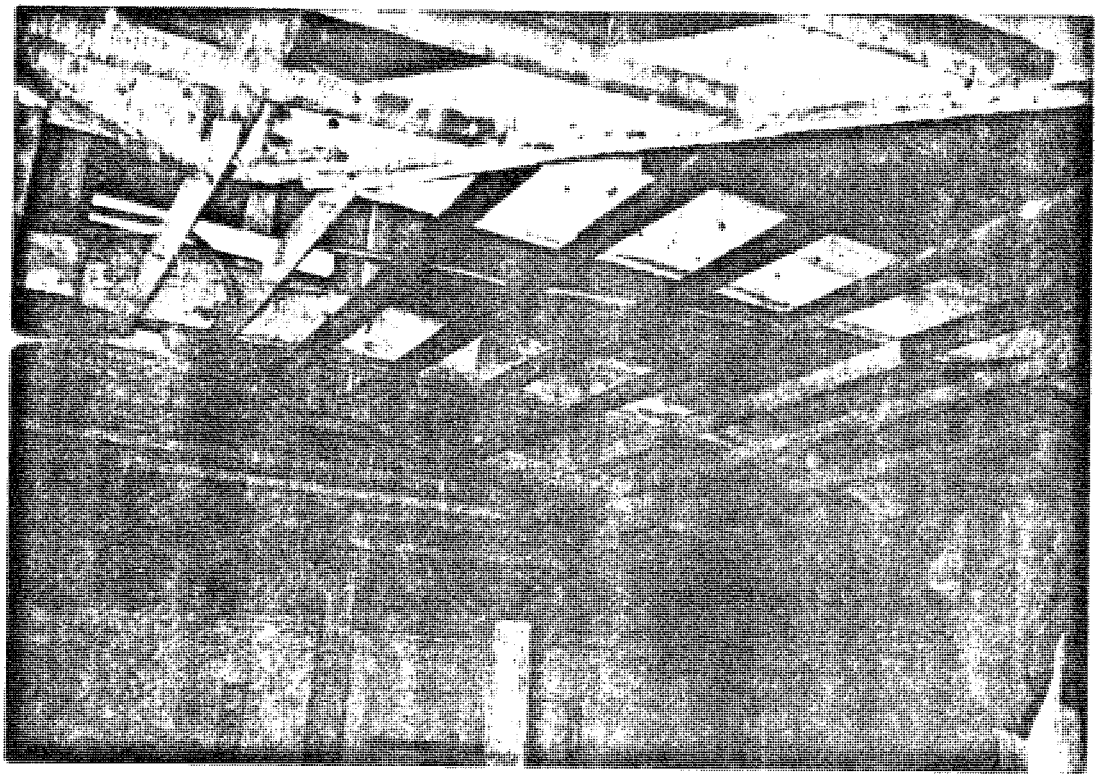
(5) INSULATION

(6) CONCRETE SLAB WITH E.W. NET

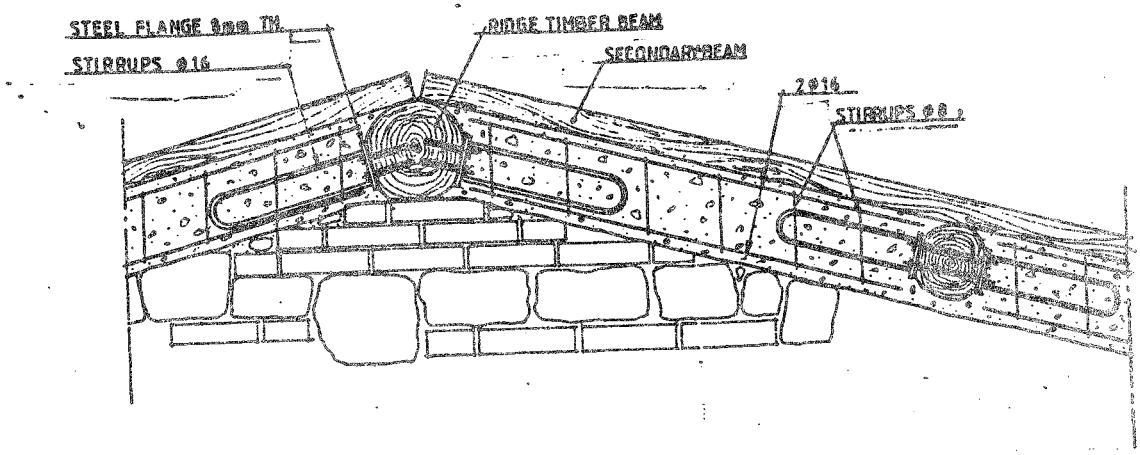
- FIG. 4 -

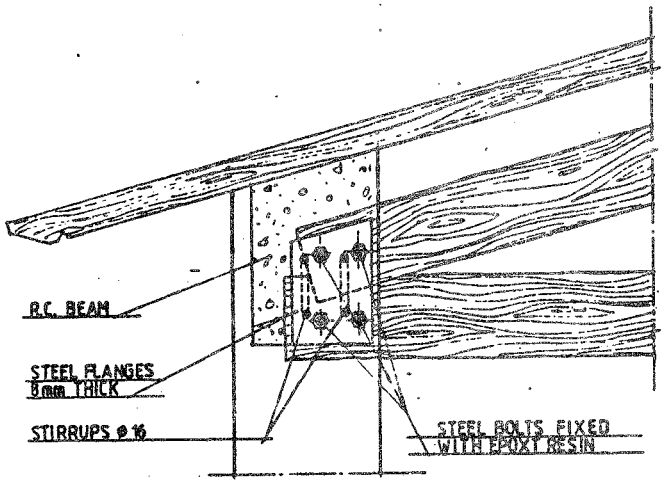


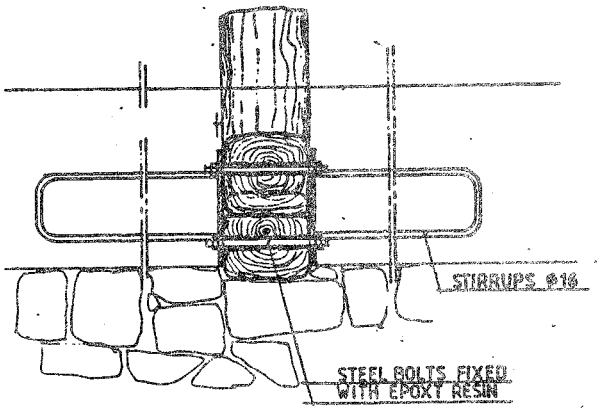
- FIG. 5 -

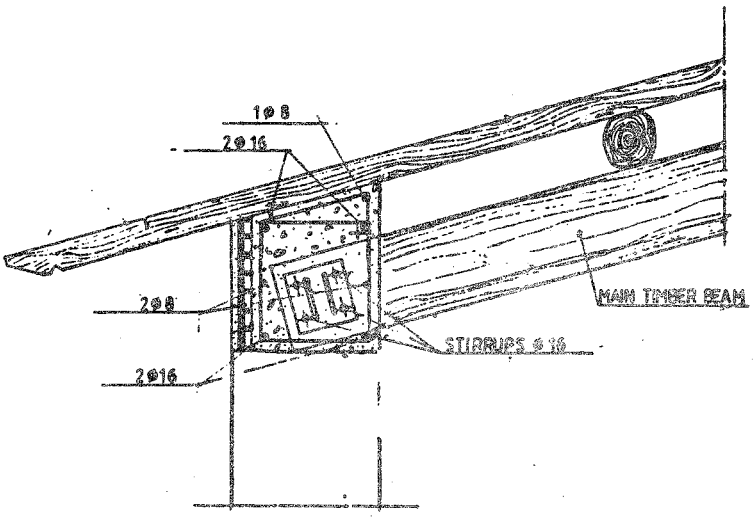


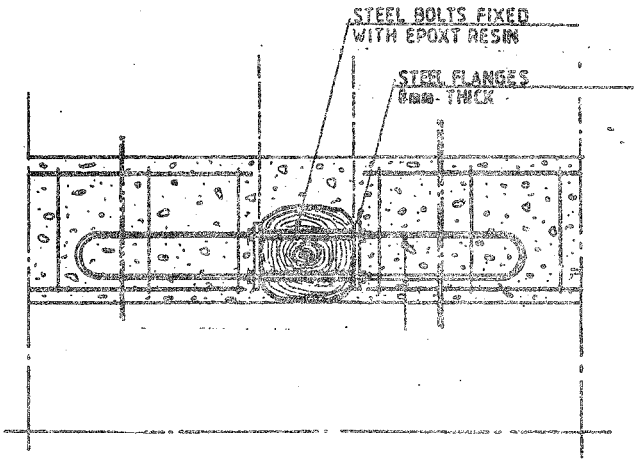
- FIG. 6 -


STEEL FLANGE 8mm TH.
STIRRUPS ø16
RIDGE TIMBER BEAM
SECONDARY BEAM
2ø16
STIRRUPS ø8

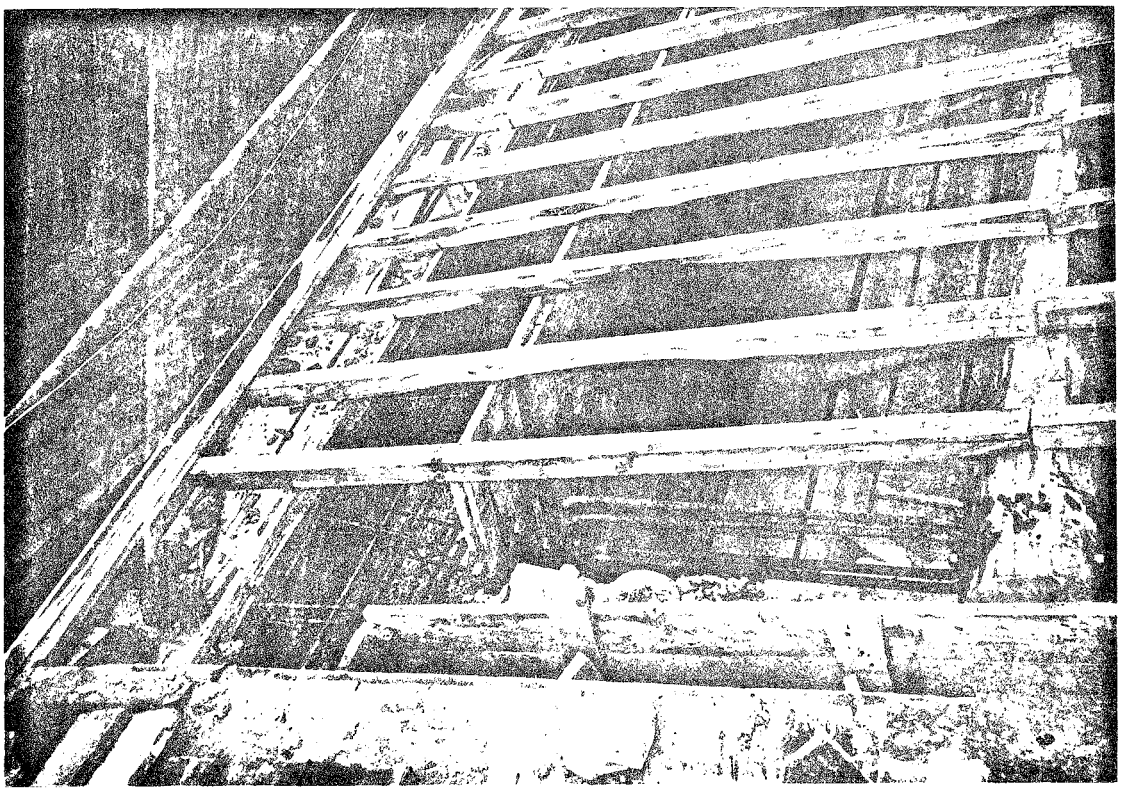

R.C. BEAM
STEEL FLANGES
8mm THICK
STIRRUPS ø16
STEEL BOLTS FIXED
WITH EPOXY RESIN


STIRRUPS ø16
STEEL BOLTS FIXED
WITH EPOXY RESIN


1ø8
2ø16
2ø8
2ø16
MAIN TIMBER BEAM
STIRRUPS ø16


STEEL BOLTS FIXED
WITH EPOXY RESIN
STEEL FLANGES
8mm THICK

- FIG. 7, a, b, c, -



- FIG. 7, d -



- FIG. 8 -

CIB-W18/19-15-5

INTERNATIONAL COUNCIL FOR BUILDING RESEARCH STUDIES AND DOCUMENTATION

WORKING COMMISSION W18 - TIMBER STRUCTURES

NON-DESTRUCTIVE VIBRATION TESTS ON EXISTING WOODEN DWELLINGS

by

Y Hirashima
Forestry and Forest Products Research Institute
Japan

MEETING NINETEEN
FLORENCE
ITALY
SEPTEMBER 1986

NON-DESTRUCTIVE VIBRATION TESTS

ON EXISTING WOODEN DWELLINGS

by

Yoshihiko Hirashima

Forestry and Forest Products Research Institute

Ministry of Agriculture, Forestry and Fisheries

Japan

1. Introduction

The history of Japanese wooden structure dates back to several thousands years ago and it is intertwined with the history of natural disasters such as earthquake, typhoon and snow.

Ever since the beginning of the history, Japan has experienced more than 430 deadly earthquakes. She has also been lashed by annual typhoons with, in some case, the maximum wind velocity of 70m per second. Some cities on the Japan Sea coast have recorded snow fall as deep as 3.8m.

According to the 'Plate Tectonics Theory', the latest theory in seismology, the huge base rock is thrusting from the Pacific Ocean side to Japanese archipelago at the rate of several centimeters per year and is moving under it. This tectonic movement gives constant stress to the crustal structure of Japan, and the strain or the energy thus accumulated is periodically released as earthquake. This theory explains why big earthquakes occur repeatedly.

The countermeasures against these typhoons, snow fall and earthquakes, which attack Japan almost every year or once in several years, are very important in designing wooden structures.

Recent residential dwellings are being constructed compling with the regulations, which include simplified design methods, with sufficient

structural performance. This structural performance, however, is considered that it will vary decreasingly with time.

Japanese climate, humid and hot in summer, accelerate the decay of structural members of timber in house and the repetition of dry and wet condition cause the looseness of joints.

It is one of the problem, which should be solved urgently, to develop the non-destructive method to evaluate the structural performance against horizontal forces such as earthquake and wind.

Some non-destructive tests trying to evaluate the structural performance have been conducted on olden houses by using a vibration generator.

The goal of the research series is to estimate the ultimate strength of the construction under horizontal load by using the characteristics obtained from small amplitude vibration tests.

In this paper, the applicability of general vibration theory for a two-storied structure with viscous damping is discussed with the test results obtained from a vibration test using a light-weight vibration generator specially developed to this project.

2. Theory

We shall begin the general theory of forced vibration of a two-storied building.

Fig.1 shows the model of two-storied building with viscous damping. It is assumed that the mass of vertically half of wall concentrate to the nearest floor or ceiling level. The building is deformed only by shear. Any bending is not considered. In the case of two-storied building subjected to external forces P_1 and P_2 the general vibration equation is expressed as follows:

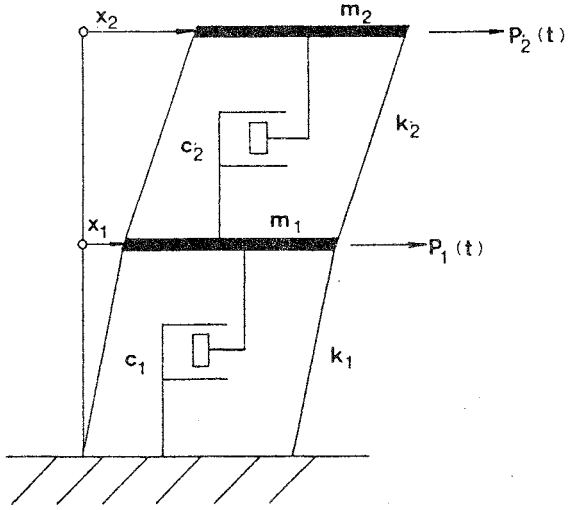


Fig.1 Modeling of two-storied building with viscous damping.

$$\begin{bmatrix} m_1 & 0 \\ 0 & m_2 \end{bmatrix} \begin{bmatrix} \ddot{x}_1 \\ \ddot{x}_2 \end{bmatrix} + \begin{bmatrix} c_{11} & c_{12} \\ c_{21} & c_{22} \end{bmatrix} \begin{bmatrix} \dot{x}_1 \\ \dot{x}_2 \end{bmatrix} + \begin{bmatrix} k_{11} & k_{12} \\ k_{21} & k_{22} \end{bmatrix} \begin{bmatrix} x_1 \\ x_2 \end{bmatrix} = \begin{bmatrix} P_1 \\ P_2 \end{bmatrix} \qquad (1)$$

where m_1: mass of 1st story

m_2: mass of 2nd story

$c_{11}, c_{12}, c_{21}, c_{22}$: expressed by coefficients of damping c_1 and c_2 as follows:

$c_{11} = c_1 + c_2$, $c_{12} = -c_2$

$c_{21} = -c_2$, $c_{22} = c_2$

$k_{11}, k_{12}, k_{21}, k_{22}$: expressed by spring constant k_1 and k_2 as follows:

$k_{11} = k_1 + k_2$, $k_{12} = -k_2$

$k_{21} = -k_2$, $k_{22} = k_2$

$\ddot{x}$: d^2x/dt^2

$\dot{x}$: dx/dt

Now let us consider the vibration test using a vibration generator having an eccentric moment, $m_0 r$, mounted at the top of second story.

Using the circular frequency ω in a complex number expression, external force P becomes

$$P = e^{i\omega t} \begin{bmatrix} 0 \\ m_0 r\omega^2 \end{bmatrix} \tag{2}$$

Solving eq.(1), we obtain the displacements of each story as follows:

$$|x_1|^2 = F_{11}^2 Q_{11}^2(\omega) + 2F_{11}F_{12}Q_{12}^2(\omega) + F_{12}^2 Q_{22}^2(\omega) \tag{3}$$

$$|x_2|^2 = F_{21}^2 Q_{11}^2(\omega) + 2F_{21}F_{22}Q_{12}^2(\omega) + F_{22}^2 Q_{22}^2(\omega) \tag{4}$$

where

$$Q_{jj}^2(\omega) = \frac{\left(\frac{\omega}{\omega_j}\right)^4}{\left\{1-\left(\frac{\omega}{\omega_j}\right)^2\right\}^2 + 4h_j^2\left(\frac{\omega}{\omega_j}\right)^2} \qquad (j=1,2)$$

$$Q_{12}^2(\omega) = \frac{\frac{\omega^4}{\omega_1^2\,\omega_2^2}\left[\left\{1-\left(\frac{\omega}{\omega_1}\right)^2\right\}\left\{1-\left(\frac{\omega}{\omega_2}\right)^2\right\} + 4h_1h_2\frac{\omega^2}{\omega_1\omega_2}\right]}{\left[\left\{1-\left(\frac{\omega}{\omega_1}\right)^2\right\}^2 + 4h_1^2\left(\frac{\omega}{\omega_1}\right)^2\right]\left[\left\{1-\left(\frac{\omega}{\omega_1}\right)^2\right\}^2 + 4h_2^2\left(\frac{\omega}{\omega_2}\right)^2\right]}$$

$$F_{11}=\frac{m_0 r\, X_{11}X_{21}}{M_1} \quad , \quad F_{12}=\frac{m_0 r\, X_{12}X_{22}}{M_2}$$

$$F_{21}=\frac{m_0 r\, X_{21}^2}{M_1} \quad , \quad F_{22}=\frac{m_0 r\, X_{22}^2}{M_2}$$

$X_{11}, X_{21}, X_{12}, X_{22}$: element of characteristic unit vector of vibration system.

$$M_j = \sum_{r=1}^{2} m_r x_{rj}^2 \qquad (j=1,2)$$

h_1, h_2: damping factor of 1st or 2nd story

In the case of free vibration, we need to consider neither external force nor viscous damping. Consequently, eq.(1) becomes as follows:

$$\begin{bmatrix} m_1 & 0 \\ 0 & m_2 \end{bmatrix} \begin{bmatrix} \ddot{x}_1 \\ \ddot{x}_2 \end{bmatrix} + \begin{bmatrix} k_{11} & k_{12} \\ k_{21} & k_{22} \end{bmatrix} \begin{bmatrix} x_1 \\ x_2 \end{bmatrix} = \begin{bmatrix} 0 \\ 0 \end{bmatrix} \tag{5}$$

From this simultaneous differential equation, we obtain the following frequency equation which can determine the circular frequency, ω.

$$(m_1\omega^2 - k_{11})(m_2\omega^2 - k_{22}) - k_{12}k_{21} = 0 \tag{6}$$

Solving this equation, we can obtain the primary and secondary natural frequencies.

3. Testing

3.1 Test building

The building tested is a residential house which has been served in practical use for three years after construction.

The construction system of the test house is light frame construction based on the system introduced from north America to Japan about ten years ago.

The plan of the test house is shown in Fig. 2 not including an annex connected to the main building. The connection between annex and main building was released at a testing step. The elevation of the house is shown in Fig. 3.

Peripheral wall of the house is composed of 2 inch by 4 inch studs with gypsum boards connected inside and structural plywood with plastered lath-mortar outside.

Internal wall is composed of same dimension studs with gypsum boards installed on both sides of the studs. The thickness of both sheathing of plywood and gypsum board is 12mm. Sheathings are connected to studs by nailing of CN50 for plywood or GN 40 for gypsum board. Nailing schedule on both sheathing of plywood and gypsum board is 100mm in peripheral of the sheet and 200mm along the intermediate studs.

Wire lath is connected to plywood sheathing by staples. Mortar is plastered about 21mm in thickness on it.

Roof of the house is constructed with rafters and plywood sheathing with asbestos cement slate as roofing materials. No decay was seen in the wooden members at the survey after testing.

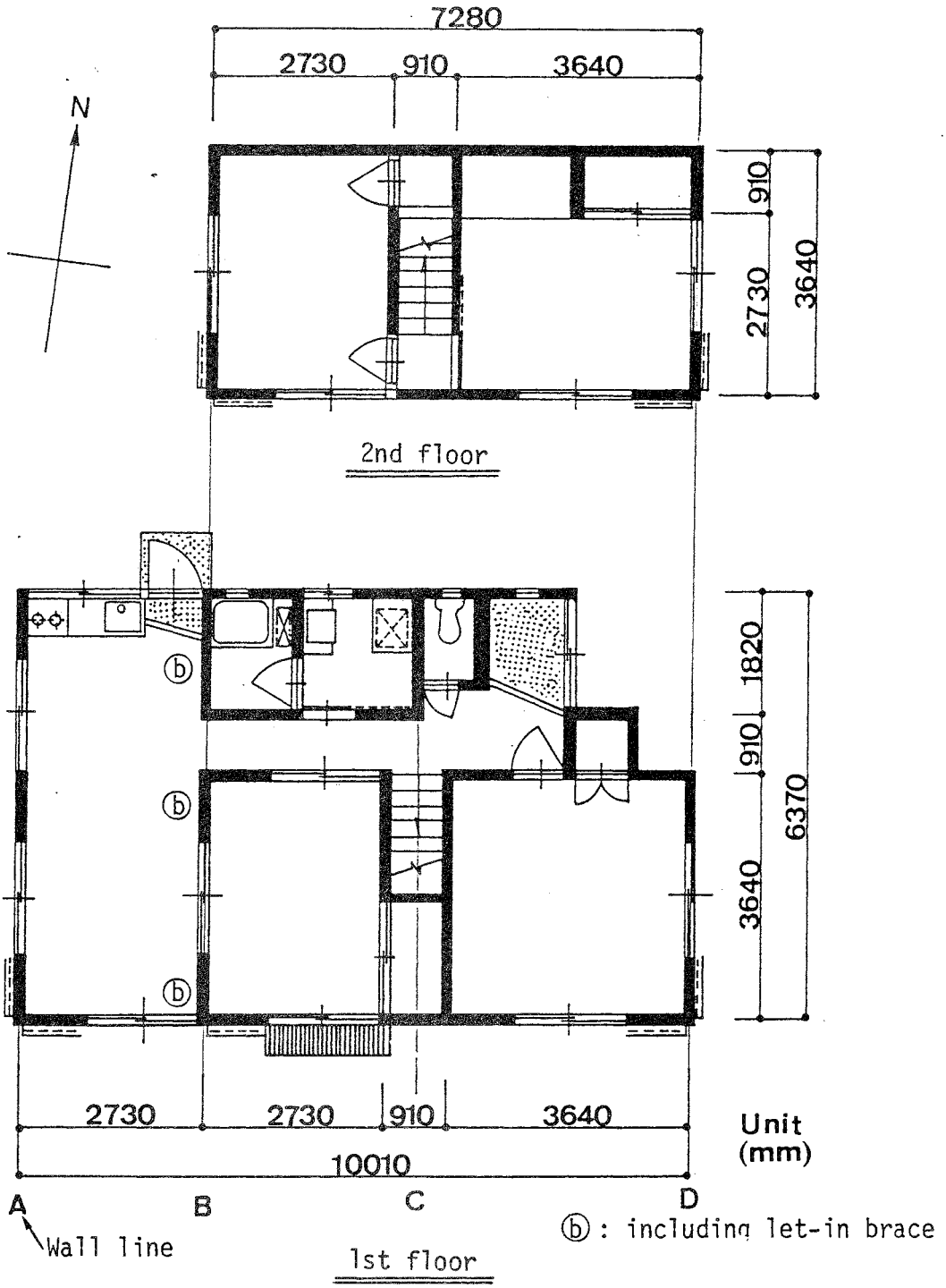
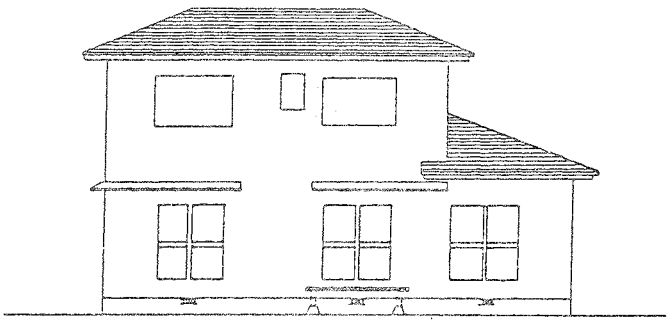
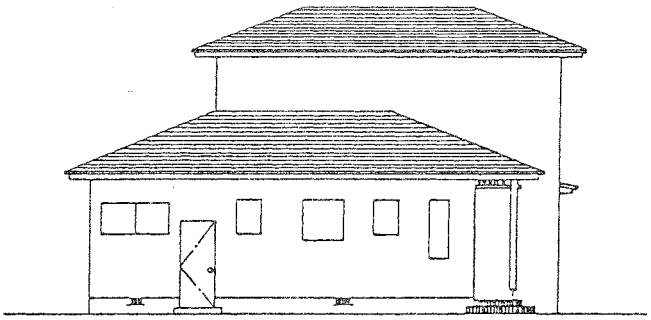


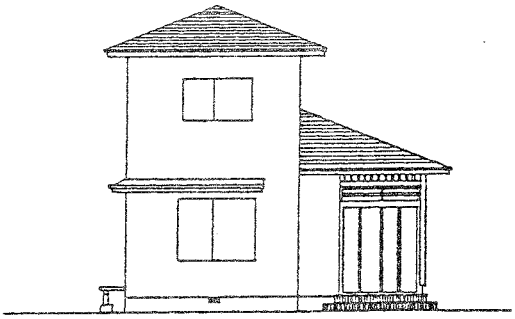
Fig.2 Plan of test house



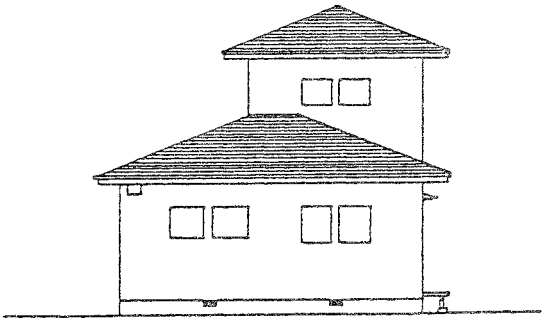
South



North



East



West

Fig.3 Elevation of test house

Table 1 Description of testing

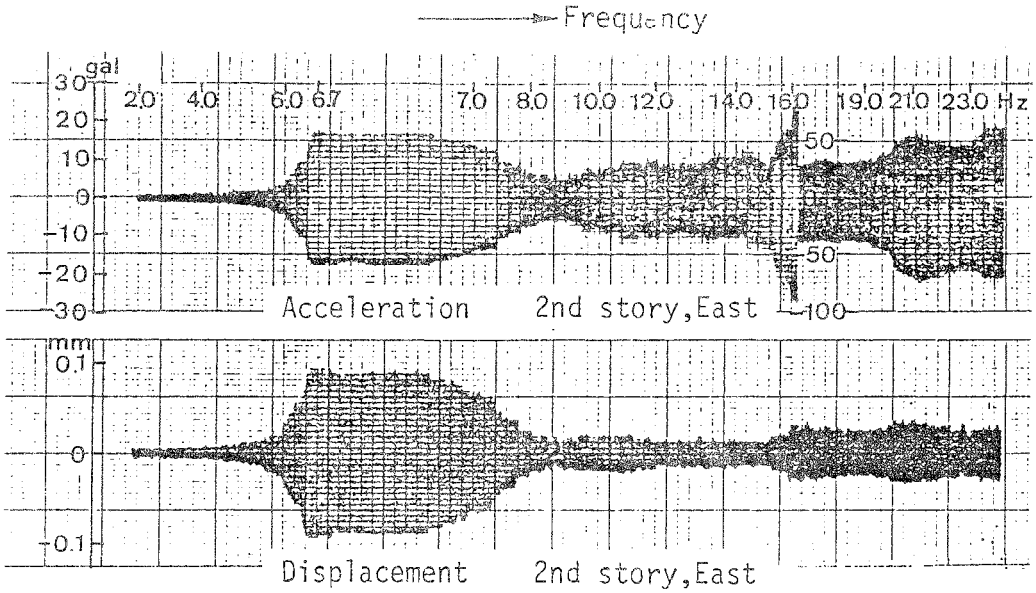
Experiment	Location of generator mounted	Direction of vibration	Test conducted:
S- 1	Second floor	Span direction	on house as it stands.
R- 3	"	Ridge direction	"
R- 4	Ceiling joist of second story	Ridge direction	"
S- 5	"	Span direction	"
S- 6	"	"	after separation of annex from main construction.
S- 7	"	"	after removing wire lath-mortar of 4P* in length in wall line D in 2nd story.
S- 8	"	"	after removing wire lath-mortar of 4P in length in wall line B in 2nd story.
S- 9	"	"	after removing wire lath-mortar of 4P in length in wall line D in 2nd story.
S-10	"	"	after removing wire lath-mortar of 7P in length in wall line A in 2nd story.
S-11	"	"	after removing gypsum board of 2P in wall line A plus 1P in wall line D in 1st story.
S-12	"	"	after removing plywood of 2P in length in wall line D in 2nd story.
S-13	"	"	after removing plywood of 2P in length in wall line B in 2nd story.
S-14	"	"	after removing plywood of 2P in length in wall line D in 1st story.
S-15	"	"	after removing plywood of 3P in length in wall line A in 1st story.
S-16	"	"	after removing gypsum board of 6P in length in wall line B in 1st story.

* 1P means module length 910mm.

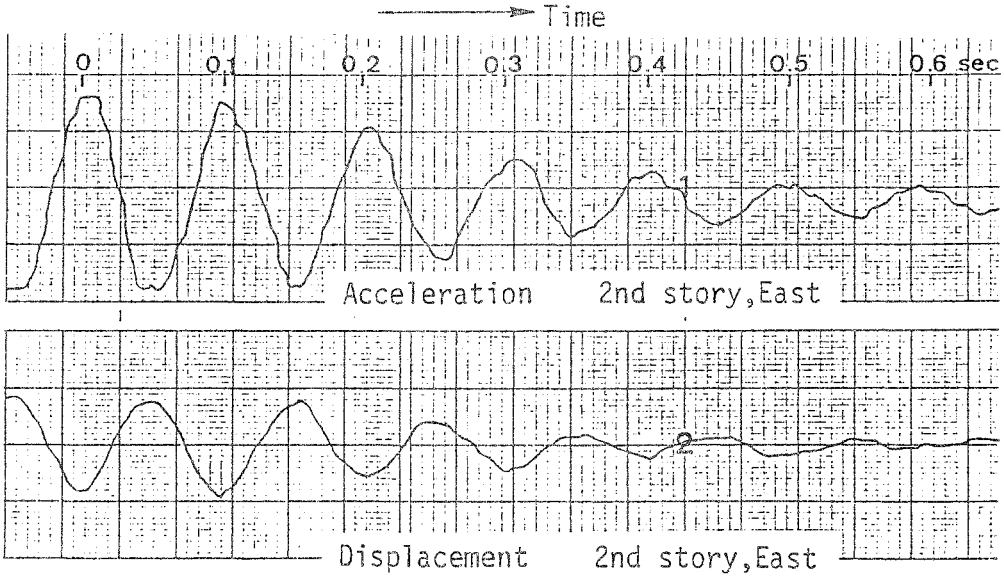
3.2 Test procedures

A special vibration generator has been developed to the purpose of non-destructive testing. Some different disturbing forces are available by changing the eccentric mass connected to a rotary disc of the machine. 4kgW.cm of eccentric moment was employed in this test.

The weight of the machine is about 40kgW. The weight of the generator enables us to mount it easily at any place in the building. The generator was mounted by bolts on the second floor or ceiling joists of second story according to the purpose of tests.



(a) Response of forced vibration



(b) Wave form of free vibration

Fig. 4 Examples of response obtained from forced vibration test (a), and wave form of free vibration (b).

At first, the generator was mounted on the second floor applying the force in the span direction of the building. Then the force applied in the ridge direction.

After these experiments, the machine was mounted on ceiling joists of second story. These experiments, experiments from S-1 to S-5 as shown in Table 1, were conducted on the house as it standed.

After these preliminary tests, several vibration tests were conducted on the building removing some parts of wall according to the test procedures as shown in Table 1.

The frequency of rotation of the machine disc was increased gradually from 2 Hz to about 20 Hz monitoring the response of the building by using oscillation recorder.

Some pickups of vibration, servo type acceleration pickup, were fixed on the east and west ends at the top of each story.

From the monitoring record, the frequency where the maximum amplitude was appeared was determined as the resonance one. An example of the wave form of response was show in Fig. 4(a).

Then the rotation of the machine was held at the resonance frequency determined previously to a steady state. After the steady state at resonance, the rotation of the machine was stopped by turning off the power switch to vibrate the building freely. Fig. 4(b) shows one of the samples of decaying wave form of the free vibration.

These tests were conducted at each experiment step in order to analyze the effect of wall on the dynamic characteristics of the building.

After the completion of test, nail joint specimens were cut from walls of plywood or gypsum board to obtain the information about the load-slip relations of joint. Shear tests on nail joint connecting sheathings to a stud were conducted at the laboratory later on.

4. Results and discussions

Table 2 shows acceleration and displacement measured in a state of primary resonance explaining the very small amplitude vibration of these tests, as well as the damping factor calculated from decaying wave form of free vibration.

Table 2 Acceleration and displacement at primary resonance, and damping factor obtained from free vibration

Experiment	Acceleration(gal)		Displacement (10^{-3} mm-pp)		Damping factor	
	1st story	2nd story	1st story	2nd story	1st story	2nd story
S- 1	-	9.6	36	47	0.096	0.066
R- 3	-	9.7	46	52	0.083	0.069
R- 4	-	16.9	64	80	0.072	0.072
S- 5	-	16.7	57	80	0.066	0.082
S- 6	9.2	19.6	49	92	0.053	0.051
S- 7	8.2	21.1	65	127	0.046	0.051
S- 8	7.3	22.6	64	134	0.052	0.054
S- 9	11.0	18.3	78	133	0.048	0.049
S-10	10.1	18.1	80	133	0.041	0.044
S-11	9.2	18.9	80	149	0.040	0.040
S-12	8.2	20.2	75	172	0.036	0.040
S-13	7.3	20.8	72	198	0.037	0.034
S-14	8.2	21.4	79	202	0.033	0.035
S-15	8.2	20.9	81	196	0.036	0.034
S-16	8.6	17.1	96	181	0.033	0.035

Table 3 Comparison of experimental value of resonance frequency with theoretical one.

Experiment	Resonance frequency (Hz)			
	Experiment		Theory	
	Primary	Sencondary	Primary	Secondary
S- 1	10.0	19.6	–	–
R- 3	10.2	–	–	–
R- 4	10.1	20.5	–	–
S- 5	9.8	19.0	–	–
S- 6	9.6	15.5	9.0	17.7
S- 7	9.1	14.5	9.1	17.2
S- 8	8.9	18.0	9.1	16.5
S- 9	8.3	17.3	8.9	16.4
S-10	8.0	17.3	8.6	16.3
S-11	7.9	16.0	8.4	16.2
S-12	7.6	16.0	8.3	15.4
S-13	7.3	14.1	8.1	14.5
S-14	7.3	14.0	7.9	14.3
S-15	7.3	14.0	7.6	14.1
S-16	6.7	12.8	6.6	13.6

Table 3 shows the resonance frequencies measured at each test steps as well as the theoretical ones. The primary resonance frequency was calculated using the wave form of free vibration, and the secondary one was determined by using the response wave of 1st story. It is evident that both of the primary and secondary resonance frequencies decreases as the wall length in the building decrease following the steps of experiment.

Theoretical values of frequencies shown in Table 3 were computed as the following procedures.

First of all, the spring constants of each kind of wall are determined for that sheathed with plywood (both of plywood sheathing and plywood sheathing with lath-mortar), that sheathed with gypsum board and that with bracing.

Fig.5 shows the load-slip curves of nail joint for different sheathings obtained from the shear test using the test specimens cut from the test building. The slope of the curve required for the calculation of the deformation of wall to determine the spring constant was obtained using the data of 0.05mm slip and the corresponding load.

For the calculation of deformation of wall, the previously derived method was used, even it was developed as a non-linear calculus (3).

Thus the spring constant k per unit length (m) were obtained as follows:

1248kg/cm for plywood sheathing wall
212kg/cm for gypsum board wall
2885kg/cm for plywood plus lath-mortar wall

In these calculations measured data of the modulus of rigidity were used as 4500kg/cm² for plywood and 6850kg/cm² for gypsum board. For lath-mortar infinity was used. In the comparison of the constants from this test with those obtained from similar previous test, there appeared a very big difference on gypsum board. The relaxation of nail joint occurred at the test specimens of gypsum board. Therefore the data from these test specimen of gypsum board were not considered as the representative, and were rejected. Instead of these data, the previously tested data (1) were

employed being showed in Fig. 5. Using this curve, the spring constant of gypsum board wall became 797kg/cm.

Using eq.(6), the spring constant of gypsum board wall can be figured out substituting the remaining those of each wall including that with bracing, mass of each story and the resonance frequencies from tests.

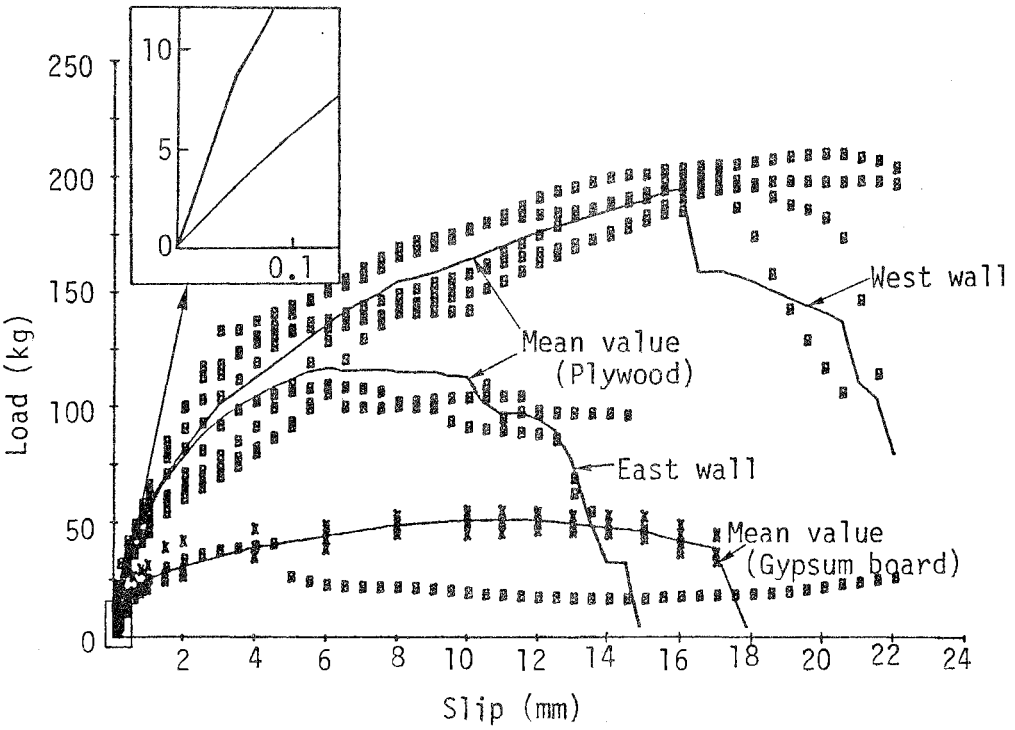


Fig.5 Load-slip curve of nailed joint of different sheathing cut from test house.

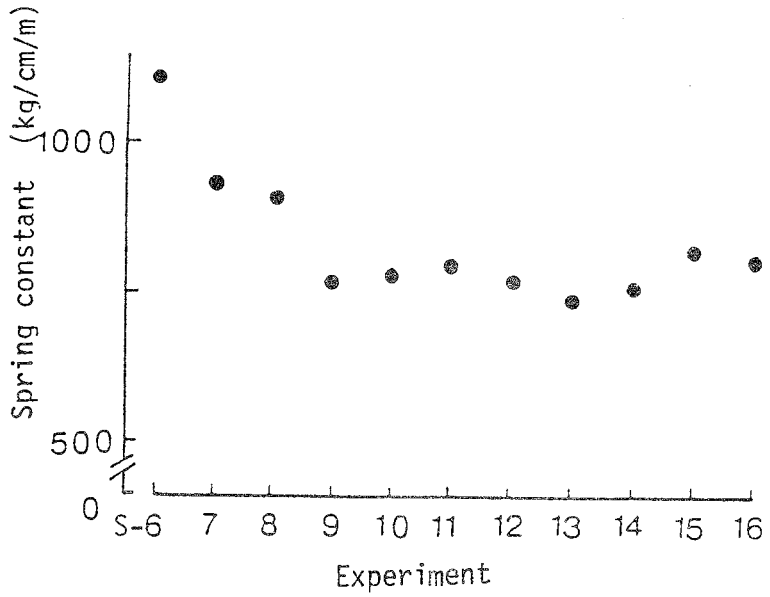


Fig.6 Spring constant of wall sheathed with gypsum board computed by using resonance frequency of experiment.

Previous test data of 155kg/cm was employed as the spring constant of wall with bracing (4).

Results of computation are shown in Fig. 6. On the steps of experiment after S-9, existing little effect of lath-mortar including effect of wall at openings, relatively steady value of 776kg/cm was obtained. This value is close to 797kg/cm obtained before.

Using the spring constants of each wall thus obtained and the mass of building estimated by survey of members and calculation, the response curve of displacement now can be computed from eqs. (3) and (4).

Fig.7 shows the computation results of the displacement response of different experiment steps as well as experimental curves.

There are slight differences between theoretical value and experimental one on the resonance frequencies and the amplitudes at resonance.

It is considered that the difference between them are caused by the inaccuracy of evaluation of spring constant of each wall and the mass of building, including the effect of wall not counted in the stiffness like small walls at openings.

It can be said generally, however, that the computation method for response of forced vibration derived from the ordinary vibration theory is applicable to the wooden buildings though the differences from experiment should be examined in more detail.

Fig. 8 shows vibration modes at primary and secondary vibration as well as the ratio of amplitude of second story to first one. According to the theory, the ratio of amplitude of second story to first one takes a constant value at anytime whenever the building vibrates in the characteristic frequencies. From Fig. 8, it can be seen that this condition is satisfied excluding the small amplitude near zero of the first story.

5. Conclusion

In this paper the ordinary theory of vibration was discussed by using the test results from small amplitude vibration tests.

From this, it can be said that the theory is applicable to wooden buildings within a small amplitude like this test, and that the response of wooden buildings is able to be predicted by using the data of the distribution of mass and spring constants of each wall constructing the structure, obtained from the data of joint characteristics and material data and the calculus of deformation of wall.

References

(1) Hirashima,Y et al - Vibration tests on existing wooden dwellings (II), Proceedings of the annual meeting of Japan Wood Research Society, 1983

(2) Tajimi,H - Theory of vibration of buildings, Corona Publishing Co.Ltd., Tokyo 1974

(3) Kamiya,F - Theoretical studies on racking stiffness and strength of wooden sheathed walls, Transaction of the Architectural Institute of Japan, No.309 1981

(4) Hirashima,Y et al - The performance of wooden frames with bracings for horizontal shearing force and their structural analysis (I)- Racking tests of wooden frames, Jour. of the Japan Wood Research Society, Vol.27, No.12 1981

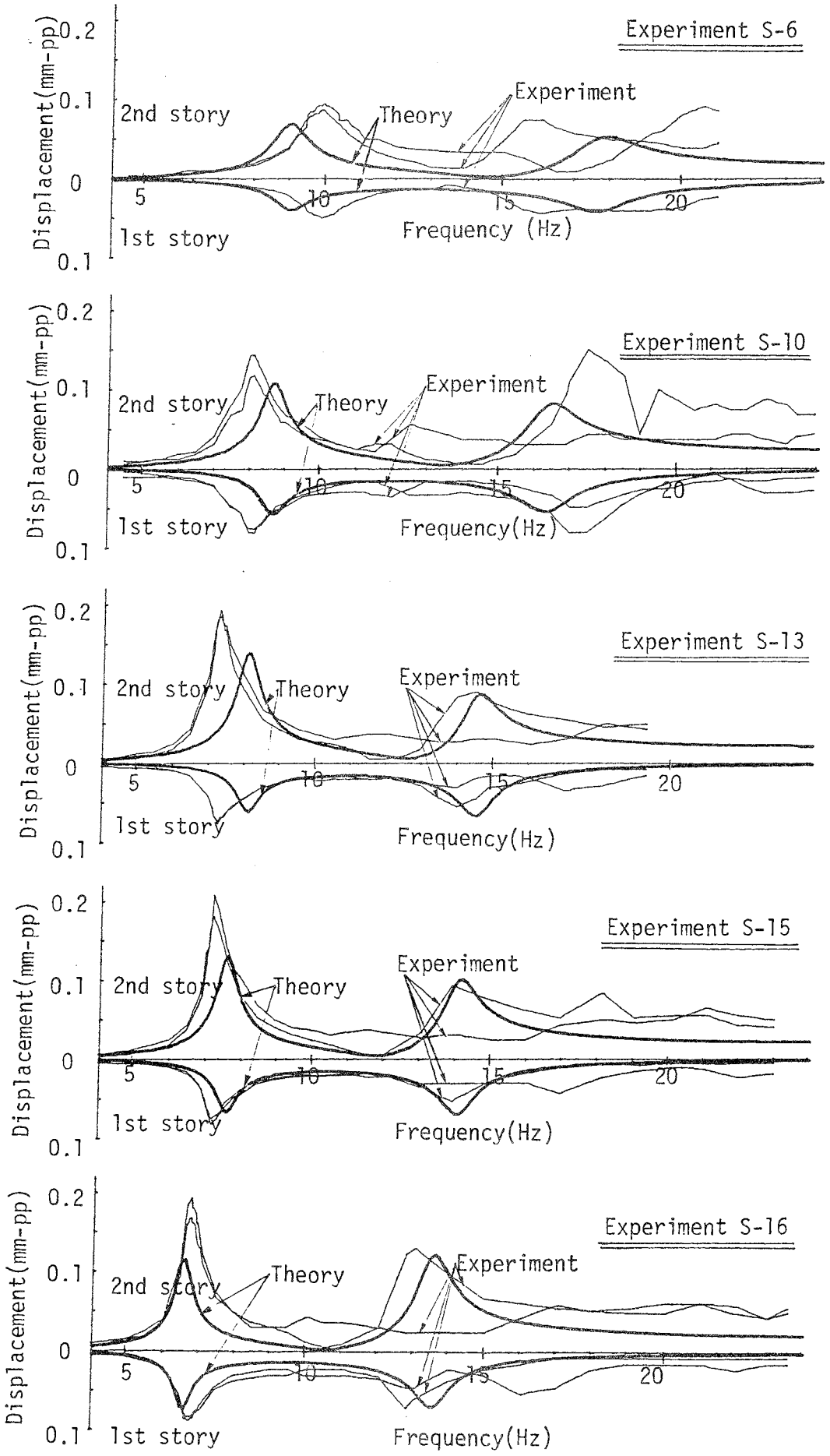


Fig.7 Displacement response curve of different experiment step showing both of experimental value and theoretical one.

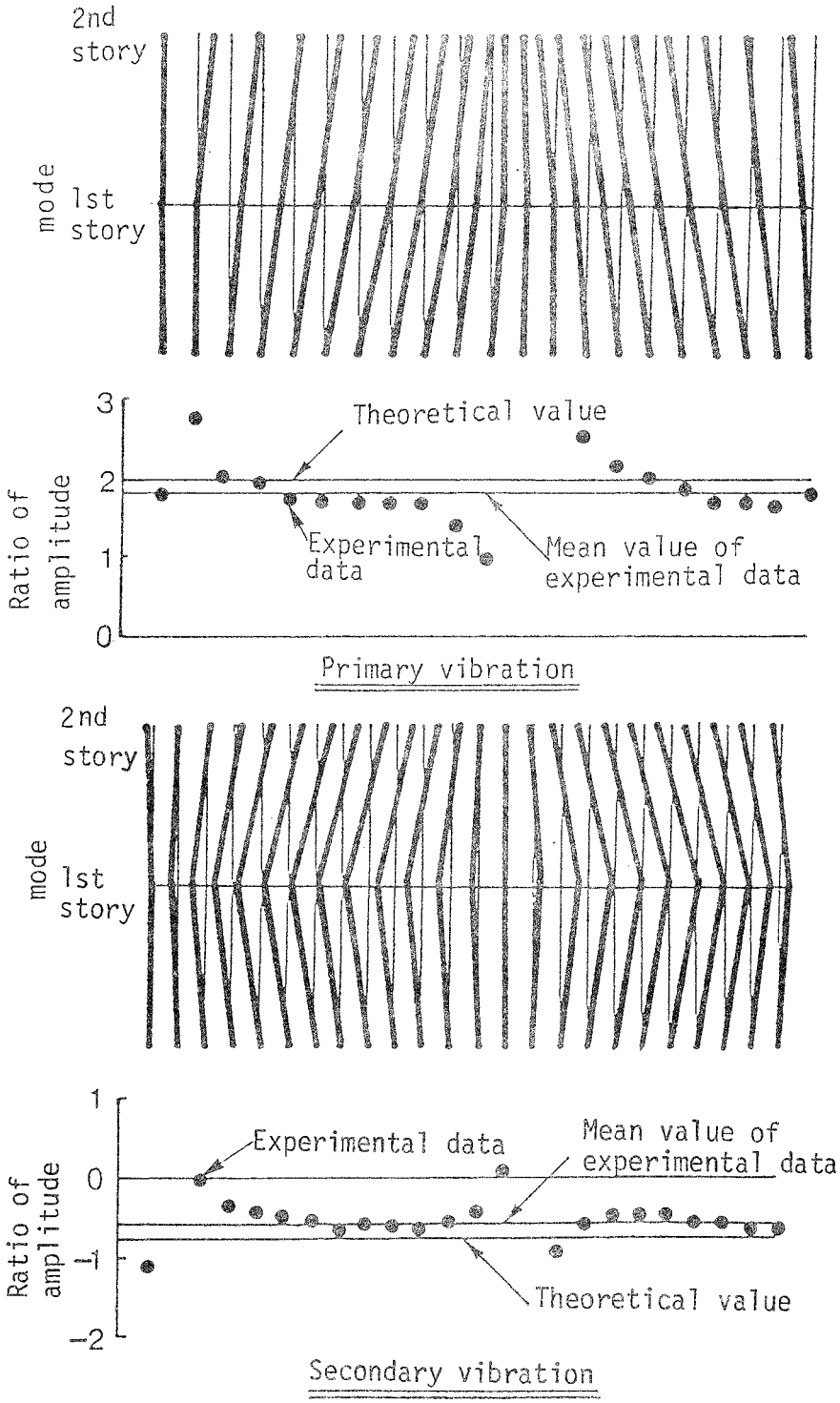


Fig.8 Vibration mode and amplitude ratio of 1st story to 2nd story at primary or secondary vibration.

CIB-W18/19-16-1

INTERNATIONAL COUNCIL FOR BUILDING RESEARCH STUDIES AND DOCUMENTATION

WORKING COMMISSION W18 - TIMBER STRUCTURES

SIMULATION OF FIRE IN TESTS OF AXIALLY LOADED WOOD WALL STUDS

by

J König
Swedish Institute for Wood Technology Research
Sweden

MEETING NINETEEN
FLORENCE
ITALY
SEPTEMBER 1986

Abstract

The results from tests of axially loaded wood studs are presented. During the tests material was removed by planing, thus simulating the charring in the case that the stud is exposed to fire on one side only. The studs were placed between stiff, non-rotating endplates. The stud ends were allowed to rotate and thus the axial load was able to change its location and decrease load excentricity. A test procedure is proposed for the determination of fire resistance of load-carrying wood-stud walls.

1. Introduction

In Sweden and several other countries the building regulations stipulate that the external walls in small one-family houses should resist fire for 30 minutes. In the case of loadbearing external walls the wall must be able to carry the design load during this time-period, and the same requirement has also to be satisfied by the components which form supports and stiffen the wall.

The majority of external walls used in Sweden are wood-stud walls which are built up of timber studs with cladding on both sides. During recent years a number of light-weight studs have been introduced. The most common one is a stud where the flanges are built up of wood and the web is built up of fibre board.

In Sweden today it is most usual to determine the fire resistance of load-bearing wood-stud walls by performing full scale fire-tests. A real wall exposed to fire is loaded by both axial and transversal loads. In order to facilitate testing the Swedish code gives a simple rule which says that the effect of transverse loading can be simulated by an excentricity of the axial load /1/. For small houses this excentricity has to be at least 20 mm. The code implies, though it does not expressly state, that the location of the axial load remains the same during the whole fire test. As can be expected, it is often not possible to satisfy the requirements for fire resistance under these conditions.

In order to elucidate the mechanical behaviour of axially loaded wood studs exposed to fire, a series of tests were conducted. The charring of the timber was replaced by planing on one side of the stud. The three other faces of the stud were assumed to be protected from fire by mineral wool and the sheating.

The aim of the fire simulation was not to consider the thermal effects of fire on the mechanical properties of the wood material but rather to gain an understanding of the mechanical behaviour of a wood stud with a view to developing a rational method of calculation. The thermal effects can be determined separately.

A complete description of this study will be found in /2/.

2. Performed tests

Totally 8 tests were conducted. Six of the specimens were formed by 2,4 m long 45 x 120 mm timber studs of the Swedish grade "Ö", which has a characteristic bending and compression strength of 15 N/mm2. Two of the specimens were 200 mm deep light-weight studs of the same length with 45 x 45 mm timber flanges and 6 mm thick fibreboard webs. For the solid studs short pieces of 45 x 120 mm timber were used as sole and head plates (specimens 1 - 6). In the case of light-weight studs (specimens 7 and 8) special light-weight members were used as sole and head plates.

In order to study the effect of different support conditions cellular rubber air-tightening profiles were attached to the sole and head plates. In half of the tests the lower support plate was given an inclination of 3,5 % in order to simulate the effect of the deflection of the roof truss or of an uneven foundation as site concrete. This inclination is larger than can normally be anticipated. The support conditions of the specimens are shown in Fig. 1.

The specimens were placed in a test rig with stiff, non-rotating, support plates, thus allowing the specimen to deform dependent on the support conditions. By using three load cells under the lower support plate it was possible to determine the location of the axial load.

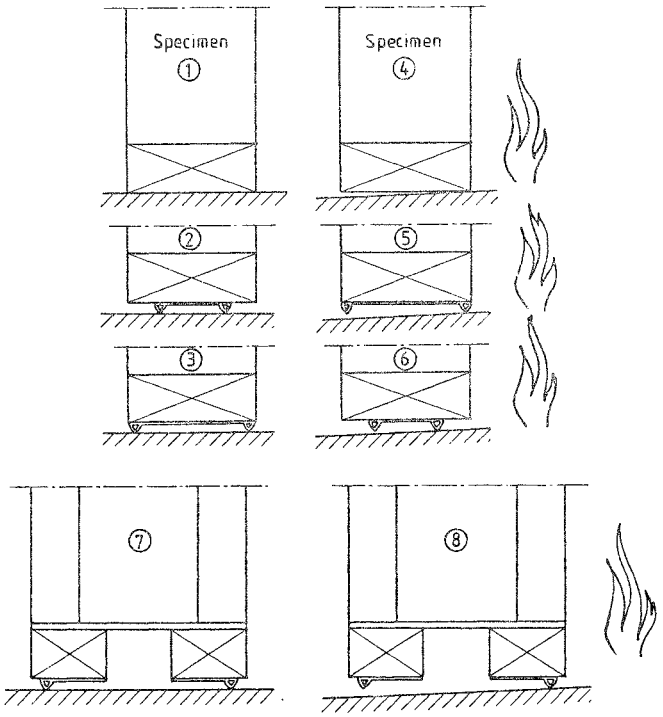


Figure 1. Support conditions. The support plate at the upper support is horizontal for all specimens.

In order to determine the bending stiffness the specimens were loaded with two transverse point loads and the displacements measured as shown in Fig. 2.

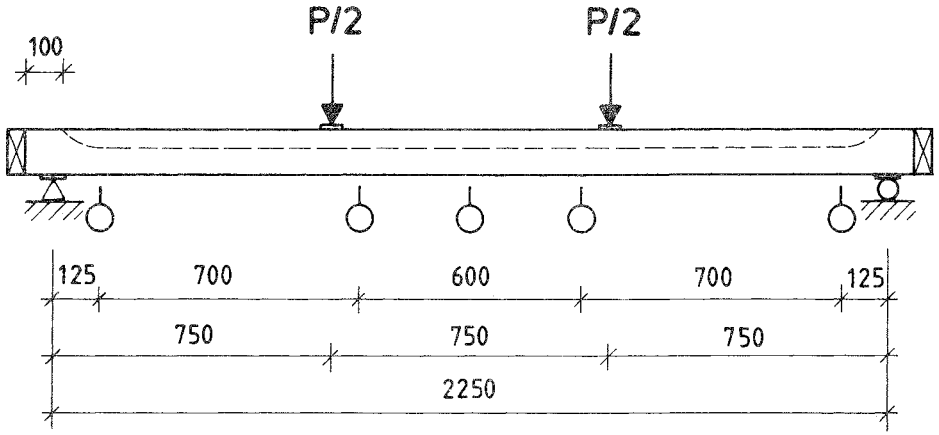


Figure 2. Application of loads and gauges for determination of bending stiffness.

The following procedure was adopted for all the tests. First the specimen was loaded with the transversal forces until a mid-span-deflection of 5 mm was reached after about two minutes. Immediately after this the specimen was unloaded and placed in the test rig for axial load. Buckling in the weak direction was prevented by bracing. The axial load was applied until the maximum load N_{max} was reached after not less than four minutes. The maximum load was held constant for five minutes and the stud was unloaded again. The load-values of the three load-cells and the mid-deflection were registred in steps of 1 kN and, when the maximum N_{max} was held constant, every minute.

After unloading a 5 or 10 mm thick layer of the stud was removed by planing, except for the regions close to the ends. This is shown on the broken curve in Fig. 2. The procedure of loading and planing was continued until the stage of collapse was reached. Normally the ultimate load N_n was lower than the maximum load N_{max}. The test results for the collapse stage and the stage before are given in Table 1.

The maximum load N_{max} was chosen slightly lower than the allowable load. This was calculated with respect to buckling in the case of specimens 1 to 6 and with respect to compression perpendicular to the grain in the sole plate in case of specimens 7 and 8.

Typical curves for axial load versus mid-deflection are shown for all stages of specimen 4 in Fig. 3 and for the collapse stage of specimens 1 - 6 in Fig. 4. It can be seen that the deflections, before ultimate load is reached, are largest in specimens with 70 mm wide rubber profiles and smallest in specimens without rubber profiles. In each of these pairs the deflection was larger when the lower support had an inclination.

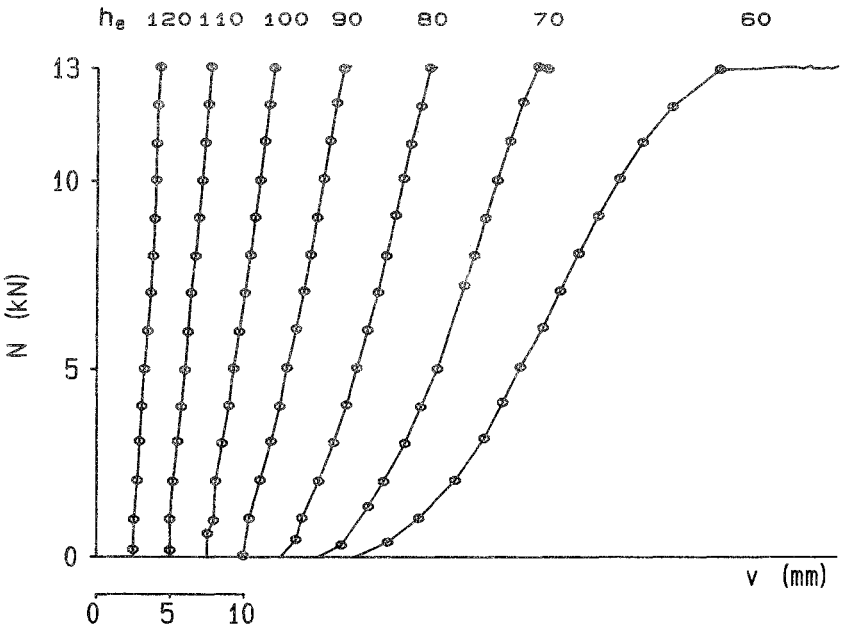


Figure 3. Axial load versus mid-deflection for all stages of specimen 4.

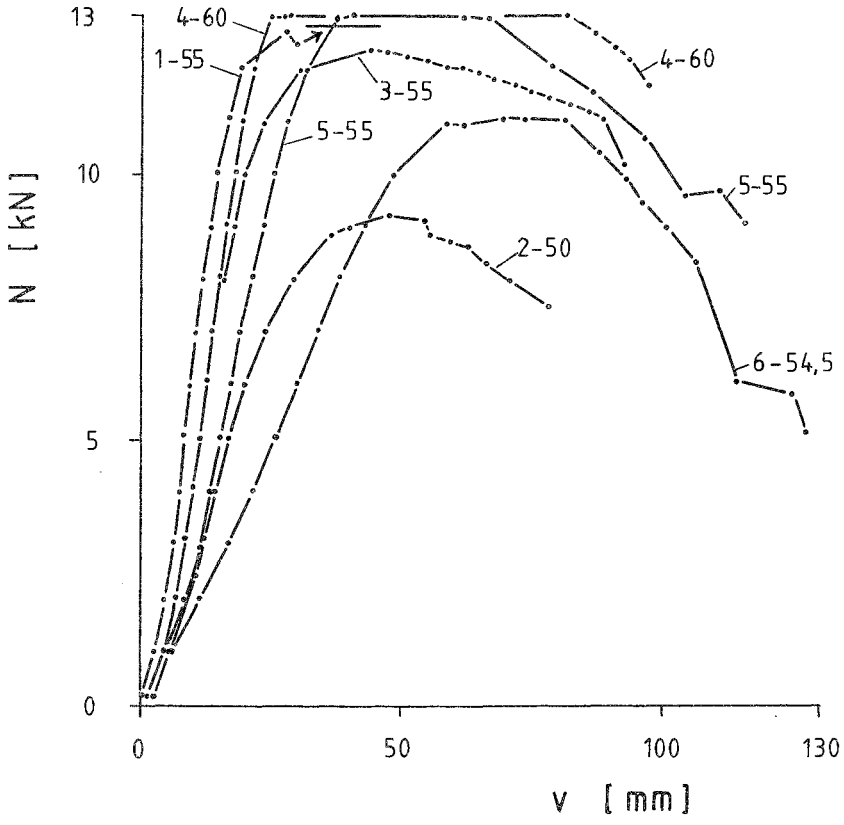


Figure 4. Axial load versus mid-deflection for collapse stage of specimens 1 - 6.

Typical curves for the location of the axial load and the geometrical centre of gravity of the mid-section of the stud, see the explanations in Fig. 5, are shown in Fig. 6. The curves for the other specimens are not shown here. The location of the axial load in the ultimate section is about the same for specimens 1 - 6, see Table 1, whereas its location is variable for the initial full section, depending on the stiffness and geometrical conditions at the supports. The specimens 7 and 8 also show a similar behaviour.

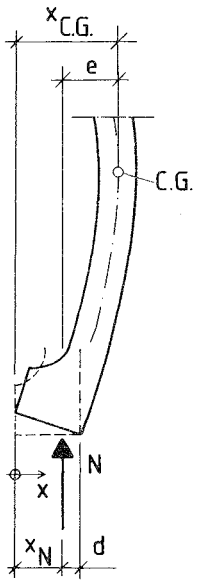


Figure 5. Location of the axial load and the geometrical centre of gravity of the mid-section.

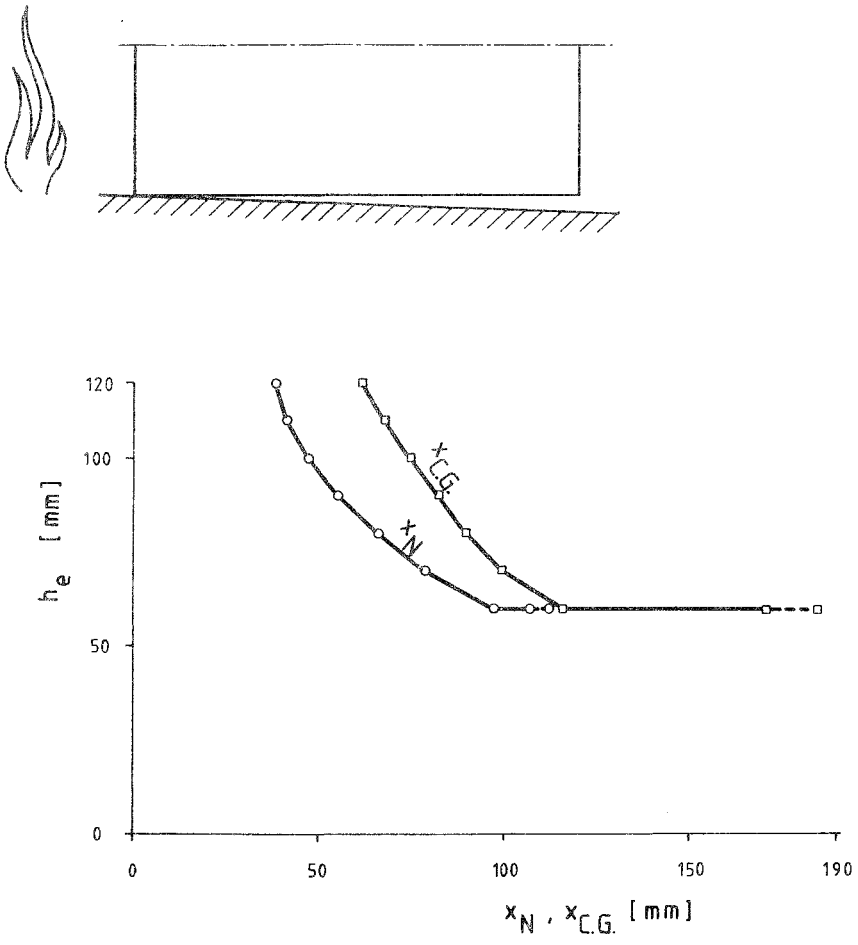


Figure 6. Location of the axial load and the geometrical centre of gravity of the mid-section at different stages of specimen 4.

The displacement of the axial load during the test is caused by the rotation of the stud ends. Thus the load excentricity, that is the distance between the two curves in Fig. 6, becomes smaller than is normally assumed in the case of column buckling with fixed end-hinges.

3. Comparison of test results and theoretical calculations

In the CIB Structural Timber Design Code /3/, section 5.1.7, a buckling curve is given for calculation of axial load-bearing capacity of columns. Using the bending stiffnesses which were determined by means of the tests with transverse loads, the theoretical load-bearing capacity N_{cd} was calculated for the specimens 1 to 6, see Table 2. In this table

the slenderness ratios λ are also given.

In these calculations the modulus of elasticity used was the mean value of all stages of the specimen. The gauge length was 2.0 m, see Fig. 2. As the specimens had no obvious imperfections, these were chosen to equal 1/1000 of the length. The CIB buckling curve gives results which are considerably on the safe side compared with the test results. These results can be expected since the buckling curve was derived assuming fixed end hinges.

4. Conclusions

The support conditions of a column with end hinges can be more favourable in a structure than they normally are assumed to be in calculations or tests. Axially loaded wood studs behave in such a manner when their slenderness ratios are large. By means of the large rotation of the stud ends, the axial load is allowed to move in the direction of the deflection. The influence of support conditions as intermediate layers of cellular rubber profiles and the inclinations of support or roof trusses is negligible when the slenderness ratio is large. These conditions are particularly pronounced in case of fire causing charring only on one side of the stud. The assumption that the axial load has a fixed location will give very conservative results.

The following outline of procedure for determining fire resistance of load-bearing wood stud walls with both axial and transverse loads is proposed. Since the thermal effects on stiffness and strength of small size timber components are not yet known to the author, fire tests under load still seem to be inevitable. The following steps should be taken:

1. Fire-testing of a wall unit under load. The wall unit is placed in a test rig with fixed end plates, allowing the

upper and lower wall ends to rotate. The axial load should be choosen to be close to the design load. If the wall unit has not collapsed after the specified period of fire resistance, the fire is put out and the axial load increased until collapse load is reached. The collapse behaviour, ductile or brittle, is registred. The profile of effective, residual cross-section is measured.

2. Specimens made of one stud plus effective parts of cladding are made. The stud has a cross-section which is approximately equivalent to the residual cross-section of the fire-tested studs (step 1).

3. "Cold tests" of one part of the specimens with axial load are undertaken until collapse. The ultimate load should normally be lower than the ultimate load obtained from the fire test.

4. "Cold tests" are conducted on the other part of the specimens with transverse load until collapse.

5. Assuming that the thermal effects on bending strength are approximately the same as in the case of axial compression of the stud, the bending capacity during fire can be calculated by decreasing the result from the "cold tests" in the same proportion as was obtained from comparison of the test results from step 3 and 1.

6. Now the load bearing capacity for combined axial and transverse loads can be determined by using the interaction formula

$$\frac{N}{N_d} + \frac{M}{M_d} \leq k$$

where N_d is the characteristic axial load bearing capacity obtained from step 1 and M_d is the characteristic moment bearing capacity determined as described above. The coefficient k should be chosen between 0.9 and 1.0.

The use of this method offers the advantage that different load combinations can be chosen and expensive fire testing minimized.

TABLE 1. Test results at and before collapse.

Specimen	Depth at collapse stage h_e mm	Depth before collapse stage[a] h_e mm	Maximum load N_{max} kN	Ultimate load N_u kN	Time N_u was held	Location of load N_u d mm
1	55	60	13,0	12,80	0	18,8
2	50	60	13,0	9,22	0	15,2
3	55	60	13,0	12,36	0	17,9
4	60	60	13,0	13,00	2 h,4 min	10,3
5	55	55	13,0	13,00	8 min	19,0
6	54,5	60	13,0	11,07	0	17,7
7	85	110	18,0	12,92	0	15,4
8	135	160[b]	18,0	17,81	0	23,7

a) In this stage the maximum load was held for at least 5 minutes.

b) Without flange.

TABLE 2. Comparison of experimental and theoretical axial load capacity

Specimen	N_u	λ	N_{cd}	$\frac{N_u}{N_{cd}}$
	kN		kN	
1	12,80	157	10,51	1,22
2	9,22	173	6,82	1,35
3	12,36	157	10.21	1,22
4	13,00	144	11,58	1,12
5	13,00	157	11,88	1,09
6	11,07	158	10,55	1,05

m = 1,175

s = 0,110

49

Literature cited

/1/ Byggnadsdelars bärförmåga vid brand. PFS 1984:1. Rules for approval of loadbearing capacity for building elements subjected to fire. The National Swedish Board of Physical Planning and Building.

/2/ Report to be published by the Swedish Institute for Wood Technology Research. Tentative title "Simulering av brand vid provning av axialbelastade träreglar".

/3/ CIB Structural Timber Design Code, CIB Report, Publication 66, Working Group W18, 1983.

CIB-W18/19-17-1

INTERNATIONAL COUNCIL FOR BUILDING RESEARCH STUDIES AND DOCUMENTATION

WORKING COMMISSION W18 - TIMBER STRUCTURES

LOAD FACTORS FOR PROOF AND PROTOTYPE TESTING

by

R H Leicester
CSIRO Division of Building Research
Australia

MEETING NINETEEN
FLORENCE
ITALY
SEPTEMBER 1986

LOAD FACTORS FOR PROOF AND PROTOTYPE TESTING

by

R.H. Leicester
(CSIRO Division of Building Research,
Melbourne, Australia)

SUMMARY

Load factors for proof and prototype testing are derived by calibration with existing structural design codes. This calibration is done on an element by element basis, even though the testing is in general applied to multiple member structures.

The load factors take into account uncertainties of loads and strength, duration of load effects and the test configuration.

INTRODUCTION

Definition of Tests

There are two important classes of load tests that may be used as acceptance tests for structures. The first is the *proof test* of an existing structure; a satisfactory test result in this case indicates a basis of acceptance only for the test structure. The second type of test is a *prototype test* on a sample of N structures; in this case a satisfactory test result may be used as a basis for the acceptance of all structures in the population to which the prototype test structures belong.

The test load, denoted by S_{test}, will be specified in the form

$$S_{test} = k_C k_D k_U \, S_{design} \qquad (1)$$

where S_{design} denotes the specified design load for the structure, and k_C, k_D and k_U are load factors to account for the loading configuration, duration effects, and uncertainties and natural variabilities in material and load properties.

In the case of proof testing, the acceptance criterion is that the proof tested structure must be capable of withstanding the specified test load without signs of distress. In the case of prototype testing, the criterion for acceptance to be used in this paper will be that the weakest structure in the sample must demonstrate the ability to withstand the specified proof load without signs of distress.

For the suite of draft limit states codes in Australia, the design load is specified as the greater of the following

$$S_{design} = 1.25\ G_{nom} + 1.5\ Q_{nom} \qquad (2a)$$

$$S_{design} = 1.25\ G_{nom} + 0.4\ Q_{nom} + W_{nom} \qquad (2b)$$

where G_{nom} denotes the dead load, Q_{nom} denotes a live load (having a 5% chance of exceedance in 50 years) and W_{nom} denotes a wind load (having a 5% chance of exceedance in 50 years).

Reliability Basis

There are many rational procedures for the derivation of load factors. For example methods based on cost-optimisation techniques, such as those derived in a previous paper (Leicester, 1984), provide a framework for linking together many reliability based decisions. However a fundamental difficulty with the use of many of these methods is that important data, such as the tail characteristics of statistical distributions, are not available, and in fact may never be so.

Because of this deficiency in the available data, it is probable that any practical method of selecting test loads will need to be very dependant on calibration procedures that are aimed at producing relative rather than absolute values of reliability. The most obvious basis of calibration is to select target reliabilities that are comparable with those obtained through the use of existing structural design codes.

One immediate consequence of this decision is that target reliabilities need to be stated in terms of individual structural elements rather than of total multiple member structures. Thus the procedure to be used for a multiple member structure is that the load factor set $k_C k_D k_U$ is obtained for each structural element in turn, and then the largest value thus obtained is the one to be inserted in equation (1).

UNCERTAINTY FACTOR k_U FOR PROTOTYPE TESTING

General

In the following, prototype testing will be considered as a method of deriving the design strength of a multiple member structure, i.e.

$$R_{M,design} = S_{design} \tag{3}$$

where $R_{M,design}$ denotes the design value of R_M, the strength of a multiple member structure.

The design strength will be stated in terms of a structural coefficient ϕ_M defined by

$$R_{M,design} = k_C k_D k_U \phi_M R_{M,0.05} \tag{4}$$

where $R_{M,0.05}$ denotes the five-percentile value of R_M.

The test load will be used to provide a lower bound estimate of the five percentile strength from

$$R_{M,0.05} = S_{test}/\gamma \tag{5}$$

where γ is load factor to be determined.

Equation (1), (3), (4) and (5) show that the uncertainty factor k_U can be derived from

$$k_U = \gamma/\phi_M \tag{6}$$

The following section indicates methods of selecting suitable values for γ and ϕ_M.

Load Factor γ

In Appendix II it is shown that the five-percentile value $R_{M,0.05}$ may be conservatively estimated by selecting a load factor γ such that

$$\gamma = \left[\frac{\ln(1-c)}{N \ln(0.95)} \right]^{V_M} \tag{7}$$

Where the c-fractile denotes the intended confidence level of the estimate and V_M denotes the coefficient of variation of R_M.

For a 75 per cent confidence level, equation (7) leads to

$$\gamma = [27/N]^{V_M} \tag{8}$$

and for a 90 per cent confidence level, equation (7) leads to

$$\gamma = [45/N]^{V_M} \tag{9}$$

A confidence level of 75 per cent is usually considered appropriate for the derivation of the characteristic values of strength for structural elements. However as indicated in the discussion in Appendix III, the use of a 90 per cent confidence level may be more correct.

Structural Coefficient ϕ_M

Within the rough concepts of first order reliability theory (Ravindra and Galambos, 1978), the design strength of a structure may be taken to be given by

$$R_{M,design} = k_C k_D k_{com} R_{M,mean} \exp\{-0.6\beta V_M\} \tag{10}$$

where $R_{M,mean}$ and V_M denote the mean value and coefficient of variation of R_M, β denotes a safety index and k_{com} denotes a 'committee factor'. The committee factor is an arbitrary multiplying constant, applied simultaneously to both loads and strength, and does not affect the level of structural safety.

Equation (4) and (10) lead to

$$\phi_M = \frac{k_{com} \exp\{-0.6\ \beta\ V_M\}}{\{R_{M,0.05}/R_{M,mean}\}} \tag{11}$$

Because this derivation is based on first order reliability theory, a lognormal distribution of strength is assumed in the application of equation (11).

The calibration of equation (11) to Australian limit states codes is discussed in Appendices IV and V, and the following parameter values were obtained,

$k_{com} = 0.9$

β = 4.0, for beams and columns
= 6.0 for connector systems.

Substitution of these values into equation (11) shows that to a good approximation

$$\phi_M = 0.90 - 0.45\ V_M \qquad (12a)$$

for beams and columns and

$$\phi_M = 0.85 - 0.95\ V_M \qquad (12b)$$

for connector systems.

Uncertainty Factor k_U

Values of k_U, computed using equations (6), (8) and (12), are shown in Table 1. To use this table it is first necessary to select suitable values of coefficient of variation for the various structural elements. The values shown in Table 2 can be used for this purpose.

TABLE 1
UNCERTAINTY FACTOR k_U

Sample size, N	k_U					
	Beams, columns			Connectors		
	V_M=0.1	V_M=0.2	V_M=0.3	V_M=0.1	V_M=0.2	V_M=0.3
1	1.6	2.4	3.5	1.8	2.9	4.8
2	1.5	2.1	2.9	1.7	2.6	3.9
5	1.4	1.7	2.2	1.6	2.1	2.9
10	1.3	1.5	1.8	1.5	1.9	2.4

Note: A confidence level of 75 per cent was used for the sampling factor γ.

TABLE 2
LIKELY VALUES OF COEFFICIENTS OF VARIATION
(Standards Association of Australia, 1986)

Structural element	Likely coefficient of variation* (%)
Timber members	
bending strength	25 - 40
tension strength	30 - 50
compression strength	15 - 25
Finger joints	
bending strength	15 - 25
Connector strength	
nailed joints	15
split ring connectors	15

* Where a range of coefficients is shown, the large values apply to timber grades containing larger natural defects.

UNCERTAINTY FACTOR k_U FOR PROOF TESTING

The simple concepts used for defining the uncertainty factor for prototype testing may be extended to include proof testing. In this case the structure is assumed to have a strength equal to the applied proof load, and to have zero variability. From equations (9) and (11) this leads to $\gamma = 1.0$, $\phi_M = 0.9$ and hence from equation (6)

$$k_U = 1.1 \qquad (13)$$

DURATION FACTOR k_D

The duration factor k_D is to take into account the fact that the properties of timber structures may change over a period of time, or alternatively the fact that the response of a structure to long duration loads may be different to the response obtained in a short duration load test.

For long duration loads, the factor k_D based on the draft recommendations of AS 1720 (Standards Association of Australia, 1986) are given by

$$k_D = k_{D1}\, k_{D2} \qquad (14)$$

where the factors k_{D1} and k_{D2} are given in Table 3 and 4.

TABLE 3
DURATION FACTOR k_{D1}

Duration of load*	k_{D1}		
	Timber members	Metal connector systems	
		Failure in wood	Failure in metal
5 seconds	1.0	0.9	1.0
5 minutes	1.0	1.0	1.0
5 days	1.0	1.2	1.0
5 months	1.1	1.3	1.0
5 years	1.3	1.5	1.0
50 years	1.8	1.8	1.0

* 'Duration of load' refers to the duration of the shortest load in a load combination.

TABLE 4
DURATION FACTOR k_{D2}

Structural component	k_{D2}	
	Seasoned timber	Unseasoned timber
Tension members	1.0	1.0
Beams		
- fully restrained	1.0	1.0
- partially restrained	1.1	1.4
Columns	1.1	1.4
Metal connector systems		
- failure in wood	1.0	1.2
- failure in metal	1.0	1.0

CONFIGURATION FACTOR k_C

Configuration factors k_C are required to compensate for the fact that either loads or strengths may not be correctly modelled during load tests.

Test structures are often modified by simplifying their buckling restraint or load sharing systems. Sometimes only a part of the structure is modelled, and some parts may be temporarily reinforced during a test. Loads are usually simplified both with respect to their spatial distribution and their time-varying characteristics.

The configuration factor depends on many considerations and hence a comprehensive discussion theron is outside the scope of this brief paper.

CONCLUDING COMMENT

The procedure developed herein is based on selecting a test load in the format given by equation (1).

To do this, each structural element in turn is examined and the appropriate load factors k_C, k_D and k_U derived; the largest multiple factor k_C, k_D, k_U obtained is the appropriate one to be used in equation (1). For structural acceptance, the test load must be carried without distress by a proof tested structure or by every tested structure in a sample of prototypes.

It is outside the scope of this paper to discuss the use of proof and prototype testing as a basis for acceptance. However it may be worth mentioning that in general the use of a pure prototype testing procedure is inefficient when applied to timber structures. This is because the high variability of some timber elements, together with the small sample sizes tested means that a large margin of safety must be used to allow for the fact that the structures tested may be stronger than average.

Usually a prototype test of a timber structure is undertaken when there is some uncertainty concerning a particular failure mode, such as that associated with a complex joint. If this is the case, then it is acceptable to consider only the load factors relevant to that failure mode or to reinforce the structure in such a way that failure can occur only in the structural mode under investigation; in such an event, the acceptance of the remainder of the structure must be based on conventional design computation procedures.

ACKNOWLEDGMENTS

The author is indebted to Ms Fran Geermans for undertaking the computing required for this paper.

APPENDIX I - THE WEIBULL DISTRIBUTION

The Weibull distribution (Benjamin and Cornell, 1970) is useful for obtaining approximate solutions to reliability problems. The cumulative distribution function of a random variable X may be written

$$\Pr\{X > x\} = \exp\{-\alpha(x/X_{mean})^m\} \tag{A1}$$

where X_{mean} denotes the mean value of x and the parameters α and m are related to the coefficient of variation V_X by

$$V_X^2 = \{\Gamma[1 + (2/m)] / \Gamma^2 [1 + (1/m)]\} - 1 \tag{A2}$$

$$\alpha = \Gamma^m [1 + (1/m)] \tag{A3}$$

in which Γ denotes a gamma function.

To a good approximation α and m may be taken as

$$\alpha = 0.555 + 0.445\ V_X \tag{A4}$$

$$m = V_X^{-1.09} \tag{A5}$$

APPENDIX II - DERIVATION OF γ

The load factor γ may be considered as defined by

$$R_{est} = R_{M,min}/\gamma \tag{A6}$$

where R_{est} is an estimate of $R_{M,p}$, the p-fractile of R_M and $R_{M,min}$ is the minimum value of R_M in a sample of size N.

From equation (A1)

$$Pr\ \{R_M > x\} = \exp\ \{ - \alpha\ (x/R_{M,mean})^m\} \tag{A7}$$

and it follows that

$$Pr\ \{R_{M,min} > x\} = \exp\ \{- N\alpha\ (x/R_{M,mean})^m\} \tag{A8}$$

By definition

$$1 - p = Pr\ \{R_M > R_{M,p}\} \tag{A9}$$

Furthermore, if the c-fractile denotes the confidence level of the estimate of $R_{M,p}$, then

$$1 - c = Pr\ \{R_{est} > R_{M,p}\} \tag{A10}$$

Equations (A6) - (A10) lead to

$$\gamma^m = \ln(1-c)/N\ \ln(1-p) \tag{A11}$$

Equation (7) is derived from equation (11) by introducing the approximation $m \approx 1/V_M$; this approximation is based on equation (A5).

The skewness of distribution of strength usually lies between those of the lognormal and Weibull distributions. Thus these two distributions are used to assess the effectiveness of equation (7). This is done in terms of an accuracy factor AF defined by

$$AF = R_{est,c}/R_{M,0.05} \tag{A12}$$

where $R_{est,c}$ denotes the c-fractile of R_{est}; the c-fractile is the target confidence level. Ideally the accuracy factor would be set at unity if the distribution of R_M were known exactly.

The accuracy factor is shown in Figure 1 for 75 and 90 per cent confidence levels. It is seen to be conservative for both types of distribution, but not unduly so if R_M happens to be a Weibull distribution.

APPENDIX III - CHOICE OF CONFIDENCE LEVELS

In terms of first order reliability theory, the target safety index β_{target} may be written

$$\beta_{target} = \frac{\ln \{R_{M,mean}/S_{mean}\}}{\sqrt{V_M^2 + V_S^2}} \qquad (A13)$$

where $R_{M,mean}$ and S_{mean} are the mean values of resistance and load and V_M and V_S are the corresponding coefficients of variation.

However, since the choice of the acceptable load is based on the five percentile value $R_{M,0.05}$ estimated according to equation (A6), the true safety index β is given by

$$\beta_{target} = \frac{\ln \{(R_{M,mean}/S_{mean})\ \lambda\}}{\sqrt{V_{est}^2 + V_M^2 + V_S^2}} \qquad (A14)$$

where

$$\lambda = R_{est,c}/R_{est,mean} \qquad (A15)$$

in which $R_{est,c}$, $R_{est,mean}$ and V_{est} are the c-fractile, mean value and coefficient of variation of R_{est}.

Equations (A6), (A8) and (A15) lead to

$$V_{est} = V_M \qquad (A16)$$

$$\lambda^m = \frac{\ln(1-c)}{\alpha} \qquad (A17)$$

Figure 2 shows safety indices computed from equation (A14). The input assumptions used are V_S=0.3 and β_{target} = 4. The graphs indicate that for large coefficients of variation it may be necessary to use a 90 per cent level of confidence in estimating $R_{M,0.05}$.

APPENDIX IV - DERIVATION OF k_{com}

The value of $k_{com} = 0.9$ used in this paper was chosen on the basis of several reliability studies on Australian limit states codes. However a simpler method is available if it is assumed that k_{com} is given by

$$k_{com} = 1/k_{u,proof} \tag{A18}$$

where $k_{u,proof}$ is the uncertainty factor in proof testing. This uncertainty factor may be obtained through cost-optimisation concepts. Use of these concepts (Leicester, 1984) lead to

$$S_{test} = k_C \, k_D \, S_{mean} \left[\frac{\ln(C_{FS}/C_{FP})}{\alpha_s}\right]^{1/m_s} \tag{A19}$$

where C_{FS} and C_{FP} refer to the cost of failure in-service and during proof testing respectively, and α_s and m_s refer to values of α and m for the applied load S.

Equations (1), A(18) and (A19) then lead to the required value of k_{com}. To obtain a value of $k_{com} = 0.9$, the parameters used were $C_{FS} = 300\ C_{FP}$, $V_S = 0.15$, $S_{design} = 1.25\ k_u\ G_{nom}$, $S_{mean} = G_{mean}$, $G_{nom} = 0.95\ G_{mean}$.

APPENDIX V - DERIVATION OF ϕ_M

In limit states codes, the criterion for the strength limit state of an element is

$$k_C k_D \phi_e R_{e,nom} = S_{design} \quad (A20)$$

where ϕ_e nd $R_{e,nom}$ are the material coefficient and the nominal strength specified for an element. From equations (3) and (4) the strength of an element as part of a multiple member structure is defined by

$$k_C k_D \phi_M R_{M,0.05} = S_{design} \quad (A21)$$

Equations (A20) and (A21) lead to

$$\phi_M = \phi_e R_{e,nom}/R_{M,0.05} \quad (A22)$$

Several current drafts of Australian limit states codes were examined and the specified values of ϕ_e and $R_{e,nom}$ were combined with estimated values of $R_{M,0.05}$ to produce values of ϕ_M. These are shown plotted in Figure 3. The same graph shows values of ϕ_M computed according to equation (11). It is seen that the graphs for safety indices of 4.0 and 6.0 are not unreasonable for structural members and for connectors respectively.

APPENDIX VI - REFERENCES

Benjamin, J.R. and Cornell, C.A. (1970). *Probability Statistics and Decision for Civil Engineers*. McGraw-Hill Book Co., New York, USA.

Leicester, R.H. (1984). Closed form solutions for cost-optimised reliability. Proc. of IUTAM Symposium on Probabilistic Methods in the Mechanics of Solids and Structures, Stockholm, June.

Ravindra, M.K. and Galambos, T.V. (1978) Load and resistance factor design for steel. *Journal of the Structural Division*, Proc. of ASCE 104, ST9, pp. 1331-1354, Sept.

Standards Association of Australia (1986). AS 1720 Timber Structures. Part 1 - Design Methods. Draft No.6. Standards House, Sydney, Australia.

APPENDIX VIII - NOTATION

c	= confidence level, c-fractile
C_{FS}	= cost of failure in-service
C_{FP}	= cost of failure during proof testing
exp{}	= expotential
G	= dead load
G_{nom}, G_{mean}	= nominal and mean value of G
k_C	= factor for test configuration
k_{com}	= committee factor, equation (10)
k_D	= factor for duration effects
k_{D1}, K_{D2}	= components of k_D
k_U	= factor for uncertainty in load and structural properties
$k_{U,proof}$	= value of k_U for proof testing
m	= parameter for a Weibull distribution, equation (A2)
m_s	= value of m for load
N	= sample size
p	= fractile value for characteristic strength
Pr{}	= probability of an event
Q_{nom}	= specified floor live load
R_{est}	= estimate of characteristic strength
$R_{est,c}$	= estimate of characteristic strength with c-fractile confidence
$R_{e,nom}$	= nominal strength of an element

R_M = strength of a multiple member structure or element therein

$R_{M,mean}$ = mean value of R_M

$R_{M,design}$ = design value of R_M

$R_{M,0.05}$ = five percentile value of R_M

$R_{M,p}$ = p-fractile value of R_M

$R_{M,min}$ = minimum value of R_M in a sample of size N

S = load

S_{design} = specified value of S

S_{mean} = mean value of S

S_{test} = value of S for required test load

V = coefficient of variation

V_{est} = value of V for R_{est}

V_M = value of V for R_M

V_S = value of V for S

W_{nom} = specified value of wind load W

α = parameter for a Weibull Distribution, equation (A3)

α_s = value of α for S

β = safety index

β_{target} = target value of β

γ = load factor defined by equation (5) and (A6)

Γ = gamma distribution

ϕ_e = material coefficient, equation (A20)

ϕ_m = structural coefficient, equation (a21)

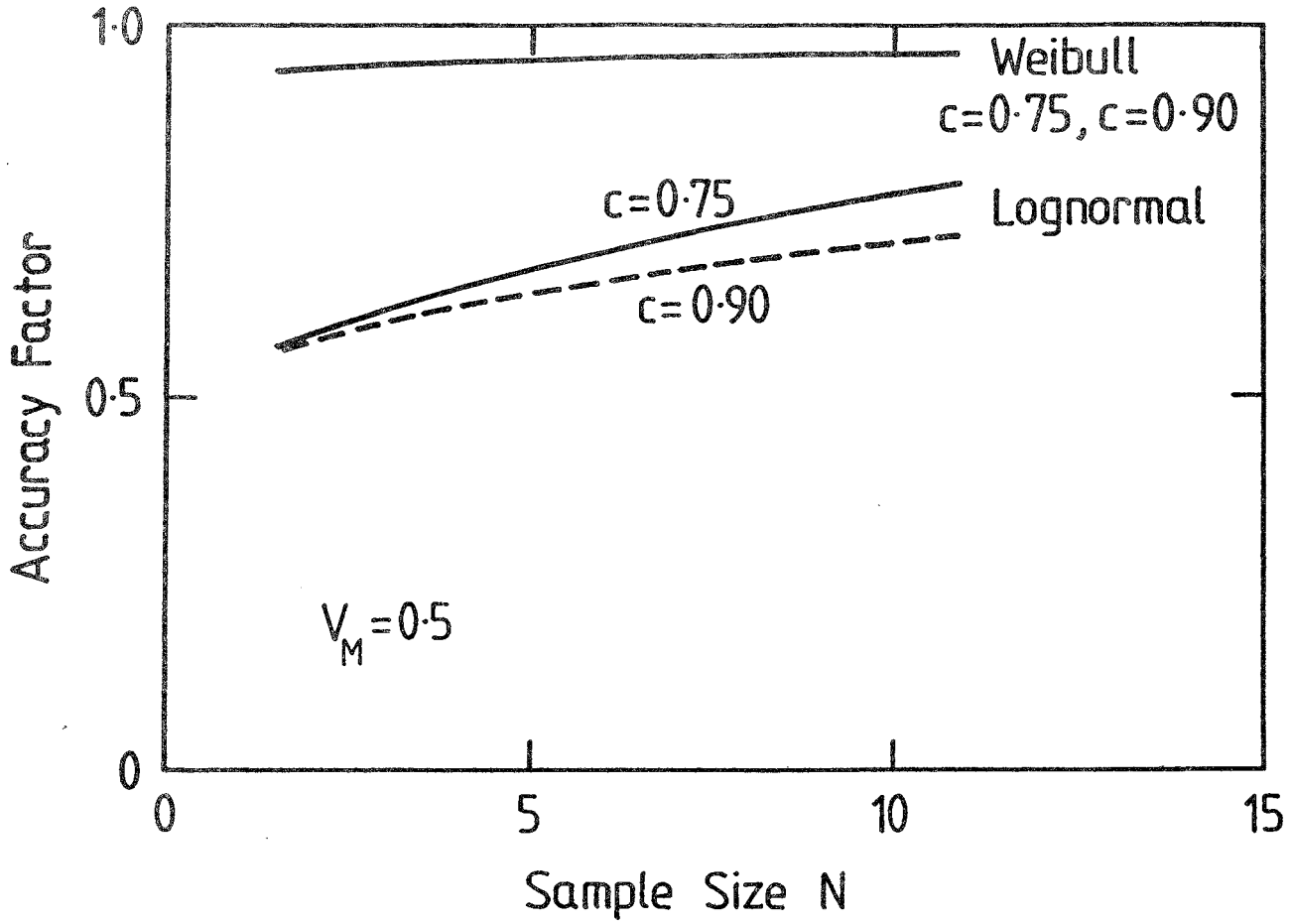


Figure 1. Effect of sample size on the accuracy factor defined in equation (A12)

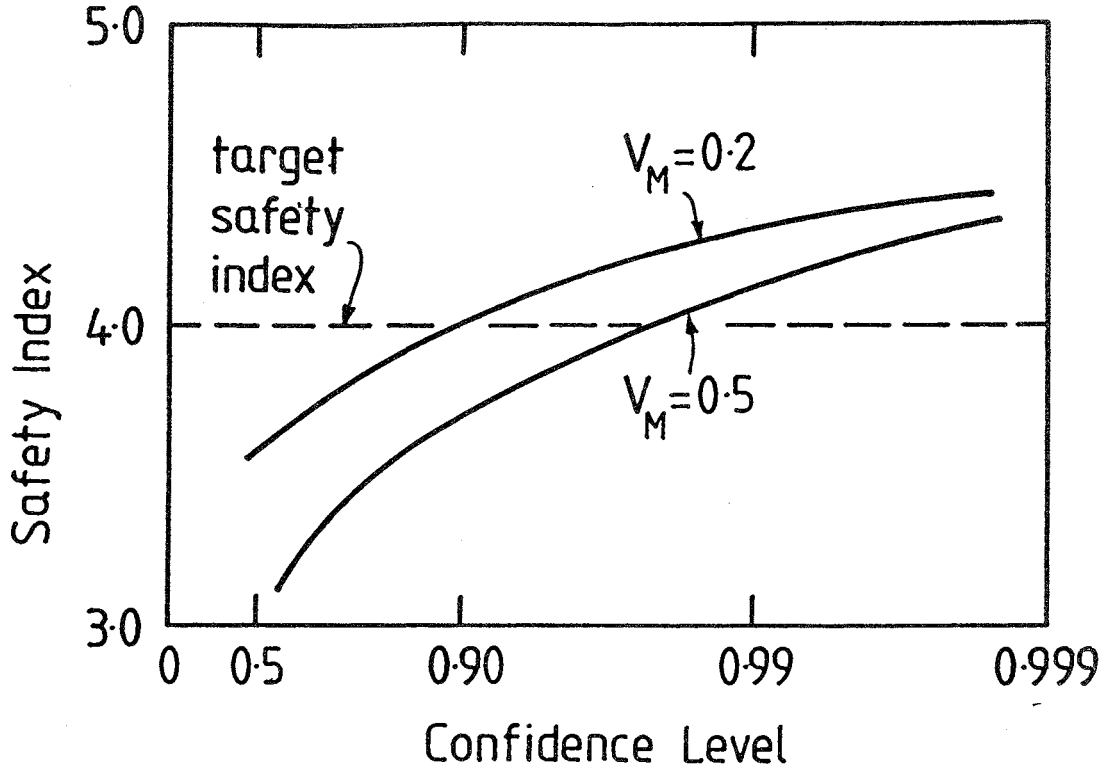


Figure 2. Effect of confidence level on the safety index (Weibull distributions)

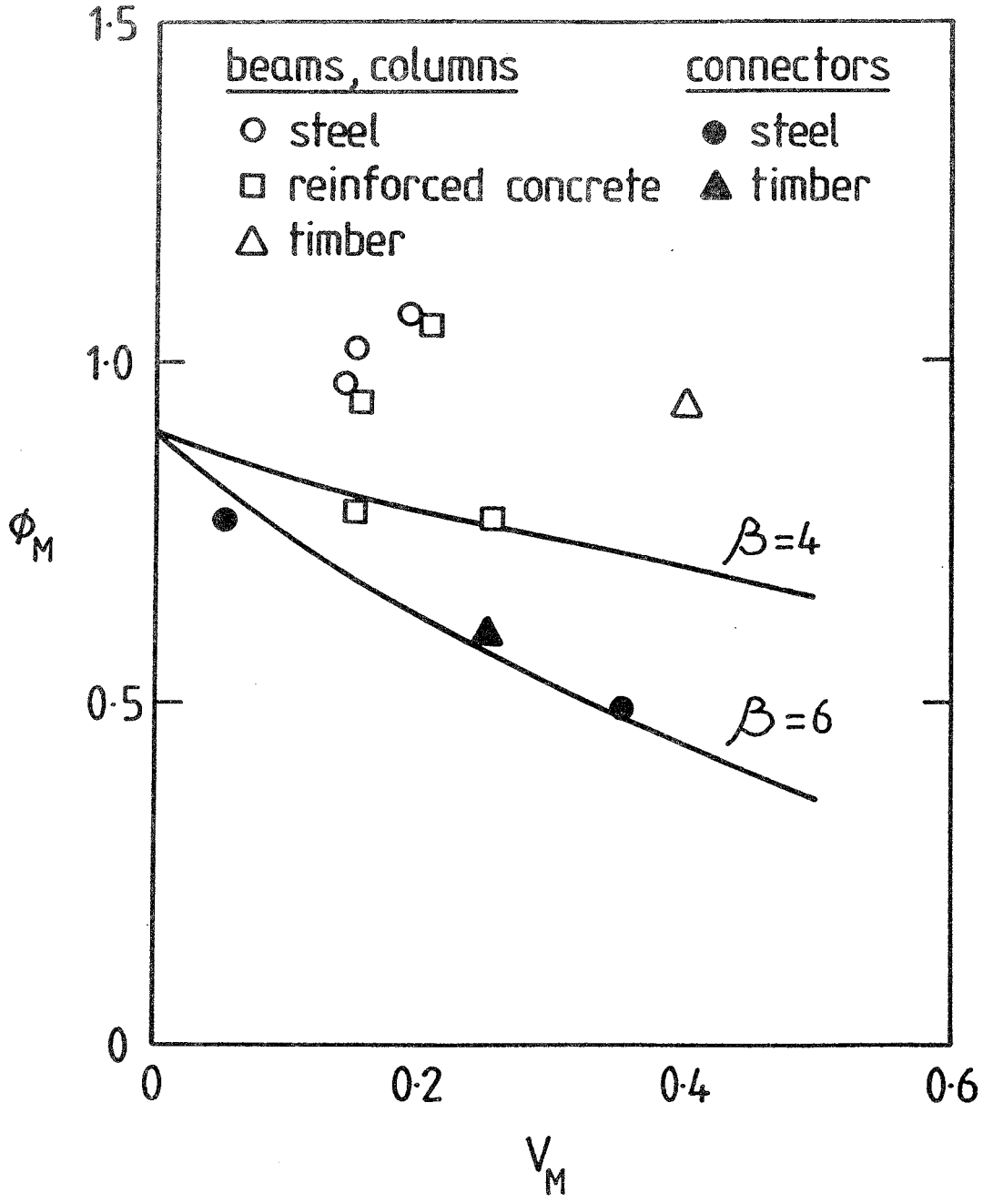


Figure 3. Derived values of the structual coefficient ϕ_M

CIB-W18/19-102-1

INTERNATIONAL COUNCIL FOR BUILDING RESEARCH STUDIES AND DOCUMENTATION

WORKING COMMISSION W18 - TIMBER STRUCTURES

EUROCODE 5 - REQUIREMENTS TO TIMBER -

by

DRAFTING PANEL EUROCODE 5
H Brüninghoff, P Crubilé, J Ehlbeck, H J Larsen, J Sunley

MEETING NINETEEN
FLORENCE
ITALY
SEPTEMBER 1986

INTRODUCTION

The section on requirements to the timber in the draft for Eurocode 5 deviates from the corresponding section in the CIB Structural Timber Design Code, and the Drafting Panel has found that it would be of value to discuss its content and presentation in CIB W18.

It is therefore reproduced below.

CODE REQUIREMENTS

Principles: Timber shall be stress graded in accordance with rules ensuring that the properties of the timber are satisfactory for use and especially that the strength and stiffness properties are reliable.

The grading rules shall be based on a visual assessment of the timber, on the non-destructive measurement of one or more properties, or on a combination of the two methods.

Strength and stiffness values shall where possible be determined by standardised short-term tests in accordance with ISO 8375.

The test material shall be a representative sample of the reference population, and the test specimens cut from the test material shall contain a strength reducing grade determining defect. In tests for the determination of the bending strength the length with constant moment shall contain a strength reducing grade determining defect, and the edge placed in tension shall be chosen at random.

Rules for application: Characteristic strength and stiffness values: Examples on the material properties for a number of species and grades are given in Annex 8.

The material properties for a series of strength classes C 1 - C 10 are given in Annex 9.

ANNEX 9 STRENGTH AND DENSITY CLASSES FOR TIMBER AND FINGER JOINTED TIMBER

A 9.1 Strength classes

The strength and stiffness values for a series of strength classes C 1 - C 10 are given in table A 9.1 a.

The bending strength applies to a beam with a depth of 200 mm. The tension strength applies to a member with a width (i.e. greatest cross-section dimension) of 200 mm.

A species/grade combination may be assigned to a strength class in accordance with table A 9.1 b.

Table A 9.1 b. Classification rules

grade classification for each property				resultant assigned
$f_{m,k}$	$f_{t,0,k}$	$f_{c,0,k}$	$E_{0,mean}$	strength class
C_x	C_x	C_x	C_x	C_x
C_x	C_x	C_{x-1}	C_{x+1}	C_x
C_{x+1}	C_x	C_{x-1}	C_{x-1}	C_x

C_x means that the characteristic value is greater or equal to the characteristic value required in table 3.1.2 for class C_x

A 9.2 Density classes

The density of wood without defects for a series of density classes D 300 - D 800 is given in table A 9.2.

Table A 9.1 a. Strength classes. Characteristic values and mean E-values in MPa

		Strength class									
MPa		C1	C2	C3	C4	C5	C6	C7	C8	C9	C10
bending	$f_{m,k}$										
- visually graded		12.0	15.0	18.0	21.5	25.0	28.5	38.0	48.0	60.0	75.0
- machine graded		11.0	14.0	17.0	20.0	23.0	26.0	35.0	44.0	55.0	69.0
tension par. to grain	$f_{t,0,k}$	7.0	9.0	11.0	13.0	15.0	17.0	24.0	30.0	38.0	48.0
compression par. to grain	$f_{c,0,k}$	13.0	15.0	17.0	19.0	22.5	26.0	30.0	38.0	48.0	60.0
shear	$f_{v,k}$	1.7	1.9	2.0	2.1	2.4	2.7	3.8	4.8	6.0	6.0
Modulus of elasticity, mean	$E_{0,mean}$	7000	8000	9000	10000	11000	12000	13500	17000	22000	27000

Table A 9.2. Density classes. Characteristic density

Density class	D 300	D 400	D 500	D 600	D 800
Characteristic density in kg/m^3	300	400	500	600	800

A species/grade combination may be assigned to a density class if the characteristic density is higher than or equal to the value of the class.

A 9.3 Characteristic strength values

Characteristic strength values are given in table A 9.1 a and A 9.3 a.

Bending strength is related to a depth of 200 mm and tension strength to a width (i.e. greatest cross-section dimension) of 200 mm. If the depth or width respectively is h the bending strength or tension strength should be multiplied by k_h

$$k_h = \left(\frac{200}{h}\right)^{0.2} \qquad \text{(A 9.3)}$$

Tabel A 9.3 a. Characteristic strength values perpendicular to the grain in MPa

		Density class				
		D 300	D 400	D 500	D 600	D 800
tension perp. to grain	$f_{t,90,k}$	0.3	0.4	0.5	0.6	0.8
compression perp. to grain	$f_{c,90,k}$	6.0	7.0	8.0	11.0	13.0

For instability calculations (lateral instability, columns, buckling) the ratio $E_{0,k}/f_{c,0,k}$ and $E_{0,k}/f_{m,k}$ should be taken from table A 9.3 b.

Table A 9.3 b. The ratio $E_{0,k}/f_{c,0,k}$ and $E_{0,k}/f_{m,k}$ for use in instability calculations

strength class	C1	C2	C3	C4	C5	C6	C7	C8	C9	C10
$E_{0,k}/f_{c,0,k}$	370	370	370	370	340	320	320	320	320	320
$E_{0,k}/f_{m,k}$	410	370	350	330	310	300	250	250	250	250

The shear modulus G_{mean} should be taken as $E_{0,mean}/\boxed{16}$.

The modulus of elasticity perpendicular to the grain $E_{90,mean}$ should be taken as $E_{0,mean}/\boxed{30}$ for softwoods and as $E_{0,mean}/\boxed{15}$ for hardwoods.

A 9.4 Examples

Table A 9.4 gives some softwood species and grades meeting the requirements of classes C1 - C6 given in table 3.1.2 together with the density class. For the botanical names reference is made to Annex 6.

Table A 9.4. Strength and density classes densities for some softwoods

	strength class				density class	
	C1	C2	C4	C6	D 300	D 400
European						
whitewood, redwood		S6	S8	S10		S6-S1
North American						
douglas fir-larch, hem-fir		S6	S8	S10		S6-S1
spruce-pine-fir		S6	S8	S10		S6-S1
douglas fir-larch, hem-fir		No. 1, No. 2	Sel.		No.1 No.2	Sel.
spruce-pine-fir		No. 1, No. 2	Sel.		No.1	Sel.
western whitewood (USA)	No. 1, No. 2	Sel.			No.1,Sel. No.2	
southern pine (USA)		No. 1, No. 2 No. 3		Sel.	No.1 No.2 No.3	Sel.

S6, S8, S10: Grades according to ISO/DP CCCC
No. 1, No. 2, No. 3, Sel(ect): Joist and plank grades according to NLGA 1979 or NGRDL 1975.

CIB-W18/19-102-2

INTERNATIONAL COUNCIL FOR BUILDING RESEARCH STUDIES AND DOCUMENTATION

WORKING COMMISSION W18 - TIMBER STRUCTURES

EUROCODE 5 AND CIB STRUCTURAL TIMBER DESIGN CODE

by

H J Larsen
Danish Building Research Institute
Denmark

MEETING NINETEEN
FLORENCE
ITALY
SEPTEMBER 1986

EUROCODE 5 AND CIB STRUCTURAL TIMBER DESIGN CODE

H.J. Larsen, Danish Building Research Institute

1 INTRODUCTION

Eurocode 5, Timber Structures, 1985, drafted for the Commission of the European Economic Community, is based on the CIB Structural Timber Design Code (CIB, 1983), in the following called the CIB-code. There are, however, differences, due to technical and theoretical developments in the span of time between the two documents and due also to Eurocode 5 being an operational code for direct use by the designers, whereas the CIB-code is a model code to be used by code writers.

In the following are described some of the differences between the two documents, and proposals for new sections to be incorporated in both documents are put forward.

The items treated are

3 Safety system and partial coefficients
4 Columns
5 Tension perpendicular to the grain
6 Shear
7 Plane frames

Section 2 gives the notation used. Section 8 is a list of references.

2 NOTATION

Apart from the general notation set out in CIB-code to which reference is made, the following symbols are used:

G	Permanent action
Q	Variable action
	Total load on a beam (shear design)
R	Resistance capacity
S	Action effect
W	Section modulus
$f_{c,0}$	Compression strength parallel to the grain
	$f^{o}_{c,0}$ corresponding to $\lambda = 0$
h	height of structure
k_c	Column factor
	k^{o}_{c} corresponding to $f^{o}_{c,0}$
k_{dis}	Distribution factor
	$k_{dis,v}$ for shear
k_{eu}	Euler factor
	k^{o}_{eu} corresponding to $f^{o}_{c,0}$
k_l	length factor
k_{mod}	Modification factor taking into account moisture content and duration of action
k_{vol}	Volume factor
	$k_{vol,v}$ for shear
k_{wei}	Shape factor
n	Safety factor (global)
γ	Partial coefficient
	γ_g on permanent action
	γ_q on variable action
	γ_M on resistance
η	Eccentricity factor
ϕ	Angle of inclination
ψ	Reduction factors to actions

3 SAFETY SYSTEM AND PARTIAL COEFFICIENTS

The safety system corresponds to the one described in ISO 2394, i.e. it is a limit state system and the partial coefficient method is used.

In the following only the simplest case is discussed i.e. where the safety verification can be made by comparing the action effect, S, with the corresponding resistance capacity R.

In Eurocode 5 this comparison is written as

$$S_d \leq R_d \tag{3.01}$$

where S_d is the design value of the action effect and R_d is the design value of the resistance capacity.

S_d is the effect from combinations of permanent actions G and variable action Q and the fundamental combination for ultimate limit states is

$$\gamma_g G + \gamma_{q1} Q_1 + \gamma_{q2}\psi_2 Q_2 + \gamma_{q3}\psi_3 Q_3 \ldots\ldots \tag{3.02}$$

where

G	is permanent action, normally mean value
Q_1, Q_2, Q_3	are variable actions with their characteristic values (code values)
$\gamma_g, \gamma_{q1}, \gamma_{q2}$	are partial coefficients on g and q respectively
ψ_2, ψ_3	are reduction factots (≤ 1) taking into account that it is unlikely that more than one variable action will act with its characteristic value at a given time.

The design resistance is found as

$$R_d = k_{mod} R_k / \gamma_M \tag{3.03}$$

where

R_k	is the characteristic resistance capacity (short term)
k_{mod}	is a factor taking into account the effect on strength parameters of the duration of the load and the moisture content in the structure
γ_M	is a partial coefficient (material factor).

The Coordination Group for the Eurocodes has rather arbitrarily prescribed

$$\gamma_g = 1.35$$
$$\gamma_q = 1.50 \qquad (3.04)$$

and the Drafting Panels for the different Eurocodes have then been asked to propose values for γ_M, and for Eurocode 5 also for k_{mod}.

The values proposed by the Drafting Panel for Eurocode 5 are mainly based on a calibration to existing design practice, which in most countries is the permissible stress method. By this $\gamma_g = \gamma_q$, and the (global) safety factor is n:

$$n = \gamma_M / k_{mod} \qquad (3.04)$$

Only in a few codes is n given explicitely, just the permissible stresses are given.

An exception is Canada, where for permanent load and interior conditions

$$n = \frac{4}{3}\,\frac{16}{9} = 2.4 \qquad (3.05)$$

In the draft for the German code (Draft DIN 1052, 1984) n is given directly only for some panels. Related to the mean value n = 3 is prescribed. Assuming a coefficient of variation of 0.10 it corresponds to

$$n \sim 3(1 - 2 \cdot 0.10) = 2.4 \qquad (3.06)$$

In the British code (BS 5268, Part 2, 1984) only permissible stresses are given. By comparing them with the published characteristic values for different species and grades, a value of about

$$n = 2.3 \qquad (3.07)$$

has been found.

In the Nordic countries the partial coefficient system has been used for many years, and the partial coefficients have been fixed on the basis of the results from the use of the so-called safety index method, see (NKB, 1978).

The Nordic values correspond to γ_M-values in the range of 1.5 (for permanent load) to 1.95 (for variable loads) with k_{mod} = 0.6 for high-grade material, and k_{mod} = 0.75 for low-grade material. This gives n-values between 2.0 and 3.25.

In France permissible stresses have been devided from the mean resistance R_{mean} with a safety factor of 2.75. It is proposed in future to use

$$n = 2.28 \tag{3.08}$$

on the R_k for all load durations and combinations for solid timber.

The Drafting Panel has decided to aim at n = 2.4 for normal structures, and with a variable load equal to the permanent load, and has proposed to use

$$k_{mod} = 0.8 \tag{3.09}$$
$$\gamma_M = 1.4 \tag{3.10}$$

corresponding to $n = 1.35 \cdot 1.4/0.8 = 2.36$ for permanent load and $n = 1.5 \cdot 1.4/0.8 = 2.63$ for variable long term loads.

A 10 per cent reduction is proposed for structures where the consequences of failure are not serious, e.g. for some farm buildings and sheds, warehouses, lighting masts and secondary structural members. A 10 per cent reduction is also proposed for machine stress graded timber to take into account the reduced variability as compared to visually graded materials.

k_{mod} = 0.8 is a rather high value compared to todays practice where k_{mod} is taken at about 0.55 - 0.60, values that are supported by the tests performed in Canada, USA and a number of European countries.

The arguments for the high value of k_{mod} are that in practice the stress level will be much lower than in the tests in the major part of the life time of the structure. And k_{mod} = 0.6 would give values of γ_M of about 1, i.e. a lower value than the one proposed for steel and much lower than the one for concrete (where $\gamma_M \sim 1.5$).

It is however obvious that there is a great need for research into the safety of timber structures.

4 COLUMNS

The design of columns in Eurocode 5 is based on the CIB column formulas. Its derivation is given in (Larsen, 1973). In Eurocode 5 some modifications, however, have been introduced to make the design especially of short columns, more economical. The main purpose of this section is to desrcibe these modifications. Further the background for the proposed values of the eccentricity factor is given.

4.1 Concentrically loaded columns

In brief the design of simply supported, concentrically loaded columns in the CIB-code and Eurocode 5 is based on the following assumptions:

a) The axis of the columns has an initial sinusoidal curvature corresponding to a maximum eccentricity of the axial force of

$$e = \eta\, r\, \lambda \qquad (4.1.01)$$

where

r is the core radius. ($r = W/A$ where W is the section modulus and A the area of the cross-section)

λ is the slenderness ratio: $\lambda = l_c/i$, where i is the radius of gyration. ($i = h/\sqrt{12}$ for a rectangular cross-section).

η is an eccentricity factor, which is discussed in 4.3.

b) The behaviour is linear-elastic until failure

c) Failure takes place when

$$\sigma_{c,0}/f^{o}_{c,0} + \sigma_m/f_m = 1 \qquad (4.1.02)$$

$f^{o}_{c,0}$ is the compression strength corresponding to $\lambda = 0$.

These assumptions lead to the requirement that the stresses should satisfy the following condition:

$$\sigma_{c,0} \leq k^o_c f^o_{c,0} \tag{4.1.03}$$

where

$$k^o_c = 0.5 \left[1 + (1 + \eta\lambda \frac{f^o_{c,0}}{f_m})k^o_{eu} - \sqrt{(1 + (1 + \eta\lambda \frac{f^o_{c,0}}{f_m})k^o_{eu})^2 - 4k^o_{eu}}\right] \tag{4.1.04}$$

and

$$k^o_{eu} = \frac{\pi^2 E_0}{f^o_{c,o}\lambda^2} \tag{4.1.05}$$

The compression strength $f_{c,0}$ in the CIB-Code and Eurocode 5 is, in accordance with ISO 8375, determined by test specimens with a slenderness ratio of about 20, i.e. according to (4.1.01) with an initial eccentricity of $e = 20\eta r$, see figure 4.1. In the following the increase in eccentricity due to the deflection is disregarded. This is on the safe side.

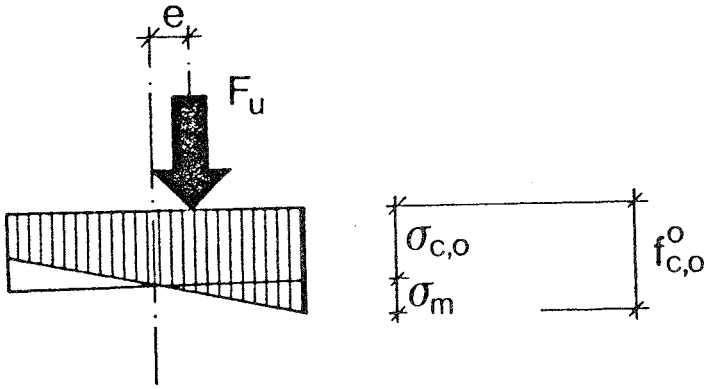


Figure 4.1

Using (also on the safe side) the following simplified failure criterion:

$$\sigma_{c,0} + \sigma_m = f^o_{c,0} \tag{4.1.06}$$

where

$$\sigma_{c,0} = F_u/A = f_{c,0} \tag{4.1.07}$$

$$\sigma_m = F_u e/W = f_{c,0}\ \eta\ r\ \lambda\ A/W \tag{4.1.08}$$

then

$$f^o_{c,0} = f_{c,0}(1 + \eta\ \lambda) = f_{c,0}(1 + 20\eta) \tag{4.1.09}$$

Inserting $f^o_{c,0}$ in (4.1.03-05) leads to the following design criterion:

$$\sigma_{c,0} \leq k_c f_{c,0} \tag{4.1.10}$$

with

$$k_c = 0.5(1 + 20\eta)\left[1+(1 + \eta\lambda(1 + 20\eta)\frac{f_{c,0}}{f_m})\frac{k_{eu}}{1+20\eta} - \sqrt{(1+(1 + \eta\lambda(1 + 20\eta)\frac{f_{c,0}}{f_m})\frac{k_{eu}}{1+20\eta})^2 - 4\,\frac{k_{eu}}{1+20\eta}}\right] \tag{4.1.11}$$

$$k_{eu} = \frac{\pi^2 E_0}{f_{c,0}\lambda^2} \tag{4.1.12}$$

For practical reasons Eurocode 5 further requires

$$k_c \leq 1 \tag{4.1.13}$$

4.2 Laterally loaded columns

The following assumptions are made additional to those for concentrically loaded columns.

d) There is a lateral load acting in the direction of one of the main axis of the cross-section giving a moment varying sinusoidally from 0 at the ends to M in the middle. M corresponds to a bending stress of σ_m.

Assuming a sinusoidal moment curve can in some cases be on the unsafe side. For the worst case - the axial load acting with equal end-eccentricities - it is on the conservative side to replace σ_m by $\frac{4}{\pi}\sigma_m$ in (4.2.01).

e) The column will deflect in the direction of the load.

The laterally loaded column will behave as a concentrically loaded column with an initial eccentricity of (e + M/F), where F is the axial force.

It is found that the following condition should be satisfied, see (Larsen, 1973).

$$\frac{\sigma_{c,0}}{k_c f_{c,0}} + \frac{\sigma_m}{f_m} \frac{1}{1 - \frac{k_c \sigma_{c,0}}{k_{eu} f_{c,0}}} \leq 1 \qquad (4.2.01)$$

where k_c and k_{eu} are given in (4.1.11 - .12)
Often (4.1.16) is replaced by

$$\frac{\sigma_{c,0}}{k_c f_{c,0}} + \frac{\sigma_m}{f_m} \leq 1 \qquad (4.2.02)$$

The relative error (on the unsafe side) by this simplification corresponds to $\Delta a/a$ in figure 4.2 a.

This simplification is not proposed in Eurocode 5.

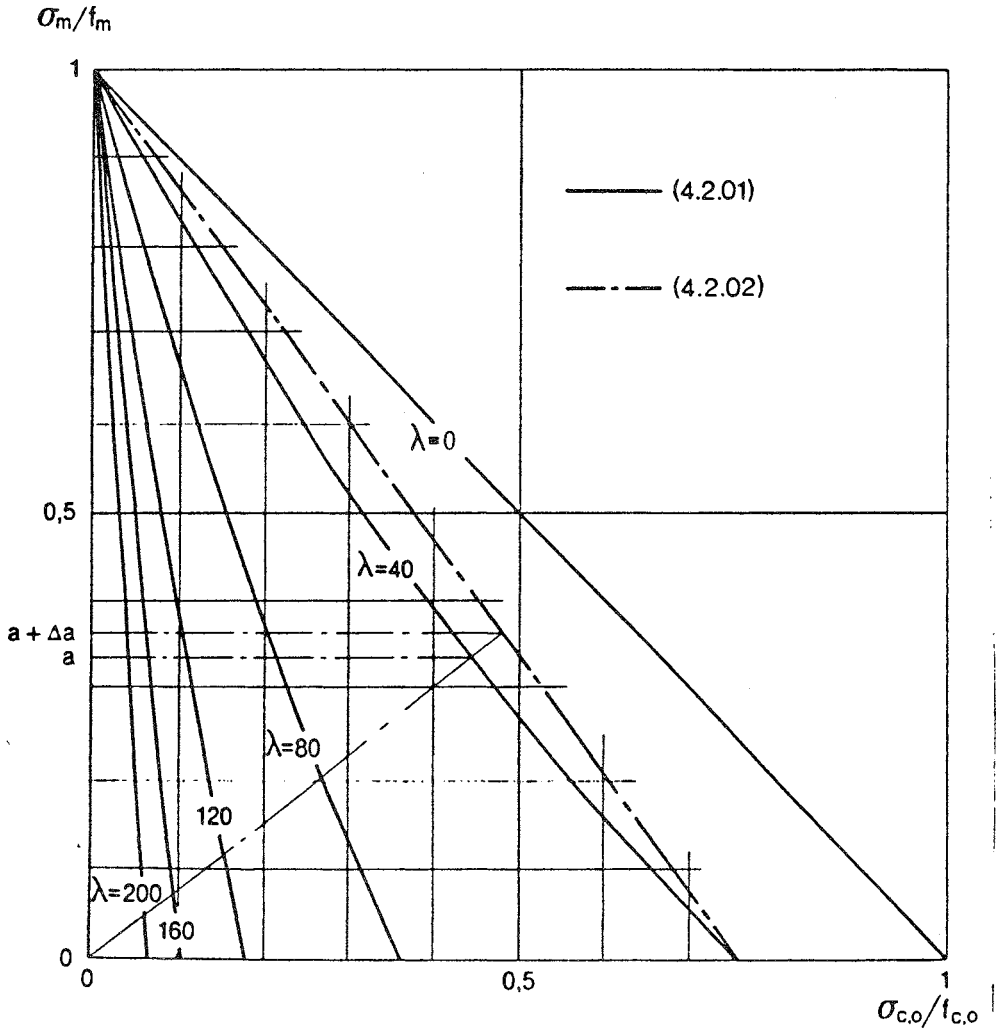


Figure 4.2 b. Acceptable combinations according to formula (4.2.01) and (4.2.02) of $\sigma_{c,0}/f_{c,0}$ and σ_m/f_m. The λ-values are given on the curves.

In some cases assumption e) is not fulfilled. As an example the column shown in figure 4.2 c can, depending on the distance between the lateral supports, fail by vertical deflection, by lateral deflection or by a combination hereof. This phenomenon is studied in (Larsen and Theilgaard, 1979), and it is shown to be a good approximation to use (4.2.01) with k_c corresponding to the larger λ for the two directions, i.e. for the column in figure 4.2 c with rectangular cross-section the minumum of $l\sqrt{12}/h$ and $l_{brac}\sqrt{12}/b$.

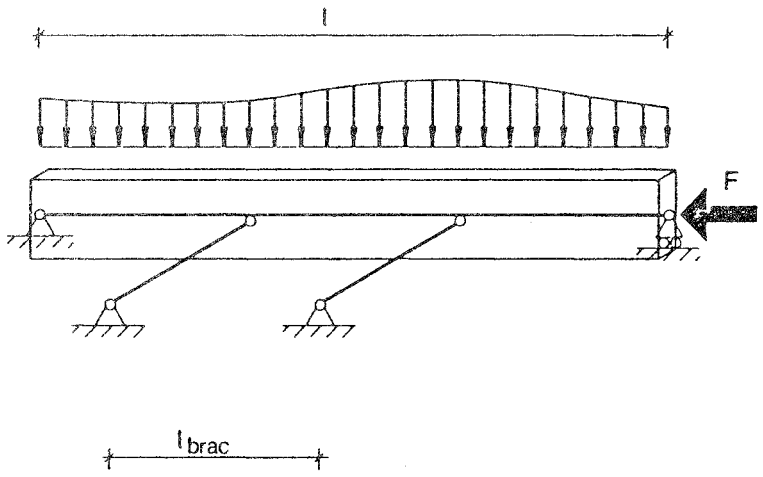


Figure 4.2 c.

4.3 Eccentricity factor

The basic parameter is the eccentricity factor η defined by

$$e = \eta \cdot r \lambda \qquad (4.1.01)$$

In (BS 5268, Part 2, 1984) e is given as

$$e = \frac{1}{300} = \frac{1}{300} \frac{i}{r} r \frac{l}{i} = \frac{6}{300 \cdot \sqrt{12}} r\lambda = 0.0058\ r\lambda \qquad (4.3.01)$$

i.e

$$\eta = 0.0058.$$

The same value has been found for structural timber by the tests described in (Larsen and Theilgaard, 1979). For glued laminated columns $\eta = 0.004$ has been found.

In (DIN 1052, Teil 1, 1969) k_c is tabled for ordinary columns. The table for structural timber corresponds very closely to the one that would result from formula (4.1.11) with $\eta = 0.005$. For glued laminated columns much smaller η-values are assumed.

For structures not covered by the tables in (DIN 1052, Teil 1, 1969) e is given as

$$e = 0.10r + \frac{2}{a} k\lambda \qquad (4.3.02)$$

with
a = 500 for glued laminated columns
a = 400 for structural timber, high grade
a = 250 for structural timber, low grade.

The constant in (4.3.02) which complicates the calculations, is not consistent with the definition of the compressive strength. For $\lambda = 0$ it leads to the requirement $\sigma_{c,0}(1 + 0.10) \leq f_{c,0}$ instead of $\sigma_{c,0} \leq f_{c,0}$. With $\eta = 0.005$ for glulam and $\eta = 0.006$ (0.009) for structural timber, high grade (low grade) formula (4.3.01) and (4.3.02) give the same values for $\lambda = 100$.

In Eurocode 5 the following values have been proposed:
- For structural timber

$$\eta = 0.006 \qquad (4.3.03)$$

corresponding for a rectangular cross-section to an initial eccentricity of 1 300 of the length.
- For glued laminated timber columns

$$\eta = 0.004 \qquad (4.3.04)$$

5 TENSION PERPENDICULAR TO THE GRAIN

5.1 General

For some of the strength properties - e.g. tensile strength perpendicular to the grain and shear strength - there is a marked size effect. This effect can be explained by Weibull's fracture theory for brittle materials, see (Weilbull, 1939) and (Barrett, Foschi, and Fox, 1975). According to this theory the distribution function of a property x is

$$F(x) = \begin{cases} 0 & \text{for } x \leq \varepsilon \quad (5.1.01) \\ 1 - \exp\left[-\left(\frac{x-\varepsilon}{\delta}\right)^{k_{wei}}\right] & \text{for } x \geq \varepsilon \quad (5.1.02) \end{cases}$$

where

k_{wei} is the shape parameter
δ is the scale factor
ε is the location parameter, i.e. the minimum possible value.

In the following it is assumed that $\varepsilon = 0$, i.e. the socalled 2-parameter Weibull distribution is used:

$$F(x) = 1 - \exp\left[-\left(\frac{x}{\delta}\right)^{k_{wei}}\right] \quad (5.1.03)$$

This will overestimate the size effect, i.e. be on the safe side, for volumes bigger than the reference volume V_0 of 0.02 m^3, see below. This will usually be the case.

Consider now a volume V_1 of a material where (5.1.03) applies to all sub-volumes and assume that the stresses are

$$\sigma_1(x,y,z) = \sigma_1 \cdot G(x,y,z) \quad (5.1.04)$$

where σ_1 is the magnitude of a characteristic stress in the distribution described by G. Then the probability of failure P is

$$P = 1 - \exp\left(-\int_{V_1} \left(\frac{\sigma_1 G}{\delta}\right)^{k_{wei}} dV\right) \quad (5.1.05)$$

A volume V_2 affine to V_1 has the same stress distribution, but with σ_2 as the magnitude of the characteristic stress. If the two volumes have the same probability of failure, it follows from (5.1.05) that

$$\sigma_1^{k_{wei}} V_1 = \sigma_2^{k_{wei}} V_2$$

or

$$\frac{\sigma_2}{\sigma_1} = \left(\frac{V_1}{V_2}\right)^{1/k_{wei}} \tag{5.1.06}$$

i.e. the strength (defined by a fractile) is inversely proportional to the stressed volume to the power of $1/k_{wei}$.

Equation (5.1.07) also shows that two volumes with different stress distributions have the same strength if

$$\int_{V_1} \sigma_1(x,y,z)^{k_{wei}} dV = \int_{V_2} \sigma_2(x,y,z)^{k_{wei}} dV \tag{5.1.07}$$

The parameter k_{wei} is related to the variability of the strength in question, which is relatively independent of species, and a constant value of $k_{wei} = 5$ has been assumed in Eurocode 5. Test values range from about 4 to about 6.

In Eurocode 5 clause 5.1.3 the following requirements are given.

They follow directly from the above, remembering the definition of $f_{t,90}$ as the strength of a uniformly stressed volume V_0 of 0.02 m^3.

"The following condition should be satisfied:

$$\sigma_{t,90,d} < k_{vol}\, k_{dis} f_{t,90,d} \tag{5.1.08}$$

where k_{vol} (≤ 1) takes into account the effect of the size of the stressed volume V, and k_{dis} the effect of the distribution of the stresses.

For a stressed volume, V, k_{vol} can be taken as

$$k_{vol} = \left(\frac{V_0}{V}\right)^{1/k_{wei}} \tag{5.1.09}$$

where $V_0 = 0.02\ m^3$ and $k_{wei} = 5$ can be assumed for softwoods.

For a uniformly stressed volume $k_{dis} = 1$.

For a volume V with a varying stress $\sigma_{t,90} = \sigma\ (x,y,z)$ with a maximum value of σ_{max}

$$k_{dis} = \frac{\sigma_{max}}{\frac{1}{V} \int_V \sigma(x,y,z)^{k_{wei}}\, dV)^{1/k_{wei}}} \qquad (5.1.10)$$

5.2 Curved beams

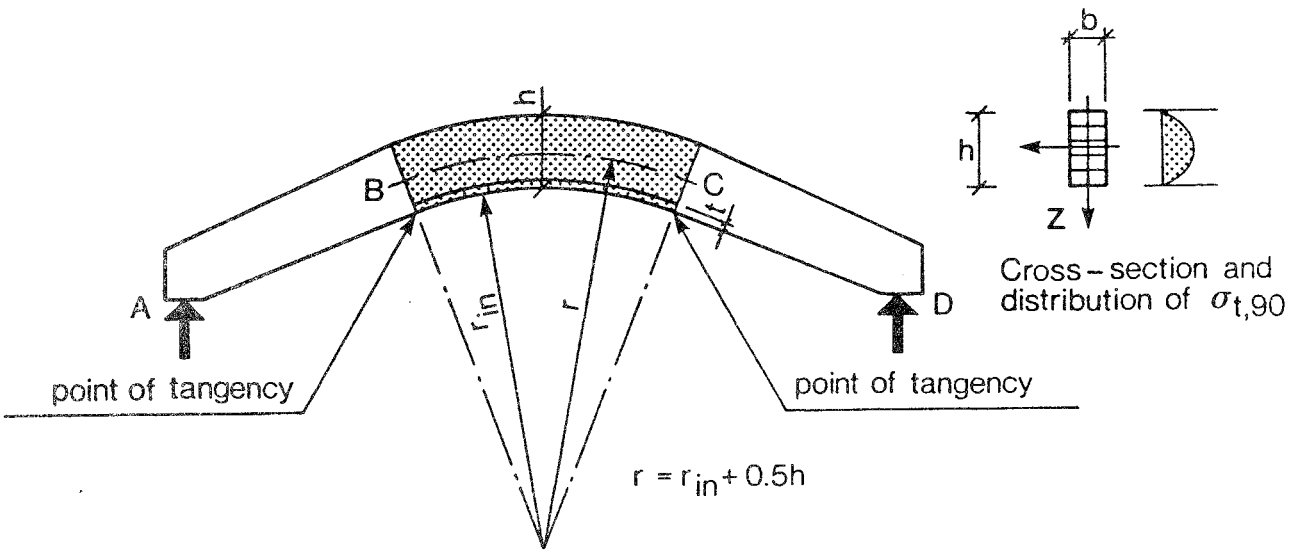


Figure 5.2 a.

In a section of a curved beam where the moment is M, the maximum stress perpendicular $\sigma_{t,90,max}$ to the grain is with good approximation

$$\sigma_{t,90,max} = \frac{1.5\ M}{r\ b\ h} \qquad (5.2.01)$$

and the distribution over the depth is parabolic.

In Eurocode 5 it is required that the tensile stresses calculated by (5.2.01) shall satisfy the following condition:

$$\sigma_{t,90,max} \leq k_{vol}\ k_{dis}\ f_{t,90} \qquad (5.2.02)$$

The volume factor

$$k_{vol} = \left(\frac{V_0}{V}\right)^{1/k_{wei}} \qquad (5.2.03)$$

is explained above.

The distribution factor k_{dis} for a constant moment can be found by inserting into (5.1.10).

$$\frac{\sigma}{\sigma_{max}} = 1 - \left(\frac{2z}{h}\right)^2$$

$$1/k_{dis} = \left(\frac{1}{h}\int_{-0.5h}^{0.5h}\left(1 - \left(\frac{2z}{h}\right)^2\right)^5 dz\right)^{0.2} = 0.366^{0.2}$$

$$k_{dis} = 1.22 \qquad (5.2.04)$$

For curved beam with uniformly distributed load, i.e. parabolic variation along the beam of the moments and thus also of the tension perpendicular to the grain

$$k_{dis} = 1.22^2 \sim 1.5 \qquad (5.2.05)$$

5.3 Tapered and cambered beams

With one exception the values given in Eurocode 5 correspond to those of Canada (CAN 3 - 086 - M80, 1980) although the presentation is slightly different as regards the volume to be used for the volume factor. The derivation of the Canadian values are given in (Fox and Foschi, 1970).

The exception is for cambered beams and uniformly distributed load, where the Canadian rules would correspond to $k_{dis} \sim 2$. In Eurocode 5 a value of $k_{dis} = 1.7$ has been given to bring a better agreement with recent German tests.

6 SHEAR

For beams of structural timber the traditional shear design method is used. According to established practice in many countries loads close to the support are only taken partly into consideration.

For glued laminated timber beams a method proposed by Foschi and Barrett, see e.g. (Foschi and Barrett, 1977) and (Foschi, 1985), is used. The method is based on the same assumptions as for tension failure perpendicular to the grain, i.e. the failure is brittle failure corresponding to a 2-parameter Weibull distribution and with the same shape factor, i.e. $k_{wei} = 5$.

According to Eurocode 5, the shear strength, f_v, is assumed to correspond to the strength of a uniformly distributed volume of 0.08 m^3. If the shear strength is determined on a simply supported beam with a concentrated load in the middle, the reference volume is 0.1 m^3, because of the parabolic variation of the stresses over the depth, cf. (5.2.04).

According to Eurocode 5 the total design load Q_d on the beam (i.e. not the shear force) shall satisfy the following conditions

$$Q_d \leq k_{vol,v}\, k_{dis,v} k_l (\tfrac{4}{3}\, b\, h\, f_{v,d}) \qquad (6.01)$$

$k_{vol,v}$ takes into account the effect of the size of the stressed volume, $k_{dis,v}$ takes into account the effect of the distribution of shear forces and k_l the effect of the length.

The length factor is

$$k_l = 1/(1 - 2h) \qquad (6.02)$$

and takes into account the influence on the stress distribution at the support or under the loads where the stresses are smoothed out.

The volume factor

$$k_{vol,v} = (\frac{V_0}{V})^{1/k_{wei}} \qquad (6.03)$$

and the distribution factor

$$k_{dis,v} = \frac{0.5\ Q_d}{(\frac{1}{l}\int_l [hV_d/h(x)]\ k_{wei}(h(x)/h)dx)^{1/k_{wei}}} \qquad (6.04)$$

corresponds to (5.1.09) and (5.1.10).

Examples on $k_{dis,v}$ are given in an annex to Eurocode 5. $k_{dis,v}$ may safely be taken as 0.5 for a beam with a loaded cantilever and as 1.0 in other cases.

It should be underlined that the proposed method in most cases will lead to a more economic shear design, and that by taking explicitely into account the size effect, the special rules for end notched glued laminated beams have been left out.

7 PLANE FRAMES

The following new section in the CIB-code and Eurocode 5 is proposed.

The stresses caused by geometrical and structural imperfections - i.e. deviations between the geometrical axis and the elastic centre of the cross-section due to e.g. material inhomogenities - and induced deflection shall be taken into account.

This may be done either by regarding the parts between points with zero moment as laterally loaded columns, cf. Eurocode 5 sections 2.10.4 and 5.1.10 or by the following method:

The imperfect shape of the structure shall be assumed to correspond to an initial deformation which is in approximate affinity to the relevant deformation figure and can be found by applying an angle ϕ of inclination to the structure or relevant parts, and an initial sinusoidal curvature between the modes of the structure corresponding to a maximum eccentricity e, see figure 7.01.

ϕ shall as a minimum be taken as

$$\phi = \boxed{0.005} \qquad \text{for } h \leq 5 \text{ m} \tag{7.01}$$

and

$$\phi = \boxed{0.005}\sqrt{5/h} \qquad \text{for } h > 5 \text{ m} \tag{7.02}$$

where h is the height of the structure on the length of the member, in m.

e shall as a minimum be taken as

$$e = \boxed{0.003}\, l \tag{7.03}$$

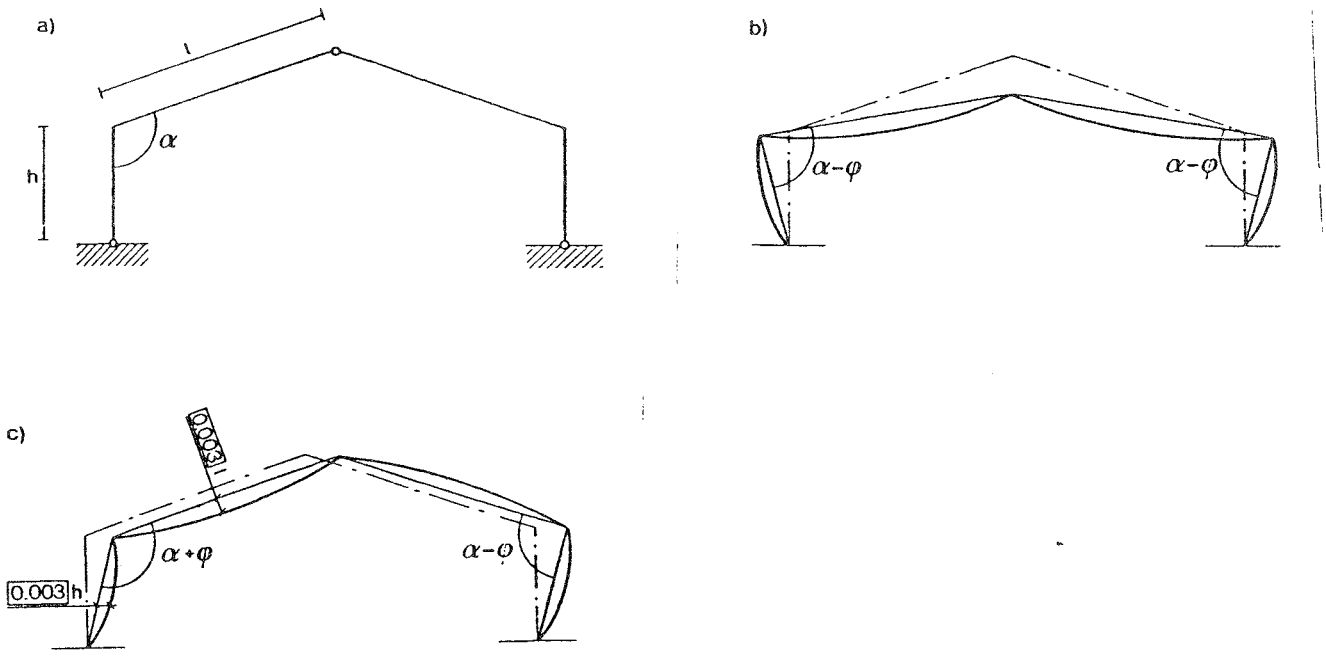


Figure 7.01. An example of assumed initial deflections for a frame (a) corresponding to symmetrical load (b) and non-symmetrical load (c).

For the three-hinged frame shown in figure 7.02 the following approximate method may be used.

For the load cases giving maximum bending stresses in the curved part (in point D) the part AE (E is the point where M = 0) is treated as a laterally loaded column. The free column length is taken as l_{AE}, or - if this will give a higher slenderness ratio - as the distance between the points, where the frame is held against lateral deflection.

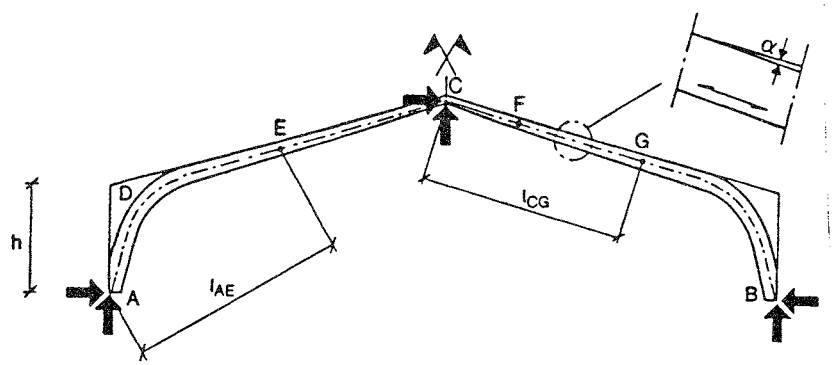


Figure 7.02. Three-hinged frame of glued laminated timber.

The following condition should be satisfied:

$$\frac{\sigma_{c,d}}{k_c f_{c,0,d}} + k_{in} \frac{\sigma_{m,d}}{k_{inst} f_{m,d}} \leq k_r \qquad (7.04)$$

where k_{in} an k_r are given in Eurocode 5 (5.1.12 b-g) and k_{inst} in section 5.1.6.

For the load cases giving maximum bending stresses in the straight part (in point F) the part CG (G is the point where M = 0) is treated as a laterally loaded column. The free length is taken as l_{CG} or - if this will give a higher slenderness ratio - as the distance between the points where the frame is held against lateral deflection.

The following condition should be satisfied:

$$\frac{\sigma_{c,d}}{k_c f_{c,0,d}} + \frac{\sigma_{m,d}}{k_{inst} f_{m,d}} \leq$$

$$\frac{1}{(1-4.4\ \tan^2\alpha)\ \sqrt{(\cos^4\alpha + \sin^2\alpha\cos^2\alpha(f_{m,d}/f_{v,d})^2 + \sin^4\alpha(f_{m,d}/f_{c,90,d}))^2}} \qquad (7.05)$$

cf. Eurocode 5 (5.1.11d) and (5.1.9b).
α is the angle between the grain and the upper fase of the beam, se figure 7.02.

8 LITERATURE

Barrett, J.D., Foschi, R.O. & Fox, S.P., 1975: Perpendicular to the grain strength of Douglas-fir. Proceeding of International Union of Forestry Research Organizations, Wood Engineering Group, Delft.

BS 5268, Part 2, 1984. Structural use of timber.

Can 3-086.1-M 80, 1980: Canadian Standards, Code for Engineering Design in Wood.

CIB, 1983. Conseil International du Bâtiment. CIB Structural Timber Design Code. CIB Report Publication 66.

DIN 1052, Teil 1, Draft August 1984. Holzbauwerke, Berechnung und Ausführung.

DIN 1052, Teil 1, 1969. Holzbauwerke. Berechnung und Ausführung.

Eurocode 5, 1985. Common Unified Rules for Timber Structures. Report prepared for the European Communities.

Foschi, R.O. & Fox, S.P., 1970: Radial stress in curved timber beams. Journal of the Structural Division, Proc. ASCE, Vol. 96, No. S 110.

Foschi, R.O. & Barrett, D., 1977: Longitudinal shear in wood beams: a design method. Canadian Journal of Civil Engineering, Vol. 4, No.3.

Foschi, R.O., 1985: Longitudinal shear design of glued laminated beams. CIB W18 paper 18-10-2.

ISO 2394, General Principles on the reliability for structures, 1986.

ISO 8375. Solid timber in structural sizes - Determination of some phusical and mechanical properties.

Larsen, H.J., 1973. The design of solid timber columns (CIB W18 paper 2-2-1).

Larsen, H.J. & Theilgaard, E., 1979. Laterally loaded timber columns. ASCE, Journal of the structural division. Vol. 105, No. ST 7.

NKB, 1978. Nordic Committee on Building.
NKB-Report No. 36. Recommendation for loading and safety regulations for structural design.

Weilbull, W., 1939. A statistical theory of the strength of materials. Swedish Royal Institute. Eng. Res. Proc. Stockholm.

CIB-W18/19-102-3

INTERNATIONAL COUNCIL FOR BUILDING RESEARCH STUDIES AND DOCUMENTATION

WORKING COMMISSION W18 - TIMBER STRUCTURES

COMMENTS ON THE FORMAT OF EUROCODE 5

by

A R Fewell
Princes Risborough Laboratory
United Kingdom

MEETING NINETEEN
FLORENCE
ITALY
SEPTEMBER 1986

COMMENTS ON THE FORMAT OF EUROCODE 5

By A R Fewell, PRINCES RISBOROUGH LABORATORY, 1986

INTRODUCTION

Development continues in the European Economic Community on a suite of structural design codes, known as Eurocodes, for all major construction materials. These codes use a limit state partial factor format that has some severe shortcomings as pointed out by Armer and Mayne[1] and Fewell and Pierce[2]. Whilst there are other points in the draft Eurocode 5 which cause concern this paper restricts its comments to the question of format to focus attention and attempt to awaken opinion on the subject before change becomes more difficult. The fact that the format for the design equation proposed in the draft Eurocode 5 for timber can be successfully calibrated to produce design solutions acceptable to each country is not disputed. However it is the desirability of having a format that includes rationally determined factors and is flexible enough to incorporate future needs, that gives rise to the comments detailed here.

CODE OBJECTIVES

It is intended that the Eurocodes will be used by the building profession for drawing up competitive tenders and will be, or will form the basis of, regulating documents in some countries. The Eurocodes therefore need to be precise but must not stifle the designers innovative instincts. To enforce a set of rules with various factors and coefficients having irrational values and unclear definitions, restricts the designer from using his ingenuity and prevents him from having a feel for the degree of safety in his design and the likely consequences of any innovative departures from past experience. Furthermore, because it is in everybody's interest that there should not be frequent changes to the general Eurocode format, the format should be capable of incorporating the results of current and future research. It is therefore important that the codes should offer a basic framework capable of coping with the above points and capable of future development without major change.

PRL56-86

THE CURRENT DRAFT EUROCODE 5 (EC5)

In its simplest form the Eurocode design equation format is

$$\gamma_G G + \gamma_Q Q \leqslant k_{mod} f_K/\gamma_M$$

where: f_K is the characteristic stress

G and Q are the permanent and variable actions respectively

γ_G and γ_Q are the partial coefficients that not only reflect the uncertainties of the loads G and Q but include unquantifiable uncertanties in the assessment of action effects

γ_M is a partial coefficient that not only reflects the uncertainty of the characteristic strength but includes uncertanties due to the model, differences between material properties in the structure and those in standardised tests, variations in geometrical properties, and in Eurocode 5 γ_M even includes a consequence factor

k_{mod} is a factor to allow for the effects of load duration and moisture content

The full format provides coefficients for combinations of loads etc, but it is not necessary to give those details here.

The definitions of the partial coefficients result in irrational values being assigned to these and other factors to achieve levels of safety compatible with current codes. For example Larsen[3] admits that the partial coefficients have been prescribed arbitrarily and that the value for k_{mod} is higher than can be justified by current research.

It is inevitable that in each country the acceptability of values for the various factors and coefficients will be judged by calibration against national codes. Indeed it is necessary for the Eurocode and each national code to give similar design solutions if the official objective requiring international tenders based on Eurocodes to be competitive with those based on national codes, is to be achieved. With the above format involving the imprecise definitions it will be a simple task to make the adjustments to achieve similar design solutions to national codes. However the result would be values as in EC5 which for the reasons given above are of limited value. Furthermore because of the arbitrary and subjective division of numerous, and in some instances unknown, uncertainties into the various

coefficients and factors, it would be a problem to know what to adjust should research enable particular uncertainties to be quantified. This problem is compounded by the fact that γ_F should be material independent and would need the committees for all materials to agree before a change could take place.

Summarising, the current proposed format would:

a result in irrational values to many of the coefficients and factors, due to imprecise definitions;

b prevent engineers from gaining a feel for the uncertainties and safety of their structures;

c make it difficult to achieve the Eurocode objective of competitive tendering, whether designs are based on the national code or Eurocode;

d make it difficult to develop the Eurocode by incorporating the results of research. This problem is compounded by the fact that the partial coefficients and characteristic values for actions should be material independent.

THE PROPOSED FORMAT

One aim of the partial factor format is to allocate the various uncertanties to the associated parts of the design equation and therefore permit a more appropriate level of safety, producing more economic structures. The number of factors is not a problem because of computers but it could be reduced by combining certain factors or properties provided it does not restrict the designers innovation or ingenuity.

Coefficients must be determined on a rational basis and (except for γ_D) cover a single source of variability. Where there is insufficient data to determine a particular coefficient then this has to be estimated and acknowledged as such. This also has a benefit in that it pinpoints areas for future research.

The proposed format, again in its simplest form is

$$\gamma_G G + \gamma_Q Q \leqslant k_{MC} k_{DOL} f_K / \gamma_M . \gamma_D$$

where G, Q and f_K are as previously given

γ_G and γ_Q are partial coefficients reflecting solely the uncertainties of individual actions

γ_M are partial coefficients reflecting solely the uncertainties of individual strength properties

γ_D is a partial coefficient reflecting all other uncertainties uncertainties including an element of calibration.

When research isolates and evaluates an effect or uncertainty included in γ_D then, if thought beneficial, it could be taken out of γ_D and treated separately.

CONCLUSION

It seems illogical that the Eurocodes should adopt a format with the intention of achieving some high ideals involving safety, flexibility and economy and then end up determining most of the coefficients or factors by what amounts to guesswork because the details and definitions in the format have not been thoroughly thought out. Furthermore this puts enormous constraints on future development of the Eurocodes and the inclusion of results from research, because of the interdependence of all factors and coefficients in the design equation.

The problems could be overcome by:

a defining each partial coefficient (except γ_D) to cover <u>one</u> source of variability;

b defining γ_D to include all remaining uncertainties and be the only repository for any adjustments for calibration. If research should identify and quantify a hitherto unknown effect or cause of uncertainty then it may be taken out of γ_D and listed separately;

c quantifying the consequence factor separately, if it can be justified at all;

d developing a rational procedure and using available data to quantify the partial coefficients and factors where possible. Where values have to be estimated this must be acknowledged.

At first glance the issues raised here may seem of little consequence because of our lack of knowledge of many of the design factors and the difficulty in seeing where research will produce arguments for change. But if the irrational values for many of the factors in EC5 which were quantified to relate to existing design solutions remain, then the interdependence of all these factors will make future developments difficult and deny the designer the right to assess the level of safety in his structures.

We need a format which gives us a flexible framework in which timber structural design can develop unhindered. I am sure many of us know the difficulties of changing national codes; to change a published Eurocode will be many times more difficult.

REFERENCES

1 ARMER G. S. T. and MAYNE J. R. On the format of modern codes of practice for structural design. BRE 1986. To be published by CIB.

2 FEWELL A. R. and PIERCE C. B. Considerations for the development of a UK limit state design code for timber. BRE 1986.

3 LARSEN H. J. Eurocodee 5 and CIB structural timber design code IUFRO/CIB.W18 paper 19-102-2.

CIB-W18/19-102-4

INTERNATIONAL COUNCIL FOR BUILDING RESEARCH STUDIES AND DOCUMENTATION

WORKING COMMISSION W18 - TIMBER STRUCTURES

NEW DEVELOPMENTS OF LIMIT STATES DESIGN FOR THE NEW GDR TIMBER DESIGN CODE

by

W Rug and M Badstube
Academy of Building, Institute for Industrial Buildings
German Democratic Republic

MEETING NINETEEN
FLORENCE
ITALY
SEPTEMBER 1986

New Developments of Limit State Design for the New GDR Timber Design Code

By W. Rug and Dr M. Badstube,
Academy of Building of the GDR, Institute for Industrial Buildings
Berlin, 1986

Contents

1. Introduction
2. Limit States
2.1. Limit States of the Load-Carrying Capacity (GZT)
2.2. Limit States of the Usability (GZN)
3. Sorting by Strength Grades
4. Basic Values of the Design Strengths
5. Adaptation Factors
5.1. Adaptation Factor γ_{m1} for Long-Term Behaviour
5.2. Adaptation Factor γ_{m2} for Cross-Sectional Height
5.3. Adaptation Factor γ_{m3} for Curvature of Timber
5.4. Adaptation Factor γ_{m4} for Aggressive Media
6. Further Research
7. References (Bibliography)

1. Introduction

An improved exploitation of the mechanical properties of timber and timber material requires the continuous improvement of the calculation and design methods or the introduction of new methods, respectively.
The change from design methods adopting admissible stresses to methods adopting limit states in timber construction is an initial step towards a probabilistic safety concept. As compared with the method by admissible stresses, the method by limit states renders it possible to cover and record more exactly by calculation the degree of loading of the built-in material subject to the actual state of utilization. Thus, the exploitation of the available materials can be improved.

Reference /1/ reports the beginning of the research work in this field.
Other papers (see references /2/ to /5/) have been published recently.

The present state of preparation of the future Timber Design Code is being described hereinafter. The results and findings were provided by implementing a close co-operation and teamwork between the GDR research institutions and establishments concerned.
The work and activities performed hitherto resulted in defining initial regulations for the future design code, such as - inter alia - for the symbols and definitions, standard and basic values of the design strengths as well as the adaptation factors. The structural arrangement of the design code is being specified on the model of the ISO and CIB Codes (see references /6/ and /7/) and according to the GDR Codes and Standards being applicable at present /8/. The designations comply in the main with those of the ISO Code /6/ (see Table 1).

2. Limit States

The limit states are distinguishable into the following two types :-

(A) limit states of the load-carrying capacity (GZT)
(B) limit states of the usability (GZN)

2.1. Limit States of the Load-Carrying Capacity (GZT)

During the whole service life of a building or structure, the maximum possible stress and loading must be smaller than or equal to the minimum possible loadability of the material concerned.
An exceeding of this limit state results in a complete unserviceability or failure of the timber structure.
The checks of the GZT limit states include the following :-
- strength of the loadbearing members
- strength of the connections
- stability of the loadbearing members
- overturning, lifting of the building/structure, and the like.

The checks of the GZT limit states can be established by means of equation (1) for the design values, by means of equation (2) for the internal forces, or by means of equation (3) for the stresses.

$$S \leq R_F \qquad (1)$$

or $$M;\ N;\ V \leq R_M;\ R_N;\ R_V \qquad (2)$$

or $$\sigma \leq R \qquad (3)$$

S = design value of the load
R_F = design value of the acceptable load
M, N, V = design values of the internal forces
R_M, R_N, R_V = design values of the acceptable internal forces
σ = design value of the stresses
R = design value of the strength

The design values of the loads are calculated by means of equation (4).

$$S = \gamma_n \left(\sum_{i=1}^{n} F_i^n \cdot \gamma_{f,i} + \psi \sum_{j=1}^{m} F_j^n \cdot \gamma_{f,j} \right) \qquad (4)$$

with $i = 1 \ldots n$ being the index for continuous and long-term actions/influences
$j = 1 \ldots m$ being the index for short-term and sudden actions/influences
γ_n according to Table 2 from /14/
ψ according to Table 3 from /15/
γ_f according to Table 4 from /15/

The design values of the internal forces and stresses are provided by analogy with this.

The design value of the strength is provided by means of equation (5).

$$R = R^{o} \cdot \Pi \cdot \gamma_{m,i} \qquad (5)$$

R^{o} = basic value of the design strength

$\gamma_{m,i}$ = adaptation factors

2.2. Limit States of the Usability (GZN)

During the whole service life of a building or structure, the deformation of the construction due to the standard loads must be smaller than or equal to its limit value according to the design/project. An exceeding of this limit state restricts the utilization of the construction as specified by the design/project.

$$u \leqq u \qquad (6)$$

$$\text{with } u = \sum_{i=1}^{n} u_i^n + \Psi \sum_{f=1}^{m} u_j^n$$

With u_i^n being the deformation due to the standard value of a continuous or long-term action/influence

u_j^n being the deformation due to the standard value of a short-term action/influence

The checks of the GZN limit states include the following :-
- deformation of the loadbearing members
- vibrations/oscillations of the loadbearing members
- positional changes of the building/structure

3. Sorting by Strength Grades

The reliability and efficiency of the design methods in timber construction can be increased considerably by adding in future the sorting parameters of mechanical sorting such as volume weight (bulk specific gravity) and modulus of bending elasticity to the sorting parameters of the hitherto prevailing visual sorting such as knots, splits, grain deviations, wingiess and the like. Looking at the coefficients of correlation

between sorting parameters and strength properties as shown in Table 5, one will see that the modulus of bending elasticity on the one hand and the knottiness and volume weight on the other hand have the same correlation with the strength properties.
The highest correlation with the strength properties is being provided by the modulus of bending elasticity in connection with the knottiness. A comparison with line 1 of Table 5 shows that the mechanical sorting is superior to the visual sorting.

Internationally, a classification/grading of the timber is being effected according to the characteristic strength which nowadays is consistently defined as 5 % quantile of a three-parametric Weibull distribution if the characteristic values were determined by tests in structural timber dimensions. The characteristic strength corresponds to the standard value of the design strength.

In general, the characteristic strength of faultless specimens is being determined by means of the normal distribution. 6

4. Basic Values of the Design Strengths

The basic values of the design strength are being derived from the standard values of the design strengths (5 % quantiles).

$$R^{o} = \frac{R^{n}(0.05)}{\gamma_{m,o}} \cdot K_{mod}$$

with $K_{mod} = k_e \cdot k_t$

K_{mod} = modification factor for transforming the design strength to normalized grades of moisture and load duration
k_e = modification factor as to climatic grade
k_t = modification factor as to load-duration grade
$\gamma_{m,o}$ = material factor

The material factor $\gamma_{m,o}$ is a partial safety factor consisting of several single factors (see Table 6) by means of which the possible uncertainties in the actual behaviour of the construction or structural unit, respectively, and the calculation/design results shall be covered.

In the GDR, material factors were not yet defined since further basic and fundamental studies and investigations are still required. This is the reason why initially only the standard values of the strengths are being indicated. Table 7 includes the standard values for individual types of stress and strain checked and tested by means of experiments.
The standard values are indicated for structural timber being sorted visually according to the quality grade of same, for structural timber being sorted mechanically according to the specific strength grade (see Figure 1).
Concerning glued laminated timber, in future 6 grades will be included in the Code. The structure/design and arrangement of same is shown in Figure 2. The individual grade 1 to 3 layers of the boards are being sorted visually whereas those of grade 4 to 6 are being sorted mechanically (see Table 8).

Tests and experiments to determine the basic values of the grades 4 to 6 of glued laminated timber are being prepared at present.

5. Adaptation Factors

The adaptation factors $\gamma_{m,i}$ cover the systematic deviations or variations in the strength and deformation behaviour of the structural timber and glued laminated timber, of the timber fasteners and of the constructions occurring under real conditions of stress and strain.
The following 4 adaptation factors will be taken into consideration in the future Timber Design Code :-

$\gamma_{m,1}$ = adaptation factor as to long-term behaviour
$\gamma_{m,2}$ = adaptation factor as to cross-sectional height
$\gamma_{m,3}$ = adaptation factor as to curvature of timber
$\gamma_{m,4}$ = adaptation factor as to aggressive media

5.1. "Long-Term Behaviour" Adaptation Factor $\gamma_{m,1}$

It covers the complex influence exercised by magnitude of loading, duration of loading, moisture of timber, and temperature.

Based upon the references /2/ and /9/, 3 moisture grades, 3 time grades and 2 temperature grades will be included in the future Code (see Tables 9a to 9d) in order to determine the adaptation factor $\gamma_{m,1}$. The adaptation factor decreases with an increasing duration of loading and temperature (see Table 10).

5.2. "Cross-Sectional Height" Adaptation Factor $\gamma_{m,2}$

Table 11 indicates the adaptation factor $\gamma_{m,2}$ for structural timber and glued laminated timber subjected to flexural load. The reduction of strength begins above h = 200 mm for structural timber and above h > 300 mm for glued laminated timber. According to reference /9/, the adaptation factor $\gamma_{m,2}$ for glued laminated timber is also in line with the actual Code which is still based upon the method of the admissible stresses (see Table 11).

5.3. "Curvature of Timber" Adaptation Factor $\gamma_{m,3}$

Due to curvature, a reduction of the flexural strength of the structural timber or glued laminated timber takes place (see Table 12). The reduction occurs in accordance with the Swiss Code /12/.

5.4. "Aggressive Media" Adaptation Factor $\gamma_{m,4}$

The adaptation factor is being indicated in Tables 13a and 13b for structural timber and glued laminated timber subject to the degree of load, stress and strain imposed by the aggressive media (such as - e.g. - salts, acids, bases, vapours, gases).

Timber is resistant to weak acids with normal room temperature and to alkaline solutions of a low concentration. A corrosive action will occur only due to strongly acid and strongly alkaline solutions. In general, no timber corrosion is to be expected within the pH-value range of $2 < pH > 11$ /10/. With the majority of chemicals in a solid, liquid and gaseous state, the corrosive action decreases in the course of time and a destruction occurs only within the zone near the surface.

Investigations of timber beams installed in old structures of the potash industry resulted in observing a strength reduction caused by K 40 type potash salt only in the boundary/end zone of 10...20 mm (with an age of the structure concerned amounting to 54 years).
Separate investigations of pine-wood test specimens taken from a conveyor bridge being 54 years old showed that there were considerable differences in strength between the boundary and inner zones which were caused by the action/influence of nitro-chalk (see Figure 3).

The cross-sectional dimensions influence the corrosive action of the aggressive media. This is the reason why the adaptation factors were defined subject to the cross section of the timber. However, the corrosive action is also influenced by protect-ive/preservative systems being applied additionally (see the Tables 13a and 13b).

6. Further Research

In order to prepare the future GDR Timber Design Code by adopt-ing the method of limit states, comprehensive studies and in-vestigations are still required with structural timber and glued laminated timber as well as with timber connections/ fasteners.

The tests planned until 1988 will serve to determine standard and basic values of the design strength, standard and basic values of the modulus of elasticity and shear modulus, and to determine adaptation factors (see Table 14).
The investigations to determine standard and basic values of the design strength are concentrated on research activities and papers concerning the strength of structural timber and glued laminated timber subjected to flexural load and compress-ive stress as well as of nailed and dowelled connections.

The research activities and papers to determine adaptation factors are concentrated on the long-term behaviour adaptation factor, including the influence of the moisture of timber, the cross-sectional height in case of glued laminated timber, and aggressive media.

7. References (Bibliography)

/1/ Rug, W.
Research on Problems of Limit States Design in Preparation of the New GDR Code
Academy of Building of the GDR, Institute for Industrial Buildings, Berlin 1985

/2/ Badstube, M.; Rug, W.
Erarbeitung der ingenieurtheoretischen Grundlagen für den Standard "Holzbau, Tragwerke, Berechnung nach Grenzzuständen"
(Preparation of the engineering-theoretical fundamentals for the Code "Timber Construction, Loadbearing Members, Calculation by Limit States")
Academy of Building of the GDR, Institute for Industrial Buildings,
Research Report, Berlin 1985

/3/ Zimmer, K.-H.; Lißner, H.
Zur Bemessung von Holzkonstruktionen nach Grenzzuständen
(On the Design of Timber Structures by Limit States)
Wiss. Zeitschrift der TU Dresden (Scientific Periodical of the Dresden University of Technology),
Dresden 34(1985)1, pp. 65-72

/4/ Zimmer, K.-H.
Zur Bemessung von Holzkonstruktionen nach Grenzzuständen
(On the Design of Timber Structures by Limit States),
12th Congress, Vancouver, B.C. Reprint from the Final Report, Zurich 1985

/5/ Apitz, R.
Beitrag zur Bestimmung der Festigkeitskennwerte von Bauholz bei Biegebeanspruchung für die Bemessung nach der Methode der Grenzzustände
(Paper on the Determination of the Strength Parameters of Structural Timber under Flexural Load for the Design by the Method of Limit States)
Ingenieurhochschule Wismar, Dissertation A (Wismar Engineering College; Grade "A" Dissertation), Wismar 1985

/6/ ISO-TC-165-N, 1983-05-11
Timber Structures, Design; First Working Draft, June 1983
ISO, Technical Committee 165

/7/ CIB-W18-Code
CIB-Structural Timber Design Code, sixth edition, January 1983, CIB-Report 1983, Publication 66
Working Group W 18, Timber Structures

/8/ Code/Standard TGL 33 135 - Blatt (sheet) 1
Holzbau, Tragwerke, Berechnung, Bauliche Durchbildung
(Timber Construction, Loadbearing Members, Calculation, Structural Design)
Ausgabe Januar 1984, Verlag für Standardisierung
(edition of January 1984, Standardization Publishers),
Leipzig/DDR

/9/ Vorschrift (Instruction) 174/85
Holzbau; Tragwerke; Berechnung; Bauliche Durchbildung
(1. Änderung von TGL 33 135 /01)
(Timber Construction; Loadbearing Members; Calculation; Structural Design (1st Modification to TGL 33 135 /01))
Mitteilungsblatt der Staatlichen Bauaufsicht
(Bulletin of the State Building Supervision Authority)
Berlin 9(1985)10/11, pp. 82-84

/10/ Mörath, E.
Die Widerstandsfähigkeit der wichtigsten einheimischen Holzarten gegen chemische Angriffe
(The Resistivity of the Most Important Domestic Kinds of Wood against Chemical Attacks)
Mitteilung des Fachausschusses für Holzfragen beim VDI
1933, Heft 5
(Information of the Committee of Experts for Timber Problems with the VDI 1933, Number 5)

/11/ Erler, K.
Untersuchungen an alten Holzkonstruktionen in der chemischen Industrie
(Investigations of Old Timber Structures in the Chemical Industry)
3. Internationales Symposium "Holz in Baukonstruktionen"
(3rd International Symposium "Timber in Building Constructions), Bratislava/Czechoslovakia 1984

/12/ Schweizer Norm (Swiss Code)
SIA 164, Zurich 1981

/13/ Glos, P.; Schulz, H.
Stand und Aussichten der maschinellen Schnittholzsortierung
(State and Prospects of the Mechanical Sorting of Sawn Timber)
Holz als Roh- und Werkstoff (Wood as Raw Material and Stock), Berlin(W) 38(1980), pp. 409-417

/14/ Späthe,
Zuverlässigkeitskonzeption für tragende Konstruktionen
(1. Entwurf)
(Reliability Concept for Loadbearing Structures (1st draft
Academy of Building of the GDR, Institute for Heating, Ventilation and Structural Theory), Berlin 1985

/15/ DDR-Norm:
TGL 32 274, Lastannahmen für Bauwerke
(GDR Code/Standard: TGL..., Design Loads for Buildings and Structures)
Ausgabe Mai 1979, Verlag für Standardisierung
(edition of May 1979, Standardization Publishers),
Leipzig/DDR

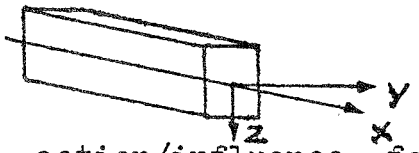
/16/ DDR-Norm:
TGL 25106/01, Prüfung von Holz, Probennahme und allgemeine Festlegungen
(... Testing of Timber, Sampling and General Regulations)
Ausgabe Juli 1979, Verlag für Standardisierung, Leipzig/DD
(edition of July 1979, Standardization Publishers...)

/17/ DDR-Norm:
TGL 25106/01, Bestimmung der Biegefestigkeit bei statischer Belastung
Ausgabe Juli 1979, Verlag für Standardisierung, Leipzig/DDR
(GDR Code/Standard: TGL..., Determination of the Flexural Strength with Static Loading
edition of July 1979, Standardization Publishers, Leipzig/GDR)

12

Table 1: Designations

symbol	dimension	designation
l	(m, mm)	length, effective span
b	(mm)	width
h	(mm)	height
t	(mm)	thickness
r	(mm)	radius
d	(mm)	diameter
a	(m, mm)	spacing/distance
e	(mm)	eccentricity
α	( )	angle
$\varkappa$	$(\frac{1}{mm})$	curvature
A	(mm^2)	area
V	(mm^3)	volume
J	(mm^4)	moment of inertia
W	(mm^3)	moment of resistance
S	(mm^3)	static moment
i	(mm)	radius of inertia
λ	(-)	slenderness coefficient
φ	(-)	buckling coefficient
u	(mm)	displacement
ϑ	($^\circ$)	torsion
x,y,z		coordinates



F	(kN,N)	action/influence, force, load
F^n	(kN,N)	standard value of the action/influence
W	(kNm, Mn)	work
m	(kg)	mass/weight
	$(\frac{kg}{m^3})$	density/specific gravity
t	(h,s)	time
T	($^\circ$C)	temperature
u	(%)	moisture of timber
	(%)	relative air humidity
M	(kNm,Nmm)	moment, flexural moment
N	(kN,N)	longitudinal force
V	(kN,N)	shear force, lateral force
p	$(\frac{N}{mm^2})$	pressure/compression
σ	$(\frac{N}{mm^2})$	normal stress
τ	$(\frac{N}{mm^2})$	shear stress
ε	(-)	strain/extension
γ	(-)	shear angle
ν	(-)	Poisson's coefficient

symbol	dimension	designation
E	$(\frac{N}{mm^2})$	modulus of elasticity
G	$(\frac{N}{mm^2})$	rigidity modulus
S	$(\frac{N}{mm^2})$	stress and strain, design value of the actions/influences
R	$(\frac{N}{mm^2})$	loadability, design value of the strength
R^n	$(\frac{N}{mm^2})$	standard value of the design strength
R^o	$(\frac{N}{mm^2})$	basic value of the design strength
γ_n	-	valency factor
γ_f	-	load factor
	-	combination factor
γ_{mo}	-	material factor
γ_m	-	adaptation factor

- superscripts (high indices)

n	-	standard value
o	-	basic value

- subscripts (low indices)

t	-	time
T	-	temperature
m	-	flexure/bending
tor	-	torsion
t	-	tension
c	-	compression
v	-	shear
E	-	Euler
crit	-	critical
inst	-	instable
x,y,z		in the direction of the axes or around the axes x,y,z
0		in parallel with the grain/fibre
90		perpendicularly to the grain/fibre

Table 2: Reliability Grades and Valency Factors acc. to /14/

Reliability grade	Consequences of exceeding a limit state of the load-carrying capacity	Consequences of exceeding a limit state of the usability	Buildings / structures	Valency factor γ_n 4)
I	High danger to human lives and very serious economic consequences	very serious impairment of the utilization, serious economic consequences	Safety-relevant structures in construction of nuclear power plants Dams/barrages Railway bridges Loadbearing structures of theatres, cinemas, schools, railway stations, grandstands of sports facilities and other buildings/structures in which crowds are frequent Loadbearing structures of museums containing irretrievable treasures	1.0 1) 1.1 2)
II	Danger to human lives and/or considerable economic consequences	Impairment of the utilization, considerable economic consequences	Residential buildings, public and social buildings, industrial buildings as far as not included in reliability grade III Central warehouse and storage buildings for the population's supply, for technical equipment of great value and the like	1.0 1)
III	No danger to human lives and insignificant economic consequences	Insignificant impairment of the utilization, insignificant economic consequences, easy repairability	Warehouse and storage buildings for commercial products/goods, fertilizers, building materials, chemicals and the like Greenhouses, lighting columns/masts Structural units/components of secondary importance and insignificant consequences in case of failure even if the total building/structure is included in the reliability grades I or II	0. 1) 0. 3)

1) Is applicable in case of limit states with the occurrence of the failure state being announced in advance.

2) For safety-relevant structures in the construction of nuclear power plants.

3) If the period of utilization is < 5 years.

4) In case of limit states with a sudden failure not being announced in advance, $\Delta\gamma_n$ is to be increased by the amount $< \gamma_n = 0.05$

Table 3 : Combination Factor acc. to /15/		
Load combinations	Number of the short-term loads	ψ
Basic combination[1)]	1	1.0
	2 or 3	0.9
	>3	0.8
Special combination[2)]	≥ 1	0.8
1) maximum load, without sudden load 2) maximum load, including sudden load		

Table 4 : Load Factors acc. to /15/[2)]	
Type of load	Load factors γ_f[1)]
Dead load	1.1 0.9[2)]
Live load	1.4[3)]

1) Are applicable only to the limit state of the load-carrying capacity.
For the limit state of the usability, $\gamma_f = 1.0$ if there should not be any specific regulations.

2) Is to be applied if the reduction of the loading should have an unfavourable effect.

3) Other values can be found in /15/.

Table 5: Coefficients of correlation between sorting criteria and strength properties, determined with boards and planks made of European pine wood acc. to /13/

	Sorting parameter	Correlation with flexural strength R_m	tensile strength R_t	compressive strength R_c
1	Visual sorting acc. to DIN 4074	0.5	0.6	0.4
2	Volume weight (specific bulk gravity)	0.5	0.5	0.6
3	Annual ring width	0.4	0.5	0.5
4	Knottiness	0.5	0.6	0.4
5	Grain deviation	0.2	0.2	0.1
6	Modulus of bending elasticity E_m	0.7-0.8	0.7-0.8	0.7-0.8
7	Volume weight and knottiness	0.7-0.8	0.7-0.8	0.7-0.8
8	Modulus E_m and volume weight	0.7-0.8	0.7-0.8	0.7-0.8
9	Modulus E_m and knottiness	0.8	0.8	0.8

Table 6: Synopsis on single factors and their significance in the material factor

Single factor of $\gamma_{m,o}$	Significance of the partial safety factor
$\gamma_{m,o,1}$	Takes the uncertainty in the determination of the material parameters (between tested material and building construction) into consideration
$\gamma_{m,o,2}$	Takes the uncertainty in the design model caused by material or geometry parameters, but also by material-dependent influences into consideration
$\gamma_{m,o,3}$	Takes the efficiency of the check performed during the manufacture into consideration

Table 7: Standard Values of the Design Strengths and of the Modulus of Bending Elasticity E_m for Structural Timber and Glued Laminated Timber

$\left(R^n_{(0.05)} = f_{k(0.05)}\right)$

loading/ stress and strain		softwood (spruce/fir, pine, larch)										hardwood (stalk oak) (sessile oak) (red beech)
		structural sawn timber			glued laminated timber						round timber	
		quality grade acc. to TGL			strength grade							
		I	II	III	1	2	3	4 [1)]	5 [1)]	6 [1)]		
Flexure/ bending	$E_{m,50\%}$	11500	10000	9000	12500	11000	11000				12000	13000
	$E_{m,5\%}$	8200	7100	6500	9000	7100	7100				8500	9000
	R_m	24	22.0	19.0	34	26	26				26.5	40.0
Tension	$R_{t,0}$	16.0	14.5	12.0	22.5	17.0	17.0				14.5	24.0
	$R_{t,90}$	0.5	0.4	0.3	0.5	0.4	0.3				0.40	0.6
Compression	$R_{c,0}$	21.5	20.0	18.0	30.5	23.5	23.5				22.8	30.0
	$R_{c,90}$	8.0	7.0	6.0	11.5	8.0	8.0				7.0	10.0
Shearing-off	$R_{v,0}$	2.5	2.25	2.0	3.0	2.50	2.5				2.50	5.0
Shear force from lateral force	$R_{v,90}$	3.3	3.0	2.7	4.0	3.25	2.25				3.25	6.7

1) Layers of boards are being sorted mechanically; strength values will be available only in 1987.

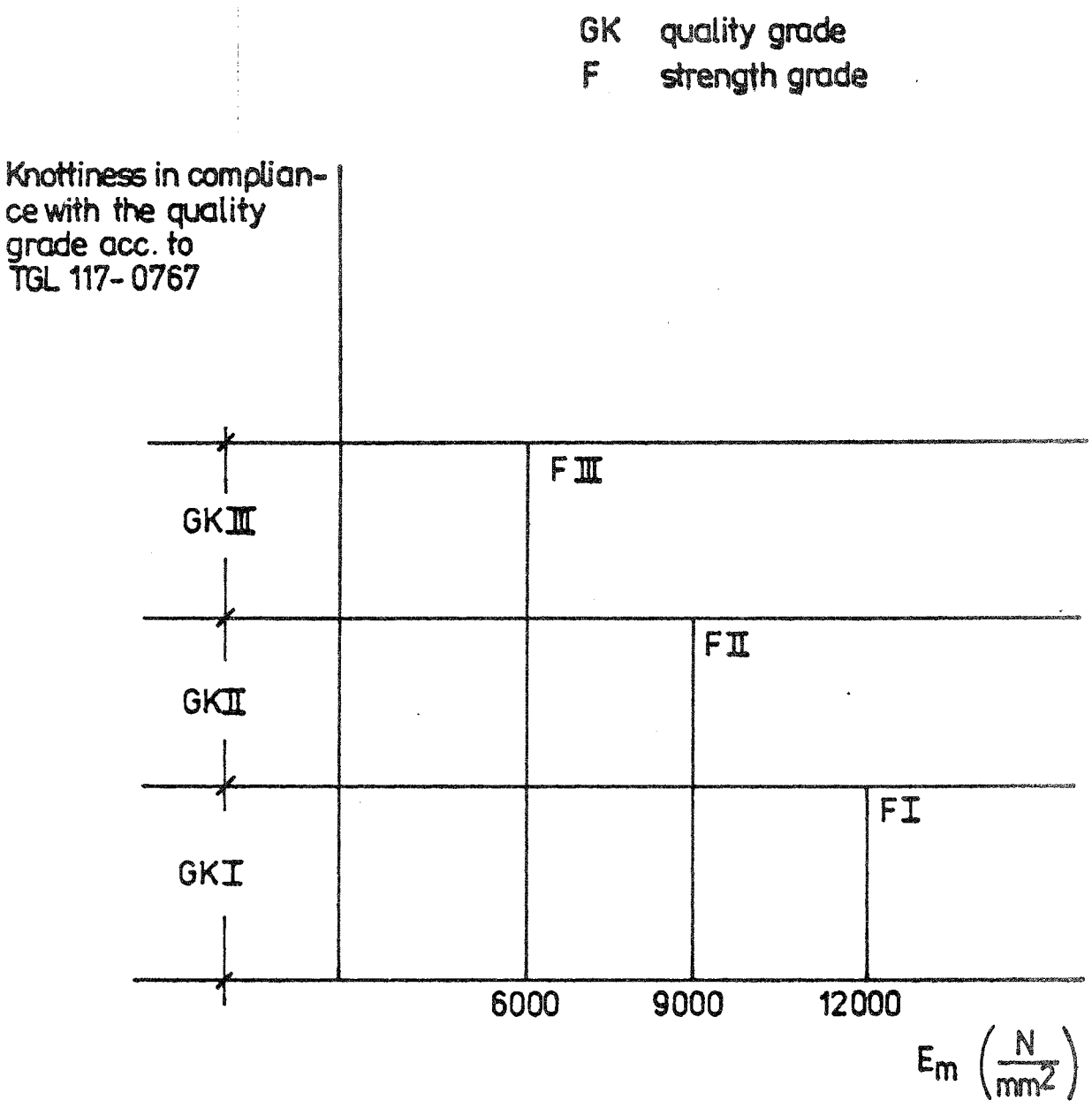


Figure 1: Strength grades of structural timber or layers of glued laminated timber.

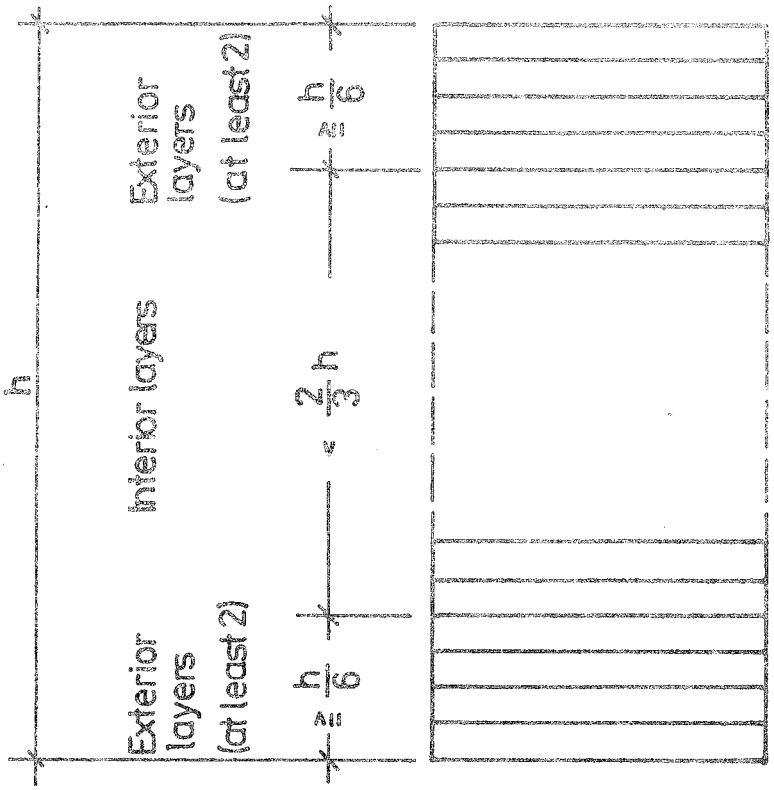


Figure 2: Design of the glued laminated timber

Table 8: Design of the new grades of glued laminated timber

design		BSH 1	BSH 2	BSH 3	BSH 4	BSH 5	BSH 6
sorting of the layers		visually	visually	visually	machine	machine	machine
exterior layers	kind of timber	NSH GK I,II	NSH GK II	NSH GK I,II	NSH F I	NSH F II	NSH F II
	KZV(mm)	≧ 250	≧ 250	≧ 0	≧ 250	≧ 250	≧ 250
interior layers	kind of timber	NSH GK I,II	NSH GK III	NSH GK I,II	NSH F III	NSH F III	NSH F II
	KZV(mm)	≧ 250	≧ 0	≧ 0	≧ 0	≧ 0	≧ 0

KZV finger joints staggering
BSH glued laminated timber
NSH sawntimber - scots pine, sitka spruce, or larch
GK quality grade; F - strength grade

Table 9a : Moisture Grades			
moisture grade (FK)	moisture of timber u (%)	case of application to structures made of structural timber or glued laminated timber	K_e
FK 1	$\leq$ 18	enclosed buildings/structures with and without heating, enclosed ventilated animal shelter buildings without heating, open and partially open roofed-over buildings/structures	1.0
FK 2	$18 > u \leq 24$	free-standing loadbearing systems/ members without any protection against climatic influences	0.93
FK 3	> 24	structures being subjected to an immediate influence/action of water	0.8

Table 9b : Time Grades		
time grade	duration of the load action	K_t
A	continuous and / or long-term	0.67
B	short-term	0.83
C	instantaneous	1.0

Table 9c : Load Combinations			
load combination	time grade		
	A	B	C
A + B	A $\geq$ 85 %	A < 85 %	-
A + C	A $\geq$ 85 %	-	A < 85 %
A + B + C	A $\geq$ 85 %	C $\leq$ 15 % A < 85 %	C > 15 %
A etc. is the load percentage of time grade A of the total load etc.			

Table 9d: Temperature Grades		
temperature grade (TK)	temperature range T (°C)	K_T
TK 1	≤ 35	1.0
TK 2	$>35 < 100$°C	0.85

Table 10 : Adaptation Factor γ_{m1} "Long-Term Behaviour" for GZT Limit States						
time grade	moisture grade (FK)					
	FK 1		FK 2		FK 3	
	temperature grade (TK)					
	TK 1	TK 2	TK 1	TK 2	TK 1	TK 2
A	0.75	0.64	0.7	0.6	0.6	0.51
B	0.9	0.77	0.85	0.72	0.75	0.64
C	1.1	0.94	1	0.85	0.9	0.77

12

Table 11 : Adaptation Factor γ_{m2} "Cross-Sectional Height" for GZT Limit States with Flexural Load		
cross-sectional height h (mm)	structural timber	glued laminated timber (BSH)
≤ 200	1	1
$200 > h \leq 300$	0.95	
$300 > h \leq 500$	-	0.95
$500 > h \leq 800$	-	0.9
$800 > h \leq 1500$	-	0.85
>1500	-	0.8
For BSH $h \geq 300$ mm: $\gamma_m = \left(\frac{300}{h(mm)}\right)^{\frac{1}{9}}$		

Table 12: Adaptation Factor γ_{m3} "Curvature of Timber" for GZT Limit States

$\frac{h}{r}$	0	$2 \cdot 10^{-3}$	$4 \cdot 10^{-3}$	$6 \cdot 10^{-3}$	$8 \cdot 10^{-3}$	10^{-4}
γ_{m3}	1	0.92	0.83	0.76	0.68	0.6

r is the radius of curvature of the timber

h is the thickness of the timber or - in case of glued laminated timber - of one layer

Table 13a: Degree of Loading of Structural Timber and Glued Laminated Timber

degree of loading	aggressive action	example [1]
B 1	none/very low	For FK 1 with 0.5-20mg of SO_2 in $1m^3$ air
B 2	medium	For FK 1 with 20-100mg of SO_2 in $1m^3$ air
B 3	high	For FK 2 with 100-500mg of SO_2 in $1m^3$ air

[1] Other regulations are indicated in reference /6/.
FK - moisture degree

Table 13b: Adaptation Factor γ_{m4} "Aggressive Media" for GZT and GZN Limit States

degree of loading	γ_{m4}	remarks
B 1	1	
B 2	0.8	For boards, laths/battens, planks
	1	For square timber and BSH without protective/ preservation system
B 3	0.4 - 0.5	For boards, laths/battens, planks
	0.8	For square timber and BSH without protective/ preservation system
	$0.9^{1)} - 1^{2)}$	For square timber and BSH with protective/ preservation system (e.g. "Kombinal", tar epoxy resin)

GZT - limit state of the load-carrying capacity
GZN - limit state of the usability

1) in case of impregnation with oily preservatives such as, e.g. - "Kombinal TD"

2) In case of impregnation with highly efficient protective/ preservation systems such as tar epoxy resin.
In case of a continuous influence of high temperature, e.g. according to temperature grade II, a highly efficient temperature-resistant coat (e.g. of tar epoxy resin) must be applied.

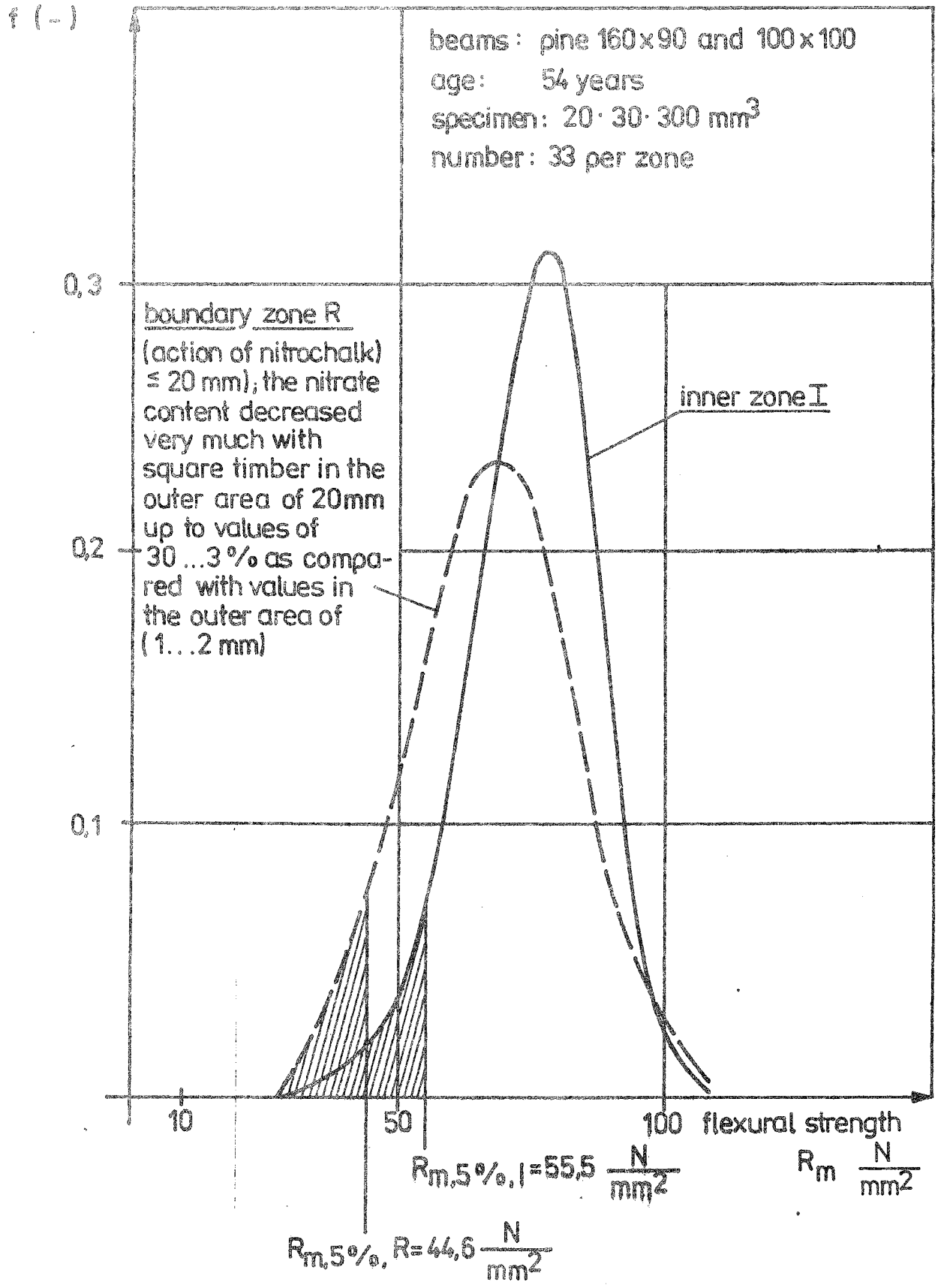


Figure 3 : Weibull distributions of the flexural strength of old timber

Table 14: 1986 - 1988 Research Programme

Research task №	Research objective
F 1	Basic values for structural timber subjected to flexural and compressive loading/stress (buckling)
F 2	Adaptation factor "Long-term behaviour" for structural timber subjected to flexural and compressive loading/stress (buckling)
F 3	Adaptation factor "Aggressive media" for structural timber subjected to flexural load
F 4	Basic values for glued laminated timber subjected to flexural load
F 5	Adaptation factor "Long-term behaviour" for glued laminated timber subjected to flexural load
F 6	Adaptation factor "Cross-sectional height" for glued laminated timber subjected to flexural load
F 7	Adaptation factor "Moisture of timber" for glued laminated timber subjected to flexural load
F 8	Basic values for the nailed connection with nails sized 3.4 x 90, subjected to shear stress/load
F 9	Basic values for the screwed connection with hexagonal wood screws sized 8 x 90, subjected to shear stress/load
F 10	Basic values for the dowelled connection with "KRD A80"-type key ring dowels subjected to shear stress/load

CIB-W18/19-105-1

INTERNATIONAL COUNCIL FOR BUILDING RESEARCH STUDIES AND DOCUMENTATION

WORKING COMMISSION W18 - TIMBER STRUCTURES

TROPICAL AND HARDWOOD TIMBER STRUCTURES

by

R H Leicester
CSIRO Division of Building Research
Australia

MEETING NINETEEN
FLORENCE
ITALY
SEPTEMBER 1986

155RHL.2/280886 JCP/137-74

CIB W18B

TROPICAL AND HARDWOOD TIMBER STRUCTURES

by R.H. Leicester

(CSIRO, Melbourne, Australia)

1. INTRODUCTION

The CIB working group, W18B, was recently formed with the intention of complementing the excellent work already undertaken by the working group W18 (now W18A) in the development of engineering procedures for timber construction. The following is a discussion on possible activities of W18B.

Two useful actions for W18B are

- the development of technology for construction with tropical and hardwood timbers;

- the transfer of timber engineering technology to developing countries.

A third role of W18B would be to encourage the choice of tropical and southern hemisphere venues for CIB meetings, to complement the meetings held in Europe and North America.

Obviously it will be essential for W18B to have close technical and administrative links with W18A. However it will also be necessary for W18B to develop interaction with other groups concerned with technological aspects of construction with tropical timbers. These would include ISO TC165, the International Research Group on Preservation and the various specialist groups of IUFRO Division 5 (e.g. P5.01 Properties and Utilization of Tropical Hardwoods, P5.04; Production and Utilization of Bamboo and Related Species and S5.03 Wood Protection).

Successful technology transfer to developing countries will depend to a large extent on building communication links with appropriate organizations concerned with the technological welfare of these countries. UNIDO and FAO are two of the most significant organizations in this regard. The various regional standards groups such as the Pacific Area Standards Congress could be useful. Finally, it is of interest to note that IUFRO has a Special Coordinator for Developing Countries.

2. DEVELOPMENT OF TECHNOLOGY

The most obvious basis for selecting topics for study is to focus on those aspects of construction with hardwoods and tropical timbers that are different from those of softwoods.

At the outset the utilization of hardwood timbers presents a difficulty in that they are frequently derived from multiple species forests; forests containing more than 100 species per hectare, or mills with a

log inventory of more than 100 species are not uncommon. These lead to special problems either with species identification, or with the utilization of species mixtures. Tropical and hardwood forests also contain species and species groups with unusual properties; examples of these include eucalypts, rubber wood, coconut wood and bamboo.

Hardwoods are often used in the unseasoned state because of their slow drying characteristics. This together with their large growth stresses, high shrinkage (tangential shrinkage of up to 15 per cent for some eucalypt species) necessitates the use of very careful detailing, particularly with regard to the minimization of splitting at connectors.

Hardwood timbers differ from softwood timbers in several aspects such as the occurrence of brittle heart and large kino veins. Monocotyledous (e.g. bamboo and coconut wood) have a structure markedly different from that of both hardwood (dicotyledon) and softwood (conifer) timbers. The high density of some hardwoods creates special connection problems. In glued joints there are difficulties in ensuring wood failure and hence the long term durability of the joint; with metal connectors, failure often occurs in the metal and hence a brittle joint is obtained. 'Collapse' susceptible hardwoods exhibit abnormally high creep when loaded in the unseasoned condition.

Special technologies need to be developed to assist the needs of developing countries. In particular it is important to develop simple technology methods for the utilization of mixed species of hardwood forests. These methods usually turn out to be less efficient than those used in developed countries; however these methods will enable the immediate utilization of the available timbers. (Since the hardwoods are

often several times stronger than the softwoods used in developed countries, the loss of efficiency associated with the use of simple technology may be of little practical consequence). The use of proof grading and nail-laminating techniques can do much to minimize the adverse effects of uncertainty and high variability associated with the use of simple technology methods. Expensive testing requirements may often be avoided through the use of conservative decisions, such as the omission of expensive air-conditioning in tropical laboratories.

Probably the technical developments that are most useful to developing countries are classifications based on grouping methods; these may be applied to all technical specifications such as those for structural properties, loadings, climate, timber sizes etc. In this way technical advice can be given in terms of a limited set of grouped specifications. Thus the quantity of technological to be transferred is minimized and easily used.

3. TRANSFER OF TECHNOLOGY

3.1 General

The most critical aspect of technology transfer to developing countries is to choose the technology to be transferred. A cursory examination of the problem soon reveals that there is a wide range in these requirements. To effectively assist developing countries it will first be necessary to undertake a survey to ascertain the nature of the timber resources, the available professional and industrial capabilities appropriate to timber construction, the quality of existing building

regulations, design standards and quality control, and of course the relative costs of various building materials (both in terms of indigenous and foreign currency expenditure).

For developing countries it is important to show how timber construction fits in with the remainder of the building infrastructure, and not to give an impression that all aspects of building should be attempted in timber. For example, in many situations it may turn out to be suitable to adivse that timber be used used only for the primary structural frame, or that the use of timber be avoided in the case of high decay hazard situations.

A reasonable objective for the CIB W18B working group would be to draft the following for distribution and use in developing countries

- a manual on timber technology
- a handbook of standard construction
- an engineering design manual.

In the intial attempt, it is proposed that these documents be formulated at the simplest level, with directions and references for later use as the level of technology improves. They should be set up so that eventually a transition may be made to the full application of ISO standards where relevant.

3.2 Manual on Timber Technology

This manual should be a simple review of the current state-of-the-art in timber technology. In addition to a brief introduction on the structural characteristics of timber, it should cover all aspects that are related

to the design of timber structures. These would include topics such as the selection and specification of timber, sawmilling, drying, durability and preservation, gluing and metal connectors, construction, inspection and maintenance.

3.3 Handbook of Standard Construction

This handbook would give span-size Tables, and associated connector details, for timber frame construction in houses and simple industrial and agricultural buildings. No computations would be required to use the Tables. All input parameters such as timber properties, load class, and climate would be stated in terms of grouped classifications.

3.4 Engineering Design Manual

The purpose of the proposed manual is to introduce an instant design capability in timber engineering to a developing country that previously had none. It will be assumed that the country has engineers that have been trained in the basic concepts of structural engineering, but who have no prior knowledge of timber as a structural material.

The four essential Parts of the manual will be the following:

Part 1. Terms and Definitions

Part 2. Classification Procedures

Part 3. Design Code

Part 4. Worked examples

For countries with a limited background in structural design technology the following additional Parts may be required,

Part 5. Structural analysis

Part 6. Minimum design loads

Finally the following two Parts could be added to stretch the design capability of the manual,

Part 7. Composite structures

Part 8. High hazard loads

In addition to the above, it is desirable that a commentary be prepared, explaining the technical background of the various Parts of the manual, and stating the structural performance expected of designs that comply with the recommendations.

4. OPERATIONAL PROCEDURES

The operational procedure for W18B to achieve the objectives discussed above have not yet been decided, and any suggestions on the matter would be welcome. Some of the objectives may be most conveniently achieved through small working parties while others are obviously more suited to discussion in open forums. The achievement of effective interaction with developing countries will depend largely on obtaining access to funds for enabling the necessary meetings to occur.

Minutes of IUFRO Division 5
Local S5.02 group meetings
held in Ljubljiana, Yougoslavia
September 8-12, 1986

First meeting

Tuesday, September 9, Room FF5, 15:00 - 19:00

A) Round table discussion

Participants introduce themselves and indicate their major topic of interest in the wood engineering area.

Name of participant	Major topic of interest
B. Madsen (Canada) - *Chairman*	Structural behavior of lumber
A. Schniewind (U.S.A.)	Mechanical behavior of wood
R. Leicester (Australia)	Timber structural codes
B. Takanoi (Japan)	Wood physics
P. Glos (F.R. Germany)	Wood as a building material
P. Colclough (Ireland)	Physical and mechanical properties of lumber
S. Kurjatko (Czecholsovakia)	Wood drying
J.A. Janssen (Netherlands)	Mechanical properties of bamboo
M.O. Laakkonen (Finland)	Timber as building material
T. Tan (Malaysia)	[Student]
T. Stam (Malaysia)	Glued - laminated timber
A. Takahashi (Japan)	Noises in houses
M. Samson (Canada) - *Rapporteur*	Machine stress-rating
A. Abbott (Great Britain)	Glued - laminated timber
L.L. Palka (Canada)	Mechanical properties of wood
B. Kasal (Czecoslovakia)	Timber structures
C. Bozjag (Czecoslovakia)	Wood properties
A. Mansour (Iran)	Timber design
C. Christian (Peru)	Housing

Total: 19 participants

B) Review of current research topics in laboratories around the world

Name of participant	Current research topics
P. Glos *(F.R. Germany)*	1- Effect of environmental pollution on wood structure 2- Duration of load in lumber in tension and compression 3- Glued joints 4- Visual and machine grading rules
A. Takahashi *(Japan)*	Impact noise problems
P. Colclough *(Ireland)*	1- Data bank on physical and mechanical properties of lumber 2- Visual grading rules 3- Metal plate joints 4- Low-cost machine grader 5- Wood quality of standing trees 6- Small log utilization for glued-laminated beams
J.A. Janssen *(Netherlands)*	1- Creep in bamboo 2- Mechanical properties of bamboo 3- Joints in bamboo structures 4- Trusses
M.O. Laakkonen *(Finland)*	1- Timber composite structures 2- Renforced concrete with wood
B. Kasal *(Czecoslovakia)*	1- Deterioration from air pollution 2- Physical properties of wood
C. Christian *(Peru)*	1- Use of timber in Latin America 2- Visual grading of lumber
M. Samson *(Canada)*	1- Model prediction of grading machine performance 2- Automaic detection of slope of grain in lumber

Name of participant	Current research topics
A. Abbott *(Great Britain)*	1- Joints 2- Pannel products 3- Test methods for plywood 4- Non-destructive testing of poles 5- Improving glued-laminated beams
L.C. Palka *(Canada)*	1- Reliability based design 2- In-grade testing 3- Joints 4- Grading
A. Schniewind *(U.S.A.)*	1- Mechanical properties of wood 2- Wood trusses 3- Combined stresses
R. Leicester *(Australia)*	1- Timber codes 2- Fasteners 3- Properties of Radiata Pine 4- Laminated veneer lumber 5- Micro-wave grading
B. Takanoi *(Japan)*	1- Grading rules 2- Dynamic properties of wood 3- Timber codes 4- Duration of load effects for connectors 5- Creep behavior under snow loads
B. Madsen *(Canada)*	1- Mechanical grading 2- Size effets 3- Earthquake loads

Second Meeting

Thursday, September 11, Room FF5, 10:00 - 12:30

	Speaker	Short title
Oral presentation 1	R. Leicester	Bolted joints
Discussion	R. Leicester	Design criteria for joints
Oral presentation 2	R. Leicester	Proof grading
Oral presentation 3	M. Samson	Grading machines-dynamic effects
Discussion	P. Glos	Deriving characteristic strength properties

Attendance: 13 people

Third Meeting

Friday, September 12, Room FF5, 14:00 - 16:30

	Speaker	Short Title
Oral presentation 1	J. Janssen	Creep in bamboo
Oral presentation 2	A. Takahashi	Impact noises in buildings
Oral presentation 3	M.O. Laakkonen	Windmill towers from wood poles
Oral presentation 4	L.C. Palka	Creep in truss plates
Oral presentation 5	E. Varoglu by L. Palka	Model for roof trusses
Discussion	P. Glos	Wood Quality

The Chairman proposed different schedules for next group meeting. The Chairman will consult group members about their preference and will inform the members on the location and date of the next meeting.

Attendance: 14 people

Marcel Samson

LIST OF IUFRO-S 5.02 PAPERS/LJUBLJIANA 1986

T Arima; N Maruyama and M Sato:
Creep of Wood, Wood-Based Material and Wood Composite Building Elements at Various Conditions

Y M Ivanov and Y Y Slavik:
On the Extrapolation of Short-Term Wood Strength to Structure Service Life

J J A Janssen:
Creep and Recovery in Bamboo

R H Leicester:
SAA Draft Standard on Proof Grading

L C Palka:
Creep and Load Duration of Truss-Plate Joints in Tension

M Samson:
Dynamic Behavior of Lumber in Stress-Grading Machines

E Varoglu and F Lam:
Reliability of Trusses

INTERNATIONAL UNION OF FOREST RESEARCH ORGANISATIONS

GROUP S 5.02 - TIMBER ENGINEERING

CREEP OF WOOD, WOOD-BASED MATERIAL AND WOOD COMPOSITE BUILDING ELEMENTS AT VARIOUS CONDITIONS

by

T Arima; N Maruyama and M Sato

LJUBLJIANA
JOUGOSLAVIA
SEPTEMBER 1986

THE 18th IUFRO WORLD CONGRESS 1986

Creep of wood, wood-based material and wood composite building elements at various conditions

Arima, T., Maruyama, N. (Division of Forest Products, Faculty of Agriculture, Shizuoka Univ., 836, Ohya, Shizuoka, 422, Japan) & Sato, M. (Building Research Institute, Ministry of Construction, 1 Tatehara, Oho-cho, Tsukuba-gun, Ibaraki-ken, 305, Japan).

Abstract

This study evaluates the time-dependent deflection of wood, wood-based materials and wood composite building elements under various loading conditions and in various humidity conditions.

A power law was used to evaluate creep deflection under constant loading for the wood containing knots and clear, wood-based materials, composite beams and trusses. Based on the power law model, the rate of relative creep to initial deflection under constant and changes in loadings at low stress level such as snow load on the roof was determined by the super-position theory and the cumulative deflection due to intermittent loading periods summed together.

The time-dependent strength known as duration of load concept was also discussed based on a relationship between strength and stiffness and the inflection or fracture point of creep curve.

Changes in relative humidity may cause more severe creep deflection to occur than constant humidity. The reaction of materials in creep testing may be seen to vary with amount of loadings and exposure conditions such as a range of humidity and periods.

I. Time-dependent deflections of wood, wood-based materials and wood composite building elements under constant loading conditions

Introduction

The creep behavior of wood and wood-based material has often been characterized by the so-called power law defined by equation (1) below.

$$\delta(t) = \delta_0 + \delta_c(t) \quad (1)$$

$$\delta_c(t) = A\,t^N \quad (2)$$

$$\delta(t)/\delta_0 = 1 + (A/\delta_0)\,t^N \quad (3)$$

where $\delta(t)$, δ_0 and $\delta_c(t)$ represents total deflection, initial deflection and creep deflection respectively and t represents time. Then the equation (3) represents relative creep.

Generally experimental results from creep tests on wood and wood-based material seem to be reasonably well fitted in a wide range of time by the power law and roughly fitted even for changing environment conditions, and we may still take advantage of the simplicity of the power law when analyzing the long-time deformation.

A power law was used to evaluate creep deflection under constant loading for the wood containing knots and clear, wood-based materials, composite beams and trusses. Based on the power law model, the relative creep was determined by equation (3).

Experimental procedure

Clear wood and wood containing knots and other defects were selected. Wood-based materials include commercial hardboard and particleboard. The specimens were center-loaded or two-point-loaded at various stress levels. Wood composite building elements such as box beam and truss were selected to compare to these specimens. These specimens were placed in a constant temperature and relative humidity room and in the room under changing conditions in actual use .

The relative creep was estimated based on the power law model to compare to the results, because loading and environment conditions for these specimens were different.

Results and discussion

The creep deflection under constant loading for the wood containing knots and clear, wood-based materials, composite beams and trusses in

the constant temperature-humidity conditions and in actual condition are shown Table 1 based on the equation (1), (2). And the estimated relative creep of 10 years and 50 years was estimated by equation (3). Some data published earlier were re-calculated by the power law model.

The creep deflection of wood , wood-based materials and their building elements is sensitive to the environment conditions, especially changings of humidity as described in many reports and later in this report. But from point of view in their actual use the power law is easy to compare the deflection in a wide range of time nevertheless variation due to changings of temperature and humidity, and effective to estimate the relative creep.

In a low stress level which is generally below the working stress the relationship between the total deformation, initial deformation, creep deformation and applied load shows a linear trend, and experimental constant N is independent upon load. In a high stress level which leads specimen to fail, a plot of log (creep deflection) versus log (time) does not show a linear trend and the total deformation is apart from the straight line given in a low stress level. Sugiyama found that the relative creep in a low stress level is independent upon load and that in a high stress level is dependent upon load, and proposed that this critical point of stress level could be defined as a creep limit.

The creep deflection in a low stress level of wood containing knots and other irregularity ,also is fitted to the power law model as be considered from the result that an experimental constant N is independent upon load in a low stress level.

The creep deflection of composite beams and trusses is considerably fitted to the power law but the total amount deflection appears to be related to the rigidity of joints as the nailed plywood gusset trussed rafters experienced the most deflection and the nail-glued trussed rafters experienced the least as shown in this report and Wilkinson's data.

Table 1 (1) Creep constants and estimated relative creep of clear wood and wood-based materials

($\delta_{10}/\delta_0 = 1 + A/\delta_0 \cdot N$)

Wood (Clear)		A/δ_0	N	δ_{10}/δ_0	δ_{30}/δ_0	Reference
Sugi	0.2	0.15~0.19	0.23~0.26	2.3	2.9~3.0	Sugiyama
	Stress 0.4 level	0.18~0.19	0.30	3.2	4.5~4.6	
	0.5	0.26	0.30	4.1	6.0	
Hinoki	~0.4	0.11~0.15	0.13~0.17	1.4~1.5	1.5~1.6	Hou
	0.5	0.15	0.23	2.0	2.5	
	0.6	0.23	0.25	2.8	3.7	
Katsura	~0.4	0.06~0.11	0.21~0.25	1.3~1.8	1.5~2.1	Mirai
	0.5	0.15	0.25	2.2	2.8	
	0.6	0.30	0.24	3.1	4.0	
	0.8	0.57	0.31	8.2	12.4	
Makamba	~0.4	0.02~0.24	0.25~0.26	1.1~2.9	1.2~3.8	
	0.5	0.65	0.23	5.3	7.5	
Shioji	~0.4	0.15~0.19	0.27~0.29	2.4~3.0	3.2~4.1	
	0.5	0.45	0.27	5.1	7.3	
	0.6	0.47	0.28	5.7	8.5	

Note:
Sugi: Cryptomeria sp.
Hinoki: Chamaecrparia sp.
Katsura: Cercidiplyllum sp.
Makamba: Betula sp.
Shiogi: Fraxinus sp.

Wood-based materials		A/δ_0	N	δ_{10}/δ_0	δ_{30}/δ_0	Reference
Plywood 3ply 6mm		0.04~0.11	0.27~0.34	1.7~2.1	2.3~2.9	Arima
Plywood //. 12mm (S.L. 3/4.3/4)		0.08	0.27	1.7	2.1	Nakai
Particle board	S.L ~0.3 U 15mm	0.16~0.22	0.16~0.22	1.6~2.2	1.8~2.7	Saito
	P 15 2/4	0.24~0.25	0.29~0.31	3.7~4.1	5.3~6.0	Nakai
	20	0.18~0.22	0.27~0.28	2.8~3.0	3.8~4.1	
	P&M 15mm S.L 0.3 / 25mm	0.19~0.37	0.17~0.37	2.1~5.4	2.3~8.9	Arima
	U 15	0.17~0.23	0.2~0.25	2.1~2.7	2.5~3.4	Arima
Hard board	W	0.70~1.06	0.34~0.35	12.4 ~18.2	22.7 ~31.4	Hou
	Dry 14	0.13~0.15	0.21~0.24	1.8~1.9	2.2~2.4	Nakai
	Dry 7	0.20~0.23	0.18~0.19	1.9~2.0	2.2~2.3	Saito

Table (2) Creep constant and estimated relative creep for wood containing knots (SUGI) in air

	δ_0	N	A	δ_{1g}/δ_0	δ_{5g}/δ_0
1	8.32	0.30	1.47	3.07	4.35
2	7.19	0.31	1.19	3.10	4.47
3	5.34	0.31	0.84	3.00	4.29
4	8.21	0.35	1.36	3.92	6.14
5	3.91	0.31	0.67	3.18	4.59
6	8.41	0.33	1.44	3.57	5.36
7	9.01	0.37	1.32	4.05	6.53
8	6.99	0.33	0.91	3.14	4.65
9	4.65	0.33	0.91	3.93	5.99
10	22.23	0.36	7.31	7.30	12.25
11	8.33	0.40	0.78	3.49	5.74
12	7.26	0.33	1.08	3.23	4.79
13	4.37	0.32	0.66	3.08	4.49
14	6.77	0.37	1.29	4.96	8.19
15	9.69	0.34	1.49	3.50	5.32
16	21.37	0.39	6.54	8.50	15.05
17	9.40	0.37	1.54	4.41	7.18
18	3.57	0.28	0.53	2.48	3.32

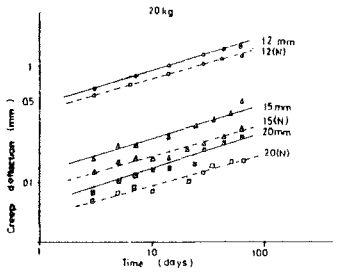


Fig. 1 (1) Creep deflection for particleboard (in constant conditioned room)

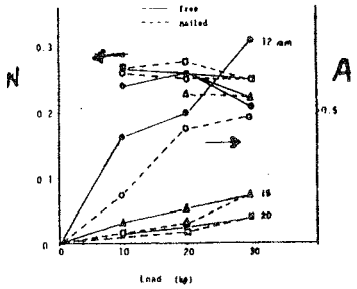


Fig. 1 (2) Relationship between A, N and load applied

Table 1(3) Creep constant ($N, A/\delta_0, \delta_0$) and estimated relative creep after 10 and 50 years ($\delta_{10}/\delta_0, \delta_{50}/\delta_0$) of roof construction

Type of roof consruction		N [1]	A/δ_0 [1]	δ_0 mm	δ_{10}/δ_0 [1]	δ_{50}/δ_0 [1]	ref.
Conventional		0.12	0.32	2.39	1.86	2.04	Arima
King-post truss (plywood gusset nailed)		0.27	0.16	1.89	2.42	3.18	
King-post truss (nail-plate)		0.21	0.092	1.31	1.51	1.72	
Fink truss (plywood gusset nailed)		0.20	0.35	2.36	2.81	3.49	
Fink truss (nail-plate)		0.26	0.094	2.55	1.79	2.21	
Truss	plywood gusset nailed	0.36	0.12	3.82	3.30	5.11	
	nail-plate	0.25	0.15	4.56	2.27	2.74	Ito
	plywood gusset nailed-glued	0.33	0.065	3.17	1.97	2.66	
Truss	plywood gusset nailed	0.26	0.23	8.4	2.94	3.95	Wilkinson
	nail-plate	0.23	0.19	7.9	2.25	2.82	
	nail-plate nailed	0.25	0.20	6.4	2.55	3.32	
	nail-plate	0.25	0.23	6.4	2.79	3.67	
	plywood gusset nailed-glued	0.24	0.10	5.6	1.72	2.05	
	plywood gusset nailed-glued	0.21	0.16	5.3	1.90	2.26	
	plywood gusset nailed-glued	0.22	0.15	6.1	1.91	2.30	
Truss	nail-plate A	0.22	0.35	9.4	3.13 (2.84) [2]	4.03 (3.40) [2]	Mayo
	nail-plate B	0.18	0.38	9.9	2.66 (2.88) [2]	3.22 (2.63) [2]	

Table 1(4) Creep constant N, A/δ_0, δ_0 and estimated relative creep of wood composite beam

Test specimen	Total load (kg)	N	A/δ_0	δ_0 mm	δ_{10}/δ_0	δ_{50}/δ_0
Box beam 2.5AB	390	0.31	0.094	1.71	2.20	2.97
3.0AB	390	0.41	0.043	2.31	2.18	3.40
	820	0.25	0.112	4.04	1.86	2.28
7×7 beam 2AB	582	0.27 (0.30)	0.17 (0.076)	4.47	2.56 (1.89)	3.40 (2.44)
2CD	390	0.26 (0.27)	0.20 (0.097)	3.01	2.69 (1.82)	3.56 (2.27)
2EF	390	0.22 (0.39)	0.23 (0.075)	3.73	2.40 (2.84)	2.99 (4.44)

II. Time-dependent deflections of wood, wood-based materials and wood composite building elements in changes of loading conditions

Introduction

After building elements are installed in building, it is subjected to many loading conditions which may affect their performance. These conditions include a constant load such as roofing materials and changes in amount of live load on the roof.

Few studies have been made to determine the time-dependent deflections of wood-based materials and trussed rafters in changes of loading conditions.

Analyses

The creep behavior of wood and wood-based material at a constant loading has often been characterized by the so-called power law as described before. But the creep behavior of wood, wood-based material and building elements in changes of loading is not well understood. We evaluate the creep in changes of loading based on three types of model as shown in Fig. 2 , .

Type of loading is a cyclic loading of low (P_0) and high (P_1) level as snow load ($P_1 > P_0$).

(1) Additional duration type

$$\delta(P_1, t) = \delta(P_0, t) + \delta(P_1 - P_0, \sum (t_{2i} - t_{2i-1}) + (t - t_{2i+1}))$$
$$\delta(P_0, t) = \delta(P_0, t) + \delta(P_1 - P_0, \sum (t_{2i} - t_{2i-1})) - \delta(P_1 - P_0)$$

(2) Maximum duration type

$$\delta(P_1, t) = \delta(P_1, \sum (t_{2i} - t_{2i-1}) + (t - t_{2i+1}))$$
$$\delta(P_0, t) = \delta(P_1, \sum (t_{2i} - t_{2i-1})) - \delta(P_1 - P_0)$$

(3) Super-position type

Generally within a low stress level , the super-position theory by Bolzman has been applied to estimation of creep in changes of loading.

$$\delta(t) = (P_0, t) + \sum \delta(P_1 - P_0, (t - t_{2i-1})) - \sum \delta(P_1 - P_0, (t - t_{2i}))$$

The estimation value of deformation in changes of loading is calculated, assuming that the creep equation is shown by power law model and the

initial deformation δ_o and A are proportional to applied load.

Results and discussion

The experimental value and calculated results of three types of model on wood-based materials and trussed rafters are shown in Fig. 3, 4 .

They seem not to be necessarily well fitted in a wide range of time but we may still take advantage of the evaluation when analyzing the long-time deformation in changes of loading.

The nail-adhesive jointed trussed rafter seems to be well fitted to the super-position type, but the nail jointed one seems not to be fitted to the estimation curve in the recovery process.

When various types of power law are used to evaluate creep deflection under constant loading and in changes of loading, the relative creeps are compared based on duration time of P_i in a year and the ratio of P_i / P_o as shown in Fig. 5, 6, 7 .

It is found that the creep deflection determined by these equations in changes of loading is reasonably smaller than that of power law under constant loading.

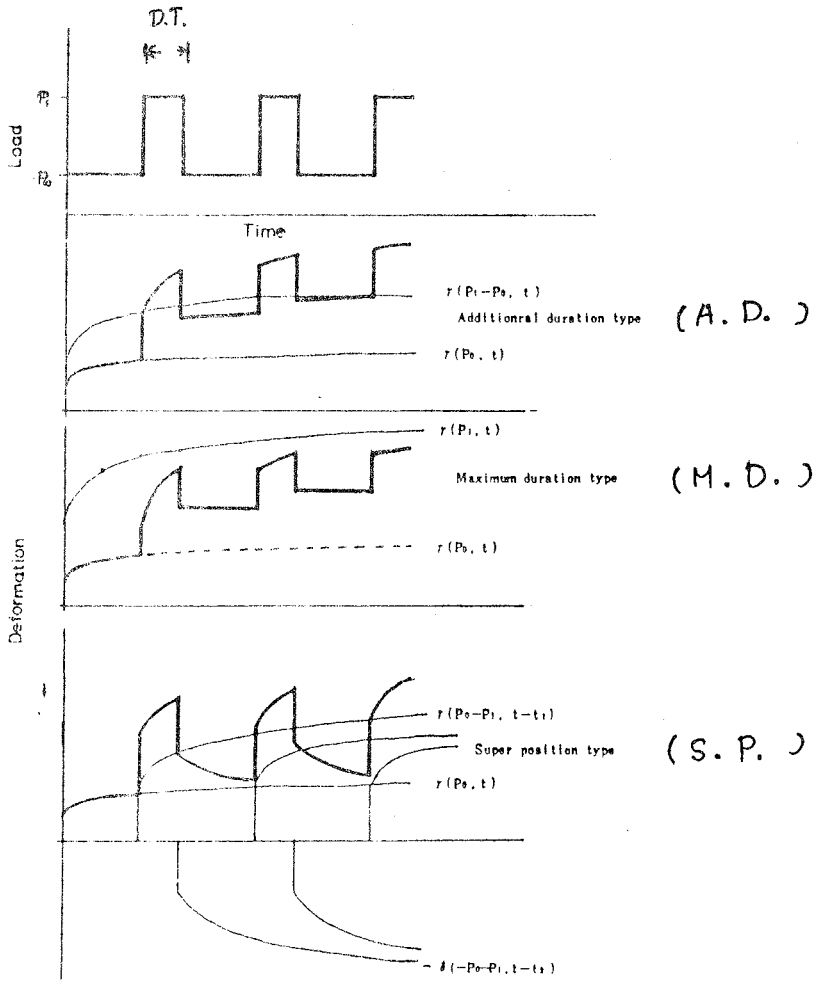


Fig. 1 Deformation model under cyclic loading

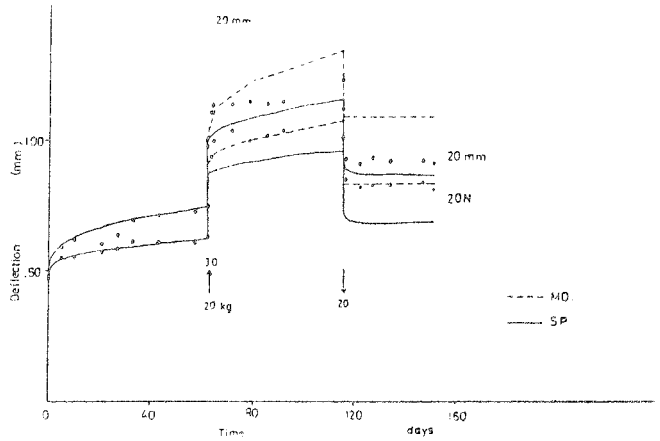


Fig. 3 (1) Deflection-time curves under cyclic loading (Particleboard 20 mm)

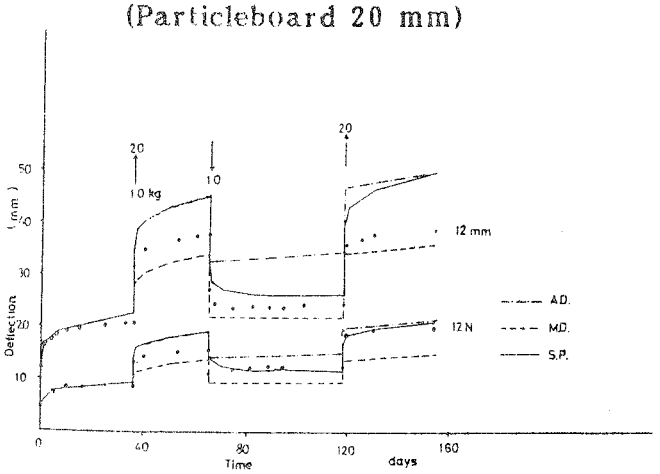


Fig. 3 (2) Deflection-time curves under cyclic loading (Particleboard 12 mm)

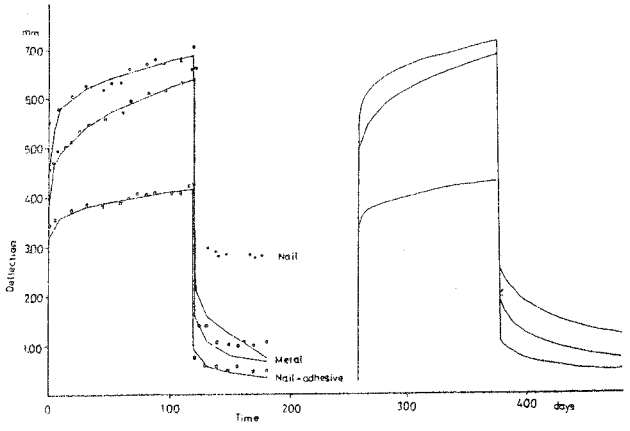


Fig. 4 Deflection-time curves under cyclic loading (Fink truss) ——— : calculated by super-position

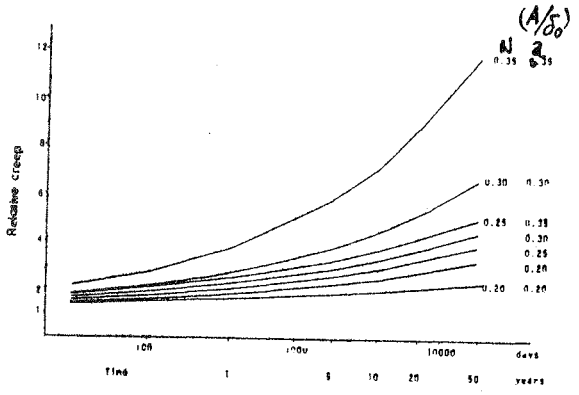
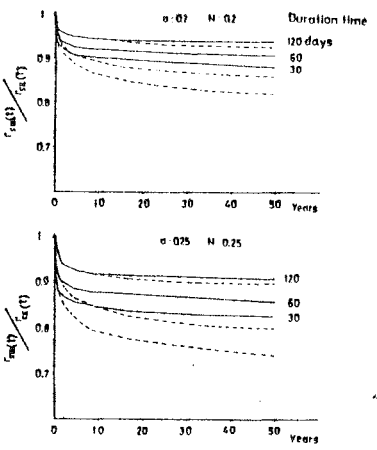
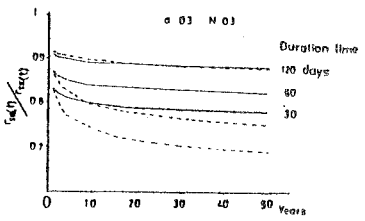


Fig. 5 Estimated rerative creep under constant loading : $\gamma_{s\,II}(t)$



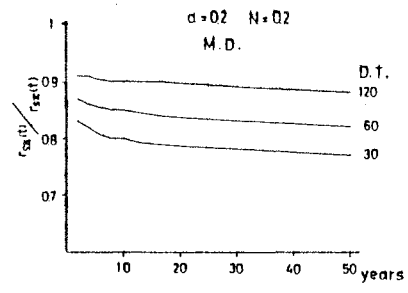


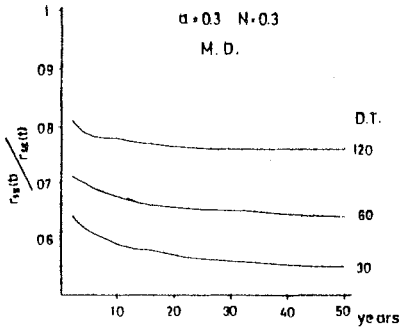
Additional duration

Super position

Fig. 6 (1)

Effect of duration time on $\gamma_{s\,III}(t)/\gamma_{s\,II}(t)$ by A.D. and S.P. (case : $P_1/P_0 = 2$)





7 - (2)

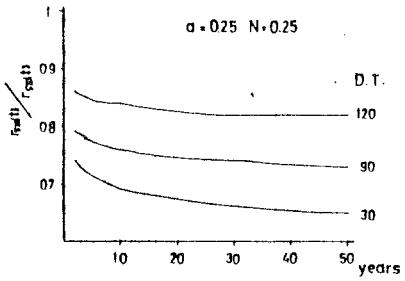
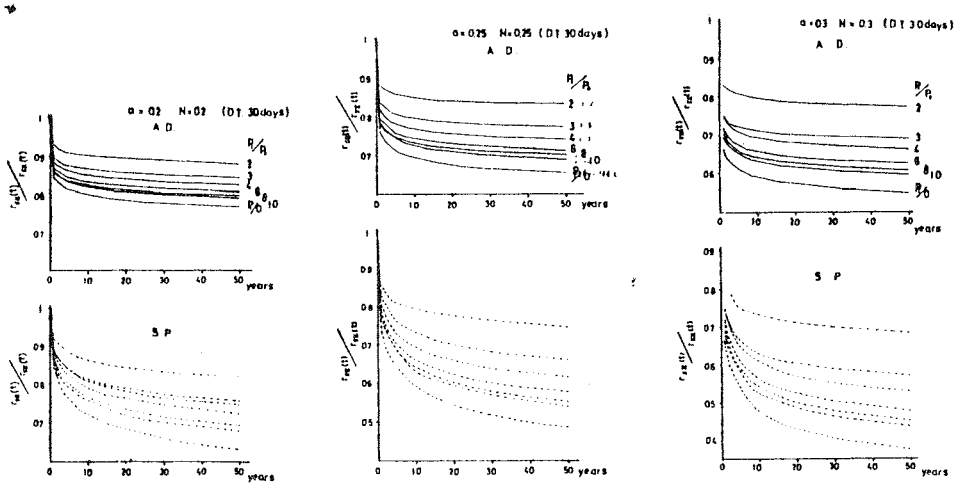


Fig. 6 (2)

Effect of duration time on $\gamma_{s\,III}(t)/\gamma_{s\,II}(t)$ calculated by M.D.



6 - (1) 6 - (2) 6 - (3)

Fig. 7

Effect of P_1/P_0 on $\gamma_{s\,III}(t)/\gamma_{s\,II}(t)$ calculated by A.D. and S.P.
(duration time : 30 days)

III. Duration of load test for wood containing knots and wood-based materials

Introduction

The most important work with regard to duration of load was carried out at the Forest Products Laboratory, in Madison, Wisconsin. The tests were carried out on small clear specimens of 1in. x 1in. Douglas Fir which were paired into matched sets. One of the specimens of pair was tested in bending at a rate of loading which would cause failure within about 5 minutes, the other was loaded with a constant load equal to a selected stress level. It was found that the time to creep failure was strongly dependent upon stress level. The findings have been applied to commercial timber containing knots and other growth irregularities for determining allowable stresses, as duration of load concept. But the mode of failure in bending is often different in the clear specimen and timber containing knots and other defects. Commercial timber often breaks caused by stress concentrations in the tension zone, whereas the clear specimen mainly wrinkles in the compression zone. Testing on 2x6 Hemlock was carried out by Madsen to ascertain the validity of applying the presently employed Duration of Load concept to commercial material. It was found that the "Duration of Load" concept is only valid for high strength material, that the time effect is strongly dependent upon stress level and no time effect is determinable at the working stress level.

There is no way to assess the true short-term strength of the long-term loaded specimens in the present experiment. Generally the pair matched specimen has been tested and stress level for long-term loaded specimen has been determined as described in many reports. This method may be useful for clear specimen, but not useful for wood containing knots or other defects. The linear regression between modulus of rupture and modulus of elasticity of specimen which is often used as a method of mechanical grading can be considerably effective to determine a selected stress level.

In this report the time-dependent strength known as duration of load concept was also discussed based on a relationship between modulus of rupture and modulus of elasticity and the inflection or fracture point of creep curve.

Experimental procedure

Wood containing knots and growth irregularity and wood-based materials were used and the modulus of elasticity was measured by applying lower stress before the creep testing.

In the part I of this study specimens were center-loaded with selected weight corresponding to 80, 85, 90, 95, 100% stress level based on a relation between modulus of rupture and modulus of elasticity on a 50 cm span as shown Table 2. Ten specimens at a stress level were subjected within one hour. Frequency of creep failure and the deflection at center was measured till the failure was occurred. And the time to failure was recorded.

In the part II load were applied at two points spaced 20 cm apart on a 50 cm span. A wide range of wood containing knots and other defects classified with modulus of elasticity were selected. The applied load was determined as the creep failure would be occurred within estimated duration time. The stress level was expressed as ratio of applied stress to estimated bending strength based on a relation between modulus of rupture and modulus of elasticity.

Results and discussion

15 The experimental data were analyzed several different ways as shown below.

1) Frequency of creep failure and stress level

The relationship between frequency of creep failure occurred within each duration time and stress level is shown in Fig. 8 and 9 . The frequency increased when the stress level and duration of time increased. It was found that the time effect is strongly dependent upon stress level and the "Duration of Load" concept for wood and wood-based materials is valid in this analyses within such high stress level.

Wood containing knots seems to fail at a lower stress level and to have shorter duration time than clear wood as shown in Fig. 9 . It could be considered that knots cause concentration of stress in high stress level or the estimated strength based on a relation of modulus of rupture and modulus of elasticity could be higher for wood containing knots. Further research is necessary to make it clear.

2) Duration time to failure and stress level

Time to failure for individual wood containing knots and clear at different stress level is plotted in Fig. 10 as shown in many reports. Time to failure is plotted on a logarithmic scale as a function of stress level based on a relation of modulus of rupture and modulus of elasticity. The regression lines for the clear specimen reported by Wood and Sugiyama are also shown. Our data in short-term are located at the up-side, that is, time to failure increases at the same stress level.

3) Classified duration time to failure and stress level calculated by a relation between applied stress and modulus of elasticity

Generally the duration of load curves are represented by the mean time to failure of each of the samples tested as a function of stress level. But a range of time to failure is considerably wide as found in many reports. We classified time to failure into definite ranges of time, such as initial, within 10 min., 1 hr., 1 day and 10 days respectively. The applied load which cause it fail within a classified time to failure and modulus of elasticity of each specimen measured before the creep testing was plotted as proportional regression line as shown in Fig. 11. The equation is shown as follows.

$$a(t_f) = \sigma(t_f) / E$$

$$a(t_f) / a(0) = (\sigma(t_f) / E) / (\sigma_0 / E)$$

$$= \sigma(t_f) / \sigma_0$$

= Estimated Stress Level

The estimated stress level for time to failure is similar to duration of load curves reported on small clear specimens and slightly higher as shown in Fig. 12.

4) Time to failure estimated from creep deflection in failure

Creep fracture is not well understood. A linear cumulative damage theory was proposed for evaluating the time-related effects of loading on strength of wood by Gerhards.

This report presents an experimental approach which may be useful for predicting time to failure.

Fig. 13 shows relationship between the creep failure deflection for particleboard and time to failure. Though the variation of creep failure deflection is considerably scattering, it seems to be independent upon time to failure. The range of creep failure deflection for wood and wood-based materials listed in Fig. 8 is shown in Table 3.

A basic assumption of the time to failure estimated here is that creep failure occurs when creep deflection reachs to the critical deflection in failure (δ_f). Time to failure (t_f) can be estimated by the creep deflection shown in a power law model. As initial deflection (δ_o) of each specimen is different, ratio of the deflection in failure to initial deflection was plotted to the estimated time to failure. The estimated values seem to be similar to the experimental values as shown in Fig. 14. The finding could be reasonably effective to estimate time to failure. The further testings should be conducted using other materials and in a full-size .

Table 2 . Specification of the bending test specimen.

	b cm	h cm	MOE ton/cm^2	MOR kg/cm^2	r
HB	5.0	1.3	20~36	113~231	0.96
PB	5.0	1.2	40~46	176~243	0.54
PW	5.0	0.9	99~128	525~737	0.42
Sugi	5.0	0.9	60~111	344~864	0.83
Beimatsu	2.0	1.5	94~145	561~955	0.59

PB:Particleboard
HB:Hardboard
PW:Plywood
Sugi:Cryptomeria sp.
Beimatsu:Douglas-fir

b : Width (cm).
h : Thickness (cm)
MOE : Modulus of elasticity (ton/cm^2)
MOR : Modulus of rupture (kg/cm^2)
r : Coefficient of correlation

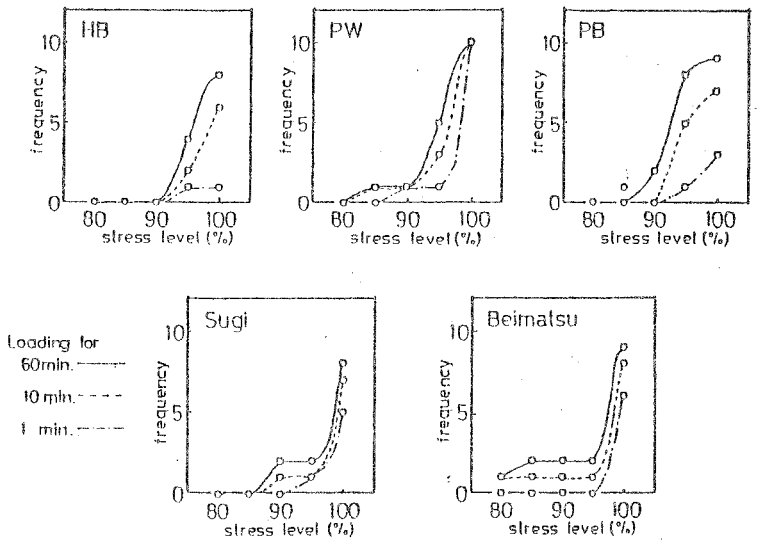
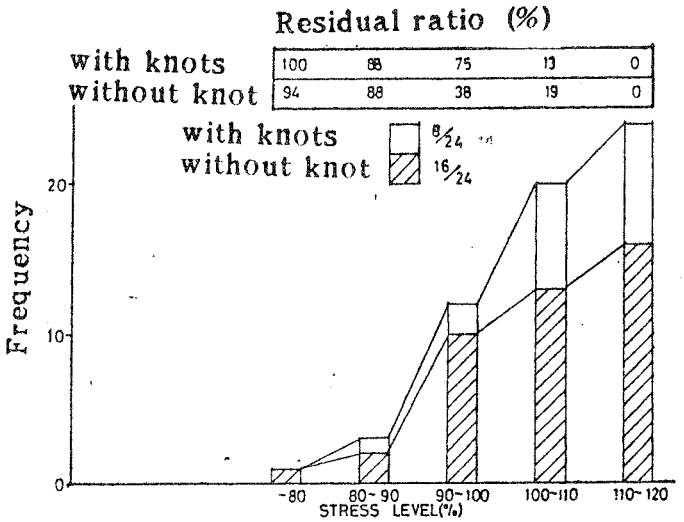


Fig. 8 Relationship between stress level and frequency of failure within loading time (wood and wood-based materials)



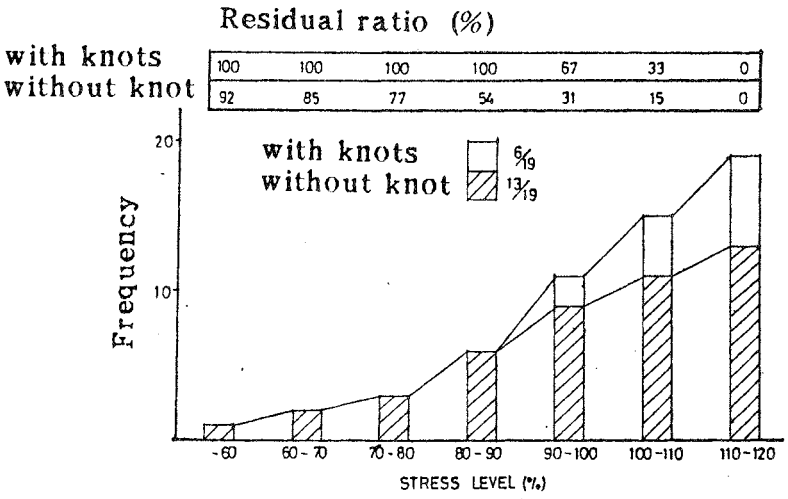


Fig. 9 Relationship between stress level and frequency of failure within loading time (wood clear and containing knots)

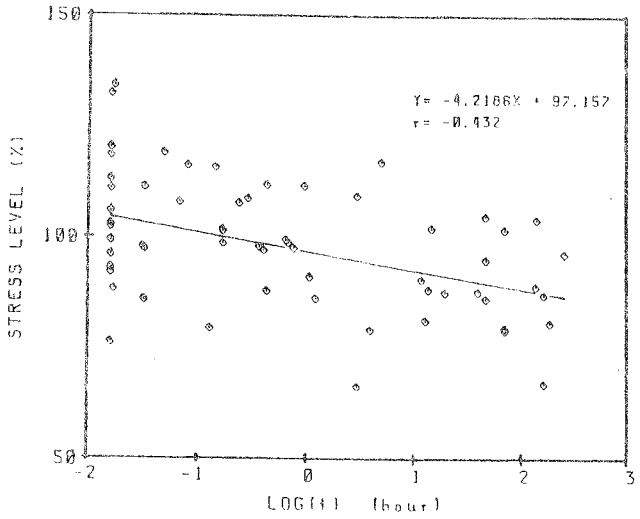


Fig. 10 Load-duration curve of wood containing knots using stress level based on MOR-MOE

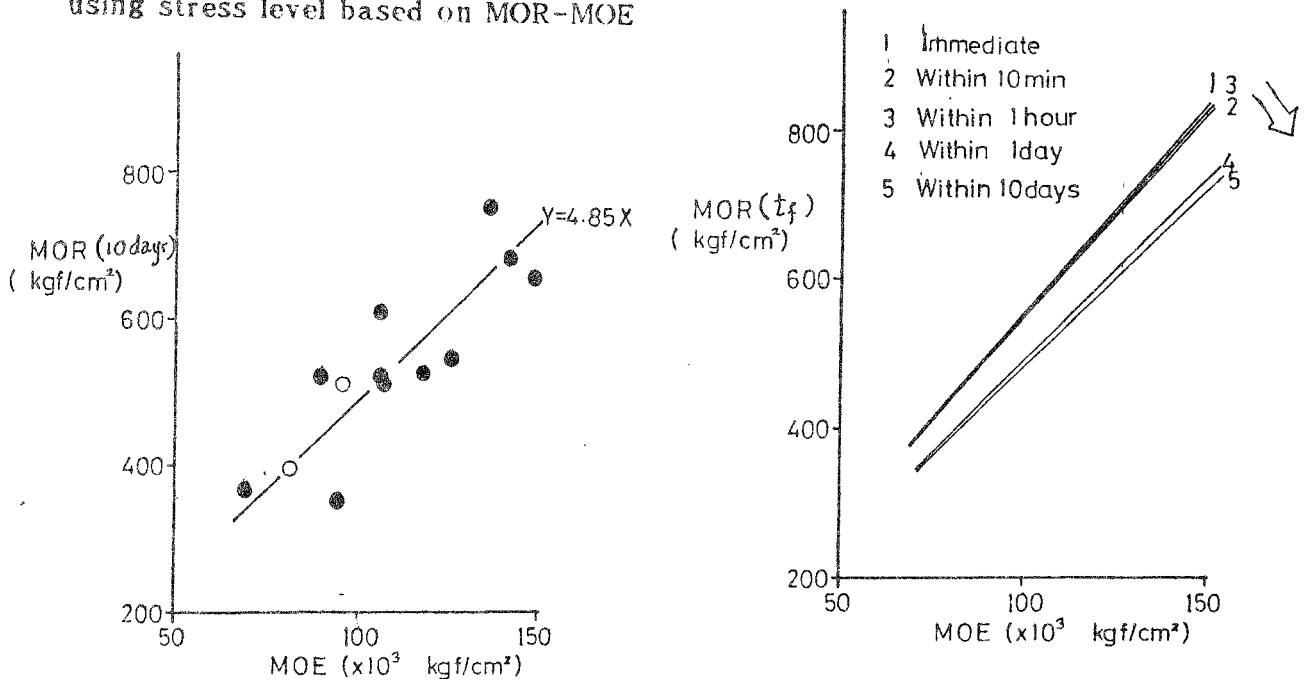


Fig. 11 Relationship between MOR (t_f) (within duration time) and MOE

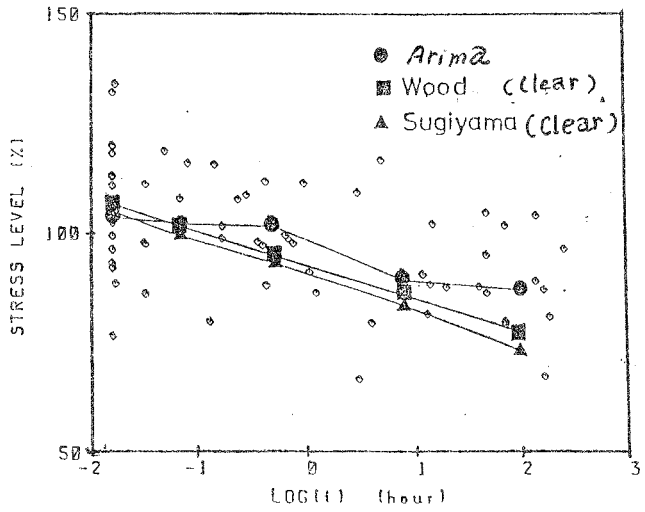


Fig. 12 Load-duration curve of wood containing knots based on relationship between MOR (t_f) (within duration time) and MOE

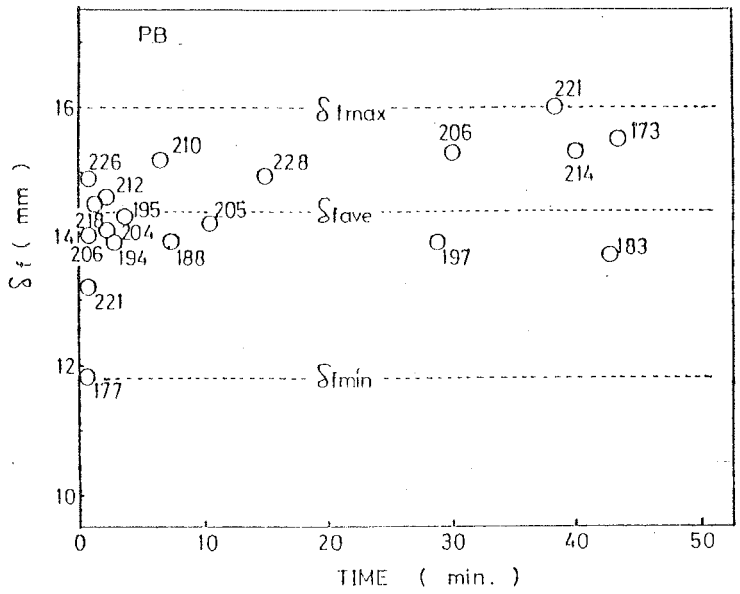


Fig. 13 Relationship between creep failure deflection and time to failure

Table 3 . Range of deflection in failure

	δ_{fmin}	δ_{fave}	δ_{fmax}
PB	11.8	14.4	16.0
PW	23.7	28.9	33.3
HB	19.8	23.6	28.2
Sugi	25.7	30.4	35.3
Beimatsu	10.8	16.0	21.6

δ_{fmin}: Minimum deflection in failure (mm)
δ_{fave}: Average deflection in failure (mm)
δ_{fmax}: Maximum deflection in failure (mm)

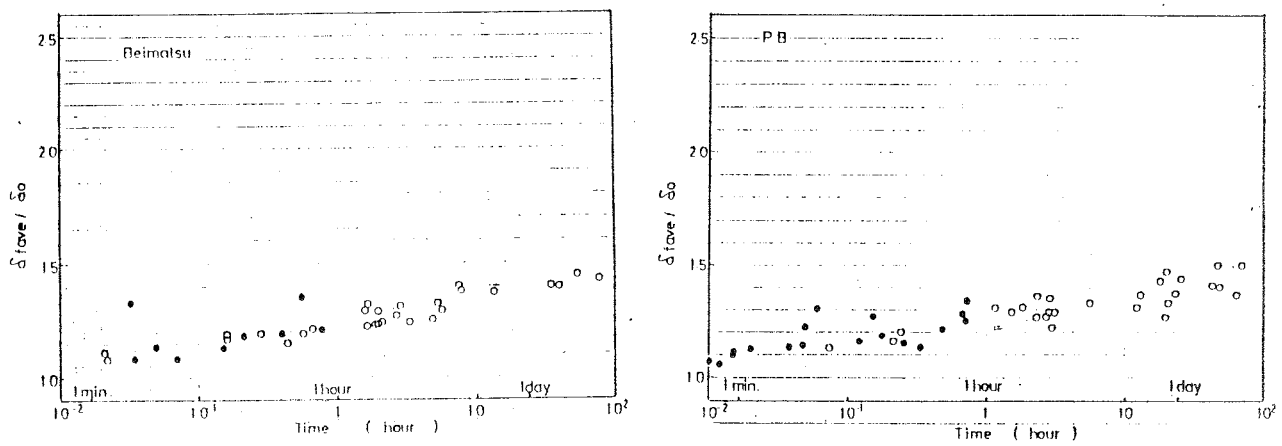


Fig. 14 Relationship between estimated time to failure based on creep deflection failure and δ_f δ_o
○ calculated, ● experimental

IV. Creep of wood, wood-based material and wood composite building elements under changing humidity conditions

Introduction

The creep behavior of wood and wood-based material under constant humidity conditions has often been characterized by the so-called power law as described. The reaction of materials in creep testing may be seen to vary with amount of loadings and exposure conditions such as a range of humidity and periods. It is found that changes in relative humidity may cause more severe creep deflection to occur than constant humidity. In this report short-term deflections corresponding to changing relative humidity and long-term deflections were experimentally observed.

Experimental procedure

Wood, wood-based material and building elements such as trusses and box beams as described earlier were subjected to changing humidity conditions in actual use. The changes of deflection were measured in detail during changing relative humidity.

Results and discussion

The deflection-time curves responded to variations of humidity in room conditions.

The experimental curves for wood containing defects seem to be roughly fitted to the power law even for changing environment conditions, and we may still take advantage of the simplicity of the power law as shown in Table4,[1(2)] when analyzing the long-term deflection.

The short-term deflections due to changing humidity conditions were observed as increased or decreased deflections in short-term based on the power law. The short-term deflections were dependent upon the difference of humidity and independent of amount of load applied as shown in Fig. 15, 16 .

In a low stress level which is generally below the working stress the total deflection would be shown as follow.

$$\delta(t, \Delta h) = \delta + A\, t^{N} + \Delta\delta(\Delta h)$$

where $\Delta\delta(\Delta h)$ is the short-term deflection due to difference of relative humidity.

Generally the equation could be fitted for wood-based materials and

wood composite elements .

The total deflections for wood-based materials decreased when relative humidity decreased as shown in many reports , while those for wood and wood composite elements which were jointed by nails or metal connectors increased when relative humidity decreased.

Table 4 Creep constants and estimated relative creep under various humidity conditions (particleboad sheathing)

条 件 Conditions	厚 さ Thickness	N	A/δ_0	δ_{10}/δ_0	δ_{50}/δ_0
恒温恒湿 Conditioned room	12	0.21～0.26	0.25～0.33	2.4～3.3	3.0～4.5
	12N*	0.16～0.26	0.16～0.38	2.4～2.8	3.1～3.7
	15	0.19～0.26	0.13～0.16	1.8～2.1	2.0～2.7
	15N*	0.22～0.23	0.13～0.16	1.9～2.0	2.2～2.4
	20	0.24～0.26	0.13～0.14	2.1	1.9～2.0
	20N*	0.25～0.28	0.10～0.12	2.6～2.7	2.4～2.6
一般空調 in air	12	0.31～0.36	0.15～0.19	3.4～3.9	5.0～6.1
	12N	0.31～0.34	0.15～0.17	3.2～3.4	4.6～5.2
	15	0.36	0.09	2.7	4.1
	15N	0.24	0.13	1.9	2.4
	20	0.26	0.09	1.8	1.9
	20N	0.24	0.13	2.2	2.4
湿潤 in wet 80～90%RH	12	0.36	0.65	13.5	23.2
	12N	0.26	0.74	7.2	10.5
	15	0.53	0.43	34.2	79.0
	15N	0.56	0.32	32.6	78.9
	20	0.40	0.77	21.5	40.0
	20N	0.33	0.27	5.1	7.9

N : nailed

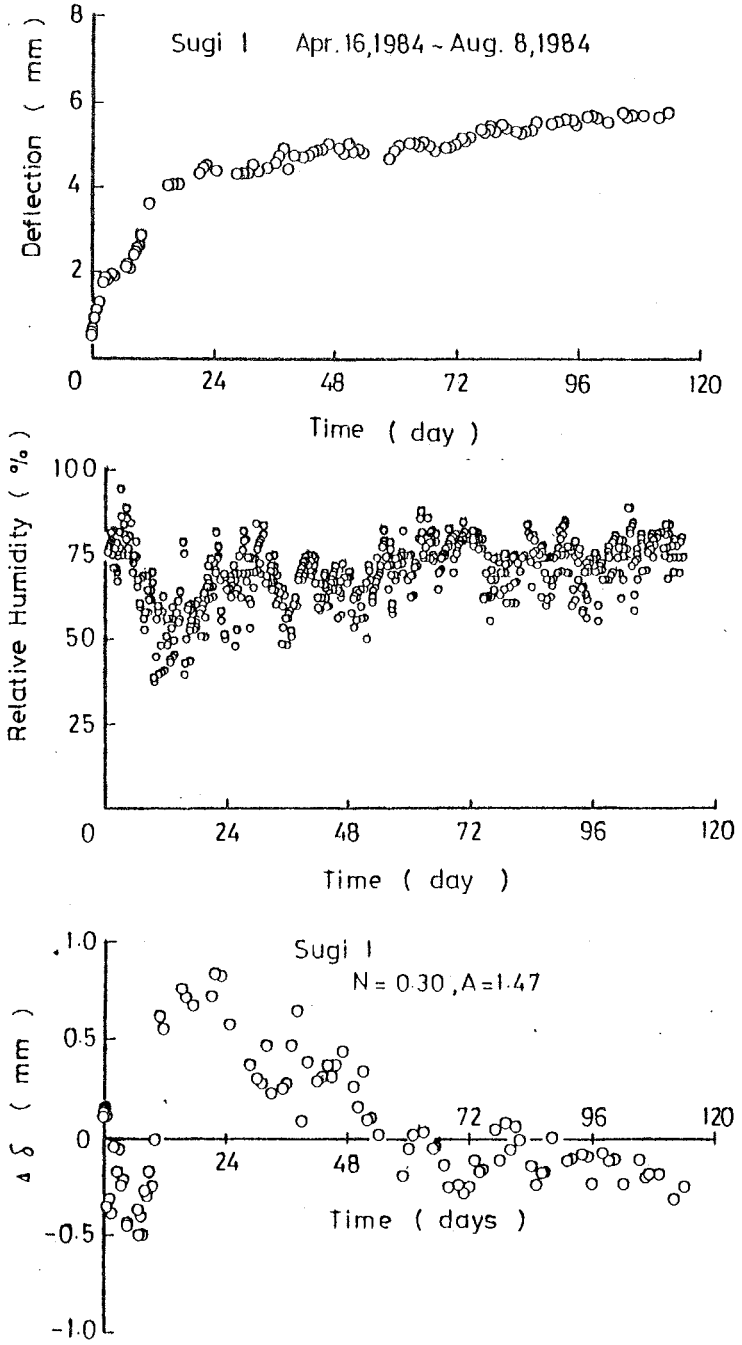


Fig. 15 Deflection-time under changing humidity conditions , relative humidity and deflection due to humidity changing

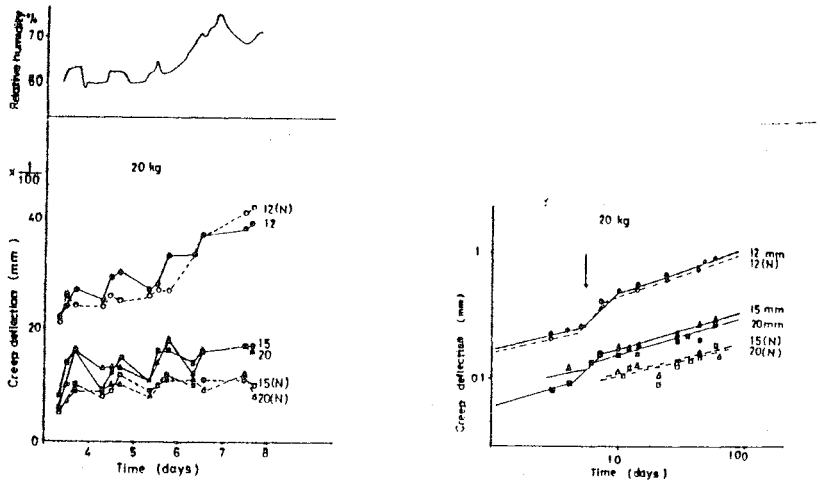


Fig. 16 Deflection-time under changing humidity conditions

Literature cited

1. Arima, T., Sato, M. and Mashita, S. : Studies on evaluation method for long-term performance of wood-based materials and elements, Report of Building Research Institute, No. 95 (1981)
2. Sugimoto, Y., Maruyama, N., Arima, T. and Okazaki, H. : Creep behavior of shelves in use, Bull. Fac. Agr. Shizuoka Univ. No. 33, 71-79 (1983)
3. Wood, L. W. : Relation of strength of wood to duration of load, U. S. For. Prod. Lab. Rep. No. R-1916, Madison, Wis. (1951)
4. Madsen, B. : Duration of load tests for dry lumber in bending, Dep. Civ. Eng., Univ. of B. C., Struct. Res. Ser. No. 3. Vancouver (1971)
5. Madsen, B. : Duration of load tests for wet lumber in bending, Dep. Civ. Eng., Univ. of B. C., Struct. Res. Ser. No. 4. Vancouver (1972)
6. Gerhards, C. C. : Effect of duration and rate of loading on strength of wood and wood-based materials, USDA For. Serv. Res. Pap. FPL283, For. Prod. Lab.,
Madison, Wis. (1977)
7. Gerhards, C. C. : Time-dependent bending deflections of Douglas-fir 2 by 4's, Forest. Prod. J. 35 (4), 18-26, (1985)
8. Gerhards, C. C. : Time-related effects of loading on wood strength, Wood Science 11 (3), 139-144 (1979)
9. Wilkinson T. L. : Longtime performance of trussed rafters with different connection systems, USDA For. Serv. Res. Pap. FPL204, For. Prod. Lab., Madison, Wis. (1978),
10. Wilkinson T. L. : Longtime performance of trussed rafters with different connection systems, USDA For. Serv. Res. Pap. FPL444, For. Prod. Lab., Madison, Wis. (1985)
11. Mayo, A. P. : Long-term performance test on trussed rafters, B. R. E. Current Paper 1/80 (1980)
12. McNatt J. D. and Hunt M. O. : Creep of thick structural flakeboards in constant and cyclic humidity, Forest Prod. J. 32 (5), 49-54 (1982)
13. McNatt J. D. : Rate- and duration-of-load behavior of Lab-made structural flakeboards, USDA For. Serv. Res. Note. FPL-0252,
For. Prod. Lab., Madison, Wis. (1985)
14. Lehmann, W. F., Ramaker T. J. and Hefty F. V. : Creep characteristic of structural panels, Proc. of 9th Washington State Univ. Symposium on Particleboard, p. 151-172 (1975)

INTERNATIONAL UNION OF FOREST RESEARCH ORGANISATIONS

GROUP S 5.02 - TIMBER ENGINEERING

ON THE EXTRAPOLATION OF SHORT-TERM WOOD STRENGTH TO STRUCTURE SERVICE LIFE

by

Y M Ivanov and Y Y Slavik

LJUBLJIANA
JOUGOSLAVIA
SEPTEMBER 1986

ON THE EXTRAPOLATION OF SHORT-TERM WOOD STRENGTH TO STRUCTURE SERVICE LIFE

by Yu.M.IVANOV[1] and Yu.Yu.SLAVIK[2]

As wood obeys to the Eq.1 of the kinetic conception of solid strength /1/

$$\log t = \log A - \alpha\sigma, \qquad (1)$$

where t is time-to-failure; σ is stress; A and α are constants at constant temperature,

so this creates a possibility of an extrapolation with certainty from short-term wood strength to long periods of time. The resultant accuracy depends on a confidential interval of the middle straight line log $t(\sigma)$ by the Eq.1 drawn through experimental points.The time-to-failure being dependent on stress is determinate by a physical process of submicrodamage accumulation /2/. Therefore, the long-term strength spread is the same as the short-term strength dispersion.

The middle straight line log $t(\sigma)$ by the Eq.1 has following confidence intervals: at tension along the grain for larch wood at uninterrupted loading (moisture content w=14,7 p.c.) $\pm$3,4 p.c. /3/; compression along the grain of pine at the same loading (w=15 p.c.) $\pm$2,10 p.c. /4/; shear in torsion of tubular specimens for hemlock fir at ramp loading (w=10-12 p.c.) $\pm$5,59 p.c. /5/ and bending of Douglas fir under long-term load with t up to 3 years (w=12 p.c.) $\pm$3,6 p.c. /6/ (confidence level 0,95 for tension, compression, shear and 0,90 for bending). The points for common lumber with defects /5,7/ are disposed nearly to the middle straight line by the Eq.1. Here the time t for tests with increasing load is defined by the formula

$$t = \frac{t'_A}{2{,}3(\log A - \log t)}, \qquad (2)$$

where t'_A is the test duration.A ramp loading with the sufficient step number equalled approximately to constant rate loading /8/.In Fig.1b the

---

1)Professor Dr.Sc.,2)Candidate Sc.,Central Research Institute for Building Structures,Gosstroi USSR,Moscow.

same data Presented by absolute values of stress σ in MPa.

The extrapolation by the straight line log t(σ) in Fig.1a is based on the constancy (at constant temperature) of the abscissa segment log A equalled to 17,1 at $\sim 20^{\circ}C$ [8]. From the similarity of the triangles (Fig. 1c) follows

$$\frac{\sigma_{lt}}{\sigma_t} = \frac{\log A - \log \bar{t}}{\log A - \log t}, \qquad (3)$$

where σ_t is the average short-term strength with log t; σ_{lt} is long-term strength for the time period $\bar{t}$.

Dividing both parts of the Eq.3 by σ_{lt} and transforming we will obtain [9]

$$\sigma_{lt} = \frac{\sigma_t}{B - C \log t}, \qquad (4)$$

where $B - C \log t = K_1$ is the long-term strength ceofficient.

Since at $t=\bar{t}$, $\sigma_t = \sigma_{lt}$ and $B - C \log \bar{t} = 1$, so the constants are

$$C_1 = (B-1)\frac{1}{\log \bar{t}}; \quad B_1 = \frac{\log A}{\log A - \log \bar{t}};$$

For example, from short-term machine testing wood specimen (at $\sim 20^{\circ}C$) with duratuin $t'_1 = 2,5$ min, $t = 3,93$ sec, log t=0,594, the long-term strength under the constant load action during 10 years is

$$\sigma_{lt} = \frac{\sigma_t}{1,98+0,114 \cdot 0,594} = \frac{\sigma_t}{1,912} = 0,52\ \sigma_t.$$

The foregoing data concern a uniform stress distribution over cross section of wood specimen (in Fig.1a and b for tension, compression and shear). Now turning to a non-uniform stress state in structure member (bending) the conditions need be considered for fairly reliable extrapolation allowing here for some peculiarities found. Let us contemplate the test data for standard wood specimens at various rate of loading up to failure (Fig.2,5)[4]: on the graph plotted with coordinates log t, σ the deviation of experimental points is distinct observed from the straight line log t(σ) after exceeding some rate of loading (or corres-

ponding log of time reduced to constant action of σ_{max} from formula (2)). The deviation of σ_{ul} noted is confirmed by the data of the vast research work on bending of lumber mark 2 conducted in Canada /10/ over wide range of ramp loading durations (Fig.2,6). The truth of this deviation was confirmed by check /7/.

Thus, the regular drop of σ_{ul} is ascertained when the rate of loading raises above some magnitude what is diametrically opposite to the usually material strength rising with accelerating force action, i.e. the paradox is present of wood behaviour in bending.

Under long-term loading considerable deflection development of wood specimen in bending is observed before failure. The latter arises after the compression crease having sprung up in extreme fibres of cross section. The appearance of the crease as exibited our experiments with bending in lever installation is immidiately followed by rapid fall of specimen bearing capacity, i.e. the crease is true primary failure deformation; after it occure the neutral axis displacement towards the tensile zone, rapid grows in turn of tension stress and rupture of extreme fibres the latter being the secondary failure deformation.

The considerable development of forced high elastic strain in extreme compression fibres of bending member is commonly for-run the crease emergence and leads to the stress relaxation due to inequality $\sigma_a > \sigma_{fe}$ and elastic core in cross section (here σ_a is the actual stress; σ_{fe} is the limit of forced high elastic deformation the rate of the latter being depend exponentially on σ /11/). The regular disposition of experimental points nearly to the straight line log t(σ) at different level of long-term load gives the ground to suppose the complete relaxation development in cross section, i.e. the fulfillment of the condition $\sigma \leq \sigma_{fe}$ and consequently $\dot{\varepsilon}_{es} < \dot{\varepsilon}_{fhe}$ (here $\dot{\varepsilon}_{es}$ is the edge strain rate and $\dot{\varepsilon}_{fhe}$ is the forced high elastic strain rate in compression fibre). If this supposition is right the grows of the edge strain rate $\dot{\varepsilon}_{es}$ in compres-

sion zone at machine test will cause reduction of both the difference $\dot{\varepsilon}_{fbe} - \dot{\varepsilon}_{es}$ and the stress relaxation rate in extreme fibre as well as the time-to-failure (i.e. time up to the instant of the compression crease appearance). This will result in the deviation of short-term test σ_{ul} downwards from the straight line log $t(\sigma)$.

$\dot{\varepsilon}_{fbe}$ grows greatly with an increase of moisture content w, for example, at the same stress σ the change of w from 12 to 30 p.c. induces the grows of $\dot{\varepsilon}_{fbe}$ by more than 2 orders. Therefore in wet wood the paradox appears at higher testing rate and with less than in dry wood deviation of σ_{ul} down from the straight line log $t(\sigma)$. This distinction can be used for direct verification of the assumption mentioned about the relaxation role in the paradox appearance. In fact the ratio of machine test σ_{ul} for dry to that for the same wet wood in compression will be more than in bending. Such an additional proof of the paradox we can get by the data of dry and green wood for species grown in the United States [12] (see Table, where are statistical characteristics: mathematical expectation $\bar{X}$, standard deviation S and coefficient of variation v, p.c.). The data listed in Table reveal the fact that moisture content affect on the value of σ_{ul} at a non-uniform stress state (bending) less than at an uniform stress distribution (compression) due to paradox in the former case. In that is concealed apparently the true cause of a diminished moisture effect on σ_{ul} obtaining from short-term bending tests.

The question now arises as to what conditions of the extrapolation to a structure service life might be in this case aiming not to underrate design stress values on account of the wood bending paradox? If edge stress levels σ_e are refered to σ_{ul} of machine tests so the paradox will manifest in higher position of the points above the straight line by the Eq.1 and the more the less the absolute σ_{ul} magnitude. Hence, the extrapolation straight line log $t(\sigma)$ has to be drawn from the axis log t point with abscissa log t=log A (at ~20°C, log A=17,1) as a middle

one trough the long-term test points. By lack of those data short-term tests ought to fulfil at decelerated loading, in particular the ramp loading with steps sustained longer time. For example, the absence of σ_{ul}-deviation down from the straight line log $t(\sigma)$ on B.MADSEN's experiments /10/ with bending lumber by 50x152 mm in cross section is provided at the time t of constant action of σ_{ul} not less than log $t \simeq 2{,}5$ (i.e.test duration $t' \approx 3{,}3$ hours).

From the above-stated it follows that design (or allowable) stresses for wood at bending on the base of machine test σ_{ul} of standard specimens or lumber were merely underestimated by the magnitude of the σ_{ul}-deviation down from the straight line log $t(\sigma)$ because of the paradox and could be raised for long-term loading. The logical deduction from the above proposed elucidation of the paradox is its direct dependence on square height of bending member cross section: the higher is the latter the more the σ_{ul}-deviation down from the straight line log $t(\sigma)$ of long-term strength. Such a decrease of σ_{ul} quite evidently corresponds to the reduction of glued laminated beams bearing capacity by the "height factor". This factor was obtained from short-term tests /13/, i.e. at the presence of the paradox which is absent under long-term load. Inasmuch as the beams designed are namely intended to serve during long times so the introduction of the "height factor" into their calculation seems not to be sufficiently substantiated.

The phenomenon analogous to the bending paradox described takes evidently place at stress concentration in wood specimens, structure members and their joints since at rapid test the relaxation rate of peak stresses could be decreased and average (over cross section area) σ_{max} (or force in joint) diminished. The same might be also owing to the stress concentration in case of a bending member failure with rupture of tensile fibres around defects.

REFERENCES

1. Zurkov S.N.,Korsukov V.E.Fisika tverdogo tela,1973,v.15,N 7.
2. Zurkov S.N.,Kuksenko V.S.,Petrov V.A. In book:Budushee nauki,1983,16
3. Perelygin L.M. Zavodskaiia laboratoriia.1938,N 1.
4. Liuboshiz M.I. Tst rate effect on the limit of plastic flow.Candid. diss.(in russ).Minsk.1950.
5. Madsen B. Forest Products Journal,1975,v.25,N 10.
6. Wood L.W. Forest Products Laboratory, NR 1916.Dec.1951.
7. Ivanov Yu.M.,Slavik Yu.Yu. Lesnoi jurnal,1981,N 2.
8. Ivanov Yu.M. Canadian Journal of Civil Enging.,1981,8.
9. Ivanov Yu.M. First International Conference on Wood Fracture.Proceedings.Vancouver.Canada.1979
10. Madsen B. Forest Products Journal,1975,v.25,N 5.
11. Ivanov Yu.M. Vysokomolekuliarnye soedineniia,1984,v.26B,N 6.
12. Markwardt L.J.,Wilson T.R.C. Strength and related properties of woods grown in the United States.Dept.Agr.,Techn.Bull.479.1935.
13. Newlin J.A.,Trayer G.W. Form factors of beams subjected to transverse bending only. National Advisory Committee for Aeronautics. Report N 181,1924.

Fig.1a Extrapolation straight line log t (σ) by the Eq.1 drawn as middle one through experimental points according to the test data for tension /1/[3/] and compression along the grain /2/[4/];shear in torsion of tubular specimens /3/[5/] and bending /4/[6/].

" 1b The same data with σ in MPa.

" 1c Scheme for long-term wood strength prediction.

" 2 Test data with various rate of loading in bending : for standard specimens of air-dry pine wood /5/[4/] and for air-dry lumber mark 2 of hemlock fir /6/[10/].

Table

Ratio of σ_{ul} in compression to σ_{ul} in bending for dry and green wood of species grown in the U.S.(/12/ Table 21)

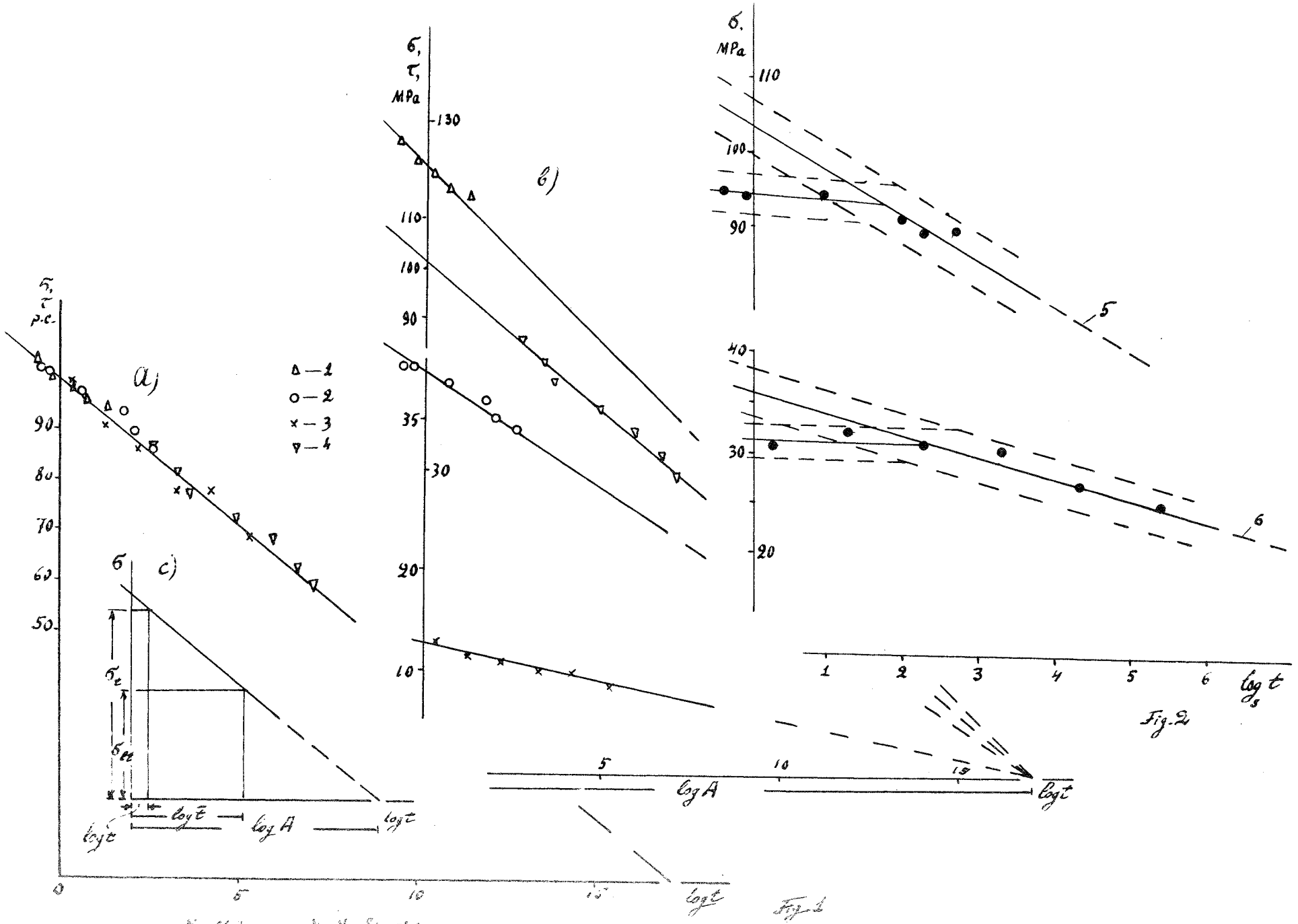
Species	Kind of testing	Moisture content p.c.	Number of average σ_{ul} values for individual species, n	Average values σ_{ul} psi.10^3 / MPa actual	edge	Statistical parameters of the ratio $\sigma_{uldry}/\sigma_{ulgreen}$ $\bar{x}$	s	v, p.c.	Estimate of difference $t=\frac{\lvert \bar{x}_1 - \bar{x}_2 \rvert}{\sqrt{(s_1^2 - s_2^2)/n}}$
Soft-woods	compression	11,8 (11,2-12,5)	43	6,44 / 45,3	-	2,02	0,237	11,7	
		30	"	3,21 / 22,6	-				$t_{0,05}=7,46 > 3$
	bending	11,8 (11,2-12,5)	"	-	10,94 / 77,0	1,68	0,187	11,1	
		30	"	-	6,53 / 45,8				
Hard-woods	compression	11,8 (11,2-12,5)	34	7,04 / 49,4	-	2,05	0,283	14,1	
		30	"	3,50 / 24,6	-				$t_{0,05}=5,50 > 3$
	bending	11,8 (11,2-12,5)	"	-	14,0 / 98,5	1,71	0,219	12,8	
		30	"	-	8,32 / 58,5				
Soft-woods a.hard-woods	compression	11,8 (11,2-12,5)	77	6,70 / 47,1	-	2,00	0,295	14,3	
		30	"	3,34 / 23.5	-				$t_{0,05}=7,36 > 3$
	bending	11,8 (11,2-12,5)	"	-	12,30 / 86,5	1,70	0,192	11,3	
		30	"	-	7,32 / 51,5				

SUMMARY

On the extrapolation of short-term wood stregth to structure service life by Yu.M.IVANOV and Yu.Yu.SLAVIK.

The extrapolation from short-term strength to long times is based on the equation of the solid strength kinetic conception to which wood obeys as it is illustrated by experimental data for tension and compression along the grain, shear and bending. The peculiarity of the extrapolation from rapid wood tests data in bending consists in decrease of ultimate strength (the wood bending paradox) after some rate of loading exceeding what ought to allow in values of design (or allowable) stresses. The underestimation (due to paradox) of the latter shown by the experimental data analysis as well as absence under long-term load of a decrease with height of the beams bearing capacity observed at short-term tests.Lit.13,ill.2.

10



Vl. M. Ivanov, Ju. Yu. Slavic.

INTERNATIONAL UNION OF FOREST RESEARCH ORGANISATIONS

GROUP S 5.02 - TIMBER ENGINEERING

CREEP AND RECOVERY IN BAMBOO

by

J J A Janssen

LJUBLJIANA
JOUGOSLAVIA
SEPTEMBER 1986

CREEP AND RECOVERY IN BAMBOO

Dedicated to prof. Koichiro Ueda, who has done so much in favor of bamboo.

dr. J.J.A. Janssen,
Eindhoven University of Technology,
P.O. Box 513,
5600 MB Eindhoven,
The Netherlands

Summary

Creep (i.e. the increase of deformation with time under load) and recovery (the decrease of deformation with time after removal of the load) has been tested for bamboo. A physical and mathematical model has been used, and the parameters in this model have been determined from test data. The validity of the model is discussed.

Introduction

Creep and recovery deals with the long term deformation, in this case the bending of bamboo. For building purposes knowledge about creep is important: one has to know not only the deformation immediately after loading, but also the deformation after 10 or 20 years of use. Research on creep in bamboo however is scarcely heard of. For the description of creep a model is always used. In the case of wood the so called Burgers model is commonly used. Because wood and bamboo are materials with similar structures, we adapt the Burgers models also to bamboo. The Burgers model is given in figure 1. (see Lindberg a.o. 1980, Lofty a.o. 1972, Kollmann 1968).

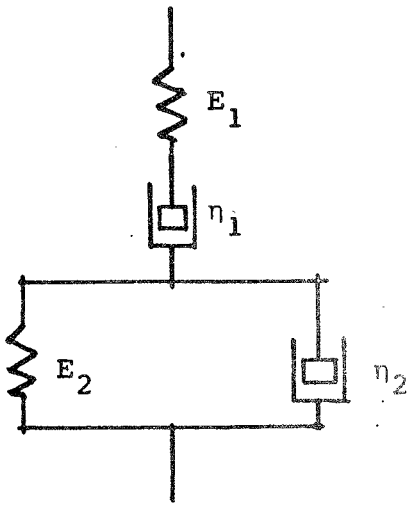


Figure 1. Burgers model.

In this model the first element, E_1, means a spring. This is the Young's modulus or the modulus of elasticity; in fact it represents the elastic straining of bond angles of molecules and also of bond lengths from their equilibrium values. Highly christalli cellulose regions in an isolated stat would have the properties of a spring. The second element, η_1, represents molecular slippage with a slip of polymer molecules past one another. In this model it is drawn as a dashpo Amorphous lignin would behave like a dashpot.
The third element, the spring E_2, represents the restoring force brought about by the thermal agitation of the chain segments.
The fourth element, the dashpot η_2, represents the resistance of the polymer chains to uncoiling and coiling.
With this model, a deformation-time-diagram will look like in figure 2.

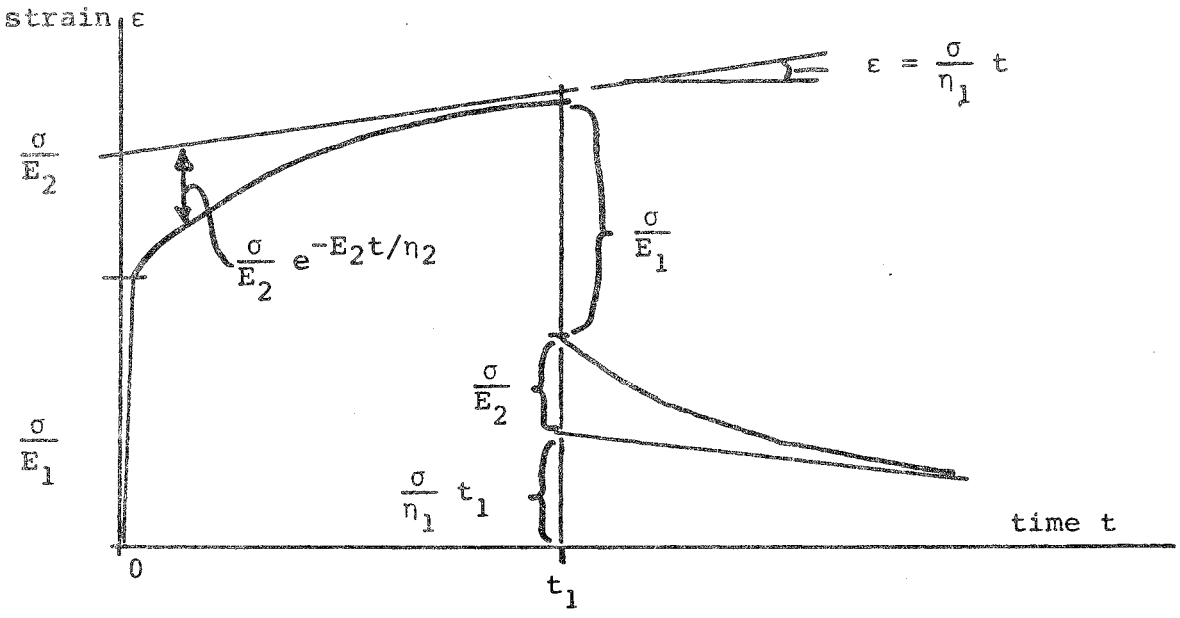


Figure 2. Strain-time-diagram.

The mathematical formula, belonging to this model, is:

$$\varepsilon(t) = \frac{\sigma}{E_1} + \frac{\sigma}{E_2} + \frac{\sigma}{\eta_1} t - \frac{\sigma}{E_2} e^{-E_2 t/\eta_2}$$

in which:

ε = the strain

σ = the stress

t = the time.

In publications on creep, several authors report about the so-called "loss-factor", called tan δ; this is simply E_1/E_2; it is the ratio between the immediate and the retarded elastic deformation (Lindberg, p. 248).

Experimental Methods

Tests have been carried out on full bamboo culms. The species is Bambusa Blumeana, from the Philippines, conditioned at R.H. 70% and 20°C. The mass per volume is 823 kg/m^3, standard deviation 119. The test method is given in figure 3 and picture 4.

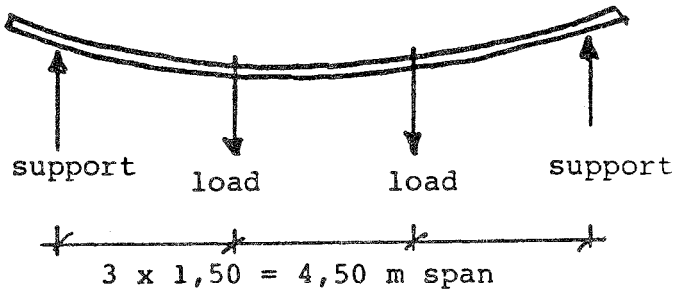
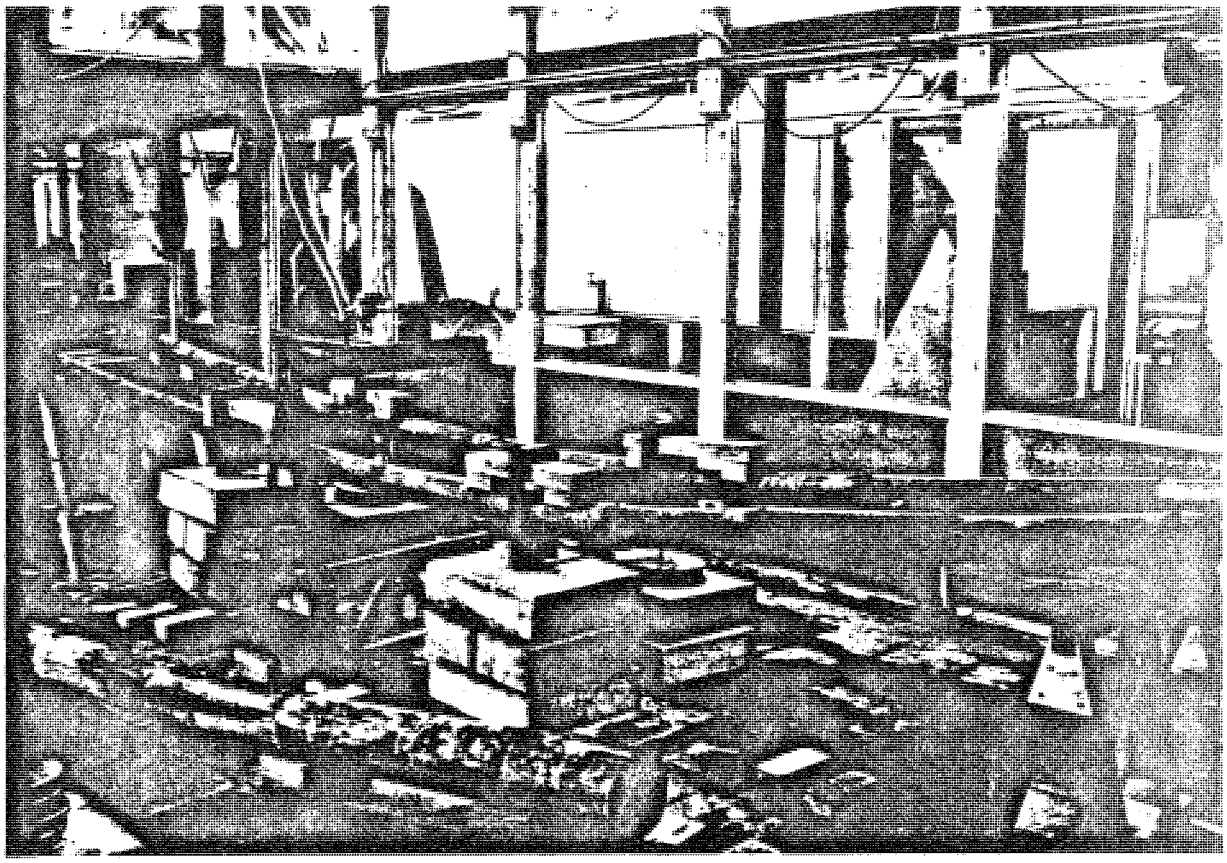


Figure 3. Test method.

The test method is a four point bending test. The deformation has been measured in the centre of the span. The load has been applied in such a way that the initial strain was about 2°/oo. Creep and recovery have been tested in two ways:

1) one hour loaded (creep), half an hour unloaded (recovery), repeated three times, total duration six hours, ten culms,
2) two months loaded (creep), one and a half month unloaded (recovery), repeated three times, total duration 14 months, 24 different culms.

This report will deal with the first test series only; the second series will be dealt with only in "Further Study"



Picture 4. Test method.

Results

A typical test result looks like figure 5.

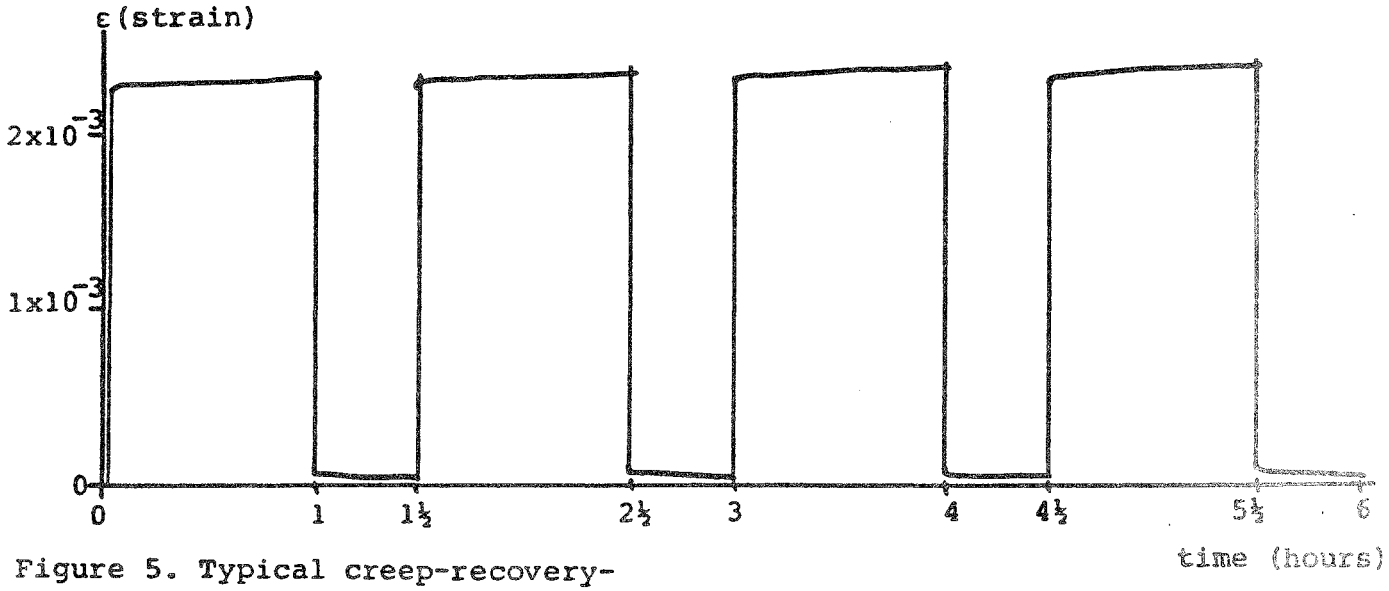


Figure 5. Typical creep-recovery-diagram.

From the data the values for E_1, E_2, η_1 and η_2 have been calculated, and compared with the mass per volume (ρ in kg/m^3, at M.C. 12 percent). These values are given in table 1.

value	mean	st.dev.	units
E_1	19450	3850	N/mm^2
E_2creep	1.66	0.50	10^6N/mm^2
E_2recov.	2.17	0.54	10^6N/mm^2
loss factor	0.01	-	-
η_1	14.4	5.9	10^9N/mm^{2}s
$\eta_2$creep	3.36	0.54	10^9N/mm^{2}s
$\eta_2$recov.	2.40	0.81	10^9N/mm^{2}s

Table 1. Results of tests.

These results have been calculated with a least-square regression. The ratio between these values and the mass per volume ρ are given in table 2.

E_1	= 2038 + 21 x ρ	r^2=.47
E_2creep	= -.5 + 0.0026x ρ	r^2=.39
E_2recov.	= .15+ 0.0025x ρ	.29
E_2creep	= .77x E_2recov.	.69
η_1	= -10.5 + 0.03 x ρ	.37
$\eta_2$creep	= - 2.2 + 0.007 x ρ	.26
$\eta_2$recov.	= - 1.2 + 0.004 x ρ	.41
$\eta_2$recov.	= 1.1 + .38 x $\eta_2$creep	.56

Table 2. Ratios between test results; units as in table 1; ρ in kg/m^3.

In the model, the value E_2 is a constant; however in the test results E_2 proved to be time-dependent, see table 3.

first hour creep	1.01	10^6N/mm^2
second	1.63	
third	1.85	
fourth	2.08	

Table 3. Values for E_2

Discussion

The value for E_1 is normal for conditioned bamboo. As to the other three values (i.e. E_2, η_1 and η_2), it seems to be impossible to find any reference. They can only be compared with values for wood (Kollmann 1968), and the ratios are as in table 4.

value	wood	bamboo	ratio
E_1	10 000	20 000	2 x
E_2	82 000	1.9 x 10^6	23 x
η_1	0.15x10^9	14.4 x 10^9	100 x
η_2	0.07x10^9	2.88 x 10^9	40 x

Table 4. Comparison of E and η for wood and bamboo.

It is rather difficult to explain these ratios. Possible parameters are:
- the mass per volume,
- the cellulose content,
- the crystallinity of the cellulose
- the angle between the microfibrils in the cell-wall, and the cell-axis

Up to now it is not clear yet how these parameters might explain the said ratios.

For building practice however it is clear that creep in bamboo can be neglected, contrary to timber.

Conclusions

Creep and recoveryin bamboo have been studied in a four-point-bending test. Results are given in table 1 and 2. For building practice, creep in bamboo can be neglected.

Further study

However, some problems remain unsolved. Firstly, the determination of η_1. This value is calculated from the slope of the curve, see figure 1. Common sense indicates that physically the best slope is as drawn in figure 6, or even steeper:

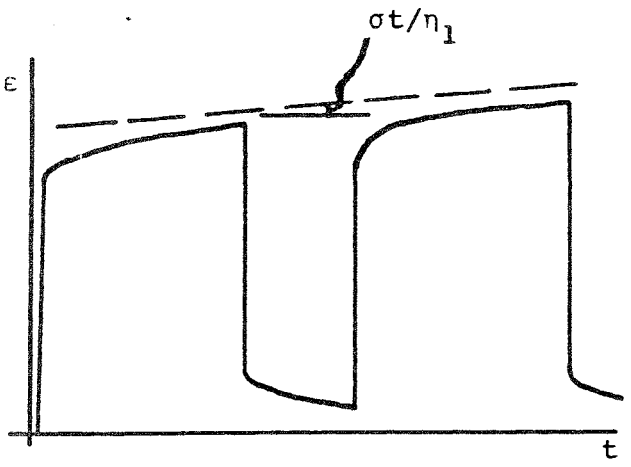


Figure 6. Best slope.

In the mathematical calculations however a less steep slope, or even a horizontal line,gives a better result in the least square regression. With other words, r^2 increases for a decreasing slope, see figure 7:

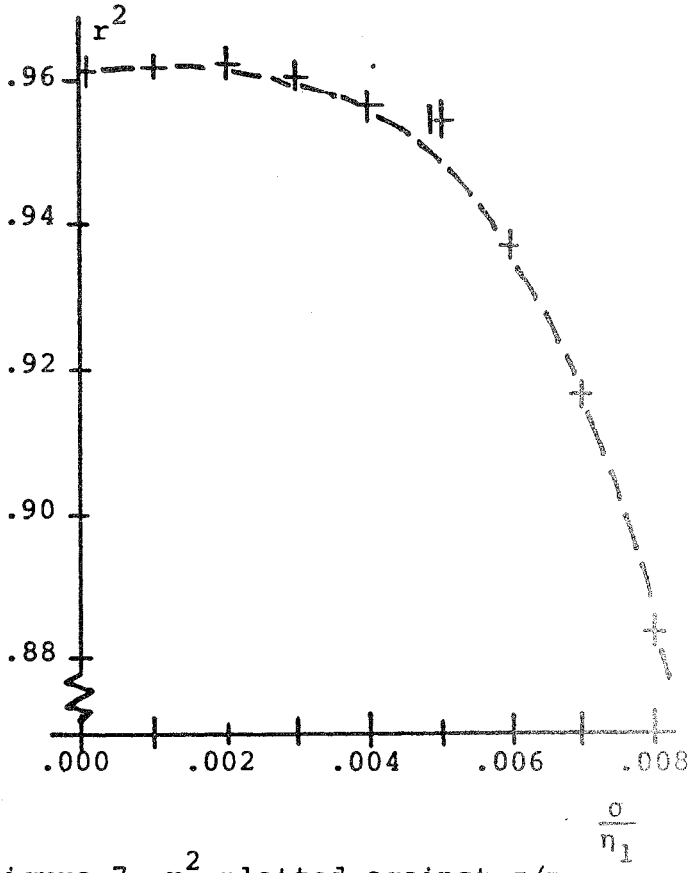


Figure 7. r^2 plotted against σ/η_1

This contradiction between the physical model and the mathematical calculation cannot be explained as yet. Also η_1 seems to decrease with time, which limits creep. In Burgers model creep has no limit.
Secondly, E_2 proves to be time-dependent (see table 3), and E_2 and η_2 prove to be different for creep and for recovery (table 1). The Burgers model (see figure 1) does not take into account these results. This means, that further study is necessary to improve the model, and to find a physical explanation.

Thirdly, we have carried out these tests not only during one hour creep and half an hour recovery, but also during two months and one and a half month respectively. In the calculations of the regression the Burgers model failed: a gap remained between the observed data and the curve calculated by regression, see figure 8.

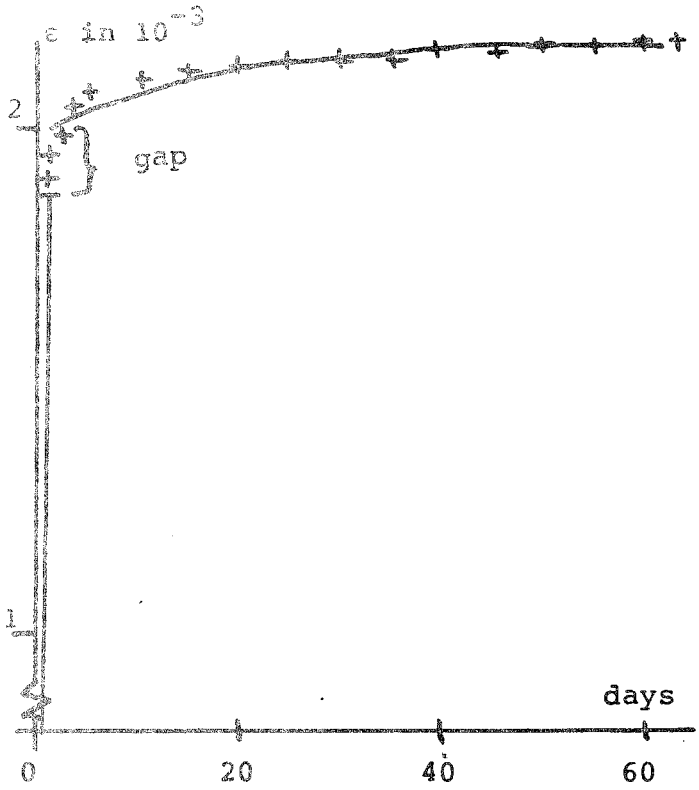


Figure 8.

In this figure the crosses + represent the observed data, and the line represents the line adapted by regression. Clearly at the left side a gap remains, which means that the Burgers model is valid for one-hour-tests only. For a duration of two months this model has to be enlarged with some time-dependent parameter(s).

As a result of this problem, we are unable to present now the results of our tests on creep and recovery with a duration of 2 and 1½ months resp. These tests have been carried out as follows:

- 8 culms, 12 percent M.C.,
- 5 culms, 12 percent M.C., with removed diaphragms, to study their influence,
- 3 culms, 12 percent M.C., with removed outer skin, to study the influence of this skin and its silica content,
- 8 culms, 9 percent M.C., to study the influence of the M.C.

Literature Cited

Bodig and Jayne, Mechanics of Wood and Wood Composites, New York 1982, ISBN: 0-442-00822-8, mainly chapter 5: "Rheological Characteristics".

Kollmann, and Côté, Principles of Wood Science and Technology, volume I, Solid Wood, pp. 315-321, Berlin 1968.

Lindberg, a.o. Rheological Models and Processing of Polymeric Materials. Kemia-Kemi (1980) no. 5, pp. 245-248, and no. 9, pp. 497-499.

Lofty, a.o. Short-term creep as related to cell-wall crystallinity. Wood and Fiber (1972) pp. 204-211.

INTERNATIONAL UNION OF FOREST RESEARCH ORGANISATIONS

GROUP S 5.02 - TIMBER ENGINEERING

SAA DRAFT STANDARD ON PROOF GRADING

by

R H Leicester

LJUBLJIANA
JOUGOSLAVIA
SEPTEMBER 1986

2

SAA DRAFT STANDARD ON PROOF GRADING

1. SCOPE

This standard describes a method of obtaining an approved stress grade of timber through proof testing. The grading procedure is described, together with quality control and quality assurance procedures. Several systems of proof grading are possible and these are divided into two primary classes. One is a full grading system, in which all pieces of timber are proof tested; the other is a hybrid grading system in which only a portion of the timber is proof tested.

2. INTRODUCTION

Proof grading is a procedure incoporating the use of a continuous proof testing machine for obtaining stress graded timber. As a piece of timber passes through the proof testing machine, it is continuously loaded on edge to a high stress level. If the piece of timber survives this stress without damage, it is deemed to belong to the stress grade of timber for which the proof grading system is set.

Sections 3-6 of this standard provides details of a recommended procedure for quality control during proof grading. This control is intended to give timber that meets a target set of structural properties but does not guarantee that these properties have been attained. As with all types of grading systems, the guarantee must be based on verification tests on the graded timber. The required verification tests are described in Section 7. Thus Sections 3-6 may be considered as recommendations for good practice while Section 7 should be regarded as mandatory to achieve conformance with this standard.

In stress grading, each piece of timber is allocated to a specific stress grade or it is rejected. If the timber is allocated to a specific stress grade, the implication is that it may be safely used with the several design properties specified in the Australian standard AS 1720. These properties are given in Appendix B. It should be noted that in addition to bending properties, other design properties such as tension strength must be guaranteed. Allocation of timber to a stress grade does not provide design information on joint strength (for which a joint group classification is required) or on compression perpendicular to the grain (for which a strength group classification is required).

It will also be noted from the methodology of the verification tests in Section 7, that the check of a stress grade is made on a population of timber, and not on a single piece of timber. Hence the term stress grade applies to a population of timber and not to a single piece.

In general the process of stress grading timber may be considered to be made up of three essential operations. These are the following.

(i) Selection of a parent population of pieces of timber.

(ii) The sorting of this parent population into sub-populations that are then designated to be of specific stress grades.

(iii) Checking the structural properties of the graded timber.

Most current grading systems place an emphasis on the method of sorting the parent population; by contrast in the proof grading procedure little is stated on the sorting method, and instead the emphasis is placed on checking. Thus proof grading may be expected to be useful in circumstances where difficulties occur in ensuring the stability of the parent population (as for example in mills that utilize multiple species) or where sorting is difficult to control (as for example where slope of grain is determined through visual grading for a dark coloured, rough sawn timber). Proof grading methods are particularly useful when it is necessary to cull out the occasional rogue piece of timber which has defects (such as compression shakes) that cannot easily be detected in sorting procedures.

The notation and definitions of special terms used in this Standard are given in Appendix A.

3. PROOF GRADING SYSTEMS

3.1 General

All types of proof grading commence by sorting the parent population into sub-populations, the intention being to qualify each such sub-population as being of a specific stress grade. Some or all of the pieces of timber in each population are then passed through a proof

testing machine, during which it is loaded on edge and continuously stressed in bending to a specified proof stress. Pieces that survive the proof stress without failure, excessive deformation or other signs of damage are deemed to qualify for a stress grade that corresponds to the applied proof stress.

3.2 Type of System

Proof grading systems may be broadly classified into full proof testing and partial proof testing systems; the latter will be referred to as hybrid grading systems. In full proof testing systems every piece of timber is proof tested. In hybrid grading systems the pieces visually (or otherwise) assessed to be the weakest 10% are proof tested.

The notation PG will be used to indicate the material of a full proof testing system, H-PG will indicate the proof tested material of a hybrid system, and H-VG the material that is not proof tested in a hybrid system.

> (Editors note. H = hybrid, PG = proof graded, VG = visually graded ... but not necessarily visually stress grade d in the formal sense).

3.3 Number of Loadings

Proof testing may be either a single pass or double pass operation. In a double pass operation each piece of timber is proof tested twice, with the alternative edge placed in tension the second time.

3.4 Orientation of the Timber

In single pass proof testing, the edge of the timber placed in tension may be either chosen at random, or it may be chosen so that the edge visually (or otherwise) assessed to be the weakest is placed in tension. These two types of testing will be referred to as having random edge and edge biased loadings respectively.

4. THE PROOF TESTING MACHINE

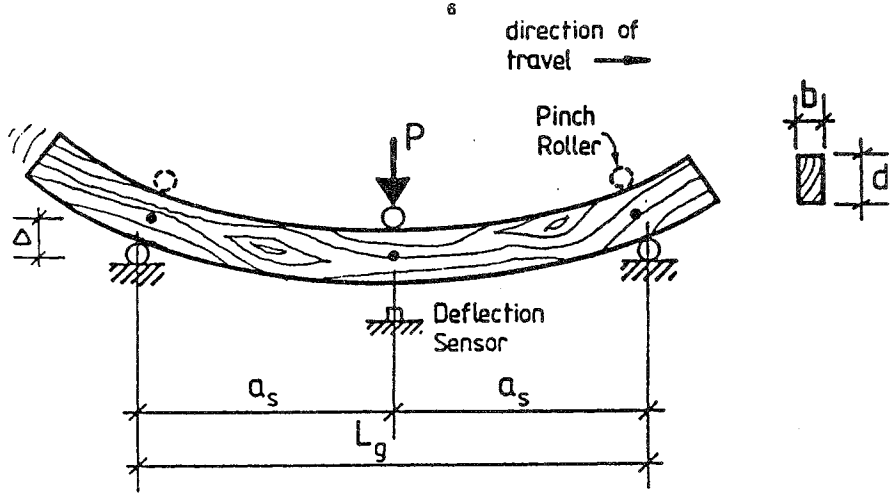
4.1 Loading Configuration

The proof testing machine may load the timber in either three point or four point bending as illustrated in Figure 1.

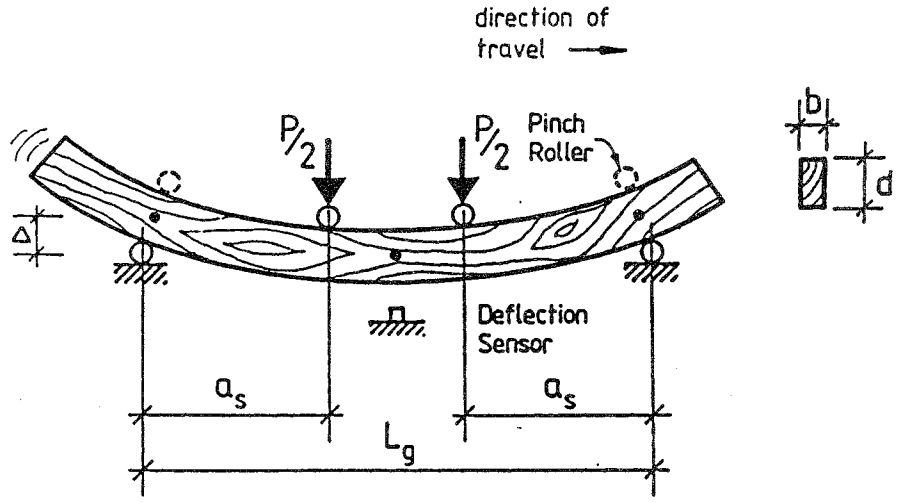
> Note. Four point bending is the preferred configuration as this reduces stress concentrations and hence damage to the timber. For similar reasons the loading wheels should be as large in diameter as possible, and also should have a soft outer rim.

4.2 Load Control

The proof testing machine in use should be capable of maintaining the applied load within +5%, -2% of any calibration setting.



(a) Three point loading



(b) Four point loading

a_s = shear span

L_g = loading span

Figure 1 Schematic illustration of loading systems

The full proof load should be applied for the total time that the timber passes through the machine, except for short lead-in and lead-out lengths. The sum total of these load-in and lead-out lengths should not exceed 200 mm per piece of timber.

4.3 Reject Switch

The proof testing machine should be fitted with a reject switch that can be activated by the grading operator or by a deflection sensor located as shown in Figure 1. Activation of the reject switch immediately unloads the timber and activates the procedures for a piece of timber classified as failed or reject.

4.4 Wheel Indent

The loading wheels of the proof tester should have raised ridges that place permanently visible indents along the compression edge of the timber during proof testing.

(Editorial Note. The drafting committee was undecided on the desirability of including the requirement, and comment is invited on this matter).

5. GRADING PROCEDURE

5.1 Presorting

The sub-populations of timber to be proof graded to a specified grade are selected from the parent population by some pre-sorting procedure.

Any parent population and pre-sorting procedure may be used to produce a given stress grade. However these must be formally specified in written documentation, and maintained constant during a given 'grade run'.

Note. The life of a 'grade run' may be chosen arbitrarily and may be a day, a year or several years. It will be seen in Section 7 that special verification procedures are required at the start of each grade run; hence it is desirable to maintain a grade run for as long as is possible.

In the hybrid grading system, the pieces of timber visually (or otherwise) assessed to comprise the weakest pieces in each grade is separated from the sub-population and designated as H-PG material, the remainder is designated H-VG material. The H-PG material is to be proof tested and shall comprise not more than 20% of the total sub-population.

(Editors note. It may not be necessary to formally visually stress grade H-VG material).

5.2 Machine Calibration

the calibration of the proof testing machine shall be checked at least once a day. A log book record of calibration should be kept.

In the case of calibration under static load condtions, care should be taken to ensure that machine friction acts in the most conservative direction during the calibration operation. For machines with pinch rollers, these should be activated to apply their normal operational pressure during the calibration operation.

Note. The best calibration is obtained if the pinch rollers are deactivated during calibration and during the application of the load in proof grading.

Note. When using a calibration bar, the method of ensuring that friction acts in a conservative direction is as follows. After a suitable calibration load has been applied on the calibration bar, the centre of the deflected bar is pushed back towards the unloaded configuration and then released slowly; the bar will then come to rest in the reqired conservative equilibrium position.

5.3 Proof Load

An estimate of the appropriate proof stress for a given grading situation is given in Appendix D. From the equations given in Appendix C, the proof stress can be converted to a proof load.

Once timber grading gets underway, the applied proof load should be altered in accordance with the findings of the verification tests specified in Section 7.

5.4 Proof Testing

During proof testing, pieces of timber that fail, show signs of damage or deflect excessively are to be rejected.

A suitable criterion for excessive deflection is a mid-span deflection of 5.0 mm plus 2.0 times the average deflection expected for timber of the target stress grade. A method for computing the average expected deflection is given in Appendix C.

(Editors Note. Timber with a coefficient of variation of 20% on MOE has a 1% chance of deflecting 1.8 times the average value. In addition a further clearance is required to allow for some spring of the timber).

During proof testing, the failure rate should not exceed 5%.

Note. If the failure rate exceeds 5%, then the magnitudes of the allowable design tension strength and stiffness of the graded timber may be poor relative to that of the bending strength.

5.5 Visual Check

If the shear span is less than or equal to 500 mm, then no visual check is needed. If the shear span is greater than 500 mm, then after proof testing, a visual check should be made that at each end of a piece of timber, for a length equal to the shear span a_s of the proof testing machine (see Figure 1), there are no defects greater than that existing in the remainder of the piece.

In addition, a check should be made that the graded timber complies with any required non-structural limitations.

Note. Examples of non-structural limitations are excessive twist, spring, bow, wane and unsightly blemishes)

5.6 Branding

Pieces of timber that are not rejected should be branded with symbols appropriate to the target stress grade, the method of grading, and the mill identification number.

5.7 Remixing

In the case of a hybrid grading system, it is necessary following the proof testing, that the H-PG and H-VG material be randomly mixed together so that the proof tested material comprises less than 20% of the total pack.

Note. In a hybrid grading system, the timber is deemed to be proof graded only after the remixing has been completed.

5.8 Quality Assurance Samples

Samples for quality assurance should be taken from the graded timber in accordance with the requirements specified in Section 7.

6. GRADING OPERATOR

The grading operator should be appropriately trained in the technique of proof grading. He should be responsible for ensuring that all aspects of the grading procedure as described in Section 5 are correctly undertaken.

7. QUALITY ASSURANCE

7.1 Responsibility

The quality assurance of proof graded timber shall be the responsibility of the timber producer.

7.2 Initial Verification

This verification is used to classify the stress grade of proof graded material. It shall be undertaken during the proof grading of the first 10 000 pieces of timber in each grade run. It shall also be undertaken each time the monitoring verification indicates a change of more than half a stress grade in the properties of the graded timber.

This verification shall be based on a sample size of not less than 400 pieces of graded timber, selected at random from the mill production. Half of the sample shall be tested in bending and the other half in tension according to the Australian Standard AS -: Evaluation of Graded Timber. The testing shall be carried out in a NATA approved laboratory.

7.3 Monitoring Verification

7.3.1 General

After the initial check has been completed, a system of continuous monitoring shall be initiated to detect any drift of structural properties away from the initially determined values.

The following describes some types of continuous monitoring that may be used.

This is applied to pieces of timber taken at random at a rate of one from every 200 pieces of proof graded timber.

7.3.2 Monitoring through use of proof testing machine

This verification procedure is described in detail in Appendix E and is essentially a rapid check on bending strength.

The test may be undertaken with the proof testing machine of the mill. The test samples may be allowed to accumulate until a convenient number have been collected for a varification run. Pieces of timber that survive the second proof test that occurs during the verification may be considered to be still acceptable as stress graded material.

7.3.3 Monitoring through laboratory tests

This is applied to pieces of timber selected at random at a rate of one from every 1000 pieces of proof graded material.

The verification is a measurement of bending strength and modulus of elasticity according to the Australian Standard AS -: Evaluation of

Graded Timber. The testing shall be carried out in an independent NATA approved laboratory.

7.4 Quality Assurance Organisation

Quality assurance organisations shall check that the verification tests as described in Section 7.2 are correctly undertaken. They will also check that production mills follow a documented procedure for presorting, that the proof testing machines are accurately calibrated, and that the branding is correct.

Note. Examples of suitable quality assurance organizations are the Radiata Pine Association of Australia and the Australian Hardwood Q.C.

APPENDIX A. DEFINITIONS AND NOTATION

A1. DEFINITIONS

Basic working stress in bending. Design stress for long duration loads, AS 1720.

Damage (to be defined)

Double pass grading. Proof grading method in which each piece of timber is proof tested twice, with alternative edges placed in tension each time.

Edge biased grading. Single pass grading in whih the edge visually (or otherwise) assessed to be the weakest is placed in tension during the proof testiing operation.

Full proof grading. Proof grading in which every stick is proof tested.

Grading operator. Person in charge of the proof grading operation.

Grade run. A grading operation applied to a sub-population of timber in which all parameters such as the pre-sorting method and the proof load are kept constant.

Hybrid proof grading. Proof grading system in which only 10% of the material is proof tested.

H-PG material. The timber that is proof tested in a hybrid proof grading

system.

H-VG material. The material that is not proof tested in a hybrid proof grading system.

Parent population. Population of timber that is presorted into sub-populations to produce various stress grades.

Presort. The sorting of a parent population into sub-populations.

Proof stress. Bending stress applied during proof testing.

Proof grading. Method of grading timber through the use of proof testing.

Proof Load. Load applied by proof testing machine.

Proof load factor. Ratio between the proof stress and the basic working stress in bending.

Proof test. Application of a large bending stress to a piece of timber to check that is has a certain minimum bending capacity.

Proof testing machine. Machine for applying a continuous proof load to timber as it passes through the machine.

Quality Assurance Organization (to be defined)

Random edge grading. Single pass grading in which a random edge of the

timber is stressed in tension during the proof testing operation.

Single pass. Proof grading method in which each piece of timber is proof tested only once.

Shear span. Distance between the support and point of load application, Fig. 1.

Sub-population. Population of timber, presorted from a parent population, and intended for proof grading to a particular stress grade.

Verfication test. Test on samples of graded timber to verify that it has certain specified structural properties.

A2. NOTATION

A_s = shear span, Fig. 1

b = tickness of timber, Fig. 1

d = depth of timber, Fig. 1

E = modulus of elasticity

f_b = bending stress

f_p = proof stress

F_b^1 = basic working stress in bending

L_g = loading span of proof testing machine

N = sample size in verification tests

P_a = acceptable failure rate in type 'B' verification tests

P_i = expected average failure rate in type 'B' verification tests

P = total load applied by the proof testing machine

Q = correction factor for sample size, equation (E2)

Δ = deflection at midspan, Fig. 1.

APPENDIX B
(Deleted)

APPENDIX C. STRUCTURAL EQUATIONS

C1. STRESS

For the piece of timber loaded as shown in Figure 1, the nominal bending stress f_b is related to the applied load P by

$$f_b = (3Pa_s)/(bd^2) \qquad (C.1)$$

C2. STIFFNESS

For the piece of timber loaded as shown in Figure 1, the deflection at midspan Δ is related to the applied load P by

$$\Delta = [(PL_g^3)/(Ebd^3)][0.75(a_s/L_g) - (a_s/L_g)^3] \qquad (C.2)$$

where E denotes the modulus of elasticity.

APPENDIX D. ESTIMATE OF PROOF STRESS

An estimate of the required proof stress f_p for a stress grade having a basic working stress in bending F'_b can be obtained from the ratio f_p/F'_b given for various cases in Tables D1-D6.

In these tables the terms structural grade nos 1 and 4 refer to timber having natural defects corresponding roughly to those permitted for structural grades nos 1 and 4 in The Australian Standards AS 2082 -: Visually Stress-graded Hardwood for Structural Purposes and AS 2858 -: Timber-Softwood-Visually Stress Graded for Structural Purposes.

Structural Grades Nos 1 and 4 correspond to 75 and 38 per cent grades of timber. It should be emphasised that the use of the terms structural grades numbers 1 and 4 are not meant to imply that the timber needs to be formally graded according to the standards 2082 and 2858; the terms are used simply to give a rough classification of the timber in terms of whether it contains large or small defects. For timber having a grade between Nos 1 and 4, interpolation may be used.

TABLE D1

PROOF LOAD FACTORS, SINGLE PASS, EDGE-BIASED
STRUCTURAL GRADE NO. 1

Shear span of proof testing machine (mm)	Timber depth (mm)	Proof load factor f_p/F'_b					
		Grading failure rate = 1%			Grading failure rate = 5%		
		Length of graded timber (mm)			Length of graded timber (mm)		
		= 2000	= 4000	= 6000	= 2000	= 4000	= 6000
450	19	2.11	1.99	1.93	2.24	2.15	2.09
450	35	2.18	2.07	2.00	2.35	2.20	2.16
450	42	2.19	2.09	2.03	2.38	2.21	2.18
450	70	2.19	2.15	2.09	2.48	2.29	2.21
450	90	2.22	2.17	2.12	2.53	2.34	2.25
450	120	2.27	2.20	2.15	2.58	2.40	2.30
450	140	2.30	2.19	2.17	2.60	2.43	2.33
450	190	2.36	2.20	2.20	2.64	2.49	2.39
500	19	2.12	1.99	1.93	2.25	2.15	2.10
500	35	2.18	2.07	2.01	2.36	2.20	2.16
500	42	2.20	2.09	2.03	2.40	2.22	2.18
500	70	2.20	2.15	2.09	2.50	2.29	2.22
500	90	2.24	2.18	2.12	2.54	2.34	2.25
500	120	2.29	2.20	2.16	2.59	2.40	2.30
500	140	2.32	2.19	2.17	2.61	2.43	2.33
500	190	2.38	2.20	2.20	2.65	2.49	2.39
600	19	2.14	2.00	1.94	2.28	2.16	2.10
600	35	2.20	2.08	2.01	2.40	2.20	2.17
600	42	2.19	2.10	2.03	2.44	2.22	2.19
600	70	2.23	2.16	2.10	2.53	2.31	2.22
600	90	2.27	2.18	2.13	2.57	2.36	2.26
600	120	2.32	2.19	2.16	2.61	2.41	2.31
600	140	2.35	2.19	2.17	2.63	2.44	2.34
600	190	2.41	2.20	2.20	2.67	2.50	2.40
800	19	2.19	2.02	1.95	2.38	2.17	2.11
800	35	2.20	2.09	2.02	2.50	2.22	2.18
800	42	2.22	2.12	2.04	2.53	2.24	2.19
800	70	2.31	2.17	2.11	2.61	2.33	2.23
800	90	2.36	2.19	2.14	2.64	2.38	2.27
800	120	2.42	2.19	2.17	2.67	2.44	2.32
800	140	2.45	2.19	2.18	2.69	2.47	2.35
800	190	2.51	2.22	2.19	2.72	2.53	2.42
1000	19	2.27	2.04	1.96	2.37	2.19	2.12
1000	35	2.39	2.11	2.03	2.66	2.24	2.18
1000	42	2.42	2.13	2.05	2.68	2.26	2.20
1000	70	2.52	2.18	2.12	2.72	2.36	2.24
1000	90	2.56	2.19	2.15	2.75	2.39	2.29
1000	120	2.60	2.19	2.17	2.76	2.47	2.34
1000	140	2.62	2.20	2.18	2.77	2.50	2.37
1000	190	2.68	2.25	2.20	2.78	2.55	2.43

TABLE D2

PROOF LOAD FACTORS, SINGLE PASS, EDGE-BIASED
STRUCTURAL GRADE NO. 4

Shear span of proof testing machine (mm)	Timber depth (mm)	Proof load factor f_p/F'_b					
		Grading failure rate = 1%			Grading failure rate = 5%		
		Length of graded timber (mm)			Length of graded timber (mm)		
		= 2000	= 4000	= 6000	= 2000	= 4000	= 6000
450	19	1.63	1.60	1.60	1.94	1.67	1.60
450	35	1.78	1.60	1.60	2.06	1.86	1.72
450	42	1.83	1.61	1.60	2.10	1.90	1.78
450	70	1.96	1.72	1.61	2.17	2.02	1.91
450	90	2.02	1.79	1.67	2.20	2.07	1.97
450	120	2.07	1.87	1.74	2.24	2.12	2.03
450	140	2.10	1.91	1.78	2.28	2.14	2.06
450	190	2.14	1.98	1.86	2.39	2.18	2.11
500	19	1.64	1.60	1.60	1.95	1.68	1.60
500	35	1.80	1.60	1.60	2.07	1.87	1.73
500	42	1.85	1.61	1.60	2.11	1.91	1.78
500	70	1.97	1.73	1.62	2.18	2.02	1.92
500	90	2.03	1.80	1.67	2.20	2.07	1.97
500	120	2.08	1.87	1.74	2.26	2.12	2.03
500	140	2.11	1.91	1.78	2.30	2.14	2.06
500	190	2.15	1.98	1.87	2.41	2.18	2.12
600	19	1.67	1.60	1.60	1.98	1.70	1.60
600	35	1.83	1.60	1.60	2.10	1.88	1.74
600	42	1.88	1.62	1.60	2.13	1.92	1.79
600	70	2.00	1.74	1.62	2.19	2.03	1.92
600	90	2.05	1.81	1.68	2.22	2.08	1.98
600	120	2.10	1.88	1.75	2.29	2.13	2.04
600	140	2.12	1.92	1.79	2.35	2.15	2.07
600	190	2.16	1.99	1.87	2.46	2.19	2.12
800	19	1.76	1.60	1.60	2.05	1.73	1.60
800	35	1.92	1.60	1.60	2.15	1.90	1.76
800	42	1.96	1.64	1.60	2.17	1.95	1.81
800	70	2.07	1.77	1.63	2.24	2.05	1.94
800	90	2.11	1.84	1.69	2.31	2.10	1.99
800	120	2.15	1.91	1.77	2.41	2.14	2.05
800	140	2.17	1.95	1.81	2.47	2.16	2.08
800	190	2.20	2.02	1.89	2.59	2.20	2.13
1000	19	1.89	1.60	1.60	2.13	1.77	1.60
1000	35	2.03	1.63	1.60	2.20	1.93	1.78
1000	42	2.06	1.67	1.60	2.23	1.97	1.83
1000	70	2.14	1.80	1.65	2.39	2.07	1.95
1000	90	2.17	1.87	1.71	2.49	2.12	2.01
1000	120	2.20	1.94	1.79	2.60	2.16	2.06
1000	140	2.22	1.97	1.83	2.66	2.18	2.09
1000	190	2.29	2.04	1.91	2.76	2.21	2.16

TABLE D3

PROOF LOAD FACTORS, SINGLE PASS, RANDOM EDGE
STRUCTURAL GRADE NO. 1

Shear span of proof testing machine (mm)	Timber depth (mm)	Proof load factor f_p/F'_b					
		Grading failure rate = 1%			Grading failure rate = 5%		
		Length of graded timber (mm)			Length of graded timber (mm)		
		= 2000	= 4000	= 6000	= 2000	= 4000	= 6000
450	19	2.11	1.99	1.93	2.24	2.15	2.09
450	35	2.18	2.07	2.00	2.35	2.20	2.16
450	42	2.19	2.09	2.03	2.38	2.21	2.18
450	70	2.19	2.15	2.09	2.48	2.29	2.21
450	90	2.22	2.17	2.12	2.53	2.34	2.25
450	120	2.27	2.20	2.15	2.58	2.40	2.30
450	140	2.30	2.19	2.17	2.60	2.43	2.33
450	190	2.36	2.20	2.20	2.64	2.49	2.39
500	19	2.12	1.99	1.93	2.25	2.15	2.10
500	35	2.18	2.07	2.01	2.36	2.20	2.16
500	42	2.20	2.09	2.03	2.40	2.22	2.18
500	70	2.20	2.15	2.09	2.50	2.29	2.22
500	90	2.24	2.18	2.12	2.54	2.34	2.25
500	120	2.29	2.20	2.16	2.59	2.40	2.30
500	140	2.32	2.19	2.17	2.61	2.43	2.33
500	190	2.38	2.20	2.20	2.65	2.49	2.39
600	19	2.14	2.00	1.94	2.28	2.16	2.10
600	35	2.20	2.08	2.01	2.40	2.20	2.17
600	42	2.19	2.10	2.03	2.44	2.22	2.19
600	70	2.23	2.16	2.10	2.53	2.31	2.22
600	90	2.27	2.18	2.13	2.57	2.36	2.26
600	120	2.32	2.19	2.16	2.61	2.41	2.31
600	140	2.35	2.19	2.17	2.63	2.44	2.34
600	190	2.41	2.20	2.20	2.67	2.50	2.40
800	19	2.19	2.02	1.95	2.38	2.17	2.11
800	35	2.20	2.09	2.02	2.50	2.22	2.18
800	42	2.22	2.12	2.04	2.53	2.24	2.19
800	70	2.31	2.17	2.11	2.61	2.33	2.23
800	90	2.36	2.19	2.14	2.64	2.38	2.27
800	120	2.42	2.19	2.17	2.67	2.44	2.32
800	140	2.45	2.19	2.18	2.69	2.47	2.35
800	190	2.51	2.22	2.19	2.72	2.53	2.42
1000	19	2.27	2.04	1.96	2.57	2.19	2.12
1000	35	2.39	2.11	2.03	2.66	2.24	2.18
1000	42	2.42	2.13	2.05	2.68	2.26	2.20
1000	70	2.52	2.18	2.12	2.72	2.36	2.24
1000	90	2.56	2.19	2.15	2.74	2.41	2.28
1000	120	2.60	2.19	2.17	2.76	2.47	2.34
1000	140	2.62	2.20	2.19	2.77	2.50	2.37
1000	190	2.65	2.25	2.19	2.78	2.55	2.43

TABLE D4

PROOF LOAD FACTORS, SINGLE PASS, RANDOM EDGE
STRUCTURAL GRADE NO. 4

Shear span of proof testing machine (mm)	Timber depth (mm)	Proof load factor f_p/F'_b					
		Grading failure rate = 1%			Grading failure rate = 5%		
		Length of graded timber (mm)			Length of graded timber (mm)		
		= 2000	= 4000	= 6000	= 2000	= 4000	= 6000
450	19	1.75	1.60	1.60	2.07	1.78	1.60
450	35	1.93	1.67	1.60	2.22	1.99	1.84
450	42	1.99	1.72	1.60	2.28	2.04	1.90
450	70	2.12	1.86	1.73	2.48	2.17	2.05
450	90	2.18	1.94	1.80	2.59	2.22	2.11
450	120	2.24	2.02	1.88	2.71	2.32	2.18
450	140	2.28	2.07	1.93	2.77	2.38	2.22
450	190	2.40	2.14	2.02	2.88	2.51	2.32
500	19	1.77	1.60	1.60	2.09	1.79	1.60
500	35	1.95	1.68	1.60	2.24	1.99	1.84
500	42	2.00	1.73	1.60	2.30	2.04	1.90
500	70	2.14	1.87	1.73	2.51	2.17	2.05
500	90	2.19	1.95	1.80	2.62	2.23	2.12
500	120	2.25	2.03	1.89	2.73	2.33	2.19
500	140	2.30	2.07	1.94	2.79	2.39	2.22
500	190	2.42	2.15	2.02	2.90	2.52	2.32
600	19	1.81	1.60	1.60	2.12	1.81	1.60
600	35	1.99	1.69	1.60	2.28	2.01	1.85
600	42	2.04	1.74	1.60	2.35	2.06	1.91
600	70	2.17	1.89	1.74	2.56	2.18	2.06
600	90	2.22	1.96	1.81	2.67	2.25	2.12
600	120	2.30	2.04	1.90	2.79	2.35	2.19
600	140	2.35	2.08	1.94	2.84	2.41	2.23
600	190	2.47	2.16	2.03	2.94	2.54	2.33
800	19	1.91	1.60	1.60	2.20	1.85	1.63
800	35	2.08	1.72	1.60	2.41	2.03	1.87
800	42	2.13	1.77	1.62	2.49	2.08	1.93
800	70	2.23	1.92	1.76	2.70	2.21	2.08
800	90	2.31	1.99	1.83	2.80	2.28	2.14
800	120	2.42	2.07	1.92	2.90	2.39	2.20
800	140	2.48	2.11	1.96	2.95	2.46	2.25
800	190	2.61	2.18	2.05	3.04	2.59	2.36
1000	19	2.05	1.60	1.60	2.36	1.89	1.66
1000	35	2.19	1.75	1.60	2.62	2.07	1.89
1000	42	2.23	1.80	1.64	2.70	2.11	1.95
1000	70	2.40	1.95	1.78	2.89	2.24	2.09
1000	90	2.51	2.02	1.85	2.97	2.32	2.16
1000	120	2.63	2.10	1.94	3.08	2.44	2.22
1000	140	2.69	2.14	1.98	3.13	2.51	2.27
1000	190	2.80	2.20	2.07	3.19	2.64	2.36

TABLE D5

PROOF LOAD FACTORS, DOUBLE PASS, RANDOM EDGE
STRUCTURAL GRADE NO. 1

Shear span of proof testing machine (mm)	Timber depth (mm)	Proof load factor f_p/F'_b					
		Grading failure rate = 1%			Grading failure rate = 5%		
		Length of graded timber (mm)			Length of graded timber (mm)		
		= 2000	= 4000	= 6000	= 2000	= 4000	= 6000
450	19	1.96	1.87	1.82	2.10	2.03	1.98
450	35	2.03	1.92	1.88	2.14	2.07	2.04
450	42	2.05	1.94	1.89	2.15	2.09	2.05
450	70	2.09	2.00	1.95	2.17	2.12	2.09
450	90	2.10	2.02	1.97	2.17	2.13	2.11
450	120	2.12	2.05	2.00	2.18	2.15	2.12
450	140	2.13	2.06	2.02	2.18	2.15	2.13
450	190	2.14	2.09	2.05	2.19	2.17	2.15
500	19	1.97	1.87	1.82	2.11	2.03	1.98
500	35	2.04	1.93	1.88	2.14	2.08	2.04
500	42	2.05	1.95	1.90	2.15	2.09	2.05
500	70	2.09	2.00	1.95	2.17	2.12	2.09
500	90	2.11	2.03	1.97	2.18	2.14	2.11
500	120	2.13	2.05	2.01	2.18	2.15	2.12
500	140	2.13	2.07	2.02	2.19	2.16	2.13
500	190	2.15	2.09	2.05	2.19	2.17	2.15
600	19	1.99	1.88	1.83	2.12	2.03	1.99
600	35	2.05	1.93	1.88	2.15	2.08	2.04
600	42	2.07	1.95	1.90	2.16	2.09	2.06
600	70	2.11	2.01	1.95	2.17	2.13	2.09
600	90	2.12	2.03	1.98	2.18	2.14	2.11
600	120	2.13	2.06	2.01	2.19	2.15	2.13
600	140	2.14	2.07	2.02	2.19	2.16	2.13
600	190	2.15	2.09	2.05	2.20	2.17	2.15
800	19	2.04	1.89	1.83	2.14	2.04	1.99
800	35	2.09	1.95	1.89	2.17	2.09	2.05
800	42	2.10	1.97	1.91	2.17	2.10	2.06
800	70	2.13	2.02	1.96	2.19	2.13	2.10
800	90	2.14	2.04	1.99	2.19	2.14	2.11
800	120	2.16	2.07	2.02	2.20	2.16	2.13
800	140	2.16	2.08	2.03	2.20	2.16	2.14
800	190	2.17	2.10	2.06	2.21	2.17	2.15
1000	19	2.12	1.90	1.84	2.18	2.06	2.00
1000	35	2.15	1.96	1.90	2.19	2.10	2.05
1000	42	2.16	1.98	1.91	2.20	2.11	2.07
1000	70	2.17	2.04	1.97	2.22	2.14	2.10
1000	90	2.18	2.06	2.00	2.23	2.15	2.12
1000	120	2.18	2.08	2.03	2.24	2.17	2.13
1000	140	2.19	2.09	2.04	2.24	2.18	2.14
1000	190	2.19	2.11	2.07	2.25	2.18	2.16

TABLE D6

PROOF LOAD FACTORS, DOUBLE PASS, RANDOM EDGE
STRUCTURAL GRADE NO. 4

Shear span of proof testing machine (mm)	Timber depth (mm)	Proof load factor f_p/F'_b					
		Grading failure rate = 1%			Grading failure rate = 5%		
		Length of graded timber (mm)			Length of graded timber (mm)		
		= 2000	= 4000	= 6000	= 2000	= 4000	= 6000
450	19	1.60	1.60	1.60	1.85	1.60	1.60
450	35	1.70	1.60	1.60	1.97	1.78	1.65
450	42	1.75	1.60	1.60	2.00	1.82	1.70
450	70	1.87	1.64	1.60	2.07	1.93	1.83
450	90	1.93	1.71	1.60	2.10	1.97	1.88
450	120	1.98	1.78	1.66	2.13	2.02	1.94
450	140	2.01	1.82	1.70	2.14	2.04	1.97
450	190	2.05	1.89	1.78	2.16	2.08	2.02
500	19	1.60	1.60	1.60	1.86	1.61	1.60
500	35	1.72	1.60	1.60	1.98	1.79	1.65
500	42	1.77	1.60	1.60	2.01	1.83	1.71
500	70	1.89	1.65	1.60	2.08	1.93	1.84
500	90	1.94	1.71	1.60	2.11	1.98	1.89
500	120	1.99	1.79	1.66	2.13	2.02	1.94
500	140	2.02	1.83	1.70	2.14	2.05	1.97
500	190	2.06	1.90	1.78	2.16	2.08	2.02
600	19	1.60	1.60	1.60	1.89	1.63	1.60
600	35	1.75	1.60	1.60	2.00	1.80	1.66
600	42	1.80	1.60	1.60	2.03	1.84	1.72
600	70	1.92	1.66	1.60	2.09	1.94	1.84
600	90	1.97	1.73	1.60	2.12	1.99	1.89
600	120	2.01	1.80	1.67	2.14	2.03	1.95
600	140	2.04	1.84	1.71	2.15	2.05	1.98
600	190	2.07	1.91	1.79	2.17	2.09	2.03
800	19	1.60	1.60	1.60	1.95	1.66	1.60
800	35	1.83	1.60	1.60	2.05	1.82	1.68
800	42	1.88	1.60	1.60	2.07	1.86	1.73
800	70	1.98	1.69	1.60	2.12	1.96	1.86
800	90	2.02	1.75	1.61	2.14	2.00	1.91
800	120	2.06	1.83	1.69	2.16	2.05	1.96
800	140	2.08	1.86	1.73	2.17	2.07	1.99
800	190	2.11	1.93	1.81	2.18	2.10	2.03
1000	19	1.61	1.60	1.60	2.03	1.70	1.60
1000	35	1.94	1.60	1.60	2.11	1.85	1.70
1000	42	1.98	1.60	1.60	2.12	1.89	1.75
1000	70	2.05	1.72	1.60	2.16	1.98	1.87
1000	90	2.08	1.78	1.63	2.17	2.02	1.92
1000	120	2.11	1.85	1.70	2.18	2.06	1.97
1000	140	2.12	1.89	1.74	2.19	2.08	2.00
1000	190	2.14	1.95	1.82	2.20	2.11	2.04

APPENDIX E. MONITORING THROUGH USE OF PROOF TESTING MACHINES

This verification procedure is intended to provide a rapid and simple check on the bending strength of graded timber.

To undertake this verification, the previously graded timber is run through the proof testing machine in a single pass, random edge mode. The proof stress f_p applied during the verification is given by

$$f_p = 2.2\ F'_b \qquad \text{(E1)}$$

where F'_b is the basic working stress in bending given in Table B1.

The expected failure rate during the proof test is given in Table E1.

The failure rate given in Table E1 is the expected value if a sample of infinite size is tested. For the cases of small sample sizes there is a possibility that the failure rate will be either larger or smaller than the average value.

In order to ensure that acceptable material is not rejected because of the sampling effect, the grading failure rate shown in Table E1 may be increased by the factor Q given in Table E2, i.e.

$$p_a = Q\ p_i \qquad \text{(E.1)}$$

where p_a is the acceptable failure rate and p_i is the expected average failure rate given in Table E1.

(Editors note. The criteria used for Table E2 is that for not more than 5% of the time will a correctly graded material be rejected by the type 'B' verification test).

TABLE E1

EXPECTED FAILURE RATE IN VERIFICATION TESTS

Shear span of proof testing machine (mm)	Timber depth (mm)	Failure rate (%)					
		Structural grade No. 1			Structural grade No. 4		
		Length of graded timber (mm)			Length of graded timber (mm)		
		= 2000	= 4000	= 6000	= 2000	= 4000	= 6000
450	19	4.63	9.31	13.14	6.29	14.37	21.93
450	35	3.01	6.04	8.53	3.64	8.32	12.70
450	42	2.64	5.31	7.50	3.09	7.07	10.79
450	70	1.84	3.70	5.22	1.96	4.48	6.83
450	90	1.54	3.10	4.37	1.56	3.58	5.45
450	120	1.26	2.53	3.57	1.21	2.76	4.22
450	140	1.13	2.27	3.20	1.05	2.41	3.67
450	190	.91	1.83	2.58	.80	1.83	2.80
500	19	4.38	9.12	12.97	5.96	14.08	21.64
500	35	2.84	5.92	8.42	3.45	8.15	12.53
500	42	2.50	5.21	7.40	2.93	6.92	10.65
500	70	1.74	3.63	5.16	1.86	4.39	6.74
500	90	1.46	3.04	4.32	1.48	3.50	5.38
500	120	1.19	2.48	3.52	1.15	2.71	4.16
500	140	1.07	2.22	3.16	1.00	2.36	3.63
500	190	.86	1.79	2.55	.76	1.80	2.76
600	19	3.85	8.74	12.65	5.30	13.48	21.08
600	35	2.50	5.67	8.21	3.07	7.81	12.21
600	42	2.20	4.99	7.22	2.61	6.63	10.37
600	70	1.53	3.48	5.03	1.65	4.20	6.57
600	90	1.28	2.91	4.21	1.32	3.35	5.24
600	120	1.05	2.37	3.44	1.02	2.59	4.05
600	140	.94	2.13	3.08	.89	2.26	3.53
600	190	.76	1.72	2.48	.68	1.72	2.69
800	19	2.70	7.96	11.98	3.95	12.29	19.95
800	35	1.75	5.17	7.78	2.29	7.11	11.55
800	42	1.54	4.54	6.84	1.94	6.04	9.81
800	70	1.07	3.17	4.76	1.23	3.83	6.21
800	90	.90	2.65	3.99	.98	3.06	4.96
800	120	.73	2.16	3.25	.76	2.36	3.84
800	140	.66	1.94	2.92	.66	2.06	3.34
800	190	.53	1.56	2.35	.50	1.57	2.58
1000	19	1.28	7.14	11.38	2.54	11.08	18.81
1000	35	.83	4.66	7.34	1.47	6.41	10.89
1000	42	.73	4.08	6.45	1.25	5.45	9.25
1000	70	.51	2.86	4.49	.79	3.45	5.86
1000	90	.42	2.39	3.76	.63	2.76	4.68
1000	120	.33	1.94	3.07	.49	2.13	3.62
1000	140	.31	1.74	2.75	.43	1.86	3.15
1000	190	.25	1.40	2.22	.32	1.41	2.40

TABLE E2

CORRECTION FACTOR FOR SAMPLE SIZE

Expected failure rate (%)	Correction Factor Q			
	N=100	N=200	N=500	N=1000
1	2.5	2.0	1.7	1.5
2	2.0	1.8	1.5	1.4
5	1.7	1.5	1.3	1.2
10	1.5	1.3	1.2	1.1
15	1.4	1.3	1.2	1.1
20	1.3	1.2	1.1	1.1

N = Sample size of proof graded material.

Editors Note. This table provides a 95% confidence that an adequate stress grade will not be rejected.

INTERNATIONAL UNION OF FOREST RESEARCH ORGANISATIONS

GROUP S 5.02 - TIMBER ENGINEERING

CREEP AND LOAD DURATION OF TRUSS-PLATE JOINTS IN TENSION

by

L C Palka

LJUBLJIANA
JOUGOSLAVIA
SEPTEMBER 1986

International Union of Forest Research Organizations
1986 Timber Engineering Meeting

CREEP AND LOAD DURATION OF TRUSS-PLATE JOINTS IN TENSION

BY

L.C. Palka

Forintek Canada Corp.

Abstract

The ultimate goal of this exploratory project is to develop an understanding of, and reliable design emthods for, both the short-term and long-term behavior of truss-plate joints in tension. To achieve these goals, development of both analytical models and experimental data is needed.

Utilizing new test data collected last year, this report provides improved estimates of creep and creep-rupture parameters from models proposed earlier, examines some relationships between static, creep and creep-rupture behavior of truss-plate joints in tension, and indicates practical consequences of the new information.

1.0 INTRODUCTION

The ultimate goals of this exploratory project were to develop a basic understanding of, and design parameters for, both the short-term and long-term behavior of truss-plate joints in tension.

The specific objectives addressed here were the examination of certain relationships between static, creep, and creep-rupture tests and model parameters; and the prediction of creep, failure time and load duration factors under constant tensile loads and ambient laboratory conditions.

In the past, engineers attempted to break complex problems into simple components, for ease of understanding and analyses. Consequently, the static, creep and creep-rupture (time-to-failure) properties of materials or systems were evaluated from completely independent tests by conventional and unrelated analytical models. In contrast, current load duration studies of truss-plate joints require the evaluation of static, creep and creep-rupture behavior of matched material samples. The resulting data base is suitable for an accurate assessment of relationships between various material properties or parameters in addition to supporting the development of conventional engineering analyses based on unrelated functions for different properties.

2.0 EXPERIMENTAL METHODS

The experimental plan for both short-term and long-term tests is outlined in Table 1. Specimen and linkage plate dimensions for each sample truss-plate joint consisting of 2 x 4 x 24-inch (38 x 89 x 610-mm) 1650f-1.5E machine stress rated dry spruce lumber, and 3x5-inch (76 x 127-mm) TTS-TL 80-tooth truss-plate are depicted in Figure 1. The test methods and the computer-controlled data acquisition systems are described elsewhere (Palka, 1983; Palka and Rovner, 1985), thus, will not be discussed here.

Statistical analyses were performed by algorithms available from the SAS-system (SAS Institute, 1982), including non-linear curve fitting and computer plotting routines. The damage accumulation model (Foschi and Barrett, 1982) was fitted to the data by algorithms developed earlier (Foschi and Karacabeyli, 1985) in the Western Laboratory of Forintek Canada Corp.

3.0 RESULTS AND DISCUSSION

3.1 Short-Term Behavior

An earlier report (Palka, 1985) concentrated on the understanding, description and prediction of short-term behavior of truss-plate joints in tension. The average measured load/slip curve and two alternate model predictions are shown in Figure 2. Relations between the cumulative distribution of static truss-plate tooth load and the nominal constant creep-load levels (ϕ: 0.60 and 0.85) are illustrated in Figure 3. The proposed static model allowed accurate prediction of the non-linear load/slip behavior of truss-plate joints in terms of basic wood, tooth and metal-plate properties and geometry. This model will not be reviewed here.

3.2 Long-Term Behavior

Updated long-term experimental data have been summarized separately (Palka, 1986). Measured and predicted values of creep under a constant tensile load ($\phi = 0.85$) and ambient laboratory conditions are depicted in Figure 4, for a single test specimen. The cumulative distribution of measured failure times during the first 18 months of the experiment is depicted in Figure 5, for the three matched groups subjected to various nominal load levels (ϕ: 0.60, 0.85 and 1.00). As discussed later in the text, failure times may be estimated for surviving specimens, resulting in the estimated cumulative distribution of failure times illustrated in Figure 6.

The long-term variables initially measured or estimated in this exploratory study are defined in Table 2, and summarized in Table 3, by nominal load level and failure status. Note that 22 creep and 18 creep-rupture specimens were culled or not tested. As shown in Figure 5 and Table 3, only 7/128 or 5.5% of the creep and 63/132 or 47.7% of the creep-rupture specimens failed through truss-plate joints during the first 18 months of testing.

3.2.1. Truss-plate joint creep

Earlier research indicated that creep S(t) or creep-rupture S(t=FT) slip or strain of most materials can be adequately described by a combination of conventional linear viscoelastic model subjected to non-linear load effects (Marin, 1962). Since displacement is measured over a 1-in (25-mm) length, tensile slip and strain of the joint are numerically identical in the imperial system of units. This approach yields a creep slip or strain predicting equation of the form

$$S(t) = [B_o + B_1 (1 - e^{-B2t}) + B_3 t] (P/Po)^n \qquad (1)$$

A commercial computer program (SAS Institute, 1982) was used to estimate the six parameters for each truss-plate joint specimen, from automatically recorded slip/time data at nominal load levels (PR=P/Po = ϕ) of 0.60 and 0.85. The goodness of fit between observed and predicted slip can be readily judged from inspection of creep or creep-rupture computer graphs, as illustrated in Figure 4. A summary of creep (surviving specimens) and creep-rupture (failed specimens) parameters is given in Table 3, together with the last measured (LS) and predicted (FS) slip and the last measured (LT) and predicted (FT) failure times. Slip is measured in thousandths of an inch and time in hours. Most creep model parameters are highly sensitive to changes in load duration, load level, and failure status or damage accumulation. Their variability from one specimen to another is also high. Therefore, most of these parameters are not likely to represent truly independent truss-plate joint properties. Indeed, each creep parameter should be considered as an interaction term, representing the combined effect of several basic wood and metal or geometric variables.

3.2.2. Creep parameters and failure time

As suggested earlier (Marin, 1962), some of the proposed creep parameters can be used to estimate both failure time FT and failure slip S(FT)=FS from

$$FT \simeq \frac{1}{n \cdot B_3 \cdot (P/Po)} \qquad \text{and} \qquad (2)$$

$$FS \simeq [B_o + B_1(1 - e^{-B_2 FT}) + B_3 . FT] \, (P/Po) \qquad (3)$$

The predicted theoretical relationships between load ratios (PR=P/Po = ϕ) and failure times (FT) for joints with a given viscous parameters (B_3 = 0.0036/hr) and three values of load effect exponent (n = 10, 25 and 50) are illustrated in Figure 7. These trends are qualitatively similar to the conventional "Madison Curve" (Wood, 1951) originally developed for small clear wood specimens in bending. As illustrated in Figures 8 and 9, truss-plate joint behavior in tension under ambient laboratory conditions, deviates substantially from theoretical predictions (equation 2). The differences between the two interpretations of the same failure time data are discussed in detail elsewhere (Palka, 1986b).

Data from the 70 failed specimens allowed estimation of a correction factor to improve the accuracy of failure time prediction from

$$MT = \beta . FT \qquad (4)$$

where $[\log \beta(FT)] = -13.100 + 3.9116 \, [\log FT]$ for $\log FT \leq 3.5$ (5)

and $[\log \beta(FT)] = 0.0$ for $\log FT > 3.5$ (6)

Thus, the viscoelastic theory appears to be valid for load durations exceeding about 3,000 hours and/or constant loads that induce load ratios below 80 percent (PR = P/Po = $\phi \leq 0.80$), as illustrated in Figure 10. The relationships between load ratios and adjusted failure time estimates based on the proposed viscoelastic creep model parameters (equation 4) are depicted in Figure 11. Inspection of Table 3 reveals that predicted failure times (FT=3,163 hours) tend to exceed observed failure times (FS=2,495 hours) by about 27% on the average, for the 63 specimens that failure under an effective relative load of PR=0.71.

3.2.3 Damage accumulation and failure time

Prediction of truss-plate joint failure time is also possible from a damage (α) accumulation model, developed initially to characterize lumber behavior (Foschi and Barrett, 1982):

$$\frac{d\alpha}{dt} = a \, e^{W_1 R_n} \left[\frac{\tau(t)}{\tau_s} - \zeta_o \right]^b + \lambda e^{W_2 V_n} \alpha \qquad (7)$$

for any specimen with an arbitrary load history $\tau(t)$ and static strength τ_s; where a, b, λ, w_1, w_2 and σ_o are model paramters to be found by calibration to short-term and long-term test data, while R_n and V_n are standard random normal variables.

Inspection of Figures 12, 13 and 14, which compare cumulative distributions of observed (measured) and predicted (simulated) failure times from the damage accumulation model, raised several unexpected questions. The major puzzle was: Why did failure times predicted from either the viscoelastic model parameters (see Table 3) or the damage accumulation model (see Figure 13) agree with measured failure times and with each other only at a fictitious load ratio of $\phi = 0.73$ instead of the initially introduced $\phi = 0.85$? This question will be examined next.

3.2.4 Joint strength increase with time

Past observations indicated (Arbek, 1979) that as the length of elapsed time between truss-plate joint preparation and static testing of the joint increases, so does the static joint strength. This may be predicted from

$$P_t = P_i + 1.51 \ln t \qquad (8)$$

where load (P_t, P_i) is in pounds and time (t) is in hours. If this trend would be true for truss-plate joints subjected to long-term loads, there would be a gradual reduction in the nominal load ratio over time, as indicated in Table 4. Predictions from the proposed viscoelastic model show a similar trend in terms of nominal load ratios with time, although there is an anomalous increase in the low load ratio.

In this context, the reduction indicated in Table 4 for the high nominal load ratio, and the possibly small or no change indicated for the low nominal load ratio by the damage accumulation model tends to verify a physical trend. The assumption that only the location parameter of the Weibull cumulative load distribution changes with time yields a constant increase in truss-plate load, similar in magnitude to the empirical time effect on static strength.

Evidently, the unidentified physical process responsible for the increase in truss-plate joint strength with the lengthening of elapsed time between joint preparation and static testing is in effect, with little change, during long-term testing also. This unusualy feature of the long-term behavior of truss-plate joints in tension has not been noticed before. Introduction of this concept would adequately answer the questions raised in the previous section. It would also provide an unexpected increase in the safety of truss-plate joints during their service life, at least under fairly constant environmental conditions.

3.2.5 Load ratios and failure times

Relationships between load ratios and failure times may be established either from viscoelastic creep parameters (equation 4 in Figure 11) or from a damage accumulation model (equation 7 in Figure 15), for truss-plate joints in tension. Inspection of Figure 16 indicates that, within the range of

available experimental data, the two alternate models predict nearly identical trends, for typical values of viscoelastic parameters, i.e. n = 15 and $0.005 \geq B_3 \geq 0.0005$. The two models, however, yield different long-term predictions beyond the range of available experimental data. The viscoelastic model assumes a slower rate of damage accumulation and does not indicate the presence of a threshold load level. Without any supporting experimental data, the true nature of extremely long-term behavior of truss-plate joints in tension has to remain an unresolved phylosophical question.

Current load duration factors in Canadian joint design codes (CSA, 1984) are listed in Table 5. These were derived for design loads assumed to remain constant during the service life of the structure or joint. Such load duration factors can be readily estimated from the load ratio versus failure time graphs developed here (see Figures 11 and 15 or 16). These factors are also listed in Table 5, for load durations commonly specified in engineering practice. Inspection of Figure 17 allows a graphical comparison of conventional load duration factors and those suggested by the two alternate models examined here, for truss-plate joints subjected to constant tensile loads under fairly constant and dry environmental conditions. Apparently, the viscoelastic model predicts more conservative load duration factors than the damage accumulation model; but the conventional (currently used) load duration factors are the most conservative for load durations of one day to ten years. On the other hand, for very short and very long load durations, the current load duration factors seem to be less conservative than the newly suggested values. No experimental data is available concerning the effect of changing environmental and load conditions upon the load duration factors of truss-plate joints in tension.

Current code rules (CSA, 1984) define allowable truss-plate joint design loads P_D as:

$$P_D = P_M/R \qquad (9)$$

where P_M represents the average static failure strength for a sample of truss-plate joints (in tension) and R is a reduction factor. Allowable design loads are assumed to act continuously on the structure for 10 years, while static tests usually last for about 6 minutes. Consequently, allowable design loads may also be estimated from the relation between load ratios and failure times (see Figure 16) by defining the reduction factor R as

$$R = P(6 \text{ minutes})/P(10 \text{ years}) \qquad (10)$$

This allows the comparison of reduction factor currently in use (R_c) with those obtained from the damage accumulation model (R_d) and from the viscoelastic model parameters (R_v):

R_c = code defined = 3.00
R_d = 1.00/0.55 = 1.82
R_v = 0.95/0.66 = 1.44

The new reduction factors would represent a 3.00/1.82 = 1.65 - fold and 3.00/1.44 = 2.08 - fold increase in allowable design loads, compared to currently accepted values. These potential gains are substantial, but would only apply to truss-plate joints under constant tensile loads and fairly constant and dry environmental conditions. The effects of cyclic loading and changing environmental conditions cannot be assessed from the experimental data provided here.

4.0 CONCLUSIONS AND RECOMMENDATIONS

4.1 Conclusions

The creep behavior of truss-plate joints in tension is accurately described by a conventional four-parameter linear viscoelastic spring and dash-pot model, subject to non-linear load effects (Equation 1).

The proposed viscoelastic model parameters seem to depend on load level, failure status and load duration; and are highly inter-correlated. Consequently, these parameters are not simple joint properties, but represent a complex interaction of several basic wood, metal and geometric variables.

Failure times under a constant tensile load can be fairly accurately predicted either from selected parameters of a viscoelastic model (Equation 4) or from a properly calibrated damage accumulation model (Equation 7).

The relationships between load ratios and failure times can also be fairly accurately predicted by either of the above models (Figure 16). Both of these models also suggest that the allowable design strength of truss-plate joints could substantially increase under fairly uniformly warm and dry environmental conditions and constant tensile loads (Equation 10).

The mechanisms responsible for increasing truss-plate joint tensile strength with the lengthening of elapsed time between joint preparation and static testing (Equation 8) seems to remain in effect during long-term testing of truss-plate joints also. This results in a gradual reduction of the nominal load ratio, hence increased service life, under constant tensile loading.

4.3 Recommendations

Continue collection of creep and creep-rupture data for truss-plate joints in tension under ambient laboratory conditions.

Explore the effects of cyclic loading and changing environmental conditions upon the static (residual), creep and creep-rupture properties of truss-plate joints in tension.

Explore relationships between static, creep and creep-rupture properties and parameters of truss-plate joints in more detail.

5.0 REFERENCES

Arbek, T. 1979. The Effect of Time on the Strength of Truss-Plate Joints. Thesis, Department of Civil Engineering, Carleton University, Ottawa, Ontario. 40p.

Canadian Standards Association. 1984. CAN3-086.1-M84: Engineering Design in Wood (Limit States Design). CSA, Rexdale, Ontario. 222p.

Foschi, R.O. and J.D. Barrett. 1982. Load Duration Effect in Western Hemlock Lumber. Journal of Structural Division, ASCE, ST7, 108:1494-1510.

Foschi, R.O. and E. Karacabeyli. 1985. User's Manual to Computer Programs for Modelling and Simulating the Long-Term Behavior of Lumber. (Draft). Forintek Canada Corp., Vancouver, B.C. 75p.

Marin, J. 1962. Mechanical Behavior of Engineering Materials. Prentice-Hall Inc., Englewood Cliffs, N.J. 502p.

Palka, L.C. 1981. Effect of Load Duration Upon Timber Fasteners: A Selective Literature Review. Report to the Canadian Forestry Service. Forintek Canada Corp., Vancouver, B.C. 58p.

Palka, L.C. 1984. Effect of Load Duration Upon Timber Fasteners: I. Building a Long-Term Tension Test Frame. II. Influence of Loading Rates on Joint Slip. Report to the Canadian Forestry Service. Forintek Canada Corp., Vancouver, B.C. 40p.

Palka, L.C. 1985. Effect of Load Duration Upon Timber Fasteners: Short- and Long-Term Models. Report to the Canadian Forestry Service. Forintek Canada Corp., Vancouver, B.C. 38p.

Palka, L.C. 1986a. Effect of Load Duration Upon Timber Fasteners: Second Data Report. Report to the Canadian Forestry Service. Forintek Canada Corp., Vancouver, B.C. 46p.

Palka, L.C. 1986b. Effect of Load Duration Upon Timber Fasteners: Short- and Long-Term Models. Report to the Canadian Forestry Service. Forintek Canada Corp., Vancouver, B.C. 35p.

Palka, L.C. and B. Rovner. 1985. Effect of Load Duration Upon Timber Fasteners: First Data Report. Report to the Canadian Forestry Service. Forintek Canada Corp., Vancouver, B.C. 59p.

Statistical Analysis Systems Institute. 1982. SAS User's Guide: Statistics. SAS Inst. Inc., Cary, N.C. 588p.

Wood, L.W. 1951. Relation of Strength of Wood to Duration of Load. United States Department of Agriculture, Forest Service, Forest Products Laboratory, Madison, WI. Report No. 1916. 26p.

Table 1

Initial Truss-Plate Joint Tests

Load Duration	Load Type	Joint Type	Test Conditions	Load Levels Nominal (%)	Code	Actual (lb.)	Replicates
Short-term	Ramp, Tension			100	0	5370	150
Long-time	Constant, Tension	Single	Ambient	85	2	4600	150
Long-time	Constant, Tension			60	1	3200	150

Long-time: The smaller of five years or the time needed to fail 50% of the test specimen.

Single: Joints made with MSR SPF lumber of one grade, and 20-guage, 3 x 5 in. steel plate with 3/8 in. deep teeth.

Ambient: Ambient laboratory temperature and humidity conditions during the test period.

100%: Average load at failure under short-term ramp loading.

Lumber: 1650f-1.5E MSR spruce.

Truss-plate: TTS-LT 20-gauge.

Table 2

Definition of Variables for Long-term Tests of Truss-plate Joints in Tension

S = [B0+B1*(1.0-EXP(-B2*T))+B3*]*[PR**PN]

FT = 1.0/[B3*PN*(PR**PN]

FS = [B0+B1*(1.0-EXP(-B2*FT.))+B3*FT]*[PR**PN]

S = TRUSS-PLATE JOINT SLIP IN 1/1000 INCH

T = LOAD DURATION IN HOURS

FT = ESTIMATED FAILURE TIME IN HOURS (Figure 2)

FS = SLIP IN 1/000 INCH CORRESPONDING TO FT (Figure 2)

B0 = INSTANTANEOUS ELASTIC COMPONENT

B1 = INSTANTANEOUS VISCOELASTIC COMPONENT

B2 = TIME-DEPENDENT VISCOELASTIC COMPONENT

B3 = LINEAR VISCOUS FLOW COMPONENT

PR = LOAD RATIO OR LOAD LEVEL (P/P_o)

PN = EXPONENT OF LOAD RATIO

RES = SUM OF SQUARED DIFFERENCES BETWEEN PREDICTED AND MEASURED SLIP VALUES

LS = LAST MEASURED SLIP VALUE IN 1/1000 INCH (Figure 1)

LT = LOAD DURATION IN HOURS TO LAST MEASURED SLIP (Figure 1)

C1=1 NOMINAL 60% LOAD LEVEL (LOW LOAD)

C1=2 NOMINAL 85% LOAD LEVEL (HIGH LOAD)

D1=0 ACTIVE SPECIMEN

D1=1 JOINT FAILED

D1=2 WOOD FAILED (CULLED)

N = NUMBER OF SPECIMENS TESTED

C.V. = COEFFICIENT OF VARIATION

Table 3

Summary of Creep Parameters by Load Levels and Failures

Variable	N	Minimum Value	Maximum Value	Mean	Std. Error of Mean	Standard Deviation	C.V.	Skewness	Kurtosis
High Active C1=2 D1 = 0									
B0	69	1.00000	20.00000	14.21739	1.08018	8.80853	61.942	-0.86944	-1.28211
B1	69	10000.00000	20000.00000	13052.27881	444.60192	3693.14094	28.295	0.82759	-0.84230
B2	69	1.50000	25.00000	4.47658	0.49382	4.10199	91.632	2.4103	8.81672
B3	69	0.50000	2.35953	0.75584	0.04588	0.38109	50.433	2.58284	7.23175
PR	69	0.67400	0.71900	0.70078	0.00106	0.00884	1.261	-0.81204	1.27359
PN	69	13.37500	16.80100	14.95651	0.06373	0.52941	3.540	0.64549	1.36268
RES	69	317.00000	95115.00000	10235.18841	1986.32515	16499.65592	161.205	3.20210	11.65981
LS	69	51.00000	199.00000	109.15942	4.04928	33.63586	30.814	0.77599	0.81543
LT	69	8659.30000	14682.50000	13197.99420	154.55803	1283.85543	9.728	-1.13361	1.05282
FS	69	74.70000	191.60000	131.94203	2.65883	22.08929	16.727	0.12226	0.98967
FT	69	8251.60000	38032.10000	21064.98261	881.10858	7319.02092	34.745	0.35704	-0.66260
High Failed C1=2 D1 = 1									
B0	63	1.00000	20.00000	13.96825	1.12322	8.91532	63.826	-0.80355	-1.39979
B1	63	10000.00000	20000.00000	11357.42463	371.38931	2947.65255	25.954	2.13132	3.26151
B2	63	1.50000	21.45800	5.20821	0.54195	4.30157	82.576	1.88854	4.17040
B3	63	0.50000	7.50000	5.84802	0.30199	2.39699	42.439	-0.89901	-0.69552
PR	63	0.67000	0.74300	0.71186	0.00149	0.01182	1.661	-0.79769	2.65167
PN	63	12.51300	16.80200	14.29390	0.08852	0.70260	4.915	0.87709	2.75810
RES	63	71.00000	156087.00000	10610.52381	3261.38748	25886.30173	243.966	4.41541	20.19397
LS	63	40.00000	266.00000	144.61905	5.30872	42.13666	29.136	0.07198	0.50606
LT	63	0.90000	12941.40000	2494.81746	470.03646	3730.61460	149.537	1.78936	1.81578
FS	63	71.60000	562.20000	165.17937	7.53380	59.79771	36.202	4.77198	31.73882
FT	63	441.90000	25862.10000	3182.66508	580.57575	4608.17716	145.708	3.85568	14.96850

Table 4. Estimated Changes in the Relative Load Level of Truss-Plate Joints in Tension with Time

Predicting Model Used	Nominal (Aug. 1, 1982) RELATIVE LOAD LEVEL	Specimen loading (Apr. 15, 1984)	First Analysis (Sep. 15, 1984)	Second Analysis (Dec. 15, 1985)
Weibull distribution	0.85	-	0.74	0.74
Static strength (Arbeck, 1979)	0.85	0.81	0.78	0.75
Damage accumulation (Foschi & Barrett, 1982)	0.85	-	-	0.73*
Non-linear viscoelastic (Palka, 1985)	0.85	-	0.75*	0.71*
Weibull distribution	0.60	-	0.53	0.53
Static strength (Arbek, 1979)	0.60	0.58	0.54	0.53
Damage accumulation (Foschi & Barrett, 1982)	0.60	-	-	?
Non-linear viscoelastic (Palka, 1985)	0.60	-	0.69*	0.68*

* Load levels providing the best fit of the model to the experimental creep data (Palka, 1985) or failue times (Foschi and Barrett, 1982).

? Insufficient data.

Table 5

Tentative Load Duration Factors for a Specific Truss-Plate Joint in Axial Tension

Load Duration Definitions	Code Load Duration Factors	Experimental Estimates*	
		Palka	Foschi
Continuous (50 years)	0.90	0.86	0.62
Normal (10 years)	1.00	1.00	1.00
Two Month (0.167 year)	1.15	1.17	1.33
Seven Day (168 hours)	1.25	1.25	1.38
One Day (24 hours)	1.33	1.27	1.45
Static (66 minutes)	–	1.36	1.67
Instantaneous (V1000 sec)	2.00	1.60	2.00

* Based on 70 joint failures within the first eighteen months of creep-rupture testing.

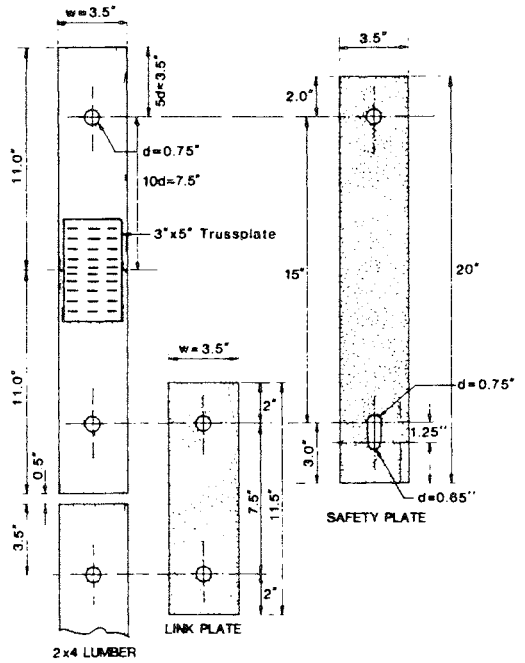


Figure 1. Specimen and linkage dimensions for testing truss-plate joints in tension.

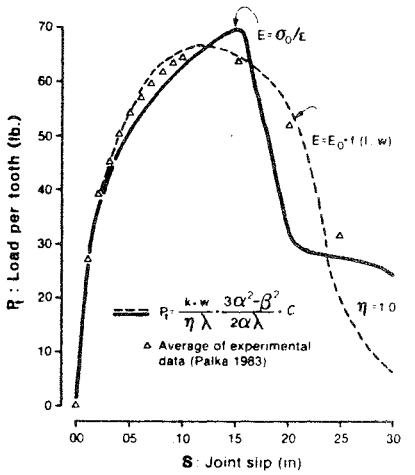


Figure 2. Measured and predicted behavior of a specific truss-plate tooth when the joint is subjected to static tension parallel to the grain.

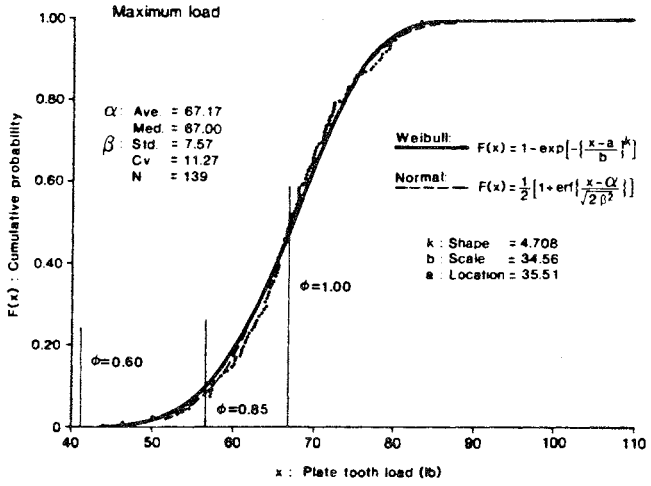


Figure 3. Cumulative distribution of maximum tooth load in 80-tooth truss-plate joints in spruce lumber.

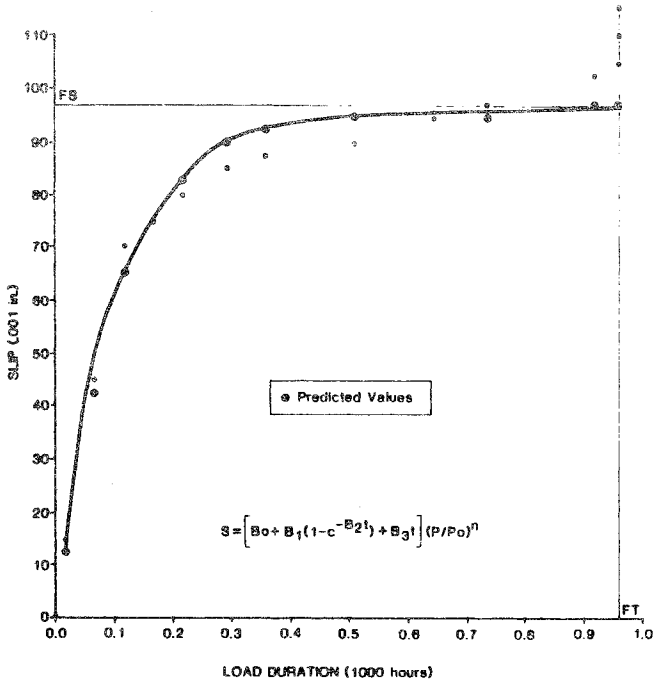


Figure 4. Measured and predicted values of creep of truss-plate joint specimens in tension under a constant load at 85% of the static strength.

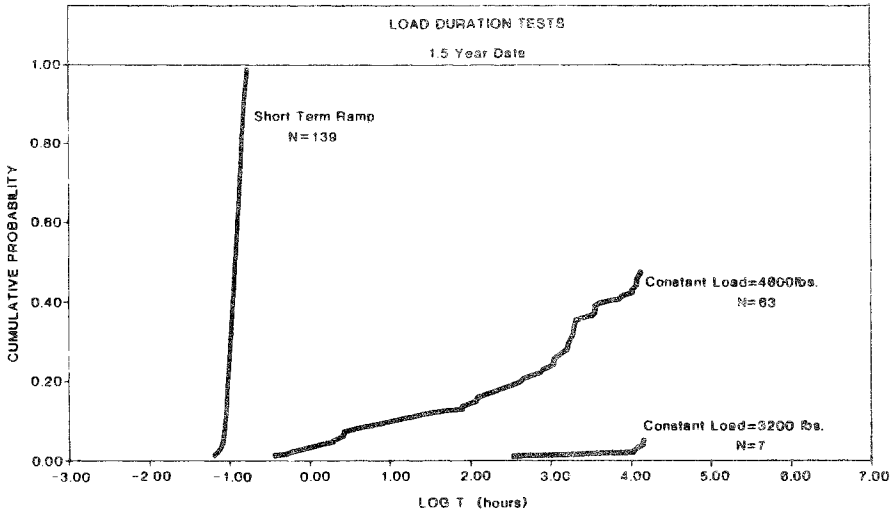


Figure 5. Cumulative distribution of measured failure times.

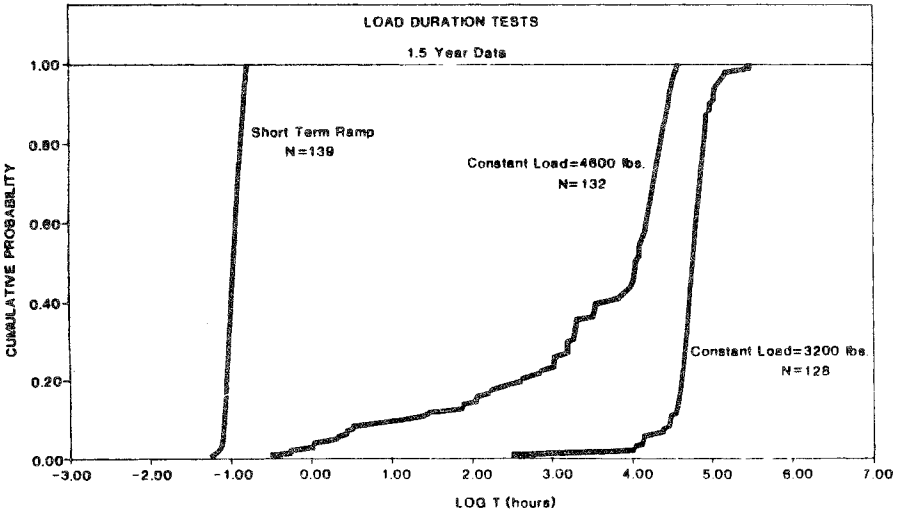


Figure 6. Cumulative distribution of measured and predicted failure times.

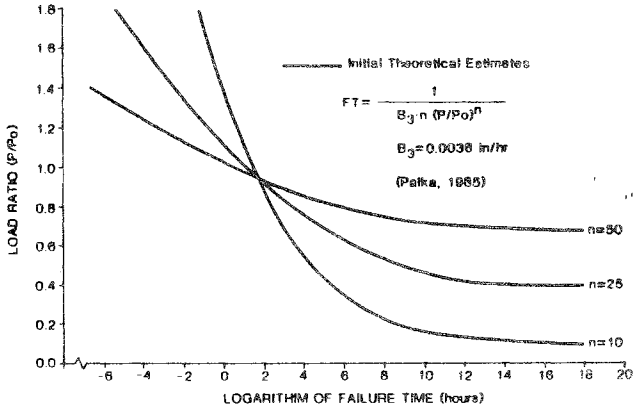


Figure 7. Initial theoretical prediction of relations between load ratio, failure time and two viscoelastic model parameters.

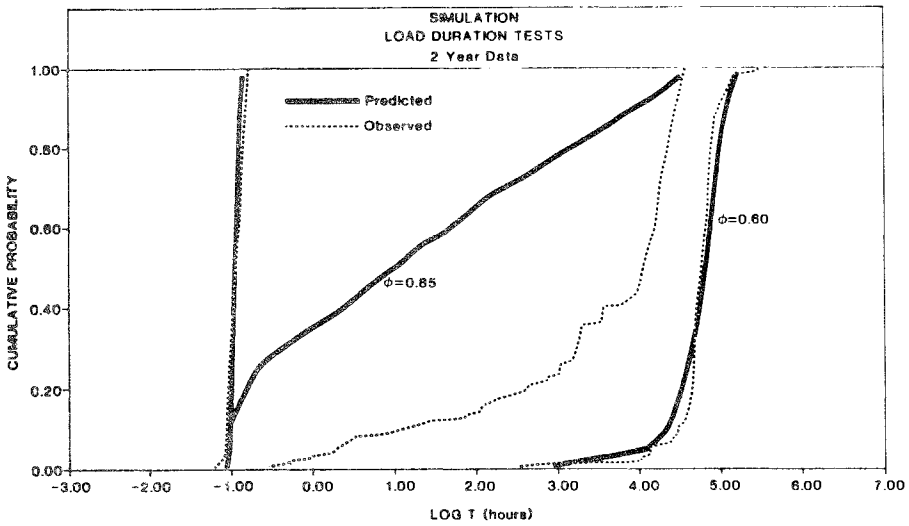


Figure 12. Predicted and observed cumulative probability of failure times at nominal and actual load ratios (ϕ).

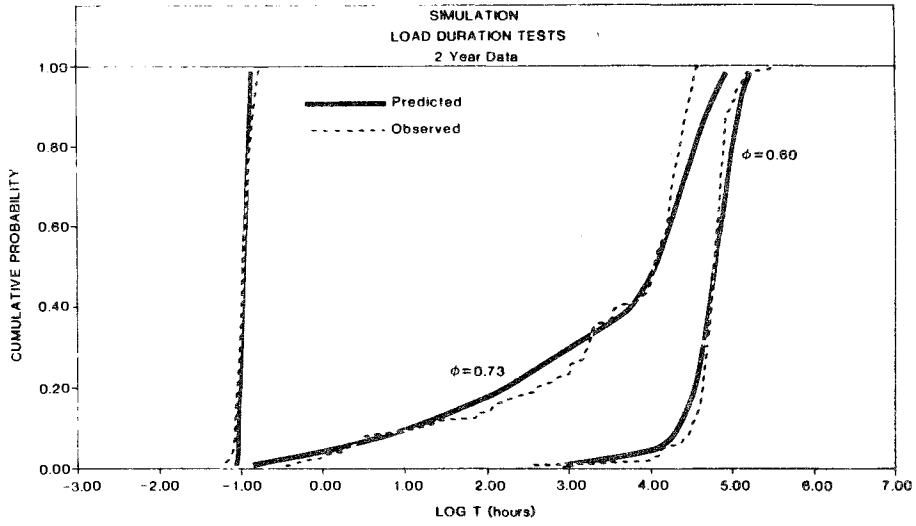


Figure 13. Predicted and observed cumulative probability of failure times at estimated nominal and actual load ratios (ϕ).

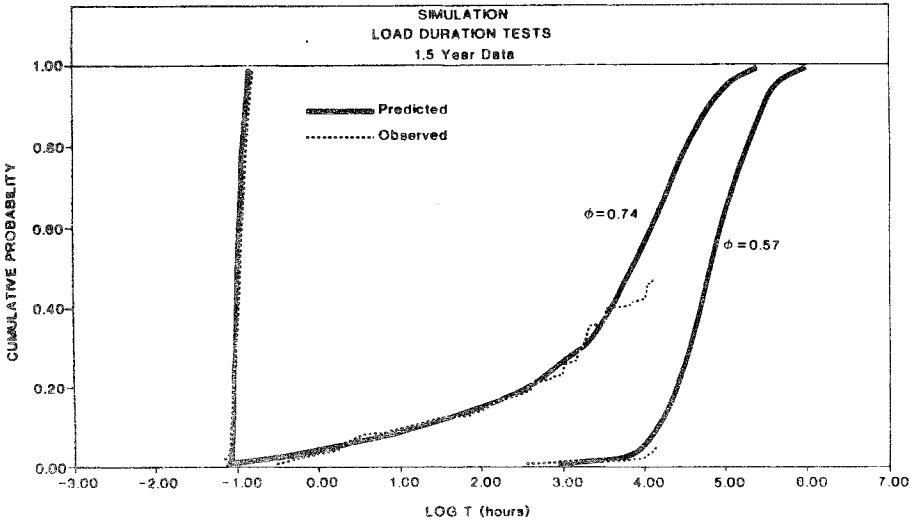


Figure 14. Predicted and observed cumulative probability of failure times.

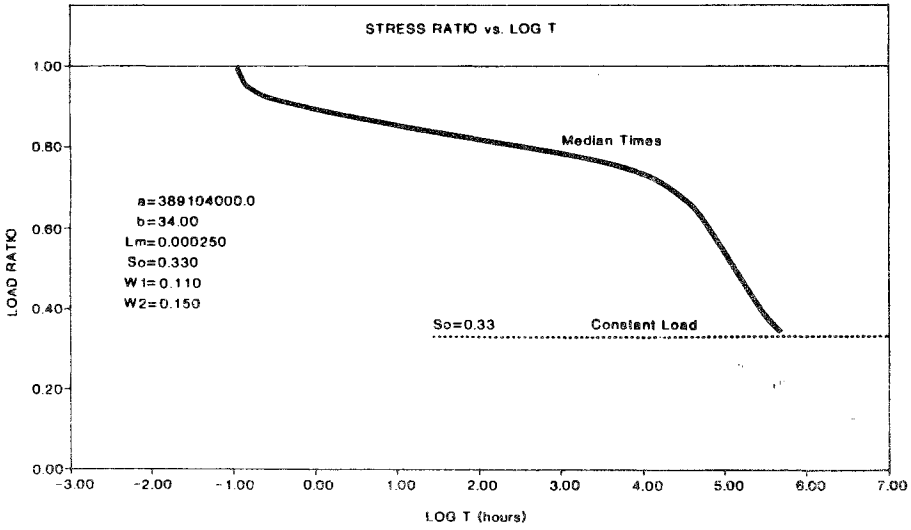


Figure 15. Relationships between load ratios and adjusted failure times based on a Damage-accumulation model (Foschi and Barrett, 1982).

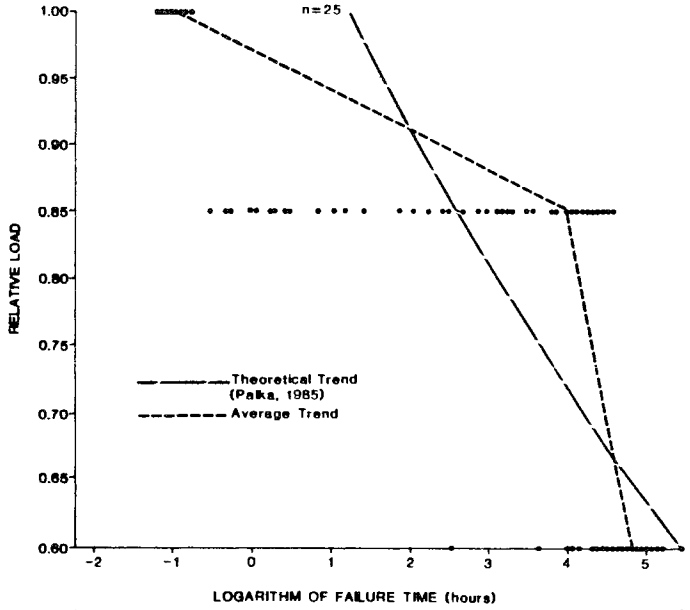


Figure 8. Load/time relationship of truss-plate joints in tension for three load conditions (Nominal).

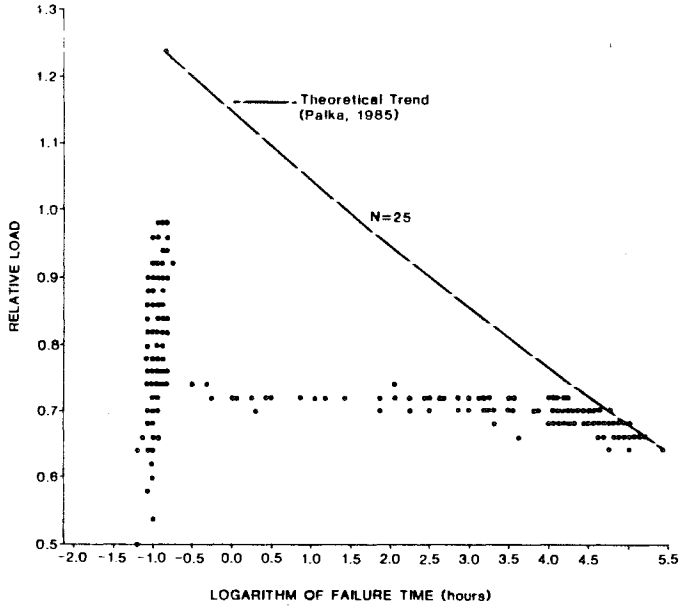


Figure 9. Load/time relationship of truss-plate joints in tension for three load conditions (Actual).

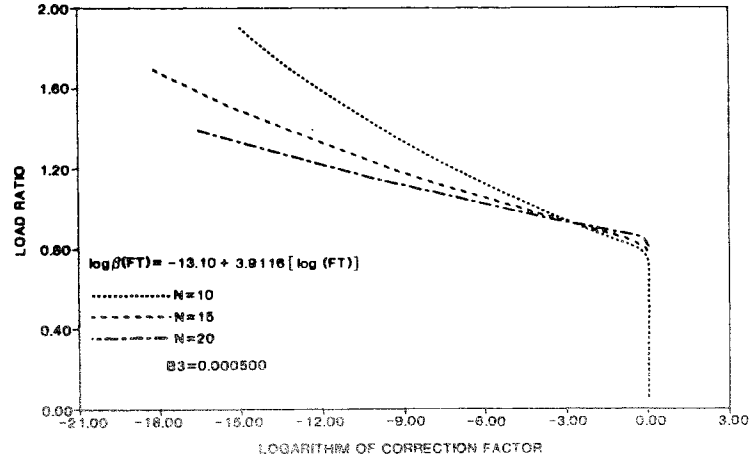


Figure 10. Relationship between load ratios and the logarithms of time-correction factors.

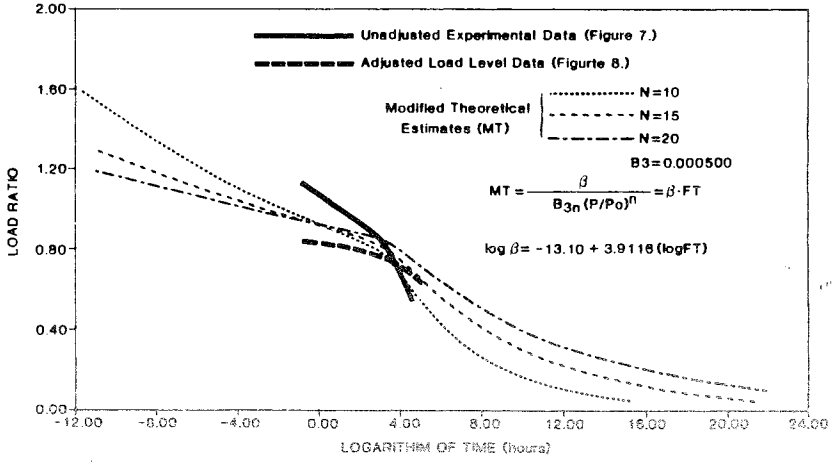


Figure 11. Relationships between load ratios and adjusted failure times based on a visco-elastic creep model (Palka, 1986).

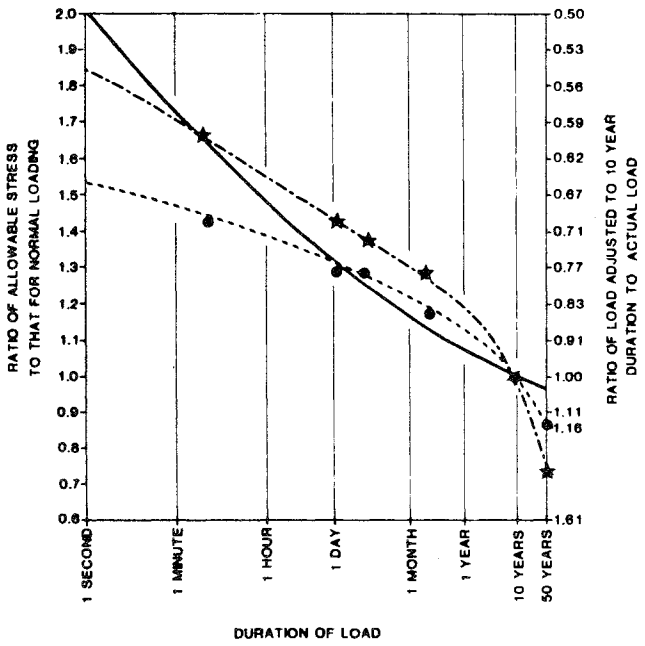


Figure 17. Proposed relation of truss-plate strength in tension under constant load to duration of load.

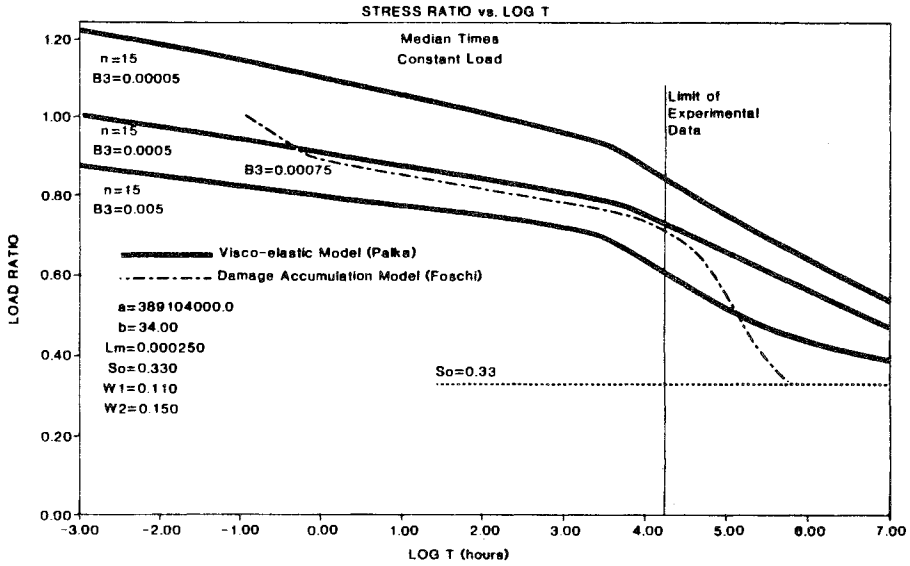


Figure 16. Comparison of predictions from a visco-elastic creep model (Palka) and from a damage accumulation model (Foschi).

INTERNATIONAL UNION OF FOREST RESEARCH ORGANISATIONS

GROUP S 5.02 - TIMBER ENGINEERING

DYNAMIC BEHAVIOR OF LUMBER IN STRESS-GRADING MACHINES

by

M Samson

LJUBLJIANA
JOUGOSLAVIA
SEPTEMBER 1986

DYNAMIC BEHAVIOR OF LUMBER IN STRESS-GRADING MACHINES

Paper presented at the
18th IUFRO World Congress
Ljubljana, Yougoslavia
September, 1986

by

Marcel Samson
Assistant Professor
Wood Science Dept.
Faculty of Forestry
Laval University
Quebec, Canada
G1K 7P4

ABSTRACT

A computer simulation model is developed for studying the dynamic behavior of uniform lumber in stress-grading machines of the constant-deflection type. Simulations carried out with the model showed that speed had no significant effect on the average modulus of elacticity measured along the lumber but largely affected modulus of elasticity values measured at individual locations. Tests conducted at 15, 150 and 315 m./min. with two machines employing different support conditions confirmed model predictions.

INTRODUCTION

Most stress-grading machines in commercial operation determine modulus of elasticity (E) of lumber from a load-deformation relationship measured in bending. Essentially, these machines differ from the laboratory bending machines in the method of loading. In a standard static test, the load or deformation is applied gradually through loading head motion on the specimen at rest, whereas in a grading machine, a predetermined load or deflection is applied to the specimen in longitudinal motion. Both methods should allow accurate measurement of E provided that the effect of speed of testing is negligible.

The operating speed of commercial grading machines has markedly been increased since their introduction in the early sixties. This

situation has raised some concerns among producers as well as users of machine stress-rated lumber about the possible effect of speed on grading machine accuracy. The present study examines the dynanic behavior of lumber in stress-grading machines as an attempt to address these concerns.

BACKGROUND

The likelihood of an effect of speed on grading machine accuracy was first indicated by Hoyle (1961). Shortly later, Pelster (1963) provided evidence of a speed of testing effect when he observed that E values measured on lumber in longitudinal motion were higher than those measured under static conditions. Reviewing the literature on the topic, Hoyle (1968) concluded that a 5 percent overestimation was to be expected, at 300 m./min., on the average E measured along a piece of lumber. His conclusion, however, has not been clearly substantiated in the more recent literature. While average E data reported by Pellerin (1976) show a 5 percent overestimation, no speed of testing effect was observed by Logan (1978).

In their analyses of the effect of speed, researchers disregarded the fact that transverse vibrations may arise in the lumber as a result of its longitudinal motion. Theoretical analysis of a moving beam reveals that natural frequencies, stability and stiffness of the beam decrease with increasing speed (Mote, 1968).

Therefore, from the vibration standpoint, increasing speed in a grading machine should lead to underestimating E, a result opposed to observations reported in the literature.

The objective of the present study was to develop a computer simulation model that could be used to predict the dynamic behavior of uniform lumber in any stress-grading machines of the constant-deflection type. A series of experiments were conducted to verify the model and to examine the effect of speed on grading machine accuracy.

MODEL DEVELOPMENT

Figure 1 illustrates the basic components of a bending-type grading machine which applies a constant nominal deflection Δ on the lumber in the middle of the span L, and measures the force P necessary to maintain this deflection. The deflection roller is installed in a housing which can pivot with respect to an axis through point A, located at a distance r from the roller axis. A load cell, idealized by a spring of stiffness constant K, is mounted directly behind the deflection roller, between the housing and the machine chassis.

The lumber can be mathematically modeled as a uniform beam in motion under the influence of a time-varying force F applied at the contact point between the deflection roller and the lumber.

Transverse vibration of this beam of modulus of elasticity E, moment of inertia I and mass density m is investigated in this study.

The governing differential equation for small transverse vibrations of this beam, developed by Samson (1986b), is

$$EI \frac{\partial^4 w}{\partial x^4} + mc^2 \frac{\partial^2 w}{\partial x^2} + 2mc \frac{\partial^2 w}{\partial x \partial t} + m \frac{\partial^2 w}{\partial t^2} - p = 0 \qquad [1]$$

where w(x,t) is the transverse displacement, p(x,t) is a distributed transverse force acting in the direction of positive z axis and c is the axial velocity of the beam . In the present application, p vanishes everywhere between the supports except at x = L/2 where is applied the point load, the expression of which, obtained from rigid body equilibrium of the deflection roller, is given as

$$F(t) = K(\Delta - w(L/2, t)) - \frac{J_A}{r^2} \frac{\partial^2 w}{\partial t^2}(L/2, t) \qquad [2]$$

where J_A is the mass moment of inertia of the deflection roller assembly with respect to the axis through A. A semidiscrete approximation was chosen as a convenient procedure for solving Eq. [1] under loading conditions expressed by Eq.[2] and arbitrary boundary conditions. In the first stage of the solution, the spatial variation of w is approximated using the concept of finite elements. Essentially, the beam is divided into an assemblage of N one-dimensional beam elements whose deflected shapes are described by cubic polynomials. This procedure leads to a system of ordinary differential equations of motion in the form

$$[M]\{\ddot{r}\} + [C]\{\dot{r}\} + [K]\{r\} = \{F\} \qquad [3]$$

where [M],[C], and [K] are coefficient matrices, and {r} and {F} are the nodal displacement and load vectors for the beam, respectively. Upon substitution of the expression for the point load and imposition of boundary conditions dictated by the type of supports used in the machine, the time-dependent Eq.[3] is solved in the second stage of the solution using the Newmark direct integration method. This procedure provides the deflection and slope of the deflected shape at any nodes at time increments Δt. The solution sought is the reaction force P, calculated from loadcell deformation as

$$P(t) = K\ (\Delta - w(L/2, t)) \qquad [4]$$

In the present model, machine output is expressed in terms of a machine-measured modulus of elasticity E_{mach}, proportionnal to P, calculated as

$$E_{mach}(t) = b\ P(t) \qquad [5]$$

where b is a constant depending on the testing geometry employed by the machine.

SIMULATIONS

Simulations were conducted with the model developed to study the effect of speed on the accuracy of two machines, referred to as Machines A and B, complying in all points with the scheme illustrated in Figure 1, with the exception of support conditions in Machine B. In Machine A, the lumber rests on roller supports, as illustrated, whereas in Machine B, the support angles are fixed to an angle $\alpha = 3\ \Delta / L$, thereby preventing any rotation at supports. Details regarding machine description and operation can be found in Samson (1986a).

Simulation output is a periodic signal $E_{mach}(t)$ given as a time series. Output signals were processed to determine signal level $\bar{E}_{mach}$, i.e. the average modulus of elasticity measured by the machine along the lumber, and signal frequency f. The ratio $\bar{E}_{mach}/E$, referred to as the offset, was also calculated to permit detecting any discrepancy between machine-measured and true E of lumber.

A sensitivity analysis revealed that parameters E, I, L, m and Δ had essentially no influence on both signal offset and frequency. This provided motivation to fix the value of these parameters in the actual simulations, leaving only parameters J_A, K, r and c for investigation. Parameters J_A, K and r are related through the expression for the natural vibration frequency of the deflection roller-loadcell system

$$f_S = \sqrt{\frac{K\ r^2}{J_A}} \qquad [6]$$

During the investigation of the combined effect of J_A, K and r, it was found more appropriate to consider the parameter f_s and study the influence of f_s on model output. Results from the simulations are summarized in Table 1 and Figure 2 for signal offset and signal frequency, respectively.

Table 1 shows that signal offset is slightly influenced by speed. The relationship between offset and speed was insensitive to variations of f_s in the 10 to 1000 Hz range, for both machines. As expected from theory, grading machines will tend to underestimate E as speed increases. However, according to Table 2, this underestimation would be insignificant (less than 0.3 %) for current high speed machines running at 400 m./min.

Information provided on Figure 2 indicates that signal frequency is affected mainly by machine parameter f_s. Speed had no influence on frequency in the 0 to 2500 m./min. range. As evident from the tight clustering of the data points around the line of equality , the model predicts that the frequency of the E_{mach} signal will correspond to the natural vibration frequency of the deflection roller - loadcell system.

EXPERIMENTAL VERIFICATION

Experiments were performed with laboratory versions of Machines A and B to verify model predictions. Span and deflection settings were 910 mm. and 4.0 mm, respectively, and the f_e value was 123 Hz for both machines. Machine runs were conducted with 38- by 89-mm. by 4.88- m. long dimension lumber specimens from three species, namely White Spruce (6 specimens), Western Hemlock (5 specimens) and Douglas Fir (5 specimens). All specimens were straight, uniform and free of major strength reducing defects. Specimens were run in two passes through Machines A and B, consecutively at 15, 150 and 315 m./min. Reaction load P was measured directly from loadcell output (without filtering) at 8.25 mm. increments along the length of the specimens. Load signals collected were converted into E_{mach} signals using Eq. [5]. Two-pass average E was determined for each run. Finally, each E_{mach} signal measured at 315 m./min. was subjected to a spectrum analysis to determine the major frequency components in the signal.

RESULTS AND DISCUSSION

Analysis of variance of the experimental data revealed that speed had no significant effect on average E within any of the species investigated, regardless of the machine employed. Therefore, experiments conducted verify theoretical expectations, established in Table 1, to the effect that the error due to speed on average E can be neglected up to 315 m./min.

Effect of speed on the ability of the grading machines to measure local E is illustrated in Figure 3 showing superimposed E profiles measured by Machine A at 15 and 315 m./min. on a typical specimen. The large amplitude profile indicated for the specimen at high speed differs markedly from the more uniform profile measured under quasi-static conditions. However, the mean trend of the high speed signal follows closely the signal measured at low speed, supporting the conclusion reached earlier about the negligible effect of speed on average E. As evident from Figure 4, power spectral density curves developed along the high speed signal show a major frequency component at around 130 Hz. This is very close to the natural frequency of the deflection roller-loadcell mechanism (f_n= 123 Hz) suggesting that this mechanism is the excitation source of the vibrations observed. Examination of frequency spectra for all high speed signals collected substantiated this conclusion.

Results from the present experiments indicate that the ability of stress-grading machines to measure local E is impaired by speed. In practice, such a situation would lead to erroneous grading in instances where low-point E, the lowest E value measured along the length of the piece, is used to grade lumber. These errors, however, could be reduced if the E signals were filtered before processing. Special attention, however, must be taken in selecting the filter in order not to cut fluctuations inherent to the lumber, such as those caused by the presence of knots and other localized defects. A study of the dynamic behavior of non-uniform lumber in stress-grading

machines would provide useful information on this matter.

CONCLUSION

Results from the present investigation indicate that the ability of constant-deflection type grading machines to measure the average modulus of elasticity of uniform lumber is not affected by speed up to 315 m./min. Speed, on the other hand, was found to reduce the ability with which the machines investigated can measure local E along the length of the lumber.

The model developed was capable to predict modulus of elasticity of lumber measured under dynamic loading conditions by two machines differing in support conditions. The close agreement which was found between theory and experiments suggests that the model could provide assistance in analysing the effect of speed for a wide range of machines operating under a wide range of conditions.

REFERENCES

Hoyle, R.J., Jr. 1961. A nondestructive test for stiffness of structural lumber. Forest Prod. J. 11(6):251-254.

-----. 1968. Background to machine stress grading. Forest Prod. J. 18(4):87-97.

Logan, J.D. 1978. Machine stress rating. Proceedings of the 4th Nondestructive Testing of Wood symposium. Vancouver, WA. Pp. 285-303.

Mote, C.D., Jr. 1968. Dynamic stability of an axially moving band. J. of The Franklin Institute 285(5):329-346.

Pellerin, R.F. 1976. Non-destructive evaluation of wood and wood products. Proceedings from IUFRO Wood Engineering Group meeting, Denmark/Norway, Paper 19.

Pelster, S. 1963. The Stress O-Matic stress rating system. Proceedings of the symposium on Nondestructive Testing of wood, Forest Prod. Lab., Madison, WI

Samson, M. 1986a. Predicted and actual performance of two laboratory stress-grading machines employing different support conditions. Wood and Fiber Sc. (in press)

------. 1986b. Effect of speed on the accuracy of stress-grading machines for lumber. Received for publication in Wood Science and Technology.

Table 1. Signal offset (E_{mach}/E) predicted by the model for both machines at selected speeds.

Machine	Speed (m./min.)				
	0	250	500	1000	2500
A	1.000	0.999	0.997	0.992	0.955
B	1.000	0.999	0.997	0.994	0.961

Captions for figures

Figure 1 Schematic representation of a bending-type stress-grading machine.

Figure 2 Relationship between signal frequency and machine parameter f_m as predicted by the model.

Figure 3 E_{mach} profiles measured by Machine A on a typical hemlock specimen at 15 and 315 m./min.

Figure 4 Dynamic spectrum of the high speed signal shown on Figure 3.

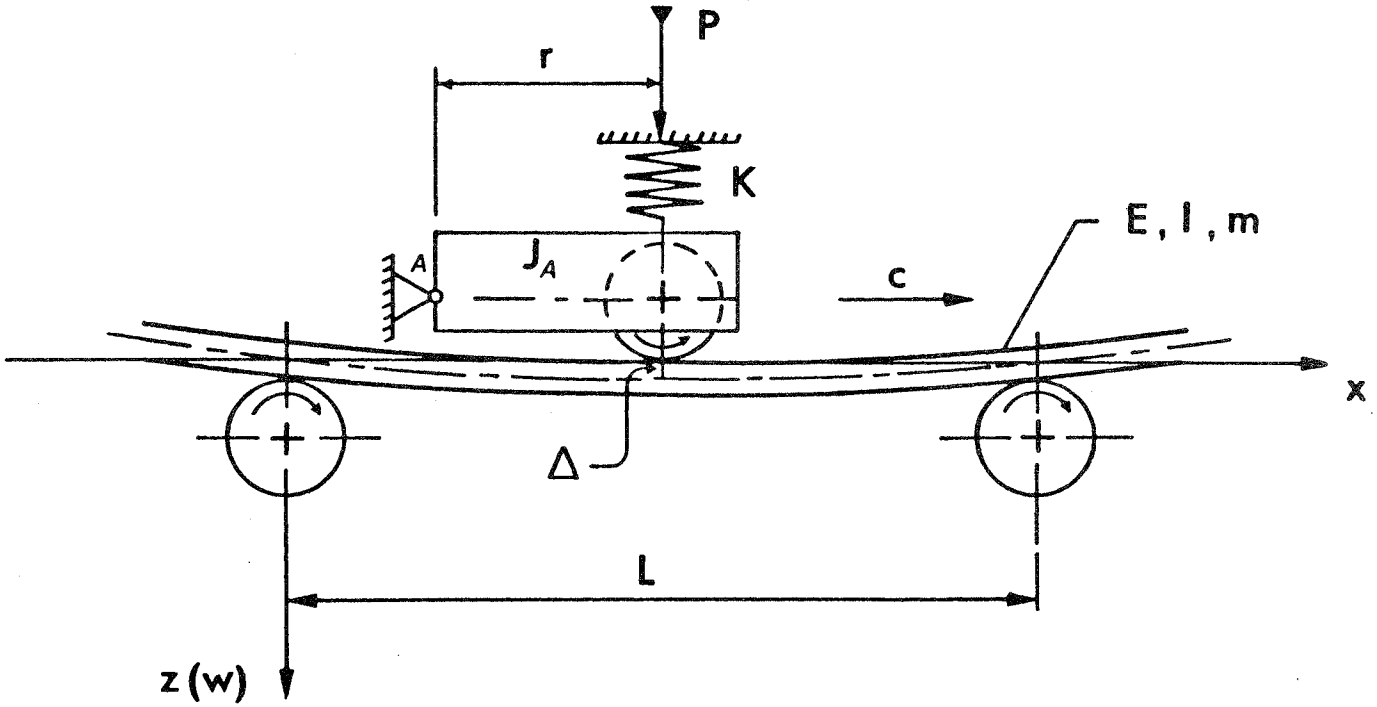


Figure 1

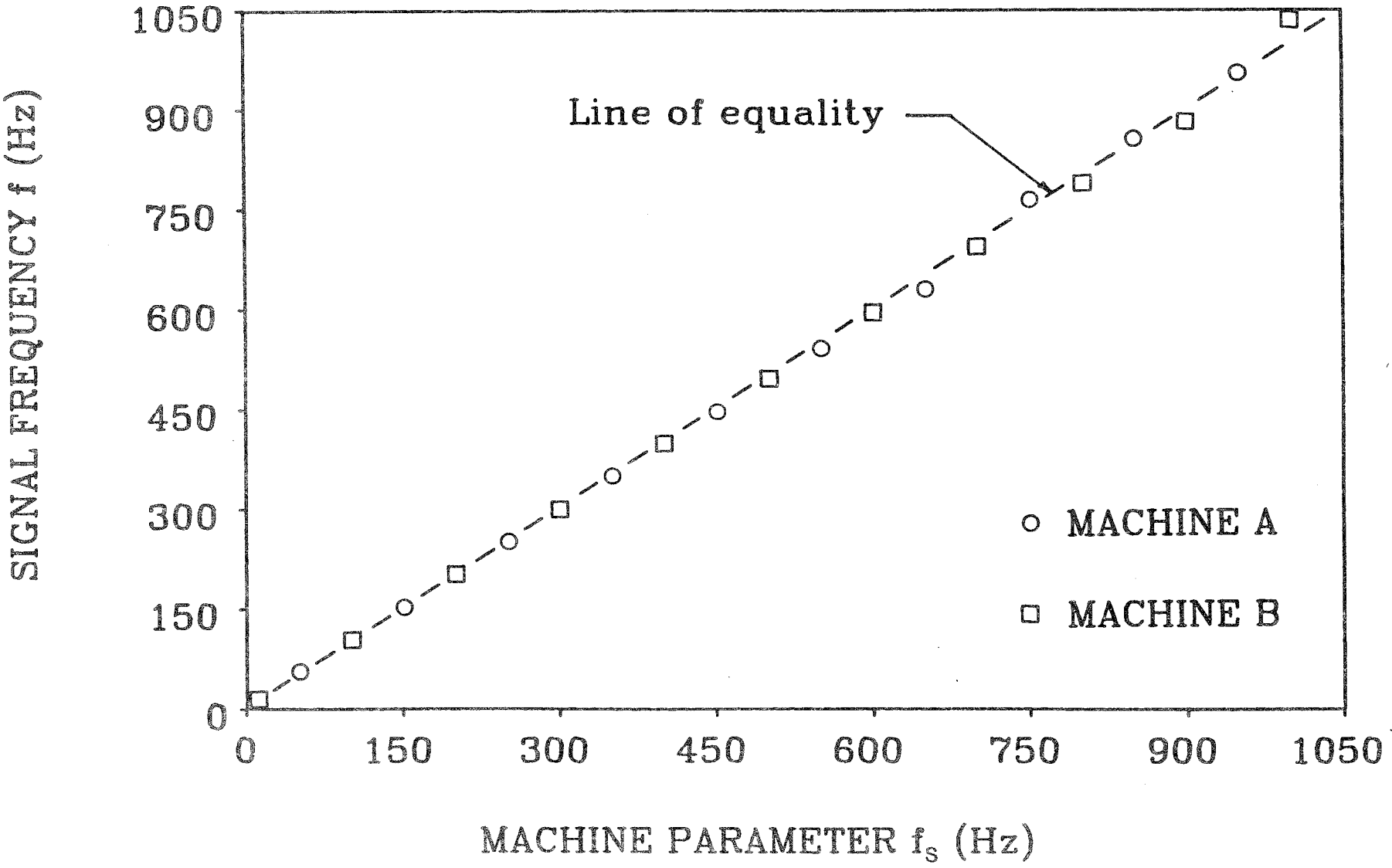

SIGNAL FREQUENCY f (Hz)
1050
900
750
600
450
300
150
0
0
150
300
450
600
750
900
1050
Line of equality
MACHINE A
MACHINE B
MACHINE PARAMETER f_s (Hz)

Figure 2

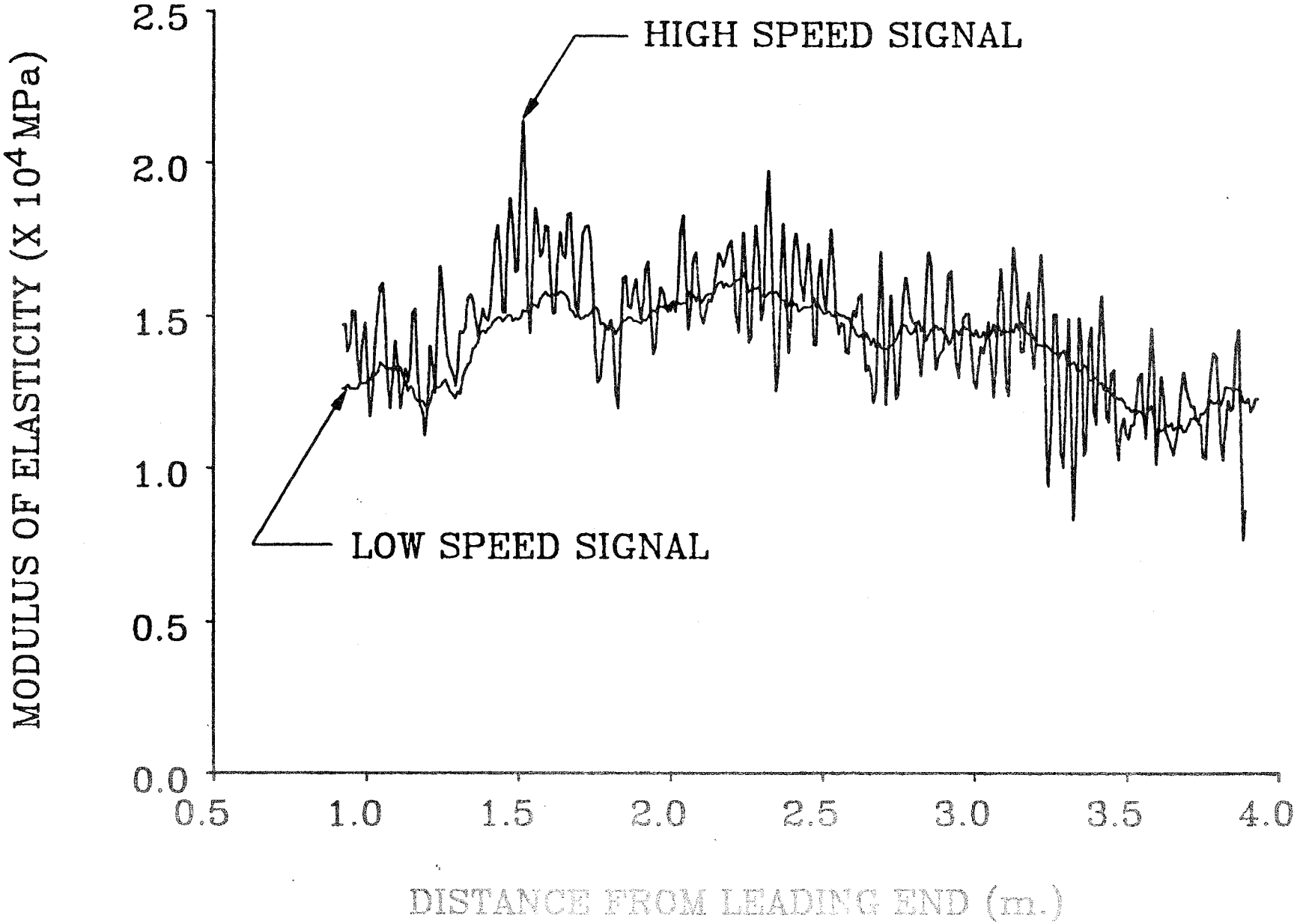

MODULUS OF ELASTICITY (X 10⁴ MPa)
2.5
2.0
1.5
1.0
0.5
0.0
HIGH SPEED SIGNAL
LOW SPEED SIGNAL
0.5
1.0
1.5
2.0
2.5
3.0
3.5
4.0
DISTANCE FROM LEADING END (m.)

Figure 3

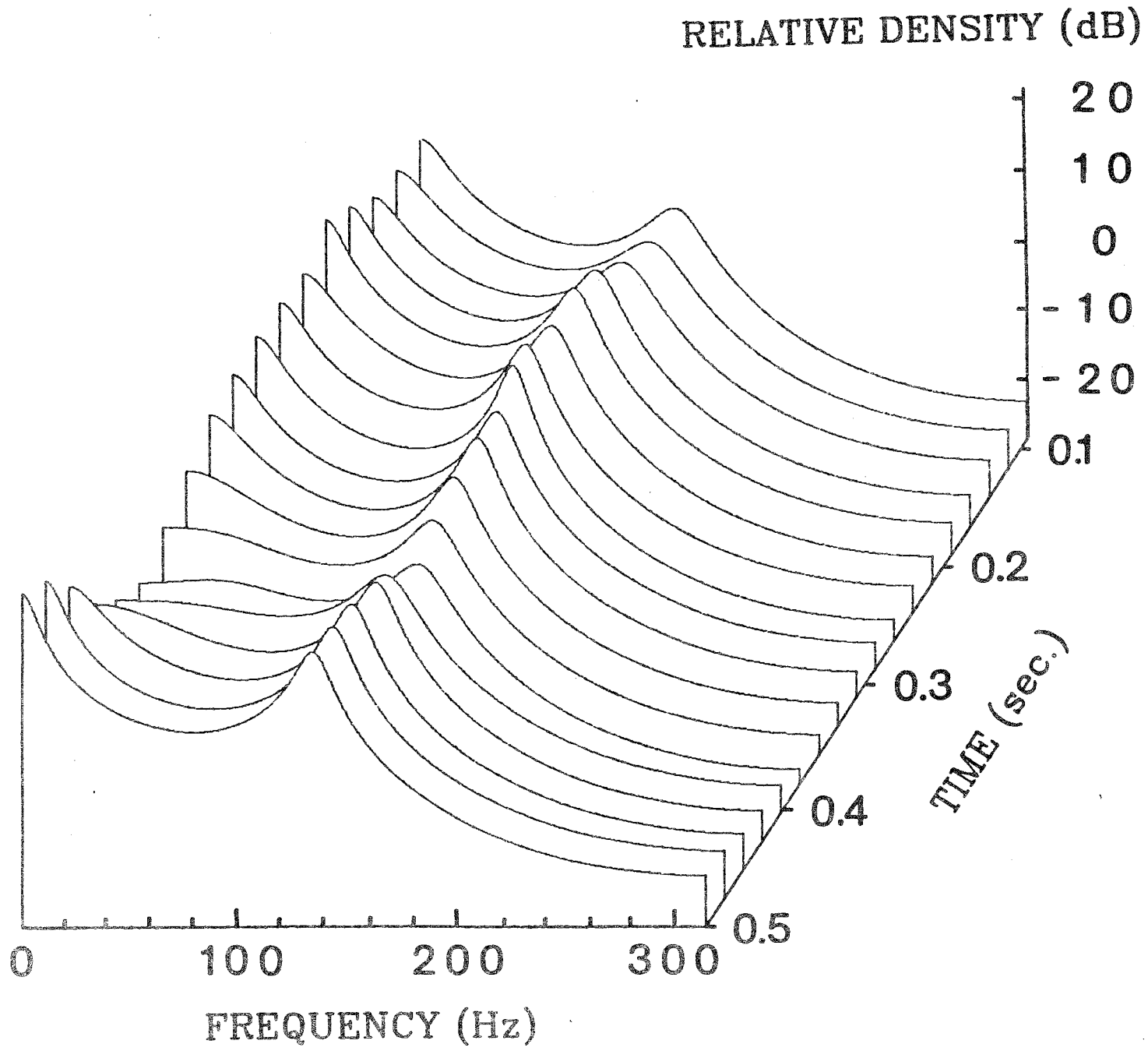

RELATIVE DENSITY (dB)
20
10
0
-10
-20
0.1
0.2
0.3
0.4
0.5
TIME (sec.)
0
100
200
300
FREQUENCY (Hz)

Figure 4

INTERNATIONAL UNION OF FOREST RESEARCH ORGANISATIONS

GROUP S 5.02 - TIMBER ENGINEERING

RELIABILITY OF TRUSSES

by

E Varoglu and F Lam

LJUBLJIANA
JOUGOSLAVIA
SEPTEMBER 1986

INTERNATIONAL COUNCIL FOR BUILDING RESEARCH
STUDIES AND DOCUMENTATION

WORKING COMMISSION W18 - TIMBER STRUCTURES
IUFRO SECTION S5.02 - TIMBER ENGINEERING

FLORENCE, ITALY
SEPTEMBER, 1986

RELIABILITY OF TRUSSES

by

E. Varoglu [1] and F. Lam [2]

Abstract

A comprehensive study of the short-term reliability of wood roof trusses is presented. Fink trusses with 4/12 roof slopes were examined. Visually graded No. 2 Spruce-Pine-Fir (SPF) and machine stress rated (MSR) 1650f-1.5E lumber, were considered in this study. Computer simulation techniques were employed to evaluate the short-term ultimate load capacity of these roof trusses. Under uniform snow loads from two locations in Canada, trusses spanning 19 to 32 ft. were examined.

Based on reliability analysis of the short-term strength limit state of these truss systems, allowable truss spans have been determined for a target reliability index of 3.5. The impact of utilization of 1650f-1.5E MSR lumber as compared to visually graded No. 2 SPF lumber in truss manufacturing have been demonstrated by the considerable increase in allowable truss spans.

1
Manager, Wood Engineering Department, Western Forest Products Laboratory, Forintek Canada Corp. 6620 N.W. Marine Drive, Vancouver, B.C. Canada

2
Research Engineer, Wood Engineering Department, Western Forest Products Laboratory, Forintek Canada Corp. 6620 N.W. Marine Drive, Vancouver, B.C. Canada

1.0 INTRODUCTION

Structural design philosophy has undergone major changes in recent years. Previous studies have demonstrated that Reliability-Based Design (RBD) offers a means to quantify safety in a better and more uniform way in comparison to allowable stress design. Subsequently, significant advances have been made in the application of RBD methods for concrete and steel structures. Although the application of RBD methods for wood structures has been limited, the current direction in structural wood design code development is towards RBD procedures.

The use of wood trusses in light frame structures represents a potentially significant share in both residential and non-residential roof construction market. It is important to develop RBD procedures for the proper assessment of safety of trusses so that more reliable and efficient use of wood in these engineered systems can be realized. A key step in the development of such RBD procedures for trusses is the utilization of computer simulation techniques to randomly generate trusses built from a given population of lumber. The short-term ultimate load capacities of these trusses under a given load configuration are determined utilizing a structural analysis computer program to establish the short-term resistance distribution of trusses assembled from a given lumber population. The amplitude of the load that these trusses will be subjected during their lifetime is also a random variable defined by the snow load information at the geographical location of the construction. By comparison of the short-term resistance distribution to the load distribution through Rackwitz-Fiessler algorithm, the reliability of the truss systems can be established. Thus, the effect of variations in the stiffness and strength properties of the lumber in the performance of wood trusses in a given location can be taken into account in a rational way.

This paper focuses on the assessment of the short-term reliability of trusses using computer simulation techniques. A comprehensive study of the short-term reliability of a Fink truss configuration with 4/12 slope, under uniform snow load has been undertaken. Preliminary experimental strength and stiffness data for visually graded No. 2 SPF lumber and the properties of MSR lumber (1650f-1.5E) are used in the computer simulations. Allowable spans are determined for a target reliability index of 3.5 associated with the strength limit state, for Vancouver and Quebec City in Canada.

2.0 THE SHORT-TERM RELIABILITY OF TRUSSES

Strength of wood depends on duration of loading. Duration of load tests for lumber in bending, compression and tension are in progress at Forintek. The results of these tests when completed will be used to study the long-term reliability of trusses. Stiffness and short-term bending, tension and compression strengths of a given grade of lumber exhibit large variability. Here, the short-term reliability of trusses under balanced snow loads has been investigated by taking into account only the variability in material properties of wood members of trusses built from a given grade of lumber.

Several truss spans, ranging from 19 to 32 ft. for a 4/12 roof slope, were examined. A representative truss configuration of a 28-ft. span is illustrated in Figure 1. The spacing of the trusses on the roof was taken as 24 in. on centre. The sizes of the truss plates are also given in Figure 1. At all joints, 18 gauge metal truss plates were used. For trusses of 32 ft. span, the single lower chord splice is replaced by two similar splices located symmetrically at a distance of eight feet from the centre of the lower chord. Also when the span is greater than 28 ft., each side of upper chord can no longer be built from a single piece of lumber; therefore, one splice is used in each side of the upper chord.

The flow chart given in Figure 2 illustrates the steps in simulations required to establish the load carrying capacity distribution for the truss family of a given span. The computer program, SIMGEN, was used to randomly generate material properties data for the truss members from a given population representing either visually graded lumber or MSR lumber. A random value of Modulus of Elasticity (MOE) and associated random bending, compression, and tension strengths selected from normal distributions were assigned to each truss component (web and chord members). For each span, material properties data for a total of 100 truss replications were generated.

The two types of material considered in this study are:

1. Visually graded, No. 2 Spruce-Pine-Fir (SPF) lumber, and
2. Machine stress rated (MSR) lumber 1650f-1.5E.

The distributions representing the variability of MOE and the short-term strengths of visually graded lumber in bending, tension and compression, as well as the correlation between MOE and the mean strengths were based on the results of in-grade type testing of the material under consideration. The same test results were utilized in the case of MSR lumber with additional constraints defined by the MSR grading rules in the random selection of MOE and strength values for the truss components. For instance, in the case of MSR lumber, the randomly generated bending strength data for components of trusses would satisfy the conditions that the fifth percentile bending strength of all the components of 100 trusses was not less than 1650x2.1 psi and the mean MOE exceeded 1,500,000 psi.

SATSIM, a simulation version of the truss analysis program, SAT, was used to perform the structural analysis of the simulation study. The structural analysis portion of SATSIM is identical to SAT; however, SATSIM has the additional capability of facilitating the simulation process by directly accessing the randomly generated member properties from SIMGEN. The theoretical background of SAT has been presented by Foschi, (1977a and 1977b) in detail, only a brief description of the program SAT will be presented here. The truss is modelled as a linear, elastic frame, joined by linear members called truss plates. The connection between the truss plates and wooden frame members is through the teeth of the truss plates. The load-deformation characteristics of the connector is assumed to be non-linear.

Each truss with randomly generated material properties and subjected to uniformly distributed load on the upper chord was analyzed. The load applied to upper chord was increased step by step until failure occured. For each replication, failure load, failure type and maximum truss deflections were recorded. The results obtained from this analysis for each span and material category are summarized in Table 1. The mean failure load is expressed as the load per unit length of the upper chord.

The failure function, G, for the strength limit state can be expressed as

$$G = R - (D+S)$$

for a given span. Here, R is the failure load (resistance) and D and G are the dead load and 30 year maximum snow load respectively for the given geographic location. The dead load was taken as 10 psf on the roof surface which corresponds to a uniformly distributed load 1.58 lb/in, on the upper chord of the truss. The snow loads for Vancouver and Quebec City were considered. Weather data provides information about the statistical distribution of the annual maximum snow depth for both cities. The 30 year maximum snow load distributions were obtained as Gumbel Type I distributions for both cities utilizing the yearly maximum snow depth distributions for both locations. The snow load in Vancouver has a high variability but low magnitude. Quebec City in contrast to Vancouver has a high magnitude and low variability. The reliability index for the failure function was calculated using the Rackwitz-Fiessler algorithm. The algorithm requires the distribution of random variables R and S in the failure function so that the slope and value of the cumulative distribution functions can be computed for any given value of the random variables. These calculations were performed numerically for R, working directly with the ranked values of failure loads obtained from the simulations. For S, Gumbel Type I distribution, as obtained from the weather data, was used for each location. The iteration for most likely failure point was stopped when two successive values of reliability safety index, β, differed less than 0.001. The reliability safety index values as a function of truss span are presented in Figure 2. The allowable spans give a target reliability index (β=3.5) were calculated, by interpolation or extrapolation and the results are presented in Table 2.

3.0 DISCUSSION OF RESULTS AND CONCLUSIONS

As shown in Table 1, truss plate failures, characterized by either tooth withdrawal or tension yielding at the links, were observed more in the visually graded truss systems of shorter-span. The same failure mode was observed almost for all the trusses built of MSR lumber. The coefficient of variation of the failure loads of MSR lumber truss systems were very small (approximately zero) because almost all of these trusses experienced connection failure at the same load step, irrespective of the variability in member properties. The joints for the truss systems of MSR lumber may be improved by increasing truss plate sizes and thicknesses, which may lead to substantial gain in the truss systems total performance.

It is clear from Table 2 that the utilization of MSR lumber results in higher allowable spans in both locations. The increase in the allowable span due to utilization of MSR lumber is about 11.7 ft for both locations.

The reliability index concept can be extended to consider the serviceability limit state of truss maximum deflection. Since the maximum truss deflections at failure were less than span/240 for all replications, serviceability limit state was not considered for this study.

4.0 REFERENCES

Foschi, R.O. 1977a. Analysis of wood diaphragms and trusses. Part I: Diaphragms. Canadian Journal of Civil Engineering. 4(3). pp.345-352.

Foschi, R.O. 1977b. Analysis of wood diaphragms and trusses. Part II: Truss-Plate. Canadian Journal of Civil Engineering. 4(3). pp.353-362.

Table 1

Failure Load and Maximum Truss Deflections

Material	Slope	Span	Failure Load		Maximum Vertical Deflection	Percentage of Connection Failure
			Mean	Coefficient of Variation		
		(ft)	(lb/in)	(%)	(in)	(%)
Visual grade No. 2	4/12	19	21.18	11.37	0.823	80
		22	17.93	12.34	0.878	81
		26	14.71	16.63	1.043	61
		28	11.85	9.48	1.196	48
MSR lumber 1650f-1.5E	4/12	24	17.79	0.0	0.803	100
		26	16.60	0.0	0.858	100
		32	9.49	0.0	1.078	100

Table 2

Allowable Truss Spans Yielding a Target Reliability Index of 3.5 for the Strength Limit State

Material	Slope	Location	Span (ft.)
Visual grade No. 2	4/12	Vancouver	19.62
		Quebec City	13.31
MSR Lumber 1650f-1.5E	4/12	Vancouver	31.36
		Quebec City	25.09

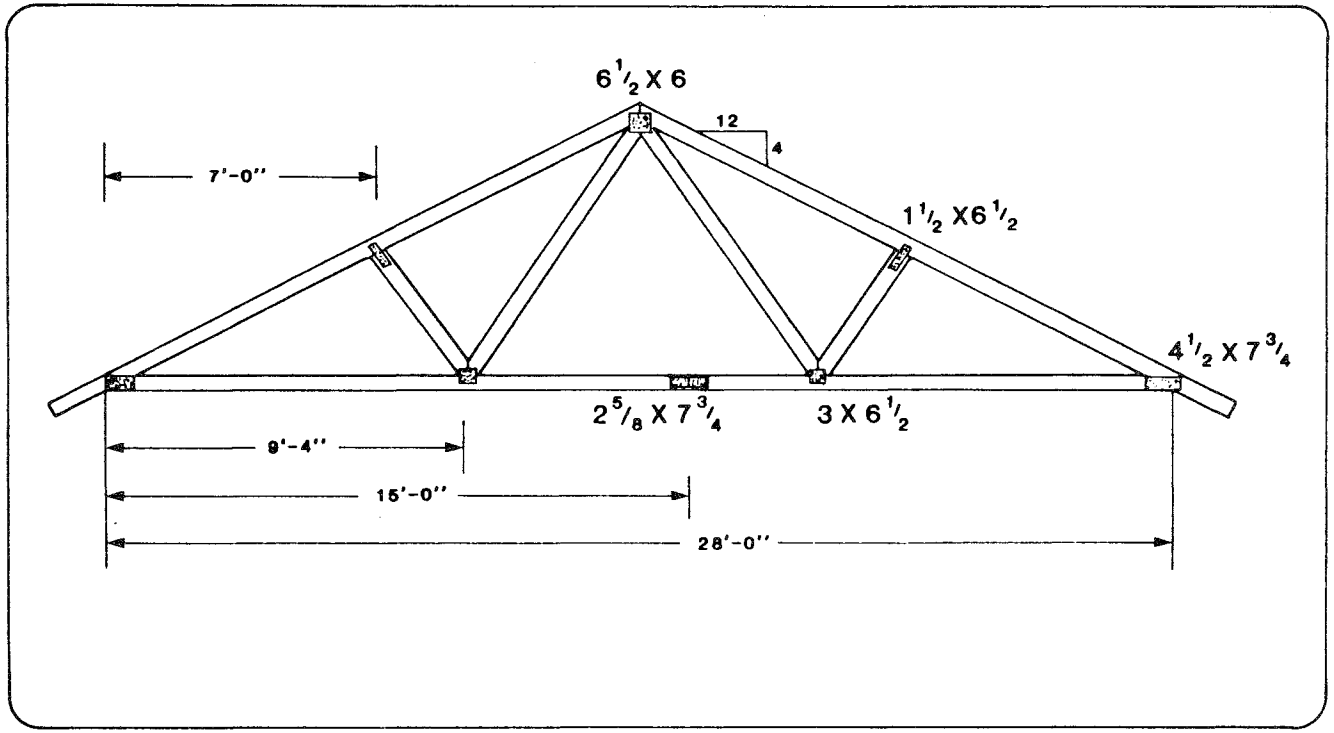


FIGURE 1. 4/12 TRUSS CONFIGURATION USED IN THE SHORT-TERM RELIABILITY ANALYSIS.

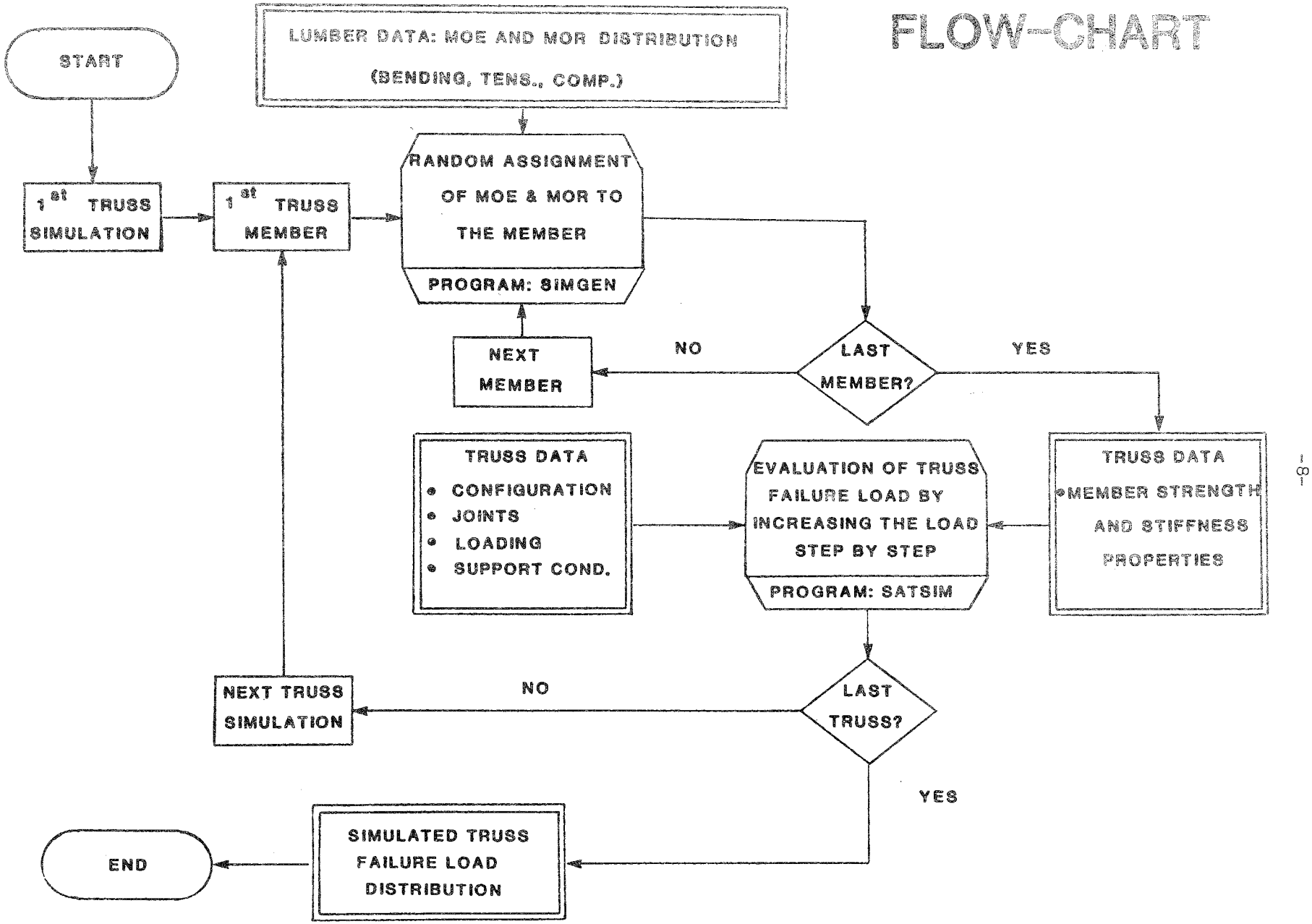


FIGURE 2. DETERMINATION OF LOAD CARRYING DISTRIBUTION OF A GIVEN TRUSS FAMILY

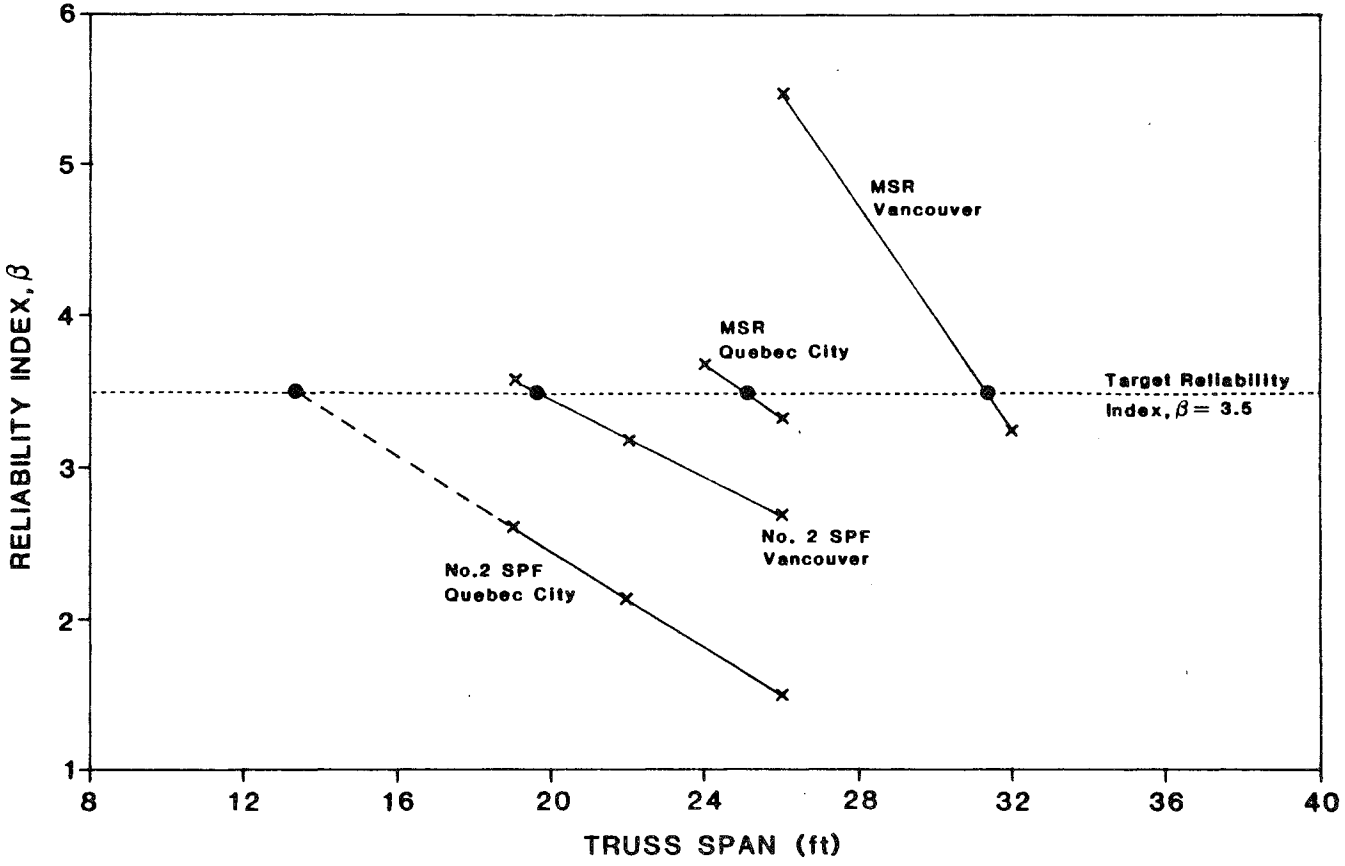


FIGURE3. RELIABILITY INDEX, β, VERSUS TRUSS SPAN FOR 4/12 TRUSSES.